BERLINER GEOGRAPHISCHE ABHANDLUNGEN

Herausgegeben von Margot Böse, Peter-Jürgen Ergenzinger, Dieter Jäkel, Hans-Joachim Pachur und Wilhelm Wöhlke. Schriftleitung: Dieter Jäkel

Heft 59

Carmen de Jong

# Temporal and spatial interactions between river bed roughness, geometry, bedload transport and flow hydraulics in mountain streams - examples from Squaw Creek (Montana, USA) and Lainbach/ Schmiedlaine (Upper Bavaria, Germany)

# Zeitliche und räumliche Wechselwirkungen zwischen Flußbettgeometrie, Rauheit, Geschiebetransport und Fließhydraulik in Gebirgsflüssen am Beispiel von Squaw Creek (Montana, USA) und Lainbach/ Schmiedlaine (Oberbayern, Deutschland).

229 Pages, 255 Figures, 7 Tables, 40 Photos

229 Seiten, 255 Abbildungen, 7 Tabellen, 40 Fotos

1995

Im Selbstverlag des Instituts für Geographische Wissenschaften der Freien Universität Berlin

ISBN 3-88009-060-2

*Carmen de Jong*

Temporal and spatial interactions between river bed roughness, geometry, bedload transport and flow hydraulics in mountain streams - examples from Squaw Creek (Montana, USA) and Lainbach/Schmiedlaine (Upper Bavaria, Germany)

Berliner Geogr. Abh., Heft 59: 1-229, Berlin 1995

BERLINER GEOGRAPHISCHE ABHANDLUNGEN

Herausgegeben von Margot Böse, Peter-Jürgen Ergenzinger, Dieter Jäkel, Hans-Joachim Pachur
und Wilhelm Wöhlke. Schriftleitung: Dieter Jäkel

Heft 59

Carmen de Jong

# Temporal and spatial interactions between river bed roughness, geometry, bedload transport and flow hydraulics in mountain streams - examples from Squaw Creek (Montana, USA) and Lainbach/ Schmiedlaine (Upper Bavaria, Germany)

229 Seiten, 255 Abbildungen, 7 Tabellen, 40 Fotos

1995

Im Selbstverlag des Instituts für Geographische Wissenschaften der Freien Universität Berlin

ISBN 3-88009-060-2

*To my grandmother, Margarete Fuchs*

*"You can never put your hand into the river in the same place twice"*
*Heraclitus*

**This thesis was awarded the IAH-IAHS Lausanne Price for 1994 (from the International Association of Hydrogeology and International Association of Hydrological Sciences) for publication in the field of Applied Geology, Hydrogeology and Hydrology.**

# Acknowledgements

I would like to express my special gratitude to my supervisor Prof. Peter Ergenzinger for all his suggestions, provoking discussions, technical innovations, active field help, joint publications, conference support and above all for the wide variety of career-forwarding opportunities he offered me in tackling never-ending heaps of international projects, translations, research liaisons e.t.c.

To my second supervisor, Prof. Hillert Ibbeken from the Department of Geology, I would like to extend my thanks for providing essential sedimentological and geological links to my work. I am also grateful for his financial support with film work during hard times.

To Prof. Dieter Rewicki of the Institute of Organic Chemistry I would like to extend my thanks for acting as my Studienstiftung mentor.

I am particularly grateful to Prof. Steve Custer from Montana State University for the laborious task of checking through my English.

I am indebted to those who made possible the invitation to the Gravel-bed Rivers Meeting in Florence, 1990 and to Prof. Luna Leopold's optimistic words which all together started the hopeful path towards my Ph.D. From the gender-specific side I am grateful to Dr. Judith Maizels from Aberdeen University for encouraging me to carry out research in the first place.

As is usual for a field-based project there are many thanks to go to many people. Since three field sites had to be covered, an inexhaustible amount of help was appreciated. In the field in Upper Bavaria I am indebted to Margarita Cruz Almanza, Neus la Roca (University of Valencia, Spain), Celso Garcia, Ramon Batalla (University of Barcelona), Marzelus Holzmann (Sozial-Pädagogische Fachhochschule Benediktbeuern), the ERASMUS students from Holland (for the unpleasant job of particle sieving) as well as Karin Möhrke, Michael von Werner, Dirk Oostwoud Wijdenes and the rest of the B.E.R.G. research group. To Michael Gross I am thankful for constructing the mini-Tausendfüssler device.

The Flußmeisterei in Benediktbeuern was an important aid in the transport and manufacture of equipment. Thanks go to the craftsmen in Benediktbeuern, especially the Seidl Timberworks and to the mayor of Benediktbeuern for special permissions. To the family Bartl I am very grateful for their annual hospitality on their picturesque farm and in particular for helping me with communications and repairs and for their patience during the nightly "rain-flood" alarms.

At Squaw Creek I greatly appreciated the help and field support given to me by Prof. Steve Custer (also for use of Departmental facilities) and his family, the office staff of the Department of Earth Sciences, Montana State University, the Swingle family, Kristin Bunte, Karin Möhrke, Michael Fischer, Artur, Dirk Ergenzinger and a number of Montana State University students. Prof. Christaller of the Department of Sensortechnik of the TFH Berlin and his assistants provided important support concerning all the electronics. To Paul Carling and his research group I am grateful for velocity data. I am also thankful for the immense amount of construction and fabrication assistance given to me by Jim Hogin of Hogin Metalworks and by John Palmer and his crew of Big Timber Works for all the construction work.

For data processing I am immensely grateful to Katja Hegewald who neatly digitised thousands of pebbles. Her diligence was unsurpassable. My thanks also go to Katja Janson, Isabella Schaltinat, Olaf Geest and Hubert Kümeke for keeping some of my supervisor's work off my back! Without the immense and painstaking help given to me by the "computer whiz-kid" Michael von Werner with all the software problems, I would never have been able to finish in time. To Karin Möhrke I am also grateful for many inspiring software hints (especially for teaching me Autocad) and quite a lot of entertainment. To Raymund Spieker I am very grateful for the professional hardware and software help he offered me at all times of the day and year.

None of my conference talks and hundreds of slides would have been of any success without the generous and often last-minute assistance from Klaus Wolfermann in the slide collection room. Rainer Willing always helped me with the complex cartography that my computer software did not achieve and also kept me up to date on all the latest departmental events. Ellen Leipner of the Photo-Reproduction Centre helped extensively and intensively with the reproduction of diagrams. In particular I would also like to thank Anne Beck for her self-replenishing office help and for checking the

final thesis version, Marlis Lindow for handling my abominable finances and Dieter Jäkel, Michael Walther, Joachim Schulz, Georg Schulz, Mr. Leonardy, Mrs Geb, Denyse Snelder and Mrs. Ackelbein for providing a pleasant and helpful stay in Berlin.

For helpful and inspiring discussions on photo-sieving analyses, I am grateful to Michael Diepenbroek, Alfred Wegener Institut, Bremerhaven as well as Alexander Barthomolä. For other positive criticisms I am thankful to Gordon Grant, Pacific Northwest Research Station, Corvallis; Simon Tait, Department of Engineering, Aberdeen University; Adrian Kelsey, Lancaster University, Murray Hicks of the National Institute of Water & Atmospheric Sciences, Christchurch; and a number of other researchers I met at the various conferences. For discussions and co-operation with the bedload data interpretations I am grateful to John Laronne, Israel.

My warmest thanks are extended to Bernhard Strackenbrock and Jutta Häser (Strackenbrock & Urban, Berlin and Seminar für Ur- und Frühgeschichte, Berlin) for managing to supplement my meagre funding in my first year by offering me translation work. They helped me develop some of my astronomical quantities of photographs and provided me with a constant supply of new ideas, programme writing assistance, the use of measuring instruments (e.g. Zeiss metric camera) and a great deal of humorous encouragement. I am also very grateful to the family Fricke for making my final stay in Berlin as pleasant and efficient as possible. My first ½ year was funded through a student research assistantship of the DFG project on the "The Fluvial Geomorphodynamics of the Lainbach in the Upper Quaternary" and by a short-term position as a research assistant in the DFG project on "Bedload Dynamics at Squaw Creek, Montana". The Studienstiftung des deutschen Volkes funded 2½ years of my Ph.D. studies and to them I am eternally grateful, not only for offering me unique and broad cultural and political opportunities, but also for the very generous funding that I acquired through them for many lavish conference visits. I am also thankful to supplements for conferences given to me through the exceptional support of the Free University of Berlin and the local conference organising committees, particularly the IAHS and the BGRG. Publication of this thesis was generously supported by the Lausanne-1994 award of the IAH-IAHS (International Association of Hydrogeologists and the International Association of Hydrological Sciences).

Lastly I would like to thank my grandmother and grandfather for all their loving and nutrient-rich support they gave to me during my research. I am also indebted to my mother Heidi for laying my geographical foundations during her long unpaid, labour-intensive years as my overseas "home-school" teacher, to Cordula for being a wonderful sister throughout and to my brother Andi for his moral support.

Berlin, 8.8.93 Carmen de Jong

# Contents

# List of Figures

## 3. Literature Review



## 4. Study Areas

## 5. Methodology



## 6. Results and Discussion

### 6.1.1 Squaw Creek 1991 & 1992

### 6.1.2. Schmiedlaine 1992



### 6.1.3. Lainbach 1992

**6.1.4 Fractal intervals of roughness in relation to grain size**



**6.1.5 The spatial variability of roughness and geometry according to channel form**

## 6.2 The spatial variability of roughness in relation to flow.

## 6.3 Temporal variability of roughness and geometry: Squaw Creek

## 6.4 Temporal variability of roughness and geometry: Lainbach

## TABLES

### 3. Literature Review



### 4. Study Areas



### 5. Methodology



### 6. Results

# 1. INTRODUCTION

Until recently there has been a lack of roughness studies with high spatial and temporal resolutions in steep, coarse-grained mountain streams during flood flows with active sediment transport (BATHURST, 1978, HEY, 1979, ERGENZINGER & STÜVE 1989, EGASHIRA & ASHIDA 1991, DE JONG 1992c). Individual processes have been examined in isolation but clearly defined interrelationships of the most important river bed interactions remain elusive.

EINSTEIN AND BARBAROSSA (1951), pioneers in the study of roughness, started by separating grain and form roughness in order to identify energy losses during roughness changes. The fluctuations in energy resulting from roughness adjustments on the river bed rely on the interactions between hydraulics, bedload transport and river bed geometry. If these parameters are generalised or averaged, large inaccuracies emerge from evaluation of energy components in the river system. Manning and Strickler first developed roughness coefficients that were later refined by Darcy and Weissbach but these coefficients define absolute roughness and do not incorporate information on grain and form roughness, or on energy dissipation which arises from bedload transfer and turbulence. Very few advances seem to have been made on this aspect of roughness since LEOPOLD, WOLMAN & MILLER (1964). Work by HAYWARD (1980), and GRIFFITHS (1989, 1981) on the dynamics of roughness in mountain streams of New Zealand are an exception. They demonstrate the importance of rapid form and flow resistance changes over mobile beds. Most emphasis in the past has had a one-sided tendency towards analysis of the influence of roughness on flow and bedload transport (both in the field and in the laboratory).

The analyses do not explore how roughness itself changes in response to the dynamics of the system. In addition, the literature does not address the role that flow and bedload play in the development of roughness and energy dissipation. Roughness has not been defined clearly and measurements have not been developed to assess the various sources of roughness.

A roughness coefficient is required that accounts for spatial and temporal changes of roughness over mobile boundaries. So far, roughness has normally been calculated before or after a flood using representative $D_{84}$ or $D_{50}$ grain size values or is merely estimated (WHITING & DIETRICH, 1990). Unfortunately these approaches conceal significant tendencies which experimental data may disclose (BAGNOLD and BARNDORFF-NIELSON, 1980). The $D_{84}$ and $D_{50}$ values are not representative of the entire grain size spectrum, nor do they indicate the changing roughness conditions during a particular time during a flood or at a particular location in space. When depending on only one representative grain size in calculating roughness, there is a danger of omitting factors that vary temporally and spatially during the course of a sediment transporting event. Thus when using flow depth over a representative grain size (BATHURST 1982 a & b, HEY 1979, EGASHIRA & ASHIDA 1991) the variability in flow depth may be obtained but changing grain and form roughness remain unknown.

There is a new approach whereby roughness can be measured with high spatial and temporal resolution. The method produces an absolute roughness coefficient ($K_3$) which correlates well with the Darcy-Weissbach or Manning coefficient and can be obtained empirically throughout the passage of a flood (ERGENZINGER AND STÜVE 1989). When calculating total roughness using the Darcy-Weissbach coefficient, all energy losses are generalised. The $K_3$ coefficient, however differentiates form and grain roughness. High resolution measurements of bedload transport and different aspects of flow hydraulics can be used to compliment the $K_3$ coefficient. In addition, factors controlling the spatial distribution of roughness and geometry can be investigated both longitudinally and laterally.

In order to analyse the interactions between roughness, geometry, bedload dynamics and flow hydraulics, both spatially and temporally, measurements should be dealt with separately. Roughness analyses have to consider the correct time-scale ALLEN (1983).

Several hypotheses have been set up under the following research structure which are to be tested during the course of the thesis. In order to examine the increasingly complex natural fluvial problems, we have to:

"Think globally, act locally" (NEWSON 1992).

## 1.1 Research Structure

This study follows the deductive approach of Carl Popper and proceeds from the problem identification, hypothesis formulation, experimental design, data collection, verification procedures and finally the formulation of laws, theories and models. The main geomorphological framework used is field observation, laboratory data analysis and theoretical office work. The primary objective is to adequately describe and explain the temporal and spatial dynamics of river bed roughness and geometry. HAINES-YOUNG and PETCH (1980) criticised this methodology because it is often characterised by uncritical acceptance of different philosophies, some of which are incompatible. This criticism led to the development of new methodologies. New methodologies and theories were introduced, keeping in mind that the advancement of many topics in geomorphology occurs in the form of paradigm shifts i.e. due to a revolution in ideas in response to dissatisfaction with the previous models (from NEWSON 1992). The need for adequate sampling is fundamental. At first all phenomena appear to be isolated. Mutual relationships can be traced only through a multiplicity of observations, combined with reasoning (HUMBOLDT 1849). The thesis has taken on a slightly, broader and more interdisciplinary approach (between geological techniques, hydrological data assessments and geomorphological interpretations).

A major obstacle to many fluvial geomorphological studies is the over-emphasis of the spatial pattern producing element which very often results in the neglect of the temporal elements. It is difficult to contend that spatial pattern descriptions actually constitute a process theory when gaps still exist in temporal descriptions. A possible cause for this error is that in the analysis stage, the objective is often not adequately defined. Another origin may be the scale problem where small scale processes are extrapolated inappropriately to large scale natural processes. An interactive roughness/bedload/flow dynamics model from the Squaw Creek data was set up to enable explanations and predictions. Predictions were tested at the Lainbach and refined.

As once stated by Schaeffer, a famous geography philosopher, "geomorphologists often accept too quickly the notion that all things are unique but that they have common characteristics and behave in common ways. It will become evident within the progress of the thesis that the same principles do not apply to all similar processes. Nevertheless, principles are better than simple description and indeed if a geomorphological idea is to be meaningful, it must consist of a verifiable scientific method. The model and relationships in my thesis are hypotheses and may be falsified in future if data supports rejection.

# 2. AIMS

The study explores the influence of bedload transport and flow hydraulics on the spatial and temporal dynamics of bed roughness and geometry in mountain streams.

In order to investigate these complex interrelationships, each topic is treated separately. A new relative roughness coefficient, $K_3$, is applied in the spatial and temporal roughness analyses. Detailed analyses of the highly variable natural fluid and sedimentary interactions are performed in the three mountain streams instead of using an estimated mean shear stress value to predict and describe river bed dynamics. Finally, the spatial and temporal interrelationships between roughness, geometry, flow dynamics and bedload transport are summarised in the new F.A.S.T. (Fluid And Sediment Transfer) model.

## 2.1 Hypotheses to be tested:

### 2.1.1. Spatial patterns of bed roughness

- How do longitudinal and lateral grain and form roughness change in relation to one another? Do these changes persist over different temporal and spatial scales? These questions will be analysed on two gravel bars and in the channel at Squaw Creek (1991/1992), on one bar in the Schmiedlaine (1990/1991/1992), and along the bar and channel in the Lainbach (1992).

- What influence does flow hydraulics and/or bedload dynamics have on the spatial dynamics of river bed roughness? This question will be analysed for the same locations and in the same time sequence as above.

- Can a river bed can be adequately described in fractal terms? If so, does a relationship exist between grain size distributions and associated fractal distributions.

- How can roughness elements such as clusters best be described so as to distinguish such features from adjacent material? Is the size difference between clusters and adjacent material significantly influenced by flow and/or bedload transport.

- Is the spatial variability of form and system roughness related to bend curvature?

### 2.1.2 Spatial variability of roughness in relation to flow

- Can roughness elements such as clusters be used as flow indicators? Do these roughness elements represent a different flow phase from that of the surrounding open-bed material. This question will be investigated for the Schmiedlaine and Squaw Creek.

- How does flow influence the planimetric and cross-sectional shape of roughness elements and their angle of imbrication?

### 2.1.3 Temporal patterns of bed roughness and geometry

- Are there relationships between the dynamics of roughness, channel geometry and water surface topography?

- Do roughness and geometry change continually or in phases during unsteady flow? Are these changes dictated by bedload transport and/or flow hydraulics. This will be investigated at Squaw Creek (1991/1992) and Lainbach (1992).

- A model is proposed to differentiate possible phases of river bed and roughness adjustment in response to water surface dynamics. FAST (Fluid And Sediment Transfer), will be formulated and tested at Squaw Creek, and applied to the Lainbach where all parameters other than bedload transport are known.

# 3. LITERATURE REVIEW

## 3.1 Research Applications

Drastic changes in the erosion, transport and deposition of valley sediments are expected in response to the threat of climatic change. The mobility of these sediments is strongly dependent on the stability of the river bed which is ultimately determined by roughness and geometry conditions. There is an urgent need to reduce resulting hazards such as increased erosion of man-made structures in higher altitude regions, increased amounts of sediment deposition in urban areas and changes in the amount and composition of sediment in the lower areas of deposition. In order to evaluate drainage area protection, detailed studies are required on sediment dynamics, river bed stability and flood hydraulics in active mountain torrents. During floods there are large temporal and spatial fluctuations in bedload transport. There are particular dangers which result from the generation of large-scale roughness elements such as log jams. The monitoring of coarse bedload movement is important for the analysis of changing roughness characteristics in relation to total sediment yield, reservoir filling rates, bridge erosion and vulnerability of fish-spawning habitats (ERGENZINGER & CUSTER 1983). A knowledge of the spatial distribution of roughness impacts on river-bed characteristics is essential in ungauged catchments for the determination of stage discharge relations, water and sediment discharge, the mean annual flood and to reconstruct paleo-flow hydraulics (SIMONS et al 1965, CLIFFORD et al 1992). The flood hydraulics which include less familiar processes such as secondary circulation (BATHURST et al 1979) and the temporal variations of friction velocity determine the onset of bedload transport (HAIZHOU & GRAF, 1993) and are important for channel design, river protection and flood routing.

### Definition of mountain stream

There are few continuous measurements of the dynamic nature of natural mountain torrents. Up to now, much work has concentrated on sand-bed rivers and meanders but work on straight, coarse reaches has been limited. Mountain torrents are characterised by large-scale form roughness created by large boulders and cobbles. Their geometry is largely dictated by step-pool topography which is dependent on large boulders, woody debris and bedrock outcrops (LISLE 1986, KELLER & TALLY, 1979). Gradients are steep (>2%) and cross-sectional geometries have high width to depth ratios. Bedload transport is of a fluctuating, intense nature which is dominantly supplied by hillslope processes. Stream hydraulics are influenced by large-scale form roughness (GRANT et al 1990) creating high energy losses (BATHURST 1978), critical to super-critical flow and disrupted velocity profiles (JARRETT 1984, WIBERG & SMITH 1987, HAIZHOU & GRAF 1993, YALIN 1992). The local morphology of the stream bed is controlled by small (approx. 10 $m^3s^{-1}$) floods which occur mainly in the early summer months in response to snow melt or orographic rainfall. Major channel forming events consist of infrequent catastrophic floods with high magnitude and low frequency (GRANT 1990, DE JONG 1992b) e.g. the extreme flood in the Lainbach valley of 30th June 1990 with a recurrence interval of 150 years (DE JONG 1992b).

### 3.1.2 Problems in the study of spatial and temporal dynamics of roughness

In most studies the temporal and spatial variability of roughness is not measured directly. As a result analysis depends on the generalising assumptions produced by substitution. BATHURST (1982a&b), BRAY (1982) and Whiting & DIETRICH (1990) refer to numerous friction/resistance formulae for roughness and test their ideas statistically using existing data sets in order to arrive at optimal empirical functions. They deal with local averages only, so that a lack in spatial and temporal roughness variability persists. Unfortunately the observation BRUSH (1965, p.2) made is often ignored "roughness is a derived quantity and not a known or predictable independent quantity". In this study, shear stress will not be relied on, instead measurements of bedload, water surface gradients, river geometry and adjustment and a relative roughness coefficient ($K_3$) will be applied. The distribution of shear stress cannot be determined successfully by theoretical methods due to the composite roughness and non-uniform shape of natural channels (KNIGHT & McDONALD, 1979).

Despite the major advances on river bedforms and roughness in relation to geometry, much remains to be learned about extreme grain sizes, unsteady flow and high bedload transport rates (ALLEN 1983). Most importantly the link between bedform development and fluid characteristics requires analysis. Because of the unsteady nature of bedload transport, data acquisition is needed at several time scales.

Extensive studies on the spatial and temporal dynamics of roughness have been carried out in the flume. But no studies in nature have been undertaken to explain why roughness should increase or decrease at a particular time or at a particular space. Flume studies remain very limited in their applicability to natural systems since they do not account for important variability in grain size distributions, grain sorting, bedform diversity, gradient, turbulence, discharge range, flume dimensions (hydraulic geometry), erodibility of flume banks and existence of hillslope interactions. The grain size distribution in steep mountain environments cannot be reconstructed from uniform grain mixtures, nor is it possible to extrapolate results, such as Froude numbers for these highly fluctuating fluvial processes. In addition complex natural behaviour influencing roughness development such as secondary flow circulation which is determined by certain width to depth ratios (YALIN 1992) and the dynamics of bedload transporting phases (BRIDGE 1991, BUNTE 1992a&b, CARSON & GRIFFITHS 1987, DE JONG & ERGENZINGER 1992, DRAKE et al 1987, ERGENZINGER 1988, ERGENZINGER et al 1994, GOMEZ 1983, et al 1989, JACKSON & BESHTA 1982, KUHNLE & SOUTHARD 1988, REID & FROSTICK 1986, SHIH & KOMAR 1990) cannot be adequately described in the flume. In short, the role that roughness plays in mountain streams is highly variable, both spatially and temporarily and this variability cannot be replicated under simplified flume conditions.

## 3.2 Spatial variation of roughness

### 3.2.1 Hierarchies and patterns of roughness

In natural torrents, river bed arrangement is a very important determinant of the spatial interactions between bedload dynamics, river bed roughness and flow adjustments. These are in part dependent on the actual grain size distribution, on grain shape and river bed gradients as well as valley shape. The scales of roughness and associated river geometry play differential roles in determining flow resistance and controlling non-uniformities in sediment transport (GRANT et al 1990, WHITTAKER and JAEGGI 1982, ERGENZINGER et al 1994).

Nonetheless, there is still a major deficiency in the description and analysis of the formation and patterns of coarse-material bedforms such as clusters, transverse ribs and arcs, boulder berms and levees and their interaction between river geometry in coarse mountain environments. Regardless of this deficiency, the range in spatial variability of roughness in coarse-grained rivers has been summarised in Table 1 after CHIN (1989), GRANT et al (1990) and ROBERT (1990). In the literature reference is made primarily to sand bedforms and artificial bedforms in the flume followed by a sudden jump in scale to boulder and step-pool systems. The scanty acknowledgement of gravel and cobble bedforms cannot be justified. Coarse material has an important influence on sediment transport and hydraulic characteristics of streams and rivers.

A distinct hierarchy exists in roughness units ranging from single grains to clusters, step-pools and finally the actual river morphometry. Thus single bed particles and their associated hydraulic micro-environments form assemblages of micro- and macro-bedforms which in turn influence the reach and collectively the river's longitudinal profile (GRANT et al 1990). Even at the largest roughness scales, i.e. unit roughness, there are important scales of variation (GRANT et al 1990) in relation to the extreme variability in grain size distributions and local slopes. Hierarchies of bedforms are thus related to a range of flow depths, flow regimes and availability of sediment (ALLEN 1968).

These investigators have shown that the spacing of channel units is not random. Step spacing is inversely proportional to the bed slope and the steepest bedforms consists of the $D_{90}$ of the local grain size distribution (GRANT et al 1990). Well developed channel units such as bars are absent from channels that have gradients steeper than about 4° due to constraints of width to depth ratios and low ratios of flow depth to particle size. Instead step-pool systems characteristically form under conditions of a low sediment supply. The spacing of channel bedforms, such as pools and riffles, has been confirmed to be a function of channel width, lying anywhere between 2-7 channel widths (CHURCH & GILBERT 1975, GRANT et al 1990, LEOPOLD & WOLMAN 1957, RICHARDS 1978). Indeed, channel bedform spacing depends on slope gradient, so that steeper channels

Table 3.1 Spatial variability of different scales of roughness

| Grain roughness | References | Form roughness | Length * (parallel to flow) | References | Unit roughness | Length* (parallel to flow) | References |
|---|---|---|---|---|---|---|---|
| single particles | Komar and Li 1986 | clusters | $10^{-2}$-$10^{0}$ | O'Loughlin 1969 Brayshaw 1983, 1985, Clifford 1992, Hassan 1990, Johannson 1963, Teisseyre 1977, Dal Cin 1968 , Reid 1983 de Jong 1992 a,b&c 1993 | riffles and pools | $10^{-1}$-$10^{0}$ | (Leopold et al 1964, Yang, 1971, Richards 1976, 1978a, 1978b, Robert 1990, Keller and Melhorne 1978, Milne 1982b Beltaos 1982 Bathurst 1982 Ashida 1981 Knighton 1983 |
| | | transverse ribs | $10^{-1}$-$10^{0}$ | McDonald and Banerjee 1971, Koster 1978, Allen 1982, McDonald and Day 1978 | minor steps | $10^{-0}$-$10^{1}$ | Hayward 1980, Whittaker 1987b, Sawada et al 1983 Heede 1981 Church & Jones 1982 |
| | | arcuate ribs | | | rapid, cascade | | (Grant et al 1990) |
| | | | | | steps and pools | | Bathurst 1978, Bowman 1977, Whittaker 1982, 1987a, 1987b, Whittaker and Jaeggi, 1982a &b Petts & Foster 1985 Ergenzinger 1990, 1992, Egashira 1991, Graf 1989, Grant, 1990, 1992 Chin 1989, Robert 1990, Clarke and Hansen 1985 |

* lengths measured in terms of channel width

have more closely spaced bedforms. Large boulders also dictate the spacing of pool systems. Ultimately unit size is dependent on the distribution of bedrock (which influences the location of steps), channel constrictions and local coarse material inputs (GRANT et al 1990, MILNE 1982a, 1982b). Large-scale boulder log jams for example, are situated at the upper end of the bedform scale and are mostly dependent on transport-limited non-fluvial material such as large boulders and logs from debris inputs (GRANT et al 1990, DE JONG 1992b). The rare incidence of coarse-material transporting events indicates that the hydraulic conditions under which these bedform systems evolved are dependent on high magnitude, low recurrence interval events (GRANT et al 1990).

### 3.2.2 Fractal intervals and scales of roughness

Fractals describe a physical division (from the Latin verb *frangere* or splitting up, breaking into irregular pieces as in *fraction*) into ever smaller intervals from infinitely large intervals (MANDELBROT 1987, TURCOTTE 1992). Fractal intervals are assumed to be an appropriate measure for describing the chaotic nature of roughness. Fractal intervals determine a range of scales over which the statistical properties of an entity remain self-similar. Fractal analyses of the hierarchy of bedforms on the river bed have revealed that transitions in roughness are scale dependent (FURBISH, 1987, ROY & ROBERT 1990). Work by

CLIFFORD et al (1992) and ROBERT (1990) has demonstrated that in natural river sediments, two fractal bands of roughness exist. These fractal bands are clearly separated by transitions which are attributed to a change in scale from grain to form roughness.

The authors also suggest that a selection of longer step lengths would emphasise the fractal dimension of the slope (gradient) component in rivers. If a short river reach is selected, then the slope is associated with a local measure of resistance to flow only as in ROBERT (1990). The river reach should therefore be long enough to include at least one geomorphic unit even if this means more work! In short, this implies that reach lengths should be long enough to develop a mean slope and assess its variance (BRAY 1982).

Fractal intervals define the transitions between form and grain roughness and so must depend in part on the grain size distribution. However little attention has been given to the distribution of roughness in relation to grain size (see MILNE 1982b), especially within a reach scale or for small gravel/cobble streams. Neither have the different types of roughness and geometry been systematically investigated for different rivers and river reaches in relation to the local grain size.

Another shortcoming is the lack of cross-sectional and longitudinal roughness comparisons, which are again related to the grain size and type of bedforms. Fractal analyses of roughness distributions in different environments and different orientations should improve our spatial knowledge of such roughness distributions.

### 3.2.3 Measurements of roughness and geometry

#### 3.2.3.1 Micro-profiling

Conventionally, roughness has been measured from the local grain size distribution (BRAY 1982, BATHURST 1982 a&b, GRIFFITHS 1981, HEY 1979). These measures are inadequate since they do not reflect the bed arrangement, hiding, and the projection (degree of exposure) of particles which have an important influence on the initial and selective movement of grains (FENTON & ABBOTT, 1977, PARKER et al 1982, ANDREWS 1983, KOMAR 1987, KIRCHNER et al 1990). Thus the resistance of roughness to flow is related to the pattern and spacing of roughness elements (BAYAZIT 1978).

In addition, BAYAZIT (1983) and KOMAR & LI (1988) found that the agreement of the roughness coefficient $K_S$ and grain size is not perfect in nature. Accurate determination of roughness has been a major problem in engineering and sedimentary investigations (HEY & THORNE, 1983), and it is clear that an efficient sample size and consistent method is required (WOLCOTT & CHURCH, 1991). Measurements of the vertical profiles (c-axes) are important since the velocity distribution has been proven to depend on the vertical orientation of the clasts (WIBERG & SMITH, 1991). Micro-profiling is thus an essential technique to measure roughness.

Measurements of roughness are typically spatially limited since they are taken only at metre intervals, rather than over an entire reach and then are restricted to the longitudinal profile, with no data collected on the cross-sectional profile. Measurements must take into account large differences in relationships between form and grain roughness for different rivers due to the effects of micro-bedforms. A multiplier function for each characteristic grain size is therefore required (CLIFFORD et al 1992). In order to derive such a multiplier of grain size distribution different techniques for measuring the particle c-axis projection can be applied.

The spatial variation of bed elevation can be determined using a micro-profiling technique whose setup and application varies with researches. No standard method exists. The bed profile can be scanned directly from a micro-profiler in the field (FURBISH, 1987, ROBERT 1988, 1991, CLIFFORD et al 1992) or re-produced by means of pins and photographed in the field, so that exact positions can be digitised later in the lab (DE JONG 1992d) or be profiled with sophisticated steel frames and adjustable spring legs as used for testing rock roughness (McCARROLL 1992). Less satisfactory and less efficient techniques include resin sampling of the surface (BUFFINGTON et al 1992).

More sophisticated techniques that do not disturb the flow field and sample the river bed in far shorter time intervals include flat water echo-sounders and high frequency sonars (DINGLER et al 1977). Extreme difficulties are encountered when applying echo-sounders in active mountain torrents rather than in gentler and deeper lake and harbour environments for which they were designed. A special flat-water echo-sounder developed for the field (Lainbach and Squaw Creek) by the company Dr. Fahrentholz failed due to signal disturbance by turbulence, air bubbles and shaking of the sounding body which confused the depth recordings.

#### 3.2.3.2 Quantification of textural particle characteristics

Approaches to the measurement of grain sizes by sieving and other similar techniques dependent on the measurement of b-axes or by weight (WOLMAN 1954, LEOPOLD et al 1964, WOLCOTT & CHURCH, 1991) are widespread in the literature. Description of roughness by grain size alone has its limitations however, since it does not take account of the degree to which particles project into flow.

In addition the lack of accurate grain size description techniques has often lead to oversimplifications or estimations of roughness properties in those cases where the river bed could not be sampled otherwise. This has been largely overcome by the new photosieving technique developed for the analyses of textural particle characteristics (DIEPENBROEK, 1992, DIEPENBROEK et al 1992, DIEPENBROEK and DE JONG 1993, IBBEKEN, 1974, IBBEKEN and SCHLEYER, 1986). This 2-D surface sampling technique may at first appear to be disadvantageous. It is actually advantageous when viewed in the light of incipient particle motion which is restricted to the surface layer and does not include the 3 dimensional particle size due to hiding and particle exposure (KLINGEMANN and MATIN, 1993). The technique allows accurate and rapid description of individual particles by means of the analysis of vertical photography of the river bed. Particles are digitised and their outlines approximated to an ellipsoid, assumed to be the particle's optimal shape, by means of a Fourier analysis. The description of the particle outlines allows not only very precise a and b axis descriptions but also the determination of particle rounding, surface area and degree of orientation. A special computer program developed by BARTHOLOMÄ and DIEPENBROEK analyses these properties.

### 3.2.4 Limitations of traditional flow resistance equations

Flow resistance is produced by the effects of form drag of sediment particles, their disposition in the channel, channel shape, bedform drag and sediment movement effects (BATHURST 1982 a & b, ROBERT 1990). As LEOPOLD, WOLMAN & MILLER (1964) pointed out, roughness has to be clearly differentiated in terms of grain, form and flow resistance. This includes the resistance of particles, bedforms and channel geometry (EINSTEIN & BARBAROSSA 1951, BOGARDI 1974, GRAF 1971). Flow resistance affects the mean velocity of flow that can be calculated from the shape of the velocity profile which in itself can be quantified as a function of resistance factors (BRAYSHAW et al 1985).

There are two commonly used equations for roughness, Manning and Darcy-Weissbach. One formulation of Darcy-Weissbach is that roughness depends on bed slope and geometry. One formulation of Manning is that roughness depends on the hydraulic radius and surface slope.

Although widely used, Mannings roughness has considerable limitations (JARRETT, 1984). The Manning equation was developed for uniform flow and seriously over- and underestimates roughness in high gradients and shallow flows. Another limitation of the equations is that no attempt is made to determine the effects of secondary flow on flow resistance (LEOPOLD, WOLMAN & MILLER 1964). Also, Darcy-Weissbach and Mannings equations only predict average reach roughness rather than local roughness. Below is an example of the Darcy-Weissbach equation, an improved version for mountain torrents:

$$\sqrt{\frac{8}{f}} \equiv \frac{v}{(gRS)^{1/2}}$$

where v = velocity, g = gravity, R= hydraulic radius and S=Slope. It allows indirect estimation of velocity and discharge which is essential in many natural and paleo-environments.

Many impressive combinations of $D_{50}$, $D_{84}$ and $D_{90}$ have been used to estimate flow resistance and emphasise the important influence of large particles (LEOPOLD et al 1964, CHURCH et al 1990), yet no appropriate combination has been achieved. Since the c-axis of a particle lies in the vertical and is therefore responsible for shear friction (JOHANSSON 1963, BATHURST et al 1982) it is appropriate to substitute this variable in flow resistance functions for natural river sediments. So far studies of this kind have only been carried out by GALAY and ROBERTSON & WRIGHT, as mentioned in BRAY (1982), and by ROBERT (1990) and DE JONG (1992c & d).

Flow-generated bedforms constituting form roughness form an integral part of the sediment transport process (DINGLER et al 1977) and are indicators of ancient environments of deposition. Ideally, flow resistance equations should consider the relative submergence of particles (BATHURST et al

1982) and the maximum particle size moved (COSTA 1983). Although imbrication is generally not accounted for, this property of fabric is important since such fabrics change the entrainment threshold (BRAYSHAW et al 1983, BRAYSHAW 1985).

Flow resistance is increased through bedforms and boulders and as a result of sediment movement. In turn, flow resistance has been recognised as having an important influence on the generation of turbulence (WANG et al 1993). BATHURST (1978) showed that when roughness elements project through flow, flow resistance is determined mainly by form drag. The effects of roughness elements on flow are most intense when roughness size is equal to flow depth (BAYAZIT 1982).

Roughness geometry, obtained by micro-profiling (section 3.23) is important since it is determines the magnitude and dimensions of eddies shed in their wake. Semi-variograms and zero-crossing techniques have been used to estimate mean velocity using the friction factor obtained from water depth and grain size information (CLIFFORD et al 1992). For these natural rivers, an empirical constant was applied to represent effective roughness lengths. Since the sorting of surficial material has a more significant influence on roughness than mean particle size (ROBERT 1988b), the assemblage of particles into bedforms has to be investigated separately from the rest of the bed material.

This problem can be addressed by the $K_3$ coefficient. This coefficient is a specific roughness parameter calculated from the maximum vertical difference between three adjacent points (ERGENZINGER & STÜVE 1989, DE JONG & ERGENZINGER 1992, ERGENZINGER 1992) which allows grain and form resistance to be separated.

$$K_3 = \max (x_1 \ldots x_3) - \min (x_1 \ldots x_3)$$

The $K_3$ coefficient depends on particle size, shape and spacing as well as relative roughness. It brings to light the complexity of specific roughness changes during flood events.

Similarly the $K_3$ technique (ERGENZINGER & STÜVE 1989, ERGENZINGER 1992, DE JONG & ERGENZINGER 1992, DE JONG 1992c) can be used as an empirical measure of roughness. The $K_3$ relative roughness measurement depends on bedform amplitude in a similar way to the zero-crossing technique and differs from the semi-variogram which analyses spatially dependent random variables (ROBERT 1988, ROBERT 1991, CLIFFORD et al 1992). Two roughness scales can be identified from these measuring techniques, that of grain and that of form roughness. Few studies up to now actually account for the empirically measured roughness length (CLIFFORD et al 1992). Such lengths include grain roughness effects (e.g. around large particles), form roughness effects, such as bars, and site characteristics (e.g. step-pools).

As GESSLER (1990) pointed out, increases in the $K_S$ roughness coefficient beyond the maximum particle size during bed armouring result from changes in the turbulent velocity i.e. a reflection of changing grain arrangement. CLIFFORD et al (1992) incorporate the relation between the b and c axis (shape) of a particle, the largest grain size and the bedform dimensions. The result is three resistance formulae which include total, grain and form resistance. The total resistance equation:

$$v^2 = \frac{8gRS_e}{f'+f''}$$

represents a combination of the Froude number together with an addition of grain and form roughness as the denominator. In the grain resistance

$$\sqrt{\frac{8}{f'}} = \frac{v}{\sqrt{gRS_e}'} = 5.76 \ln\left( \frac{12.27R}{kg} \right)$$

equation, where k is the value obtained from the semi-variogram and in the form resistance equation,

$$\sqrt{\frac{8}{f''}} = \frac{1}{\sqrt{\frac{C_d}{2} \bullet \frac{k_f}{l_f}}}$$

where l is obtained directly from a micro-profiler.

Thus, as BRAY (1982) stated, the effects of bedforms are not adequately accounted for when applying traditional resistance equations and improvements are necessary in this field. In future, more work is required on the fundamental characteristics of roughness and its measurement.

## 3.3 Flow hydraulics

### 3.3.1 Spatial interactions between the distribution of roughness and flow

This thesis also attempts to explore the influence of flow on roughness. In the literature most studies concentrate on the influence of roughness on flow but not the reverse. If the opposite is to be analysed, then particle orientation, vertical and horizontal bed arrangement need to be considered. Orientation studies for coarse sediments are still lacking in the literature, apart from work carried out by TEISSEYRE (1978), BRAYSHAW et al (1983), DAL CIN (1968) and JOHANNSEN (1963). Other studies have been limited to finer grained fabric analysis. Orientation studies are important since they provide information on patterns of currents as well as processes and mechanics of transport (ALLEN 1982b).

Comparisons with flume experiments (GRANT et al 1990) show that steps form where large particles are deposited under hydraulic jumps whose physical obstruction cause abrupt decreases in velocity. Boulders protruding above the bed favour the formation of hydraulic jumps (BATHURST et al 1979, KIEFFER, 1985). For a step to form, flow has to be equal to the $D_{max}$. The regularity of step-pool systems has not been explained so far but may be comparable to the longitudinal sorting of sediment into "smooth", low gradient and "congested", high gradient zones as suggested by ISEYA & IKEDA (1987) in the flume. Sediments segregate into these zones because high concentrations of fines increase local bedload transport rates of coarse particles by reducing grain roughness and providing a smooth transport surface. Coarse particles are transported until they encounter an obstacle or other obstruction deposited under a standing wave, where grain roughness is increased and a gravel jam or cluster occurs. The mechanism can be compared to the kinematic wave theory of LANGBEIN & LEOPOLD (1968).

#### 3.3.1.1 Influence of fluid vortices/von Karman fluid vortex street on bedform growth

Fluid flow moves by translation and rotation into vortices (PRESS & SCHRÖDER 1966). The vortex field consists of a system of vortex lines which induce the circulation. In viscous fluids the periodic production of vortices from bodies subject to flow are defined as the Karman fluid vortex street (VON KARMAN 1912), shown in Fig 3.1. This process originates behind an obstacle where an increase in pressure causes velocity to become negative and the flow direction to change into a backstream (PRESS & SCHRÖDER 1966, SPURK 1990, BRAYSHAW et al 1983). Upstream of the obstacle a pressure maximum is achieved which causes a pressure gradient to develop downstream of the obstacle. Pressure changes occur not only in the direction of flow but also transverse to it (KARCZ 1968) thus creating centrifugal forces. The vorticity produced has a strong downward component creating a diving motion of the fluid into the familiar horseshoe vortex which moves up again downstream of the obstacle where the pressure is lower (PRESS & SCHRÖDER 1966). This forces the vertical velocity profile to change from convex to concave which in turn results in the release of vortices into the mainstream. So much energy is lost through friction in the obstacle stoss that downstream of the obstacle the Bernoulli pressure cannot increase any longer. A flow re-attachment zone is achieved from which the vortices are carried away by the flow in counter-rotating, alternative pairs from one side of the obstacle to the other, causing the Karman fluid vortex street.

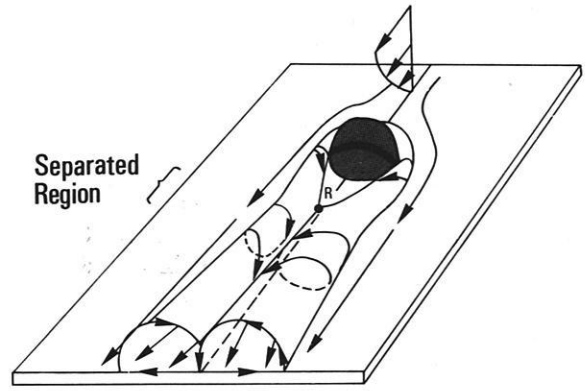


**Fig. 3.1** Vortex production/eddy shedding form the fluid Karman vortex street. (after PAOLA et al 1986). R=Reattachment point.

Where there is local lift, an oscillation of the vortex occurs, followed by bursting, ejection and a sweep (or inrush) which effects the entire boundary layer (GRASS 1991, SUTHERLAND 1967). The movement of the vortex into a high velocity area enhances vortex stretching. This process of vortex development near an obstacle is the most likely cause of regular flow structures. Large-scale turbulence i.e. flow cells are formed where small-scale vortices pull

up. Particle entrainment has been used as a technique for exploring the structure of these turbulent spots. When roughness is very close to each other, the eddies shed by roughness elements are confined to pockets between the elements and flow becomes uniform outside (BAYAZIT 1982). But no information is available on bursting phenomena near large roughness elements.

Work has been carried out on the influence of turbulence on sediment transport in marine environments but a discussion on this will be omitted due to the unconfined nature of marine flows. Also, few experiments exist on the formation of bedforms in coarse media but some data can be transferred from sandy media. On sand beds flow can possess a certain periodicity in crossstream direction due to the influence of secondary circulation (SPURK 1989, YALIN 1992). Once a local discontinuity exists, the behaviour of flow and its turbulent structure changes. This process "promotes" eddy shedding and more frequent burst-forming eddies. The break-up of one burst triggers the formation of the next. The bedforms that originate at the discontinuity sections are the imprints of these burst sequences. Bedforms are created by bursts effecting grain dislodgment. The growth of bedforms causes the total growth of bed roughness and thus a reduction of the Darcy-Weissbach friction factor and Froude number (PARKER & SUTHERLAND 1990).

These burst-generated bedforms are perpetuated as steps. The smaller their period (i.e. lesser bursts), the smaller the bedform. In short, bedforms are produced by the coalescence of a series of smaller bedforms. The bedform growth terminates when the largest bedform has been produced. The maximum width of a vertical burst in plan is twice the bedform height. Erosion occurs at the beginning of the bedform and deposition at the end where a regulation of streamlines is attempted by the flow. If standing waves persist long enough, bedforms are initiated. The steepness of the bedforms are of flow-induced origin. Flow shapes its lower boundary until an ideal steepness (imbrication) is reached. An increase of the D/h (grain size/bedform height) can only be achieved if there is a decrease in the imbrication angle.

#### 3.3.1.2. Morphological adaptation of obstacles/ clusters to flow

The adaptation/organisation of particles on the river bed into various types of bedforms is important when considering their ability or disability to become entrained. Of these the formation of clusters (TEISSEYRE 1977, DAL CIN 1968, BRAYSHAW 1984, CLIFFORD 1992, DE JONG 1992a, REID et al 1992) in coarse environments has been most neglected. FAHNSTOCK (1963) defines clusters as imbricated boulders that form at high flow during high bedload transport, when large particles are set in motion. These clusters become "islands" either due to the scour of adjacent channels or due to decreases in discharge. Few studies have described the process of cluster break-up in detail. There is some evidence that flow velocities can increase on the edges of clusters during flood flows. This process can remove stoss and lee particles effected by lift and drag forces while the obstacle remains in place acting as locus for sediment exchange (BILLI 1988, DE JONG 1992a). This reflects the importance of near-bed turbulent velocity effects on micro and macro-roughness. Micro-form spacing is therefore a phenomenon of microform geometry which in itself is effected by eddy shedding and the deposition or erosion of single particles.

The results from the natural experiments show that coarser grain particles may actually be entrained at lower shear stress (KOMAR 1987) and finer grain sizes require higher shear stress due to hiding effects. This has implications for the stability of bedforms, since preferential entrainment of larger clasts may even occur within cluster structures (BILLI 1988, DE JONG 1992a). Individual interpretations on this theme differ (BRAYSHAW et al 1983, CHURCH 1985) and measurement difficulties may obscure some results.

KOMAR (1987) suggests nevertheless that flow competence can be estimated from selective entrainment relationships. Entrainment depends not only on the particle size but also on their relation to surrounding grains. This re-affirms the need for a relative roughness co-efficient. Particle arrangement may cause a lowering of shear stress necessary for entrainment, thus larger particles projecting further into the field of velocity and are more likely to be subject to lift forces (ERGENZINGER & JÜPNER 1992).

Obstacles are important three-dimensional elements in river bed microtopography (Fig. 3.1) since they determine flow patterns and the subsequent development or destruction of bedforms. The pattern of erosion around obstacles depends on flow depth, Reynold's numbers, orientation and position of the obstacle to flow, obstacle size i.e. width, height and percentage of total length of obstacle with maximum protrusion, as well as shape (KARCZ, 1968, ALLEN 1982a, DE JONG 1991, 1992a, PAOLA et al 1986, STATZNER 1988). Skin friction accounts for differential development of stoss and wake

characteristics (PAOLA et al 1986). Downstream of the obstacle's flow re-attachment area the skin-friction magnitude is approx. 20% greater than its adjacent free-stream value whilst to either side of the obstacle, skin-friction values are lower. This explains why the obstacle's area of influence to flow limits the length- and width-wise development of scour hollows and/or depositional tails.

Depositional and erosional processes downstream of the obstacle depend on the obstacle height (PAOLO et al 1986). Thus tall cylindrical obstacles will cause scour pits rather than depositional tail ridges. In biological experiments carried out with macro invertebrates at quasi-natural flow conditions, bodies that protruded furthest into the flow created the steepest velocity gradients (STATZNER & HOLM, 1989). This region is associated with the highest rate of abrasion and lift.

The area of scour around an obstacle does not extend as far downstream under low flow as under high flow (SPURK 1990, KARCZ 1968). Thus at low Reynolds numbers (e.g. 20) the separation zone occurred at 1.8 times the obstacle height in length whereas under high Reynolds numbers (e.g. 6500) flow separation occurred only at 9 times the obstacle height (STATZNER 1988). By comparison with his biological obstacles, an optimally adapted shape to flow would have low Reynolds numbers, high protrusion and steep wake angles since this combination would reduce friction drag, minimise lift and maximise pressure drag.

Since the Reynolds number is related to particle size, small obstacles acting as candidates for cluster formation should have different shapes and imbrications to larger ones adapted to the three potential forces acting on them. Traditionally it was thought that the more streamlined the obstacle was, the better the morphological adaptation to flow, the more the reduction in drag and the smaller the scour. LDA (Laser Doppler Anemometer) measurements carried out by STATZNER (1988) showed that streamlining was dependent on particle size, thus small obstacles should be hemispherical in shape in order to reduce friction drag whilst larger ones can be streamlined to reduce pressure drag. This should have implications for the natural shape of clusters.
If the obstacle lies normal to flow it will cause a U-shaped scour crescent that begins with an upstream scour slope and ends with long tapering tails that form in conjunction with reduction in velocity (KARCZ 1968). The upstream hollow often allows material to rest against the particle's obstacle i.e. forming a cluster under coarse material conditions. Cluster formation is strongly dependent on fluid forces. The appearance and dimensions of the cluster will depend on the spacing of the obstacles on the river bed. There is considerable interference between patterns of flow deformation around closely spaced obstacles or bedforms. When the ratio of inter-obstacle distance to obstacle diameter exceeded 12, no flow interference occurred. When this ratio diminishes, the wake zone of the obstacles becomes disturbed by the stoss zone of the obstacle downstream of it, so that the scour crescent is inhibited into a shallower and smaller shape than normal. The geometrical length of scour depends on the duration of scour i.e. after a certain period of time, a maximum length of scour is achieved. The geometry of the obstacle marks is determined by secondary flow patterns induced by the obstacle itself. In sandy gravel mixtures, obstacle shadows may assume the shape of a longitudinal ridge produced by deposition or a longitudinal furrow produced by erosion or indeed a multiple arrangement of ridges/furrows.

The natural diversity of clusters has not been examined very closely up to now. Comparison with fine-grained media show that depositional ridges can form under various conditions (PAOLA et al 1986), although they may be more limited in coarse-grained environments. In the tested relationships, tail lengths are usually not longer than 2-10 obstacle heights. One possible reason for deposition of ridges longer than assumed from the obstacle-wake relationships may be changes in current direction as a result of bedload deposition. STATZNER & HOLM (1989) also found in their experiments that in streamlined obstacles, the orientation of the obstacle to flow influenced the extent of the dead water zone, whereby the greatest extent was achieved when flow came from the side. Another explanation could be obtained from changes in the wake structure induced by small flow depths or strong sediment transport (ALLEN 1982a). Changes in flow depth will bring about alterations in the vorticity i.e. vorticity will become predominantly vertical and elongate the depositional zone. The strength of sediment transport alone may not be as decisive in extending the ridge as the modification of the unknown skin-friction patterns.

#### 3.3.1.3. Turbulent fluctuations in response to varying roughness scales

Although the influence of obstacles on flow cannot be directly measured in the field during floods, micro-profiling of the river bed supplies important parameters with which to define the stability of individual particles, their influence on surrounding bed arrangement and flow. VON KARMAN &

RUBACH (1912) pioneered work on the creation of flow separation and fluid vortex streets in relation to obstacles in the flume. Nearly 80 years later, three-dimensional field analysed velocities provide some indirect identification of eddy shedding and energy loss produced from large grains and micro-forms (CLIFFORD et al 1992). Velocity measurements were analysed by stochastic modelling of periodic oscillation frequencies. Both short and longer interval fluctuations were present. The frequency of eddy shedding is not only dependent on the near velocity field but more importantly on the diameter of the obstacle (SCHLICHTING 1970, SPURK 1989). Under increasingly higher Reynolds numbers the length of the eddy produced increases (SPURK 1989). In addition the micro-form element height has a more significant influence than flow depth. In flume experiments, the lift force was found to be dependent on the gap ratio between particles i.e. the distribution and spacing of roughness. (WILLETTS & NADDEH, 1987).

## 3.4 Temporal variations of roughness and geometry

### 3.4.1 Temporal variation of roughness

Temporal variability of roughness is very rapid and extreme during the passage of flood events (ERGENZINGER & STÜVE 1989, DE JONG & ERGENZINGER 1992, DE JONG 1992c). This change, along with fluid turbulence and bed sediment transport, causes roughness measurement problems. The grain coefficients are not invariant during the course of a flood (WHITING & DIETRICH 1990), since there is an increase in resistance due to moving grains and an associated energy loss. Pioneering studies by LEOPOLD & MADDOCK (1953) found that changes in channel geometry, average velocity and the Darcy-Weissbach friction factor correlated well with the discharge. Results of average $K_3$ roughness values from the Lainbach (in 1988, see ERGENZINGER & STÜVE 1989) support this conclusion and indicate that increases in flow depth and flow velocity are related to discharge.

At the Lainbach, decreases in the $K_3$ co-efficient occurred in the main channel with increasing discharges but on the bar, roughness increased during decreasing discharges (ERGENZINGER & STÜVE 1989, ERGENZINGER 1992). With an increase in discharge, there was an increase in energy and power, reconstructed from the relationship between gradient and flow resistance. In energy terms, high discharges with low roughness conditions have a tendency to become more equilibrated than low flows with high roughness.

HAIZHOU & GRAF (1993) determined ways in which to measure friction velocities and applied them to natural hydrographs using Coleman's 1962 data. The friction velocity was usually higher on the rising flood limb with a maximum immediately before the peak followed by descending values on the falling limb. This may be of importance when considering phases of bedload transport. Since the peak amount of sediment transport is usually reached on the rising flood limb, this may be an interactive process with correspondingly high friction velocities. In addition roughness values as measured in flume and natural studies usually sink to their lowest values during this phase (VINCENT 1967).

### 3.4.2 Temporal variation of channel geometry

Unfortunately analyses of channel geometry in straight reaches are generally lacking and what literature there is, is confined to sand-silt channel bends. Nevertheless bed topography is generally related to the amount of bedload throughput, the bedload transport rate and direction, each of which is governed by the three-dimensional flow (ENGELUND 1974, IKEDA & NISHIMURA 1985). Models of bed-flow interactions in the flume are limited in that they consider bed material transport as a continuity instead of an sporadic pulsed process (ERGENZINGER et al 1994). Modelling of bed topography should integrate the following variables: 1) geometrical properties of channel form i.e. hydraulic radius, slope and roughness, 2) mean hydraulic variables i.e. velocity, critical velocity, depth and 3) properties of bed material i.e. particle diameters, roughness co-efficient-efficient (IKEDA & NISHIMURA 1985).

Processes of erosion and deposition are key factors in controlling adjustments in channel geometry. The instability of hydraulic geometry (PHILLIPS 1990) has been recognised but only at at-a-point positions and with data based on the Darcy-Weissbach coefficient. The three-dimensional interrelationships between hydraulic geometry and sediment transfer are not yet fully understood (PHILLIPS 1990, KNIGHT 1989). In order to understand these adjustments, high-resolution temporal investigations are necessary. Such measurements have been exclusively carried out in the laboratory flume.

Simulations of high gradient, step-pool mountain streams have revealed that the erosive capacity of the system reaches a maximum when the pools are almost full of sediment (WHITTAKER & JAEGGI 1982). Energy dissipation is at its lowest during this phase, enabling high flow velocities and consequentially high sediment transport and erosive capacities to develop. This would be similar to peak sediment transport phases in natural streams. HAYWARD (1980) describes this as the period when the pools are drowned and most lateral channel adjustment is occurring.

No studies so far have correlated the geometry and valley shape to the individual development of roughness elements as this is not possible in the flume. It is unknown for example how the water surface gradient during changing flood discharges correlates with the bed gradient. Such measurements are necessary since it is under particular Froude numbers (< 1) (ERGENZINGER 1987, DE JONG 1992e) and water/bed states that certain types of roughness develop. Neither have studies attempted to describe how amounts of erosion and deposition can change over individual segments of the river bed and how this influences not only roughness but also how these in turn are influenced by bedload transporting processes.

Sediment supply is an important determinant of the stability of river beds. Thus as sediment supply declines, river geometry will tend to stabilise itself (HEY 1987). Periods of erosion and deposition cause flow regimes and sediment transport to change in response to temporal and spatial changes in channel geometry and bed material size. Reach processes that have been developed for flow resistance and sediment transport apply to average channells (HEY 1987). In these models fixed width and plan shapes have been assumed independent of changing input conditions. When sediment supply decreases the bed will erode, whilst increases causes aggradation.

## 3.5 Flow dynamics

### 3.5.1 Flume measurements and theory

Open-channel flow behaves critically, subcritically or supercritically. This state is determined by the distribution and expenditure of energy (PRESS & SCHRÖDER 1966). Froude numbers are used in this context as a dimensionless criterion for flow description. When the Froude number =1, a minimum of energy is expended and flow is critical. Studies of the effects of roughness on flow structure

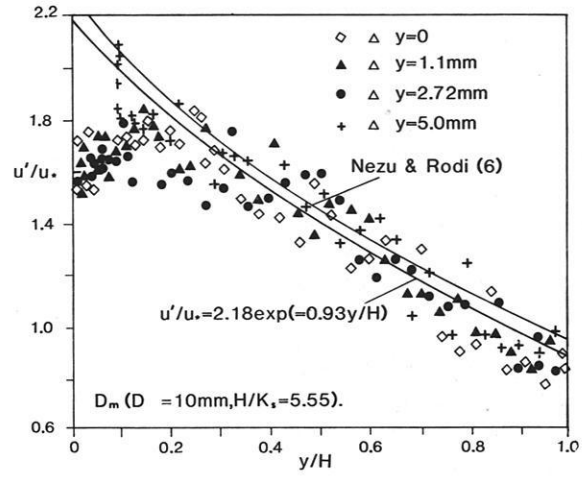


**Fig. 3.2** Vertical velocity distribution under high roughness, non-uniform beds.

and degree of turbulence through time and space have been adequately investigated in the flume. Pioneer studies on the influence of smooth and rough walls on the flow were made by NIKURADSE (1933). Investigations followed on influences of boundary roughness on turbulent intensities of open channel flow by RICHARDSON & MCQUIVEY (1968) among others. NAKAGAWA et al (1988) found that turbulence was not significantly influenced by boundary roughness once measured at sufficient vertical distance from the bed. This is due to the differential subdivision of the vertical velocity profile. The region closest to the bed consists of a viscous sub-layer, followed by a transition region and the turbulent zone. To explore these ideas, WANG et al (1993) carried out experiments on a fully rough bed at Reynolds numbers higher than 80 (Fig. 3.2). When $H/k_S$ was less than one over a uniform gravel bed, where $H$ was the water depth and $k_S$ was the roughness height, roughness was large and the vertical distribution of $u'/u_*$ was shown to be uniform (BATHURST 1985), where $u'$ stands for the rms value of the streamwise fluctuation velocity and $u_*$ for the friction velocity. As expected, roughness caused the flow turbulence to increase.

With decreasing roughness height relative to water depth however, roughness has far less influence on the velocity distribution and the vertical velocity distribution does in fact become similar to that of a smooth bed. On non-uniform beds, a similar vertical velocity distribution is obtained for the longitudinal turbulent intensity. The $u'/u_*$ distribution is primarily effected by the maximum gravel size rather than by the type of gravel bed. This has to be kept in mind for the interpretation of investigations over natural gravel beds in the Results Chapter.

## 3.5.2 Natural measurements and theory

Turbulence is so complex and studies in natural fluvial situations are so limited that the topic in this thesis has been simplified to investigations of the influence of large-scale turbulence i.e. secondary flow structures on sediment movement and visa versa. Investigation of hydraulic influences on the development of roughness during the course of a flood event are still lacking. This is in part due to the difficulties encountered in carrying out continuous high-resolution spatial and temporal measurements of flow velocities and structure under natural conditions. Measuring devices comparable in accuracy to those used in the flume usually fail in the field. Thus highly sophisticated LDA (Laser Doppler Anemometers) (NEZU & RODI, 1986, WANG et al 1993) are impossible to operate under highly turbid and turbulent natural flood situations. Detailed flow characteristics either have to be reconstructed after floods or compared to flume studies. Thus in order to reconstruct general flow structures and their possible interactions with bedload and river-bed roughness, field workers resort to indirect factors such as the water surface structure that remain measurable during all flood stages. The literature on flume studies indicates that the water surface is an inseparable part of the flow structure that also reflects the roughness structure on the river bed. Under natural conditions the water surface can also be shown to reflect the nature of secondary circulation or flow cells (LEOPOLD 1982).

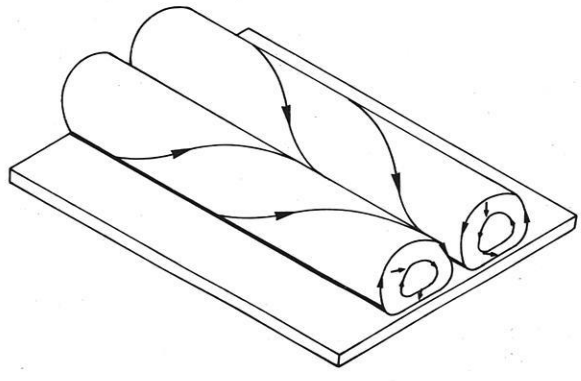

**Fig. 3.3** Flow cell development after GÖRTLER (1945).

### 3.5.2.1 Water surface configurations and secondary circulation

The measurement and modelling of secondary flow is essential in natural streams since it affects dispersion, diffusion, stream meandering, sediment transport, distribution of boundary shear stress, flow resistance and velocity distributions, bed and bank erosion and development of channel morphology. (BATHURST et al 1979, BHOWMIK 1982). Many definitions exist for secondary flow (Fig. 3.3). They were first identified as the Taylor-Görtler type (GÖRTLER 1941), then taken up by EINSTEIN and LI (1958). Secondary flow can best be defined as a persistent component of velocity that is neither parallel to nor tangential to the centreline of the channel or to the bed slope (BHOWMIK 1982, KARCZ 1981 and MOSS et al 1982).

In principle, two kinds of secondary flow circulation can develop, either stress-induced i.e. in straight channels where streamwise vorticity is produced directly from the flow as a result of bed topography or skew induced in relation to pre-existing vorticity in channel bends. When such circulation develops, flow will rotate towards or away from itself in a cross-channel direction, thus creating flow cells which propagate into a spiral vortex, travelling in a downstream direction with the current (GIBSON 1909, BATHURST et al 1979).

Of special interest is the development of flow cells in straight reaches. This condition is representative of the Lainbach and Squaw Creek study reaches. Some of the most important pioneering studies made on the existence of flow circulation in straight channels include STEARNS (1883), CUNNINGHAM (1883) and GIBSON (1909). Sophistications of their work followed by EINSTEIN & LI 1958, VANONI, (1946), LEVIAVSKY, (1955) and LEOPOLD, (1982). Of the limited work carried out in straight channels, MOSS et al (1982) found very close relationships in sand-bed channels between secondary flow and channel scour or deposition. They noticed that where water levels were lowered, scour occurred and where it was raised, flow was divergent at the bed, causing small trenches to be eroded. Positive feedback led to increased scour and channel enlargement. Although flow cells were found in far shallower sandy media, they assume that on coarse beds the effects of friction are very large causing high vertical velocity gradients and the same probability of development of secondary flow cells. They do however emphasise the general inexperience in coarse environments under deeper flows.

Although it is well known that water surfaces are

superelevated in channel bends (YEN & YEN 1971, DIETRICH et al 1979, LISLE 1986, BRIDGE & JARVIS 1992) studies in straight natural channels remain scarce and do not cover short-term spatial and temporal scales (KIEFFER 1989, LEOPOLD 1982). This is due to the lack of acknowledgement of the existence of the interactions between bedload and river bed dynamics in straight reaches.

Measuring instruments for such studies are under-developed or are totally lacking (BHOWMIK 1982) apart from limited visual and geodetic observations. Such shortcomings are unfortunate since the water surface may in many natural cases offer the only means for interpreting flow dynamics. Water surface measurements are relevant since water superelevation is influenced by helical flow motion and channel bed topography in channel bends (YEN & YEN 1971) as well as in straight reaches (ERGENZINGER & DE JONG 1992, LEOPOLD, 1982).

#### 3.4.2.2 Restriction of flow cell development by roughness and river geometry

A minimum water depth is required for the development of flow cells. This observation explains cell decay during certain flow phases (THOMPSON 1986). Models presented by CHIU (1982) and THORNE & HEY (1979) indicate that flow cells will develop whenever the three components of shear force are not in equilibrium. EINSTEIN & LI (1958) found that secondary currents could be produced by time-average components of flow as well as by some components of turbulence. At the water surface flow cells are reflected as ridges and troughs with respect to flow convergence and divergence. Water converges at the surface causing a depression zone of maximum velocity below the surface which is deflected to the channel edge. At the bed surface, the flow moves in the opposite direction thus enabling a complete circulation to form.

HELLSTROM (1948) notes that secondary flow velocities are about 12% of the mainstream velocity. This has been reinforced by studies made in Squaw Creek in 1991. In channels with width to depth ratios of between 5-20, only two flow cells will develop and where mid-channel flow diverges at the water surface, this will cause a single upward bulge (see studies by WAIRD in LEOPOLD et al 1964). ERGENZINGER, DE JONG & CHRISTALLER (1994) note that under a width to depth ratio of 40, a minimum water depth of 30 cm is required for the development of 4 or more flow cells. Hey et al (1975) demonstrated that during low flow on the River Dove, England, with a width to depth ratio of 30, more than 4 flow cells could exist but that only two were left during high flow because bed roughness was drowned. Sediment was thought to concentrate in longitudinal ridges (or proto-bedforms) where flow is divergent at the bed.

### 3.5.3 Measurement

Secondary circulation itself can be measured directly or indirectly, i.e. either from water surface measurements or from the flow itself. In order to identify flow cells, the water surface should be sub-divided into 2 or even 3 components, thus longitudinal, vertical and lateral. In the widely used roughness formulae, the water surface is often not measured and a surrogate mean river bed level is taken instead. Important parameters necessary for the determination of flow cells include the channel cross-section, discharge, depth, water surface profiles and primary velocity distribution parameters. Even so, measurements for straight reaches during the course of a sediment-rich flood event are rare.

The most direct method includes measurements made with three-directional electro-magnetic (EMS) current meters (BATHRUST et al 1977, CHIU 1982, THORNE & HEY 1979, HAMMAN DE SALAZAR 1992, SAUNDERSON 1992) which measure both the cross-channel and downstream velocity components. The indirect method includes measurements or observations of the water surface. EMS measurements in natural river channels have been of limited success, the literature is confined to marine studies (WILLIAMS et al 1989).

Some important information can be drawn from flood studies made in the meandering channels of the Kaskaskia River, Illinois (BHOWMIK 1979) where the position of the thalweg changed between high and low velocity flow in accordance with the changing magnitude and characteristics of secondary flow. HEY (1975) observed that during low flow, secondary currents could not develop due to the flow geometry and distribution of roughness elements but that higher stages are ideal for flow cell development. These will modify the hydraulic geometry through differential erosion and deposition. As a result of these limitations, simulations of flow development in straight channels have dominated the flume studies (EINSTEIN & SHEN 1964, ASHMORE 1982). The width to depth ratios in flumes can never imitate natural river conditions due to wall effects and lack of differentiation in bed topography.

## 3.6 Bedload transport

### 3.6.1 The effects of bedload transportation on formation of different roughness types

The roughness type that develops on a river bed is clearly dependent on bedload processes. This has led to process-differentiated definitions of armoured versus paved gravel beds (BRAY & CHURCH 1980, ANDREWS & PARKER 1987, GESSLER 1965). Investigations have been somewhat limited by inadequacies of representative areal descriptions of the river bed (SUTHERLAND 1987, DIEPENBROEK & DE JONG 1993, IBBEKEN & SCHLEYER 1986). It should be clear which of these processes are dealt with in definitions of bedforms and river bed arrangement.

An armoured bed consists of a heterogeneous mixture of sediment subject to flow that is capable of actively transporting most grain sizes in the absence of an upstream sediment supply (BRAY & CHURCH 1980, ANDREWS & PARKER 1987). PROFITT (1983) showed that the actual process of armouring not only entails the erosion and transport of particles but also the rearrangement of the particles making up the bed. During the process of armour or pavement formation there is a tendency for small grains to settle between the larger ones which causes a decrease in local grain friction and higher velocities (DIETRICH et al 1990). Armoured beds usually form where rivers actively transport material. The grain population of its bed surface is the same as the sub-surface. Larger particles will slowly become immobile as the bedload transport rate decreases and form a protective covering. Armouring is thus a process of bed coarsening through winnowing out of fines causing general bed degradation. Flume experimentation reveals that mobile armour layers that form during bedload transport of non-uniform sediments are very similar to the static armour layers that form by selective erosion of clear (sediment-free) water flows (PARKER & SUTHERLAND 1990, SUTHERLAND 1987). Static armour layers develop when none or very few of the coarsest size fractions available for transport and they can only become mobile in the presence of sediment.

A paved bed is the result of surface material in motion only during extreme events (BRAY & CHURCH 1980). In a paved bed the surface is larger than the sub-surface (LEVIASKY 1955, ANDREWS 1983). The distinctive larger material remaining on the surface is the result of selective entrainment of finer grain sizes. Paved beds are usually the result of rivers flowing over bouldery material that they are only rarely capable of transporting (BRAY & CHURCH 1980). PARKER & KLINGEMAN (1982) argue that as coarse grains become more abundant on the bed surface due to winnowing of fines, equal mobility is achieved. Sheltering effects (EINSTEIN 1950, PROFITT & SUTHERLAND 1983) help to protect the sublayers and increase tendencies towards equal mobility. However, ANDREWS & PARKER (1987) and KUHNLE & SOUTHARD (1988) found that a pavement occurred even when most sizes were transported and sediment supply was unlimited. Even so, sediment supply reduction causes changes in bedforms and confinement of active bedload transport to a narrow band where the bed surface is finer (DIETRICH et al 1990) and adjacent surface coarsening. High rates of bedload transport enable the surface cover to become mobilised into thin bedload sheets which alternate with congested, smooth and transitional zones (ISEYA & IKEDA 1987).

Thus in a paved bed the size distribution of the bedload may remain similar to the sub-surface but the surface material remains much coarser. The relative abundance of coarse particles means that there is greater exposure and therefore greater probability of material entrainment (ANDREWS & PARKER 1987, HASSAN 1990). At low bedload transport the interchange of particles occurs between the sediment, bed and flow in a layer one grain thick (ANDREWS & PARKER 1987). Topographically induced flow causes divergence and cross-channel transport with a reduction in sediment supply and coarsening of the surface. According to ANDREWS & PARKER 1987 and HASSAN 1990, the pavement is usually not destroyed during flood events due to the sporadic movement of bedload. The depth of material reworked is usually quite shallow i.e. not more than 30 cm (HASSAN 1990).

### 3.6.2 Effects of different roughness arrangement on bedload transport thresholds

The nature of the river bed influences particle entrainment thresholds. Conventional shear stress formulas are limited since they are not considered as part of grain and bedload processes (PETIT 1990). If shear is to be reconstructed from roughness, the problem of roughness determination from naturally mixed sediments (LARONNE & CARSON 1976, LEOPOLD & EMMETT 1981) and from bedforms remains (ALLEN 1983, ALLEN 1982A,

BATHURST, GRAF, & CAO 1982, BILLI 1988, BLUCK 1987, BRAYSHAW 1984, BRAYSHAW, FROSTICK, & REID 1983, CARLING, & READER 1982, CLIFFORD, ROBERT, & RICHARDS 1992, DAVIES 1982, DE JONG 1991, DE JONG 1992 a, b & c, ERGENZINGER 1988, GOMEZ, NAFF, & HUBBELL 1989, HASSAN, & REID 1990, JOHANSSON 1963, LEWIN 1976, MCDONALD, & BANERJEE 1971, MILNE 1982, NADEN & BRAYSHAW 1987, REID et al 1985, REID 1992, ROBERT 1990, TEISSEYRE 1977, THOMPSON 1986). Standard threshold curves cannot be applied to gravel movement in mixed sediments due to factors which cause selective grain entrainment (KOMAR & LI 1986). Notably, in mountain streams, in addition to grain shape and size, high bed slopes and low ratios of depth to grain size also play a role in entrainment (ASHIDA & BAYAZIT 1973, BATHURST et al 1982).

With an increase in flow strength, the different sizes and shapes of particles ultimately determine grain pivoting angles, and are important determinants of entrainment thresholds. The pivoting or friction angle is important for the initiation of grain movement since the grain will tip out of its resting position once the particle's weight is overcome by the fluid drag force. Thus the entrainment of spheres is followed by smooth ellipsoids (effective in rolling), by angular grains and lastly by imbricated ellipsoids (effective in achieving high imbrication angles, KOMAR & LI 1986). The rollability of the grain depends on the ratio of the $D_c/D_b$ (shortest over intermediate axis). This is due to the grain angularity which determines the degree of grain interlocking and grain projection which in effect determines the tendency towards entrainment (FENTON & ABBOTT 1977). In addition, the grain's pivoting or friction angle (BUFFINGTON et al 1992) depends on the ratio of the size of the pivoting grain to that of the grains upon which it rests. The pivoting angles of spheres decrease with increasing particle size. Varying grain imbrication creates different geometries for grain pivoting and entrainment. The higher the imbrication angles, the more the particle interlock and the higher the pivoting angle.

Friction angles (LI & KOMAR 1986, KIRCHNER et al 1990) and relative grain protrusion have been measured both for semi-natural river beds in the flume during bedload transport and for natural beds without bedload transport (BUFFINGTON, DIETRICH & KIRCHNER 1992) in order to derive critical boundary shear stress. Limitations due to the effects of grain burial and near-bed velocities are usually not considered. WIBERG & SMITH (1987) showed that grains of widely differing grain sizes had approximately the same minimum critical boundary shear stress. In terms of bedload transport this result supports equal mobility of grains (PARKER & KLINGEMAN 1982).

Results from natural river beds reveal that there is a dependency of friction angles on the degree of surface sorting. It has also been demonstrated that, in contrast to the laboratory results, smaller grains are more actively entrained (ANDREWS & ERMAN 1986, ASHWORTH & FERGUSON 1989, KUHNLE & SOUTHARD, 1988, HASSAN, 1990, HASSAN et al 1984, 1990).

### 3.6.3 Measurements of temporal and spatial variation of bedload transport

Bedload transport needs to be measured at high temporal and spatial resolutions if it is to be related to dynamical roughness changes. MILLER & LEOPOLD (1963) were among the first researchers to emphasise the need for short interval measurements of bedload and river bed adjustment in space and time along fixed cross-sections. Due to the difficulties encountered in measuring bedload transport in coarse-grained mountain channels, high resolution studies have almost without exception been limited to the laboratory. Natural studies have on the whole been hindered by insufficient development of measuring techniques. The result has been short, averaged, at-a-point measurements which often bypass the aim of measuring continual, short-term bedload fluctuations. With high relative roughness the resting periods during bedload transport increase significantly. Step lengths should therefore be dependent on roughness rather than discharge.

#### 3.6.3.1 Laboratory measurements

Bedload measurements in the laboratory have produced evidence for the erratically fluctuating "pulsed" nature of bedload transport (WHITTAKER & JAEGGI, 1982, ISEYA & IKEDA, 1987, GOMEZ 1983, et al 1989). Even though this non-uniformity in sediment motion has not been fully explained, there is evidence to suggest that turbulence and sediment storage play a role (ERGENZINGER et al 1994, REID et al 1986).

Although the detailed interaction of particles has not been measured in nature, particle collisions should influence the development of roughness. In aeolian

transport, collision has been found to be an important mechanism which influences grain saltation and surface re-sorting (WILLETTS & RICE 1986) due to momentum exchange. Grain shape has a marked effect on collision. Although the saltation amplitude increases after collision, inter-grain collisions are less effective in sustaining saltation for material which is more platy and bladed, than for more rounded, compact material.

### 3.6.3.1 Natural measurements

Most natural measurements of bedload have been carried out with Helley-Smith (BRIDGE 1991, CARSON & GRIFFITHS, 1987, GOMEZ 1983, 1989, ISEYA & IKEDA. 1987, JACKSON & BESHTA 1982, KUHNLE & SOUTHARD 1988, FERGUSON et al 1992 REID & FROSTICK 1986, SHIH & KOMAR 1990) or vortex tube samplers (TACCONI & BILLI 1987). Occasionally, motion picture studies have been undertaken (DRAKE et al 1987) or pressure traps (LARONNE & DUNCAN 1992), piezometric measurements (BÄNZIGER & BURSCH 1990) or bedload nets (BUNTE 1992b). The most sophisticated techniques include the development of magnetically sensitive sills (ERGENZINGER 1985, ERGENZINGER 1988, ERGENZINGER & CONRADY 1982, ERGENZINGER & CUSTER 1983, REID et al 1984). The reliability of the widely used Helley-Smith sampler is doubtful since it enables neither continual temporal nor spatial samples to be taken and may actually miss major pulses of material. The direct power functions suggested by some authors between discharge and bedload transport are therefore dubious.

The naturally pulsed nature of bedload has been noticed by a number of researchers (HOEY 1992, LEKACH and SCHICK, 1983, CUSTER et al 1986, BUNTE 1986; see also all citations in section 3.6.2). In these cases, a post-peak sediment pulse was monitored and their formation interpreted in terms of the kinematic wave theory suggested by LANGBEIN & LEOPOLD (1968).

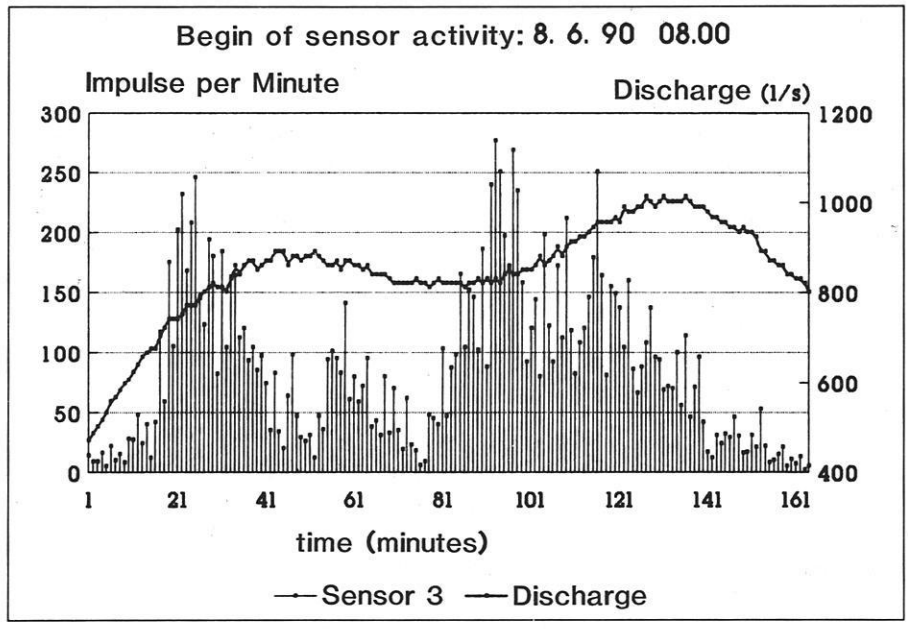


**Fig. 3.4** Relationship between discharge and bedload transport for the Ehrlenbach registered by hydrophone measurements (after BÄNZIGER & BURSCH, 1991, p.2).

## 3.7 Interactions between roughness, channel geometry, flow and bedload movement

The interrelationships between roughness, geometry, flow and bedload transport have rarely been summarised in studies of straight reaches (ERGENZINGER et al 1994, ERGENZINGER & DE JONG 1992). Other evidence can only be discussed in the light of bend studies (BRIDGE & JARVIS 1982) but the finer grain sizes and different flow hydraulics limit comparisons. An interesting observation is their suggestion that flow resistance reaches a maximum when bed topography is stable at about the 2/3 of peak discharge. This relationship may request a means of energy conservation.

Bedload transport feedback processes regulate the spatial concentration of bedform roughness i.e. pebble clusters (HASSAN & REID 1990, DAVIES & SUTHERLAND 1980). Clusters influence bed mobility by causing form drag which requires the adjustment of shear stress due to division of resistance into form and grain components (CLIFFORD et al 1992). When dimensionless shear stress is correlated with form roughness at initiation of bedload transport at Turkey Brook (REID et al 1986), results indicate that particles are more mobile at the beginning of the hydrograph. Prior to breaking its armour layer at the beginning of bedload transport, the river bed experiences shear which is delayed by the development of form roughness.

Studies by LEOPOLD (1982) in the Colorado River by photographically documenting dye movement form an important early work on the correspondence of flow cell circulation and spacing to bedload streets or preferred sediment transport routes (Fig. 3.5). Before that, EINSTEIN & LI (1958) stated that cross-components could develop without the presence of sediment but that sediment transport could significantly influence their nature. The wandering nature of these flow cells in straight reaches were attributed to the alternative deposition of pools and riffles (LEOPOLD 1982, KELLER, 1972, HEY 1979 and THOMPSON 1986). Bedload will preferentially move along the channel margins and is dependent on the fluctuating cross and down channel movement of the flow cells (LEOPOLD 1982, ERGENZINGER et al 1994).

It is difficult to determine what factors most influence the processes linking bed roughness, bedload transport and flow dynamics. In order to answer this question one must consider the process of bedload transport, which is inherently important in causing changes in roughness and bed configuration (DE JONG 1992c, ERGENZINGER et al 1994). The regulation of the intensity of bedload transport is determined to some extent by the bed gradient in steep mountain torrents. With a doubling of gradient, the potential for bedload transport increases fourfold (FORSTER et al 1993). In addition there are large variations in energy losses during a flood event due to the effects of the large grain-size spectrum. This observation explains the irregularity of bedload transport and its independence on the discharge curve (see Fig 3.4).

HASSAN (1990) found in his studies that aggradation and degradation of the river bed were subject to extreme spatial variability. Scour and fill processes were interactive so that exposed particles were buried and moved in close proximity during the same flood event. The burial depth frequency was similar for all flood events, suggesting an equilibrium threshold in erosion and deposition. RICKENMANN (1992) found that discharge events in the Ehrlenbach did not achieve erosion depths of more than 0.5 m. Thus the overall configuration or river geometry had been maintained, even if local changes in the arrangement of the river bed were substantial. No clear relationship could be established between bedload transport rates and discharge. Only once average values were considered for the fluctuating bedload transport rates during floods spread over a couple of years could a relationship be established with the discharge.

Although it has been mentioned that there is evidence for dynamic variations in bed roughness between floods and within floods, no detailed measurements have been attempted. EMMETT (1975) points out that bedload transport is related to the water surface configuration and discharge. But various stages in roughness formation are most probably related to bedload transport (BATHURST 1982a&b). Thus when sediment is transferred at high rates, roughness is reduced since transport is most effective over a smooth surface (ERGENZINGER et al 1994). As the sediment load increases, flow resistance decreases. In the final flood stage, as sediment transport decreases, bedforms become fully developed, flow resistance is highest and large-scale roughness exist. This decrease in roughness during high rates of bedload transport and increase in roughness during low rates of transfer has recently been confirmed in the flume (TAIT et al 1992, LAMBERTI & PARIS, 1992). Flow resistance has therefore been recognised to vary directly with sediment load and probably not with discharge.

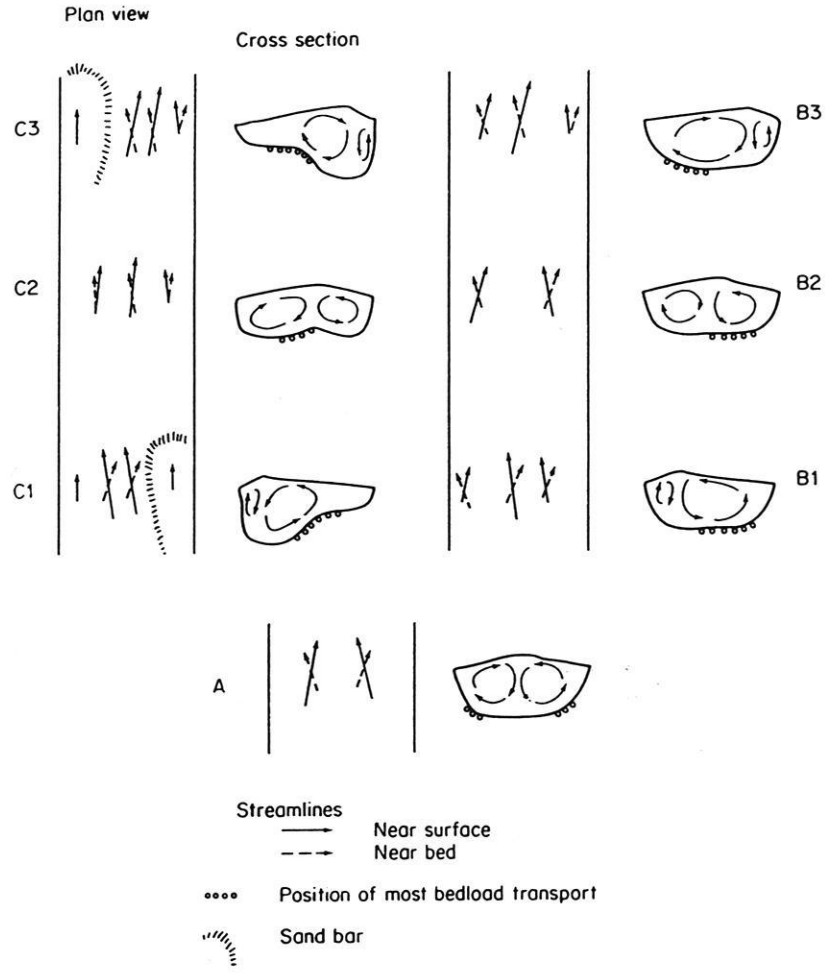


**Fig. 3.5** Streamline direction at surface and at bed with corresponding secondary circulation patterns in cross-section (after LEOPOLD 1982).

# 4. STUDY AREAS

The three study areas selected will be treated separately. In each case criteria for selection included a heterogeneous, coarse-grained gravel-bed, steep gradients and the occurrence of active, sediment transporting summer floods. Table 4.1 summarises the three study areas:

## 4.1 Squaw Creek

Squaw Creek is situated in the Gallatin Range of the Rocky Mountains 42 km south of Bozeman, Gallatin County, Montana, USA (see Fig. 4.1). The Squaw Creek measuring site is just above the confluence with the Gallatin River, which eventually forms the Missouri. Details on the catchment, sedimentary and hydraulic characteristics can be obtained from Table 4.1. The head waters of Squaw Creek flow through a formerly glaciated valley. Above the measuring site it alternates from braided to step-pool and even a narrow canyon cut into Paleozoic and Mesozoic sedimentary rocks. The vegetation consists mainly of *Picea engelmannii, Pseudotsuga menziesii, Pinus contorta* (conifers) and *Artemisia* and *Juniperus* shrubs.

### 4.1.1. Geology

Squaw Creek drains an area which contains andesitic volcanic and intrusive rocks (55%), pre-Cambrian gneiss (25%), Paleozoic limestone, sandstone and shale (20%) (Fig. 4.2). The high percentage of magnetite (7.4%) contained in the andesites was the main reason for the establishment of the measuring site since bedload transport monitoring is dependent on magnetically induced signals (ERGENZINGER, CHRISTALLER and DE JONG 1994). In fact, 76% of the bedload is of volcanic origin.

### 4.1.2 Flood Hydrology

Details of the hydrological regime of Squaw Creek are given in BUNTE (1991). The hydrological patterns are dictated by snow-melt. The topography of the catchment and climatic conditions (Table 4.1) enables snow to persist for many months (6-9 annually). The main snow-melt season lasts from the end of April to the beginning of July (Fig. 4.3) During this period major flood and sediment transporting events occur, with average peak discharges of $6.8 m^3 s^{-1}$. Squaw Creek was a US Forest Service gauging station for over 30 years (ERGENZINGER and CUSTER 1983).

**Table 4.1** Catchment details of Squaw Creek, Lainbach and Schmiedlaine.

| CHARACTERISTICS | SQUAW CREEK | LAINBACH | SCHMIEDLAINE |
|---|---|---|---|
| **Drainage area** | 105.7 $km^2$ | 15.5 $km^2$ | 9.4 $km^2$ |
| **Drainage length** | 20.3 km | 5.5 km | 3.4 km |
| **Max. elevation** | 3154 m | 1800 m | 1800 m |
| **Gradient (average)** | 0.025 | 0.02 | 0.05 |
| **Drainage density** | 0.99 $km/km^2$ | 2.1 $km/km^2$ | 1.6 $km/km^2$ |
| **Annual precipitation (snow)** | 457 mm | 761.4 mm | 761.4 mm |
| **Annual precipitation (rain)** | 356 mm | 728.6 mm | 728.6 mm |
| **Forest cover (%)** | 50 | 79.1 | 75.3 |
| **Channel width (average)** | 8 m | 5 m | 3 m |
| **Channel depth (average)** | 0.3 | 0.2 | 0.3 |
| **Avererage flood Q (at study site)** | 6.8 $m^3 s^{-1}$ | 20.1 $m^3 s^{-1}$ | 14.6 $m^3 s^{-1}$ |
| **Average Q (study site)** | 0.35 | 1.03 | 0.54 $m^3 s^{-1}$ |
| **$D_{50}$ (bar surface, study site)** | 34 mm | 73 mm | 86 mm |
| **$D_{84}$ (bar surface, study site)** | 56 mm | 140 mm | 170 mm |

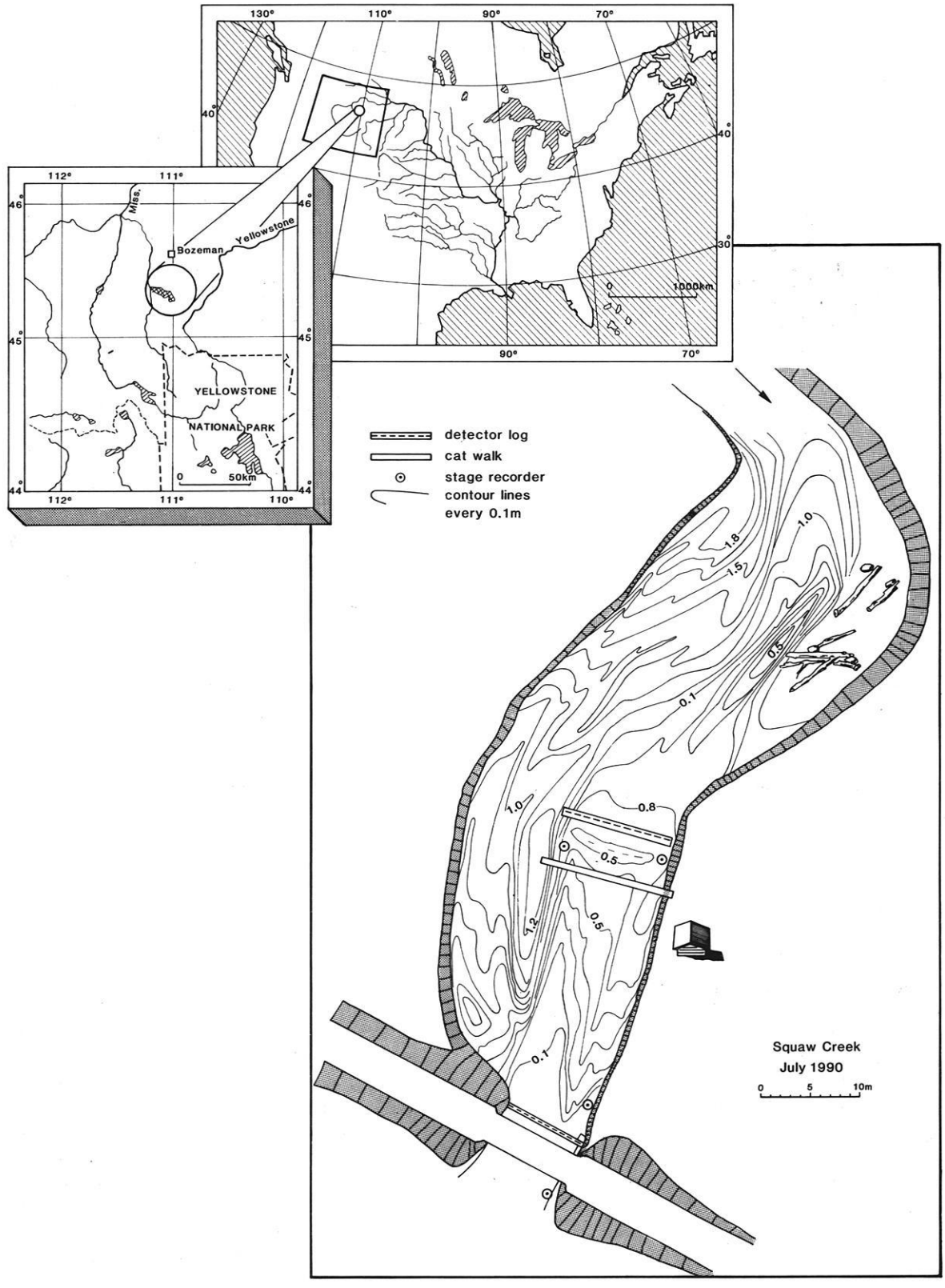


**Fig. 4.1** Location of the Squaw Creek study area.

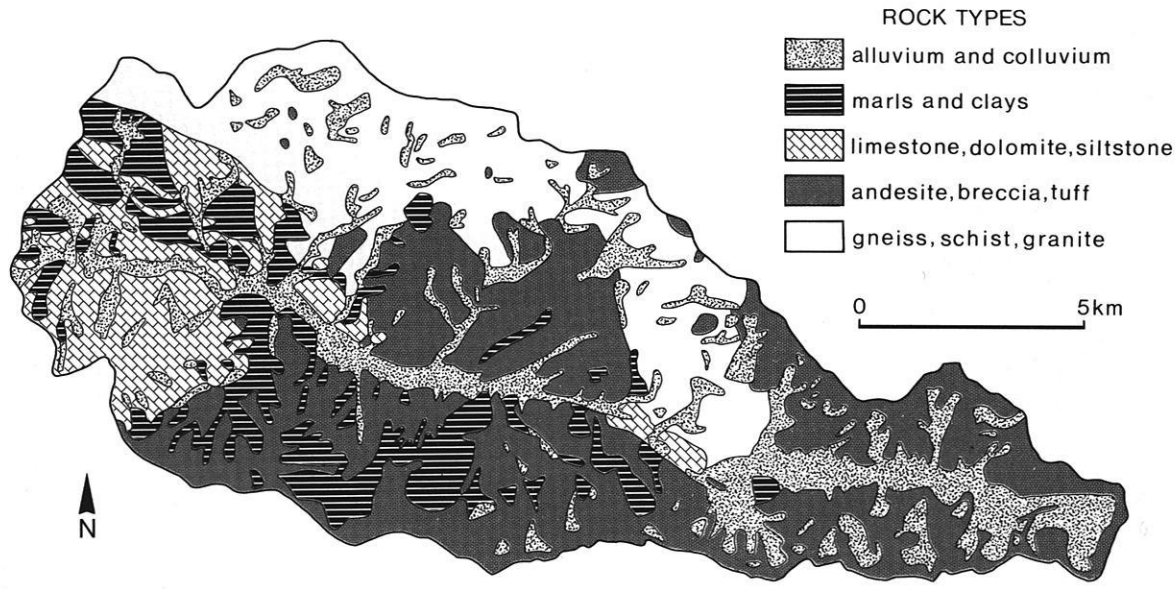


**Fig. 4.2** Geological map of Squaw Creek indicating the variety of geological types and predominance of volcanic rocks.

In some years, snow melts after very warm periods before spring or snow melts slowly and discharge is not augmented by rain. Under such circumstances, spring flood discharge can be insufficient for bedload transport. The flood hydrograph is thus dictated by the amount of snow, rates of snow melt and in rarer incidences by the amount of rain or rain on snow. Such a combined event can lead to exceptional discharges (ERGENZINGER and CUSTER 1983), Fig.4.4.

### 4.1.3 Topography and Sedimentology

The study site consists of alternating riffle and pool zones which lie along a fairly straight measuring reach (Fig. 4.5). The diagram shows Squaw Creek in 1992 after a geodetic survey was made. It has to be emphasised that the straight geometry of the reach is important in controlling sedimentary and hydraulic processes. Two gravel bars lie within the reach, one an elongated and slightly vegetated medial bar of straight geometry active during all bedload producing floods, the other a lateral bar, slightly crescentic in shape and only active during very high discharges. The medial gravel bar will be referred to as the "old" gravel bar, while the lateral bar will be referred to as the "new" gravel bar since it was rebuilt during the 1991 flood event (Fig. 4.5).

The sediment sizes at Squaw Creek have been summarised in Table 4.1 (CUSTER et al 1987). Fig.

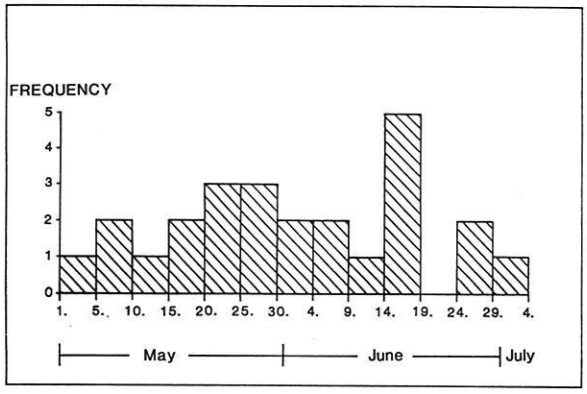


**Fig. 4.3.** Temporal distribution of maximum annual floods between 1959-1986 (after BUNTE 1991).

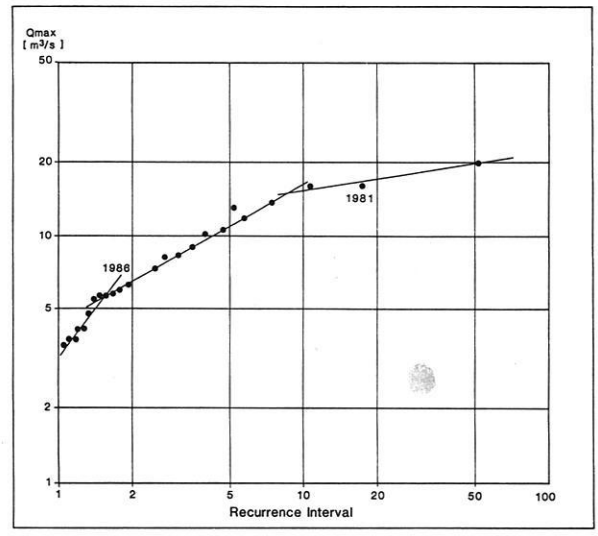


**Fig. 4.4** Recurrence intervals for the maximum annual discharge between 1959-1986 (after BUNTE 1991).

4.7 gives an indication of the grain size distribution obtained from the photo-sieving method on the new gravel bar. Whilst the new bar has fairly rounded particles (Fig. 4.6 a), the old bar (Fig. 4.6 b) has slightly more angular material. Both bars nevertheless display clustering.

## 4.1.4 Measuring installations

The measuring site has two magnetic sills 30 m apart from each other for bedload movement detection (Fig. 4.5). The Tausendfüssler device is situated approximately 3 m downstream of the upper sill. This distance is sufficient for any turbulence or standing waves created by the upper detector log to be dissipated. Stage recorders are located at 5 locations along the river banks and the intakes for the upper and lower hoses for measuring the water level gradients are indicated below the upper detector log and along the old bar.

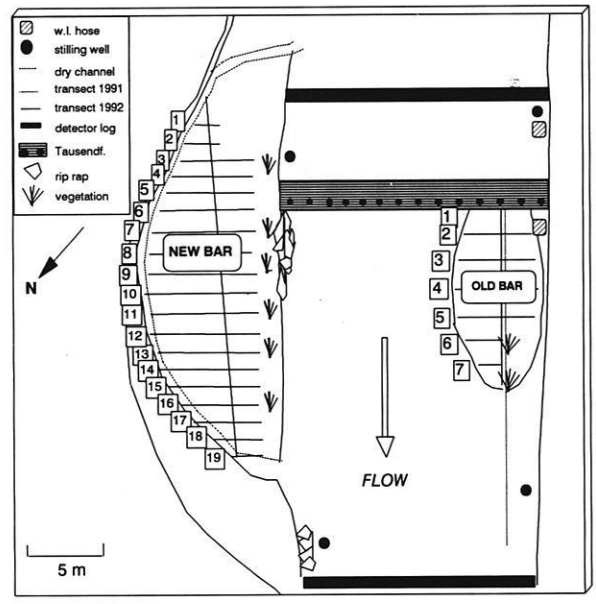


**Fig. 4.5** The Squaw Creek measuring site indicating Tausendfüssler bridge, magnetic bedload monitoring sills and stage measurement sites (stilling wells).

a)

b)

**Fig. 4.6** **a)** Upstream view of old bar (Fig. 4.5). Note that old bar not only has higher particle roughness but also roughness induced by vegetation. The photo-sieving device can be seen at the distal end of the bar. Notice problem of partial bar submergence. In the background the macro-Tausendfüssler device is visible. **b)** Upstream view of new bar with more rounded and homogenous sediment. Note small channel to the left of the bar, proximal end (left, background) lining vegetated banks and vegetated ridge artificially strengthened by rip rap on right, to which Tausendfüssler is attached.

## 4.2 Schmiedlaine

The Schmiedlaine is a tributary of the Lainbach River in Upper Bavaria at the northern edge of the northern Limestone Alps, 70 km south of Munich (Fig. 4.8). The Schmiedlaine measuring site is located just above the confluence with the Lainbach (ERGENZINGER 1992). Details on the catchment, sedimentary and hydraulic characteristics can be obtained from Table 4.1. The Schmiedlaine constitutes an extremely interesting example of river bed arrangement and geometry in a stream with high curvature and bedrock confined bends (Fig. 4.9 a & b).

Unlike Squaw Creek, the bed material is very angular, gradients and valley slopes are steep (average 8%) and there is greater variability in the grain size spectrum. In addition valley side inputs from small rills, debris flows and slumps form an active part of sediment supply. The forest cover is denser and more extensive than at Squaw Creek, which creates an additional organic input and the formation of log jams. Vegetation consists mainly of spruce, deciduous and mixed wood.

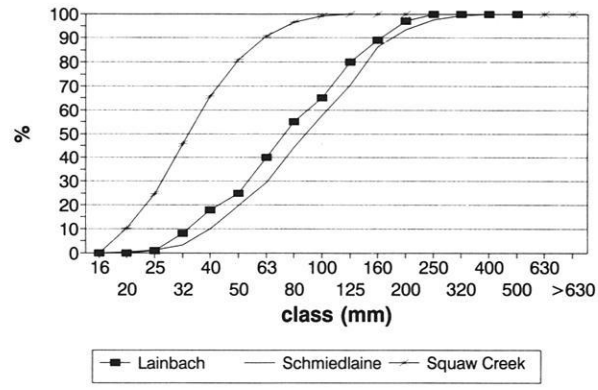


**Fig. 4.7** Cumulative grain size distributions obtained by photo-sieving at Squaw Creek (Montana), Schmiedlaine and Lainbach (Upper Bavaria).

### 4.2.1 Geology

The geology of the Schmiedlaine is very diverse ranging from Quaternary glacial and glaciolacustrine sediments to Mesozoic marls, sandstones, conglomerates, shales, slates and limestones (DOBIN 1985, ERGENZINGER 1992, BECHT 1989, DE JONG 1992b). The lower Schmiedlaine is divided into three main reaches: a straight bedrock reach in the steep, upper parts; a meandering valley confined boulder-bed reach with debris flow inputs and shale outcrops in the medial reaches and finally a meandering valley with major deposition and tendencies to braid. It is in the last reach that the main measuring site is situated.

### 4.2.2 Flood Hydrology

Details of flood hydrology are given in Table 4.1 and in BECHT (1989). Large floods occur as a result of short thunderstorm events in July and August produced by the orographic effects of the Benediktenwand, a highly elevated rock face (1800m). Such locally induced rainstorm events can create high magnitude floods such as the event of 30th June 1990 with the highest recorded discharge so far of 75 $m^3s^{-1}$ (Fig. 4.10).

Average annual discharges lie around 1 $m^3s^{-1}$ while the maximum observed discharge to date (30th June 1990) peaked at about 75 $m^3 s^{-1}$. During very dry years the possibility of a sediment transport event, requiring a threshold discharge of 5 $m^3s^{-1}$, is severely limited, as was the case in 1992.

### 4.2.3 Topography and Sedimentology

The study site consists of a braided bar reach, with a gradient of approximately 2% (Fig. 4.9 a & b, Table 4.1). Unlike the main Lainbach river, the Schmiedlaine has remained a natural torrent and has not been modified by any check dams. Slopes are very steep and provide immediate sediment inputs. The medial bar selected for study is adapted to the high angle of valley curvature. Sediment is of a very coarse-grained and angular nature (see Table 4.1 and Fig. 4.7). The results show that the Schmiedlaine has a far coarser grain size distribution than Squaw Creek. A series of coarse-grained cobble-boulder berms are located at the upper bar edge parallel to the outer channel curvature. The bar surface consists almost solely of gravel bedforms i.e. highly imbricated clusters, transverse ridges interspersed with organic matter. The main channel contains a step-pool system with standing waves and riffles.

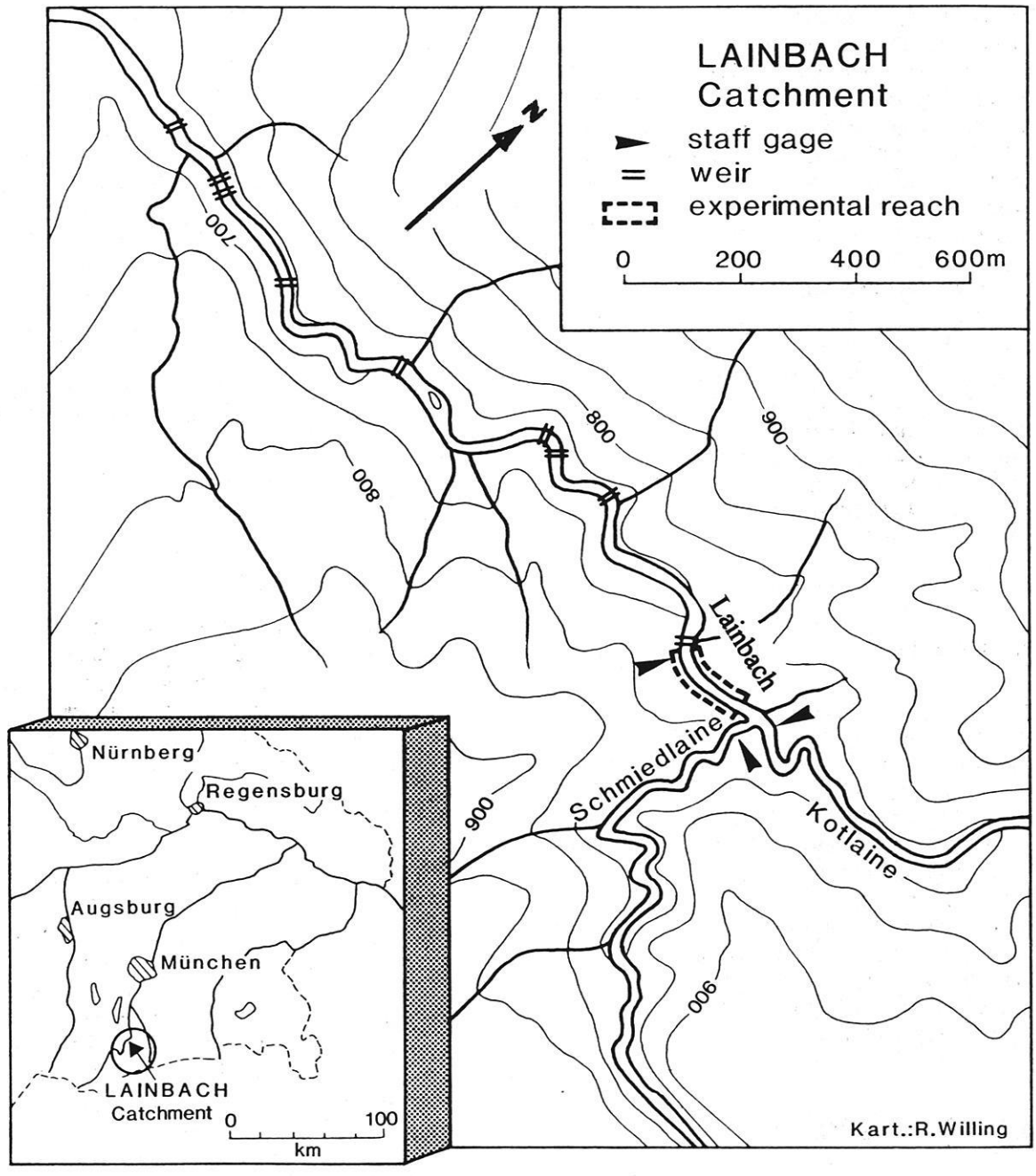


**Fig. 4.8** Location of the Schmiedlaine and Lainbach study sites.

a)

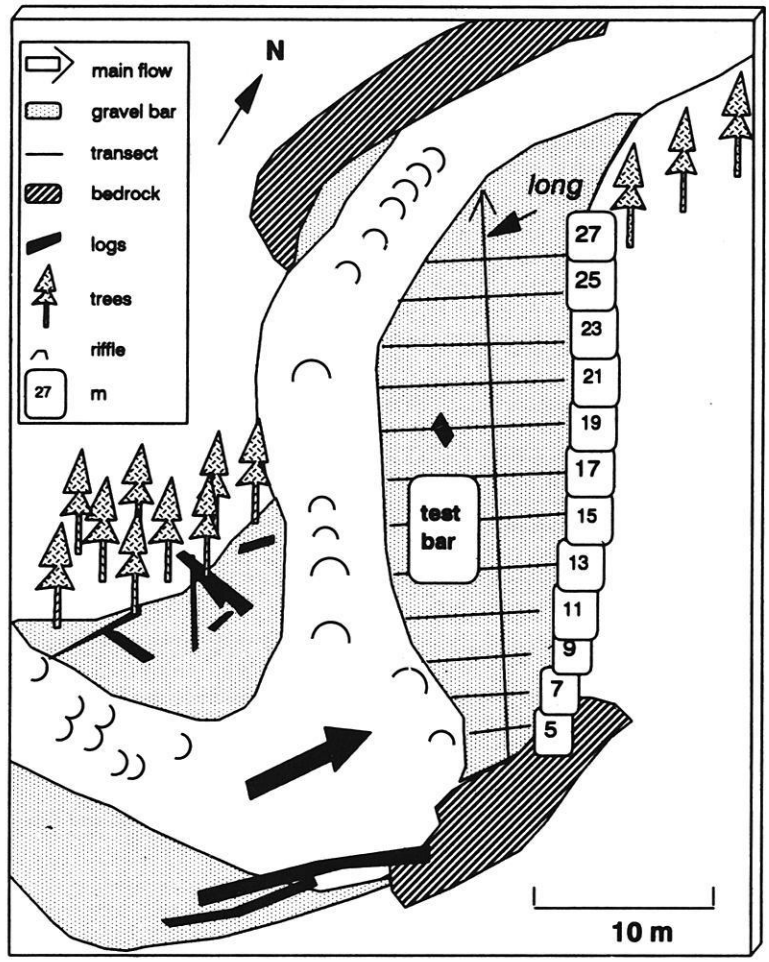


b)

**Fig. 4.9** **a)** Study site in braided lower reach of the Schmiedlaine, 1992. Notice high curvature bend, inner bend deposition of logs and large boulders. Longitudinal and cross-sectional transects (5-27) are marked in relation to distance downstream. **b)** Oblique photograph of study site at same angle of observation. Notice outer bend berm deposition (light-coloured gravel bars opposite wooden debris in inner bend) equivalent to transects 5-17 on the map.

### 4.2.4 Measuring installations

The site has permanent tie-in-points for mini-Tausendfüssler and photo-sieving surveys (see Ch. 5. Methodology). Discharges were reconstructed from the main measuring site on the River Lainbach.

## 4.3 Lainbach

The Lainbach is a tributary of the River Loisach which contributes to the River Isar. The measuring site (Fig. 4.8) lies just below the confluence of the Schmiedlaine (described above) and the Kotlaine. Details on the catchment, sedimentary and hydraulic characteristics can be obtained from Table 4.1 and (ERGENZINGER 1992, ERGENZINGER & STÜVE 1986, FELIX et al 1988). Vegetation characteristics are similar to the Schmiedlaine. The Lainbach valley is broader than the Schmiedlaine and less steep (2% average gradient). The channel is a step-pool system.

### 4.3.1 Geology

The catchment consists of sedimentary rocks from the flysch in the north and the Allgäu and Lechtal nappes in the south. The steep E-W striking walls of the Glaswand and Benediktenwand along the southern divide consist of Wetterstein limestone. The central parts of the basin consist of unconsolidated Quaternary tills approx. 150 m in thickness transported into the basin by the Loisach glacier during several advances. At the Lainbach measuring site, the bedload material consists of the inputs from the Schmied- and Kotlaine. The bed material consists mainly of Quaternary glacial and glaciolacustrine sediments as well as marls, sandstones, conglomerates, shales, slates and limestones (ERGENZINGER 1992, BECHT 1989, DE JONG 1992b).

### 4.3.2 Flood Hydrology

The flood regime of the Lainbach is similar to that of the Schmiedlaine (Table 4.1). Average annual discharges lie around 2 $m^3s^{-1}$, with a maximum estimated peak discharge of 200 $m^3 s^{-1}$.

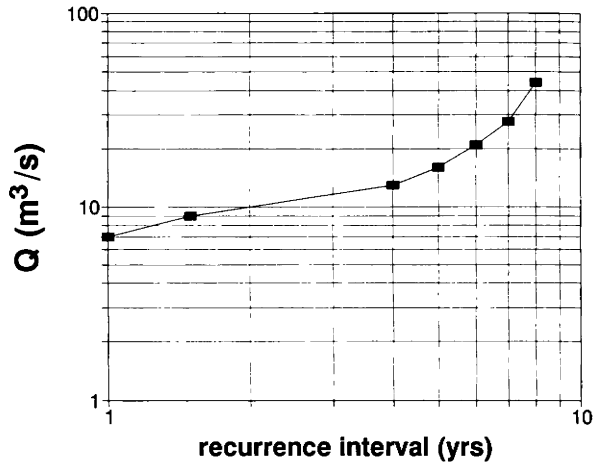


**Fig. 4.10** Recurrence intervals for the maximum annual discharge between 1975-83 for the Lainbach (FELIX et al 1988).

### 4.3.3 Topography and Sedimentology

The Lainbach consists of a step-pool system, created both by the local geology and by large boulders. Unlike the Schmiedlaine, the Lainbach has been modified by an extensive series of check dams. It is only at the measuring site that the river bed has been preserved in its natural state. In Fig. 4.7 the grain size distribution refers to the finer-grained gravel bar and channel at the measuring site. If the entire step-pool sequences are analysed along the Lainbach, the grain size distribution becomes far coarser but still lies to the left of the Schmiedlaine. The measuring site where roughness and geometry were observed consists of a 5 m by 15 m area which includes one step and part of a pool in the main channel as well as one lateral bar (Fig. 4.11). The main criterion for selecting the measuring site was its comparability with Squaw Creek in that it is in a straight reach.

### 4.3.4. Measuring site

The study site consists of two Tausendfüssler measuring bridges, 5 m apart and 15 m long (Fig. 4.11). Attached to each bridge is the Tausendfüssler installation with an additional mobile longitudinal bridge between them (marked over the main channel). Flow velocities, water depth and surface topography could be determined from these fixed locations. In addition water level recorders were installed at and below the measuring bridges. Longitudinal and cross-sectional transects taken with the mini-Tausendfüssler are marked.

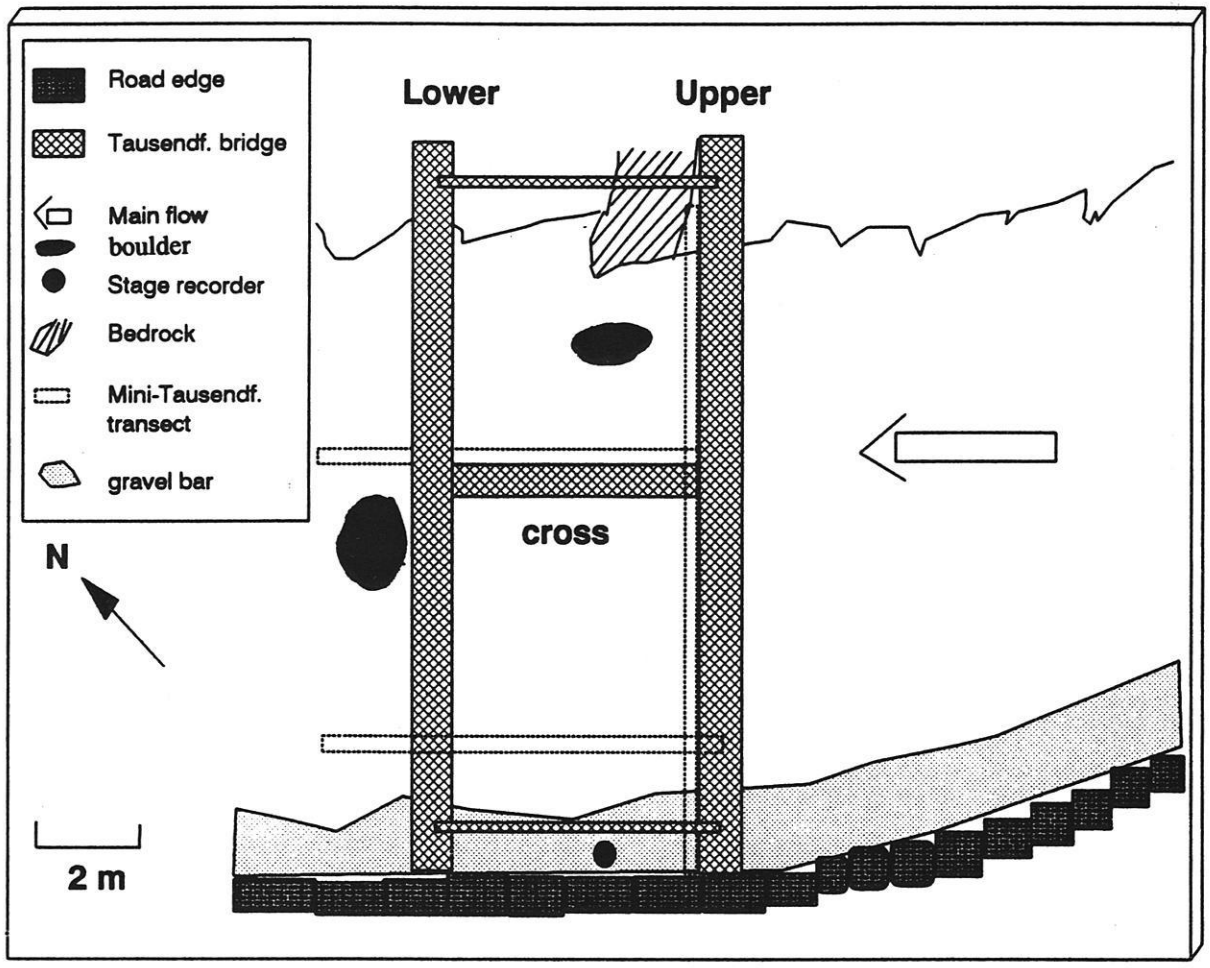


**Fig.4.11** Study site on the Lainbach River just below the confluence of the Schmied- and Kotlaine. Notice that it is a nearly straight reach just as at Squaw Creek. The channel dominates the cross-section with only a narrow bar. As at Squaw Creek, the entire channel width is submerged during a flood. Notice that the spatial detail roughness can be sampled using the two cross-sectional and additional mobile longitudinal bridge.

# 5. METHODOLOGY

Measurements of spatial and temporal changes in roughness and geometry were carried out during the field seasons of 1990, 1991 and 1992 both at Squaw Creek, Schmiedlaine and Lainbach. At Squaw Creek, temporal changes were measured in accordance with project funding in 1991 but could not be obtained for 1992 due to a lack of flood events during the field season. In contrast, spatial measurement data were gathered both for 1991 and 1992. Since spatial measurements can be executed ubiquitously, the Schmiedlaine could be sampled both in 1990, 1991 and 1992. Due to the destruction of all measuring equipment during a catastrophic 150 year R.I. flood in the Lainbach valley in 1990, no temporal measurements could be taken in the Lainbach for 1990. In addition no continual flood measurements were carried out in the Lainbach in 1991, therefore only 1992 will be considered.

## 5.1 Measuring the spatial variability of bed roughness and geometry

Problems encountered in the areal measurement of roughness have been mentioned frequently in the literature (SUTHERLAND 1987). "Detailed surveys of river beds" have been proposed (DIETRICH et al 1988). Analyses of the spatial variability of roughness and geometry require an accurate description of the river bed (ERGENZINGER & STÜVE 1987). Factors considered in this study include particle projection, imbrication, bedform shape, particle size and area distributions, orientations and rounding. These geomorphologic and granulometric analyses of the river-bed were achieved with the help of geodetic and photogrammetric surveys.

In order to determine the role that roughness elements such as clusters play on the river bed, separate analyses for clusters and the surrounding material were carried out (Figs. 5.1 a & b, 5.4, 5.6, and in Section 6.2 - 6.56 a&b). Clusters were identified (following DAL CIN 1968, TEISSEYRE 1977, BRAYSHAW 1984, BILLI 1988, REID & FROSTICK 1986, DE JONG 1992a) as an assemblage of 2 or more neatly organised, imbricated particles, limited both in section and in plan to an approximate ellipsoid and forming a "deviation from the general bed level readily detectable to the eye" (BRUSH 1965). Each cluster is assumed to contain an obstacle clast and a stoss or stoss and lee-side accumulation of grains.

a)

b)

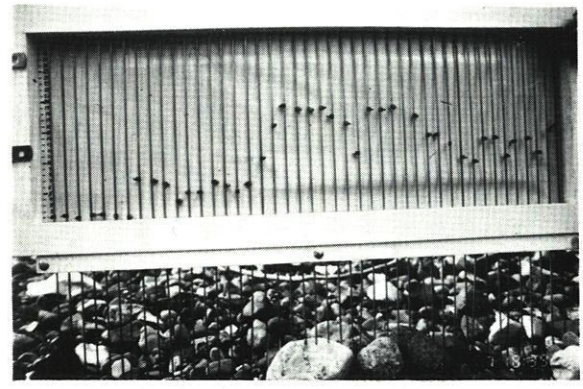

**Fig. 5.1** The mini-Tausendfüssler (bed profiling device) held in long profile over a typical cluster both in **a)** the Schmiedlaine (1991), flow from left to right and **b)** Squaw Creek (1991), flow from right to left. Needles are 2cm apart and cover a 90cm length. The frame is 30cm high. Notice differences in grain size, grain rounding and angles of imbrication.

### 5.1.1 Micro-profiling

To determine the empirical roughness values, the relative projection of particles must be measured with high resolution. Micro-profiling of the river bed not only enables the determination of relative roughness which forms the basis of form drag (SHEN et al 1990) but also the degree of projection, the angle of imbrication, and the shape of individual bedforms in relation to surrounding material. A new instrument, the mini-Tausendfüssler device (Fig. 5.1) is introduced (DE JONG 1992c, DE JONG 1992d) for this purpose. The mini-Tausendfüssler micro-profiles roughness by means of vertical needles positioned at 2 cm intervals. The technique requires the microprofiler to be levelled with two bubble levels, one in the horizontal and one in the vertical, at each measurement location.

An exact vertical outline of the bed structure shows up on the mini-Tausendfüssler with the help of screws displayed against graph paper. A photograph is taken of the entire device and its underlying topography using a wide-angled lens (20mm). This technique allows one sample to be taken per minute. Later the photograph is enlarged and is digitised using an AUTOCAD program and the scales indicated on the graph paper.

At Squaw Creek, mini-Tausendfüssler profiles were carried out both in 1991 and in 1992 along the old (left) and new (right) gravel bar (Fig. 4.5 & 4.6, Ch. Study Areas). Profiles were taken both along longitudinal and cross-section transects, the cross-sections were 2 m apart. The length and number of profiles are given in Table 5.1. On the old bar, the longitudinal profile in 1991 extended not only over the entire bar length starting from the Tausendfüssler bridge but it also extended beyond the bar into the channel to the lower detector log. In contrast, the 1992 profile extended only along the bar top.

Profiles were also sampled at the macro-Tausendfüssler bridge in 1991 and 1992 in the same manner as the standard macro-Tausendfüssler cross-profile during flood measurements. In 1991 the Tausendfüssler profile extended along the bar and only as far as the channel/bar interface due to high water levels (Fig. 4.5, Study Areas) whereas the profile covered the entire bar, interface and channel width in 1992 (Fig. 5.11).

In the Schmiedlaine, mini-Tausendfüssler profiles were taken twice in 1991 and once in 1992 over the same gravel bar (Fig. 4.10, Ch. 4. Study Areas) and along the same longitudinal and cross-sectional transects. A single end-to-end longitudinal profile was sampled in addition to cross-sectional profiles at 2 m intervals. Mini-Tausendfüssler measurements were limited to the gravel bar due to large flow depth and flow strength in the water and the difficulties of bed surface verification in the water.

At the Lainbach, mini-Tausendfüssler profiles were measured only in 1992 (Fig. 4.12). Longitudinal profiles, each 10 m long, were taken along the main channel and bar and one cross-sectional profile, 10 m in width, along the upper Tausendfüssler bridge.

Mini-Tausendfüssler profiles were always overlapped in order to ensure accurate end-to-end reconstruction of the river bed. In addition, each mini-Tausendfüssler profile was corrected for height. Mini-Tausendfüssler profiles were taken in the same direction and along the same profiles as the photo-sieving samples (section 5.1.2).

**Table 5.1** Annual details on the location, direction, number and length of Mini-Tausendfüssler profiles taken at each study site.

| Study Area | Date | Location | Direction | No. of long profiles | Total length (m) | No. of cross profiles | Total length (m) |
|---|---|---|---|---|---|---|---|
| Squaw Creek | 7/5/91 | Tausendfüssler | cross | - | 7 | - | - |
| Squaw Creek | 14/5/91 | old gravel bar | long/cross | 1 | 18 | 4 | 25 |
| Schmiedlaine | 3/7/91 | gravel bar | long/cross | 1 | 19 | 15 | 22 |
| Squaw Creek | 20/5/92 | new bar | long/cross | 1 | 23 | 21 | 91 |
| Squaw Creek | 7/5/92 | Tausendfüssler | long/cross | 1 | 10 | 1 | 10 |
| Squaw Creek | 18/5/92 | old bar | long/cross | 1 | 8 | 7 | 33 |
| Schmiedlaine | 29/7/92 | gravel bar | long/cross | 1 | 33 | 12 | 112 |
| Lainbach | 4/10/92 | Tausendfüssler | long/cross | 2 | 12 / 12 | 1 | 12 |

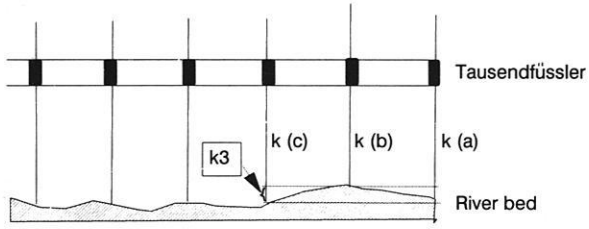


k3 = max [k(a); k(b); k(c)]- min [k(a); k(b); k(c)]

**Fig. 5.2** Calculation of the $K_3$ coefficient from the Tausendfüssler micro-profiling device.

*5.1.1.1 Geometry*

The x and y co-ordinates obtained for each point from the mini-Tausendfüssler device were used to reconstruct the river bed topography. The geometry of the river bed was reconstructed at 2 cm intervals for all the long and cross profiles on the gravel bar and in the channel at all three study sites. The profiles had to be corrected manually for overlap and were then fitted end-to-end. In addition, all gravel bars were surveyed geodetically.

*5.1.1.2 Calculation of particle projection ($K_3$)*

The data obtained from the mini-Tausendfüssler profiles were used to calculate the relative roughness or projection. Projection was calculated from a moving average value of the vertical height difference between three adjacent topographical points using the $K_3$ coefficient (ERGENZINGER & STÜVE 1989). The principal of the technique is similar to that applied for the macro-Tausendfüssler and is illustrated in Fig. 5.2.

*5.1.1.3 Reconstruction of 3-D roughness*

With the $K_3$ (2 cm) data obtained from the maximum vertical difference between 3 mini-Tausendfüssler points, each 2 cm apart, a three-dimensional roughness model was constructed for the old bar in 1991 and 1992 and the new bar in 1992 at Squaw Creek as well as the test bar in the Schmiedlaine in 1992. For each mini-Tausendfüssler sample, the maximum $K_3$ value was utilised in the plot which consisted of a series of cross-sectional profiles typifying roughness conditions over the entire bar.

*5.1.1.4 Roughness frequency analysis*

Frequency distributions were calculated from the $K_3$ data for all river beds sampled, since average $K_3$ values may be misleading. The spacing of roughness is important since it relates to the resistance of flow (BATHURST 1978). In the Schmiedlaine, a class size of 1 cm was used for the horizontal intervals up to the 0.24 m size class whereas at Squaw Creek roughness was classified at 5 mm intervals up to the 0.18 m size class due to the finer grain sizes. Longitudinal and cross-sectional frequency distributions were considered from each individual mini-Tausendfüssler profiles, each sample therefore covered 90 cm of the river bed. Individual longitudinal frequency were considered in the longitudinal sample and for comparison purposes, an average distribution was calculated from the whole cross-section in the cross-sectional samples. This enabled the longitudinal and cross-sectional frequencies to be compared directly. Due to the larger sample size, the cross-sectional distribution was smoother.

*5.1.1.5 Fractal intervals*

In order to describe the organisation of the river bed and transitions between different roughness types, fractal intervals were calculated (ROBERT & RICHARDS 1988). Using the $K_3$ approach the river bed was analysed at ever increasing $K_3$ intervals. The lowest interval was given by $K_3$ (2) calculated directly from the primary data set at 2 cm spacing. This was followed by $K_3$ (4) calculated from every other topographic measurement point of the mini-Tausendfüssler pins at 4 cm distance from each other. The following intervals included $K_3$ (6), $K_3$ (10), $K_3$ (20), $K_3$ (30), $K_3$ (40), $K_3$ (50),$K_3$ (60), $K_3$ (70), $K_3$ (80), $K_3$ (90), $K_3$ (100), $K_3$ (200), $K_3$ (300), and $K_3$ (400). For each of the intervals above, an average $K_3$ value was calculated for that interval calculated along the whole measuring section. Little difference was obtained between the maximum, standard deviation and average $K_3$ value for each distribution. The intervals were calculated for the entire length and width of the gravel bars at Squaw Creek, Schmiedlaine and Lainbach to ensure an adequate sample size. Since the sample size (n = number of samples) decreases exponentially from 1400 data points to only 3 with increasing $K_3$ intervals, the 100-400 cm intervals should produce less resolution. To counteract this loss, the interval calculation was repeated by shifting the starting point each time. The final value obtained consisted of an average value obtained from these separate calculations. Even though the n value was very small, the difference between measurements in the end was negligible (± 1 cm).

In all following spatial roughness analyses, the $K_3$ (2) value was utilised whereas in all temporal analyses, the $K_3$ (10) was used (Section 6.3). Fig. 5.3 shows the relation between the lateral distribution of $K_3$ (2) and $K_3$ (20) at the Squaw Creek macro-Tausendfüssler bridge in 1991. $K_3$ (20) was chosen for illustrative purposes since it is already within the form category. Its spatial distribution is less accurate than the $K_3$ (10) interval which marks the transition between grain and form roughness. The basic pattern of roughness is maintained but the detail is lost at the higher $K_3$ (20) interval. Since there is a correlation of 0.7 for the two distributions, the $K_3$(2) value was selected for all further analyses. In section, the $K_3$ (2) value represents grain roughness whereas the $K_3$ (20) already lies in the form roughness category.

*5.1.1.6 Imbrication*

Imbrication measurements should reveal information about the potential stability of grains (BUFFINGTON et al 1992, KOMAR and LI 1986). The imbrication of particles was obtained directly from the topographical image of the river bed by measuring the angle that the particle formed in relation to the horizontal on longitudinal Tausendfüssler profiles (Fig. 5.1). Separate measurements were carried out for clustered and open-bed particles. The difference between clustered and open-bed material gives information on the relative mobility of grains. Each single particle was considered along the long profile of the new bar at Squaw Creek (273 particles) and the bar in the Schmiedlaine (129 particles due to larger particle size). Considering every cluster along the transect, 24 clusters were processed at Squaw Creek and 17 in the Schmiedlaine which were up to 1m in length. The ratio of the angle between clusters and surrounding material was determined and correlated with the $D_{84}$ and the maximum $K_3$ (2) value since clusters are assumed to occupy the coarsest fraction of the bed.

An ellipsoid was described around each cluster from the slope of the first to the slope of the last particle inclusive of the maximum height (z) (Fig. 5.2). An

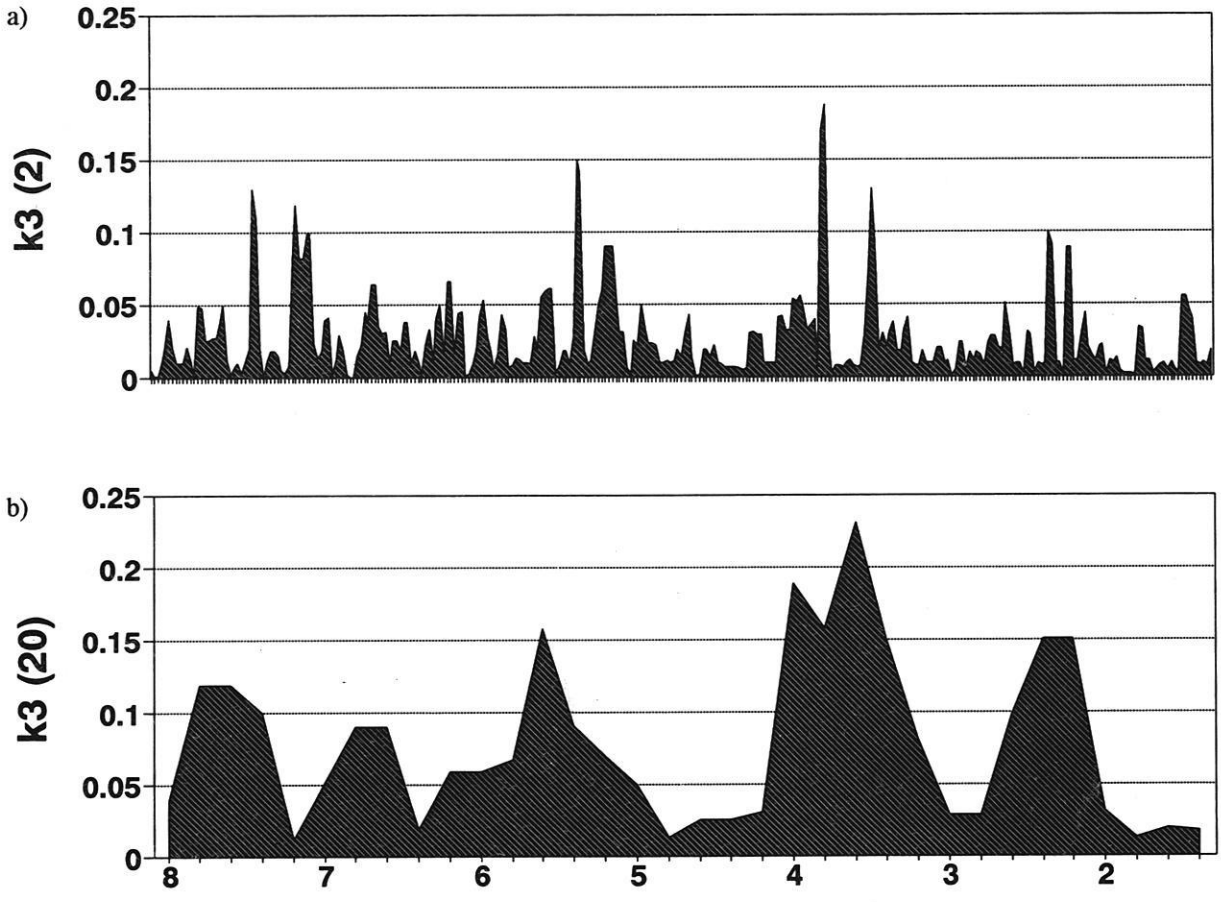


**Fig. 5.3** Comparison between the lateral distribution of a) $K_3$ (2) and b) $K_3$ (20) at the Squaw Creek macro-Tausendfüssler bridge in 1991.

ellipsoid is the best approximation to the natural cluster shape in order to reconstruct flow dynamics. The a and b axis was determined for the ellipsoid both in section and in plan and the ratio of a/b calculated for each cluster. By defining each cluster as an ellipsoid, the frequency of roughness (cluster) spacing could be determined.

## 5.1.2 Photo-sieving

A new method of photo-sieving (IBBEKEN 1974, IBBEKEN and SCHLEYER 1986, DE JONG 1992a, DIEPENBROEK 1992, DIEPENBROEK & DE JONG 1993) was applied in order to reproduce the spatial roughness characteristics of the armoured layer. Clustered and open-bed (non-clustered) material were considered separately. This method enables complete and undisturbed sampling of the surface layer of the river bed by means of vertical photograph at a given scale (Fig. 4.6 a in the Chapter Study Area; Fig. 5.4). A camera is attached to the top of the frame, enabling a vertical photograph to be taken of the river bed, inclusive of the lower frame which is demarcated with scale. This ensures a systematic and large sample (WOLCOTT & CHURCH 1991) to be obtained in a short time. Sampling error is also minimal.

In the laboratory each single particle presented on the photograph was digitised with a mouse on a graphics board and processed with the Photo-Sieving Program developed by Alex Bartholomä and Michael Diepenbroek of the Geology Department, Free University of Berlin (Fig. 5.5). The minimum particle size digitised was 13 mm. When digitising the particles, the entire outline of the particle was considered even if it had to be projected underneath another particle covering it. The results were checked by manual sieving at a selected location on the bar top. Manual sieving samples of the surface revealed a $D_{50}$ of 80.15 as compared to the $D_{50}$ of 45.16 obtained by photo-sieving. The coarseness of the sample demonstrates that the finer grain sizes were truncated in the manual sample. Other studies have also supported the inaccuracy and truncations of manual samples (DIEPENBROEK 1992).

Photo-sieving was carried out along longitudinal and lateral profiles on the new and old gravel bars at Squaw Creek in 1991 and 1992 (see Fig. 4.5, Ch. Study Areas) and on the lower gravel bar of the Schmiedlaine in 1990, 1991 and 1992 (see Table 5.2 & Fig. 4.10, Ch. Study Areas). In 1991, a total area sample was taken of the old and new bar at Squaw Creek and of the bar in the Schmiedlaine. In 1992 the samples were taken along the same locations and intervals as the mini-Tausendfüssler profiles. No photo-sieving was attempted in the Lainbach test reach since it is covered with too much water. Data were obtained from the gravel bar below the test site.

In the Schmiedlaine, the approximate number of particles covering a photograph is estimated at 150 (Fig. 5.6). At Squaw Creek the average number of particles in a photograph is approximately 700 (Fig. 5.4). This not only allowed the measurement of grain size but also the area covered by a particle, its rounding and orientation to be accurately determined for each single particle presented in each photograph. Cluster density was calculated as the average number of clusters per $m^2$. The sample size for the Schmiedlaine was approximately 5000 particles in 1990, approximately twice 5000 particles in 1991 and 8000 in 1992. At Squaw Creek the sample size was approximately 8000 particles for the old bar and 20,000 particles for the new bar in 1991, and 10,000 particles for the old bar and 30,000 for the new bar in 1992. Only the new bar will be considered for photo-sieving since the old bar was covered by too much water to obtain a representative picture of its roughness arrangement.

**Table 5.2** Annual details on the location, direction, total sample area and size of the photo-sieving sample together with actual sample area and size processed (open-bed) as well as sample area and size of clusters and cluster particles. Cluster area is expressed as average area in $m^2$ covered by one cluster. Flow orientation sample used for separate study on particle orientation (Section 6.2.1).

| Study Area | Date | Location | Direction | Total sample area ($m^2$) | *Open-bed area ($m^2$) | Flow orient. sample | *Open bed grain sample | Cluster particles (no.) | Cluster bedform (no.) | Cluster particle area ($m^2$) | Cluster density ($m^2$) |
|---|---|---|---|---|---|---|---|---|---|---|---|
| Schmiedlaine | 7/7/90 | test bar | long | 37.80 | 30 | 2,000 | 1,374 | 191 | 17 | 2.95 | 1.61 |
| (pre/post-flood) | 18/7/90 | test bar | long | 45.36 | | | | | | | |
| Squaw Creek | 3/5/91 | old bar | long/cross | 45.36 | | | | | | | |
| | 7/7/91 | old bar | long/cross | 56.70 | | | | | | | |
| Schmiedlaine | *3/7/91* | test bar | long/cross | 60.48 | 15 | 5,000 | 1,339 | 54 | 12 | 3 | 0.56 |
| Squaw Creek | 22/5/92 | new bar | long/cross | 76.86 | 49.14 | 30,000 | 17,156 | 324 | 79 | 1.14 | 0.8 |
| Squaw Creek | 3/5/92 | old bar | long/cross | 49.14 | | | | | | | |
| Schmiedlaine | 30/7/92 | test bar | long/cross | 64.26 | | | | | | | |

** sample processed from total (clusters not included).*

*5.1.2.1 Grain size determination*

Grain size analyses of poorly sorted material common in mountain torrents cannot be obtained in representative quantities through conventional methods. Methods such as those described in BUFFINGTON et al (1990) where grain sizes were "determined by randomly lowering a hand-held needle (while the operator looked away) onto the surface and measuring the selected grain size" clearly require improvement. The photo-sieving method (IBBEKEN 1986, IBBEKEN et al 1992, DIEPENBROEK & DE JONG 1993) was used to calculate grain size distributions from the grain b-axes after the Wolman method (WOLMAN 1954). Grain size is calculated by transformation of the particle's projected outline into a series of Fourier coefficients. The particle outline is correlated with its best approximating ellipse (assumed to be the particle's ultimate shape after transport, Fig. 5.7) which is obtained from the second harmonic of the Fourier spectrum. More elaborate details on the Fourier analysis can be obtained from DIEPENBROEK 1993 and DIEPENBROEK et al 1992.

Thus for each digitised clast, the longest and shortest axes of the particle's approximation to an ellipsoid is calculated. This is equivalent to the grain's a- and b-axis since the shortest axis (c-axis) cannot be determined from vertical photography. Grain size distributions are then calculated by number from the b-axis distribution. With the photosieving programme, the grain sizes are classified according to the Wentworth classes ($\phi$), which deviate from the DIN 4022 description. The particles were classified according to the following Wentworth table:

**Table 5.3** Wentworth table for particle size

| | | |
|---|---|---|
| sand | up to | 2 mm |
| pebble | up to | 64 mm |
| cobble | up to | 256 mm |
| boulder | more than | 256 mm. |

The photosieving method provides much larger sample sizes, is also more accurate, and can be analysed quickly. In one hour, the equivalent of 300 kg of sediment can be analysed and factors in addition to grain size can be determined.

**Fig. 5.4** Example of a photo-sieving picture taken at Squaw Creek. Notice material is much more rounded than in the Schmiedlaine (Fig. 5.6) and that cluster assemblages have smaller number of particles. Blue particles are marked as clusters and treated separately in all investigations.

The grain size information was compared to the $K_3$ roughness data in order to validate the new coefficient. The $D_{16}$, $D_{50}$ and $D_{84}$ were chosen as dynamical indicators of roughness. The $D_{84}$ was chosen rather than the $D_{95}$ since above the $D_{84}$ the distributions did not differentiate enough (Fig. 4.7, Ch. Study Area). Since the finer grain sizes are not truncated in the photo-sieving samples, the $D_{16}$ would still represent a dynamical value. In all comparisons of grain size and $K_3$ roughness, the $K_3(2)$ i.e. the smallest possible interval was taken in order to represent all minor roughness variations. There is a very good relationship between the $K_3$ (2), (10) and (20), but much detail is lost at the higher intervals. The $K_3$ (2) value was selected to reproduce the most details.

Clusters could be considered separately from surrounding material with the photographic technique. This means that the grain size distributions

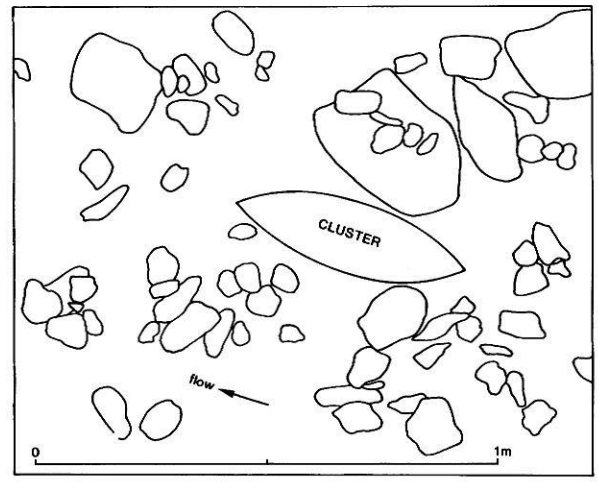


**Fig. 5.5** Example of a digitised diagram obtained from the photo-sieving technique in the Schmiedlaine.

**Fig. 5.6** Example of a photo-sieving picture taken in the Schmiedlaine. Notice coarse-grained, angular material, suitable for clustering. Red particle assemblages indicate clusters, orange individual particles indicate loose test particles (not treated in the thesis) and remaining distribution indicates surrounding open-bed material.

and other grain parameters (such as grain area described in the following section) were determined for each single cluster and compared to the surrounding material. At Squaw Creek, 80 clusters were considered in 1992 over an area of 47.88 $m^2$. This is the equivalent density of 1 cluster per 0.6 $m^2$. In 1990 at the Schmiedlaine, 18 clusters were considered over 22.68 $m^2$, equivalent to 1 cluster per 1.26 $m^2$. In 1991, 12 clusters were considered in the Schmiedlaine over 15.12 $m^2$ which is also equivalent to 1 cluster per 1.26 $m^2$. In the Schmiedlaine (Fig. 5.6) cluster density is twice that of Squaw Creek (Fig. 5.4). The samples processed represent only half of the total samples taken.

### *5.1.2.2 Grain Area Determination*

Due to the difficulties encountered in measuring grain areas, the role of area in natural river beds has been neglected. Even so, the importance of the area of the river bed that is covered by large blocks is significant as a flow resistance parameter. River bed arrangement is significant both for high and for low flows. Since form drag on an object is a function of several parameters which include the area projecting into flow (BATHURST 1978), the measurement of grain areas is a necessity. The photo-sieving method was introduced (DE JONG 1992c, DIEPENBROEK & DE JONG 1993) as an appropriate technique for determining grain areas.

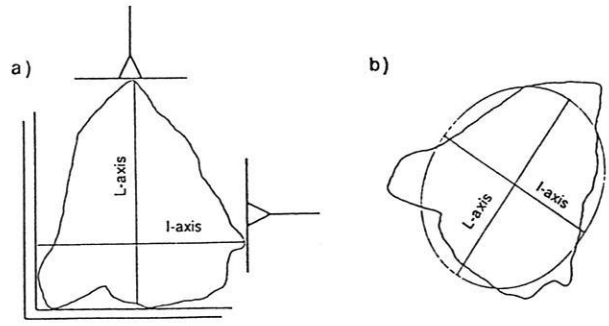


**Fig. 5.7.** Measurement of a particle's main axes using a) mechanical sieving and b) photo-sieving.

### *5.1.2.3 Grain orientation*

Detailed grain orientation studies in the literature have also been neglected due to the labour involved in manual orientation measurements in the field. The photo-sieving technique provides the opportunity for rapidly and accurately calculating the orientation of individual particles according to the grain's a-(long) axis (Fig. 5.7). The orientation of a particle

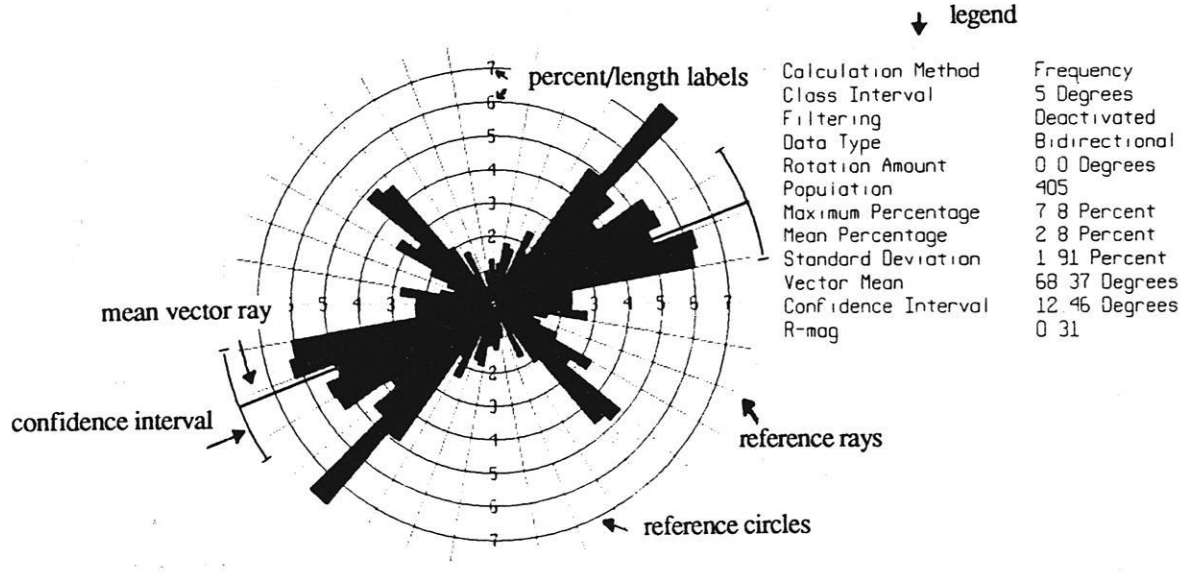


**Fig. 5.8** The statistical calculations carried out by the ROSE program. The vector mean obtained from the orientation distribution was used to calculate average flow directions.

corresponds to the orientation of the ellipse which is calculated from the phase angle of the second harmonic (DIEPENBROEK et al 1992, DIEPENBROEK 1992, DIEPENBROEK & DE JONG 1993). Since all photographs were taken parallel to the main flow direction along the bar, it was not difficult to determine the particle orientations.

Orientation data were processed and plotted using the ROSE program by ROCKWORKS (Fig. 5.8). The program calculated the class frequency of orientations at 10 degree intervals, assuming uni-directional flow and plotted them as rose diagrams. The program carried out statistical calculations which showed the maximum and mean percentage presented by each class, the standard deviation from the main flow direction, the vector mean, confidence interval and r-magnitude.

At each cluster site, the orientation of each cluster was calculated separately from the average orientations of the surrounding open-bed material. The orientation of a cluster was obtained from the whole cluster. Results were combined and plotted on a geomorphologic orientation map (DIEPENBROEK & DE JONG 1993).

*5.1.2.4 Grain rounding*

The photosieving program presents a new evaluation of grain rounding from the complete harmonic spectrum of the Fourier series. All major curvatures of the particle, as well as the relative position of corners and edges are considered in relation to the final ellipsoidal shape. Average grain rounding values were compared for clustered and open-bed material.

### 5.1.3 Gradient

The relation between gradient and roughness size has been mentioned briefly in the literature (ERGENZINGER & STÜVE 1992, GRANT 1990, OSTERKAMP 1978, WIBERG & SMITH 1987, LEOPOLD 1992, DE JONG 1992b). The largest types of bedforms are expected in high gradient river reaches, such as steps or steep bedrock canyons. Gradients were recorded with a theodolite in 1990 and with a GEODIMETER in 1991-1993 from more than 50 cross-profiles along a 2 km section of the Schmiedlaine. In addition, local gradients along the gravel bars were extracted from mini-Tausendfüssler long profiles.

### 5.1.4 Curvature

The degree of river curvature and the amplitude of the bend play a decisive role in the distribution and size of roughness. The radius of curvature was obtained from river sections along a detailed geomorphological map, reproduced from 50 cross-sections (Fig. 4.9, Ch. Study Areas).

## 5.2. Measuring temporal variability of roughness and geometry

### 5.2.1 Bed profiling

Measurements of temporal changes in roughness and geometry were carried out with the macro-Tausendfüssler device (ERGENZINGER 1990, ERGENZINGER 1992, DE JONG 1992c&d, DE JONG & ERGENZINGER 1992) at Squaw Creek and in the Lainbach (Fig.5.9 & 5.10). The macro-Tausendfüssler device probes the river bed at 10 cm intervals according to a fixed vertical reference level (Fig. 5.2) attached to a measuring bridge constructed from scaffolding. Each roughness measurement is taken manually with a rod inserted sequentially through a tube until it touches the river bed. The height difference between the end of the rod and the reference level can be obtained with an accuracy of +/- 1cm. This method ensures undisturbed measurements not only of the water surface but also of the river bed. Water surface measurements are obtained at the same time as the bed profile at 50 cm intervals. The advantage of the method is that river bed roughness and water surface irregularities can be measured at closely-spaced spatial and temporal intervals throughout a passage of a flood without mechanical failure up at discharges less than 10 $m^3 s^{-1}$. The cross-profile of the river bed is plotted for each measuring interval together with the water surface.

An average cross-section took approximately 30-45 minutes. Changes of the river bed were determined at hourly intervals for the entire flood and at half-hourly during the very active periods. Two 24 hour periods are referred to from Squaw Creek for the 23/24th of May 1991 and 5/6th June 1991 respectively. No measurements could be taken during 1992 due to the total absence of a flood event during the field season. One 24 hour period was measured at the Lainbach on the 22/23rd July 1992. At both Squaw Creek and Lainbach each profile consisted of 115

**Fig 5.9** The Lainbach measuring site with its two cross-sectional bridges seen obliquely during a flood event in 1991. Mobile longitudinal bridge was not installed at the time. Flow is from right to left. Upper bridge at right, lower bridge at left. Bridges are 5 m apart. Notice large standing wave above lower bridge caused by large boulder.

Tausendfüssler points, whilst the long profile at Lainbach constituted 50 points. At Squaw Creek data was obtained from a single Tausendfüssler profile whilst at Lainbach, measurements in 1992 were obtained from an upper and lower bridge as well as from a longitudinal bridge (Fig. 4.12 , Ch. Study Areas).

### *5.2.2.1 Determination of roughness*

In order to determine changes in roughness during the entire flood period at hourly intervals, a $K_3$ coefficient (ERGENZINGER & STÜVE 1989) was calculated for each point along the entire profile (see Fig. 5.2 & Fig. 5.11). This parameter enables grain and form roughness to be evaluated as separate parameters (DE JONG 1992d, DE JONG and ERGENZINGER 1992c). $K_3$ coefficients were averaged for the left and right bars, main channel and the channel-bar interface for each cross-section (Fig. 5.11). For each measurement period, the extent of the bars, channels and channel-bar interface were defined separately from their geometrical configurations at that time. This procedure allowed the spatially varying

**Fig. 5.10** The "macro-Tausendfüssler" device in operation at Squaw Creek. Notice parallel tubes attached to the measuring bridge through which rod is being inserted (BERG-commandeur Ergenzinger working).

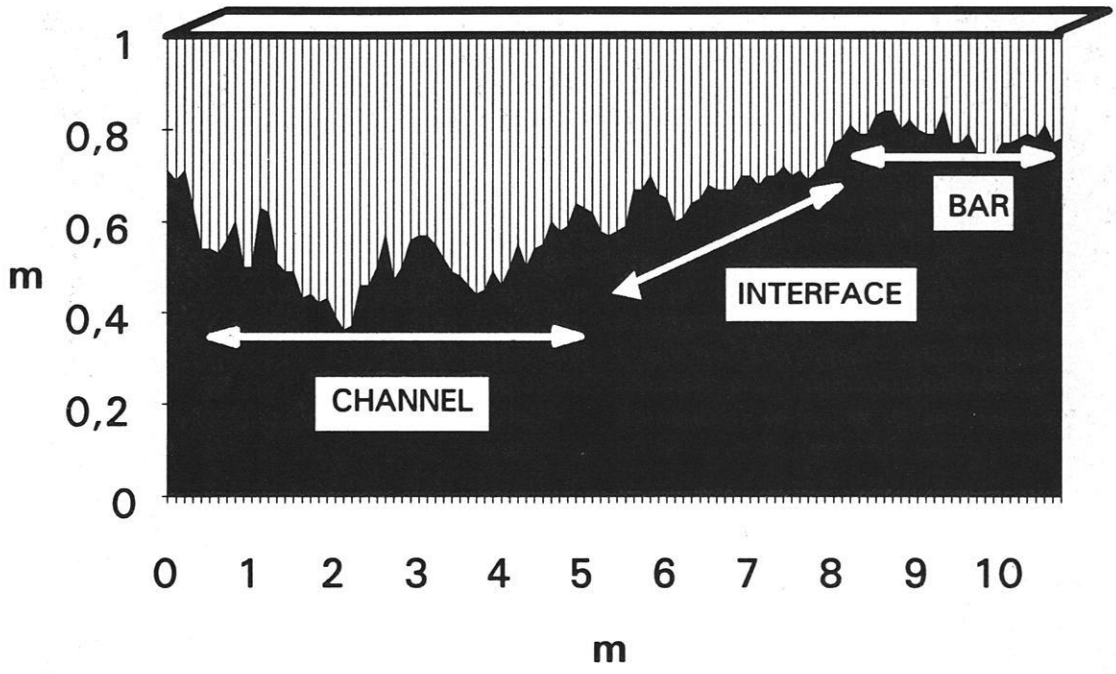


**Fig. 5.11** Cross-sectional profile of the Macro-Tausendfüssler at Squaw Creek indicating sub-division into bar, channel and channel-bar interface. These three sub-divisions are also used to calculate geometrical changes during the course of the flood. Vertical scale is exaggerated by a factor of 6.

dynamics of the roughness to be monitored during the course of an entire flood wave.

*5.2.2.1 Determination of bed geometry*

River bed and water level changes were calculated separately to clarify some of the processes controlling geometry. Change (adjustment) was calculated from the vertical amount of erosion or deposition at each Tausendfüssler point between one measuring session and the next. Changes in water surface configuration were calculated in the same way. River bed and water surface adjustment was calculated for all the flood events (see section 5.2.1), including the upper and lower Tausendfüssler bridges at Lainbach. In addition, the area of change between one measuring session and the next was calculated as a standardised value in order to determine temporal adjustments in river bed geometry. At each Tausendfüssler point the vertical changes occurring at that point between one measurement session and the next was defined as the amount of erosion or deposition and multiplied by a factor of 10 (for the 10 cm intervals) to introduce area. In addition the measurements had to be standardised into hourly intervals since the Tausendfüssler measurements were taken at irregular time intervals. The resulting area of change per hour was averaged and differentiated by location into bar, interface and channel as for the $K_3$ values (Fig. 5.11). Phases of river bed erosion and deposition could be clearly differentiated.

## 5.3 Measuring the temporal and spatial variability of flow

### 5.3.1 Water surface topography

The structure of flow could be determined indirectly from measurements of the water surface. Water surface structure was obtained at the same time as the Tausendfüssler measurements at 50 cm intervals (Fig. 5.11). Distinct surface waves could be detected from vertically exaggerated water surface plots. The information acquired was also used to calculate the difference in water level from one measuring session to the next according to erosion or deposition. The character and length of existence of such surface waves revealed some of the hydraulic dynamics occurring in the flow. Sometimes it may be difficult to separate grain from form roughness since a large boulder can constitute the same amount of roughness as a cluster element consisting of a series of large cobbles. Eventually, however, the large boulder may be transported away as a single grain.

### 5.3.2 Velocity

At Squaw Creek, one-directional velocity measurements were taken in profile as near as possible to the bed both with Seba velocity rotors, consisting of three small propellers and with gangs to five velocity rotors mounted vertically on a single wading rod (from Dr. Carling, Freshwater Biological Institute). Velocity measurements, lasting for one minute, were taken every 50 cm across the Tausendfüssler measuring bridge simultaneously to the bed profiling sessions. Two-dimensional velocity was measured in the x and y direction with three electro-magnetic current meters mounted on a special frame in order to form a triangular measuring field.

At the Lainbach, velocity measurements were taken using the same procedure as at Squaw Creek. In 1992, velocity measurements were taken along both the upper and lower bridge and along the longitudinal mobile bridge. No stage recorder was installed in the Schmiedlaine since the discharge curve at the location immediately above the confluence with the Lainbach is very similar.

### 5.3.3 Stage

The location of the stage recorders for Squaw Creek are indicated in Fig. 4.5 (Study Areas). Stage was recorded continuously from floats installed inside the stilling wells, connected to the river with 2 m long tubes. Stage recorders were installed on the right and left river banks just below the upper detector sill and on the right and left banks just above the lower detector sill, as well as on the left bank below the lower detector sill.

Water surface gradients (Fig. 5.12) were determined with water level hoses. Two hoses were installed, one at the upper end of the measuring reach below the upper detector sill on the left bank, 17 m in length and the other above the lower detector sill. Both ends of the hoses were bent upwards and attached together to a ruler scale at the lower detector sill. River water was allowed to flow through the hoses by gravity and the difference in water levels between the upper and lower hoses was recorded as the water gradient. The water levels were read off at 1-2 hour intervals.

At Lainbach (Fig. 4.11, Ch. Study Areas), stage recorders were installed both between the upper and lower measuring bridges and approximately 40 m below the measuring site.

## 5.4 Measuring the temporal and spatial variability of bedload transport

At Squaw Creek, bedload measurements were monitored electronically during flood flows using two magnetically sensitive sills inserted across the entire width of the river bed and situated 30 m apart from each other (Fig. 5.13). Detailed descriptions of the method can be obtained in ERGENZINGER, DE JONG & CHRISTALLER (1993) and SPIEKER & ERGENZINGER 1990). The technique is based on the Faraday principle for recording pulses created by naturally magnetic particles passing over the sills. Each time a magnetic particle passes a sill, a signal is created which is recorded on the computer in the measuring hut (Fig. 5.14). The lower size class detectable lies around 15 mm. Approximately 70% of the material at Squaw Creek is magnetic, thus ensuring a large sample of bedload to be detected.

Each of the sills contains magnetically sensitive coils subdivided into 2 parallel rows each containing 6 segments, thus 6 in the upper and 6 in the lower row. The lower segments were installed in order to countercheck the functioning of the upper segments and to differentiate signals created by passing magnetic particles from signals created by thunderstorms. The photograph in Fig. 5.15 shows part of the uncovered upper sill with its parallel rows

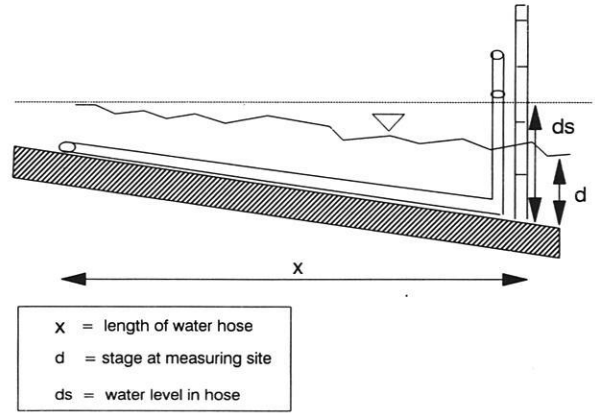


**Fig.5.12** Measurement of water surface gradients with the hoses (after BUNTE 1992).

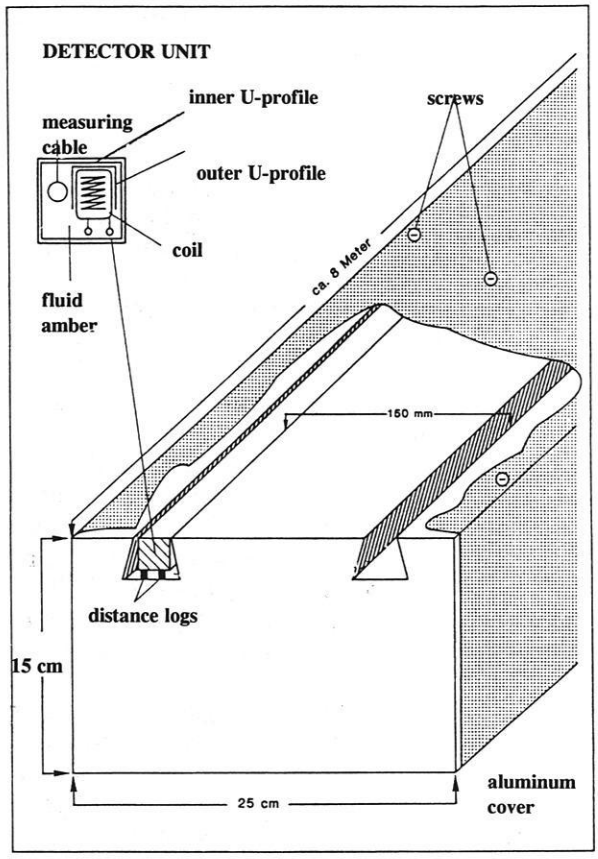


**Fig. 5.13** The set-up of the magnetically sensitive bedload monitoring system at Squaw Creek. Bedload signals created by the passage of individual particles over both the upper and lower sills were continually recorded.

of sensors in repair at the time. In 1991 the upper sill consisted of five segments and the lower sill consisted of six segments. This not only allowed all the incoming and outgoing magnetic particles to be monitored within the reach but also enabled the bedload dynamics to be compared with their respective location on the bar, interface and channel. Bedload measurements could be calculated at hecto-second intervals continuously throughout the 24 hour flood event. Bedload data were processed at 1 second, 10 second, 1 minute, 5 minute, 10 minute, ½ hour and 1 hour intervals. No difference was obvious between the 5 and 10 minute intervals when plotted for the entire 24 hour event. For convenience of comparison with the roughness and geometry data, bedload transfer was averaged over 10 minute intervals for the flood events.

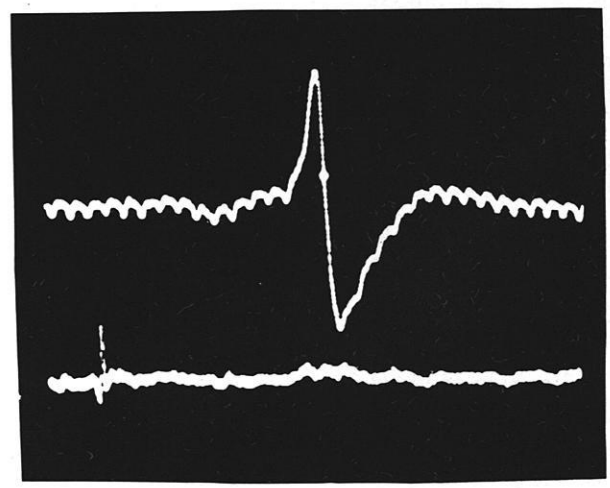

**Fig. 5.14** A signal produced by a magnetic particle passing over the upper detector log.


**Fig. 5.15** The upper detector log partially uncovered during repair works. On the left and right aluminium covers protect the magnetically sensitive coils. The river has been dammed with a double row of sacks in order to divert water onto the new bar to enable repair works. Peter Ergenzinger and Steve Custer at work.

# 6. RESULTS & DISCUSSION

## 6.1. The spatial variability of grain and form roughness on gravel bars

### 6.1.1 Squaw Creek 1991 & 1992

#### 6.1.1.1 New bar

*6.1.1.1.1 Bar geometry*

Bar geometry was derived from Mini-Tausendfüssler data plotted at 2 cm intervals, both along longitudinal and cross-sectional profiles (Fig. 6.1). The example of the new bar at Squaw Creek is illustrated in detail since it could be processed in terms of fractal calculations, grain size distributions, imbrications and flow orientations. The bar shape is limited by the maximum lateral expansion possible into the vegetated banks (see Fig. 4.6b in Ch. Study Areas). The bar formed as a result of the 1991 flood of 5-6th May; before that it was rarely flooded and infrequently reworked due to limitations of lateral flow expansion during medium sized floods. The new bar consists of a small side channel along its right bank (left on the cross-sectional diagram, Fig. 6.1), a mid-bar topographical high running along the whole length of the bar (highest point on cross-section, Fig. 6.1), a second minor channel to its left and finally an artificial ridge strengthened with rip-rap along the border to the main channel. Cross-profiles were only taken on the bar, not on the rip-rap ridge. The long profile (Fig. 6.1) demonstrates that Squaw Creek has a low gradient relative to the other study sites (<2%), with a higher gradient at the proximal and distal ends of the bar. This is related to the curvature of the typically crescentic shape of the lateral bar. Grain roughness seems to dominate, given by the sharp individual peaks. Major steps are absent and bedforms are widely spaced.

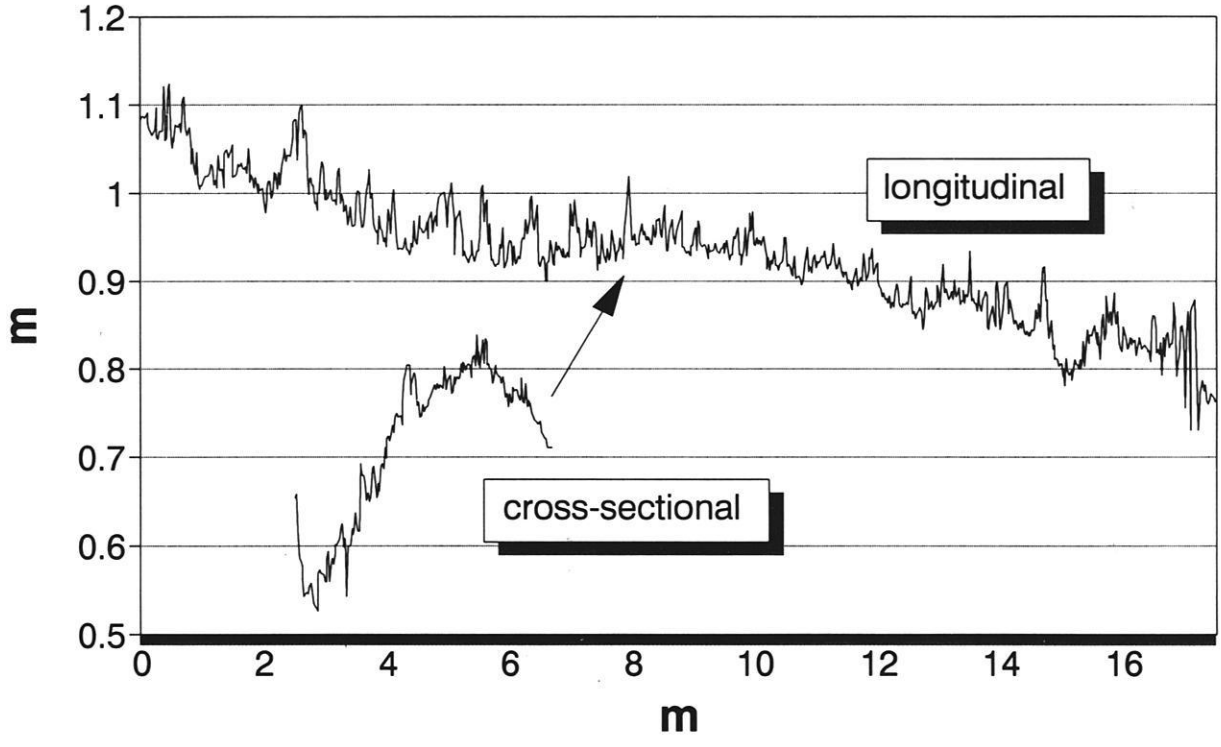


**Fig. 6.1** Topography of the new gravel bar at Squaw Creek, Montana. The longitudinal section has been plotted together with a cross-section superimposed below at the same scale. The cross-section was taken at the 8 m location looking upstream.

In the cross profile, plotted at the same scale as the long profile (Fig. 6.1), lateral gradients are far more drastic as the bar builds up to its maximum at the crest.

#### *6.1.1.1.2 Analysis of particle projection ($K_3$)*

Calculations of $K_3(2)$ coefficients along the long profile of the new bar show that roughness values are widely spaced due to the relative homogeneity in particle shape and size. This type of material is generally inappropriate for dense, imbricated particle arrangement. Fig. 6.2 is an illustration of a typical mini-Tausendfüssler profile taken on the proximal end of the bar. Grain roughness dominates and bedform assemblages up to 4 particles are evident. Form roughness i.e. the development of clusters is most dominant on the new bar but not as well developed as in the other study areas (See later sections). On the whole, roughness keeps a homogenous profile and maximum $K_3$ (2) values lie below 0.12 m. Since flow depths were insufficient for major bedload transport, roughness values on this bar remained lower than on the old bar which is more centrally located (Section 6.1.1.2). Longitudinal roughness has to be well adapted to flow in order to minimise resistance. As a rule, the particles behind an obstacle can never project higher into the flow than the ellipsoid formed around the obstacle itself. In order to avoid entrainment, particles are arranged in descending order of projection in front of and behind of the obstacle.

The cross-profiles show that roughness protrudes as separate grains which are adapted to the hemispherical shape of the bar (Fig. 6.3). Single

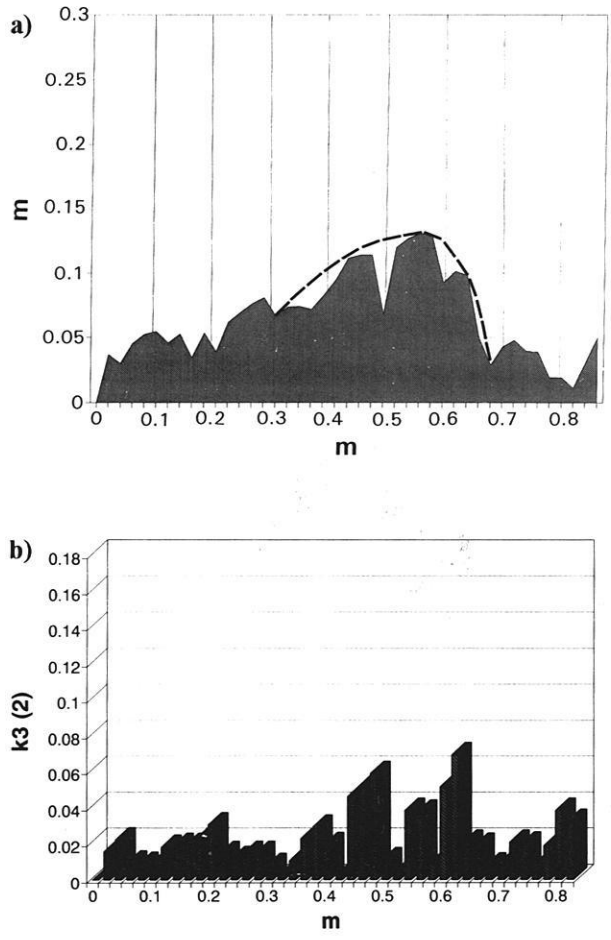


**Fig. 6.2** Mini-Tausendfüssler taken in: **a)** long profile with **b)** respective $K_3(2)$ distribution along the new bar in 1992. Flow is from L. to R.

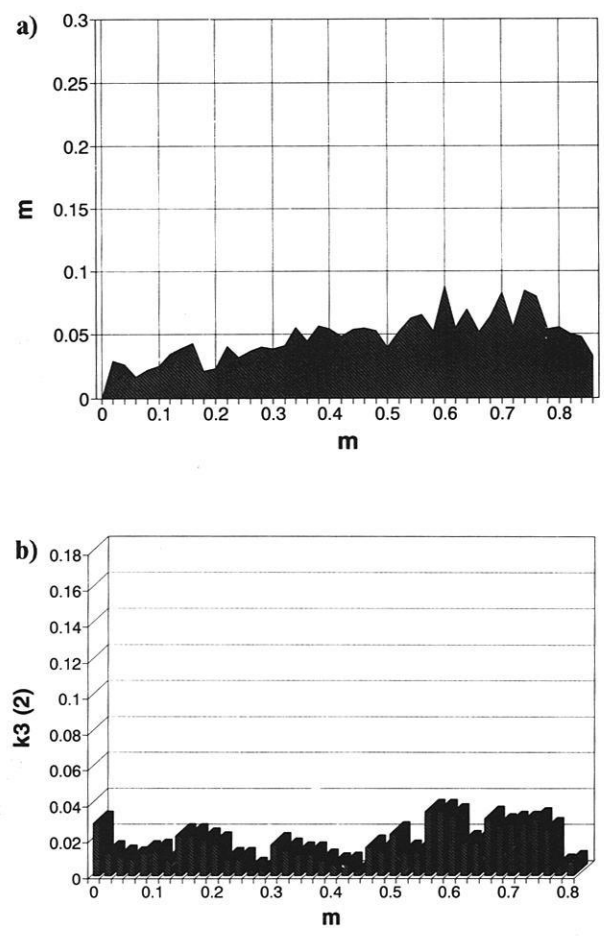


**Fig. 6.3** Mini-Tausendfüssler taken in: **a)** cross profile with **b)** $K_3(2)$ distribution along the new bar, 1992. View is looking upstream.

grains like the spikes on a rake, separate flow at fairly regular intervals.

*6.1.1.1.3 3-D roughness model*

On the new bar, the roughness distribution is interesting due to the crescentic shape of the bar (Fig. 4.5 in Study Area). Roughness is largest along the topographically higher ridge i.e. on the bar top along the 7 m line in the cross-section (Fig. 6.4). In the small side channel, which concentrated flow during the flood, roughness values are high in accordance with maximum grain size (3 m line, left in Fig. 6.4).

Continuity of roughness is well developed on the bar top and in the side channels. This suggests that a particular roughness type acts as a nucleus of attraction for the following build-up of roughness. Roughness clearly increases to a maximum, followed by a decrease away from this point towards the bar edge. The smooth megaforms obtained in this way are particularly well adapted to flow. Thus as flow spreads over the bar, flow will concentrate in the side channels and result in a preferred build-up of large roughness. Flow is deflected both laterally and longitudinally away from the low energy, low roughness zones into these high roughness areas.

In the main side channel, bedload transport will be most active and cause the preferred deposition of its largest size fraction. Over the bar top, bedload will become obstructed by large obstacles of roughness existing under shallow flow and deposit material in this lower energy zone to form clusters of material. This overall accumulation of coarse material into clusters will result in the well-adapted, smoothly undulating mega-roughness forms on the bar. Since flow depths were low and the capacity for sediment movement was limited it is presumed that this case study reflects a unique process of roughness build-up and sedimentation during the descending limb of the flood observed from the 5-6th June, 1991.

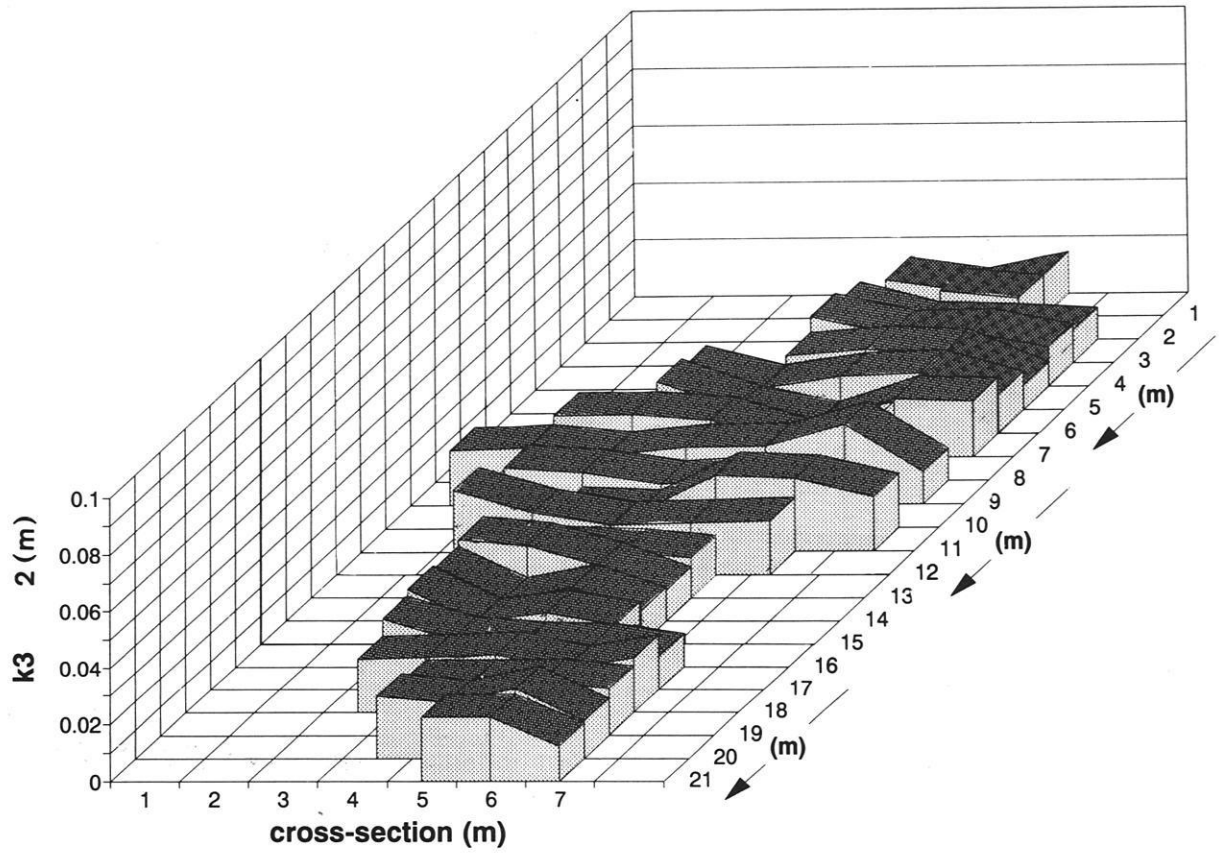


**Fig. 6.4** Three-dimensional model of roughness distribution on new bar in 1992. Flow is towards the observer. Notice lateral roughness peaks.

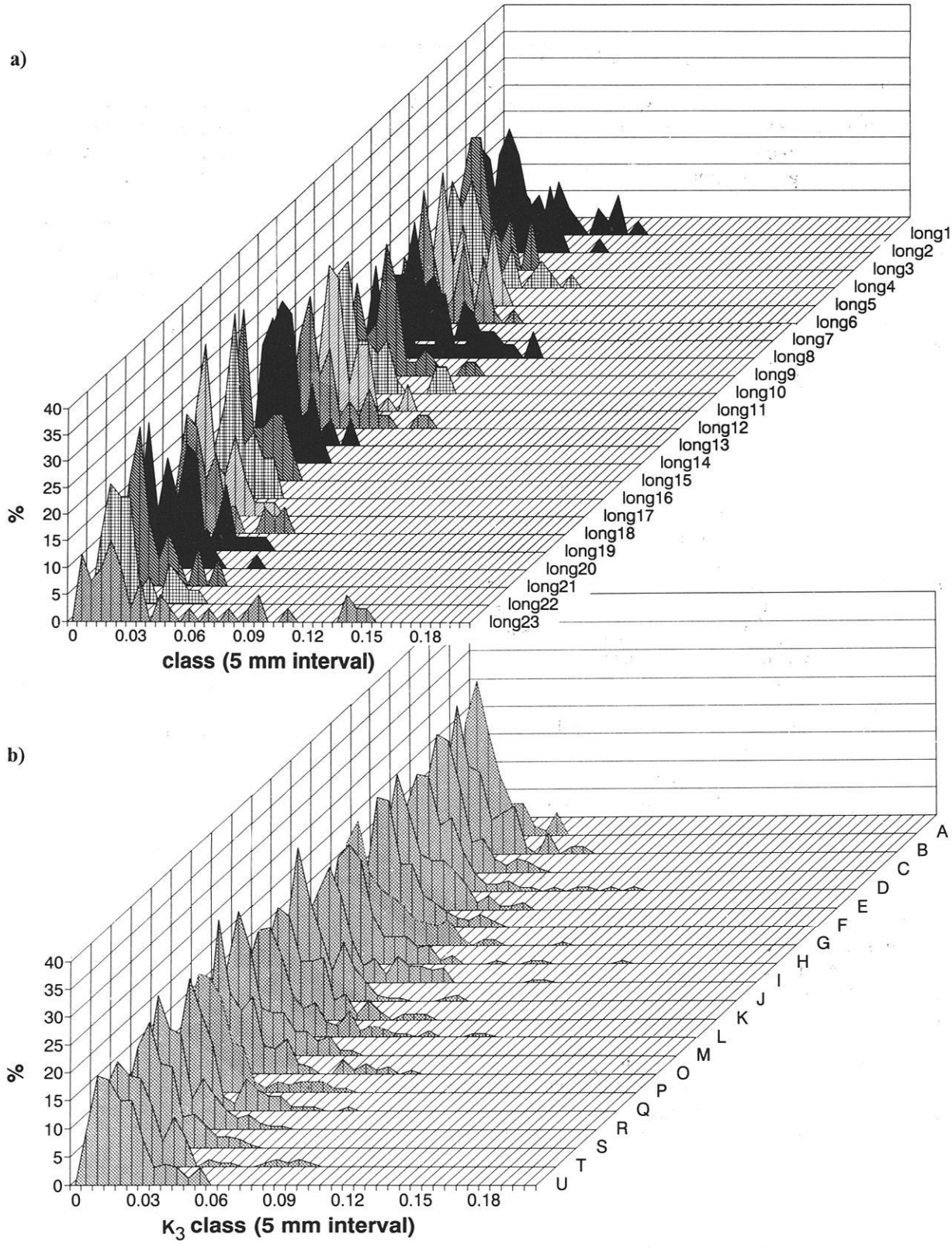


**Fig. 6.5** Roughness frequency distributions over new bar at Squaw Creek in 1991 along **a)** the longitudinal profile, one sample each and **b)** along the average cross-profiles at same level as corresponding longitudinal profile. Flow is towards the observer. Cross-sections long 4, long 8 and long 12 are equivalent to D, H and L. Notice that cross-profiles have smoother distributions because they represent an average of several cross profiles.

#### 6.1.1.1.4 *Roughness frequency analyses*

The distribution of roughness, analysed in terms of frequency is illustrated in Fig. 6.5 a & b. Each line (e.g. long 23) is a frequency distribution with the $K_3$ (0.005), equivalent to 5 mm. The size class is indicated on the x-axis. A large roughness element is plotted on the right and small to the left. In Figure 6.5.a, small roughness elements are most common, but there are a few large roughness elements especially at long 23, and at long 8 and 12. A very flattened distribution indicates large roughness, while a spiked, narrow distribution indicates minimal roughness. It is apparent that lateral roughness is much larger than longitudinal roughness. This is not due to the averaging procedure carried out. The maximum $K_3$ (2) value fluctuates between 0.06 and 0.12 m in cross-section, whereas in long section, the maximum only ranges between 0.03 and 0.1 m. Average roughness does however remain around 0.02 m in both cases. Without taking into account location long 23, roughness builds up to a maximum around location long 8 on the medial ridge so that the bar clearly becomes less coarse with distance downstream. The exception lies at the tail-end location of long 23, with the flattest distribution, produced by a single large cluster element probably originating directly from the main channel.

The frequency distributions illustrate the periodic build-up of roughness. In the longitudinal section (Fig. 6.5.a) roughness maxima (widely stretched distributions) are located at the meter marks long 1, long 4, long 8 and long 12. After that roughness decreases up to the final build-up at long 20 (with the exception of long 23). The first three maxima are also evident in the cross profiles (Fig. 6.5.b) where the equivalent pattern can be found at D, H, L, (O) and T. Both profiles have roughness peaks at the same locations and at the same 4 m intervals from each other in the proximal to medial bar ends. Thus longitudinal and lateral roughness act in similar manners.

As already described in the 3-D roughness model (6.1.1.3), these roughness distributions are subject to a systematic flux that seems to be an adaptation to flow patterns over the bar, and vice versa. A more detailed description of this interaction will be given in later sections.

#### 6.1.1.1.5 *$K_3$ roughness related to grain size/area from photo-sieving*

The grain size distribution obtained from the entire bar surface was utilised for correlation between all open-bed and cluster material as well as for reconstruction of the downstream variations in grain size along a transect.

Fig. 6.6 illustrates an example of the downstream variation of grain size along the first 6 longitudinal transects. It is apparent that there are consistent fluctuations in the distribution and a very slight decrease in grain size downstream. In order to establish the validity of the highly dynamical spatial variations of the $K_3$ roughness parameter described so far, roughness was related to the conventional grain size distributions obtained from photo-sieving. The $K_3$ was related to the $D_{16}$, $D_{50}$ and $D_{84}$ of the cumulative grain size distribution (Fig. 6.7). The highest $r^2$ correlation coefficient was obtained for the $D_{16}$ (0.73).

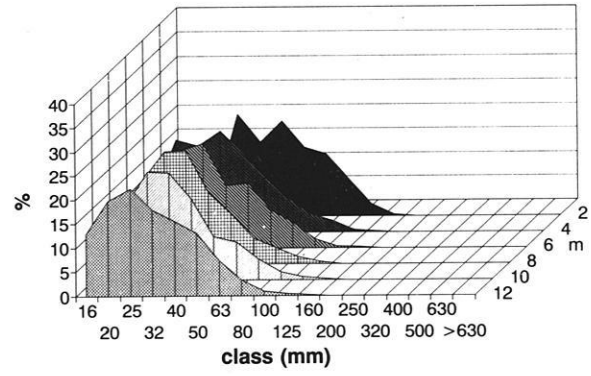


**Fig. 6.6** Downstream grain size variations along longitudinal transect. Flow direction is towards the observer.

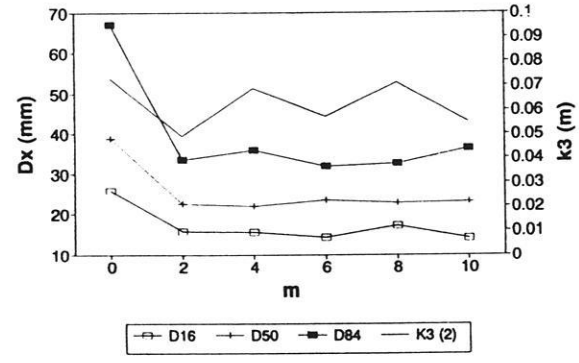


**Fig. 6.7** Relationship between $K_3$ roughness coefficient and $D_{16}$, $D_{50}$ and $D_{84}$ of the surrounding grain size distribution along the long profile of the new bar, 1992.

The $D_{84}$ had the poorest correlation with the $K_3$ coefficient, whereas the $D_{16}$ almost plotted as a straight line relationship against roughness. An approximately straight line relationship existed between the $D_{16}$, $D_{50}$, $D_{84}$ The general pattern of roughness build-up was crudely reflected in the grain size distribution. Unfortunately the relationships show that the grain size distributions are not as accurate as the pattern of $K_3$ when considering detailed studies of roughness variations. GESSLER (1990) also points out that his friction factor is independent of grain size, but is dependent on the arrangement of particles on the bed.

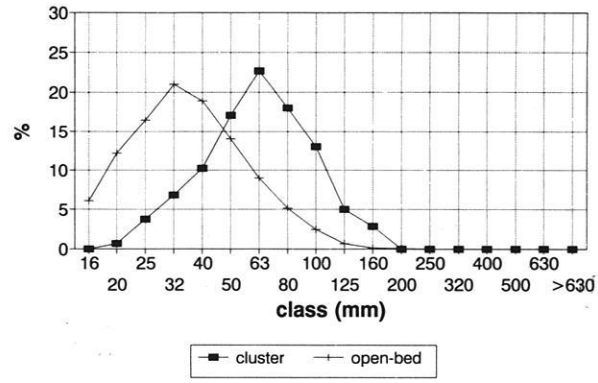


**Fig. 6.8.a** Relationship between the grain size of clustered and open-bed material on new bar, Squaw Creek 1992.

#### *6.1.1.1.6 Cluster and open-bed grain size/area comparisons*

The grain size distribution resulting from the entire surface of the gravel bar differs considerably from the size distribution produced by single clusters of material (Fig. 6.8 a). Thus whereas the open-bed material is like a Gaussian distribution (BAGNOLD & BARNDORFF-NIELSEN, 1980), clusters are heavily right skewed. This shows that although the gravel material is quite homogeneous, the two distributions indicate very separate sedimentary and hydraulic histories. Even though clusters are not distributed very densely over the river bed (80 clusters over 47.88 $m^2$ i.e. 1 cluster per 0.6 $m^2$ in relation) their effect on roughness is considerable. Since every single cluster element located in the photo-sieving sample area was considered for this study, the resulting distribution creates a clear picture of their importance. Their coarseness indicates that they must be transported under large flow strengths but deposited under receding flow. Whereas the $D_{50}$ of open-bed material lies only at 28.75 mm, that of the clusters lies at 51.50 mm. Although the grain size distribution was truncated at 16 mm i.e. in the class of 13-16mm, particles smaller than that did not actually appear on the photographs, indicating an absence of sand in nearly all cases.

The grain area distribution, i.e. the projected surface area that a particle occupies on the photo, shows that although the general bed material follows a very smooth, normal distribution, the cluster distribution has a tendency towards bimodality (Fig. 6.8 b). The obstacle clast in these roughness elements is not considerably larger than the surrounding cluster particles, indicated by the minor peak between 125-160 mm class but the cluster infill, consisting of smaller particles, clearly has a mode between the 80-100 mm class. In the 100-125 mm class there is a decrease in cluster participance.

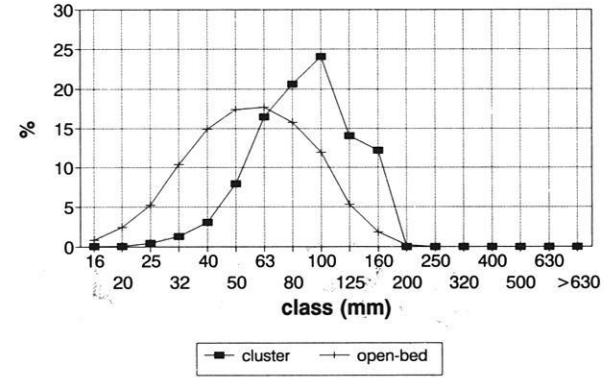


**Fig. 6.8.b** Relationship between the grain area of clustered and open-bed material on new bar, Squaw Creek 1992.

In summary, at Squaw Creek clusters occupy an essential proportion of the river bed and should exert considerable influence on flow resistance due to large size and surface areas. In addition the entire coarse sedimentary fraction of the river bed rearranges itself into clusters.

### 6.1.1.2. Old bar, 1991

#### *6.1.1.2.1 Bar geometry*

On the old bar, a longitudinal vegetated ridge running along the centre-line of the bar slopes into a small channel on its left and into the main stream at its right (see photo Fig. 4.6a) in Ch. Study Areas). Two longitudinal roughness ribs are present, becoming

higher towards the vegetated bar maximum. Due to its partial submergence during most of the field season, photo-sieving was not very successful and the main results on grain size variations, roughness and fractal analyses therefore focus on the new bar.

#### *6.1.1.2.2 Analysis of particle projection ($K_3$)*

The long profile of the old bar shows that roughness elements are far higher than on the new bar (compare Fig. 6.3 & 6.9) with the exception of the large cluster bedform on the distal end of the new bar. The cross-profiles on the old bar show that cross-sectional roughness can be clearly differentiated from longitudinal roughness. Maximal roughness reaches 0.18 m. The example in Fig. 6.10 of the proximal bar indicates that roughness consists of highly protruding individual elements, usually cropping up as single particles only. Cross-sectional gradients are more pronounced. In cross-section, particle assemblages are not necessary for minimising resistance and separate lateral arrangement of single particles becomes dominant.

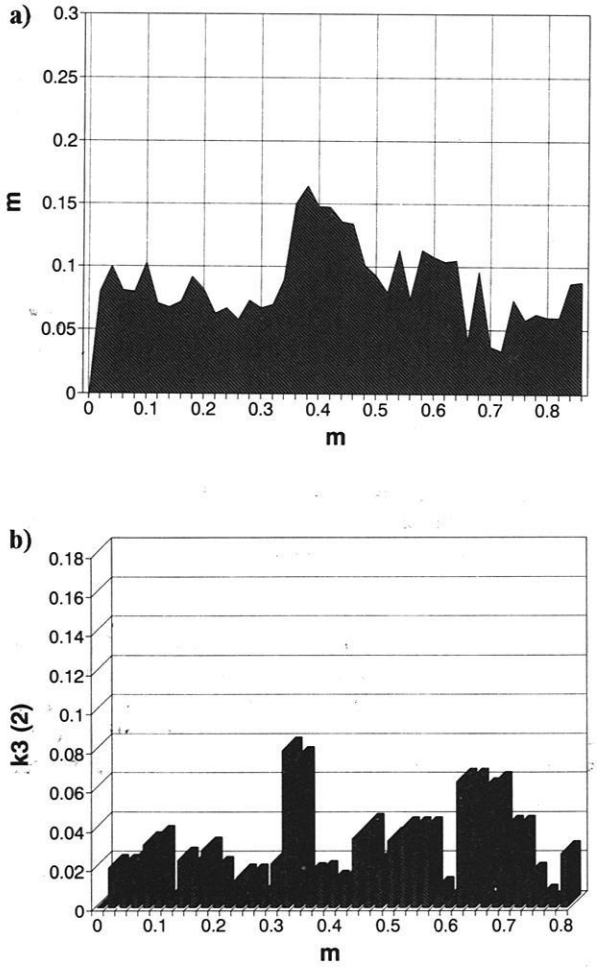


**Fig. 6.9** Mini-Tausendfüssler taken in: **a)** long profile with **b)** associated $K_3$ (2) distribution along the old bar in 1991. Flow is from right to left.

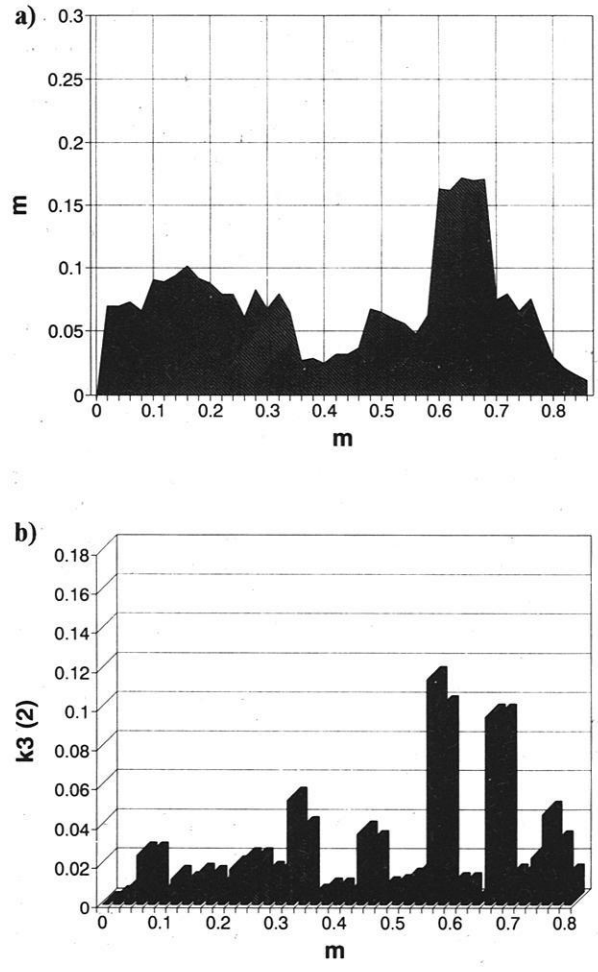


**Fig. 6.10** Mini-Tausendfüssler taken in: **a)** cross profile with **b)** associated $K_3(2)$ distribution along the old bar in 1991. View is looking upstream.

*6.1.1.2.3 3-D roughness model*

At Squaw Creek the $K_3$ (2) values for the old, medial bar in 1991 are sharply differentiated and organised (Fig. 6.11). Since a straight reach has to be considered in this case, no bend arch roughness can be present. Instead, a longitudinal rib is strengthened by the vegetated medial parts of the bar top. The ridge is visible along the 5 m mark at cross-section B and C. Roughness values increase towards the interface of the main channel. Values are relatively low in the small sandy channel running between the bar edge and the river banks at the 7 m mark. Due to its location in the reach, which allows it to become submerged during all medium-sized floods, the bar has an opportunity to develop higher roughness.

*6.1.1.2.4 Roughness frequency analysis*

Average roughness values calculated from the cross-sections and reconstructed longitudinally did not reveal any extremes in roughness (Fig. 6.12 a & b) apart from the cobble at long-2. The main factor influencing this is the lack of steep gradients and large material. Roughness values decrease from proximal to distal bar. The profiles continued in the main channel from long-11 onwards show that once in the channel, roughness values remain low, without major variations. As on the new bar, the cross profiles show significantly higher roughness, which can be explained by the same principle of flow adaptation in the long profile but flow divergence on the cross-profile.

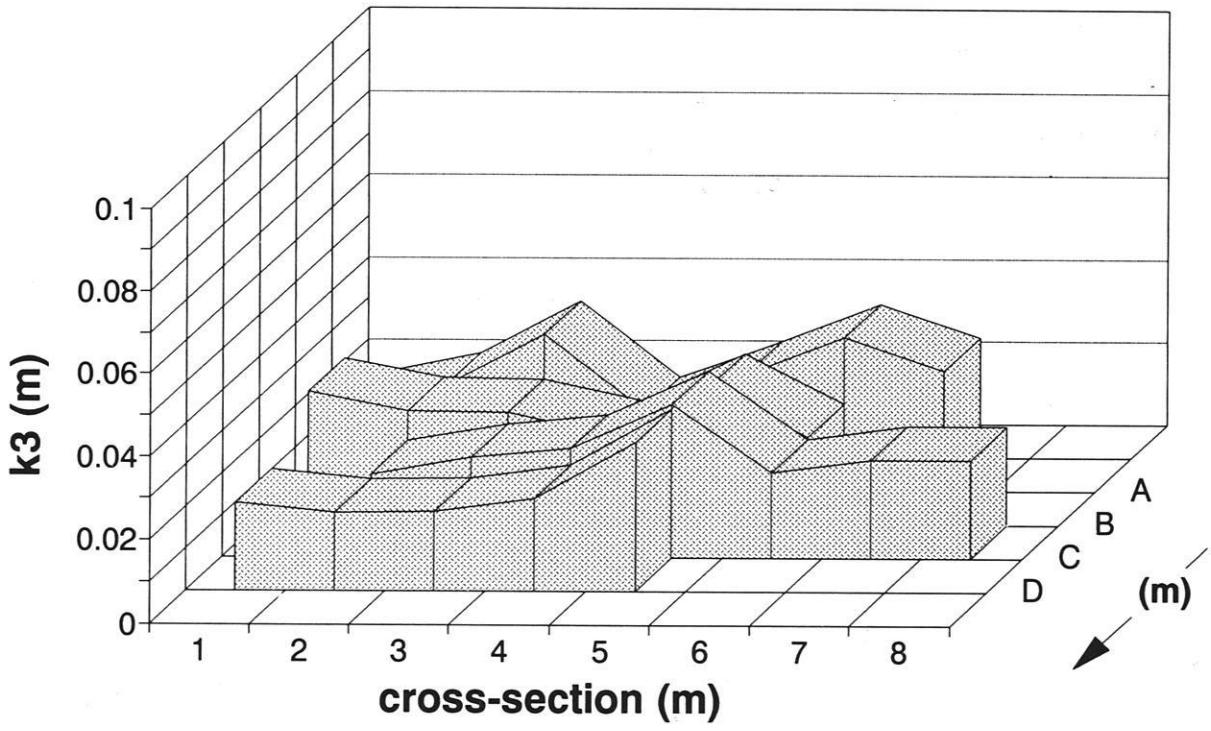


**Fig. 6.11** Three-dimensional model of roughness distribution on old bar, 1991. Flow is towards the observer.

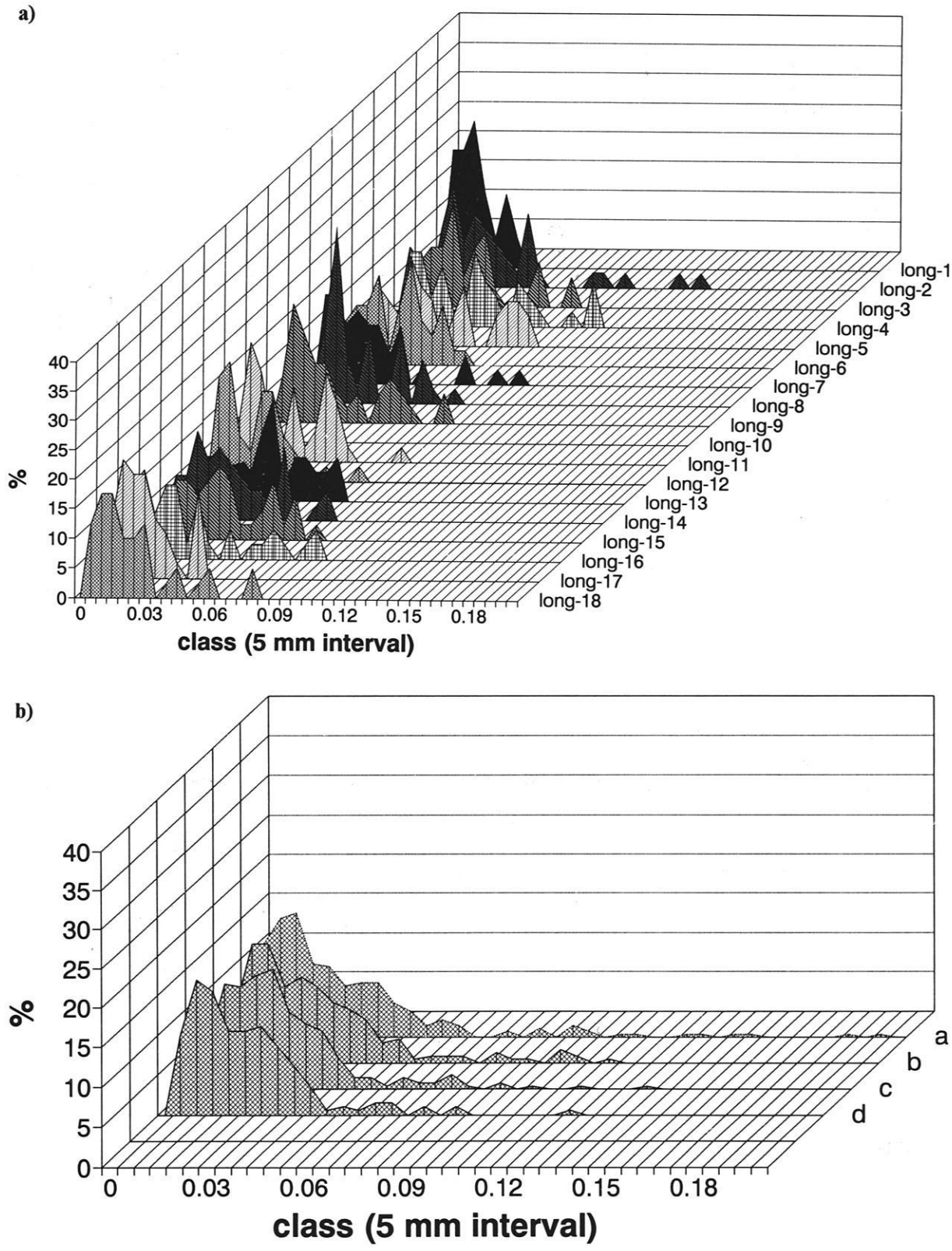


**Fig. 6.12** Frequency distribution over the old bar and its channel extension in 1991 along **a)** the longitudinal profile and **b)** along the average cross-profiles. Flow is towards the observer. Cross-sections a,b,c,d are equivalent to long 2,3,4,5 along the longitudinal section on the gravel bar. Sections long 11-long 18 include the main channel beyond the gravel bar. There is no data at long-11.

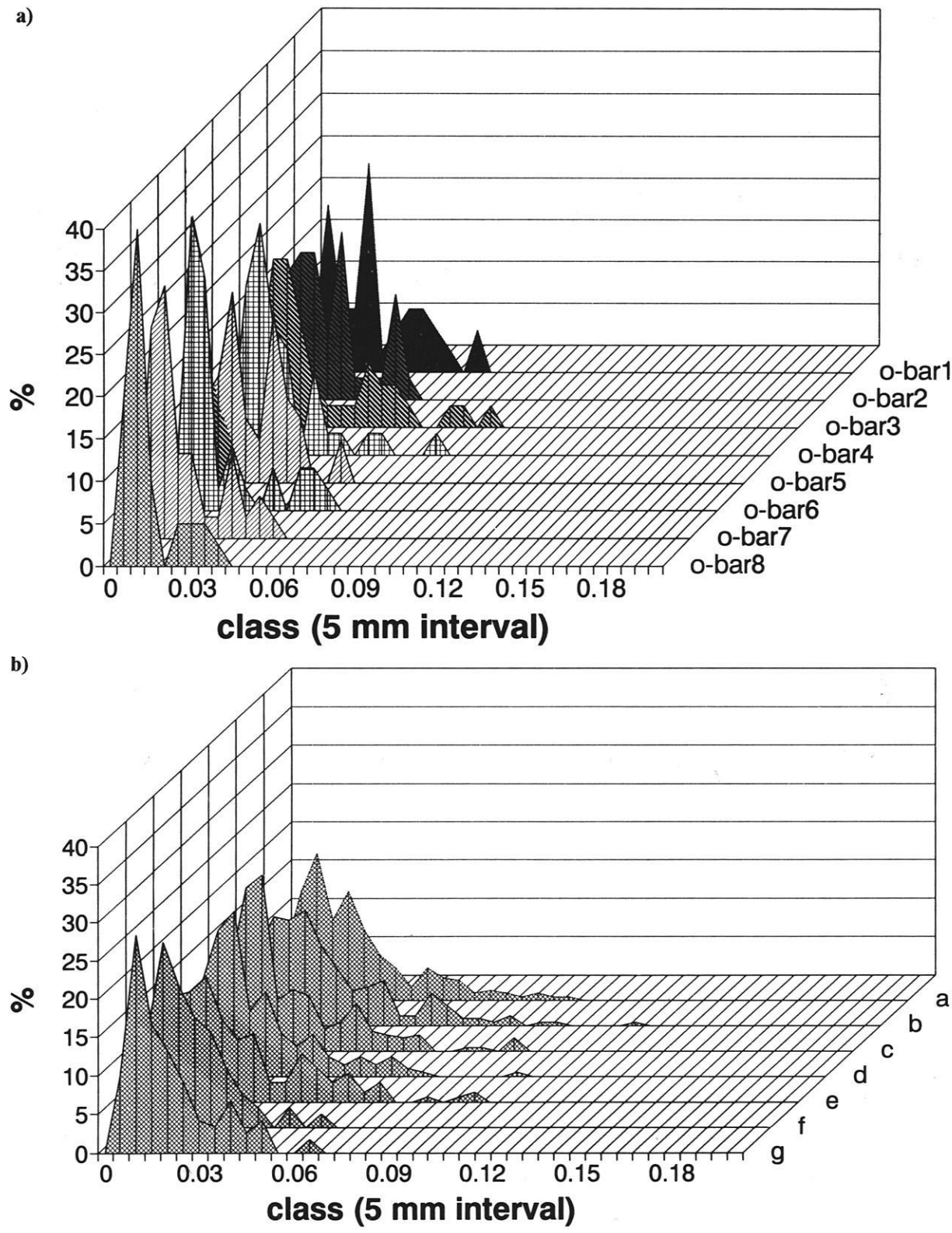


**Fig. 6.13** Frequency distribution over the old bar in 1992 along **a)** the longitudinal profile (o-bar2 is equivalent to long-2 in Fig. 6.12) and **b)** along the average cross-profiles. Average cross-profiles a-f are equivalent to longitudinal profiles o-bar2-8 (Section b in the cross-profile is equivalent to section a in the cross-profile of Fig. 6.12). Notice that roughness is much reduced in comparison to previous year (Fig. 6.12).

### 6.1.1.3 Old bar 1992

*6.1.1.3.1 Bar geometry*

The geometry of the old bar had not changed much from 1991 to 1992. The vegetated ridge in the centre of the bar was still present and the bar dimensions remained similar. The bed had however re-arranged itself into very particular patterns of roughness (described in section 6.1.1.3.3). After the floods in 1991, the bar had temporarily roughened up but by 1992, the bar had reached far lower roughness values.

*6.1.1.3.2 Analysis of particle projection ($K_3$)*

In contrast to the minor changes in bar geometry, the roughness characteristics had undergone considerable changes between 1991 and 1992. The same longitudinal profile of the old bar was considered in 1992 (Fig. 4.5 Ch. Study Areas). Although the bar had been reworked by several flood events, the overall pattern, even with the lower roughness values, remained similar to the year before (Fig. 6.14). Roughness values had become lower i.e. with only an isolated maximum of $K_3$ (2) 0.14 m. Two particle clusters consisting of two particles each are illustrated

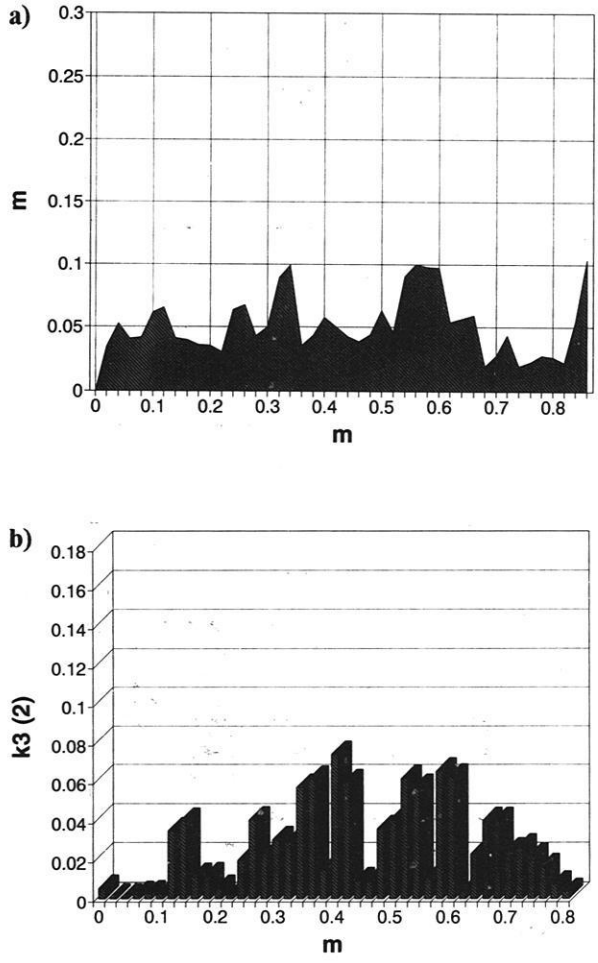


**Fig. 6.14** Mini-Tausendfüssler taken in: **a)** long profile with **b)** respective $K_3$ (2) distribution along the old bar in 1992. Flow is from L. to R.

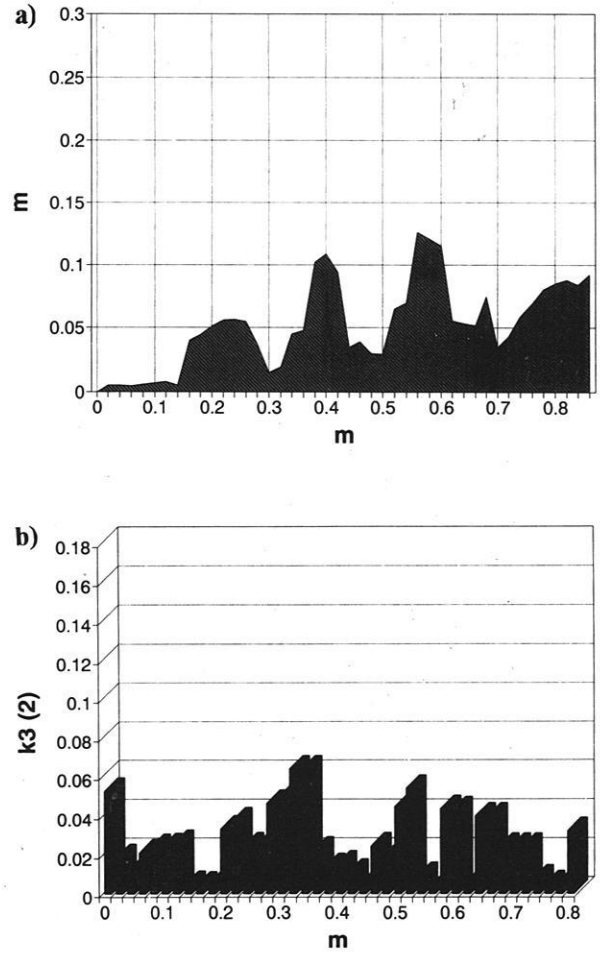


**Fig. 6.15** Mini-Tausendfüssler taken in: **a)** cross profile with **b)** respective $K_3$(2) distribution along the old bar in 1992. View is looking upstream.

in the diagram between 0 - 0.1 m and 0.2 - 0.4 m, again with the second particle resting lower than the obstacle.

In cross-section (Fig. 6.15), isolated single clasts dominate again, though projection height is lower than in 1991. Once more the role played by cross-sectional roughness in diverting flow laterally is illustrated. Since overall roughness was lower in 1992, and lateral roughness is evidently dependent on longitudinal roughness and visa versa. Lateral roughness values should logically also have been lower.

#### *6.1.1.3.3 3-D roughness model*

The 3-D roughness model in 1992 (Fig. 6.16) illustrates that $K_3$ values had become lower than in 1991 (Fig. 6.11). The ridge of high roughness is still apparent along the 5 m line. Thus the overall roughness pattern remained similar to that in 1991 except that roughness peaks were more accentuated. This indicates that roughness repeatedly arranges itself in a particular pattern according to the location of major roughness elements. This arrangement may be dictated by the development of shear waves (KARCZ 1981, HODGES 1982) on shallow (10 cm flow depth) bar tops. Shear waves (explained later in 6.1.7), form as diagonally intersecting flow threads. The streamline intersect at a nodal point, then separate again in opposite directions, only to intersect again at the next nodal point. Presumably once a particular roughness element, such as a cluster, is deposited and this shear wave pattern is initiated around it, the propagation of the shear wave downstream of and around the roughness element will force the next roughness elements to be deposited at the next nodal points. As depicted in Fig. 6.17a this in turn will influence the further spread of shear waves so that the total distribution of roughness could be explained according to the exact location and size of the roughness elements (clusters) deposited. Similar results were obtained independently during flume experiments carried out at Aberdeen University by TAIT and WILLETTS in 1992 (Fig. 6.17b). This type of diamond cluster arrangement was found during the later stages of armouring after a sharp drop in sediment transport rate which should be equivalent to the dynamics of the descending flood limb.

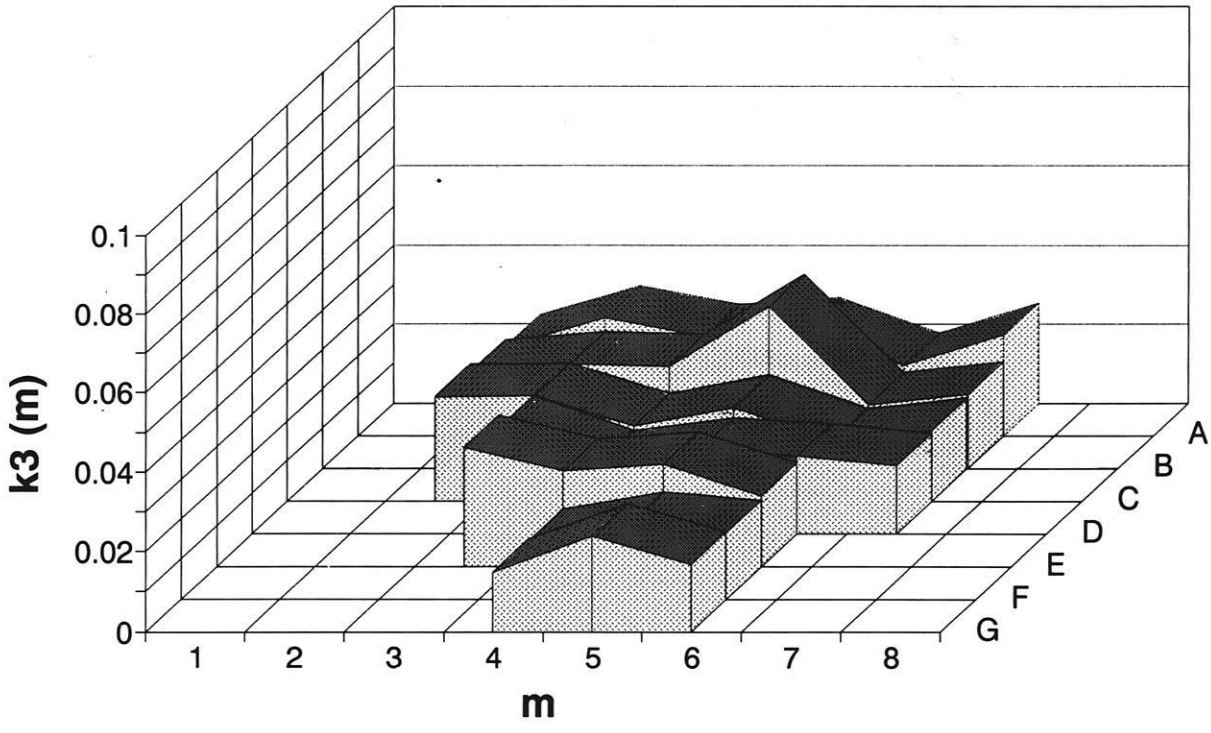


**Fig. 6.16** Three-dimensional model of roughness distribution on old bar, 1992. Flow is towards the observer. Compare to Fig. 6.11.

a)

b)

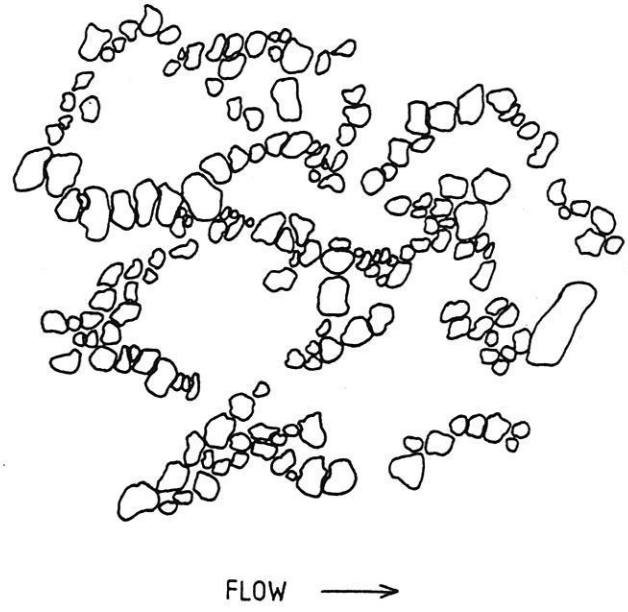


**Fig. 6.17** a) Illustration of the ring-like clusters formed on the old bar at Squaw Creek, 1992. Large roughness elements are spaced in a diagonal pattern such that material accumulates at these nodal points. b) Diagram of similar pattern obtained form laboratory experiments (after TAIT and WILLETTS 1992).

#### *6.1.1.3.4 Roughness frequency analysis*

The roughness frequency distributions in long profile indicate that the gravel bar was rougher in 1991 than in 1992 (Fig. 6.13a). The distributions are more attenuated in 1991 in contrast to the very left-skewed and spiked distributions in 1992. The location of long-2 in 1991 is equivalent to o-bar2 in 1992. The roughness peak at long 2 in 1991 and o-bar3 in 1992, together with the subsequent downstream fining apparent in both years (long 5-9 in 1991 and o-bar4-8 in 1992), shows that the overall roughness pattern is maintained.

From the cross profiles, the general downstream decrease of major roughness can be deduced both in 1991 and in 1992 (Fig. 6.13b). Roughness values remain larger in relation to the long profile. The roughness cross-profiles also indicate considerably lower roughness than in 1992. This decrease may be due to smaller grain sizes deposited such that relative roughness remains low or due to the interstitial infill of finer sediment.

### 6.1.1.4 Tausendfüssler Profile 1991 & 1992

#### *6.1.1.4.1 Bar and channel geometry*

In Fig 5.11 (Methodology) the cross-sectional profile at Squaw Creek is illustrated for 1991. A well defined large bar as well as channel area are visible, separated by a transition zone labelled as the bar-channel interface. The small bar to the left of the channel is not marked on the diagram but is considered in the calculations. A few large particles are evident. The cross-profile at the Tausendfüssler consisting of 10 cm intervals was replotted from measurements taken with the more accurate mini-Tausendfüssler at 2 cm intervals. Nevertheless, a very close correlation was obtained between the mini- and macro-Tausendfüssler profiles (0.84). As was the case for the old and new bar, the cross-profile in 1992 was no longer as rough as in 1991 and the channel area had enlarged.

#### *6.1.1.4.2 Comparison of $K_3$(2) & $K_3$(10) roughness (mini- and macro-Tausendfüssler)*

Roughness was analysed at 2 cm intervals and the resulting $K_3$ (2) compared to the standard $K_3$ (10) intervals utilised for the macro-Tausendfüssler in 1991. Plotted against each other, the two intervals showed a good correlation ($r^2$ of 0.72). This result supports the accuracy of the temporal river bed roughness measurements at 10 cm intervals. In 1991, the cross-section included very large roughness elements (Fig. 6.18a). By 1992, after several floods, the cross-profile had far lower roughness. When this cross-profile was compared to the longitudinal sections taken at the same location (Fig.6.18b & c), the long profile displayed less extreme variation in

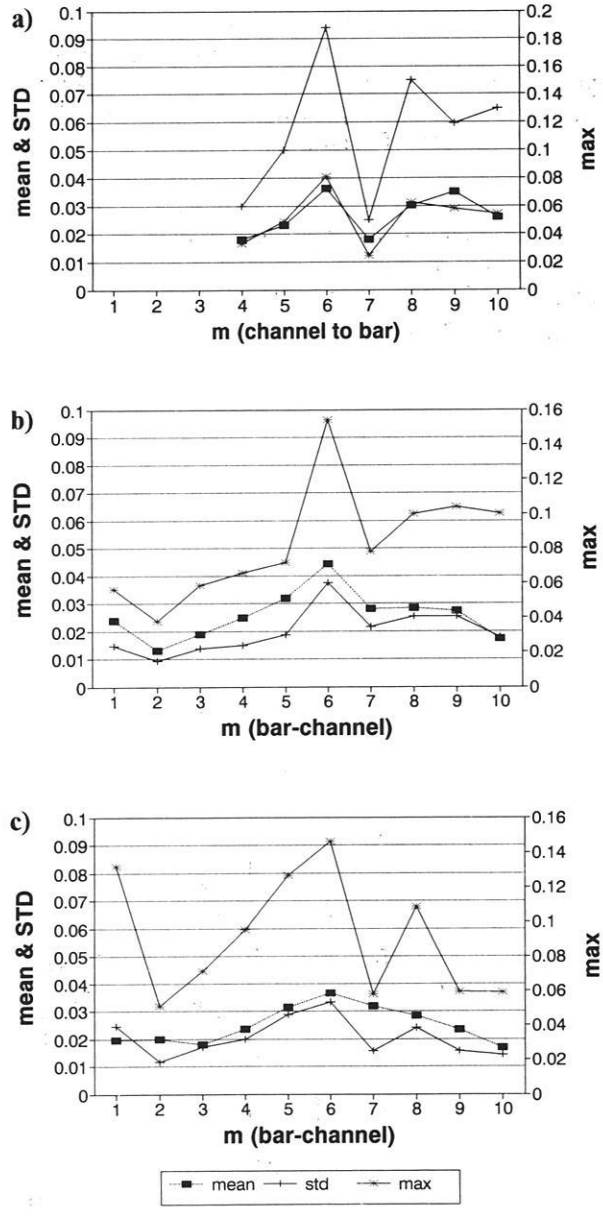


**Fig. 6.18** **a)** Cross-sectional roughness at Tausendfüssler site in 1991. **b)** cross-sectional roughness at Tausendfüssler site in 1992 **c)** Longitudinal roughness in 1992. Notice the change in scale for maximum roughness $K_3$ (10) from 1991 a) to 1992 b).

values ($K_3$ max. 0.03-0.09 m, mean 0.018-0.035 m) than the cross profile ($K_3$ max. 0.025-0.1 m, mean 0.015-0.45 m). While average roughness in cross-profile was somewhat parallel to longitudinal roughness with the same degree of variation, the maxima did not correlate. This reproduction of the roughness pattern on the bar section of the profile seems surprising since roughness had changed considerably between 1991 and 1992. Thus although roughness covered a more extreme range in 1991 compared to 1992, as verified throughout the Squaw Creek test area, i.e. for the old and new bar, the roughness pattern retained a mirror image from the year before. This may again be interpreted in terms of the shear wave idea explained in 6.1.1.3.3 for the 3-D roughness model of the old bar.

As was demonstrated on the other gravel bars, cross-sectional roughness is generally more extreme than longitudinal roughness. Considering the channel separately from the bar in 1992, the cross-sectional roughness reveals that both bars contain lower maximum roughness than the channel (Fig.6.18 b & c). The same is true for longitudinal roughness which is defined by the competence of the main channel to transport largest sediment.

#### *6.1.1.4.3 Roughness frequency analysis*

In 1991, the roughness frequency distributions of the cross-profile reflect the extremity in large roughness values (Fig. 6.19a). The roughness frequency distributions in 1992 (Fig. 19b) demonstrate that in cross-section, there are still independent peaks of maximum roughness though not nearly as large as in 1991. In the long profile (Fig. 19c) these roughness peaks are absent and the distributions are more truncated with less left skewness than in cross profile. Also the cross-sectional frequencies illustrate that roughness is higher than in the longitudinal profile. The general pattern of cross-sectional roughness is similar between the two years, especially the large block located at cross-6.

a)

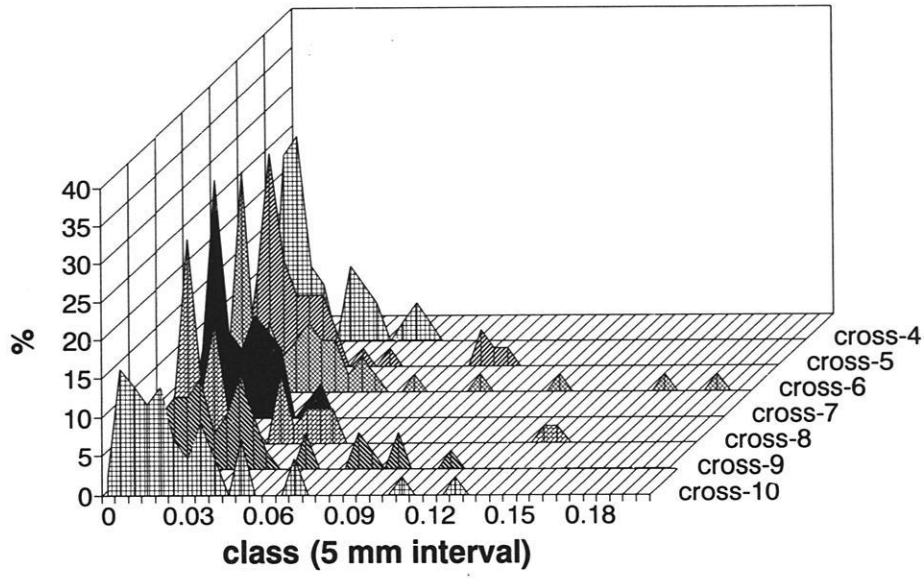


**Fig. 6.19** Roughness frequency distributions for Squaw Creek at the Tausendfüssler bridges in **a)** 1991 for the cross-section and **b)** in 1992 for cross-sectional and **c)** longitudinal profiles in 1992.

b)

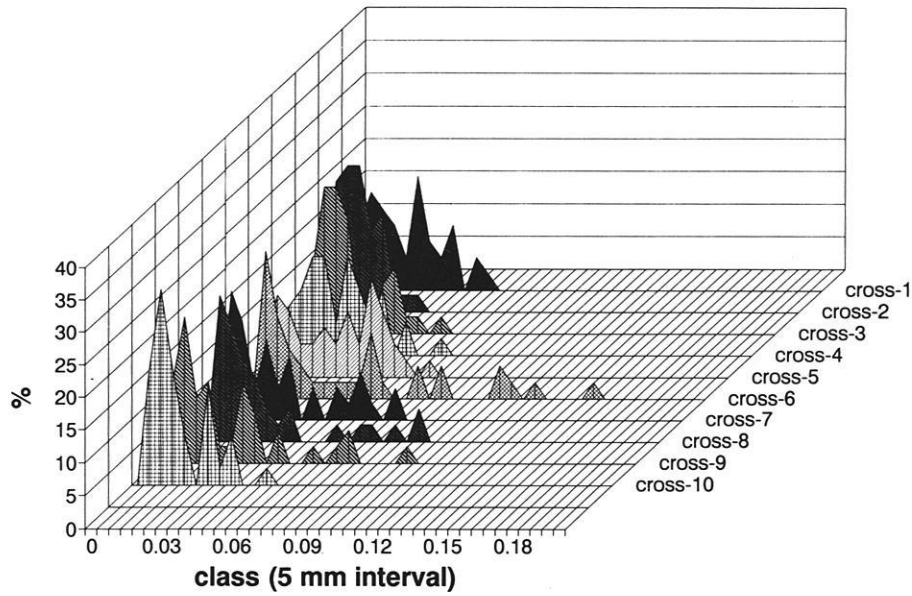
40
35
30
25
20
15
10
5
0
%
0
0.03
0.06
0.09
0.12
0.15
0.18
class (5 mm interval)
cross-1
cross-2
cross-3
cross-4
cross-5
cross-6
cross-7
cross-8
cross-9
cross-10

c)

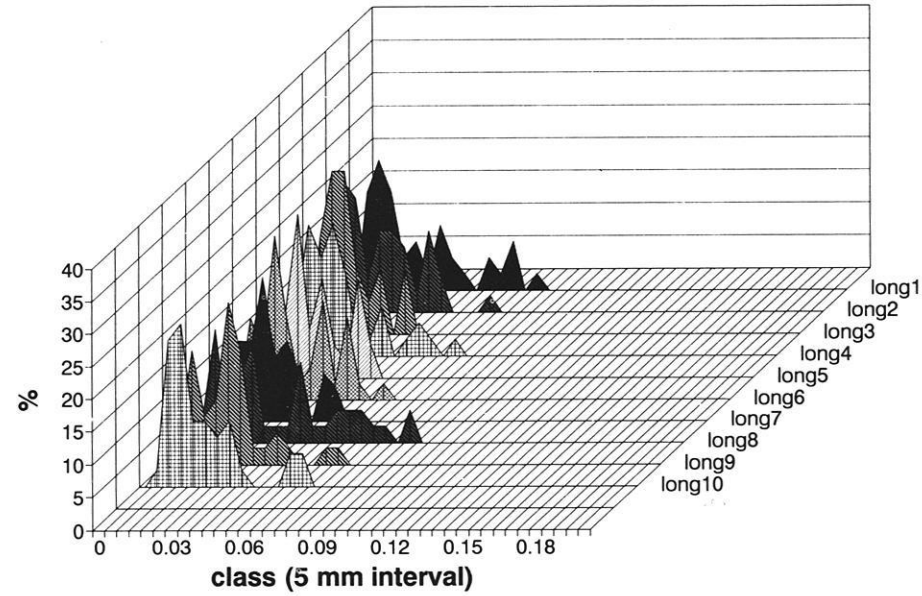
40
35
30
25
20
15
10
5
0
%
0
0.03
0.06
0.09
0.12
0.15
0.18
class (5 mm interval)
long1
long2
long3
long4
long5
long6
long7
long8
long9
long10

## 6.1.2 Schmiedlaine 1992

*6.1.2.1.1 Bar geometry*

The geometry of the lateral gravel bar was reconstructed at the same 2 cm intervals as at Squaw Creek (Fig. 6.20). Fig. 6.20 indicates the spatial order in which the micro-topography is arranged. Along the long profile, the bar reveals step and pool units i.e. three major steps that emerge at regular intervals. Each step is approximately 4 m in length. The long profile supports the concept of regular roughness elements. The long profile does not follow the usual step-pool pattern described in the literature as originating from large boulders (GRANT et al 1990). Rather, there seems to be a dominance of large roughness elements at very regular intervals that dictates the spacing of the next step (Fig.6.21 a & b). This step pattern is well developed along the straight reach between the entrance and exit of the bend. At the distal end of the bar the step system dissolves due to the position of the next bend. Thus individual grain roughness is not as spiky and pronounced as at Squaw Creek (Fig. 6.22). Rather so, smoother bedform shapes dominate that are on average 30 cm long. In cross-section, roughness consists of more spiked individual elements that have higher roughness values. As at Squaw Creek, roughness is higher in cross-profile than longitudinally.

In cross-section (Fig. 6.20) the bar is slightly hemispherical in shape (see photo, Fig. 6.21) and consists of two exceptionally high roughness areas around the 6 and 8 m marks which are related to lateral cobble berms. The berms are clearly presented under flood flows (Fig. 6.21b). These roughness structures are arch-shaped berms when viewed in plan, running parallel to the bar's relative location to the river bend (see photo Fig.4.10, Ch. Study Areas). During normal flood flows (5 $m^3s^{-1}$) these berms together with large cluster assemblages will remain the only elements protruding above the flow (Fig.6.21b). The cobble berm consists of a pure sequence of clusters. In terms of flow resistance, evidence for which was obtained from observations of the bar during flood flows (Fig. 6.21 b), cluster elements provide a coarse-grained framework for roughness structure.

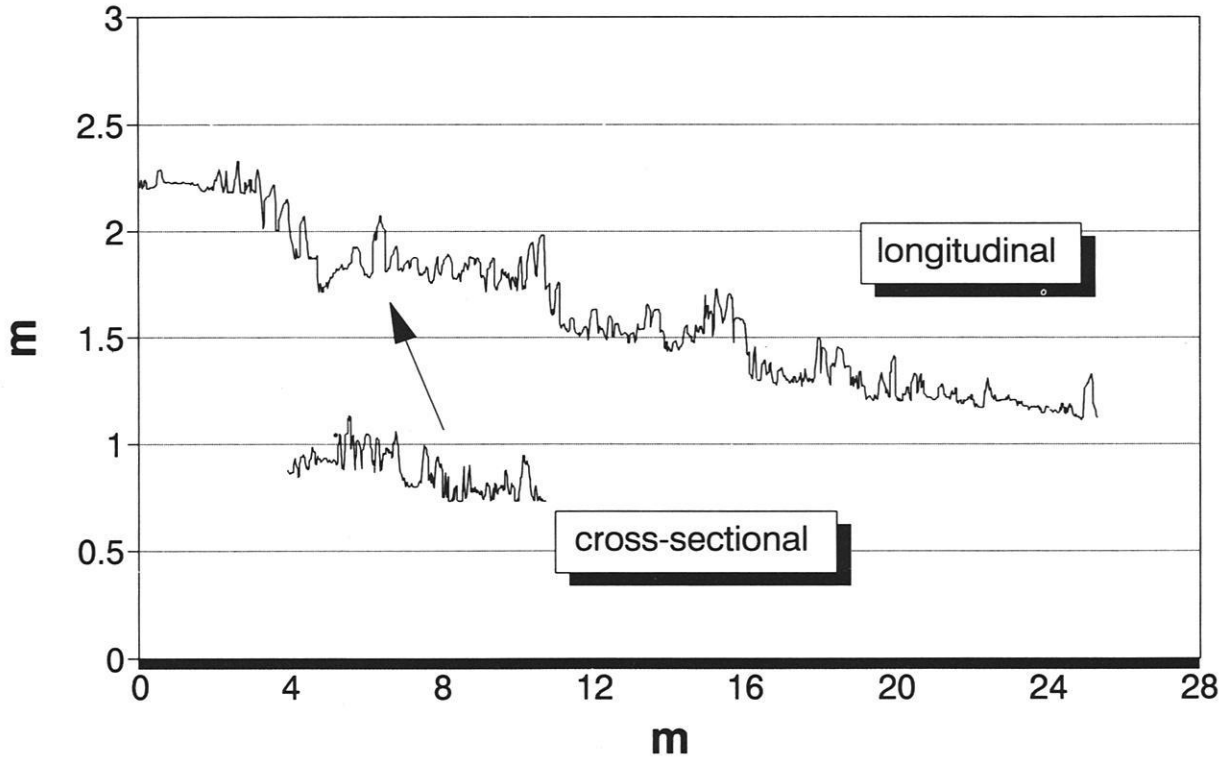


**Fig. 6.20** Topography of the gravel bar in the Schmiedlaine, Upper Bavaria. The longitudinal section has been plotted together with a cross-section superimposed below at the same scale. The cross-section was taken at the 7 m location looking upstream.

a)

b)

**Fig. 6.21** **a)** Upstream view of the river bed in Schmiedlaine during normal conditions, 1992. Notice longitudinal transect (yellow line) running over berm with red cluster in the background, main channel to the right and bedrock confined valley sides. **b)** Most of the river bed submerged during flood flow (1991). Notice double row of cobble berms in outer bend (background) and predominance of non-submerged, coarse-grained clusters (red particles).

The formation of the arch-shaped berms can be related to the recessional deposition of very coarse material during high flows (>5 $m^3s^{-1}$). Thus as stream competence decreases after bedload transport, it could well be that the first arch will be deposited in the outer bend, parallel to the overall shape of the bend. During the final stages of the flood, as stream power gradually decreases, individual berms will be deposited in sequence, parallel to each other and the bend, towards the inner part of the curve. Additional evidence to support this gradual change in competence or energy expenditure in relation to more restricted flow paths will be described later under the section of "Flow orientation".

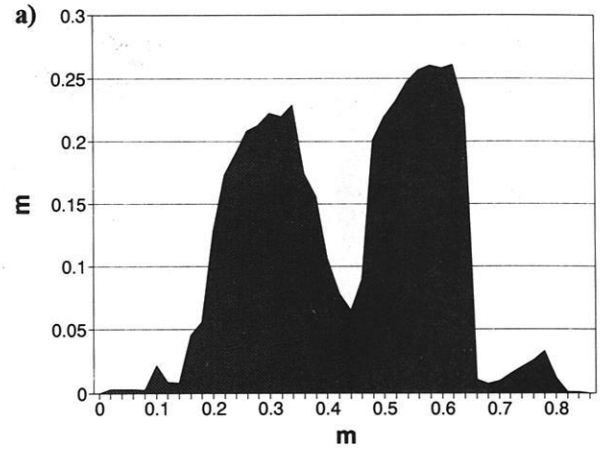


*6.1.2.1.2 Analyses of particle projection ($K_3$)*

Calculations of K3 (2) intervals carried out both longitudinally and laterally indicated distinct patterns of geometry on the bar. Figures 6.22 and 6.23 show typical examples of micro-form roughness elements in long and cross-section. As indicated by the longitudinal section, the bedform is hydrodynamically well adapted to flow (Fig. 6.22). This mega-cluster provides evidence for the way in which large grain roughness consists of a decreasing range of smaller grains and how this overall shape forms a compact assemblage. The example indicates how high projection or relative roughness is for individual grains in the Schmiedlaine compared to those at Squaw Creek, with only half the projection height. Fig.6.22 demonstrates how well adapted the large grains are to flow in that they rest at very high imbrication angles (discussed later in section 6.2) in order to avoid too much protrusion into the flow.

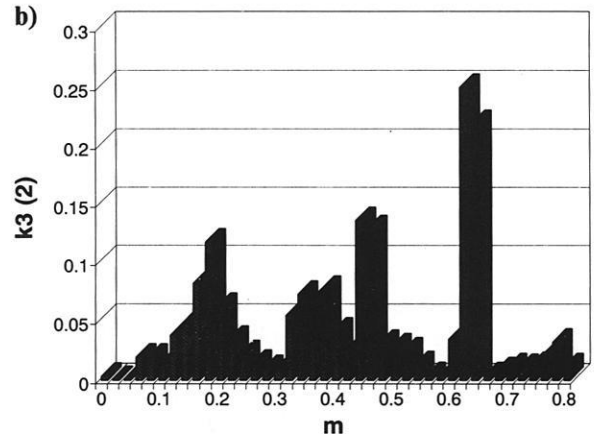


**Fig. 6.22** Mini-Tausendfüssler taken of a cluster in: **a)** long profile with **b)** respective $K_3(2)$ distribution along the bar in 1992. Flow is from left to right.

In contrast, the cross-sectional shape of the bedform indicates greater relative projection into flow, interrupted by gaps of very low roughness. The difference between these single grains and the gaps is much larger than at Squaw Creek and as expected they are also larger than in the long profile. Roughness is thus much higher and more differentiated than at Squaw Creek. This pattern repeats itself in chains, so when analysed in long profile, one roughness element will develop and then the next, periodically, maintaining low relative projection within the roughness element. In the cross-sectional analyses, the roughness elements are spaced discontinuously and at larger intervals.

Fig. 6.24 illustrates an example of how optimally single grains can be adapted to the bar form when considered in cross-section. The grains are spaced vertically and horizontally with such exactitude that they can follow the gradient of the bar without protruding above the general level. Not only does this demonstrate that flow may have ensued diagonally across the bar during recessional flows, leading to the roughness adaptations illustrated.

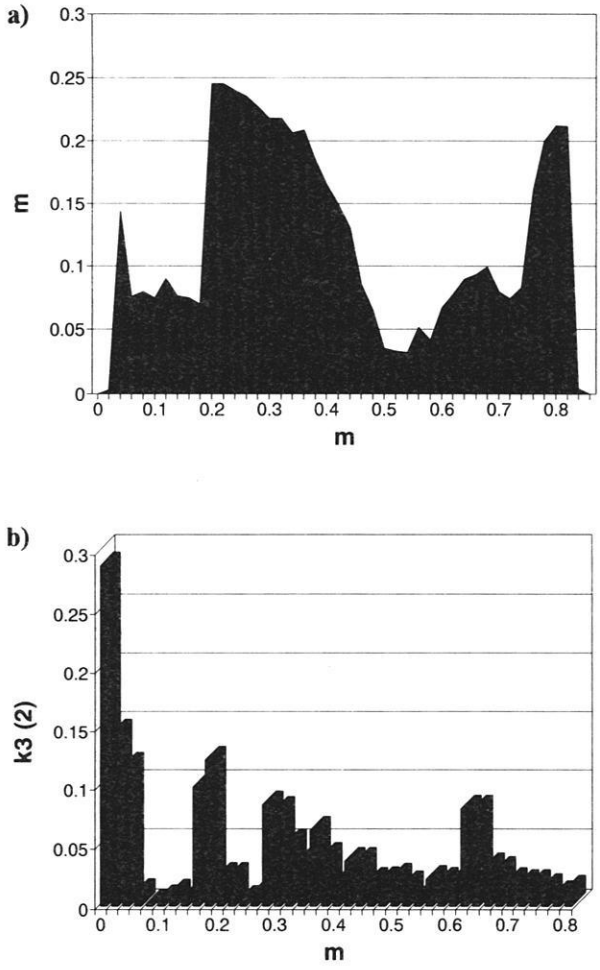


**Fig. 6.23** Mini-Tausendfüssler taken in: **a)** cross profile with **b)** respective $K_3(2)$ distribution along the bar in 1992. View is looking into flow.

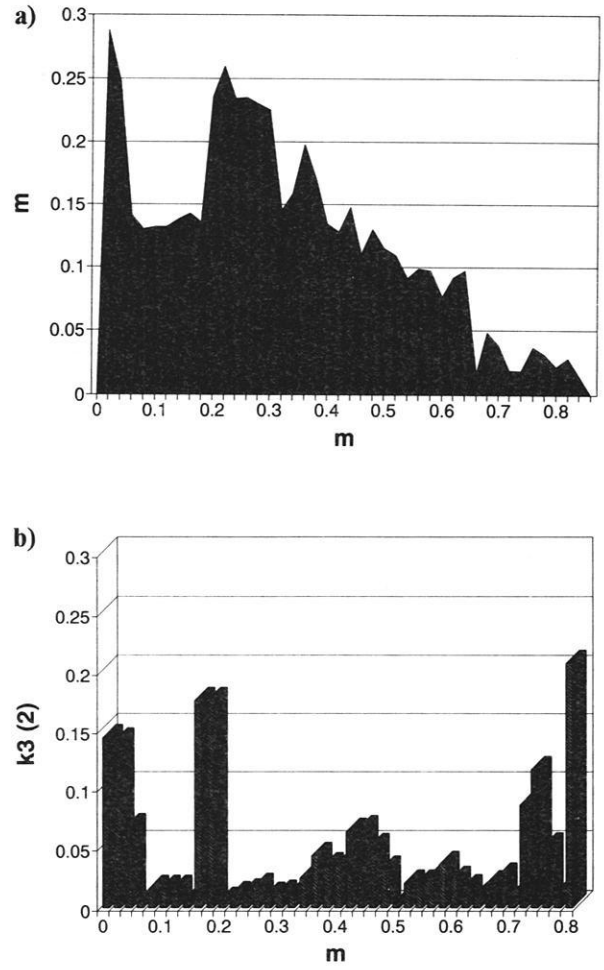


**Fig. 6.24** Mini-Tausendfüssler taken in: **a)** cross profile with **b)** respective $K_3(2)$ distribution along the bar in 1992. View is looking diagonally into flow, from channel to bar.

*6.1.2.1.3 3-D roughness model*

The $K_3$ data averaged for each Tausendfüssler profile was merged together for the entire bar to form the simplified three-dimensional roughness model (Fig. 6.25). The model shows that roughness on the gravel bar varies according to bar location, channel geometry and channel curvature. To review the curvature effects at the Schmiedlaine, please refer to Fig. 4.10 a & b (Ch. Study Areas). Thus at the upper end of the bar, where the channel is still narrow and is incidentally parallel to the sharpest part of the bend, large gravel berms, or bend arcs are evident. Not only are these bend arcs topographically higher but they also represent the largest roughness values on the bar. In the Schmiedlaine, two such bend arcs exist parallel to each other and the channel bend (photos Fig. 6.21a & b). The berms are evident in section 0, 2 and 4 m (long) at locations 4 and 7m (cross) (Fig. 6.25) which can be clearly recognised on the photos. Further downstream towards the medial part of the bar, the only comparably high roughness value is derived from a stranded log at location 10 m long and 9 m cross. The high roughness area at section 2 long, 0 cross is the result of large angular material deposited directly from the slope above the bar. The low roughness

values along the remaining left side of the bar are an indication of pool regions (photo Fig. 6.21). On the right of the model, low roughness values at the channel interface are the result of sand and fine gravel accumulations. The general roughness features on the bar are consistent, thus a dry channel can be followed downstream as well as ribs of higher roughness.

*6.1.2.1.4 Roughness frequency analyses*

All roughness frequency distributions are left skewed, whether observed in cross-section or in long profile (Fig. 6.26 a & b), which supports other natural river bed analyses (ROBERT 1990) and the results from Squaw Creek. There is a rapid decrease in the frequency of large roughness so that most of the distribution is left-skewed in shape. The distributions consist mainly of small scale or single grain roughness, followed by a small gap with an absence of medium to large scale roughness and finally the largest roughness characteristic of form roughness.

Although the long profiles have been reconstructed from one sample only (Fig. 6.26 a) they indicate a clear pattern of build-up of roughness at for example long 5, long 9, long 14/15, long 20/21 and long 27 thus in 4, 5, and 6 m steps. The roughness increase and decrease occurs gradually in each case. The regularity of roughness build-up was examined from the cross-profiles and will be discussed together with the grain size distributions under section 6.1.2.1.5. At the beginning (long 1 and 2) and at the end of the bar (long 31, long 32) a sandy patch caused the roughness values to shift to the extreme left.

In the cross-sections, roughness peaks can be found at long 5, long 11, long 17, long 19 and long 27, thus in

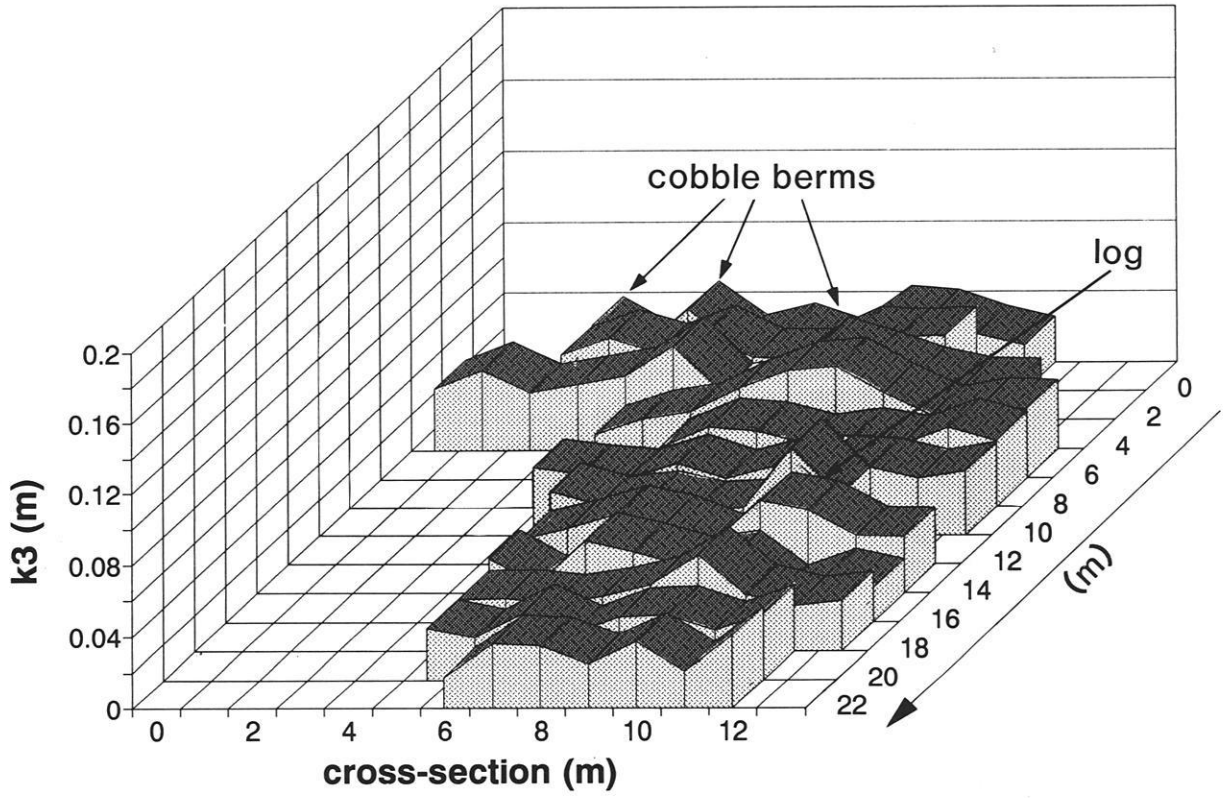


**Fig. 6.25** Three-dimensional model of roughness distribution on test bar in 1992. Flow is towards the observer. Notice that roughness scale is twice that of Squaw Creek.

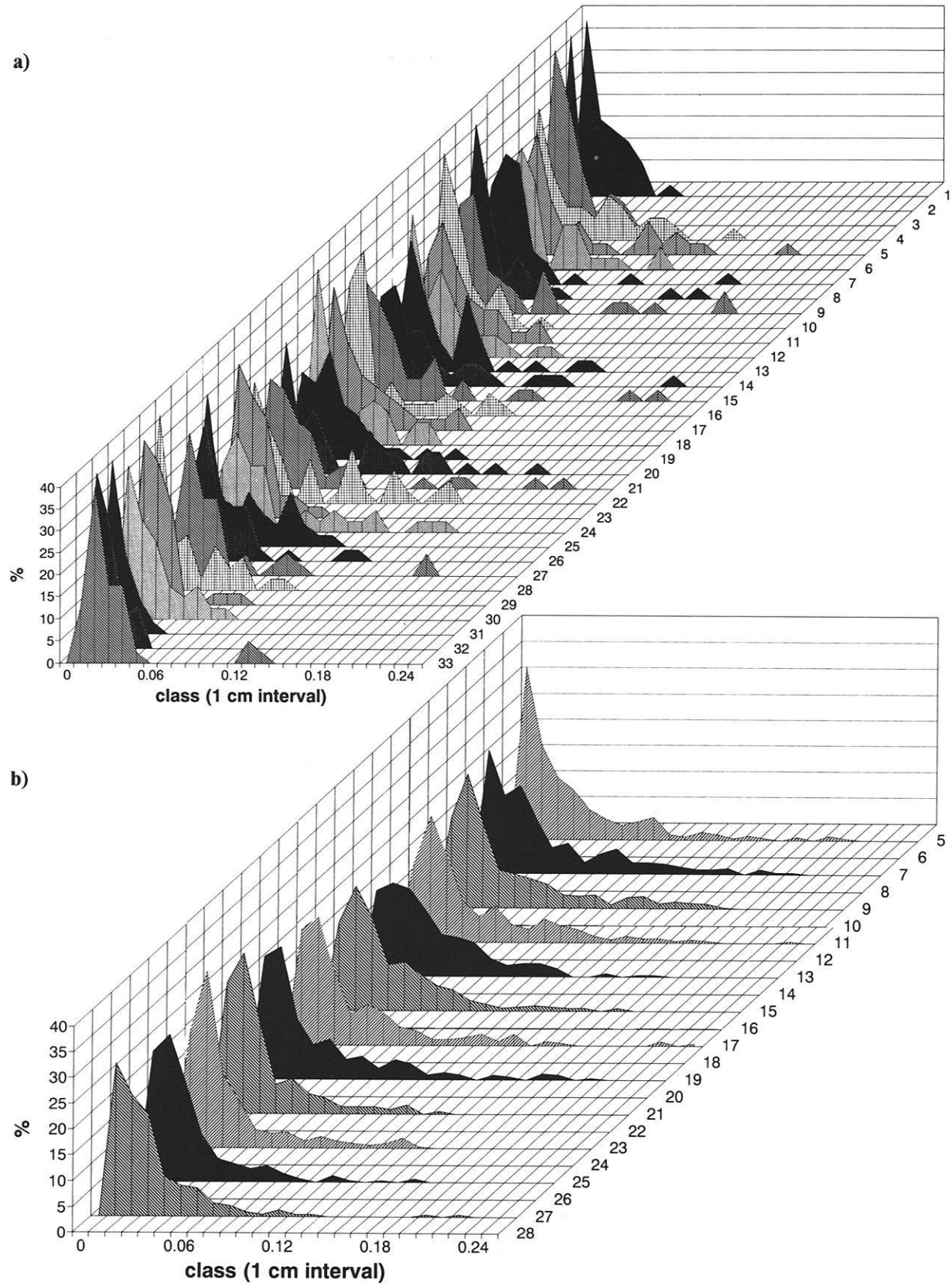


**Fig. 6.26** Roughness frequency distributions along test bar, long profile, Schmiedlaine **a)** longitudinal profile, one sample each & **b)** cross-profile with corresponding long-profile, same tone of shading. Profile 5 in a) corresponds to 5 in b) e.t.c.

6 m, 6 m, 5 m and 8 m steps (Fig. 6.26 b). Although there is some correspondence with the long profile, the roughness values do not fit as well as would be expected. This is because they take into account the entire cross-sectional spectrum and may become more attenuated as a result.

#### *6.1.2.1.5 $K_3$ roughness related to grain size/grain area from photo-sieving.*

The distribution of grain size from photo-sieving indicates that there is a downstream fining of sediment (Fig. 6.27). A coarse distal distribution at long 2 and 4 m corresponds to the cobble berm. This is visible also as a roughness increase at the 4 - 6 m location in the longitudinal profile of the roughness frequency distribution diagram (Fig. 6.26). Another coarse peak can be found at long 18 and 20. The peak at the 20 m location in Fig. 6.27 corresponds to the coarse peak at 21/22 m in Fig. 6.26. On the whole, the distributions are quite even and do not fluctuate as dynamically as the $K_3$ values. It is therefore impossible to find any tendency towards the regular roughness build-up from the grain size distributions alone.

In order to pursue the idea of roughness differentiation between long and cross profiles, photo-sieving samples taken along the same longitudinal and cross-sectional profiles were compared in terms of area samples to the projection samples obtained from the $K_3$ (2) (Fig. 6.28 a&b). The information shows that both the long and cross profiles have similar roughness relationship. The least fluctuation was

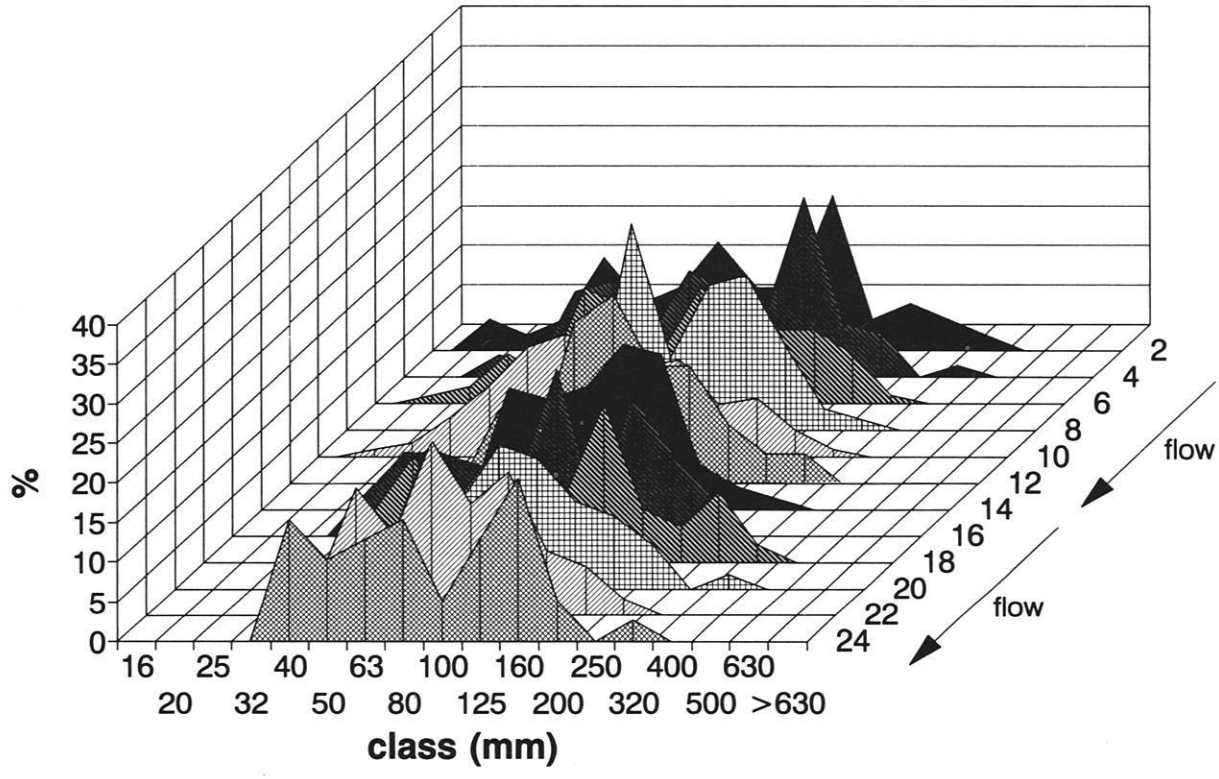


**Fig. 6.27** Downstream grain size variations along longitudinal transect. Flow is towards the observer. Distance is in m.

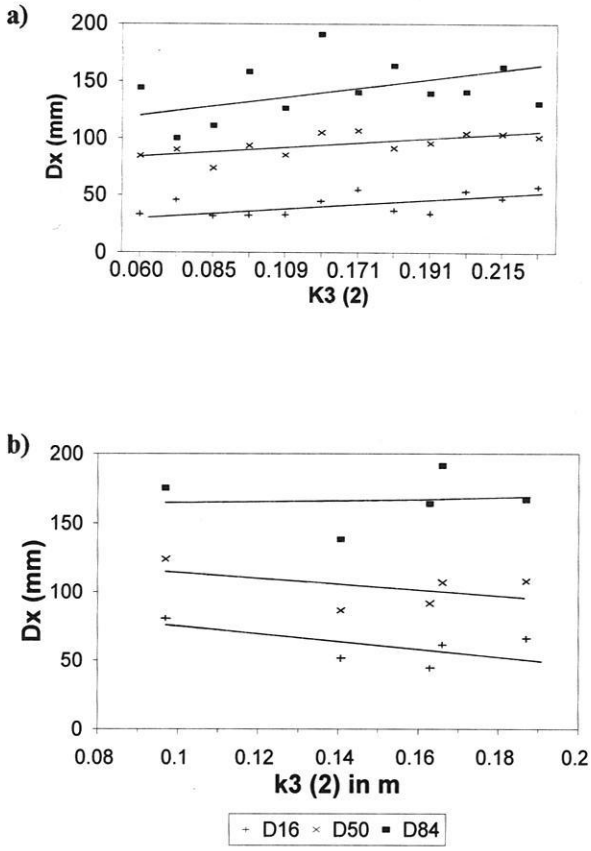


**Fig. 6.28** Direct relationship between $K_3(2)$ and $D_x$ ($D_{16}$, $D_{50}$, $D_{84}$) for entire bar for **a)** long profile (1 - 20m) and **b)** one cross-profile (1 - 4m).

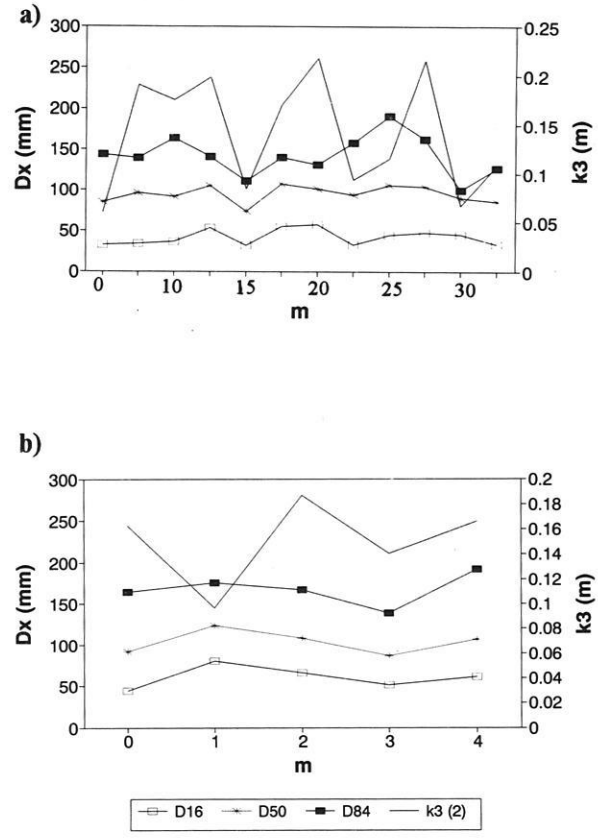


**Fig. 6.29** Relationship between $K_3(2)$ roughness coefficient and the $D_{16}$, $D_{50}$ and $D_{84}$ of the surrounding grain size distribution along the **a)** long profile and **b)** one cross profile.

presented by the $D_{16}$, as was the case at Squaw Creek. The results indicate that with an increase in roughness there is a direct and positive increase in grain size for the long profile but a slight decrease for the cross-profile. This demonstrates the effectiveness of the $K_3$ technique in differentiating roughness.

The regular step-like features reproduced by the $K_3(2)$ parameter along the first 20 m of the bar long profile, which was also mentioned in conjunction with the roughness frequency distribution, is depicted by the straight line in Fig. 6.29a. The longitudinal profile correlated with the cross profile with a $r^2$ factor of 0.77, showing that this regularity is not restricted to the long profile alone. Unfortunately the distribution is only weakly reproduced by the grain size relationships obtained from the same location. This shows that yet again the grain size is an inadequate descriptor of river bed roughness and that especially at the $D_{84}$ level fluctuations may be very high. In cross-section, (Fig. 6.29 b) the pattern given by the grain sizes is even weaker than in the long profile, even though as for the long profile the sample size was very large. These results strongly support the necessity for detailed micro-topographical measurements of the river bed rather than the simple use of grain size analyses.

Although the same long profile is plotted in Fig. 6.30 a) as in 6.29a), note that the $K_3(2)$ values can be reproduced in far more detail than the grain size distributions. Thus when the longitudinal roughness profile is reconstructed from one average value from each cross-section across the bar (Fig. 6.30a), the regularity of large roughness elements becomes even more poignant.

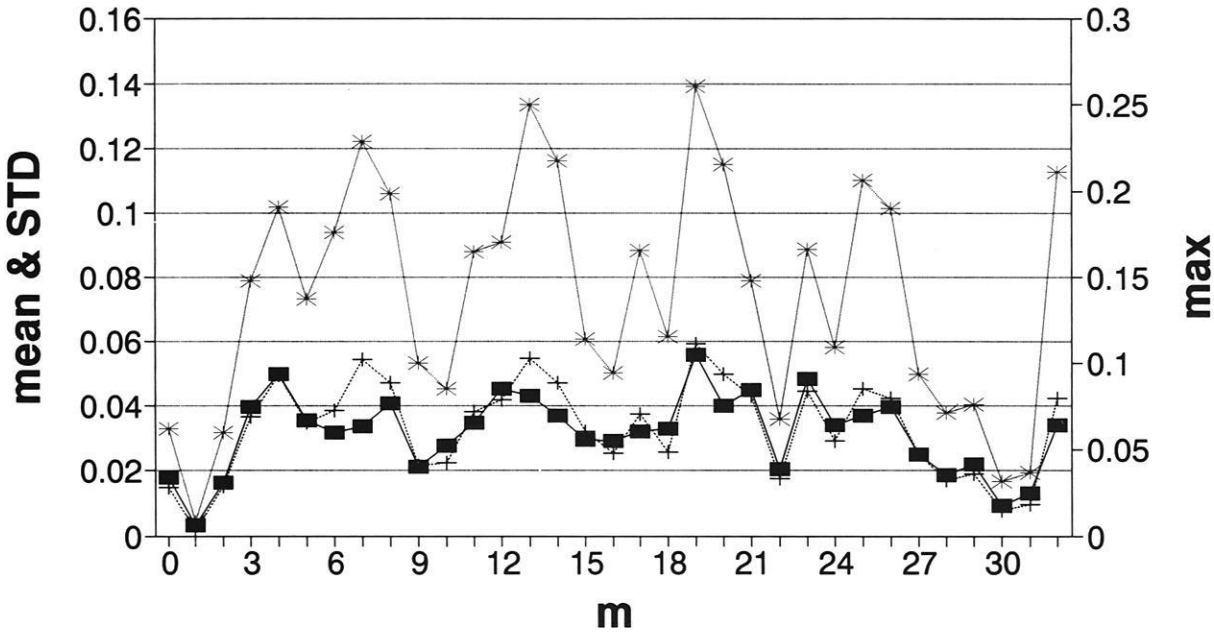


**Fig. 6.30 a)** $K_3(2)$ maximum, average and standard deviation plotted for the entire bar long profile. Flow is from left to right. Note regular spacing of 4 major peaks and minor ones infront.

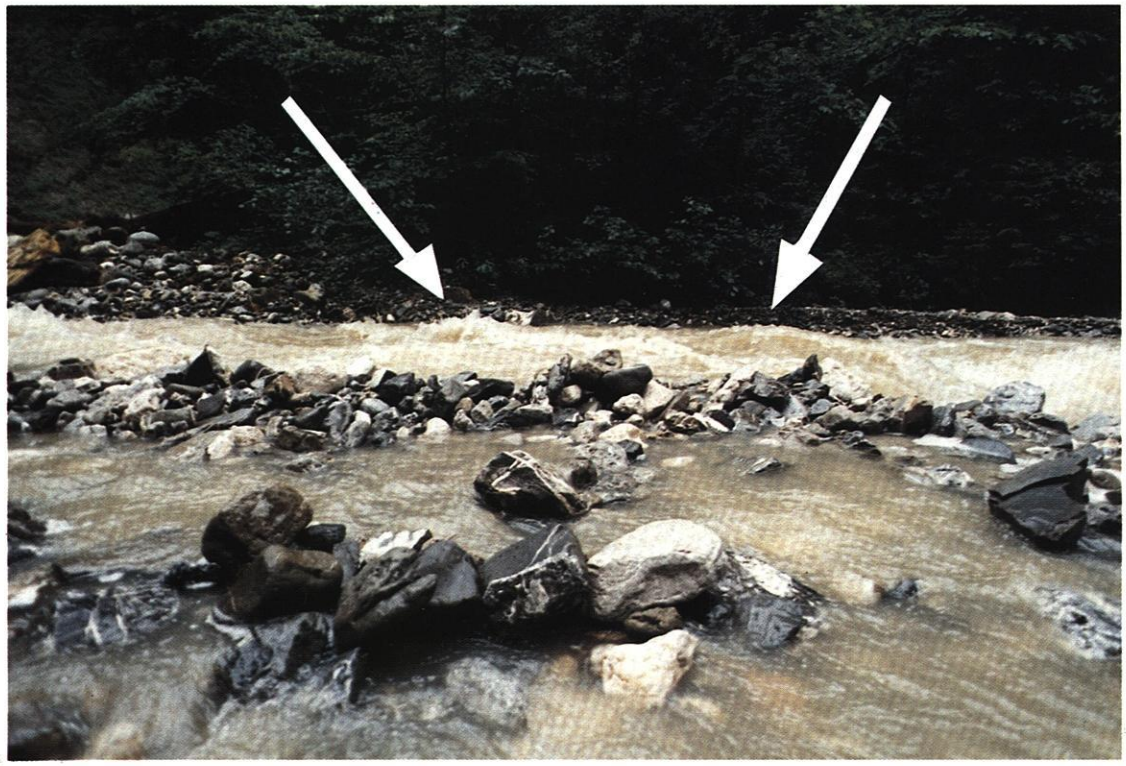

**Fig. 6.30 b)** Standing waves parallel to cobble berm, proximal bar during flood flow. Large cluster in foreground. It is postulated that the regular spacing of standing waves is responsible for the regular build-up of roughness peaks.

The distribution of maximum roughness shows that there are four major roughness peaks, with four smaller peaks superimposed in front. The average roughness values also indicate the regularity of the peaks. From visual observation, both roughness peaks recur at 6 m intervals along the length of the bar. In order to check whether discrete roughness intervals repeat themselves, the longitudinal profile was split into 6 m steps and a gliding average value calculated for the entire bar length. Not surprisingly, the average values formed a straight line, i.e. in the absence of any variance in the average values it can be hypothesised that these large roughness structures repeat their occurrence at 6 m intervals.

The regularity of the pattern is most probably due to the distribution of standing waves during the flood flows responsible for their formation (Fig. 6.30 b). By observation of a medium-sized flood in the Schmiedlaine it was apparent that standing waves in the main channel were large and regular enough to be able to influence the patterned deposition of large grain roughness. Once this nucleus of roughness has been deposited and deflected by flow, an opportunity would be given for other large material to be deposited in its vicinity. This would explain the regular build-up of the large roughness peaks. The smaller roughness peaks will most probably have formed during a succeeding smaller or weaker flood wave, taking advantage of the shelter obtained from the larger roughness peaks.

This roughness phenomenon probably is deposited in a short time span (within a couple of hours) and is dependent on high flow velocity, i.e. super-critical flow conditions and high gradients (0.04). Flow over the bar surface during a flood powerful enough to deposit the large roughness peaks would have had a depth of approximately 40 cm, i.e. barely enough to cover the particles in transport completely. Since by experience the main channel forming bedload transport does not occur at peak flow but rather during the ascending limb and very often during the recession (see 6.3.2), these roughness elements were most probably deposited during the recessional stages of flow. Additional evidence for this can be obtained from the freshly deposited cluster in the foreground of Fig. 6.30 b.

#### *6.1.2.1.6 Cluster & open-bed grain size/area comparisons (1990 & 1991)*

The changes in the spatial arrangement of roughness elements, i.e. clusters in relation to their surrounding material, is also indicative of the flow dynamics from year to year. Clusters are always coarser than their open-bed counterparts but this relationship changes annually according to flood power and sediment availability. Thus in 1990, the $D_{50}$ of the grain size distribution for clusters lay at 78.10 mm while the open-bed particles had a $D_{50}$ of only 45.16 mm (Fig. 6.31a).

A similar pattern of cluster dominance was observed in the grain area distribution (Fig. 6.31.b), where the $D_{50}$ lay at 102.32 mm for clusters and 89.07 m for the surroundings. As for Squaw Creek, the open-bed distribution remained normal, whereas the clusters were more right skewed. A combination of both data sets in the Schmiedlaine, as at Squaw Creek, would cause the total grain size distribution to shift slightly to the right.

The grain size distribution can be utilised to clarify the investigations on grain area, and since the two are mutually dependent they cannot be treated separately. The grain size distributions indicate that the cluster particles had become very much coarser in 1991 (Figs. 6.31 a & 6.32 a). Notice too that the distribution in 1991 has a slight tendency towards a depression at the peak, i.e. with the result of a double peak. This bimodal tendency is well emphasised in the grain area distributions. In 1990 the only peak for the cluster grain size distribution lay at $D_{50}$ whilst the first peak lay at $D_{30}$ in 1991 and the second peak lay at $D_{74}$. When considering the grain area the first peak lay at $D_{36}$ and the second at $D_{84}$ in 1990, while in 1991 the first peak lay at $D_{20}$ and the second peak lay at $D_{74}$. In 1990, the area that cluster particles occupied was small to medium sized i.e. in the range from 20-100 mm, with a peak in the 100-125 mm class, a small gap in the 125-160 mm grain class, followed by the bimodal peak in the 160-200 mm class (Fig.6.31 b).

Since the distribution extends further on than this peak, it can be said that cluster obstacles could reach a size of 400 mm. In 1991, after a series of floods (Fig.6.32 b), a very pronounced bimodality had been generated in the Schmiedlaine. The cluster particles had in this case become much coarser, thus they occupied the 63-125 mm class, with the peak this time in the 125-160 mm class and a sharp drop, dictated by an absence of particles in the 160-200 mm class, followed by a large peak in the 250-400 mm class. The largest obstacle particle for that year lay within this class.

The tendency towards bimodality of the grain area distribution of clustered particles in Fig. 6.31 b) and 6.32 b) is justifiable. This bimodality has already been described for Squaw Creek. In the case of the Schmiedlaine, the bimodality pattern is the reverse,

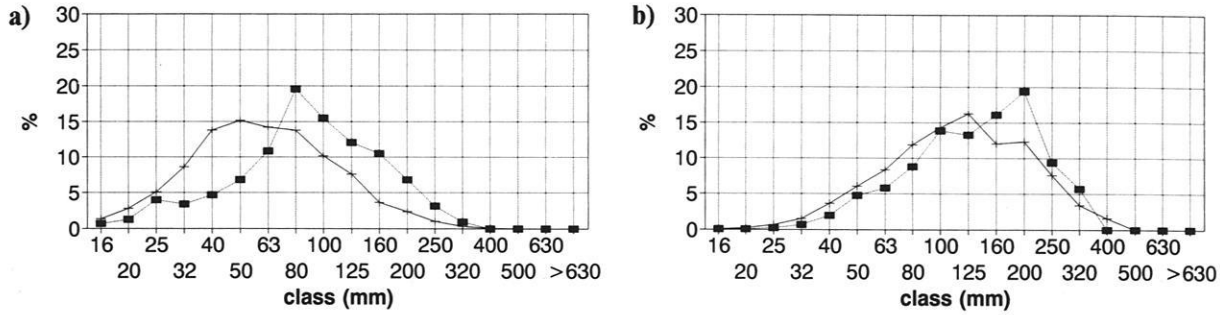


**Fig. 6.31** Relationship between clustered and open-bed material for the entire test bar, Schmiedlaine, 1990 for **a)** grain size distribution and **b)** grain area distribution.

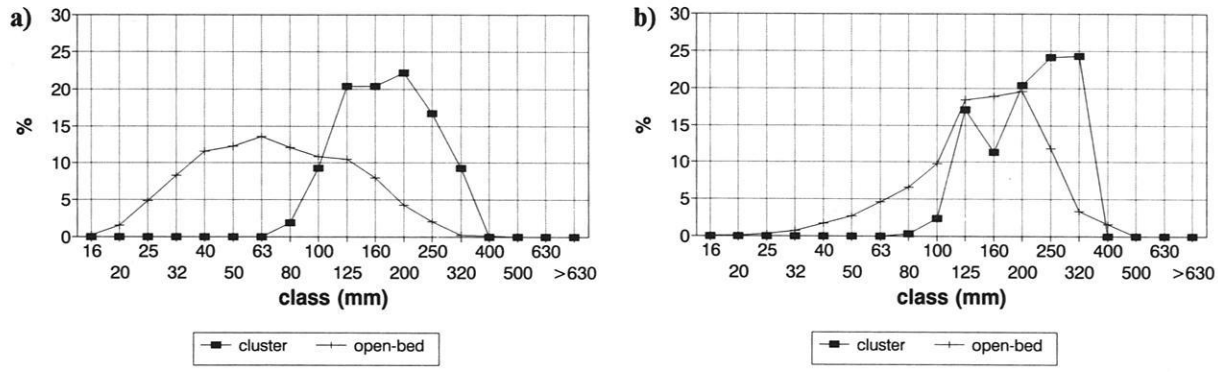


**Fig. 6.32** Relationship between clustered and open-bed material for the entire test bar, Schmiedlaine, 1991 for **a)** grain size distribution and **b)** grain area distribution.

i.e. the peak of the distribution lies in the coarser grain size classes for both the 1990 and 1991 samples. This means that clusters in the Schmiedlaine generally consist of a very large obstacle particle, followed by a sequence of finer particles. Evidence for obstacle dominance can be obtained from photos (Fig. 5.1a Ch. Methodology). At Squaw Creek this was not so well developed due to the absence of an extreme particle size range which is present in the Schmiedlaine (Fig. 5.1b Ch. Methodology). Notice that between the two years, the general grain size distribution did not change, although the characteristics of the clusters did. This phenomenon of equilibration of geometry but fluctuation in roughness has already been illustrated in detail in the example of Squaw Creek. In the Schmiedlaine, roughness changes between 1990 and 1991 are evident from the surface area occupied by the dominating clusters. As BAGNOLD & BARNDORFF-NIELSEN (1980) pointed out, the skewed grain size distribution must have been the result of larger grains being segregated out, while smaller grains have higher mobility, leaving the medium sized particles to dominate.

From these results it can be deduced that the cluster particles generally became larger and that the structure of the cluster also changed considerably between the two years. Thus an obstacle clast in 1991 was usually twice the size of the remaining infill. It is questionable whether this result was dependent on local sediment supply since the surrounding distribution had actually not changed. Rather, this change in structure must have been dependent on hydraulic conditions, capable of transporting larger particles (as obstacles) and also capable of sweeping out a rather coarse component of the previous cluster (160-200 mm).

Thus although discharge was measured only in the Lainbach at the expense of the Schmiedlaine, the paleohydraulics of the floods responsible for bar reworking can be reconstructed from the cluster open-bed relationships. Accompanying changes in the orientation of particles, described in section 6.2 further support the differences in flow characteristics.

## 6.1.3 Lainbach

*6.1.3.1.1 Geometry*

Fig. 6.33 indicates the variations in geometry plotted at 2 cm intervals along the longitudinal profile of the gravel bar and the channel in the Lainbach, together with the cross-sectional profile taken along the upper Tausendfüssler bridge (see Fig. 4.12 Ch. Study Areas).

Very large differences can be observed between the long profile on the bar and in the channel. On the bar, the gradient is constant and roughness is very smooth. In fact only two major peaks are detectable. In contrast, the channel shows a pool between an upstream and downstream step. The downstream step with reversed gradient is caused by a boulder, 1m in diameter. It is a typical step element of the regular step-pool system in the Lainbach. In the channel there is a higher range of gradients than at the Schmiedlaine and Squaw Creek due to the influence of large boulders, and finer-grained areas in between, resulting from scour and deposition (see channel, Fig. 6.33). On the bar, roughness is lower than in the channel even though the two profiles are only 4 m apart.

Fractal and sediment size analyses were restricted to the bar profile since the longitudinal section in the channel was not representative of the entire step-pool sequence. By choosing another bar, the results remained comparable with the bars at Squaw Creek and in the Schmiedlaine.

The cross-section shows a high gradient contrast between the highest point on the bars and the channel. Roughness does however remain relatively smooth and devoid of sharp contrasts. The river is confined by bedrock and an artificial wall built to protect the road at the cross-section. The valley is incised at the cross-section.

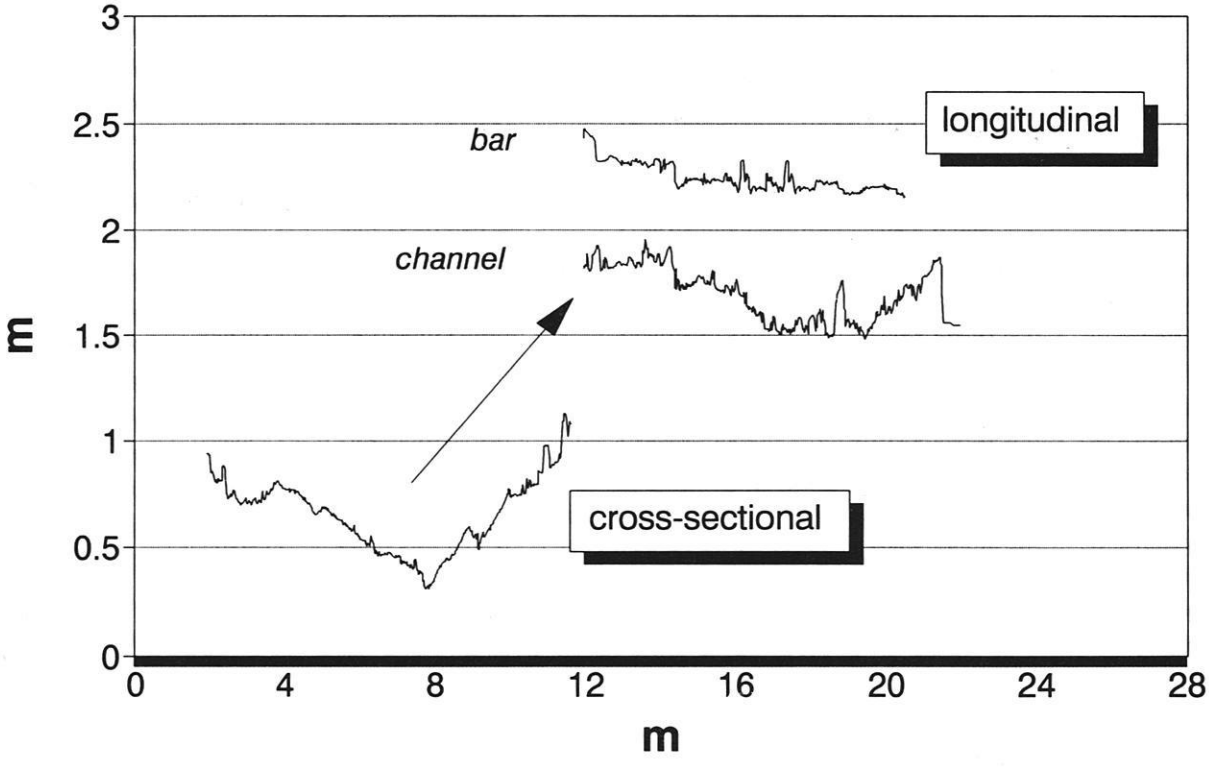


**Fig. 6.33** Topography of the bar and channel at the Lainbach, Upper Bavaria. The longitudinal sections of the channel and bar (where flow is from left to right) have been plotted together with the cross-section (of the whole system) superimposed below at the same scale. The longitudinal sections were taken 4 m apart starting at the upper Tausendfüssler bridge. The cross section was obtained along the upper Tausendfüssler bridge at the first bar and channel position.

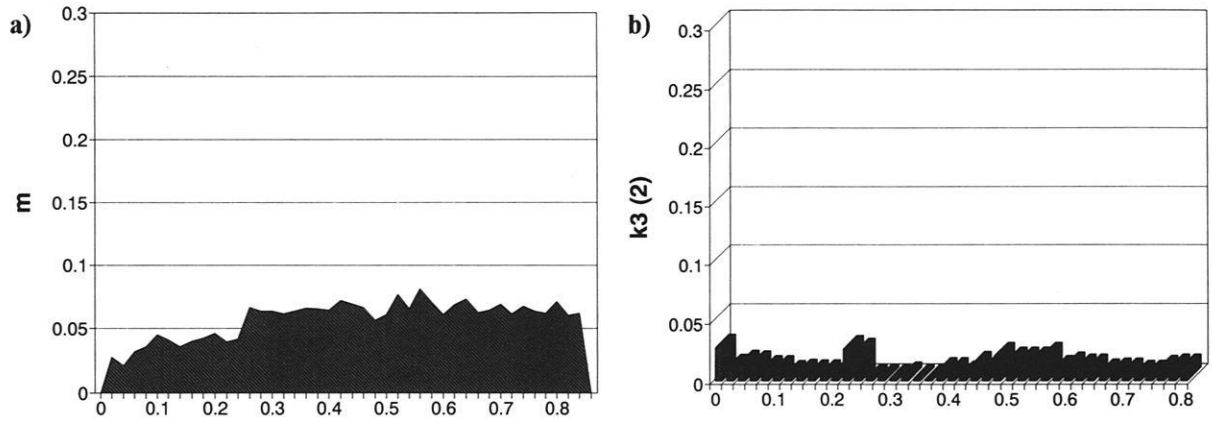


**Fig. 6.34** Mini-Tausendfüssler **a)** long-profile and **b)** $K_3$ (2) roughness on bar indicating sandy/gravelly area. Flow is from R. to L.

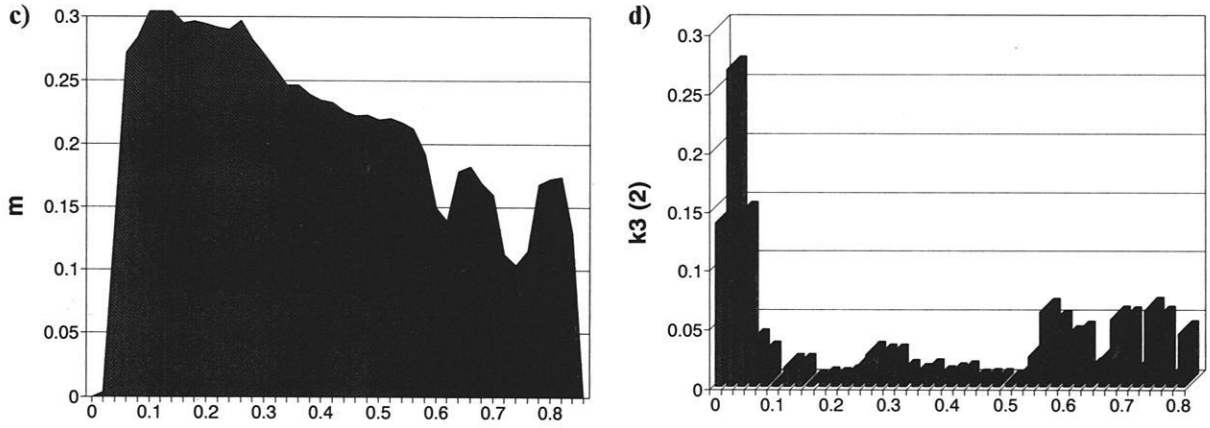


**Fig. 6.34** Mini-Tausendfüssler **c)** long-profile and **d)** $K_3$ (2) roughness in channel with large boulder, constituting step. Flow is R. to L.

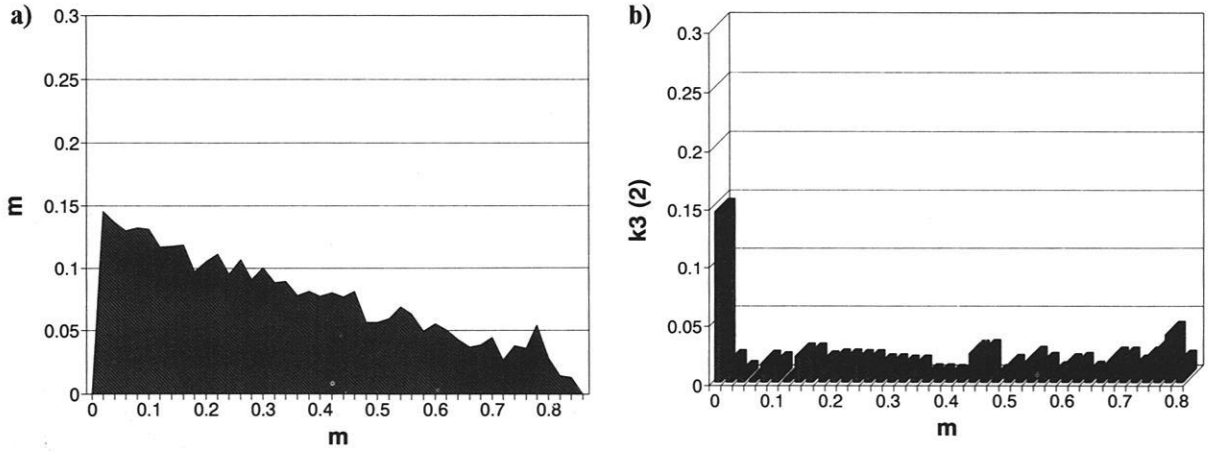


**Fig. 6.35** **a)** Mini-Tausendfüssler cross-profile and **b)** roughness at channel/bar interface. Flow is from R. to L.

*6.1.3.1.2 Analysis of particle projection ($K_3$)*

There is a larger range in roughness values at Lainbach than on the Schmiedlaine test bar because of the larger scale roughness elements and higher boulder frequency. In the long profile very low roughness values are found on the bar (Fig. 6.34 a & b). The profile is even smoother than at Squaw Creek (Fig. 6.2). In the channel (Fig. 6.34 c & d), very high roughness values, associated with boulders >1 m in diameter are interspersed with very low roughness areas composed of sand in the lee of these large boulders. In the cross-profile (Fig. 6.35) there is very little variation in relief, since grain size is very small and the bottom of the channel is generally smooth. It is noteworthy that as on the new bar at Squaw Creek (Fig. 6.3 a & b) and in the Schmiedlaine (Fig. 2.4 a & b), the lateral roughness arrangement is optimally adapted to the gradient of the bar/channel interface.

*6.1.3.1.3 Grain sizes from photosieving*

Since the Lainbach is largely covered by water, photo-sieving could not be carried out directly at the test site during the field season and was carried out downstream instead. Grain size distributions measured form the downstream areas were used only for comparison with fractal analyses of the $K_3$ data (Section 6.1.4), not for analyses of spatial roughness patterns. No grain area was therefore calculated for the Lainbach. Data from photo-sieving was obtained in 1990. The Lainbach as a very variable grain size distribution and although its step-pool system renders it coarser than the Schmiedlaine in many parts, the local grain size distribution on the gravel bar and in the channel at the test site is actually finer than in the Schmiedlaine.

*6.1.3.1.4 Roughness frequency distribution*

Fig. 6.36 a) shows the roughness frequency at the cross-a profile of the upper Tausendfüssler bridge. There are extreme values of roughness to either side of the profile (lines 1-5 and 8-12) i.e. on the bars and low roughness in the channel (lines 5-8). This pattern is also present on the micro-profile in Fig. 6.33. The generally rough situation of the bar is evident when comparing Fig. 6.36 b) and Fig. 6.36 c). In Fig. 3.6 b) the distributions are more attenuated, with some very large elements unconnected to the most frequently occurring roughness scales. This attenuation indicates that larger roughness structures such as clusters are present on the bar, as at position 9. In the channel (Fig. 6.36c) roughness frequencies are spiked, and small in scale, indicating the presence of finer material. Due to the short longitudinal distance involved at the Lainbach (5 m), there is little chance of detecting multiple-stepped patterns of roughness.

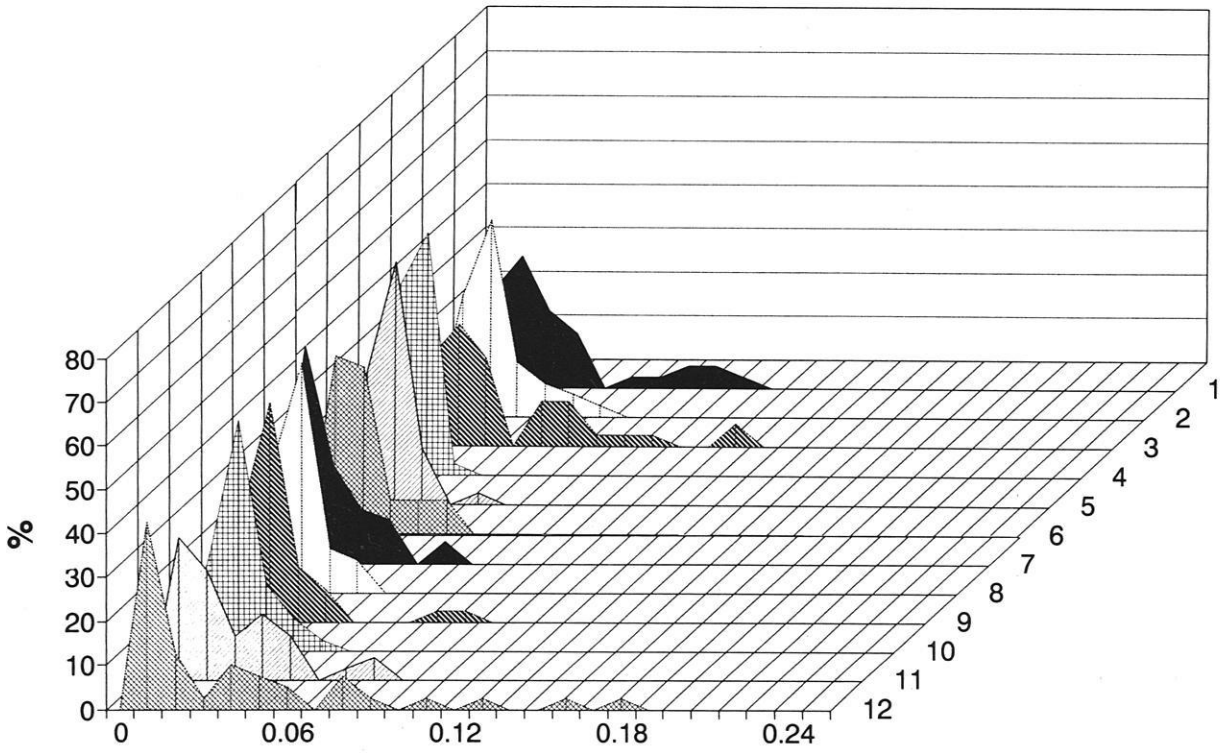


**Fig. 6.36** a) Roughness frequency distribution along upper cross-section, Lainbach 1992. Class intervals are in $K_3$ (0.01m).

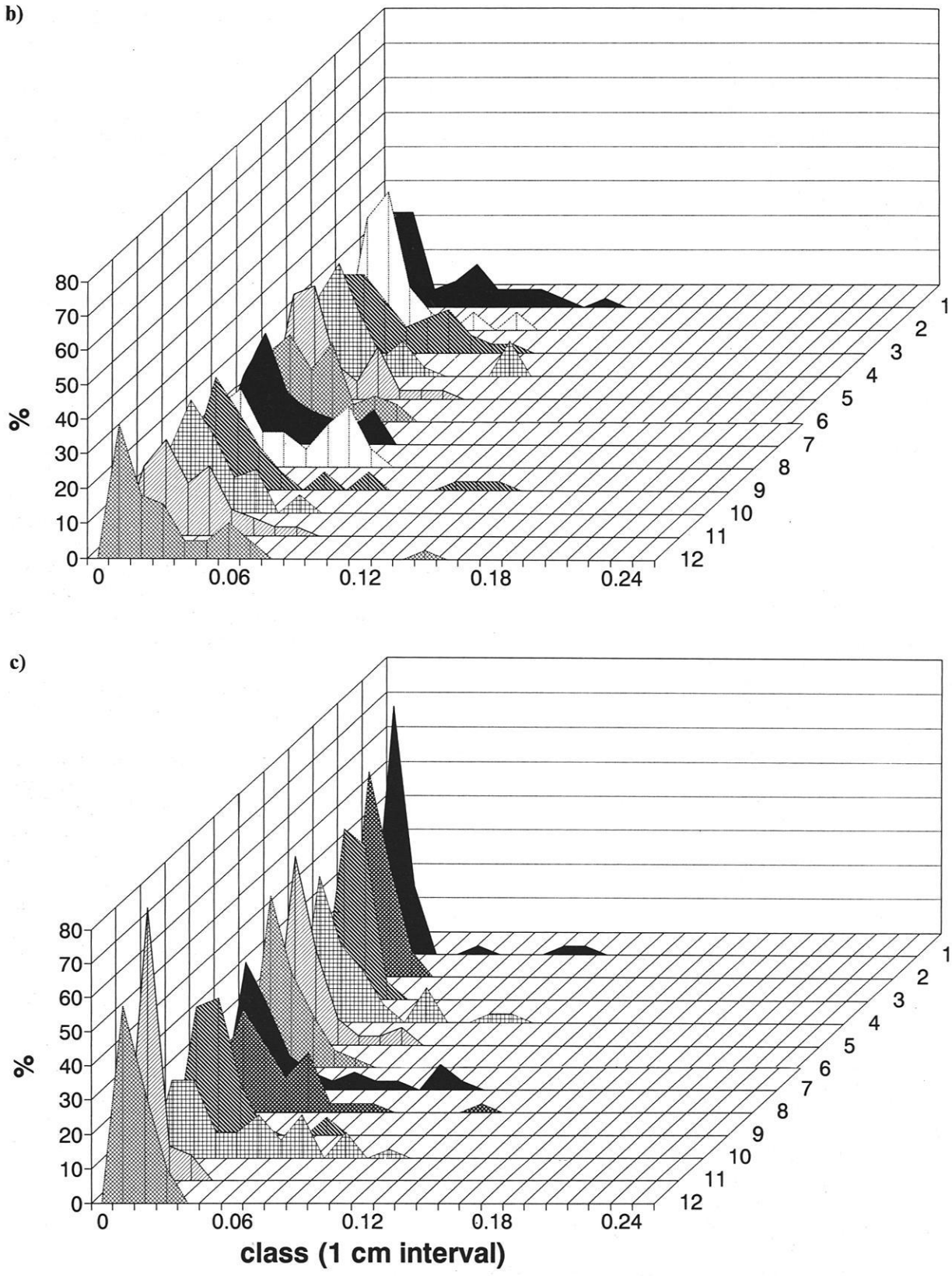


**Fig. 6.36** **b)** Roughness frequency distribution along the long profile on the bar, and **c)** along the long profile in the channel Lainbach 1992. Notice more single large roughness elements in channel, but overall finer-grained distance (more spiked).

### 6.1.4 Summary of the spatial variability of roughness

In the previous sections, 6.1.1 - 6.1.3, the spatial organisation of roughness has been dealt with in great detail; the main emphasis lies on the bars. The hydraulic conditions responsible for roughness formation shall be discussed in the context of temporal experiments undertaken on roughness change, presented in Sections 6.3 and 6.4.

From the knowledge of the actively reworked test bar studied in the Schmiedlaine over the past three years and from the new bar at Squaw Creek in 1991 and 1992, it is clear that any new bar segment or new medial bar deposited in those reaches is highly clustered and primarily clast supported at the surface. Minor flood reworking usually results in a higher percentage of fine sediment deposited in between roughness elements and causes the distance between successive clusters to increase. Thus the age and associated stability of a bar may be determinable from how densely and well packed the sediment is.

It has been pointed out that on the bar surface, standing waves and shear waves may develop under shallow flow conditions. Such flow patterns exercise the main influence on the formation of roughness elements such as clusters. In the case of both the Lainbach and Squaw Creek, roughness values were higher on the bar than in the channel. In the channel, roughness values are lower due to the influence of bedload transport and higher amounts of energy expenditure. The existence of large roughness such as cluster bedforms on the bars suggests less bedload transport than in the channel, especially during the waning stages of flow. If clusters do exist in mid-channel locations then this indicates that they also developed during the flood recession in accordance with minimum energy dissipation.

The spatial arrangement of roughness is influenced by - and influences - the development of spiral flow cells due to the divergence and convergence of flow over irregular topography. For spiral flow to develop over the river bed, a minimum flow depth is required. The water depth has to attain, on average, 3-4 times the roughness height in order for flow spirals to develop. Thus a flow depth of at least 30-40 cm is required for an average $K_3$ value of 0.1 m. Since this situation is rarely possible on the bar surface, where average flow depths only attain 15 cm during peak discharge, flow vortices cannot develop on the bar surface and are therefore limited to the main channel.

The detailed hydraulic aspects in the channel are difficult to interpret due to the limited mini-Tausendfüssler information obtained here. Temporal measurements with the macro-Tausendfüssler device do however show the importance of an ideal cross-sectional shape, which encompasses both the bars and the channel. LANE (1955) argues that half a sphere is the ideal shape in energy terms. The real-world cross-sections are however quite different. In the Schmiedlaine for example, flow is concentrated in the straight reach and it expands in the bend. At Squaw Creek the situation is much the same. Thus flow is concentrated in the straight measuring reach after the bend.

What is really important in the development of flow structure is the height difference between bar and channel and whether an interface exists or not at the time. In contrast to Squaw Creek, there is no interface developed in the Lainbach and in the Schmiedlaine. The height difference between the bar and channel for the Schmiedlaine and Lainbach streams is much larger than at Squaw Creek. At Squaw Creek, the more gradual transit from channel to bar allows for the existence of an interface. These transitions are important in considerations of flow hydraulics as influenced by their individual hydraulic geometry.

Thus while the patterns of roughness in the Lainbach can be marginally influenced by the possible development of flow cells over the bar, those in the Schmiedlaine and at Squaw Creek are purely limited to shallower shear wave and standing wave patterns. Shear waves have been experimentally observed to occur under low velocity flow during flow recession on slopes (HODGES 1982). They are discussed more fully in Section 6.2. Nevertheless it is important to point out that shear wave development explains some of the lateral and longitudinal patterns of clustering developed on the various gravel bars. Evidence for their existence comes from the observation of water surfaces during flood flows. Whereas sub-critical flow may be influenced by changes in bed configuration on the upstream side, super-critical flow will only be subject to an downstream control (ALLEN 1982). On the bar, where flow can be both sub and super-critical, the arrangement of obstacles, clusters and other bedforms may cause significant perturbations in both the upstream and downstream direction.

The importance of channel shape is reflected in the different types of channel processes. In the channel at Squaw Creek, the development of flow cells will quickly expand to the interface with a small rise in water level but even under maximum flow, the bar will barely be covered. In the Lainbach, a much larger

rise in water level will be necessary before the bars are sufficiently covered to develop flow spirals. Nevertheless deeper flow over the bars can easily develop during an average flood. Since slopes are steeper and water discharges larger in the Lainbach, increases in flow depth can be much more rapid than under the gentler gradients at Squaw Creek, where flow is accommodated by lateral spreading of water.

Another important determinant of roughness development and its invariable influence on the development of hydraulic geometry is the grain size. It is important to consider how the range in grain size influences the development of roughness. At Squaw Creek, the limited range in grain size causes little variation in the spacing, arrangement and nature of roughness elements. Quite the opposite is true for the Schmiedlaine and Lainbach. In the Schmiedlaine, the wide range in grain size enables extreme variability in roughness distribution and shape.

In itself, this suggests that extreme floods, capable of transporting a maximum range of grain size, cause the greatest diversity of roughness distribution and arrangement. During an extreme flood, there will be very low roughness in order to maximise sediment transport, but after the flood event, the river bed will be very differentiated. In energy terms, maximum amounts of bedload will be transferred during an extreme flood. With the cessation or minimisation of bedload transfer, local erosion and deposition occurs and individual roughness develops. The reason why the river bed is coarser during the recession in contrast to the peak flow cannot be explained only in terms of bedload. Due to the interrelationship with bedload transport, flow hydraulics are equally important in the minimisation of roughness during peak flow and maximisation of roughness during the recession. Thus the development of roughness during this final stage will be dependent on the starvation of bedload enabling the development of standing waves and shear waves on the bar and spiral flow in the channel.

## 6.1.5 Fractal intervals of roughness

A suitable description of roughness is essential to relate flow resistance to boundary roughness but it is difficult to systematically describe the diversity of geometric forms on the river bed (FURBISH 1987). Different scales of roughness must be adequately differentiated since they are ultimately related to the intensity of turbulence near the river bed. Two streams with the same average size may have different roughness sizes and distributions (FURBISH 1987, TAIT per. comm.). FURBISH (1987) therefore suggests that roughness should be statistically similar at different scales. In his studies he did not however differentiate between grain and form roughness nor did he account for surface packing.

Fractal analyses of increasing $K_3$ values, ranging from $K_3$ (2) to $K_3$ (400), were calculated for all three study areas along the entire reach length and width from the 2 cm basis intervals. The higher intervals $K_3$ (100-400) were calculated repeatedly from different starting positions to ensure an adequate sample size. A more detailed description of this methodology is given in section 5.1.1.5 (Ch. Methodology). The intervals were chosen so that they could cover the entire roughness range, commencing with grain roughness, through (bed)form roughness to system roughness, effected by channel shape and gradient. These transitions were determined directly from a graph at the point of break of slope i.e. at the end of an increase in slope and transition into the end slope segment (Fig. 6.37a).

Since a direct relationship exists between $K_3$ and grain size (Fig. 6.28) the $K_3$ value for a particular interval was linked with the related grain size and its cumulative percentage $D_X$. Thus if an average $K_3$ value for the $K_3$ (100) interval is $K_3$ 0.1 m along the y-axis of its fractal distribution, this is equivalent to 10 cm or 100 mm in terms of its vertical deviation in height, which is assumed to be the grain size. This measure would fall into the grain sieve class of 100-125 mm of the grain size distribution graph, which in turn corresponds to the $D_x$th percentile (along the y-axis) of that particular distribution.

### 6.1.5.1 Squaw Creek

Analyses of fractal intervals on the new bar at Squaw Creek in 1992 indicate that there are three main roughness transitions (Fig. 6.37). For the longitudinal analysis, grain roughness increases up to $K_3$ (10). The steep rise up to $K_3$ (30) represents the transition to form roughness. After that there is a sharp depression (at $K_3$ (80)), followed by an increase determined by the general gradient of the reach which represents system roughness. The cross-sectional profile follows the pattern of the longitudinal profile up to $K_3$ (80). The limit for the grain size/form transition also lies at $K_3$ (30) after which it continues rising. The form system roughness transition for the cross section

profile lies at $K_3$ (60). This demonstrates that at Squaw Creek, the cross-sectional gradient is more pronounced than the longitudinal gradient (refer to Fig. 6.1, Section 6.1.1).

When the transitions are compared to the cumulative grain size distribution, the limitations of constant conventional roughness intervals are brought to light.

a)

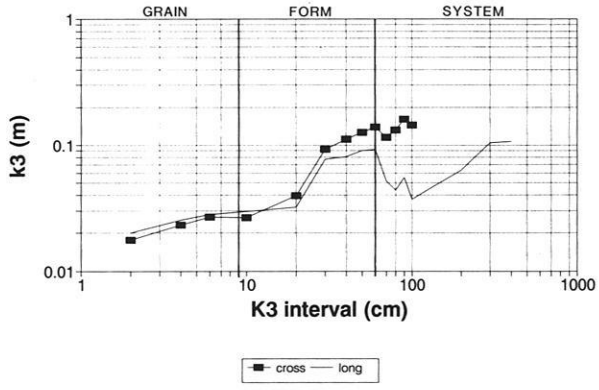


**Fig. 6.37 a)** Log-normal relationship between fractal $K_3$ intervals (x-scale) and average $K_3$ value for that interval (y-scale) for longitudinal and cross-sectional sections at Squaw Creek 1992). Notice similarity of lines up to $K_3$ (80).

b)

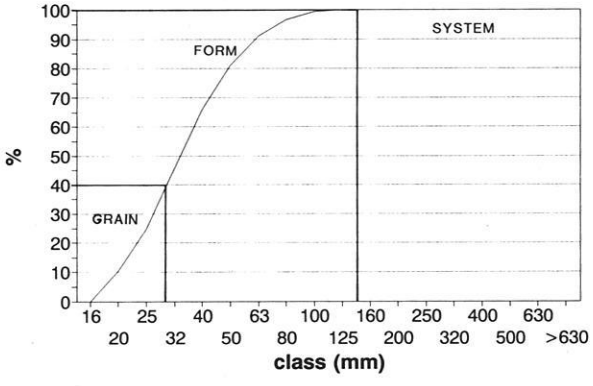


**Fig. 6.37 b)** Photo-sieved cumulative grain size distribution at Squaw Creek, 1992. Transitions from grain to form roughness lie at $D_{40}$ and from form to system roughness lie at $D_{100}$.

The transitions from grain to form $D_{40}$ and system roughness $D_{100}$ do not match conventional parameters. Conventional parameters assume $D_{50}$ and $D_{85}$ or $D_{95}$ as decisive roughness descriptors. The first transition from single grain to form roughness (Fig. 6.37) for both the long and cross profile is equivalent to a $D_{40}$ ! or a grain class 25-30mm at $K_3$ (10) with an average $K_3$ value of 0.03 m. The next transition, from form to system roughness, is equivalent to the $D_{98}$ in the 125-160 mm grain class at $K_3$ (60). Average $K_3$ values are 0.105 m for the cross-profile and 0.09 m for the long profile. This indicates that the lower percentiles are more important in dictating roughness patterns. When the fractal intervals were calculated without the lateral and longitudinal gradient effect, the relationship looked very different as early as the $K_3$ (60) interval. Thus in actual fact, the effects of gradient are important from $K_3$ (60) onwards. Without the gradient, the relationship fails to increase after form roughness and is forced to fluctuate at the $K_3$ (60) level. Considering the cross-sectional analysis, it can be seen that gradient is critical to the formation of a negative fractal relationship at Squaw Creek. Without the effects of gradient, the relationship would be positive.

The macro-Tausendfüssler interval used at Squaw Creek for the temporal measurements of roughness and geometry was pre-determined at $K_3$ (10) (ERGENZINGER and STÜVE 1989). The fractal study demonstrates that this interval is optimal for representing grain roughness at its transition to form roughness given the grain size distribution at the site.

### 6.1.5.2 Schmiedlaine

During the analyses of the fractal intervals in the Schmiedlaine, three main transitions also come to light. As expected, the longitudinal relationship rises at a steeper rate than the lateral one due to gradient effects. Again the lines run parallel to each other to the grain roughness transition, at $K_3$ (20) for the long and cross profile ($D_{56}$ grain size). After this transition, the lines still principally run parallel to each other up to the form/system transition. For both the long and cross profiles, the form/system transition begins with an ascent after the $K_3$ of (100), equivalent to a $D_{90}$ in the 160-200 mm grain class, with an average $K_3$ value of 0.16 m. In contrast to Squaw Creek, this indicates that the higher grain percentiles are more important in dictating roughness patterns. Also in contrast to

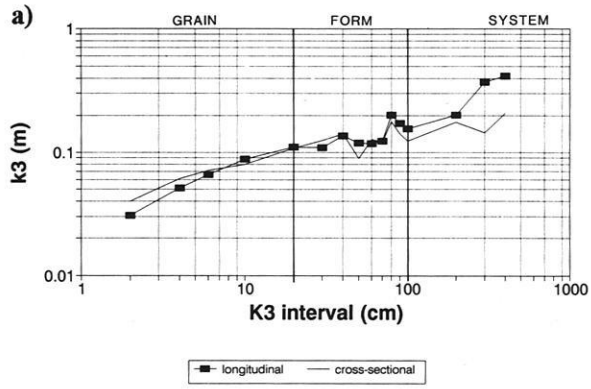


**Fig. 6.38 a)** Log-normal relationship between fractal $K_3$ intervals (x-scale) and average $K_3$ value for that interval (y-scale) for longitudinal and lateral sections in the Schmiedlaine, 1992. Notice resemblance of lines up to $K_3$ (110).

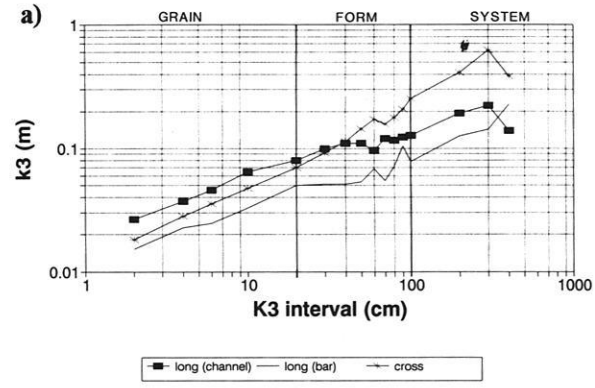


**Fig. 6.39 a)** Log-normal relationship between fractal $K_3$ intervals (x-scale) and average $K_3$ value for that interval (y-scale) for longitudinal and lateral sections at the Lainbach. Notice resemblance of lines up to $K_3$ (80).

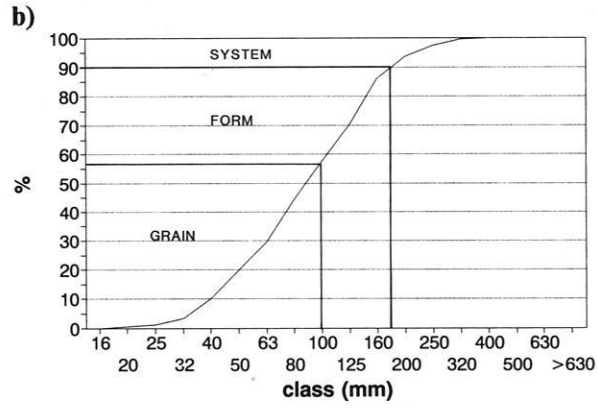


**Fig. 6.38 b)** Photo-sieved cumulative grain size distribution in the Schmiedlaine, 1992. The transitions from grain to form roughness lie at $D_{56}$ for long and cross-profile and from form to system roughness lie at $D_{90}$ for both.

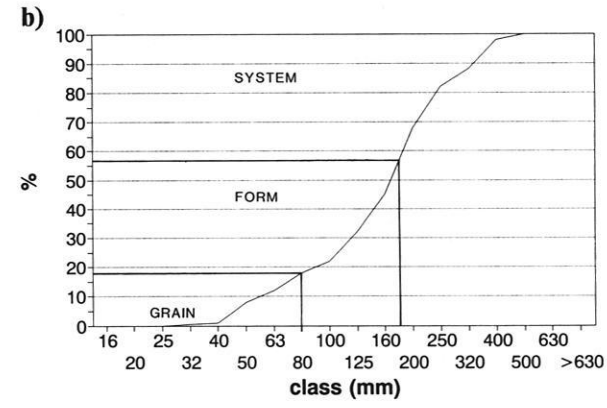


**Fig. 6.39 b)** Photo-sieved cumulative grain size distribution at Lainbach, 1992. The transitions from grain to form roughness lie at $D_{10}$, $D_{40}$ and $D_{40}$ for the channel cross, channel and bar long profiles respectively and the form/system transition lies at $D_{65}$.

Squaw Creek, the cross-sectional line rises more gently than the long profile. This interval marks the dominance of the overall gradient of the reach in the long profile and does not show up in the cross-sectional relationship since the gradient is not as pronounced in the lateral, and also due to the lateral limitation of the gravel bar. If the dimensions of the gravel bar were larger, the last 3-4 m $K_3$ intervals would be measurably higher and more representative. In addition, the $K_3$ measurements were limited to the bar. Had they been continued through the channel, higher ranges in gradient could have been incorporated into the relationship. This may have changed the relationship between the long and cross-

profile such that the cross-profile would have been more parallel to the long profile.

#### 6.1.5.3 Lainbach

At the Lainbach, the cross-sectional relationship rises more steeply than the longitudinal in the higher intervals, as was the case at Squaw Creek (Fig. 6.39a). Both the channel and bar long profiles assumed very parallel patterns. Up to a $K_3$ of (20), the cross-section and two long profiles run parallel, with the cross-sectional relationship lying exactly between the channel and bar long-profile. After the grain/form transition for the long profile of the channel and bar at $K_3$ (20), equivalent to a $D_{18}$ (Fig. 6.39 b), the relationships fluctuate parallel to each other up to the form/system transition. This transition lies at $K_3$ (100) for the channel long profile and for the bar long profile, equivalent to a $D_{20}$ and $D_{56}$ respectively. In contrast, the cross-profile does not assume its grain to form transition up to a $K_3$ of (60) or $D_{50}$ but assumes its form to system transition at $K_3$ (70) as for the channel ($D_{56}$). The reason for the difference in the cross-sectional behaviour of fractal intervals lies in the fact that the cross-sectional geometry is subject to more rapid changes in geometry over short space than the long profiles (Fig. 6.33). At the macro-Tausendfüssler site in the Lainbach, temporal measurements of roughness and geometry were also carried out at 10 cm intervals. As indicated by the fractal analysis, the $K_3$ (10) also marks grain roughness just below its transition to form roughness, at $K_3$ (20).

### 6.1.6 Summary of fractal intervals of roughness

The three studies show power functions trends can be identified for increasing roughness intervals used in the fractal calculations for all three study sites. In Fig. 6.40 a) & b) the roughness and grain size information for bar cross-sections in all three study areas has been summarised in a single plot. Fractal trends are similar both for the longitudinal and the lateral roughness

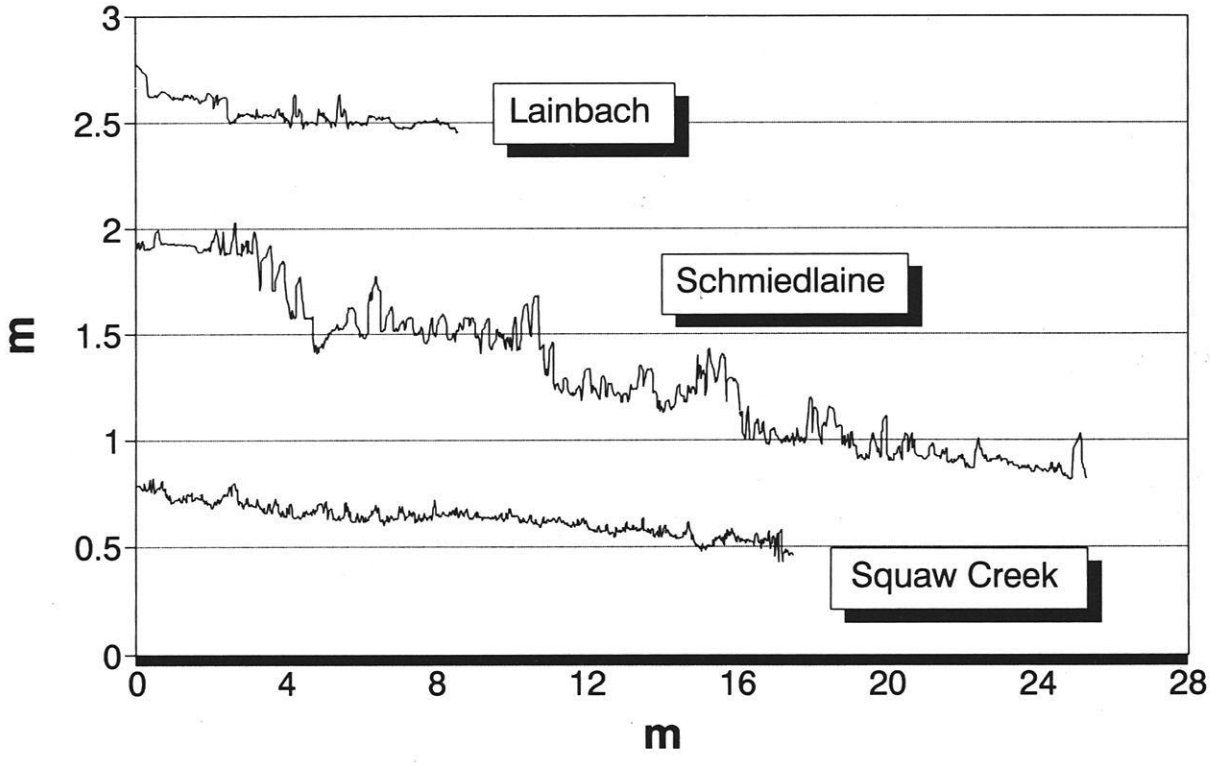


**Fig. 6.40 a)** Longitudinal topographies of Squaw Creek, Schmiedlaine and Lainbach in 1992. Notice that the Lainbach has a lower gradient than the Schmiedlaine, with only a minor step. The Schmiedlaine is steep, bedform dominated and has four clearly developed steps. Squaw Creek has a comparatively low gradient and is grain dominated.

patterns on the bars. As in CLIFFORD et al. (1992) the first two breaks of slope can be identified in each case from the data in addition, the form/system roughness transition could also be identified. In the long profile a marked fractal transition exists between what can be verified as grain roughness, i.e. single particles, to form roughness i.e. cluster bedforms and finally system or river geometry roughness i.e. where gradients reflect step and pool features. Such differentiations are important since each exerts different control over flow resistance (HEY 1988).

In the cross-profile, cross-sectional geometries and channel shape dictate the pattern of the largest fractal intervals while in the long profile, the type and gradient of river system determines the outcome. Thus step-pool systems (Schmiedlaine) will judge the location and gradient of the transition between form and system roughness, whereas lower gradient reaches (Squaw Creek) will attenuate the transition.

Viewed in long profile, the scale and steepness of the transitions correspond in each case to the grain size distribution of the river in question. The spacing of the bedforms is confined within a lower and upper limit i.e. beyond the second fractal transition the bedforms evolve from an assemblage of single particles to a whole bedform. Once they reach a maximum length the second transition is traversed to give way to river geometry or the so-called gradient effects. The larger the grain size (as in the Schmiedlaine), the higher the transition between grain to form and also form to system roughness. In the Lainbach, the channel and bar long profiles have similar patterns even though they are subject to a slight lag. Thus the transition to form and system roughness occurs at a higher $K_3$ interval on the bar since it is not influenced as much by gradient as in the channel.

Not only does the example of the Schmiedlaine show that the grain size is larger but also that the overall geometries of the long profile are subject to greater height differences. Thus the larger bedforms in the form category will already be influenced by the effects of gradient which is essential in determining the type of river system that develops. Smaller grain sizes, homogeneity of material and general low gradient at Squaw Creek explain the sudden jump at $K_3$ (20) followed by the unusual hump. At Squaw Creek, form roughness presented by clusters ($K_3$ 20-100) is not as dependent on the overall gradient as in the

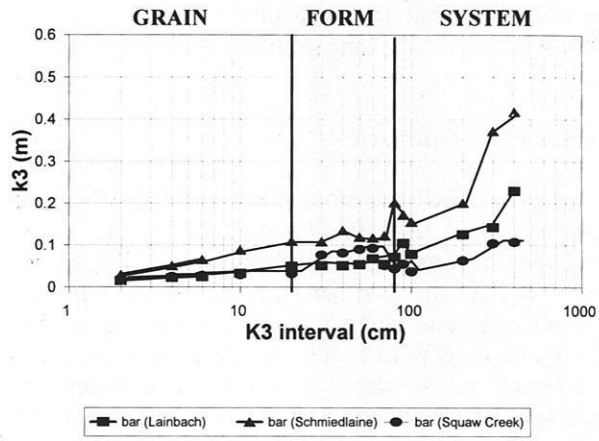


**Fig. 6.40 b)** Log-normal relationship between $K_3$ intervals and average $K_3$ value for longitudinal profiles at all three study areas. Notice resemblance between the Lainbach and its tributary Schmiedlaine with a slight lag.Schmiedlaine.

Schmiedlaine. Because bedforms are better adapted to the overall reach in the Schmiedlaine and Lainbach, the transition from grain to form roughness is smoother. There are determinable thresholds for roughness development (Fig. 6.40 c). If the slope and grain size can be determined accurately, then the location of the transition in the fractal intervals help answer the question of how the particles will be arranged in order to create a certain roughness type. Thus in the long profile (Fig. 6.40c), the slope can either be smooth and straight, or arranged into steps (as in the Schmiedlaine and Lainbach), or straight with roughness elements such as clusters superimposed (as at Squaw Creek). In cross-section (Fig. 6.40c), the profile can either be smooth and hemispherical, or smooth with integrated hummocks of roughness (as in the Schmiedlaine), or sub-divided into individual hummocks (as at Squaw Creek) or steeply sub-divided into individual bar and channel segments (as in the Lainbach).

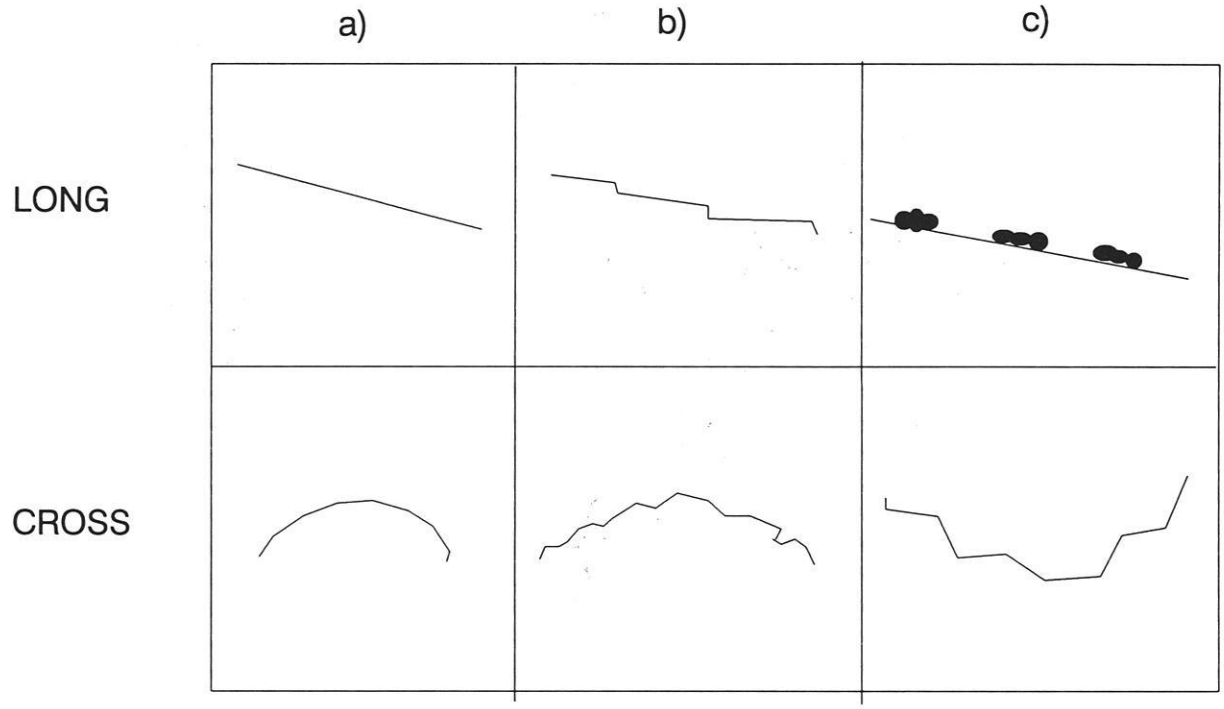


**Fig. 6.40 c)** Thresholds in cross-sectional and longitudinal gradient and shape from a) smooth, to b) stepped or form dominated (as in the Schmiedlaine to c) grain dominated in the long profile and stepped cross-section in the cross profile).

The application of the fractal intervals and associated transition thresholds are diverse but they should be used to describe roughness. Choosing an optimal sampling interval for measuring profiles has been indicated as a problem by FURBISH (1987). Since the sampling interval depends on the distribution of particle size and arrangement, it should be determined separately from fractal analyses for each fluvial reach in question. Thus each river bed will be subject to a different roughness type, allowing an optimal roughness interval to be selected by differentiating grain, form or system roughness (see Table 6.1).

**Table 6.1** Thresholds between grain, form and system roughness for all three study areas.

| Study site | Grain/form roughness (cm) | Form/system roughness (cm) | $D_x$ Grain/form | $D_x$ Form/system |
|---|---|---|---|---|
| **Squaw Creek** | $K_3$ (10) | $K_3$ (80) | $D_{40}$ | $D_{100}$ |
| **Lainbach** | $K_3$ (20) | $K_3$ (100) | $D_{18}$ | $D_{56}$ |
| **Schmiedlaine** | $K_3$ (20) | $K_3$ (100) | $D_{56}$ | $D_{90}$ |

## 6.1.7 The spatial variability of form and system roughness

This study of the spatial variability of roughness types according to channel form is based on an extensive geodetic survey with 50 cross-sections within a 2 km reach of the Schmiedlaine together with field observation and oblique aerial photography (Fig. 6.41 & 6.42). The importance of the spatial variation in bed surface texture in relation to channel form and topography was stressed by LEOPOLD and WOLMAN (1957). If energy slopes and roughness are not consistent from reach to reach, then the associated bedforms and grain sizes they encompass should vary too (BRIDGE & JARVIS 1982). But it is precisely this detailed differentiation of bedforms in the form-to-system roughness transition that is often inadequately described in the literature. For example MILNE (1982a&b), KELLER and MELHORNE (1978) and RICHARDS (1978) concentrate on the spacing of riffles, pools and point bars. None of these studies examines the grain, form or system roughness in the extremely coarse-grained and steep gradient streams characteristic of the Alpine streams. Interactions between grain size, channel and valley geometry, longitudinal gradients and flow hydraulics are all indicative of the type of bedform produced in coarse-grained streams. These characteristics need to be linked to the river bed at a reach scale, both longitudinally and cross-sectionally. A clear distinction is necessary between the bedform producing effects of cross-sectional and longitudinal geometry. The long profile has to be seen in terms of long term river bed development, whereas the cross-sections often reflect the short term dynamics (ANDREWS 1979).

Changes in bedform types must be related to the hydraulic geometry. The changing downstream relationship between width and depth fundamentally influences the sedimentary deposition (SCHUMM

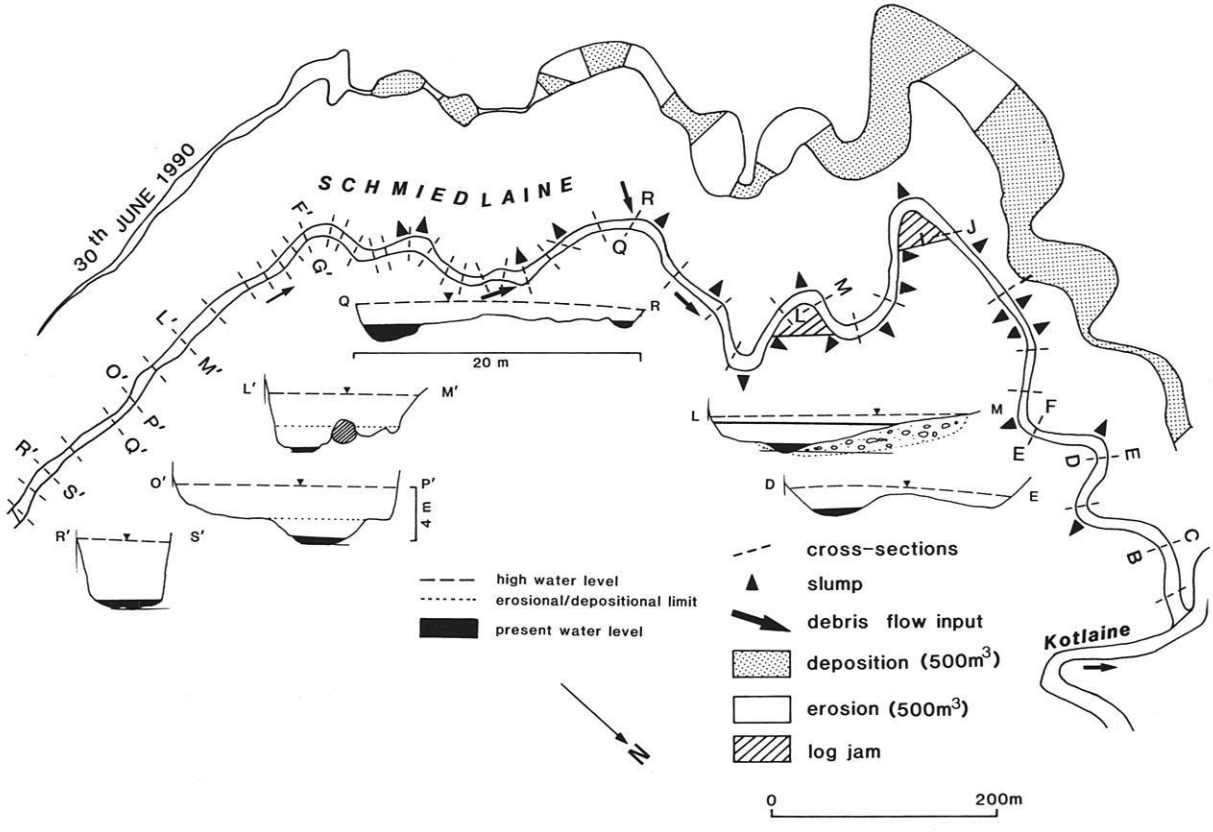


**Fig. 6.41** Detailed geomorphological map of the Schmiedlaine, indicating the three main types of reaches (straight, upper bedrock reach up to FG, meandering reach up to IJ and braided lower reach), the location of the debris flow inputs and resulting log jams. The volumes of sediment erosion and deposition mobilized during the exceptional flood of 30th June 1990 (R.I. 150 yrs) are marked as a ribbon above the reach. Corresponding examples of cross-sections marking "typical" reaches with associated maximum water levels during flows are also indicated.

1960). This behaviour can be seen at the Schmiedlaine. The hydraulic geometry changes from low to high width to depth ratio with distance downstream and the channel shape changes from symmetrical to very asymmetrical (Fig. 6.41). In the very wide meanders of the medial to lower reaches there is a tendency for a double symmetry to develop (DE JONG 1992 d). In this case the upper reach geometry is bedrock controlled. Since this upper reach is mainly erosional, bed roughness and geometry will usually consist of single "grain" roughness (see Section 6.1.5) or very large channel filling boulders, as in cross-section L'M' in Fig. 6.41. In the lower reaches, form and system (unit) roughness dominate i.e. the channel bed consists of complex bedforms, mostly depositional in nature. In the upper reaches, erosion is far more effective since scour is possible to a greater depth with a small rise in stage. Due to the higher width to depth ratios in the lower reaches, velocity has far more impact on the channel bed. The response to this process is the development of bedforms. The subsequent discussion will focus mainly on the case study of the Schmiedlaine which is characteristic of a natural mountain stream without check-dams (unlike the Lainbach) with the widest range of gradient, curvature and sedimentary material. Unlike the examples cited in the literature, the Schmiedlaine is valley-bedrock confined. As a result, bedform development is clearly controlled by sediment and hydraulic characteristics, and spatial, rather than temporal changes in planform. The Schmiedlaine also has a more extensive record of data since it was monitored over a three year period. At the beginning of the data collection period there was an extreme flood event with an approximate 150 year recurrence interval occurred (DE JONG 1992b). Although average flood discharges only attain 5 $m^3s^{-1}$, this rare event had an estimated peak discharge of 75 $m^3s^{-1}$. A detailed survey of a 2 km stretch of the Schmiedlaine enabled hydraulic geometries and average flood velocities to be reconstructed. Many of the subsequent changes in geometry and roughness during the first year relate to the readjustment of the stream after the extreme event.

Examples of form roughness range from various types of clusters (imbricate, two particle, diamond arrangements, complex clusters, multiple obstacle clusters, transverse ribs, megaclusters and cobble berms). System roughness elements observed and discussed include re-attachment bars, and normal bars, step-pools, and log jams. Sediment availability is controlled both by upstream inputs, local inputs of sediment from the slopes and inputs from long term immobile sedimentary deposits from large floods. The stable bedrock curvature induces a cross-sectional symmetry that significantly influences the river bed morphology. Thus the local bedrock controls the roughness of the river bed more than traditional processes thought to produce rhythmical sequences of steps and pools (KELLER and MELHORNE 1978).

The Schmiedlaine case study is quite unique. In contrast to KELLER and MELHORNE's (1978) work, the development and spacing of the morphology at the Schmiedlaine is also dependent on local sediment inputs, which dictate grain size. The main pre-requisite for bedform development is the degree of bend curvature. MILNE (1982) discovered that there was at least one step-pool sequence in bends longer than 10-14 channel widths. Such regularities are hard to find in the Schmiedlaine where local residual grain size distributions introduced by hyperconcentrated flow and debris flow, and influence bedform development, i.e. debris flow end-lobes and log-jams. Examples will be compared, where possible, to the Lainbach confluence and the less variable Squaw Creek. Where possible, the nature of these different types of roughness will be discussed in the light of their hydraulics. ALLEN (1983) observed that form roughness depends on the size, shape and spacing of bed waves but this direct relationship has not been explored much further for natural channels.

### 6.1.7.1 Form roughness

The form roughness that will be described in the following sections has to be considered as part of a hierarchy of bedforms (ALLEN 1968) where clusters are superimposed on the bar, transverse ribs in the channel and complex clusters form part of cobble berms and megaclusters are components of log jams. Form roughness has been separated into individual classes of clusters/transverse ribs since they are an important reflection of individual flow and sediment transport "streets" where the accumulation of bedforms into system (unit) roughness does not grow homogeneously (BAGNOLD 1956).

#### *6.1.7.1.1 Imbricate clusters*

Imbricate clusters are particle assemblages (BRAYSHAW et al 1984, BRAYSHAW 1987, LARONNE and CARSON 1976, BILLI 1988, REID et al 1992, HASSAN and REID 1990) three or more particles in length. These features form as single, highly imbricated longitudinal threads. They need not to consist of the largest material on the bar, even though this is predominantly the case. The imbricate clusters are differentiated in terms of shape, number and arrangement of particles. In steep reaches such as in the Schmiedlaine, their angle of stacking may be vertical (Fig. 6.42). In such cases particles will be

a)

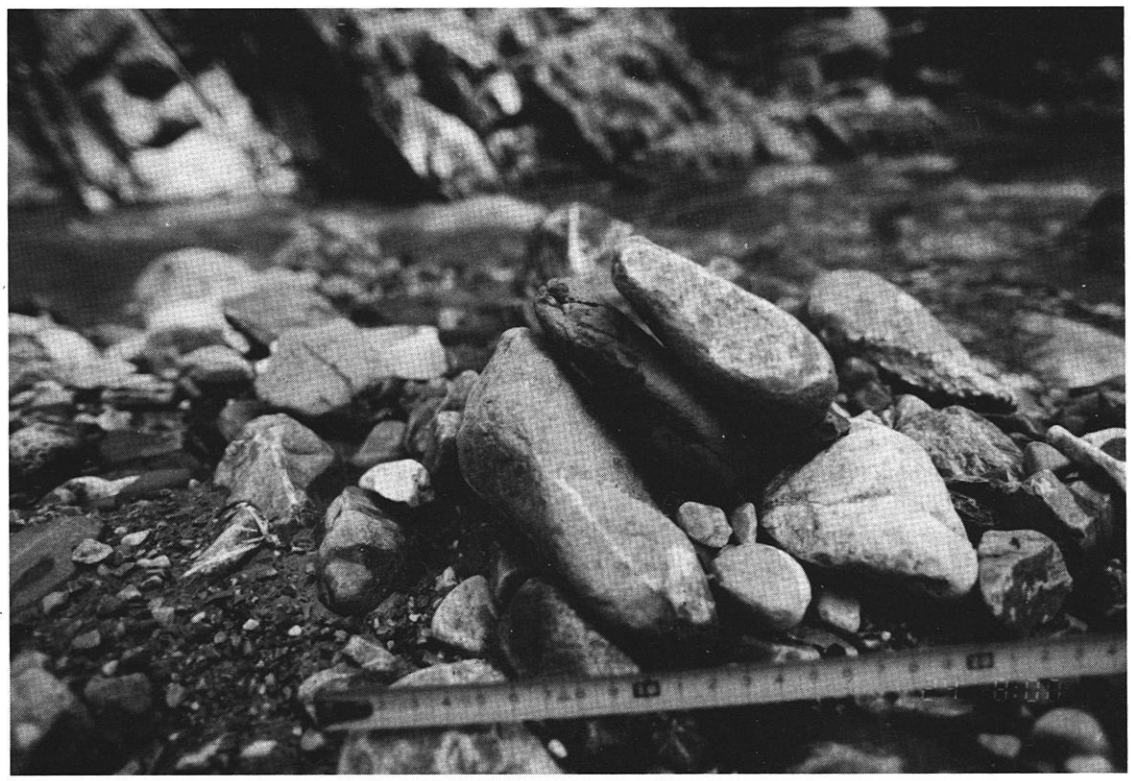

b)

**Fig. 6.42** Examples of typical imbricate clusters in the Schmiedlaine **a)** in dry channel on bar, reach above EF (see Fig. 6.41) in 1990, flow from R. to L. and **b)** in dry channel on bar, reach above IJ in 1992, flow from R. to L, **c)** in section, at channel edge, at DE in 1992, flow from L. to R. and **d)** same cluster as in c) in plan view.

c)

d)

a)

b)

**Fig. 6.43** Two-particle cluster on bar in Lainbach (see Fig. 6.44). Flow is from R. to L. **a)** in section & **b)** in plan & **c)** schematically. Note particle behind large rounded obstacle has a streamlined surface.

c)

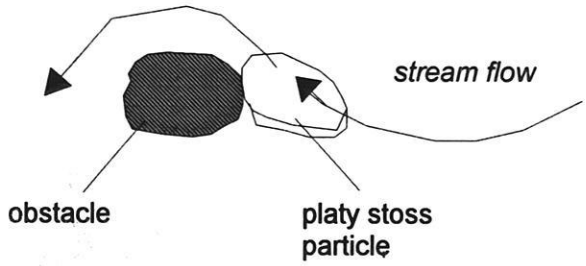


deposited behind over-sized obstacle clasts and are usually limited to 6 or fewer particles in length. Such clusters will be found as separate entities on the bar top (Fig. 6.42 a&b) or along the bar edge (HASSAN et al 1990 and Fig. 6.42 c&d). In the Schmiedlaine, they are also located in medial positions in the secondary channels that are active during high flows in the medial to lower reaches of the Schmiedlaine. This is true for small as well as mega-sized clusters. Imbricate clusters are well adapted to flow such that their ellipsoidal shapes in plan and in cross-section offer little resistance to flow (section 6.2).

They form a roughness entity that is streamlined. The semi-ellipsoidal form offers less resistance to flow than a random assemblage of single, open-bed clasts. These types of clusters occur in many environments and were found in the Schmiedlaine, Lainbach and at Squaw Creek (Fig. 6.42). They typically form in active flow regions. Further examples of typical imbricate cluster in the active channel from both Squaw Creek and Schmiedlaine are given in Fig. 6.55a-e), section 6.2.

These clusters are delicately arranged with large voids underneath the material. During floods this may induce more turbulence and lift force between the clasts. In the Schmiedlaine as at Squaw Creek and in the Lainbach, freshly deposited bar areas recently uncovered after the occurrence of a flood were densely covered with imbricate clusters, particularly at the proximal parts of the bar. Since this upper part of the bar is also usually the coarsest, this means that there will be particularly numerous particles eligible for cluster formation. As was pointed out in the previous section, the grain size distribution showed that clusters constitute the coarsest fraction of river bed.

From detailed flow orientation studies on the test bar (6.2) it was shown that flow was significantly reflected off the bedrock bend and was forced diagonally across the channel. The coarse bedforms did not follow this pattern but rather were deposited along the low energy routes during the waning flow stages. Observations and measurements suggest that the entire bar surfaces will be deposited during high flow or results from local erosion at that stage, whereas a coarse lag of material composed of clusters and similar bedforms must be deposited towards the final stage of the flood. Evidence for cluster formation during the final flood phase comes from monitoring at the Tausendfüssler bridges in the Lainbach (6.4).

#### *6.1.7.1.2 Two-particle clusters*

These occur very frequently on the finer-grained river bed, mostly in conjunction with larger particles (Fig. 6.43). They are found on most gravel bars and could possibly be immature clusters. It is noteworthy that the stoss-side clast behind the very rounded obstacle usually covers the same area but is far more platy, thus decreasing the chance for any smaller particles to be deposited behind it. At Squaw Creek and at Lainbach, these are predominant on the proximal bar tops. In the Schmiedlaine these are less frequent, restricted to low gradient reaches also since the wide variety of angular material increases the chance that longer clusters will form. Notice that in Fig. 6.43, the shape of the overall cluster is optimally adapted to flow by offering least friction. An odd-shaped or oversized stoss side particle would most probably be subject to lift forces (ERGENZINGER and JÜPNER 1992) and would be entrained by the flow. It is therefore important for the second particle to be well interlocked with the obstacle clast.

*6.1.7.1.3 Diamond arrangement of clusters*

This term has been given to the distinct diamond pattern in which imbricate or two-obstacle clusters are arranged. The pattern typically occurs on bars in a straight reach (Fig. 6.44). This type of arrangement is found only on those bars that are covered by shallow flows during floods. Thus at Squaw Creek as well as in the Schmiedlaine, clusters are not arranged directly downstream of one another. Instead, clusters are located at the right and left downstream extremities of the cluster. In the zone below the cluster the wake zone turbulence probably inhibit the direct deposition of another bedform. Diamond cluster arrangement can take on various shapes, depending on the bar gradient and shape diversity of material. As is suggested by HASSAN & REID (1990) and explained below, their spacing is an equilibrium spacing.

At Squaw Creek, the lattice-like arrangement of bedforms formed as a result of transverse and longitudinal rows of particles joining into rings. Similar ring-like diamond patterns of clusters have been produced independently in coarse-grained laboratory experiments (TAIT and WILLETTS 1992, ALLEN 1982a). Each rhomboid looks like an elongated diamond (TAIT 1993, ALLEN 1982b). Other authors have termed them stone cells (McDONALD and BANJEREE 1971, GUSTAVSON 1974) which are thought to be related to shallow flow depths. ALLEN (1982a) indicates that rhomboidal surface waves responsible for diamond cluster formation will only form at Froude numbers above 1, but he restricts his observations to sand beds and muddy beaches. KARCZ (1981) explains how obstacle-induced oblique hydraulic jumps cause the formation of rhomboidal patterns, where wave trains are refracted by an obstacle across the stream path. Centrifugal components distort the hydrostatic pressure distribution three-dimensionally so that a secondary motion causes the longitudinal acceleration of fluid and the production of the diamond pattern. Although previously described for gravel beds, the rhomboidal lattice structure of clusters can be attributed to the regular criss-crossing streamlines formed during the descending flood limb at the Lainbach and at Squaw Creek or other generally low gradient bar tops in the low energy zones between the bends of the Schmiedlaine. Their tendency to form in shallow water, on gently sloping bar surfaces with smaller, more rounded grain sizes is suggested by their existence at Squaw Creek on the old bar and from laboratory experiments (TAIT, 1993, pers comm). The large grain sizes and angular shapes, which cause particle stacking rather than flat, end-to-end arrangements, probably inhibit their formation in the Schmiedlaine. In the Schmiedlaine, clusters were mainly of the imbricate type arranged as separate entitie i.e. in an unjoined diamond pattern.

The diagonal separation of flow lines can vary according to the obstacle size and shape. Thus downstream of the re-attachment zone along the centre-line of the plain cluster obstacles, the vector

**Fig. 6.44** **a)** Diamond arrangement of clusters on a bar (right, looking upstream), with criss-crossing shear waves to the left: real-world example given by photo in the Lainbach, descending flood limb, July 23rd 1992.

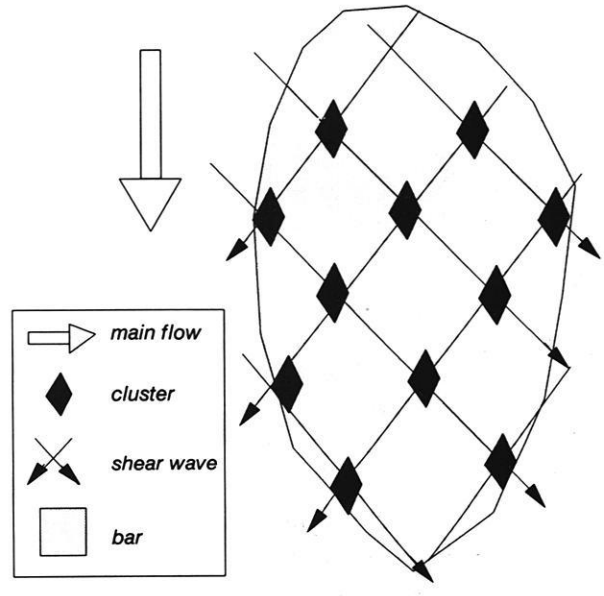


**Fig. 6.44** **b)** Model of shear wave development over gravel bar. Clusters form where shear waves intersect.

field can be divergent or erosive (PAOLA et al. 1986), (6.55 e&f, Section 6.2). Approximately one obstacle radius to either side of the centre-line, the vector field is convergent or depositional. This measure is essential in determining the location of the next cluster. Obstacles that already have a triangular tapering end could be undergoing a feedback process whereby the presence of flow interference due to their own shape will cause further extension of the interference zone (i.e. an erosive von Karman vortex street). In this case the distance to the next cluster would be even longer, since the obstacle has a larger erosive interference zone. Since the obstacle and associated cluster will not always induce an erosive effect (DE JONG 1992a), the diamond pattern in nature can be distorted. Thus where the obstacle lies transverse to flow, the wake zone will have the depositional characteristics widely cited in the literature (e.g. BRAYSHAW 1984). The influence of obstacle shape is shown in 6.55 e&f, Section 6.2.

In the literature the fundamentals of cluster deposition have not been clearly explained. If an obstacle is already located in a particular manner, one can attempt to predict where the next obstacles will be located. What is lacking to solve this problem is an explanation for the deposition of large, bedform pattern inducing obstacles in the first place. For this, shear waves have to be present so that the depositional environment can be predetermined. From photographic observations of the shallow water surface (< 10 cm) during the descending limb of a flood and from longitudinal measurements of the corresponding re-establishment of roughness elements, it is clear that shear waves are necessary for the deposition of cluster obstacles under the given sub-critical flow conditions.

HODGES (1982) has described shear waves or rhomboidal flow on slopes. These shear flowing diagonally towards one another and crossing each other at nodal points such that a diamond pattern is induced. At the intersection point, the flow velocities are reduced, thereby enabling an obstacle to become stranded. Once stranded, the obstacle determines the location of the next shear wave intersection point necessary for subsequent obstacle deposition. HODGES (1982) attributed them to the flow recessional stage, where Froude numbers were sub-critical. In contrast ALLEN (1982) attributed shear waves to super-critical flows. Temporal measurements of roughness change in relation to flow velocity and river geometry on the bar in the Lainbach and at Squaw Creek also indicate that Froude numbers have to be < 1 for the formation of shear waves. The braided structure of flow is dominant on gently sloping surfaces, explaining why they should form on the bar surfaces. Flow competence and capacity are influenced by flow depth and velocity to permit coarse sediment to settle in a diamond pattern.

Shear waves do not need to be stationary but can wander according to the movement of isolated sedimentary particles. Comparisons with flume experiments under steady flow (LAWRENCE 1987) showed that when under super-critical conditions a hydraulic jump exists over an obstacle and an obstruction is put into the flow above the obstacle, the hydraulic jump will move upstream of the obstacle and remain there even if the obstruction is removed. This shows that a temporary flow disturbance will suffice to produce a longer lasting shear wave effect even in the absence of obstacles.

*6.1.7.1.4 Complex clusters*

In contrast to the imbricate clusters, complex clusters are quite chaotic in arrangement and can be likened to a proto-bar form that is dome shaped in cross-section. They protrude higher into the flow than imbricate clusters and are also more than one particle in width. In many cases clusters have the same number of particles in length as in width (5:5) and usually consist of the same size of particles. In totality they may also be oval in shape and usually consist of the coarsest clasts on the bar, and protrude above the general bar level. Sometimes they consist of an outer wall of coarser clasts with an infill of finer material (6.45) The coarse cobble berms described in the Schmiedlaine (section 6.1.5.7, this chapter) consist almost solely of an assemblage of these clusters. These are located primarily in the sharp river bends where channel width is not restricted, i.e. in the medial to lower reaches. Specific locations include MO, KL, EF

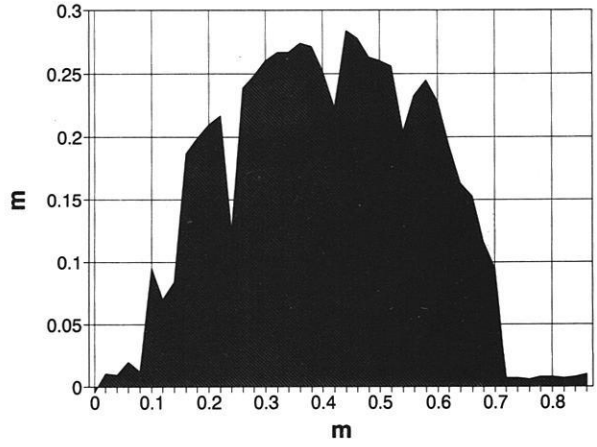


**Fig. 6.45** Mini-Tausendfüssler cross-profile of a complex cluster in the Schmiedlaine (1991).

a)

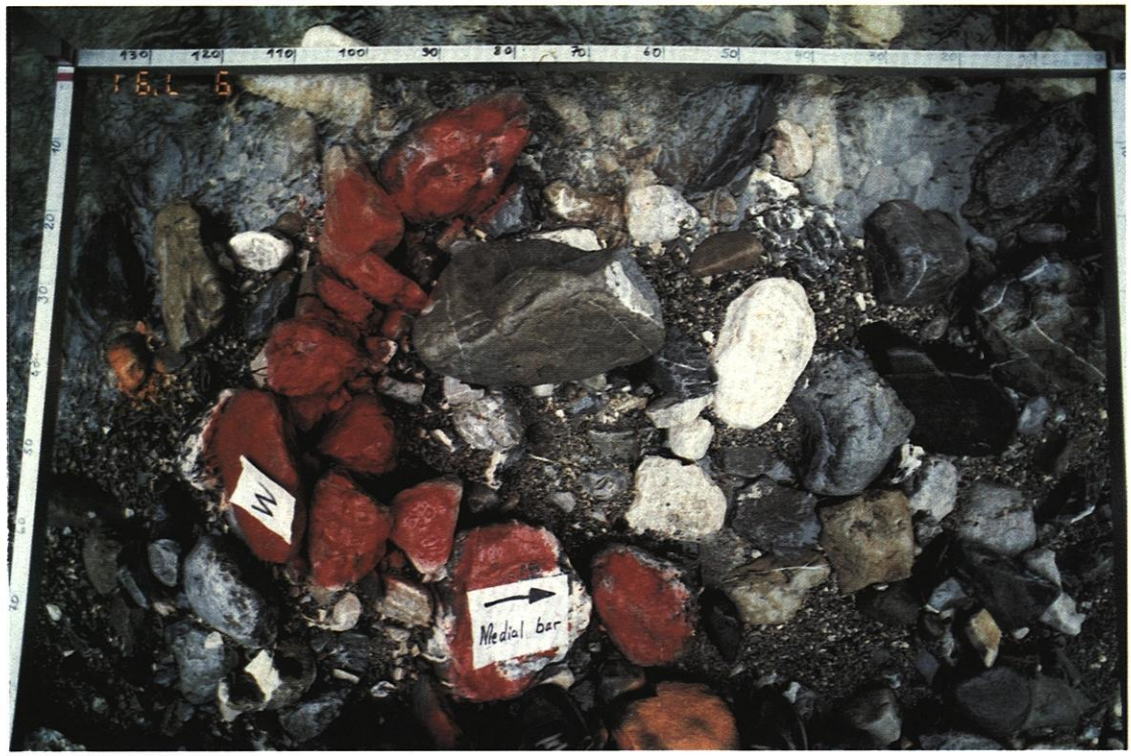


b)

**Fig. 6.46** Multiple obstacle clast in Schmiedlaine **a)** photo in plan, 1991, upper test bar and **b)** oblique photo, reach (two sections below QR, **c)** sketch (in plan) of cluster in b). Numbers are in hypothesised order of deposition.

and CD. They require high gradients (approx. 4%) and are located exclusively in the outer regions of high curvature bends.

*6.1.7.1.5 Multiple-obstacle clusters*

These anabranching, fork-shaped clusters consist of two to three rows of pebbles each locked against an obstacle clast and growing upstream towards a mutual assemblage of particles (Fig. 6.46 a, b & c). The location of the cluster in Fig. 6.46 can be refound in Fig. 6.41, mid-channel, lower part of reach e.g. at PQ and CD, in the outer bend just below the bend apex. These types of clusters were found during all years in the Schmiedlaine. It is not yet clear whether these features develop in an upstream or downstream direction. In sandy media, a single obstacle can actually cause a series of ridges to form downstream of it (KARCZ 1968).

The forks develop where very coarse material is present (> 20 cm b-axis) and where there are steep lateral bar gradients. These clusters are typically found in the active part of the channel, i.e. a further development of imbricate clusters, in the erosional part of the reach. The angle between two obstacle-induced rows of particles may attain more than 90° (Fig. 6.46a). Thus at the test bar in the Schmiedlaine, depositional cobble berms just at the beginning of the bend towards its outer edge. In the reach below, the multiple-obstacle clusters were found above the debris flow input at QR (Fig. 6.41), a two-obstacle cluster was also located in the active, erosional part of the channel. The very wide angle of division between the two rows of particles may characterise the initial stages of arcuate transverse ridge formation. Such dynamically formed bedforms are therefore restricted to high energy zones or zones of flow concentration at the entrance and exit to bends.

c)

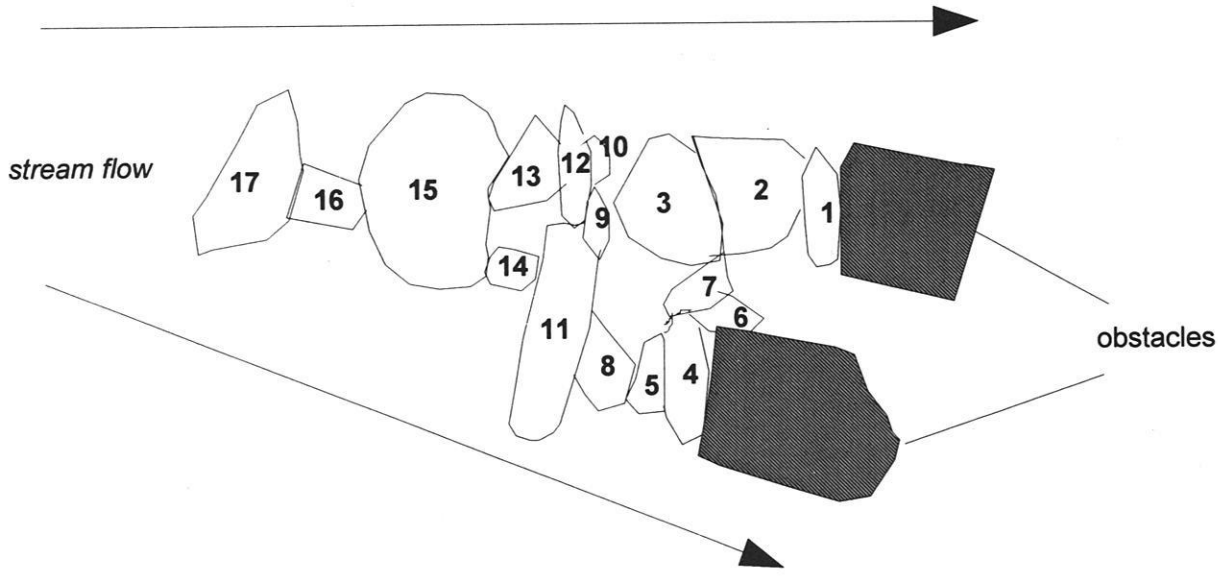

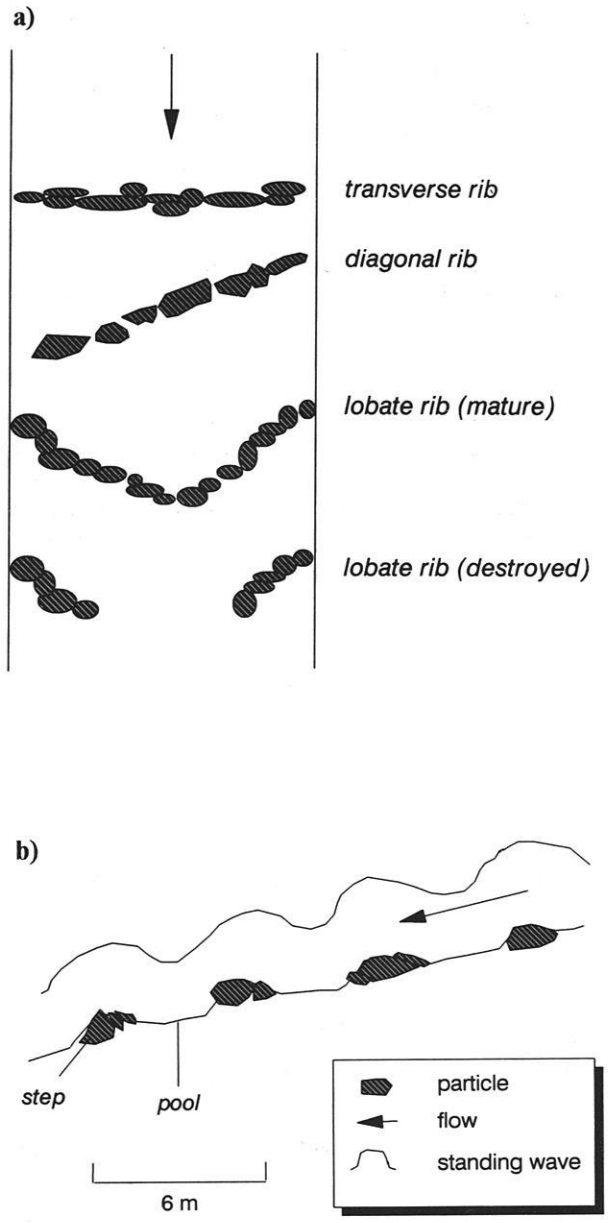


**Fig. 6.47** **a)** Pattern of formation of transverse ribs in the Schmiedlaine. **b)** in section, standing waves.

*6.1.7.1.6 Transverse ribs*

Tranverse ribs (KOSTER 1978, NADEN & BRAYSHAW 1987, McDONALD & BANJEREE 1971, BOOTHROYD & ASHLEY 1975, GUSTAVSON 1974) consist of lateral ribs of clusters. They are formed during the waning stages of flow in shallow, high energy environments indicating that they require high velocities and a high capacity of sediment transport. Transverse ribs are characteristic of low sinuosity single channel reaches with high width to depth ratios. In these cases, with the exception of work by LARONNE and CARSON (1976), transverse ribs are reported to be straight and have been restricted to glacier outwash plains where coarse ribs are found in intervening areas of silt.
In the Schmiedlaine, transverse ribs are composed entirely of coarse projecting sediment and take on four separate forms (Fig. 6.47): first, a transverse rib or minor step located perpendicular to the entire channel width, secondly a rib located diagonally across the channel, thirdly an arcuate ridge located across the channel and fourthly an arcuate ridge interrupted in mid-channel location. These bedforms are typically found at the exit to channel bends where the grain sizes are in the cobble to gravel range and flow is concentrating. Transverse ribs form preferentially in the depositional reaches; they were not found in the erosive reach. In steep and narrow channels or in the vicinity of very coarse material, transverse ribs are replaced by larger step-pool systems (Section 6.1.7.2.4).

These transverse steps are formed in areas of flow acceleration at the entrance and exit of bends, where the higher gradients allow standing waves to form. Comparisons with studies in nature (McDONALD & BANJEREE 1971) and in the flume (GRANT et al 1990) indicate a local congestion of material below standing waves may be the reason for transverse step formation. Once such a step is formed, a local standing wave develops over it and it is the amplitude of the wave that probably dictates where and in which dimensions the next step will be formed. The ribs will thus form under super-critical conditions (KOSTER 1978) which favours their occurrence on the bar tops.

Once a full standing wave is developed across the channel during the falling flood limb, a mature transverse rib will project across the entire width of the channel (Fig. 6.47a&b). In a favoured channel reach, bedforms can be found in close proximity to each other in various stages of development (see Fig. 6.47a). Incomplete transverse arcs are dissected in mid-channel location, most probably as a result of the associated higher velocities during flows superseding the event that formed them. At the entrance to pool regions between these steps flow is fully concentrated and velocities are high causing scour beneath the wave trough. The next transverse rib will thus be deposited under the succeeding standing wave. Depending on the channel configuration and plan form, different types of transverse ribs will be capable of forming. Thus where the channel is starting to curve into the bend, transverse ribs may extend

diagonally across the channel (Fig. 6.47). In other reaches where the channel is incised more deeply, the rib does not form straight across the channel but is deposited in a semi-circle which points downstream.

#### *6.1.7.1.7 Megaclusters*

Megaclusters are outsized clusters on bar tops (Fig. 6.48a&b). They are so large that they can constitute part of system roughness in the upper reaches of the Schmiedlaine. Megaclusters are dependent on local sediment supply inputs from slopes, e.g. debris flows. The particles constituting megaclusters can only be transported for short distances only. Megaclusters are depositional features and ironically they are often isolated towards the end of the bar. This was even the case at Squaw Creek, where the smoothly decreasing roughness distribution in the long profile was interrupted by the single, large cluster at the distal end of the bar. In this case flow from the main channel flooding the bar during high flow could have induced deposition. On the Schmiedlaine test bar, at CD (Fig. 6.41), the single very large cluster at the distal end of the bar, just prior to the entrance of the next bend, also formed the roughest feature on the bar.

The best example of a megacluster (Fig. 6.48b) is one km further upstream, in the reach below the influence of a debris input reach (Fig. 6.41), two cross-sections below the debris input arrow at QR. This three-metre-long cluster is not directly positioned on the proximal bar but in a large dry channel on the medial bar (Fig. 6.48c). The bar has an average gradient of approximately 5° and in this case the cluster has a major influence on flow divergence. In terms of flow direction, these types of mega-forms take on the most direct flow routes (See section 6.2). The considerable mobility of these out-sized boulders seems to be related to the very large momentum achieved. A specific process is probably responsible for the concentration of the bar's largest particles into clusters in the same position (Fig. 6.48b). The obstacle clast is again the main determinant of the shape and size of cluster formed. The obstacle probably induces super-critical flow (ZGHEIB 1990) which through vertical and horizontal energy dissipation dictates the further development of the bedform. Other types of megaclusters in the very steep medial to upper reaches of the Schmiedlaine (Fig. 6.48a) show how prone large clasts are to location-specific accumulation. Clusters, controlled by the obstacle, therefore play an important function in river bed sorting and local increases in roughness.

**Fig. 6.48 a)** Photo of megacluster in steep reach above L'M', Schmiedlaine (arm for scale). **b)** Photo of megacluster in the Schmiedlaine, reach QR. (3 m in length), **c)** Geomorphological sketch of reach below QR with megacluster. Arrows indicate flow directions.

b)

c)

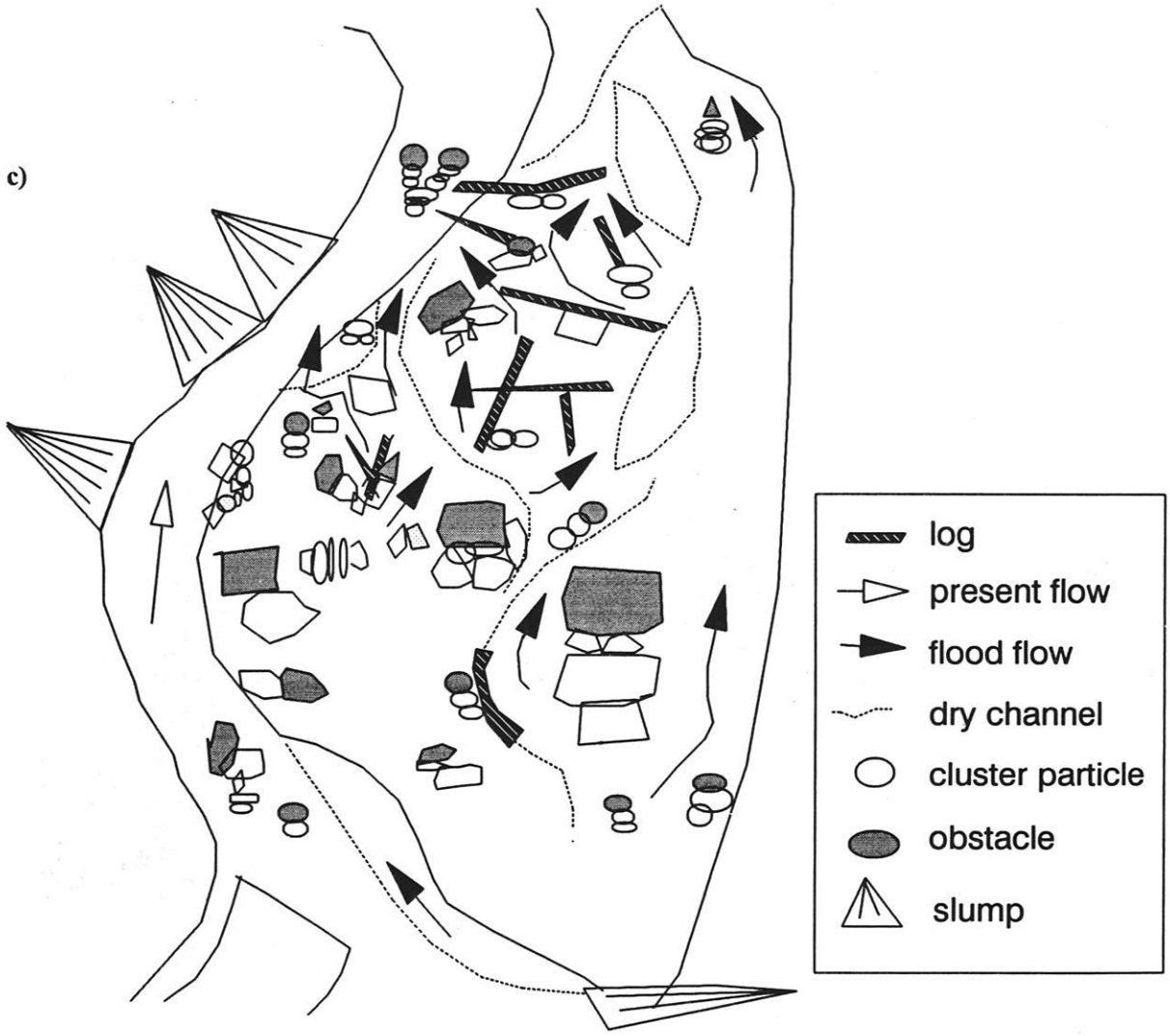
log
present flow
flood flow
dry channel
cluster particle
obstacle
slump

### 6.1.7.2 System roughness

#### *6.1.7.2.1 Cobble berms*

Cobble berms are features that are the result of an accumulation of complex clusters into arch-shaped, levee-like structures (Fig. 6.49). Their formation can be likened to those of boulder berms (CARLING 1989). In flume experiments boulder berms form under unsteady supercritical conditions and are rapidly deposited independent of sediment transport rates. From evidence gathered in the Schmiedlaine (Fig. 6.49a&b) they form as a result of sequential outer channel deposition of arch-shaped levees. Their occurrence is frequent in the very steep, high curvature bends of the Schmiedlaine (Fig. 6.41) such as at the test bar, reach CD, at NO and NM (below LM).

Since cobble berms are related to the shape of the outer bend they are not found at Squaw Creek. The coarse cobble berm in the Schmiedlaine persisted from 1991 to 1992. In 1990 similar cobble berms were located at the edge of secondary channels. Therefore it was assumed that these probably mark a recessional stage of river bed formation. The deposition of these arcuate bedforms is dependent on the radius of curvature of the flow in the bend which in turn is a function of the discharge during a single discharge event (Fig. 6.49). At high discharge, photographic documentation shows that flow will be fully developed across the channel but as it recedes, the first cobble berm will be deposited at the very outer edge of the channel. As flow recedes further, the next cobble berm in the series will be deposited adjacent to the first. This process continues three or four times until flow has retreated to its former channel limits. From detailed grain size analyses on the Schmiedlaine test bar and from photographic observations further upstream, it is evident that there is a size gradation from the outer towards the inner bend. This is not surprising since the coarsest sediment is expected to be deposited under high discharge in the outer bend, and finer material will be deposited subsequently as the energy gradient declines with falling discharge.

Due to the shape of the channel in the Schmiedlaine and the difference in water depths, it is not possible for these features to form by mid-channel flow separation. The sequential deposition of the berms ensures a smooth hydraulic transition during the waning stages of the flood. Thus according to CARLING (1989), the berms are the result of a minimisation of energy during high flow. The assertions by CARLING that sediment transport does not constitute an efficient input into their formation is probably due to the limitations of flume experiments. Although these cobble berms are stage and discharge dependent, this does not exclude the role of sediment entrainment. Sediment transport cannot occur in the first place without submergence. The gradual deposition of the sequences of berms away from the outer bend into the main stream indicates that not only discharge but also the sediment transporting capacity must be decreasing rapidly.

#### *6.1.7.2.2 Re-attachment bar*

The only extensive description of a re-attachment bar is by RUBIN et al (1990). They are narrow, elongated depositional features that are located within the channel expansion zone where a weak recirculation current developed. Although described in a larger scale study treating finer grain sizes, their formation in the outer bend where flow is beginning to expand can also be applied to the Schmiedlaine. Re-attachment bars are the same scale as cobble berms. As in the case of cobble berms, re-attachment bars consist entirely of complex and imbricate clusters. They are different from cobble berms in that they form in very narrow bends and are attached by one end to a bedrock spur. Cobble berms are not attached to bedrock spurs. This type of feature is dependent on valley curvature. Where the radius of curvature is very small, as in the case at cross-section DE, the depositional zone is so compressed that the narrow, elongate re-attachment bar is formed.

#### *6.1.7.2.3 Step-pools*

Step pool systems are found in steep, coarse-grained environments (WHITTAKER and JAEGGI 1982, CHIN 1989, ERGENZINGER 1990, ERGENZINGER 1992, GRANT 1990) and have been classified in the Literature Review more extensively.

Step-pools are not directly comparable to the more wide-spread riffle pool sequences due to the difference in grain size and the associated differences in erosion and deposition processes. In the Schmiedlaine, step and pool units are mostly found in the straight reaches or at the entrance and exit to the bend, not in the bend apices. They are found throughout the upper and medial reaches where grain sizes are large and the channel is steep. Exceptionally large steps are generally found in the higher gradient channel bends where there is higher probability of coarse sediment deposition or direct slope inputs. Steps are therefore asymmetrical in cross-profile, whilst pools are generally more symmetrical and developed in the straighter reaches. This stands in contrast to the riffle-pool patterns observed by KELLER and MELHORN (1978) and MILNE (1982).

a)

b)

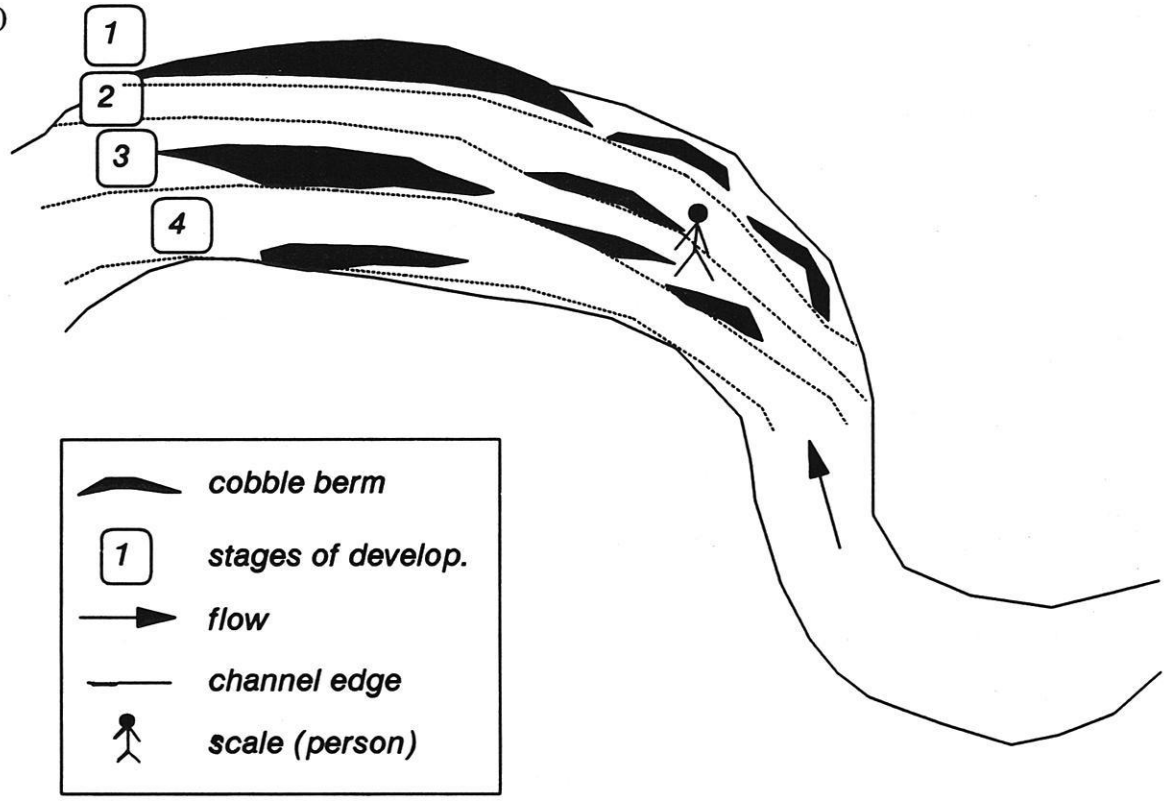


**Fig. 6.49** **a)** Photo of sequential outer bend deposition of cobble berms at reach NO (two above LM).
**b)** sketch of hypothetical formation.

The step pool patterns are not regularly spaced in the Schmiedlaine for a number of reasons. Bedforms have to be considered within their local environment since they are indeed dependent on local grain size spectrums influenced by slope inputs and longer term immobile flood deposits (GRANT et al 1990). In addition the influence of local geology interrupts regular patterns. Thus where a local input of very coarse material has been supplied into the channel, the river may be incapable of transporting it away, and steps are initiated. Since the grain size distribution is highly variable downstream (MILNE 1982b), certain locations will favour large differences in gradient and the deposition of coarse grain sizes, resulting in the formation of steps (MILNE 1982b, GRANT et al 1990).

The formation of step-pools has been attributed to processes related to standing waves just as transverse ribs are, but step pool systems are larger (GRANT et al 1990). This idea is supported by the location of step-pools within straight reaches between bends. Thus in contrast to bars, flow energies are far higher and more concentrated in the channel. Step pool formation could thus be a function of channel width, since they rarely extend into the lower energy bar zones.

The standing wave that develops over the step causes a pool to develop just downstream. In the Schmiedlaine and Lainbach, pools have been proven to be much finer-grained (ERGENZINGER & STÜVE 1989) than steps. Whereas the step and pool units will be located at regular intervals from one another, the actual distance from one step-pool sequence to the next remains highly variable and dependent on curvature. In other cases the steps will be composed of pure bedrock or other roughness elements.

It is questionable how far step-pool systems are dependent on channel pattern (LEOPOLD et al 1964, KELLER and MELHORN 1978). The 150 m long measuring reach within the Lainbach test site is nearly straight and still has a well developed step-pool system. Step pools are strong indicators of sediment-supply starvation. A large number of pools in the upper reaches of the Schmiedlaine are influenced by bedrock and the deficiency of sediment along this straight bedrock reach also explains why step-pools are predominant there. If the channel pattern does influence step-pool development, then the influence is indirect. For example there may be a greater chance of coarse material deposition in the bends and the release of large boulders into the main channel.

Experiments under natural conditions indicate that sediment transport occurs from pool to pool in the Lainbach (ERGENZINGER and STÜVE 1989), suggesting that the pools are more active than the step regions during high flows and that the step regions are actually more stable (ERGENZINGER & SCHMIDT 1990). Observations and measurement during low flows have shown that shear stress distribution is usually similar in steps and pools. Steeper steps have shallower flows which compensate for the gentler pools with higher depths. During an average flood, there is considerable difference in shear stress between step and pool areas. This could support the fact that velocity is higher in the pools than over the riffles, explaining the preferred scour in the pools and deposition of coarse material on the steps (KELLER 1971). In contrast, high flood flows have a tendency to equalize velocity in both areas, and this provides the conditions for re-shaping (ERGENZINGER and STÜVE 1989).

The longer term development of a step-pool system in the Lainbach and the Schmiedlaine was observed between 1990 and 1993. During a catastrophic flood/hyperconcentrated flow with a 150 year recurrence interval (DE JONG 1992b) most of the Lainbach and the lower reaches of the Schmiedlaine, which were formerly step-pool and became braided depositional systems. There was a general smoothing of the long profile. The long profile was straightened out due to the erosion of some steps and infill of all pools. Within only 2 weeks after the flood event, during a period of extreme re-adjustment, both the Lainbach and the Schmiedlaine started resembling a step-pool system again. This rapid re-establishment has been observed by other workers (SAWADA et al 1983, WHITTAKER & JAEGGI 1982). Step-pool formation therefore occurs after the passage of high flows and coarsening of the bed. Subsequent re-adjustment can be seen as a bed deforming process in heterogeneous material and tumbling flow (WHITTAKER & JAEGGI 1982). In the Schmiedlaine, nearly the same volumes of sediment deposited during the flood were transported away during that period. This was reconstructed from the configuration of the cross-profiles (Fig. 6.42).

For a step-pool system to develop, erosion and sediment starvation are a pre-requisite. In the Schmiedlaine and Lainbach, the starvation of sediment supply meant that the lower reaches developed higher energies due to an increase in gradient. Erosion of finer material was possible. This eventually uncovered the coarse boulders, most of which had not travelled very far and gave rise to the original step-pool system. GRANT et al (1990) similarly found that this step-pool system formed in the absence of sediment transport. High sediment

transport rates destabilised the deposition of sediment aggregations that formed candidates for step formation.

*6.1.7.2.4 Bars*

In the past bar forms have been examined primarily in sandy or gravelly meandering rivers but little attention has been given to the role that obstructions and bends play in controlling geomorphic forms in coarse-grained environments (LISLE 1986). Bars are mainly deposited in the medial to lower reaches of the Schmiedlaine where channel processes are erosionally and depositionally interactive or purely depositional. Whether a bar forms or not is dependent on the width to depth ratio. Bars develop where the ratio is high (CHANG 1980). Deposition of point bars can be directly related to bend curvature (marked as red areas on the map, Fig. 6.41). This is due to the role that sharp bends play in arresting sediment under lower energy conditions. Other reasons for bar deposition are offered by obstructions such as large, oversized boulders or bedrock promontories as in the case of the re-attachment bar, or simply a decreased energy zone related to flow expansion after a bend causing the channel to split into a braid. The role that wooden debris plays in obstructing sediment is treated separately in the section on log jams.

By visual observation and b-axes measurements at selected locations, sediment size of gravel can be linked to the radius of curvature (MILNE 1982a). Thus the largest radius of curvature exhibits the finest grain size whereas the smallest radius of curvature is related to the coarsest sediment, causing features such as log jams to develop.

Several factors control the formation of alternating bars. In addition to the varying velocities, the angle of attack (LISLE, 1986) and the radius of bend curvature is important because the interaction of flow and bend produces superelevation of water levels on one side of the channel and subelevation on the other. During the extreme flood of 30th June 1990 in the Lainbach valley (De JONG 1992b), the cross-channel difference in water level attained a gradient of up to 0.06, compared to the average 0.04 in the long profile. These extreme cross-channel gradients have very significant effects on flow trajectories and sediment transport capacities. These gradients control the extent, width and length variations of the bar forms and their variation between inner and outer bend at the Schmiedlaine. Thus in the bends, the bars are formed as a result of bend-induced secondary circulations (NELSON & SMITH 1989).

In the Schmiedlaine, the complex hydraulic geometry of the cross-sections (Fig. 6.41) causes major differences in lateral water levels during large floods (see TAKAHASHI 1991, p. 94) and in the case of debris and hyperconcentrated flows. Differences in the water levels need not even be restricted to sharp bends. In fact in the tributary Lainbach there were measurable water level differences (see 6.4) along the straight reach which correspond with secondary flow cell development. In the bends the water level difference is of course much larger under all flow conditions. The associated development of secondary circulation shapes steeper sloping bars. Flow cell development inhibits bar formation in the cells, but at the edges, bar forms will readily develop. Bars are thus associated with shallower flows where the diamond patterns of clusters suggest the predominance of shear waves. The importance of the water surface configuration in the development of bed structures was studied by LISLE (1986). The more detailed study on the spatial variability of roughness in relation to flow (6.2) in the following section emphasises the dominant role that bend curvature plays in dictating roughness and bar development.

The size and especially the shape of large obstructions determine whether or not a pool or a bar will form downstream of it. Obstructions that did not project above the surface of maximum flow and that were deposited parallel to flow, not transverse to it, caused downstream bar development. Others that were very outsized and formed a major "step" developed an erosive pool and bars upstream. In each case the bar length is dictated by the geometry of the bend. Bars only develop within the low energy zone and before the next bend commences.

This forms the basis of LISLE's (1986) model of the effects of bends and obstructions in stabilising or arresting bar migration downstream. In the actively reworked bars of the Schmiedlaine however, the configuration of the bar and channel does change and may cause the bars to occupy positions which extend further up or downstream from their previous position.

In contrast to other work, approach angles of flow are more influential than the actual obstruction in dictating bar development. This was systematically observed on the test bar as it changed between 1990 and 1992. Thus as the upstream thalweg changed, so did the position of the channel and bar, swinging away from its formally optimal position parallel to the bend. Thus the development of bedform roughness depends on the type of flow i.e. its capacity for sediment transport, entrainment, the transport conditions and the character of flow over the wavy surface (ALLEN 1983).

*6.1.7.2.5 Log jams*

The role of log jams is often neglected. Log jams are found exclusively in the sharpest channel bends of the Schmiedlaine (Fig. 6.50a) or downstream of a major debris flow input (MOSELY 1981). They form during extreme events and may also take on the shape of a debris end-lobe, or a tongue-like accumulation of large particles. Log jams and end-lobes present the problem of differentiating between the competence of the flood itself (KOMAR 1987) and the local slope or debris channel inputs. Since the material is so diverse in the Schmiedlaine, determination of source is difficult.

In the Schmiedlaine, log jams are usually the result of a large log being trapped diagonally across the bend. Other logs and large boulders soon become trapped behind. The logs will arrange themselves parallel to the obstacle log. These depositional features were studied in detail for the Schmiedlaine. The map (Fig. 6.41) indicates how log jams are associated with major areas of deposition. These major bedforms are either dependent on the local sediment supply or on the storage of large material from extreme events (GRANT et al 1990). All energy seems to be dissipated in these areas so that the largest logs and boulders become trapped. Log jams have an important influence on channel morphology and as sediment storage sites through energy dissipation (KELLER & TALLY 1979).

## 6.1.8 Summary of form and system roughness

Evaluation of the function of micro and macro-bedforms on the river bed is important for correct analysis of river bed stability. Although no active flume experiments were carried out, the data presented in Section 6.1.5 demonstrate the importance of bedform analysis in river reaches in the future. In hindsight, the observations suggest that the sorting of particles of similar shape and size into roughness assemblages such as clusters varies according to the obstacle clast and streamlines induced by cluster spacing. These factors control whether or not a cluster is stabilised. Cluster bedforms are thus particle size and shape selective. This observation has important consequences in the regular patterns of roughness formation, repeated from year to year.

Other inseparable factors which influence the arrangement of roughness are the channel bed gradient and curvature. The examples from the Schmiedlaine clearly demonstrate the dependence of bedform development on the geometry and curvature of the channel (summarized in Fig. 6.50 b)). These factors need to be included in future studies of river bed stability criteria.

The analysis of different roughness scales indicates that the sequences are not random (GRANT et al 1990). The schematic illustrations clarify the complexity of different roughness systems distributed over all reaches of the Schmiedlaine. Obviously channel curvature is an essential element which determines the length and type of bedform. Since the grain size distribution is highly variable downstream (MILNE 1982b) and this is greatly influenced by channel curvature, the characteristics of roughness and geometry cannot be simply related to downstream fining. Thus log jams and debris flow end-lobes disturb downstream fining patterns.

The channel is only stable in those areas where there is no channel migration due to widthwise bedrock restrictions. In all other cases, the channel dimensions and position fluctuated considerably, particularly in the medial to lower, highly meandering reaches with high width to depth ratios. The main difference between the catastrophic flood and that of the channel reworked by smaller floods in the preceding years, was that the thalweg attempted to straighten its route during the very extreme flood but exhibited a more meandering form in the preceding years. Form and system roughness developed accordingly. Thus large roughness was developed during the extreme events in positions not otherwise reworked during smaller floods. The different flood routing during the extreme flood can be explained in terms of sediment enrichment and energy losses during the extreme event, in contrast to the sediment-poor and energy-intensive processes during the smaller floods.

The evidence gathered from channel roughness forms, both longitudinally and cross-sectionally, suggests that micro- and macro-bedform development depends not only on channel curvature but also on complex interaction with different types of discharge and sediment transporting events (ALLEN 1983). Thus the amalgamation of perennial bedforms and high energy features has to be clearly differentiated in river morphology studies.

a)

b)

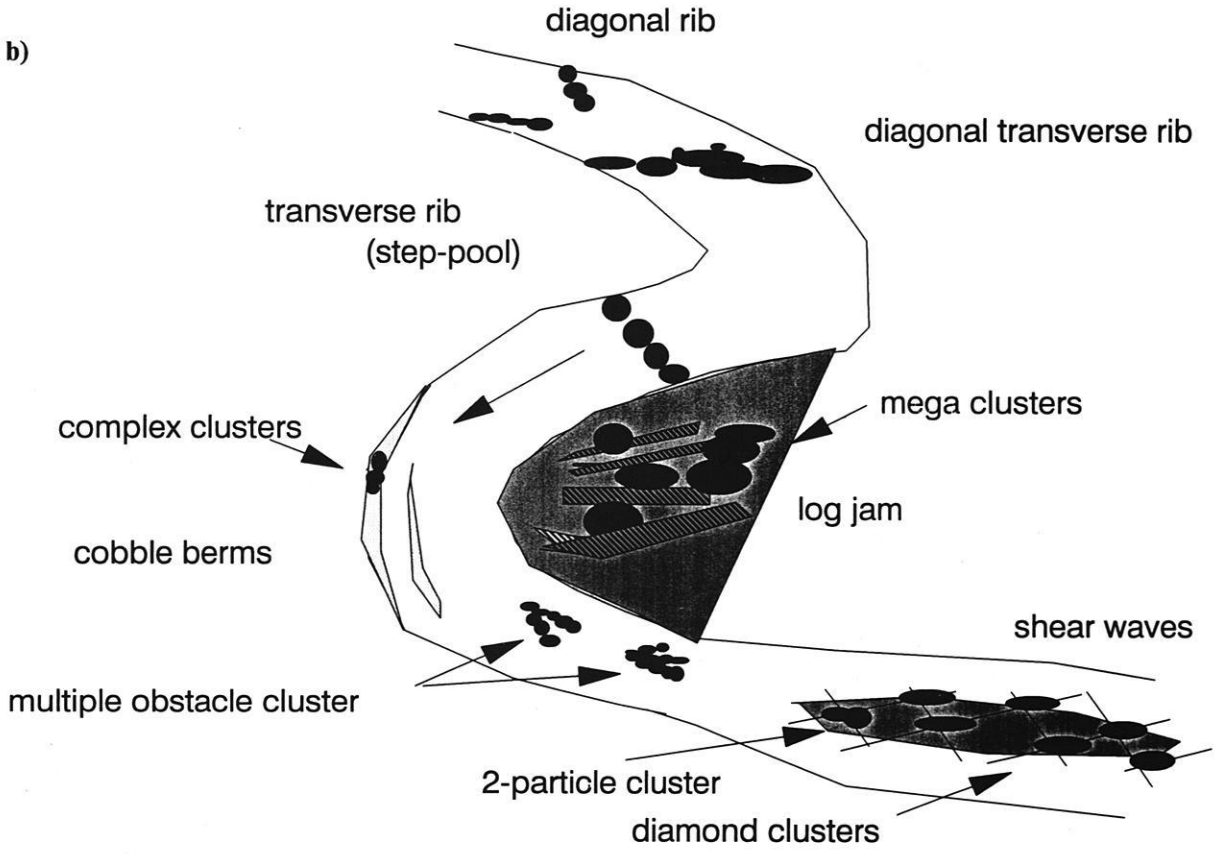


**Fig. 6.50** **a)** Photo of eroded log jam at reach IJ in the Schmiedlaine. Flow is towards the observer. Note deposition of logs and large boulders in the inner bend, and erosion in the channel.
**b)** Summary of the role of bends in the Schmiedlaine in the development of form and system (unit) roughness.

## 6.2 The influence of flow on the spatial variability of roughness

### 6.2.1 Flow orientations of clusters versus surrounding open-bed particles

The ability of flowing water to initiate particle motion is a function of particle properties and their arrangement on the river bed (SUTHERLAND 1967). Although many studies analyse the influence of roughness on flow, very few seek to explain the reverse, i.e. how flow influences roughness development. The influence of roughness on flow assumes that the roughness feature is already there, while the reverse problem explains how and why a certain type of roughness develops under various flow conditions. This will be treated both in the context of flow orientation from single particles and clusters, as well as from the cross-sectional and planimetric shape of particle clusters.

In these coarse-grained streams it is assumed that the particles are aligned parallel to flow (ALLEN 1982). But depending on the grain shape and position within a cluster, not all particles assume this direction. Many particles will rest in orientations that give them the best protection against disturbance, which explains why particle arrangement is so important in incipient motion (KLINGEMAN & MATIN 1993). Thus a cluster may consist of an obstacle lying transverse to flow (Fig. 6.55 e & f), while the remaining stoss side accumulations will be oriented parallel to flow. For this reason the entire cluster shape was utilised in the flow orientation study.

#### 6.2.1.1 Squaw Creek

The orientation of clusters was compared to the mean orientation of all surrounding material at each cluster site in order to establish former flow conditions over the new bar. As is evident from Fig. 6.51, clusters indicate very precise flow orientations. Cluster orientations were obtained from the actual outline of the cluster since the variation obtained from the single, often very rounded particles was often too high.

In the case of extreme sphericity, no preferred orientation could be obtained from the measured a-

**Fig. 6.51** Proximal part of new gravel bar, Squaw Creek. Camera was pointed upstream. Notice very distinct orientation of blue cluster particles.

axes of the material surrounding the clusters. Some orientation results were so chaotic that they had confidence intervals of 200° and even pointed upstream. Flows at Squaw Creek were not strong enough for counterflows of this magnitude to develop. Selected results of the orientation study are given in Fig. 6.52.

At each sample site, there are up to 8 clusters that all indicated very similar flow directions. Over the proximal bar, some directions point laterally across the bar due to the influence of the bend above the upper detector log. Towards the medial bar, however, flow becomes more concentrated lengthwise in adaptation to the straighter geometry of the bar. Downstream of the medial bar location, some flow arrows begin to diverge strongly towards the main channel. This is likely to indicate flow dynamics during peak flow when water levels were high enough over the bar to flow over the entire bar surface directly into the main channel with the exception of the higher, vegetated rip-rap ridge.

Further downstream, towards the distal bar, flow directions adapt to the crescentric shape of the bar and are limited by the maximum extent of the bar. They are forced diagonally into the main channel. The minor exceptions of flow pointing away from the main channel only occur near the minor channel running along the vegetated river banks (Fig. 4.5 Ch. Study Areas). Here flow would have plunged into the deeper side channel away from the bar top due to gradient effects.

What is clear from the flow arrows is that some take on the straight line route down the mid-bar, while others criss-cross to the right and left. On the one hand these diversions are influenced by two minor bars still partly uncovered during the high flows (Fig 6.64). This almost certainly indicates two stages of flow, where the arrows pointing laterally away from the mainstream would indicate high enough discharge conditions for flow, together with bedload, to pass diagonally over the minor bar tops during the descending limb whereas the straighter, less divergent arrows would indicate low energy conditions during the highest flood stages.

These interpretations are supported by active river-bed and bedload measurements in the adjacent channel and on the old bar (Section. 6.3) as well as from sequential photographs (Fig. 6.64) taken of the event responsible for their deposition. For the clusters to be deposited, low rates of bedload transport are necessary. This condition was most predominant and effective during the final stages of the flood (Fig. 6.59 & 6.60).

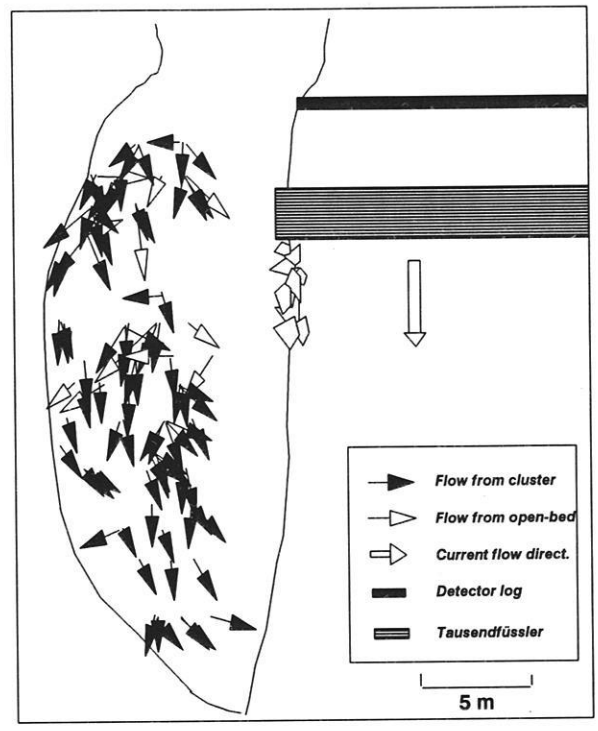


**Fig. 6.52** Mean flow orientation directions for clustered and open-bed material on the new bar at Squaw Creek, 1992. In contrast to the Schmiedlaine only selected open-bed directions could be utilised due to the extreme and erroneous range of orientations obtained from the very rounded material.

### 6.2.1.2 Schmiedlaine

Due to the coarseness and angularity of material in the Schmiedlaine, the reconstruction of flow orientations was possible both for clusters and for open-bed material. Confidence intervals for flow orientations of open-bed particles did not on average, deviate by more than 30°. The uni-directional flow directions that were reproduced showed that flow was limited to a narrow range of variation and did not spread over the entire 360° as was the case at Squaw Creek. This allowed a very novel and extensive interpretation of flow dynamics to be made. As is evident from Fig. 6.53, two very different flow histories can be deduced from clusters and open-bed particles for the flood flows of 1990. Clusters generally show straighter routes parallel to the present-day flow, while the open-bed particles tend to diverge by as much as 67° from the mean cluster orientation.

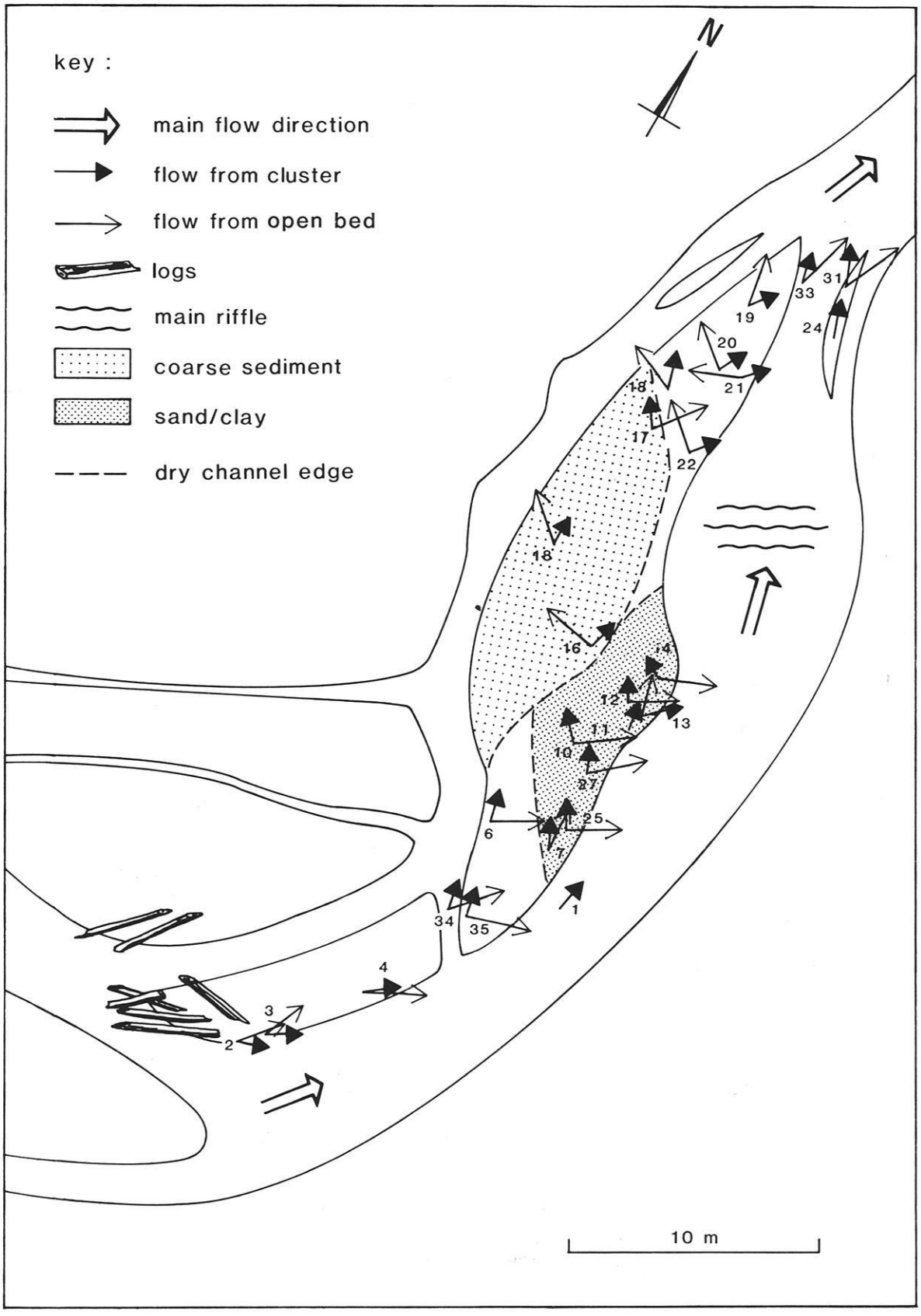


**Fig. 6.53** Mean flow orientations for clusters and open-bed material in the Schmiedlaine for 1990. Numbers mark cluster sites.

The flow arrows show that open-bed clasts were subject to flows that cut straight across the bar and channel at the proximal bar end downstream of the wooden debris. They were then sharply deflected off the bedrock valley slopes in the opposite direction, only to straighten again at the distal end of the bar. This lateral deflection amounted up to 100° in some cases. The open-bed material flow orientations are very much dependent on bend curvature. Thus at the bend entrance at the proximal end of the bar, the flow arrows still point straight across the bar. But once forced into the bend by centrifugal forces, they are subject to deflection in the opposite direction. The straightening further downstream is the result of flow confluence and concentration at the exit of the curve.

The open-bed arrows are indicative of flood energy and stage. The mutual character of the straight flow directions up to cluster location 14 (Fig. 6.53) show that high flood energy must have existed in order for equally orientated particles to have been deposited over the entire bar top. The equivalent behaviour of flow at the distal bar end is supported by a number of well spread sample sites all indicating fully developed flood flow.

In contrast the clusters, which are coarser in size than the open-bed material (see section 6.1.2.1.6), indicate that flow directions are well adapted to the individual geometries of the major and minor bars (Fig. 6.53) and are more similar to present flow conditions. BRAYSHAW (1984) also found that clusters exhibited more consistent alignment parallel to flow. Therefore clusters represent the final descending and depositional stages of the flood, as at Squaw Creek.

The data processed for the floods of 1991 indicate a similar pattern of differentiation between clusters and open-bed particles, except that the range of deviation between the two is less, i.e. only 46°. Since the clusters did not deviate as much from the open-bed material, it is postulated that the floods succeeding the major 1990 events were less powerful in 1991. In 1991, the clusters were orientated in directions very similar to the open-bed and present flow directions, so that it can be surmised that flows were not as high and fully developed over the bar surface when compared to the preceding year.

### 6.2.2 Influence of flow on cross-sectional and planimetric shape of cluster- versus open-bed particles

The shape of a roughness element, whether single grain or bedform, is significantly influenced by flow velocities and flow structure. Thus with increasing Reynold's numbers, the length of the downstream and lateral vortices increase (SPURK 1989). This considerably influences the length, height and width of the bedform produced as well as the spacing of other bedforms reflected in an ellipsoidal dimension. If at the highest Reynold's numbers ($10^6$) the separation zone is twice the length of the obstacle, then the length of the cluster must reflect these flow conditions.

#### 6.2.2.1 Squaw Creek

Fig. 6.54 a) illustrates an enlarged section of the proximal end of the new bar at Squaw Creek. Major roughness elements are widely spaced and clearly ellipsoidal in section (FURBISH 1987). The particles are stacked at high imbrication angles around or upstream of the obstacle clast. A perfect ellipse is maintained in plan view in every case, and a semi-ellipse in cross-section, such that particles will never protrude outside the general ellipsoidal outline, nor above a certain level of the river bed (see photos, Fig. 6.55 a-f). This is because particles projecting above the mean bed are more readily subject to entrainment (SUTHERLAND 1967).

The ellipsoidal form develops since an obstacle deposited on the river bed will trap a number of clasts, whose position depends on the adaptation to flow (BILLI 1988). Since the obstacle causes flow deflection either upstream or downstream of it, clusters will maintain either an upstream or downstream slope behind the obstacle (Fig. 6.42 a & b). In terms of the flow hydraulics, the cluster shape demonstrates that during an active flood, flow is not uniform over the gravel bar but rather occurs as undulating waves. These waves are very minor at Squaw Creek, probably not more than 5 cm in height and 50 cm long, as estimated from the average cluster spacing.

The limited wave size arises from the low gradient and smaller grain size. Evidence for these suggestions was supported by photographic documentation of very regular minor waves, especially visible on the distal bar (Fig. 6.64 c), Section. 6.3).

Along the long profile of the new bar at Squaw Creek, roughness elements presented by clusters are clearly differentiated from the rest of the surrounding material (Fig. 6.54a). Thus while cluster elements get deposited at high angles of imbrication (between 30 and 65°), the open-bed material is imbricated at smaller angles (between 10 and 36° (Fig. 6.56 a)). Roughness is dominated by single particle roughness

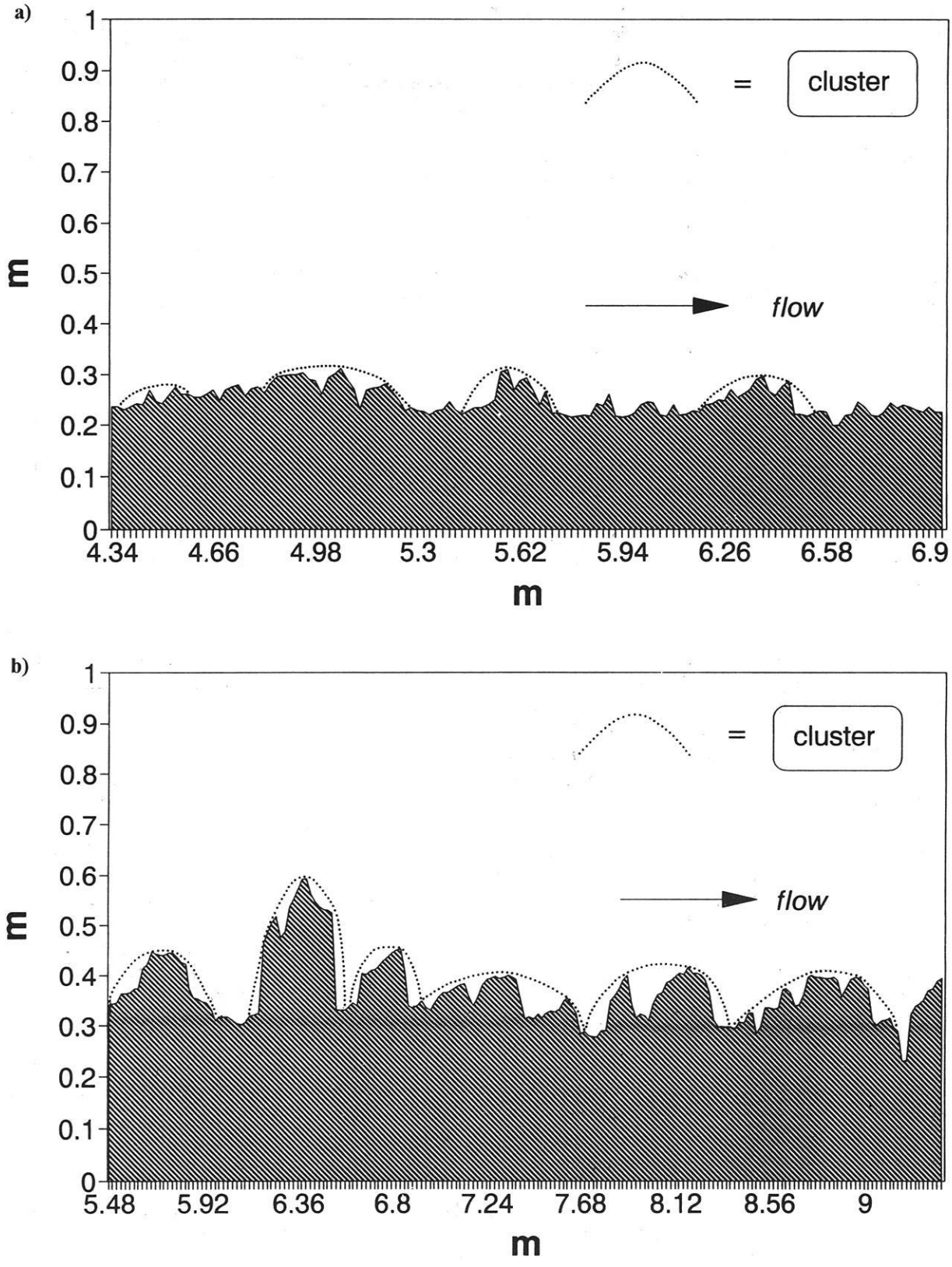


**Fig. 6.54** Longitudinal profile of **a)** the new bar at Squaw Creek and **b)** test bar in the Schmiedlaine, enlarged to show the spacing of individual roughness elements. Roughness and gradients are fairly homogeneous. Each single roughness element is demarked by semi-ellipse.

(see section 6.1.1.2) interspersed with isolated larger roughness elements. Fractal analysis (Fig. 6.37a) supports the interpretation that there is an absence of a clear transition from grain to form roughness since the roughness spacing is so large.

Particles in heterogeneous mixtures tend to cluster in a recurrent manner under the influence of flow FURBISH (1987). At Squaw Creek, large differences in imbrication, i.e. due to generally well rounded, non- clustered particles may mean that the general surface is more mobile than under the highly imbricated conditions in the Schmiedlaine. But bed stability is determined by the actual arrangement of the bed, not the high $K_3$ or high imbrication values (KIRCHNER et al 1992).

In plan an elongated ellipse becomes apparent for each roughness element (Fig. 6.55 a & b). The height and width of the roughness element hardly fluctuate and remain parallel to each other. The length of the roughness element varies considerably (Fig. 6.57 a). Cluster height and width clearly offer least resistance to flow. The length of the cluster varies but remains streamlined due to the width limitation imposed by the obstacle particle and flow conditions.

When an ellipsoid is circumscribed around the roughness feature (cluster) both in section, as a semi-ellipsoid and in plan, as a whole ellipsoid, the ratio of the height to length varies with the ratio of the width to length (Fig.6.58 a). Thus although the cluster may vary considerably in length, its length is limited by its width and height.

It has become clear that flow exercises an important control on the dimensions, shape and spacing of major roughness on the bar surface. Particles within individual roughness elements have to remain "hidden" within the general form. Any major protrusion may cause the particle to become a candidate for lift and entrainment, since lift force is often more decisive than drag force in the initial entrainment of particles stacked on coarse, porous river beds (ERGENZINGER & JÜPNER 1992). The porosity of coarse river beds enables large pressure differences to occur beneath the top cluster layer of particles so that fluid is forced up between the interstices and causes powerful lift forces to occur. Furthermore, if a particle projects very much into the flow, there is a greater potential for it to be subject to particle collision (SUTHERLAND 1987) and subsequent entrainment.

These factors limit the height and length of the cluster. Flow does not, however, limit the roughness length as much as the height, as is obvious from the very long cluster trains compared to their projection height. The limitation in height is partly the result of particle size and depletion of material. Yet flow will be active in removing particles obstructing its way laterally and vertically.

Flow will only cease to have influence on bedform width and height if the particles involved defeat flow competence. In this case flow has to diverge around the obstruction. Thus obstacle particles influence the location and extent of particle deposition in their immediate surroundings.

#### 6.2.2.2 Schmiedlaine

In the Schmiedlaine, clusters constitute nearly all of the river bed. Figure 6.54 b shows that the number of particles and obstacle size dictate the length of the cluster and its height. In order to remain streamlined, longer clusters will generally consist of smaller particles. If a particle is larger than average, a cluster only 2-3 particles long will develop. This will ensure that the overall cluster length is approximately the same as the other clusters. This ensures perfect adaptation to flow (Fig. 6.55 c & d). From the comparison of Fig. 6.55 a & b with Fig. 6.55 c & d shows that for a certain particle size, the cluster assemblages at Squaw Creek are very similar in size to those in the Schmiedlaine.

Figure 6.56 b shows that clusters are more imbricated than the non-clustered open-bed bar material but that the difference is greater at Squaw Creek than in the Schmiedlaine. The detailed longitudinal diagram (Fig. 6.54 b) clearly demonstrates that there is a continuity in cluster trains. There is hardly a particle in existence at the Schmiedlaine that is not part of a cluster assemblage. Since the bar is so highly clustered, it is not surprising that all particles have very high imbrication angles. Since nearly all grains are an inherent part of the cluster, the transition from grain to form roughness is smooth.

This observation is also shown in the fractal analysis of the Schmiedlaine bed material (Fig. 6.40 b). If the individual grains are clearly separable from the bedforms, the transition from form to grain roughness is sharper, as at Squaw Creek.

The width and height of clusters in the Schmiedlaine fluctuates fairly constantly and consists of low values (Fig. 6.57b) as at Squaw Creek. In contrast cluster length is independent of cluster height and width. In the case of exceptionally high protrusion, however, clusters are very short. Covariation of ellipsoid section and plan at Squaw Creek and the Schmiedlaine

a)

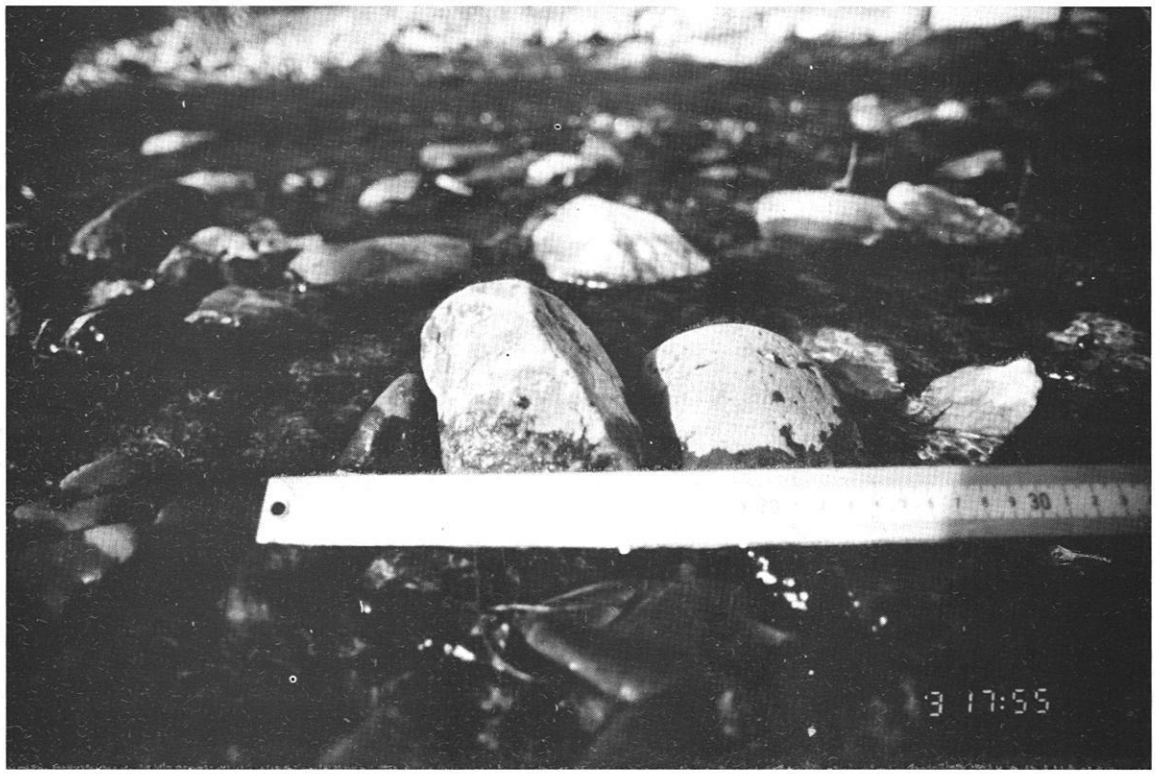


b)

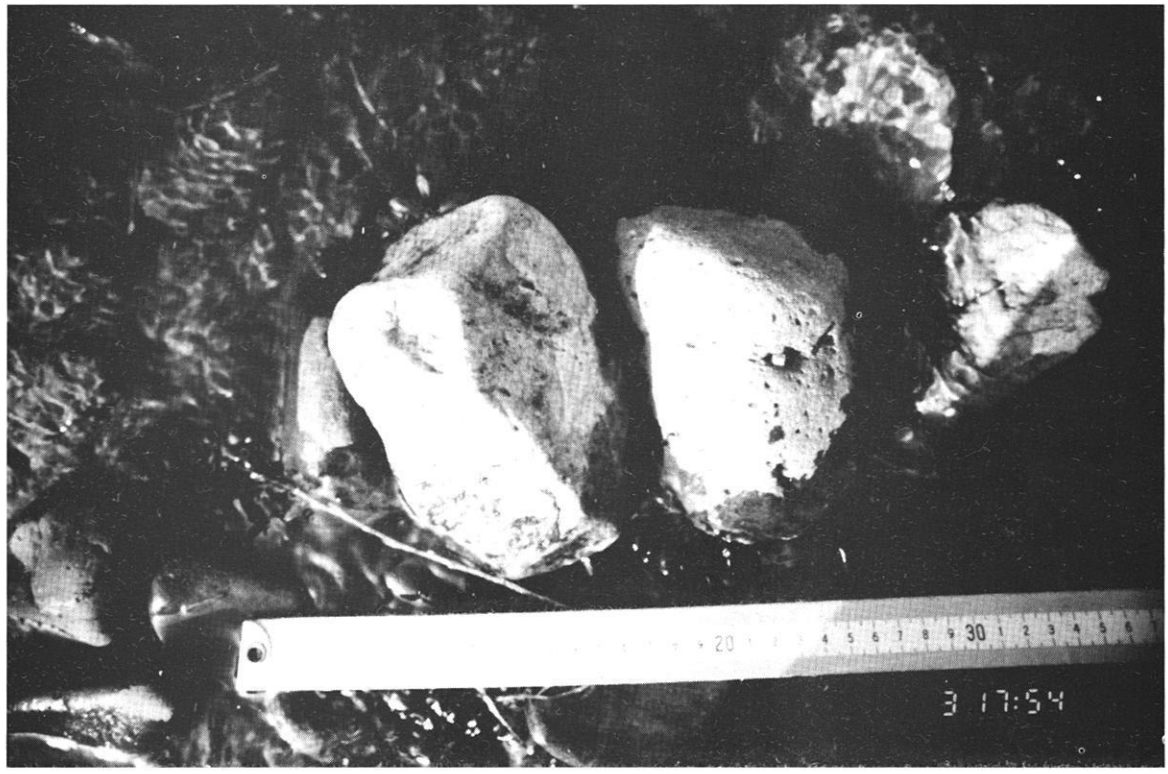


**Fig. 6.55 a)** Sectional view of imbricate cluster at Squaw Creek, 1992. Flow is from right to left **b)** Plan view of same cluster.

c)

d)

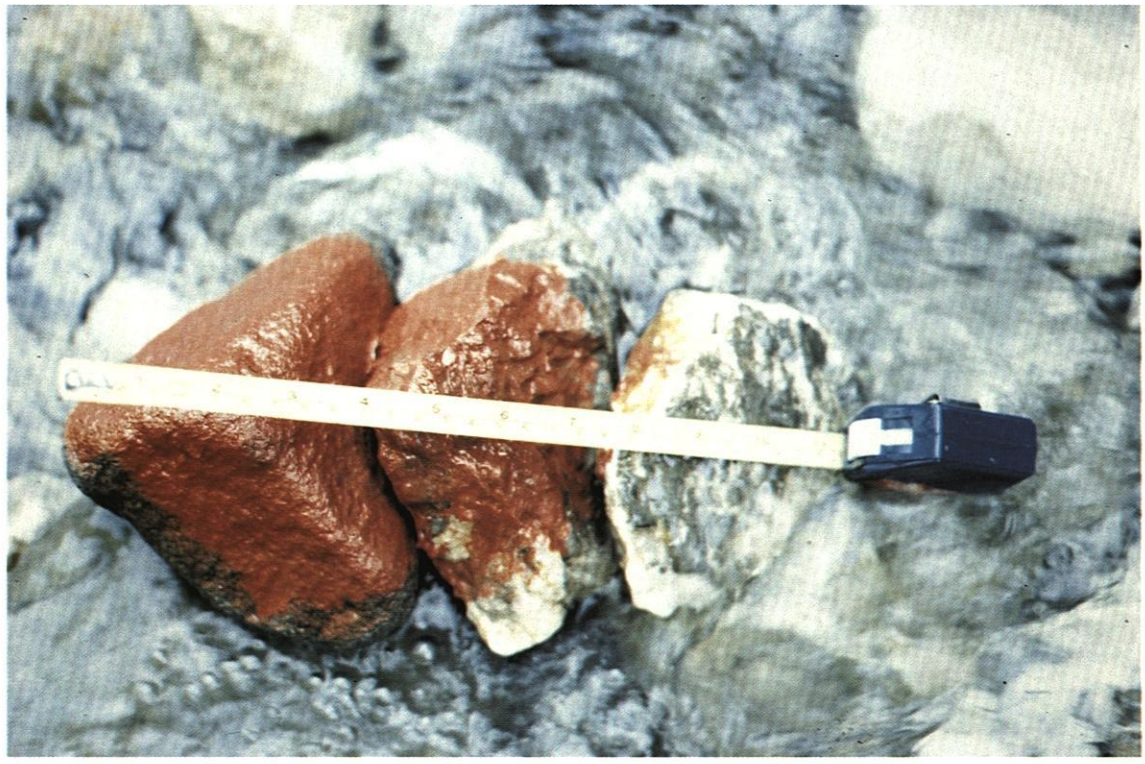

**Fig. 6.55 c)** Sectional view of imbricate cluster in the Schmiedlaine, 1990. Flow is also from right to left and **d)** plan view of same cluster.

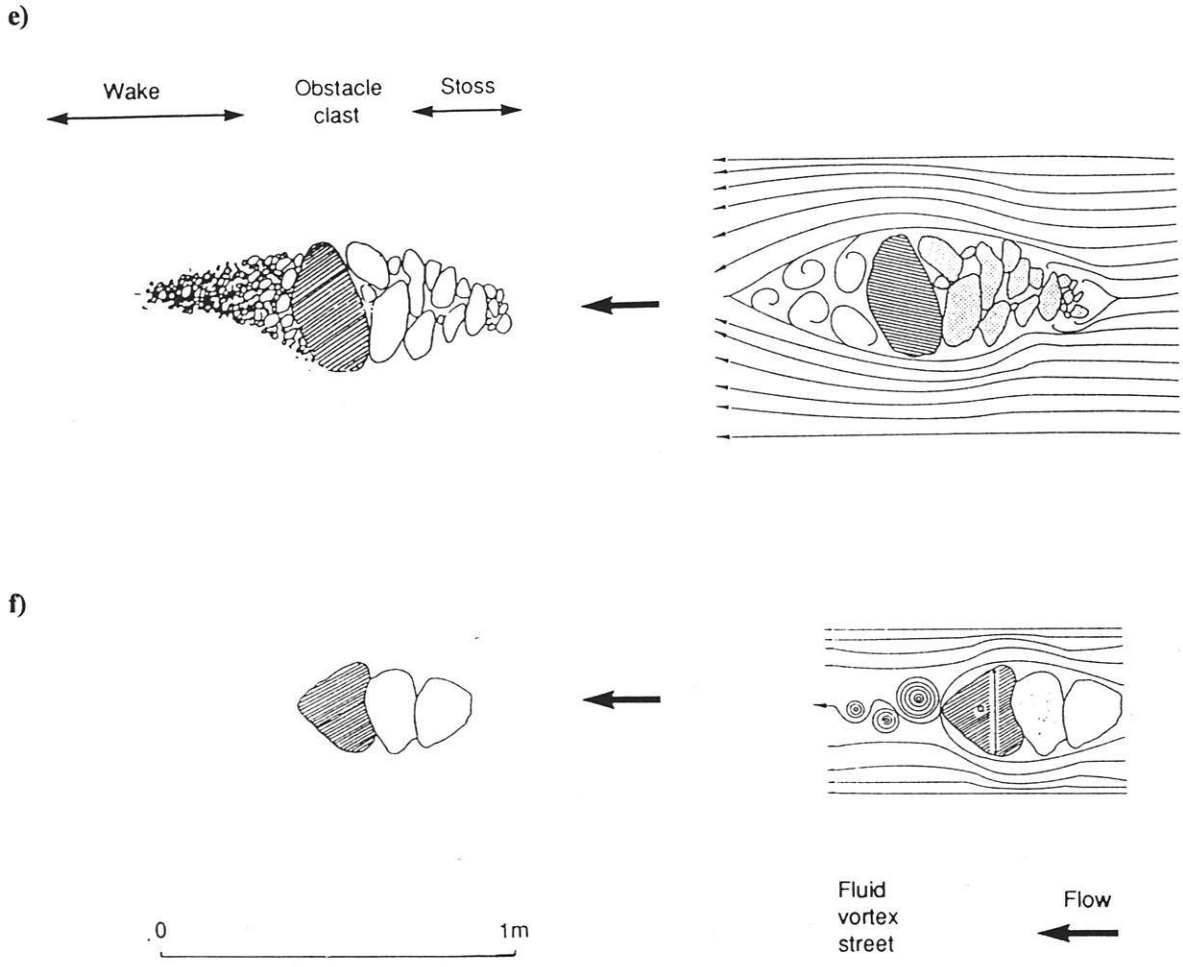


**Fig. 6.55** **e)** Streamlines formed around a transverse, obstacle with wake accumulation and subsequent cluster development and **f)** streamlines formed around a triangular tapering obstacle with erosive Von Karman vortex street (after DE JONG 1992a).

(Fig. 6.58b) shows that the two are closely dependent on one another. When the cluster is very narrow, it will not protrude very high above the bed. When the cluster is wider, it will maintain higher projection which can be interpreted in terms of greater stability with respect to flow. This stability is, however, stage dependent. During higher flow, larger sedimentary particles will be in motion, creating a higher probability of grain collision and subsequent entrainment. The larger cluster dimensions are of course directly related to particle size. The larger the particle, the greater the chance that it is part of a cluster and the more stable it will be.

### 6.2.3 Effects of particle shape on bed arrangement

The shape of the open-bed and clustered particles was determined from the photo-sieving programme. Roundness was obtained from the relationship between the a and b axes, by approximating the second harmonic of the Fourier analysis to an ellipsoid (DIEPENBROEK 1992). This ensured that the influence of sphericity was kept separate from roundness. On the whole, cluster particles in the Schmiedlaine had lower rounding coefficients than

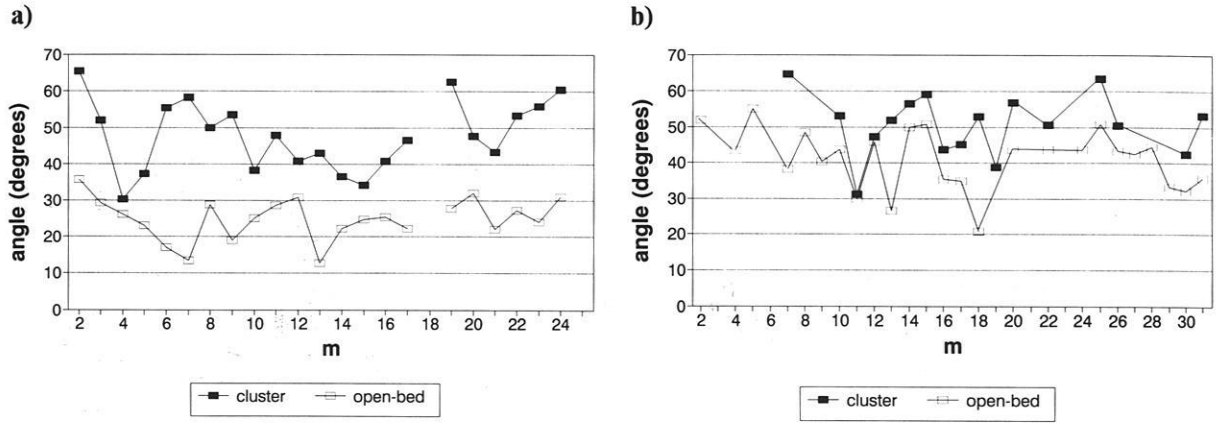


**Fig. 6.56** Downstream variation of average imbrication angles for cluster and open-bed particles for each mini-Tausendfüssler section **a)** at Squaw Creek, and **b)** in the Schmiedlaine. Flow from L. to R. No data was available for 18-19m.

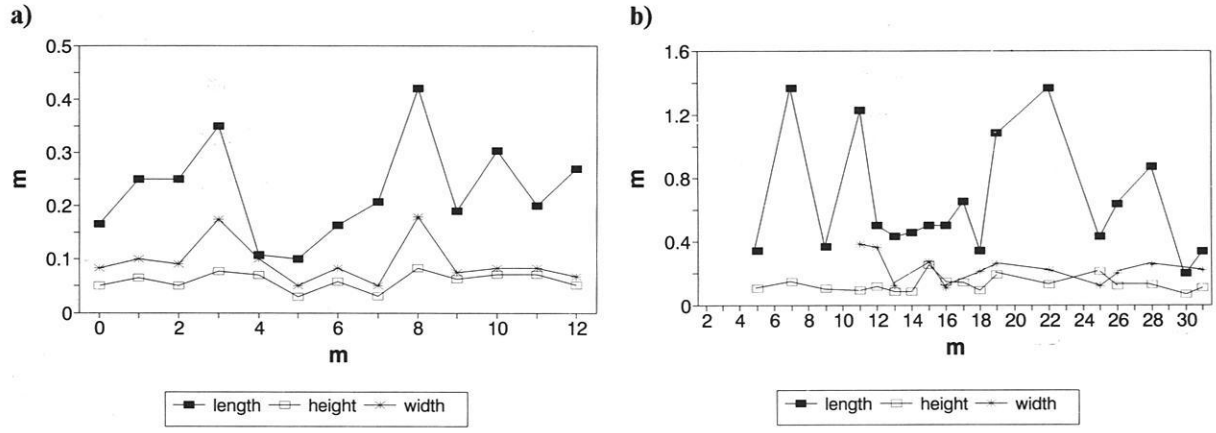


**Fig. 6.57** Cluster geometry. Variation between cluster length, width and height **a)** at Squaw Creek and **b)** in the Schmiedlaine. Note the difference in scale at the two sites.

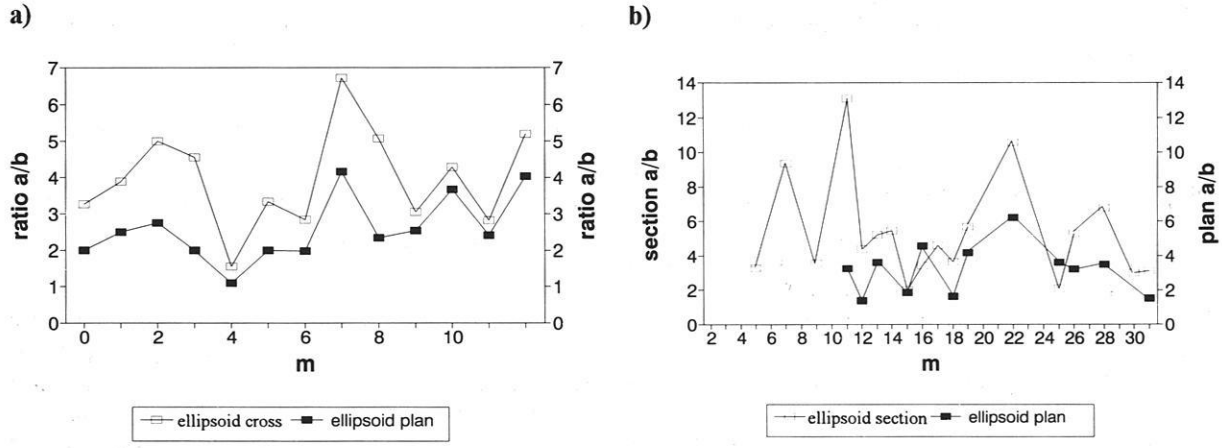


**Fig. 6.58** Relationship between the ratio of cluster ellipsoid length to height (a to b in section) and the cluster ellipsoid length to width (a to b in plan) **a)** at Squaw Creek and **b)** in the Schmiedlaine.

the open-bed material. Thus cluster particles had average rounding coefficients of 0.28, while open-bed material lay around 0.33. Both rounding values are relatively low (a value of 1 would mean total roundness). The general platiness of the material in the Schmiedlaine therefore explains why there is such a high density of clustering. Cluster particles were not always less rounded than the surrounding material, thus more rounded material was not excluded from cluster formation, if it was of the correct size and shape to fit into the cluster ellipsoid.

At the Schmiedlaine there is more frequent cluster formation because platy particles are more prone to clustering, but clusters have fewer particles (only 3-4) (DE JONG 1992e). This smaller number of particles in each cluster participance is surely a result of the particle stability difficulties which arise from the many odd-shaped obstacles.

At Squaw Creek, the very rounded material (average coefficient of 0.55 for both clusters and 0.6 for open-bed) explains why clusters are easier to form. Due to the smaller grain sizes involved, there are more clusters per $m^2$, thus a higher density of clusters but a smaller overall area covered. Squaw Creek has an average cluster density of 1.61 per $m^2$ in contrast to Schmiedlaine, which had a density of 0.8 per $m^2$ in 1990. But the actual area that clusters occupied on the river bed attained only 2% at Squaw Creek, while it attained 16% in the Schmiedlaine. This means that the more platy particles are actually better adapted to clustering. These findings contrast with the work by REID et al (1992) who argue that platy material forms longer clusters and thus decreases the density of cluster formation. In the comparative studies, at Squaw Creek and in the Schmiedlaine, the area that clusters cover on the river bed is probably more significant in controlling sediment entrainment. Thus one should be careful to differentiate between the number density of clusters and the area of the river bed covered by clusters.

### 6.2.4 Summary

Differences in imbrication are important in terms of sediment entrainment thresholds due to their influence on grain pivoting (KOMAR & LI, 1988, KIRCHNER et al 1990). Since the difference between the imbrication angles of clusters and open-bed material is large at Squaw Creek, the non-clustered material should pivot out of place more readily. In contrast, in the Schmiedlaine, where imbrication angles of both types of material is similar, higher thresholds for pivoting should exist making the material more stable.

In the Schmiedlaine, as at Squaw Creek, there is a slight trend of increasing cross-sectional a/b ratios with distance downstream (Fig. 6.58 c). In terms of bedform shape this indicates that from the initial highly protruding, hump-backed clusters on the proximal bar, clusters become more elongated with distance downstream. At Squaw Creek, this trend is also well developed. These changes in ellipsoid dimensions have implications for the downstream fining of the gravel bar. The local variation of bedforms reflects the differing roles of sediment transport and sediment trapping. Thus the sedimentary processes causing variations in bedform shape are determined more by the hydraulic conditions, cross-sectional and planimetric shape of the channel and bar than the actual distance downstream. This requires the flow to be more powerful in the proximal bar location. Not only does the ellipsoidal shape of the cluster indicate that very large particles have to be involved but also that flow has to be powerful enough to dislocate such assemblages.

In the Schmiedlaine, the bend dynamics are particularly important in this context. As flow proceeds around the bend, it has gathered much momentum and the energy produced can be dissipated in the entrainment of large particles and the formation of such large roughness elements. Further downstream, as the bar straightens in adaptation to the linearity of the reach, flow momentum is lost and the competence to carry large particles also decreases. This explains why on the whole, smaller particles will be found towards the distal bar end, capable only of achieving flattened bedforms. Preferential trapping of smaller particles in these lower energy zones also explains the gradual trend towards longer particle trains.

From the comparative analyses, it is again clear that flow is influenced by the shape of the reach as much as by particle size. These factors combine to influence the bar and channel shape and the associated type and distribution of bedforms. Thus bedform and channel shape are subject to processes that remain mutually interactive. As flow is influenced by reach dimensions, it influences the deposition or erosion of particles and causes a certain type of bedform to develop. This bedform in turn influences the local flow dynamics. If flow and channel location dictate the preferential trapping of large particles, then the deficit of large material further downstream will not only ensue as a result of complex particle clustering

further upstream but also as a result of flow patterns induced by the bedforms themselves. Conclusive evidence on the shape of the ellipsoid in section and its associated planimetric form could help clarify the problem of reconstructing the relationship between flow depth and the size, shape and location of bedforms produced.

Particle dimensions may be just as important as particle shape in determining how flow can sort and arrange the river bed. Although the general rule holds true that more platy and less rounded material is more prone to clustering, exceptions do exist if the particle is just small enough to fit into the stoss side accumulation of a cluster. Particle arrangement is subject to a positive feedback process, controlled by the ellipsoidal limitations that the cluster has to adapt to. Thus if an obstacle particle has particularly low rounding values, it will attract equally odd shaped particles in its stoss and/or lee which are less frequent, and cluster particles are reduced. If however an exceptionally large and well rounded particle comes to a halt on the river bed, it will have to find a equal number of well rounded particles to fit the dimensions of the cluster. In a fairly well-sorted river bed, this should not be too difficult.

Observation and comparative cluster analyses show that more rounded particles covered a higher density and cover a lower area of the river bed, because particle trains are longer. Platy material is more prone to clustering and enables a smaller cluster density and a higher area of the river bed (see Table below).

**Table 6.2** Cluster density in Schmiedlaine and Squaw Creek

| | **Cluster particles ($/m^2$)** | **Cluster area (%)** | **Cluster rounding** | **Open-bed rounding** |
|---|---|---|---|---|
| **Squaw Creek** | 1.6 | 2 | 0.55 | 0.6 |
| **Schmied-laine** | 0.8 | 16 | 0.28 | 0.33 |

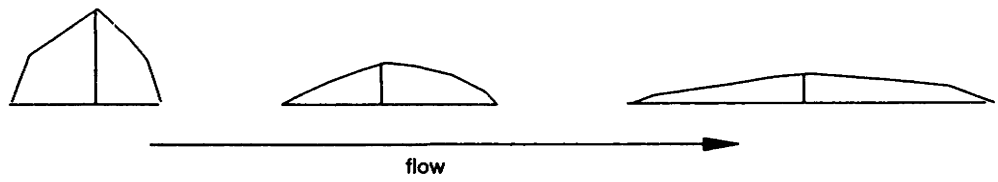


**Fig. 6.58** c) Downstream changes in ellipsoidal cluster configuration (in section).

## 6.3 Temporal variability of roughness and geometry: Squaw Creek 1991

### 6.3.1 The nature of bedload and discharge

Bedload transport studies in relation to discharge are very widespread in the literature. For the purpose of the following analyses however, only studies can be considered that have treated bedload transport as a highly fluctuating temporal and spatial process, i.e. where high resolution measurements, preferably of single particle transport, have been undertaken (ERGENZINGER et al 1993, BÄNZIGER et al 1991). The higher the measurement resolution, the clearer the pattern of bedload pulsation and its relation or non-relation to discharge. In addition, high resolution temporal measurements of river bed roughness and geometry are lacking in nature, so the present study is breaking new ground. This invariably narrows the range of comparisons to be made. The discussion of the results has to be regarded in light of unique and first-hand measurement experiences.

At Squaw Creek, the aims of the study were to obtain detailed information on the transport of single particles during an entire flood event so that any adjustment in roughness and geometry could be examined in light of discharge, velocity and bedload transport through time. The question to be tested is whether changes in roughness and geometry related more to bed load transport than to discharge. The Squaw Creek bedload measurement experiences are very unique not only because of the high resolutions and spatial range involved but also because of the existence of two separate detector sills that for the first time allow a bedload balance to be determined over a 30 m reach during a natural flood event. It has to be kept in mind that the bedload counts represent only the coarse magnetic material and not the total transport but these counts are assumed proportional to the total transport. The bedload counts represent approximately 70% of the total bedload.

Unfortunately a similar bedload detection system does not exist at the Lainbach. Nevertheless, this shortcoming allowed the model ideas developed at Squaw Creek to be applied and tested, given that all other parameters were determinable.

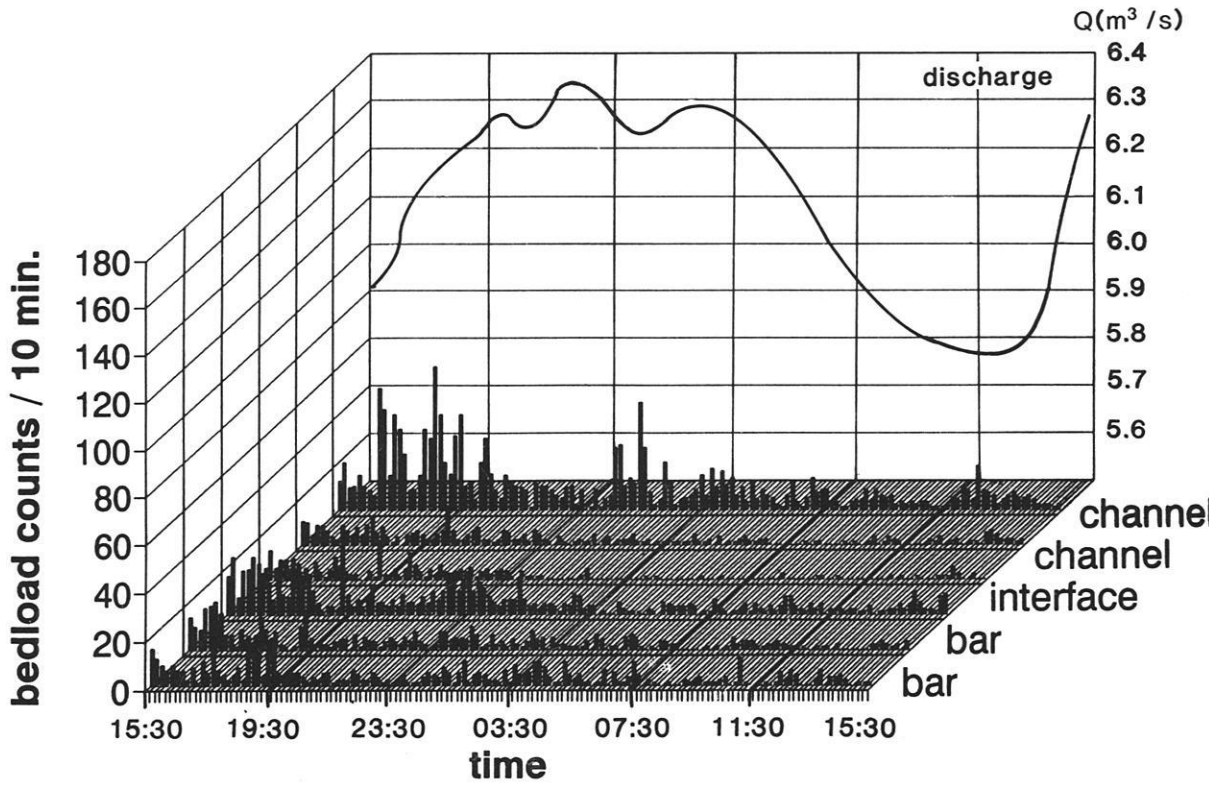


**Fig. 6.59** Bedload transport over the upper sill at Squaw Creek, 23-24th May 1991. The sill is spatially sub-divided according to its location on the channel, bar and interface (R. - L., looking downstream). Channel is located on right side, bar on left.

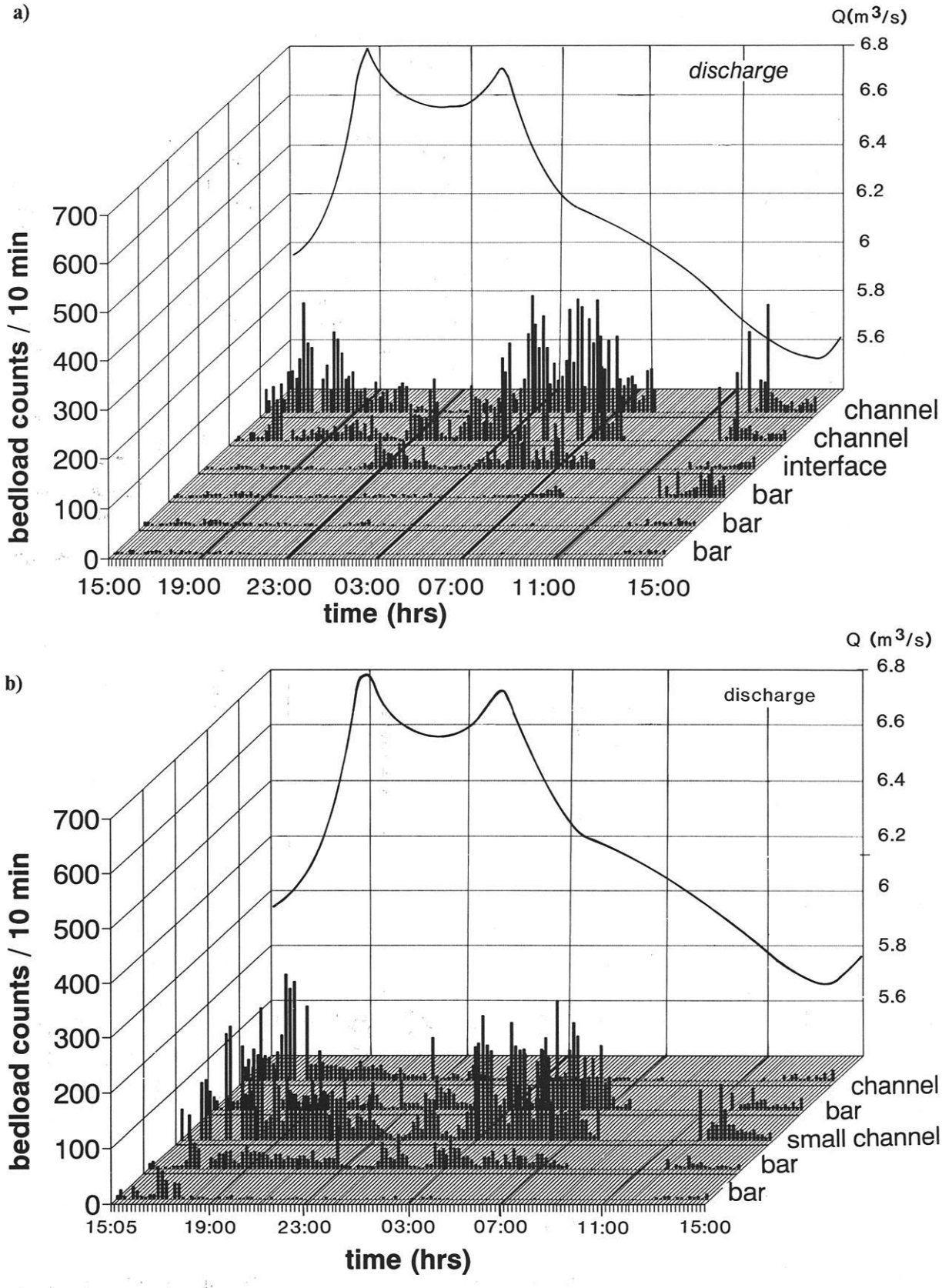


**Fig. 6.60** Bedload transport over **a)** the upper sill and **b)** lower sill at Squaw Creek, 5-6th June 1991. The sill was spatially sub-divided into channel, interface and bar. Notice that the largest pulse occurred between 04:00-06:00 over both sills with the exception of a minor pulse over the lower sill during the ascending limb.

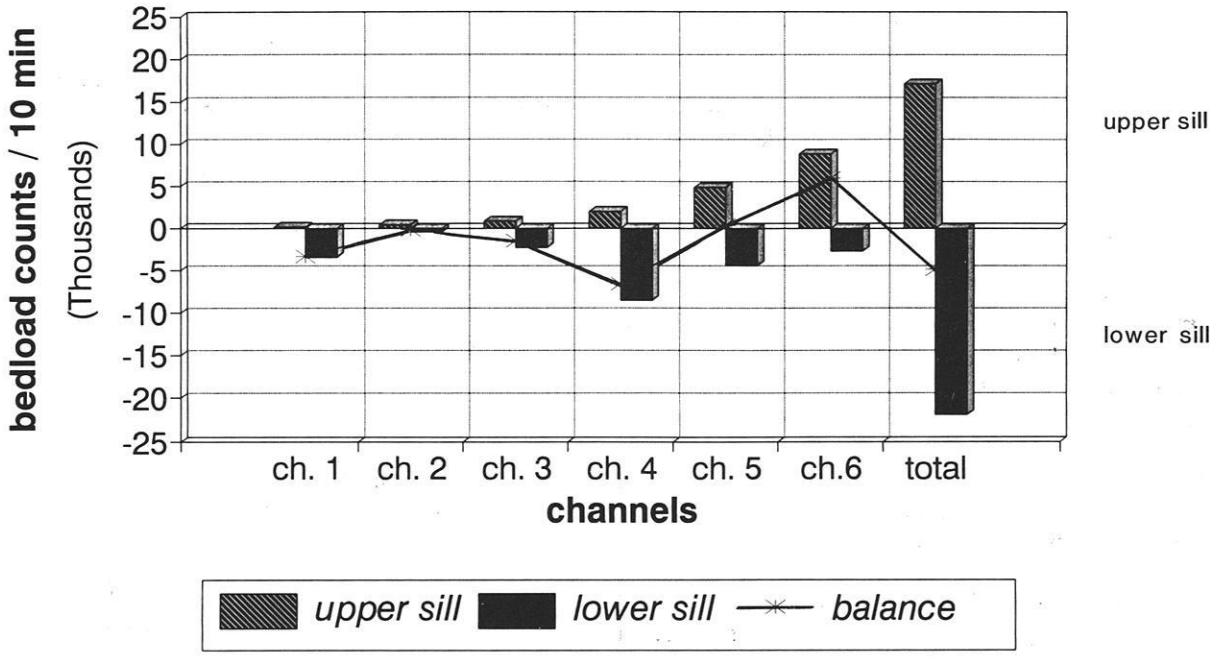


**Fig. 6.60** c) Bedload balance over each of the six detector segments (Channel 1-6) over the upper (positive) and lower sill (negative). The last bar indicates the total balance over the upper and lower sill. Notice the overall negative balance

#### 6.3.1.1 Flood of 23-24th May 1991

The flood of 23-24th May 1991 was a typical snow-melt event, with a rapidly ascending limb, an extended peak reaching 6.5 $m^3s^{-1}$ and a gradually descending limb (Fig. 6.59). The steep hydrograph rise at the end of the hydrograph marks the beginning of the next snow-melt event. Bedload measurements could only be obtained for the upper sill since the lower sill had failed. The largest pulse of bedload material ensued between 18-22:00 (Fig. 6.59). A minor pulse followed at 24:00, 04:00 and again at 13:00. The bedload data were calculated as the sum of pulses over 10 minute intervals. In order to monitor lateral variability, the sill was subdivided into channel, interface and bar. It is clear that during the event most bedload was transported through the channel during the ascending limb. During the descending limb, however, there was a considerable increase in bedload transport over the bar.

#### 6.3.1.2 Flood of 5-6th June 1991

The flood of 5-6th June was unusual in that it maintained a very long descending limb consisting of a double peak resulting from a combination of snow-melt and prolonged warm rain (Fig. 6.60 a & b). Rain-flood events are rare at Squaw Creek and the large amounts of discharge were only possible as a result of this unusual combination. The double peak allowed high water levels to be maintained during the course of the event. Bedload measurements were possible both over the upper and over the lower sill with exception of the period between 10:00-13:00 where lightening completely disrupted the electronics (Fig. 6.60 a & b). Both data sets were reduced to 10 minute summations of bedload and subdivided spatially as for the 23rd May.

Visual comparison reveals that the largest pulse of bedload did not pass the sills during peak flow. Rather, there was a small pulse of material during the ascending limb and the largest pulse dominated the descending limb of the flood over the upper sill as well as the lower sill. Although upon first observation, the lower sill gives the impression of transporting more material than the upper sill, e.g. due to its short-lived pulse right at the beginning of the flood, the largest amounts of bedload are transported within the channel and it is this that dictates the overall balance. Thus in the total, more material was transported in the channel over the upper sill than over the lower. More material exited over the lower sill during the ascending limb due to more active transport over the bars, such that there was a deficit in the total bedload

balance during the flood (approximately 4000 particle, see Fig. 6.60 c)).

This approximate balance (Fig. 6.60c) demonstrates that if more material exited over the lower sill, the 300 $m^2$ monitored reach must have been eroded. This deficit of approximately 13 particles per $m^2$ per hour constitutes only 2% of the surface armour layer which is therefore insignificant. Bedload meandered along the reach. Figure 6.60c) indicates that most bedload was registered in channel 6 over the upper sill, but on the lower sill (the equivalent of the main channel) most bedload was registered over sill 4, with smaller amounts over sill 1 and 5. Additional evidence for meandering bedload can be obtained from a frothy line (Fig. 6.64 c) which can be traced along the main bedload track from the middle (foreground) to the extreme left of the channel (background).

In summary, bedload transport is not directly related to the discharge curve. Rather, the main pulse of material is obtained during the rising flood limb and again during the descending limb. During peak discharge bedload transport nearly came to a standstill. It is not uncommon during the floods at Squaw Creek for periods to exist with a complete absence of bedload. This pulsed nature of bedload has to be kept in mind for later analyses because of important implications for bed dynamics and the general adjustment of river bed geometry. In order to examine the control of bedload on river bed geometry, bedload was summed over the Tausendfüssler measuring intervals and standardised into hourly intervals.

## 6.3.2 Dynamics of river bed roughness and geometry in relation to water surface

To date, studies concerning the detailed spatial and temporal variability of river bed roughness and geometry have been sparse. Analysis of the water surface has been totally lacking. Such gaps in measurement objectives are unfortunate since in shallow flowing mountain streams (ratio 1:33 for Squaw Creek, see YALIN 1993), the water surface is certainly a very sensitive indicator of river bed processes.

This subject will be treated in detail in the next section especially with regards to changes in roughness and adaptation of river bed geometry which has been specifically sub-divided into channel, interface and bar.

The $K_3$ roughness coefficient is used for all studies, since it is a dynamical coefficient that not only allows grain but also form roughness to be separated (DE JONG 1992c, DE JONG & ERGENZINGER 1992). Since it is a relative roughness coefficient, $K_3$ can be used as a very precise indicator of roughness conditions at a particular point during a flood. $K_3$ comparisons with the widely used Manning roughness parameter are also critically investigated.

### 6.3.2.1 Flood of 23-24th May 1991

#### *6.3.2.1.1 Temporal changes in roughness and water surface topography*

The changes in river bed geometry are very complex (Fig. 6.61). Most changes in roughness and geometry can be traced during the first and largest bedload pulse on the ascending discharge limb marked in the diagram. During the remaining flood, only very small pulses cause changes, such as at 04:00. The rest of the time is utilised for river bed adjustment back to the former conditions. The frequency of $K_3$ roughness, subdivided into 1 cm classes, was plotted in order to obtain an overview of the characteristics of temporal changes in roughness distribution. The utilisation of $K_3$ has been mentioned earlier. In Fig. 6.62 the time-sequential distribution of $K_3$ roughness can be followed for the flood of 23-24th May, 1991. Very large roughness elements exist at 17:00, 23:00, 04:00, 06:00 and 12:00, whereas extremely low roughness values were obtained at 16:00, 18:00, 02:00, and 09:00. The very low values correspond with major and minor bedload pulses. On the other hand, the roughness peaks occur during periods of river bed adjustment.

Fig. 6.63 indicates the pattern of roughness changes summarised as average $K_3$ values over the channel, interface and bar for the course of the flood event. During phases of bedload transport, roughness values are at their lowest in the channel but high over the bar. As bedload decreases, roughness builds up again. Since the interface is also an active transporting sediment area, it also has low roughness values during the beginning of the flood (up to 18:30) and again during the minor pulse at 06:00. Bar roughness is also low during the 06:00 phase but it roughens up rapidly during the final flood stages after cessation of bedload transport.

The water surface topography can be considered as an indication of the state that the river bed is in, as well as whether bedload transport events are under way.

Thus 2-3 large waves (see left diagram Fig. 6.61) are developed during the ascending limb. With the first bedload movement, the water surface becomes chaotic, i.e. sub-divided into many small waves, and gives the impression of "boiling". Once bedload diminishes or ceases the surface becomes organised into larger waves again. Figs. 6.64 a) and 6.65 a) are photographic illustrations of the ascending limb without bedload transport. The water surface is quite smooth and the waves are large and undulating. The wavy surface (Fig. 6.65) is particularly well developed over channel and interface. It is postulated that these waves, clearly differentiable from the cross-sectional water surface plots (Fig. 6.61), are due to the development of vortex-induced flow cells. They will be discussed in more detail in section 6.3.2.2.2 (Flow Cells). Over the bar the waves cannot be seen since the water level is too shallow for flow cells to develop. Appendix A1 illustrates the adjustment of river bedand water surface during the entire flood sequence.

*6.3.2.1.2 Temporal adjustment of geometry*

The temporal adjustment of geometry was calculated as the rate of erosion and deposition in $m^2$ per hour from the detailed bed topographical data. In Fig. 6.66 a), the rates of deposition have been spatially and temporally sub-divided as in the $K_3$ diagram. Least deposition occurred during the bedload transporting phase and at the end of the flood. Similar temporal and spatial patterns were reproduced by the interface and bar. In terms of erosion (Fig. 6.66 b), the opposite is true. Thus erosion peaks significantly during the large bedload pulses and decreases during the

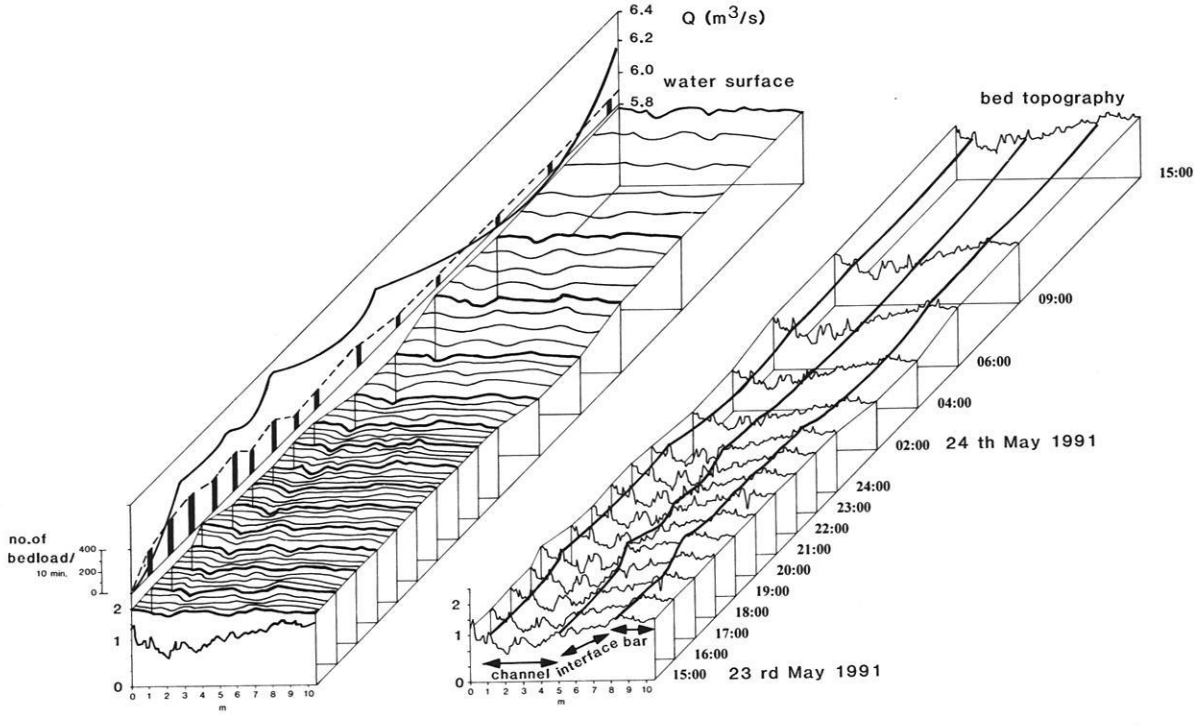


**Fig. 6.61** Temporal changes in river bed roughness and geometry at Squaw Creek during the flood of 23-24th May 1991 (right-hand diagram). The varying extent of the geometry of the right bar, interface, channel and left bar have been marked. The water surface topography (left-hand) is plotted for the same temporal intervals. Thick lines indicate measured sections, thin lines are interpolated. Discharge is shown together with amounts of bedload for the measured sections.

low/non-bedload phases. The interface responds similarly to the bar, i.e. with most erosion after the first pulse, steadily decreasing thereafter. The channel may be eroding at the expense of the interface, so that there is channel widening during the bedload pulse. This may be partially due to lateral collapse under the influence of the development of flow cells.

The total rates of adjustment (Fig. 6.66 c) show that the river bed is adjusting in three main cycles. There is much adjustment as discharge begins to increase and with the onset of bedload transport. The next increase in adjustment corresponds with the first major bedload pulse, followed by a second peak at 23:00 and with the minor pulse at 06:00. Most adjustments occur within the channel. River bed changes correspond least of all with discharge. At peak discharge, the river bed is most stable.

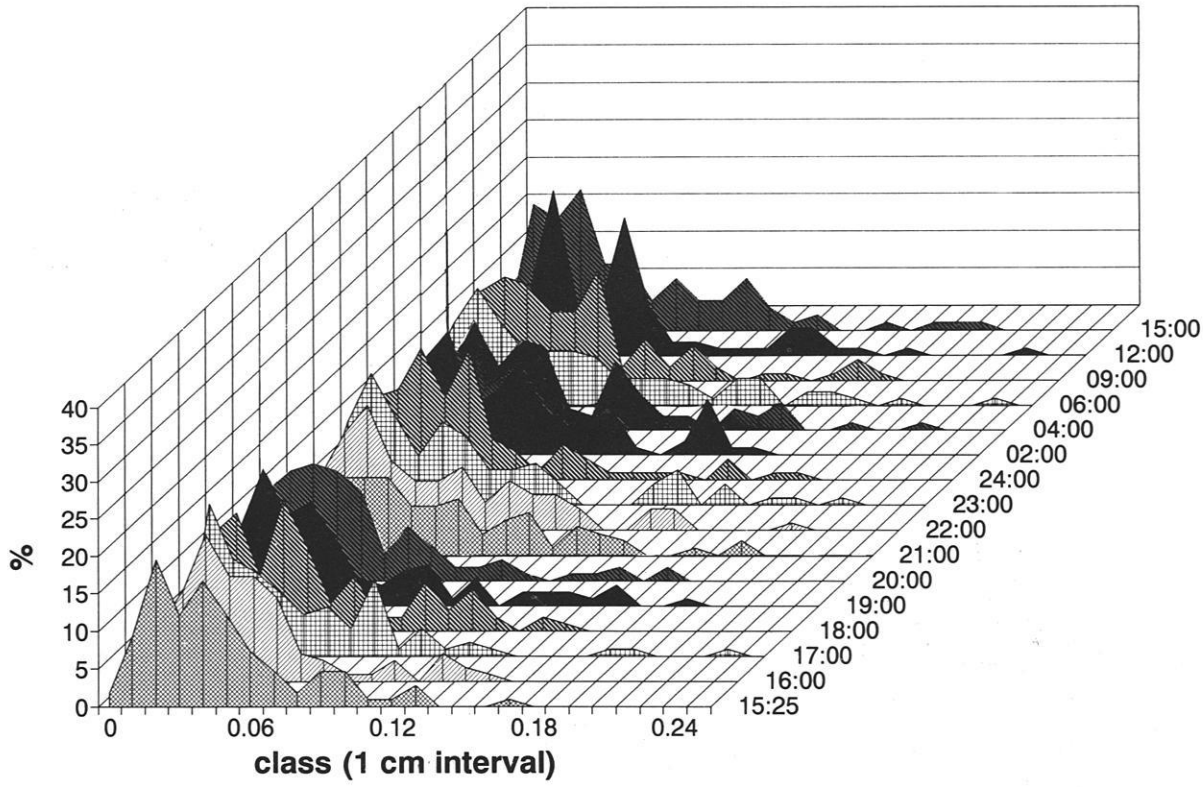


**Fig. 6.62** Temporal variations of $K_3$ frequency distribution during flood of 23-24th May, Squaw Creek 1991. Large roughness features are those appearing above the threshold line at the 0.21 m class interval.

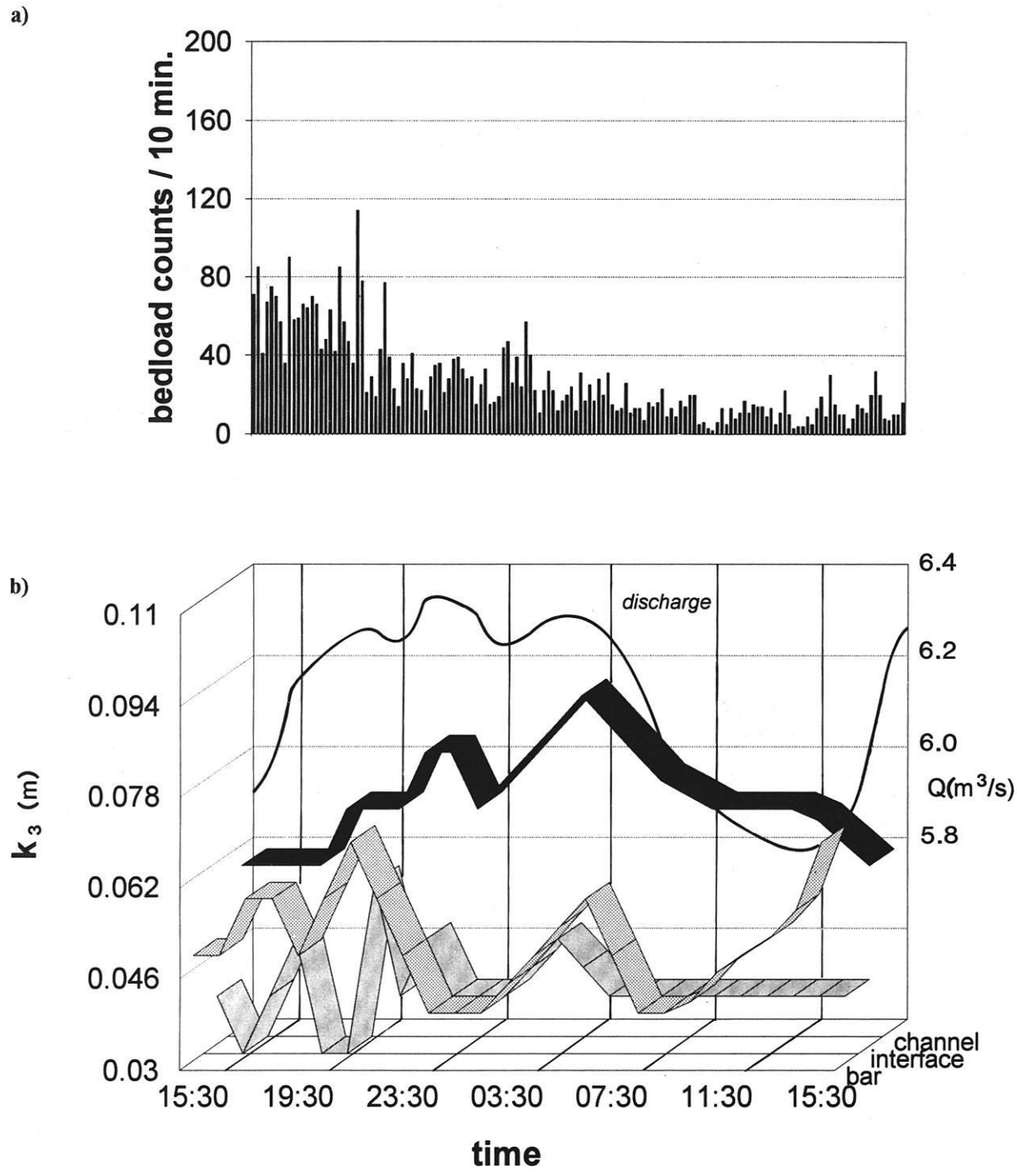


**Fig. 6.63** **a)** Temporal changes of bedload transport, summed as bedload counts over 10 minute intervals for flood of 23-24th May, Squaw Creek and **b)** temporal changes of average $K_3$ roughness values during same flood. The section has been sub-divided into channel, interface and bar.

a)


b)

**Fig. 6.64** Upstream view of water surface at Squaw Creek, **a)** 16:32, 23rd May, very little bedload, notice smooth waves, **b)** 19:11, 5th June moderate bedload pulse, notice beginning of development of shear waves **c)** 6th June 06:07, extremely large bedload pulse, notice "boiling" of water surface and large shear waves over bar and **d)** 10:04, small bedload pulse, notice still widespread development of shear waves. Bedload measurements are focused on the main channel since no data exists on the "new bar".

c)


d)

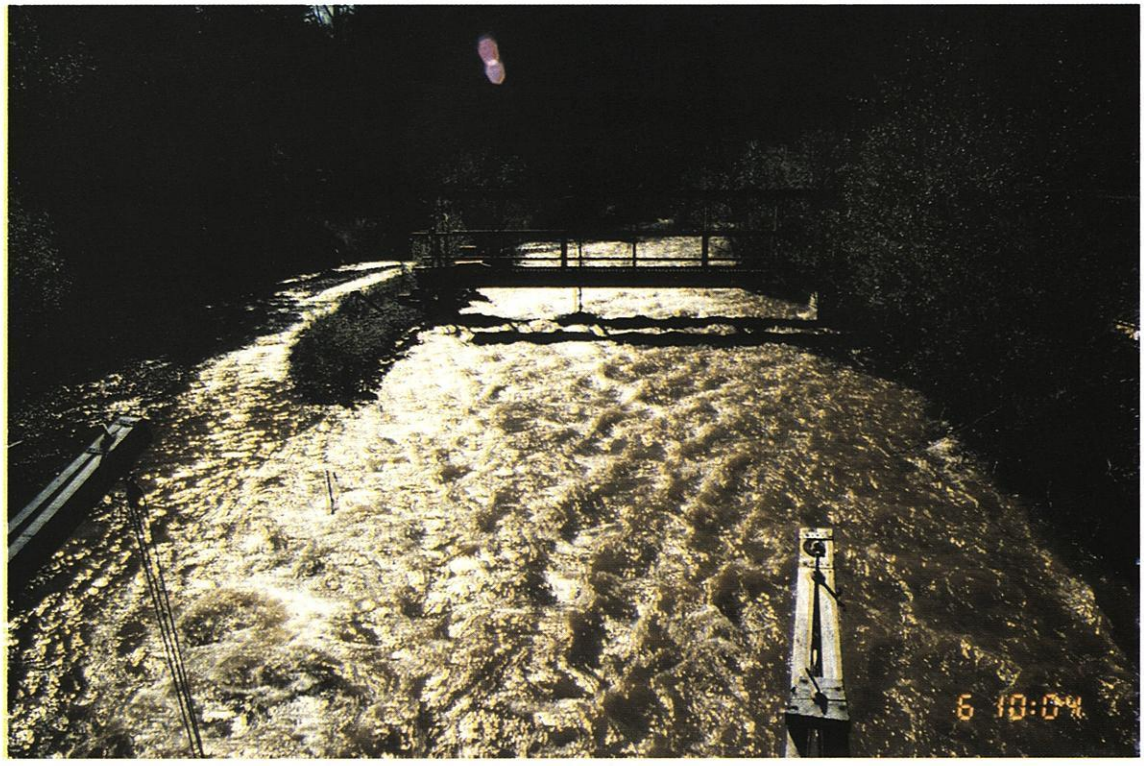

a)

b)

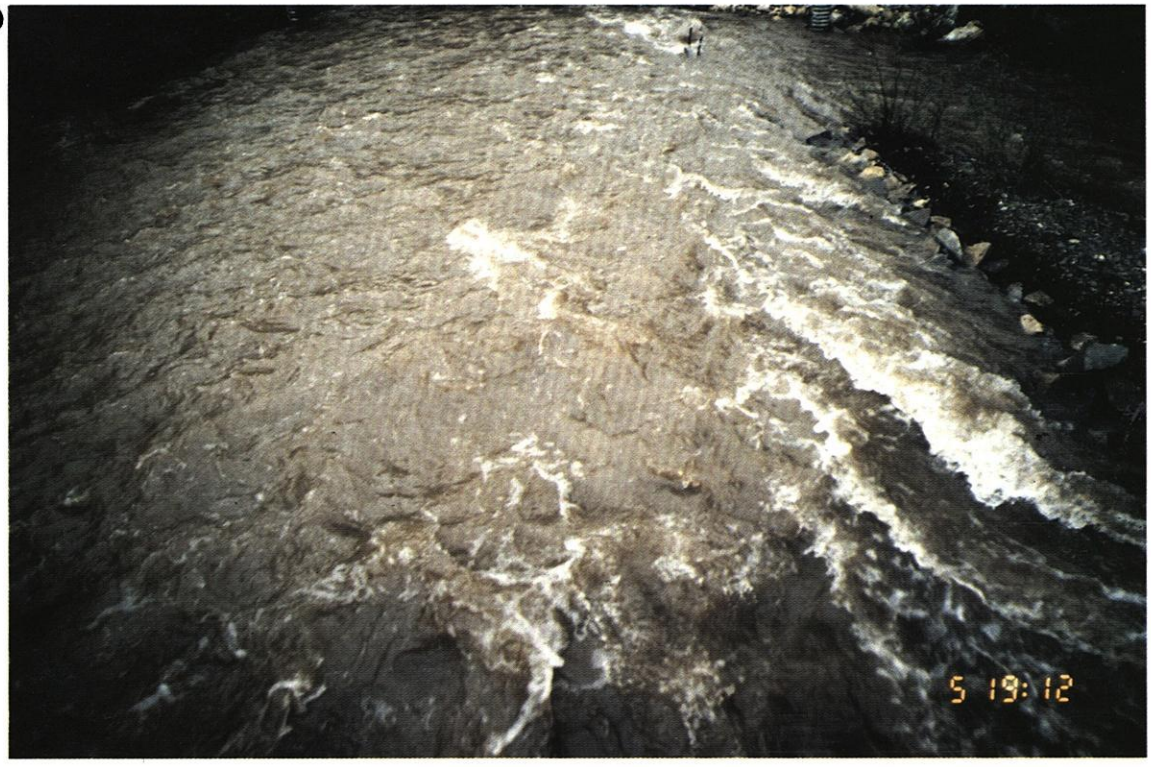

c)

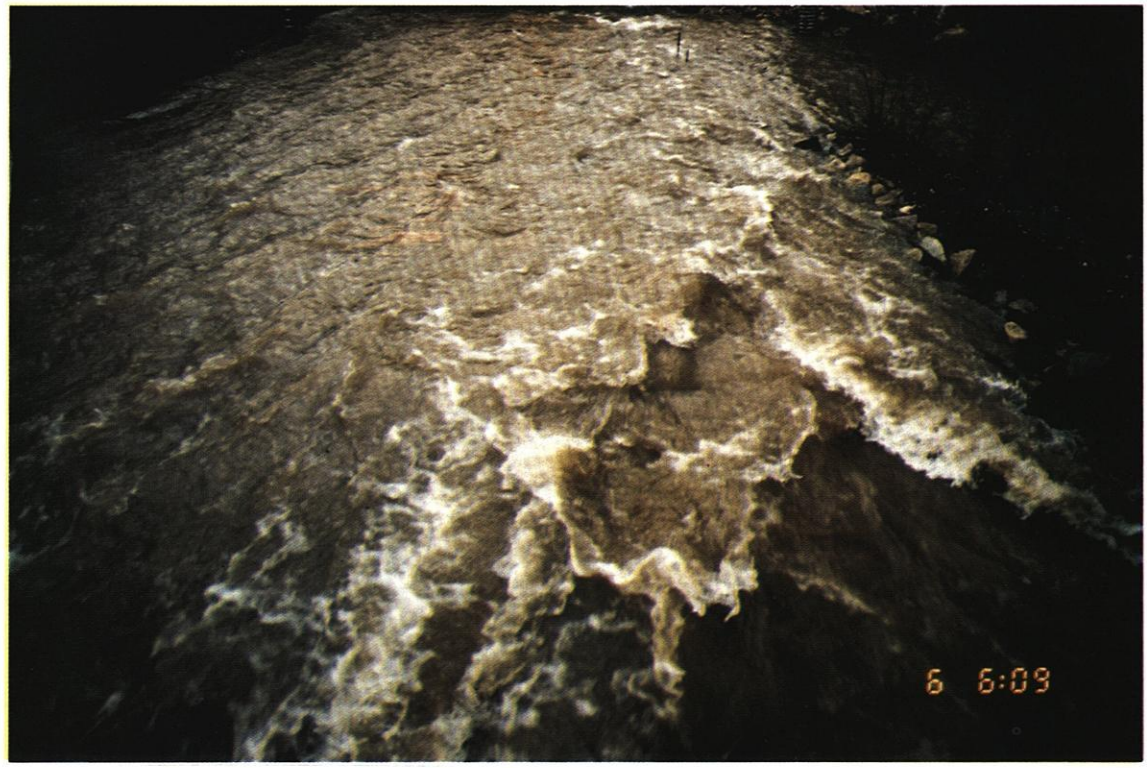


**Fig. 6.65** Downstream view of water surface from Tausendfüssler bridge **a)** on Squaw Creek, 23rd May, 1991, 16:30, very little bedload, notice little froth and wide amplitude waves, **b)** 5th June, moderate bedload pulse, water surface is "boiling", sub-divided into many smaller waves and **c)** 6th June, 06:09, extremely large bedload pulse, notice extreme "boiling" of water surface, very chaotic.

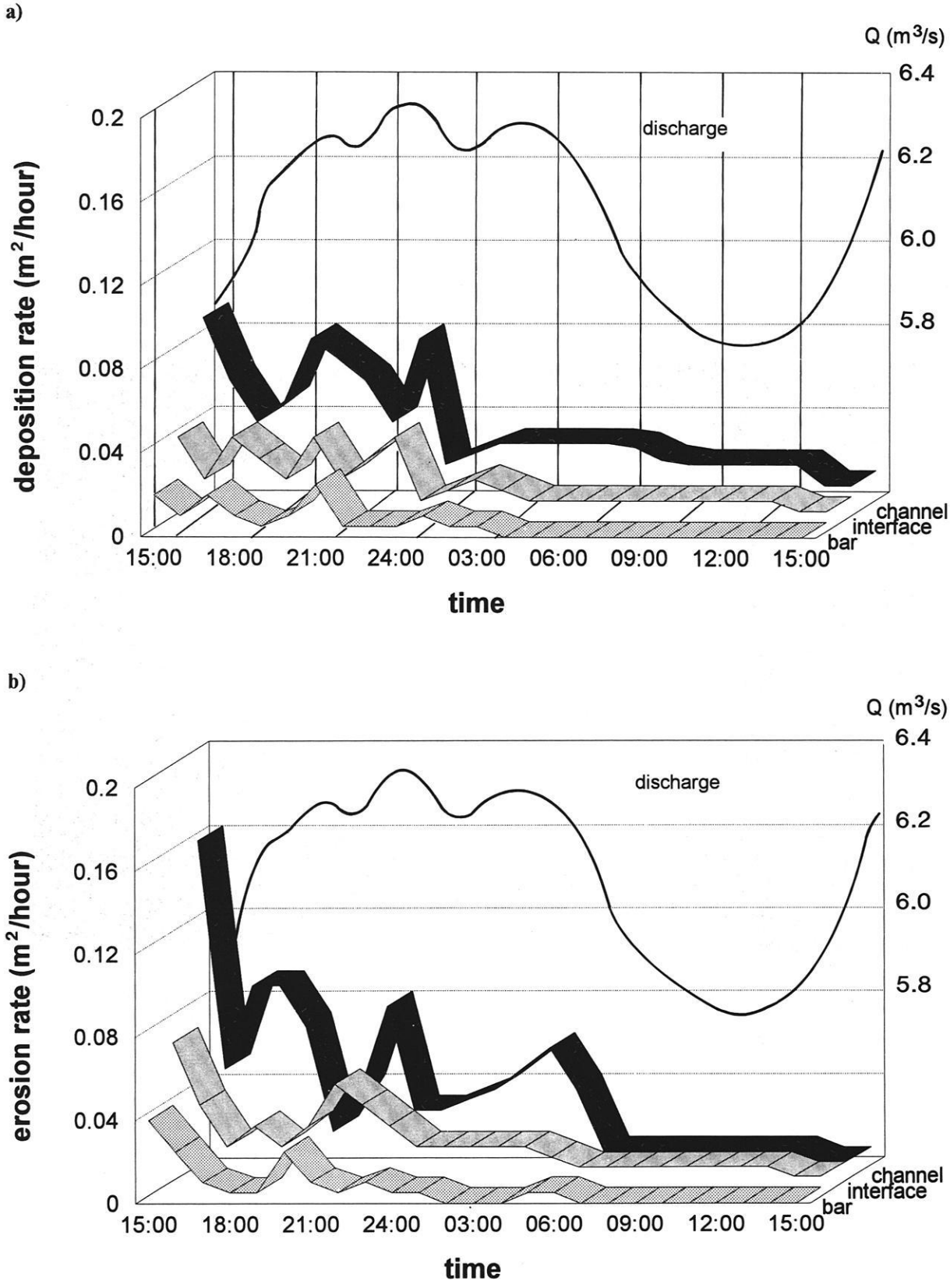


**Fig. 6.66** Hourly rates of **a)** deposition and **b)** rates of erosion, standardised over the Tausendfüssler intervals for channel, interface and bar, Squaw Creek, 23-24th May 1991.

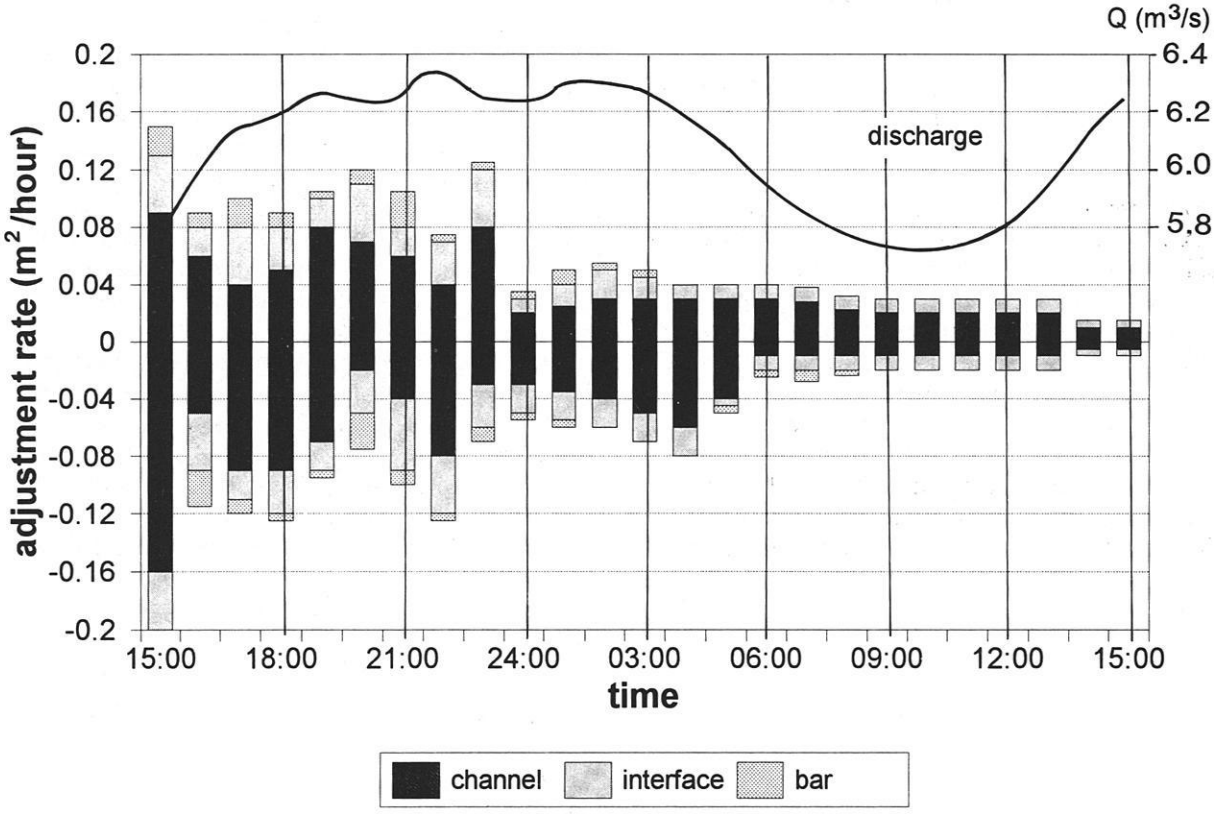


**Fig. 6.66** c) Hourly rates of total adjustment, erosion signified as negative values, deposition as positive values for channel, interface and bar.

#### *6.3.2.1.3 Comparison of $K_3$ and Manning coefficients*

The $K_3$ coefficient was compared with the Manning roughness parameter in order to test its validity against a widely used parameter (Fig. 6.67). When $K_3$ roughness is high, the Manning coefficient is low and this indicates high roughness. An inverse relationship between the two, marking a good correspondence, was obtained for the beginning of the flood until 00:00 (including the time of major bedload transport). During the morning hours (00:00 - 15:30) with low rates of bedload transport, the relation was not so good. The relation between the two parameters became less close after midnight due to less frequent and less simulataneous measurements.

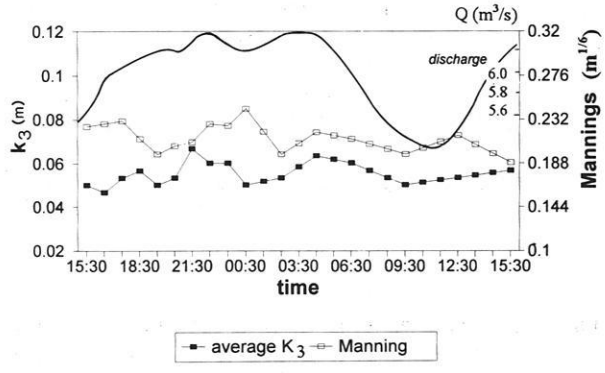


**Fig. 6.67** Comparison of $K_3$ and Manning coefficients against discharge, Squaw Creek, 23-24th May 1991.

### 6.3.2.2 Flood of 5-6th June 1991

#### *6.3.2.2.1 Temporal changes in roughness and water surface topography*

The dynamics of river bed adjustment and changes in roughness on the 5-6th June are very different from those of the 23-24th May (Fig. 6.68, 6.61). This is not only due to the different shape and magnitude of the discharge curve but more importantly due to the dynamics of bedload transport (Fig. 6.60 a)& b)). With the initiation of bedload transport, the first changes of bar and channel roughness can be detected. At 21:30 the first large change in roughness and geometry occurred. The channel became smaller and the left bar increased in size. The change can be related to the large bedload pulse, marked on the diagram. During the very low bedload transport until 03:35, the river bed seems to be adjusting back to its former conditions, (later analyses clearly support this) while very large changes in the geometry and roughness occur as an immediate response to the largest bedload pulse during the descending limb. Although bedload could not be measured in the time between 10:00-13:00 due to lightening it is obvious from the small amounts of bed adjustment that very little bedload must have moved. But at about 13:00, there is another minor pulse which caused the geometry at 15:10 to re-adjust again.

In Fig. 6.69 the temporal distribution of $K_3$ roughness shows sequences of roughness variation in a similar way to changes on the 23-24th May. Thus very high roughness can be found at 19:30, 23:30, 06:00, and 10:00. Low roughness distributions occurred at 17:25, 20:30, 00:30, 02:11, 03:45, and 06:45. Again the very peaked and left-skewed distributions are related to

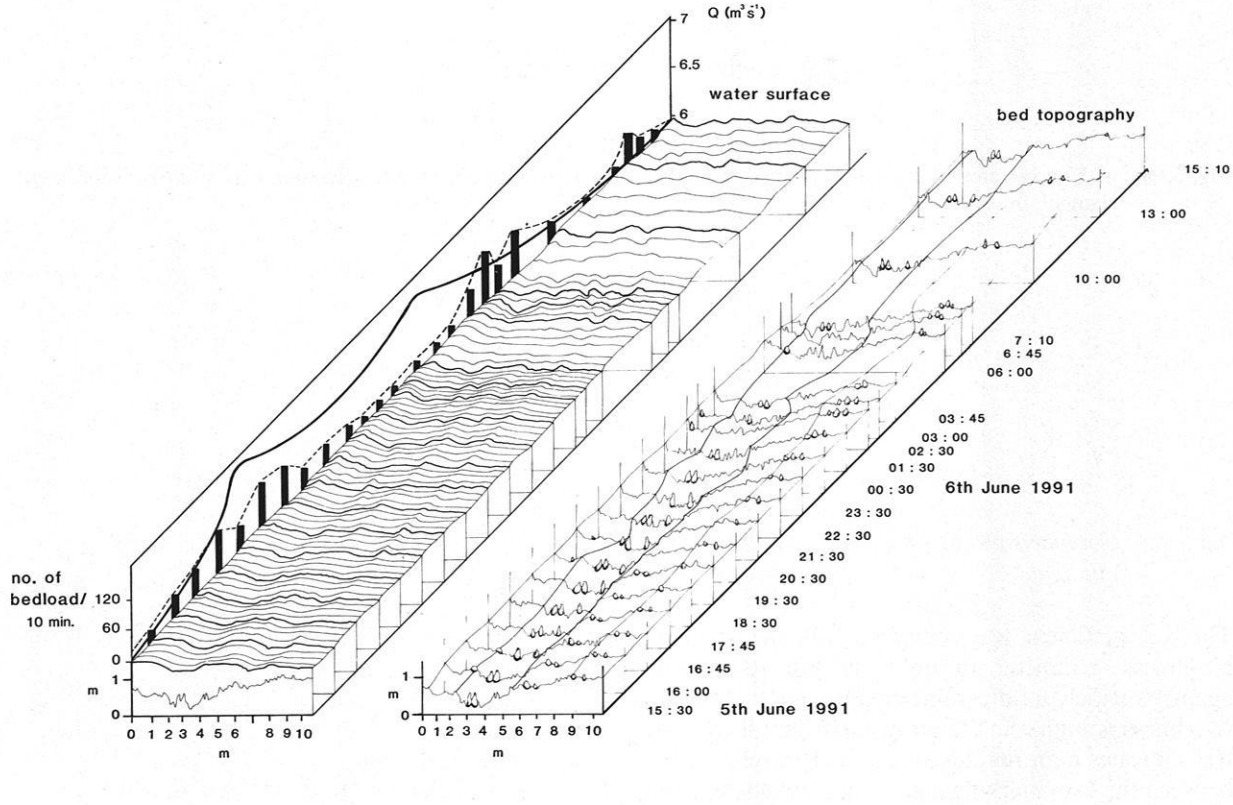


**Fig. 6.68** Temporal changes in river bed roughness and geometry at Squaw Creek during the flood of 5-6th June 1991 (right-hand diagram). Temporary stationary blocks have been marked in addition to the varying extent of the geometry of the right bar, interface, channel and left bar. The water surface topography is marked on the left-hand diagram for the same temporal intervals. Thick lines indicate measured sections, thin lines are interpolated. The discharge curve together with amounts of bedload for the measured sections have been marked for comparison.

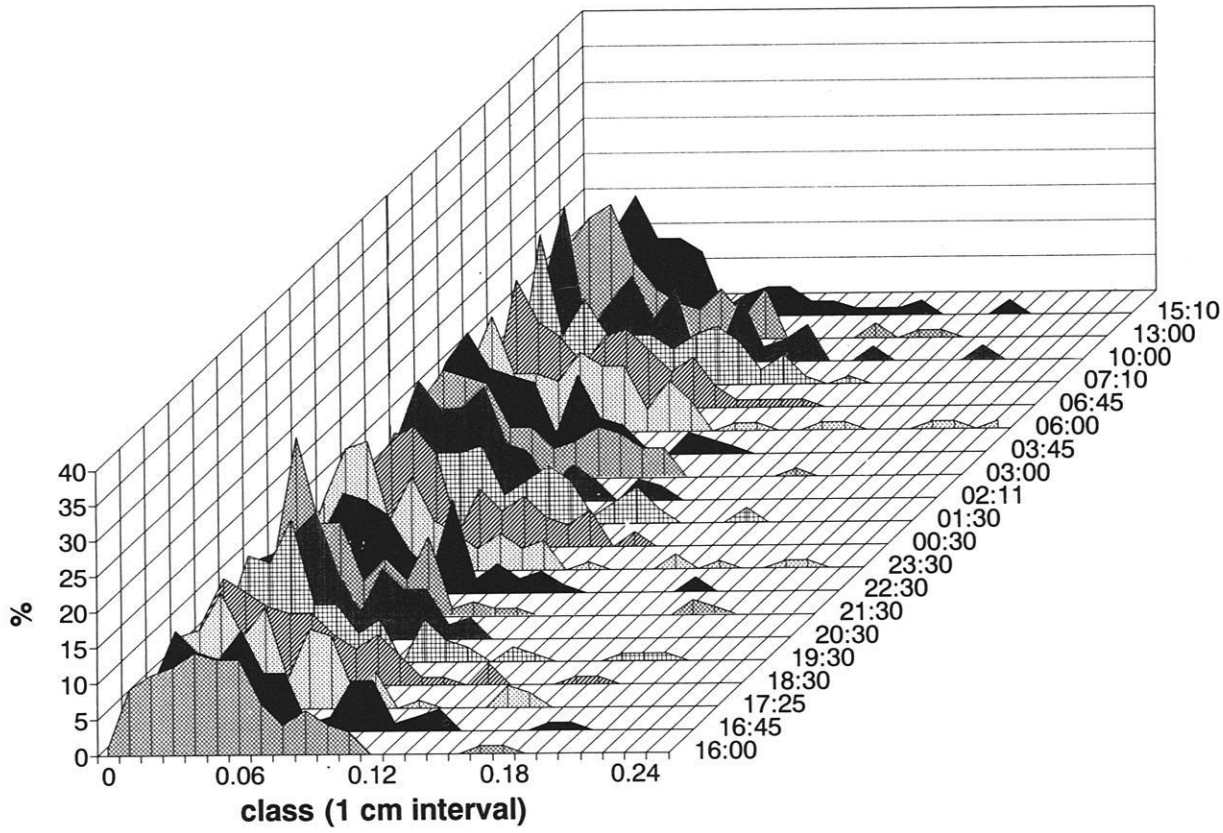


**Fig. 6.69** Temporal variability of $K_3$ roughness distribution at Squaw Creek, from 5-6th June 1991. Time sequence is from fore- to background. Class intervals are 1 cm.

large pulses of bedload. Phases with diminishing or no bedload are reflected in more rounded distributions, including very rough values.

In summary, roughness should be treated as a variable which changes with time and position on the bed. Also, there are distinct phases with high, and others with low roughness which occur totally independently of flood power but are rather so an indicator of intensive, or less intensive bedload transport. The water surface topography (Fig. 6.68) corresponds not only to the configuration of the river bed but also to the state of bedload transport. Thus during the first major pulse at 21:30 (Fig.6.60, 6.64b, 6.65b), the water surface becomes more rippled and splits into a greater number of smaller waves (see section 6.3.2.2.2). As bedload transport decreases, the wave amplitude increases again. During the 06:00-07:10 period the water surface is highly chaotic or "boiling" in correspondence to the largest pulse. Again as bedload transport diminishes, the wave pattern becomes more regulated. In Fig. 6.70 the temporal change of $K_3$ shows that roughness depends upon whether bedload is in transit or not (Fig. 6.60 b). Thus two main phases with very low roughness can be observed in accordance with the timing of the two largest bedload pulses during the event. During the times with little or no bedload, roughness increases again towards the higher values characteristic of the beginning and end of the flood.

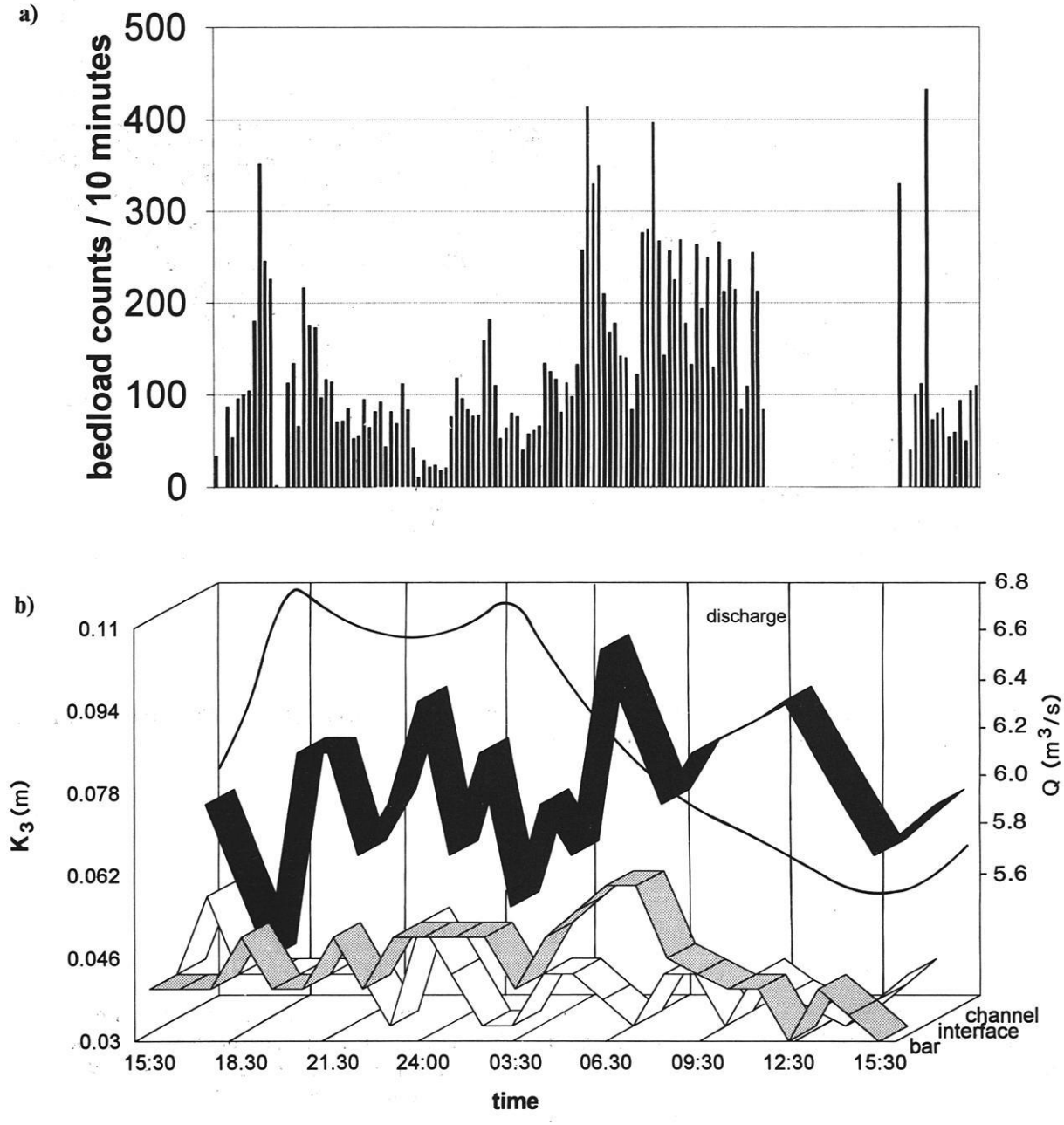


**Fig. 6.70** **a)** Temporal changes of bedload transport, summed as bedload counts over 10 minute intervals for flood of 5-6th June, Squaw Creek and **b)** temporal changes of $K_3$ during flood of 5-6th June 1991 at Squaw Creek, differentiated according to channel, bar and interface.

*6.3.2.2.2 Flow cells*

It has been recognised from both floods that the distribution of roughness is restricted to particular phases and that the water surface also behaves accordingly. If there is a clear correspondence between the two, certain lateral, spiral (vortex) circulations have to be responsible for elevating the water surface at particular locations and lowering it in others (DE JONG & ERGENZINGER, 1992, ERGENZINGER et al 1993, LEOPOLD 1982). Since roughness elements are very regulated in their spacing (see Section 6.1, Spatial Variability of Roughness), and develop during the depositional cycles in the course as non-bedload phases, the water surface has to adapt accordingly. Thus where there is large roughness, water must be converging on the bed, i.e. with little energy dissipation, and where this water is converging on the surface, upwelling will result at the water surface (Fig. 6.71). If however the roughness elements are very large, vertical turbulence will ensue that will cause a disturbance and a new arrangement of the flow cells. The upwelling has to be counteracted by downwelling to both sides. This downwelling is associated with concentration of energy on the river bed and will therefore cause erosion if it is not dissipated by more intensive bedload transport. Based on the observations of water surface and bed roughness in this study during periods without bedload transport, 4-6 waves will develop, i.e. 2-3 pairs, concentrating 2-3 surface waves (Fig. 6.68). The minimum depth required will be 30 cm; for this reason no flow cells are possible on the bar, where water depths do not exceed 10 cm.

The flow cells are visible on the photographs over the main channel (Fig. 6.64 & 6.65). Over the bar, where flow is too shallow for the development of flow cells, clear diagonal patterns are discernible, associated with the formation of shear waves. Their development is described in Section 6.1.5.3 (Spatial Variability of Form and System Roughness). Observation of water surface and the understanding of underlying causes are critical when studying river bed formation and bedform development.

A totally different picture is obtained during the bedload transporting process. Here the water surface was described as "boiling" from observations made during both flood waves (Fig. 6.64b & 6.6.5b). The river bed tended to decrease its roughness and become smooth in order to optimise sediment transfer. Any large roughness differentiation would have offered resistance to bedload movement and it was therefore

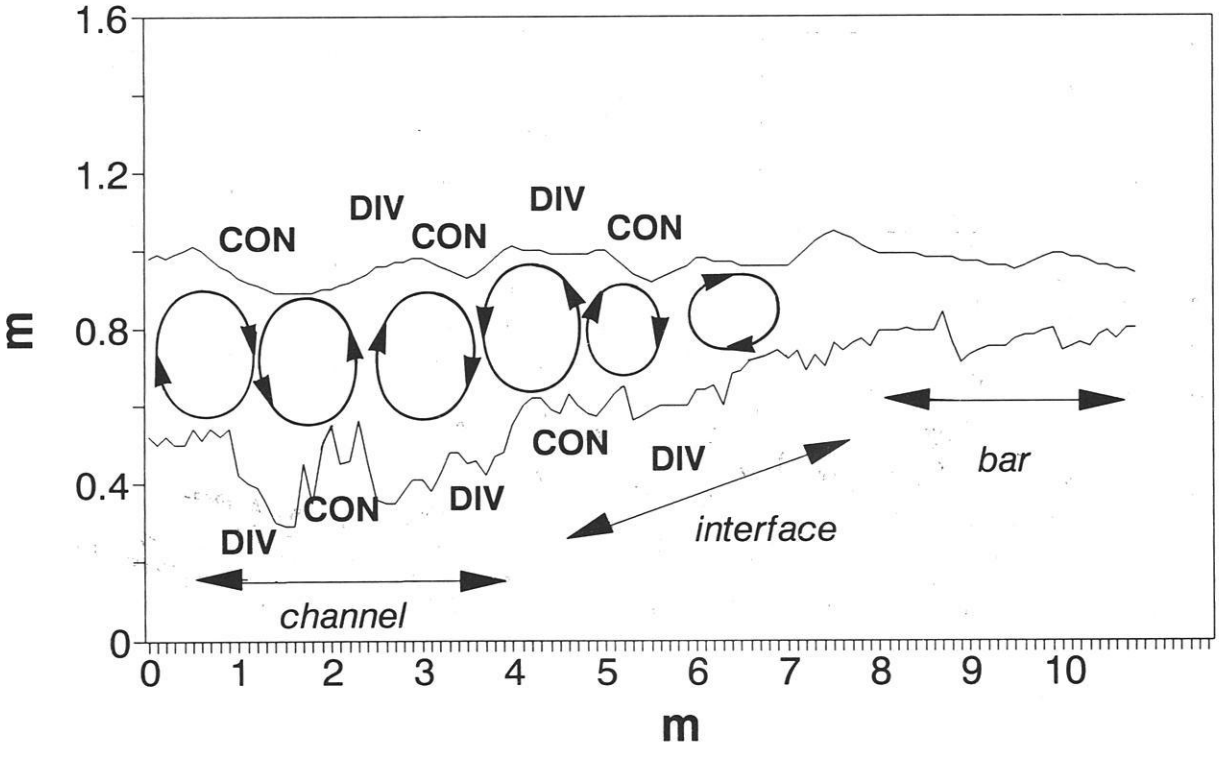


**Fig. 6.71** The development of flow cells. Where there is a large roughness element, water converges over it, causing upwelling at the surface. This leads to divergence at the water surface and corresponding downwelling on the river bed and this time convergence on the river bed.

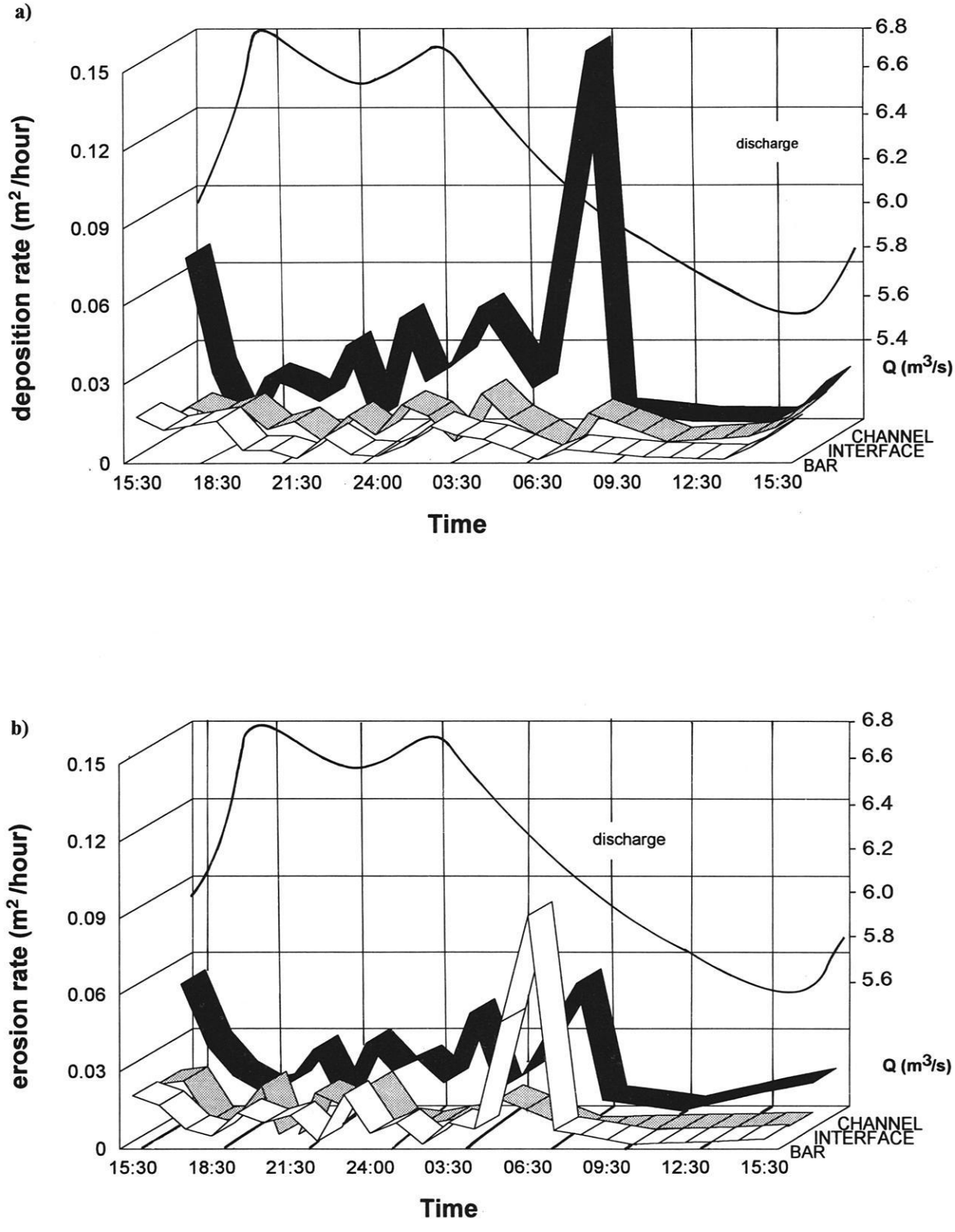


**Fig. 6.72** a) rates of deposition (per hour), b) rates of erosion and c) total rates of adjustment for channel, interface and bar, Squaw Creek, 5-6th June, 1991.

c)

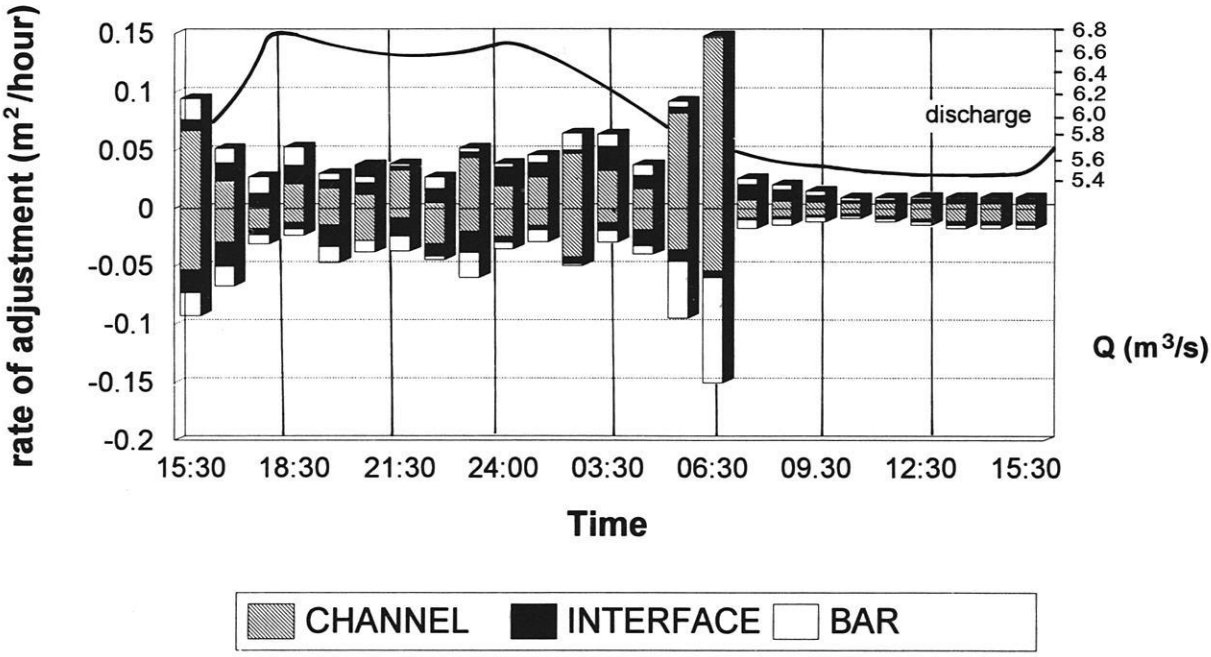


decreased in height either by removal or by infill. During these phases, the flow cells will be destroyed due to the widespread transport of bedload. Flow will become two-layered with a bottom layer merely concerned with efficient bedload transfer and a covering layer of "bedload-free" water. This "bedload-free" layer is highly turbulent and is therefore reflected as a "boiling" blanket over the river bed.

When bedload transport diminishes and becomes concentrated into a few bedload streets, flow cells will be given the opportunity to develop again, initiated from the channel banks.

*6.3.2.2.3 Temporal adjustment of geometry*

The flood of 5-6th June was anticipated to demonstrate different behaviour in river-bed adjustment due to the very delayed major bedload pulse. In Fig. 6.72a) the rates of deposition are highest during the major bedload pulse at 06:00. On the bar and interface, deposition rates occur in cycles, where the highest peak dominates during the beginning of the flood. Deposition rates do not run parallel with discharge, and at peak discharge deposition is at its lowest. Erosion rates (Fig. 6.72b) occur in steady cycles with minor, regular peaks in the phases preceding and superseding bedload transport. On the bar, erosion is highest at the time of peak bedload transport, as was the case for the flood of 23-24th May. In the summary diagram (Fig. 6.72c) it can be seen that in terms of work, most is achieved during the 06:00-07:10 bedload phase which was monitored three times during that period, both in terms of erosion and deposition. Large amounts of activity are also predominant during the ascending limb with active bedload transfer (Fig. 6.72 c). During the minor bedload pulse, approximately 4 particles were transported over the entire river width per minute, whereas during the major pulse, nearly 14 particles were transported per minute.

If the rates of adjustment are compared with rates of bedload throughput at the time (Fig. 7.73) and these dynamics are compared to discharge, then adjustment rates are controlled by bedload transport more than by discharge. This observation has serious implications on the validity of the well established shear stress criterion in determining sediment transport.

River-bed adjustment was calculated in terms of the number of particles eroded or deposited from one measurement period to the next. Bedload transport was summed for the counts over the entire upper sill,

and particle adjustment was calculated for the entire river width for the same event. Thus an hourly rate was obtained, assuming $1m^2$ of horizontal or vertical river area to be covered on average by 500 particles (from photo-sieving, see Fig. 6.74 a & b). Although the packing of material is different on the surface from that in section, it is noteworthy that, on the 23-24th May (Fig. 6.74 a), a maximum of only 38 detectable particles per hour were probably eroded over the 10 m river width at 23:00 and the same amount was deposited again during peak bedload transport (06:00). This is the equivalent of 8% of the river bed in section, thus if it is assumed that 500 particles are stacked depth-wise in the river bed, 38 particles will constitute nearly two layers of material. During the flood of 5-6th June (Fig. 6.74 b), up to 70 particles per hour were deposited at 03:45 and 80 eroded at 06:00. This is the equivalent of 16% of the armour layer or 4 sheets of particles depthwise. The 5-6th June flood event was therefore twice as effective in terms of work achieved.

The difference in adjustment should not only be dependent on grain mobility but also on the grain sizes involved. Work by BUNTE (1990) showed that during the rising limb of a flood at Squaw Creek, the grain sizes increased. The selective transport of finer material resulted in the coarsening of the armour layer. The cobbles that were left behind became increasingly projected into flow and were more likely to become entrained. These types of processes were

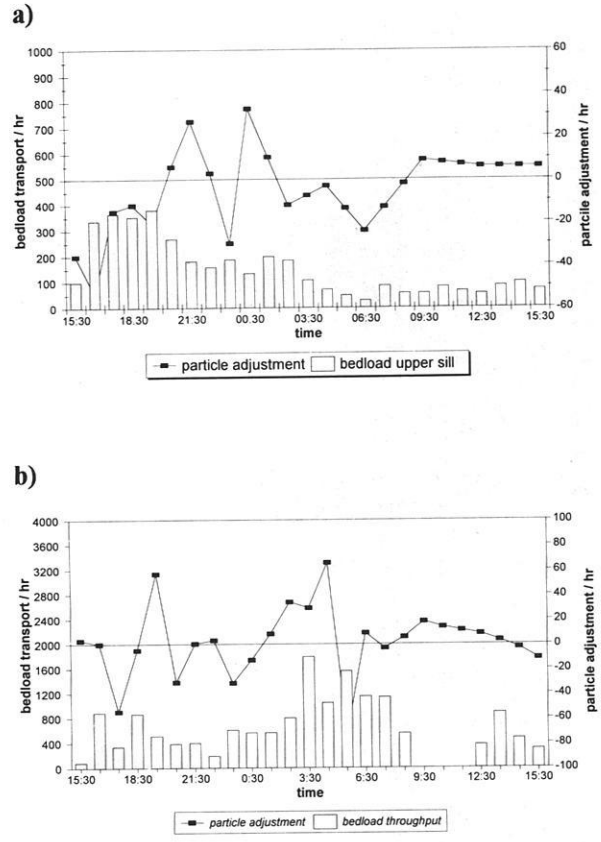


**Fig. 6.74** Bedload transport over the upper sill (in particles per hour) against cross-sectional particle throughput (calculated amount of particles being moved over particular river width per hour) for **a)** 23-24th May and **b)** 5-6th June at Tausendfüssler location calculated in terms of lateral river bed adjustment. Negative values indicate erosion and positive values indicate deposition.

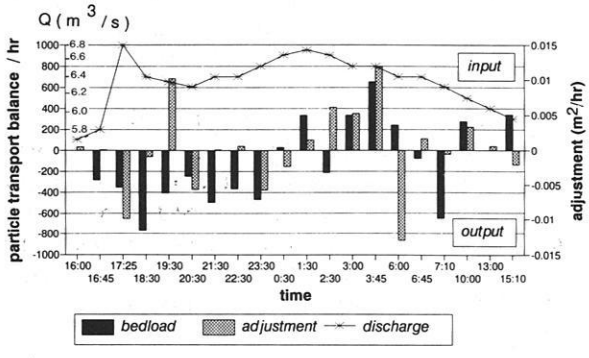


**Fig. 6.73** River bed adjustment correlated against bedload balance over both sills in relation to discharge.

described to occur only during short periods of time. Thus although the rates of particle transfer calculated were hourly, they did not guarantee that this rate was maintained throughout the entire hour. It was only at peak bedload transport that a sheet of particles could be kept in transit two or four particle layers in thickness. Since there is a dramatic difference in erosion and deposition rates during the rest of the flood, it can be stated that for the other periods, bedload under transport did not cover all of the river bed. The randomness of scour and fill during a bedload transporting event has been suggested by other workers (LEOPOLD & MADDOCK, 1953, JACKSON & BESHTA, 1982, ERGENZINGER 1992, ERGENZINGER et al 1993). They

acknowledge that if spatially differentiated changes are to occur, then bedload transport cannot be uniform over space and in time.

Most bed changes are therefore induced by single threads or micro-pulses of material. The appendices (Appendix A1, Squaw Creek, 23-24th May) clarify how very localised the changes of the river bed geometry and roughness are and how quickly the water surface will respond and vice versa.

The example of 5-6th June (Appendix A2) is a unique example of how spatially sensitive roughness and geometry changes are in relation to the bedload balance calculated between the upper and lower sills. Although there is insufficient space to demonstrate each single example, the event of 5-6th June (Appendix A2) does create a very detailed picture of the dynamics of bedload input, associated parallel adjustments of the river bed and water surface and output. Thus the characteristics of the within-reach effects of bedload transfer (i.e. whether erosive or depositional) could be related not only temporally but also spatially within a localised area. These local changes are not only due to local bedload streets but are also the joint result of flow cell development. Where a particular flow cell converges or diverges, erosion or deposition will result.

Additional proof for this mechanism of local scour and deposition comes from the detailed analyses of the structure of bedload transport at hecto-second intervals. The very small pulses of bedload that were discovered mostly travel as normally distributed groups of material. Experiments in the flume (TAIT pers. comm.) verified that bedload transport will only occur in sheets during the most intensive bedload phases. At all other times, bedload is of a localised, pulsed nature. If the pulsing of material is discussed in the context of local turbulence (EINSTEIN 1958, GRASS, 1971, 1991, SUTHERLAND 1967) then it can be concluded that the grains moved in a series of short bursts are confined to a small area. At each burst the grains move simultaneously to form the pulse observed in nature.

If bedload transport did occur as sheets of material, the structure or mere existence of these minor pulses would be very different. Associated adjustment of the river bed would also be more homogeneous and widespread. Since the dynamics of bedload movement are however very complex and interrelatable with the organisation or destruction of numerous local flow cells, the adjustments and particular roughness conditions on the river bed respond accordingly. Thus roughness and geometry changes on the river bed are directly dependent on the flushing of sediment through the system and are directly interrelated with flow cell development rather than the amounts of fluid transfer.

#### *6.3.2.2.4 Comparison of $K_3$ and Manning coefficient*

Comparison of the $K_3$ and Manning coefficients was difficult for the flood of 5-6th June since it was not possible to take velocity measurements after 00:30. Fig. 6.75 does demonstrate however that Manning and $K_3$ run inverse to each other, and they therefore indicate a good relationship, as for the flood of 23-24th May. The parameters used for the calculation of the Manning coefficient were obtained at 2 hour intervals in contrast to the hourly $K_3$ measurements. The Manning coefficient fluctuates less dynamically than $K_3$.

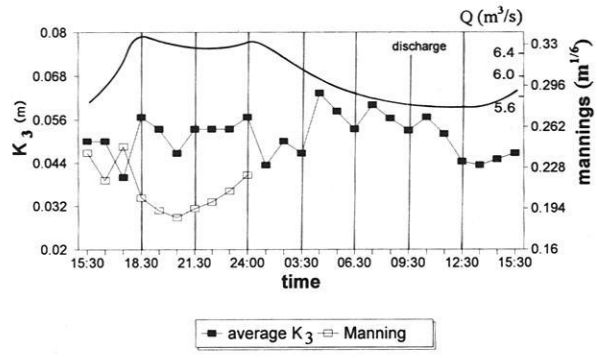


Fig. 6.75 Comparison of $K_3$ and Manning roughness coefficients for flood of 5-6th June.

#### *6.3.2.2.5 CAVE (Coefficient for Average Velocity Estimation)*

CAVE stands for the Coefficient for Average Velocity Estimation. The coefficient is part of a formula that calculates the average velocity from a modified Manning formula that is based on actual measured variables, including the $K_3$ roughness coefficient as a replacement of Manning's n. If $K_3$ is divided by the Manning coefficient, a constant of 0.25 is obtained. When u becomes the determinant of the equation, the constant value of 4 is referred to as CAVE. Exactly the same coefficient is obtained for the flood of 23-24th May. If these findings are to be used as a tool for predictability of flood dynamics or in paleohydrology, the estimation of velocity is often essential. The mean

velocity at Squaw Creek for the normal snow-melt floods can be predicted using the equation:

$$\bar{u} = 4K_3R^{2/3}S^{1/2}$$

In the same way, if velocity is known, the relative roughness and the determination of grain or form roughness can be predicted from the hydraulic radius, slope and constant of 4.

This coefficient naturally depends on grain size and the threshold of grain to form transition. The same relationship can be tested for the Lainbach flood in order to determine the grain size/roughness coefficient after the model to be tested is described.

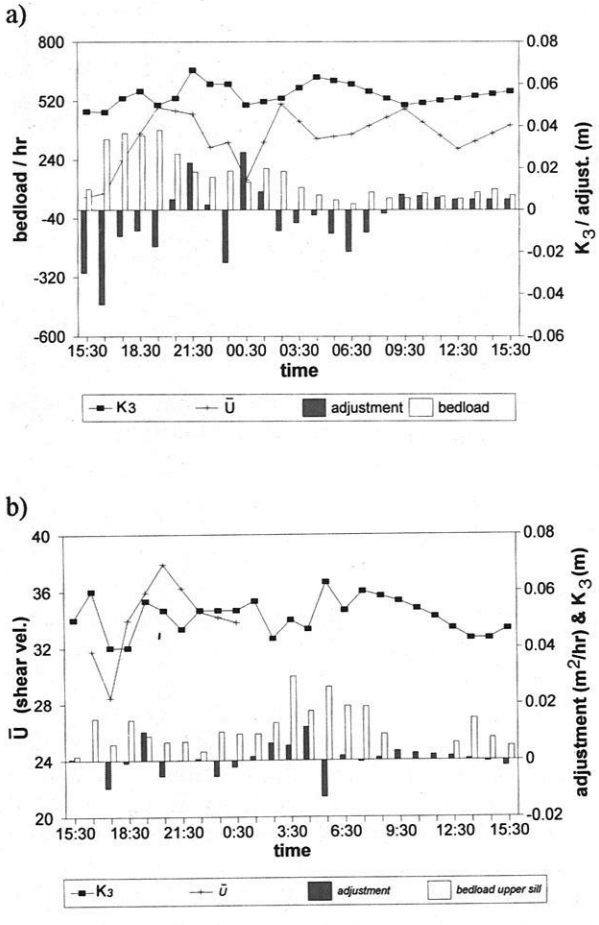


**Fig. 6.76** Temporal dynamics of $K_3$, bed adjustment, u, and bedload for **a)** 23-24th May and **b)** 5-6th June at Squaw Creek, 1991.

### 6.3.3 Interactions between roughness, geometry, bedload transport and flow dynamics: FAST (Fluid and Sediment Transfer)

When the events of 23rd May and 5-6th June are compared in terms of $K_3$ roughness, bed adjustment, average velocity and bedload transport, some very cohesive correlations can be derived. Starting with the 23rd May (Fig. 6.76a), where bedload transport is intensive, critical velocity is high and $K_3$ low. During this phase erosion predominates. Deposition occurs in the phases in between and during the descending limb. Similar relationships between transport and scour were obtained by JACKSON & BESHTA (1982). Unfortunately the event of 5-6th June (Fig. 6.76b) can only be discussed for the first half of the flood. Nevertheless when bedload is high during the first minor pulse, velocity is also high and the $K_3$ coefficient decreases rapidly.

If the interactions between river-bed roughness and geometry are to be explained in relation to bedload and flow, it is not sufficient to limit the interpretations to one lateral transect. As described earlier, bedload transport is a variable, erratic process that induces large changes in bed gradient and river bed morphology. Since the bed gradient reflects the ongoing process of erosion or deposition, the water surface has to be elevated or lowered accordingly. Thus measurements of the water surface gradient, obtained from the right and left bank, correspond with the bedload balance (Fig. 6.77). Where $K_3$ values declined, the reach was eroding (more particles exiting the lower sill) and the water surface gradient became high (0.021) on the left bank. The right bank gradient behaved similarly but only increased to 0.019. At both locations gradient increased slightly. With the second and largest pulse of bed material, there was deposition within the reach. As the extreme pulsing begins, both water levels rose sharply but as the material begins accumulating, the gradients dropped down to their absolute minima, both at 0.019.

This balance in gradient could well be the reason why no further deposition is possible and erosion must proceed. Once erosion begins and/or the temporary sediment store is being depleted, the right hand water level begins rising steeply whereas the left bank gradient is decreasing steadily. This continues up to the point where both reach the same gradient and correspond with the next minor bedload pulse. Discharge has begun to increase again at this point, marking the beginning of the next flood event.

To summarise, water surface gradients are high where there is in-reach deposition and intensive material throughput over the upper sill. Water levels drop where there is intensive erosion. The state of the river bed responds such that roughness is low when there is a pulse and roughness is high in the period in between.

These results can be summarised in the following conceptual model (FAST) standing for Fluid And Sediment Transfer (Fig. 6.78). The main inputs are bedload transport and discharge, where discharge can be regarded as a continuous process but bedload should be seen as a discontinuous, pulsed process.

Bedload discharge over time behaves erratically and is not dependent on the discharge curve. There are periods during high flow when there is no bedload transport, and periods not at the hydrograph peak when transport rates are high. Other authors have also found that bedload transport is not a direct function of discharge (HAYWARD & SUTHERLAND 1974, ANDREWS, 1979, HAYWARD 1980, REID 1986, KUHNLE 1988, BÄNZINGER & BURSCH 1990, SHIH & KOMAR 1990, BUNTE 1992, ERGENZINGER & DE JONG 1992, ERGENZINGER et al 1993).

A second element of the model relates to the interaction of bedload transport intensity and hydraulic response. FAST differentiates two hydraulic phases according to whether intensive bedload transport is under way or bedload transport is weak and localised.

Bedload interactions with flow are important. Thus during intensive bedload transport, 2 layered "chaotic" flow efficiently transports sediment but during less intensive bedload transporting phases, vortex flow develops. Most changes in roughness and river bed geometry will occur during the high intensity bedload transporting phases.

Similar sub-divisions of bedload into phases of weak and strong transport have been made by JACKSON & BESHTA (1982), though in this case, bedload intensity was classified over longer time-scales. They state that a change in bed elevation must be accompanied by a difference in bedload balance (in and out) and that there is a predictable relationship between sediment discharge and the characteristics of flow as well as available sediment. They found that irregular channel geometries are the cause of differing relationships between velocity and discharge form place to place. A dynamical equilibrium exists

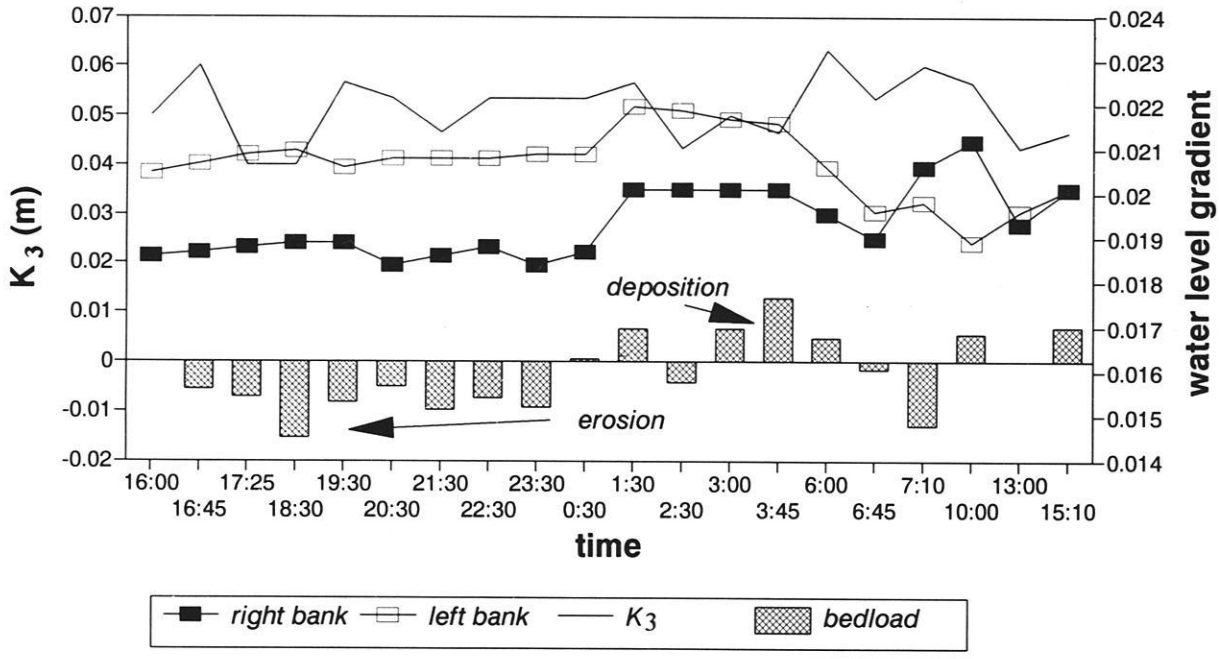


**Fig. 6.77** $K_3$ roughness against right and left bank water surface gradient and bedload balance for Squaw Creek, 5-6th June 1991.

between local geometry and bedload transport. They did however admit that stream channel processes have been insufficiently monitored for calibration and verification. The details of JACKSON & BESHTA's interpretations are uncertain because the accuracy of their Helley-Smith bedload samples is unknown. Even the more representative net sampler (BUNTE 1992) could not be applied continuously at Squaw Creek, and major bedload pulses were often totally missed or misrepresented. Clearly, point samples of bedload are problematic and this problem needs a solution.

A third element of the model, the outputs, suggests that most changes in roughness and geometry occur during intensive bedload transport. The properties of the water surface, roughness magnitude and distribution as well as the geometry of the river bed can be differentiated and quantified according to these two main phases identified in the second element of the model. Thus the water surface will tend to be of a wavy nature during the organised flow cell, weak-bedload-transporting phase. Roughness in terms of the $K_3$ coefficient will be spatially differentiated and there will be a pronounced differentiation between bar and channel. During the bedload transporting phases however, the water surface will be of a "boiling" nature, $K_3$ roughness values will be low with little spatial differentiation and the geometry of the river bed will tend to smoothen.

From the model, bedload and non-bedload transporting phases can be differentiated according to these properties. It is clear that water surface descriptions are essential in characterising the state of the river bed and bedload transport. Such types of measurements need to be treated in more detail in the future. Although the measuring set-up at Squaw Creek was extended in 1992 to accommodate detailed measurements of the water surface at 20 cm intervals with water surface sonars and tracer experiments, the lack of snow-melt events during the field-season did not allow any flood events to be monitored. The role of FAST (Fluid And Sediment Transfer model) as a possible tool in prediction of river bed roughness, flow and bedload characteristics will be treated in the next section. The FAST model will be tested in a similar mountain torrent in the Lainbach study site but under steeper gradient conditions and under higher flood flows carrying with them larger particles that cause higher effective $K_3$ roughness.

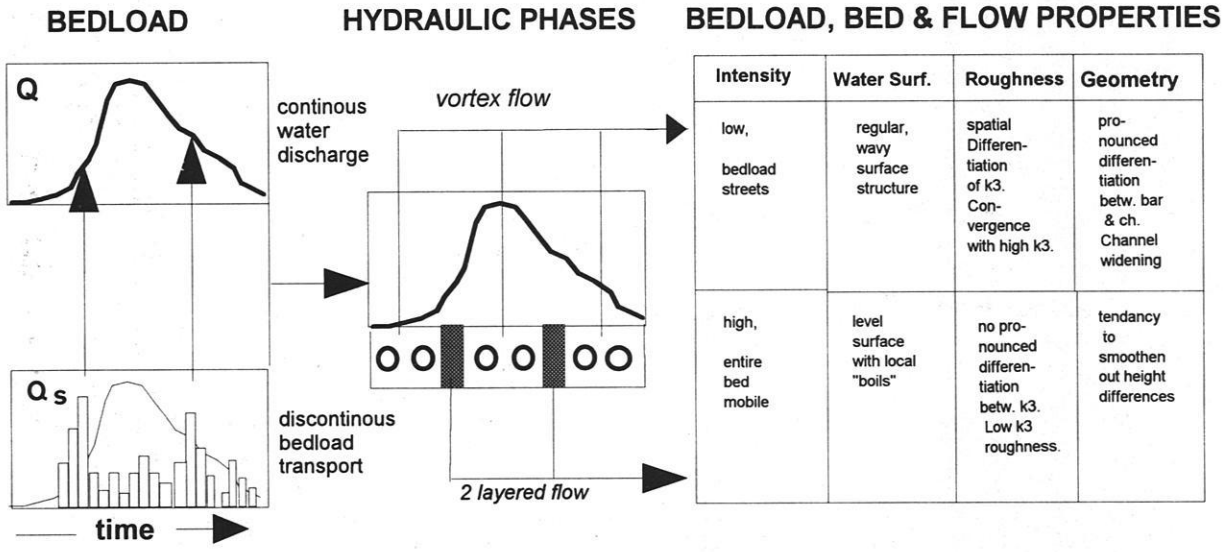


**Fig. 6.78** The FAST (**F**luid **A**nd **S**ediment **T**ransfer) model. The inputs in the first stage of the model are defined as bedload (discontinuous process) and discharge (continuous process). The effects of discontinuous bedload transport are characterised by the hydraulic phases, i.e. whether 2 layered or sub-divided into flow cells in the second stage in the model. The outputs in the third stage of the model are the associated river bed roughness and flow properties. These include the nature of the water surface, the extent and magnitude of roughness and the geometrical variations of the river bed.

## 6.4 Temporal variability of roughness and geometry: Lainbach 1992

### 6.4.1 The nature of bedload and discharge: flood of 22-23rd July 1992

Bedload transport could not be measured temporally in the Lainbach study area, since no bedload detector was in existence. The behaviour and spatial distribution of single particle tracers was investigated in turn but this did not allow comparisons to be made on an hourly or site basis.

In the Lainbach the aims of the study were to obtain detailed information on the spatial and temporal adjustment of roughness and geometry which was possible over a 50 $m^2$ area in the region between an upper, lower, and longitudinal Tausendfüssler bridge. The results could be examined in light of discharge and velocity but not with respect to bedload transfer. The question examined was whether the FAST model could be successfully applied in a different environment, the Lainbach, so that changes in the properties of roughness, geometry and the water surface could be related to flow cell existence and to the visual and acoustic observations of intensive and non-intensive periods of bedload transport. The intensity of bedload transport was noted from the banging of pebbles against the measuring rod.

The Lainbach measurement experiences are unique in that they provide simultaneous high-resolution spatial and temporal roughness and geometry data both longitudinally and laterally. Two separate Tausendfüssler bridges allow an adjustment balance to be made in terms of erosion and deposition. In addition roughness changes and the detailed spatial behaviour of vortex spirals over 5m length are reconstructed during a natural flood event.

The flood of 22-23rd July 1992 was not a typical orographic event, since it consisted of two discharge peaks, a minor one at 17:20 and a major one at 22:30. The discharge curve consisted of a gradually ascending first discharge peak (2 $m^3sec^{-1}$), a fast descent and a rapid but much higher second discharge peak (9.7 $m^3s^{-1}$), with a gradually descending limb. The double peak in discharge offered the opportunity to compare the Lainbach event to the similar event on 5-6th June, 1991 at Squaw Creek. The largest pulse of bedload material probably ensued between 21:00-23:30 based on acoustic observations made during the Tausendfüssler measurements.

### 6.4.2 Dynamics of river bed roughness and geometry in relation to water surface

So far studies concerning the three-dimensional spatial and temporal variability of river bed roughness and geometry have not been recorded for gravel-bed mountain streams nor have detailed comparisons been made to the three-dimensional water surface structure. This subject will be treated in detail in the next section especially with regard to changes in roughness and adaptation of river bed geometry and the water surface over channel and bar. The $K_3$ roughness coefficient is used for the studies in the same context as for the Squaw Creek floods. $K_3$ comparisons of the longitudinal and two cross-sectional profiles will be made with the Manning roughness parameter.

#### 6.4.2.1 Temporal changes in roughness and water surface topography

*6.4.2.1.1 Longitudinal profile*

The changes in river bed geometry in the long profile can be derived from Fig. 6.79 (right-hand diagram). Most changes in roughness and geometry occurred at 21:45 and minor changes at 17:40, during the descending limb of the first discharge peak and during the ascending limb of the second and larger discharge peak. During the rest of the flood, the configuration of the river bed and roughness re-adjusted to the initial conditions. According to the FAST model, most bedload transport will be occurring during those phases where the river bed is smoothest (17:40 and 21:45) and roughness is at its lowest.

By applying the FAST model, the water surface topography (left-hand diagram, Fig. 6.79) can be considered as an indicator of the state that the river bed is in as well as which bedload transporting phases are under way. Few large waves are developed when bedload transport is weak, which could be characterised as the phases at the very beginning of the flood at 12:00 and those from 23:30 to 10:00. The following description for changes in roughness and the water surface were obtained from the sequence of diagrams in Appendix A3. In each case the difference of the water level and river bed from one measuring session to the next was considered.

During the phase lasting from 12:00-17:20, there are three main waves. The wave trough corresponds to

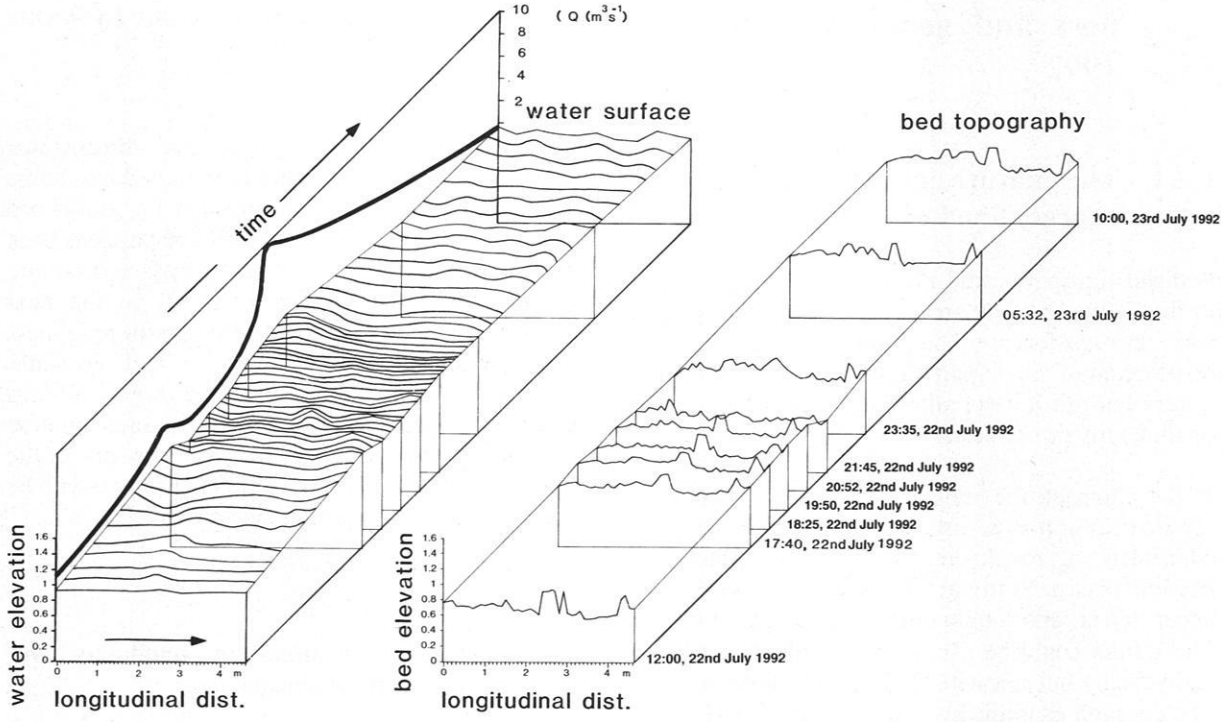


**Fig. 6.79** Temporal changes in longitudinal river-bed adjustment and geometry in the Lainbach during the flood of 22-23rd July 1992 (right hand diagram). Measurements were taken from the channel parallel bridge, between the upper and lower cross-sectional bridges. Flow is from left to right. The water surface topography is plotted on the left-hand diagram for the same temporal intervals. Vertical lines at the transect indicate measured sections, lines in between are interpolated. The discharge curve has been added for comparison.

deposition, i.e. the opposite situation to that in the cross-profile. The wave trough is over the area of minor deposition, i.e. 20 cm. Major erosion, i.e. 20 cm, corresponds to a wave peak. The maximum, vertical amplitude between waves in the long section is less than those in the cross-section. Between 17:00-18:25 there are three main waves which accompany the water level drop. The wave peak moved 20 cm upstream of the obstacle. The position of erosion corresponds with the wave crest, but erosion amounts are small.

Between 18:25-19:50 a water-surface wave built up in one location although there is otherwise a continued drop in water level. This change may reflect the deposition of a single particle, 5cm in height which caused a small wave, also 5 cm in height, to develop upstream of it. Most erosion (10 cm) occurred at the same position as the wave peak.

From 19:50-20:52 there is chaotic adjustment with the rapid water level rise. There are now 4 wave crests with associated deposition. The river bed is very irregular at this stage.

Between 20:52-21:45 there was further water level rise with only two main waves accompanied by major erosion of up to 25 cm. Only one major particle was deposited (12 cm in height) causing a wave to build-up upstream of it. Least erosion occurs at the same position as the second wave peak. Between 21:45-23:35 there was rapid deposition in accordance with the further build-up of the two waves.

From 23:35-05:32 there was a major drop in water level (up to 40 cm) and channel re-adjustment. Most erosion occurs at the wave trough. From 05:32-10:00 major re-adjustment is under way, and the profile changes back toward the initial configuration. A large

cluster (an obstacle clast and two stoss particles) was deposited. This cluster assemblage that was present in a similar shape and length at the beginning of the flood was eroded between 20:00-21:00, deposited again and once more eroded in the 23:00-05:00 phase, each time at about the same location. Observation calls into question the concept of how stable clusters really are and whether clusters are just as prone to particle exchange as the surrounding open-bed material.

As water depth increases, there was an elevation change similar to the larger scale changes observed by KIEFFER (1984). She notes that as discharge increases over a hydraulic jump sub-critical conditions are achieved due to increases in water depth over the obstacle (water velocity approximately constant), until the wave eventually disappears. This behaviour should not be confused with the bedload transporting phase at the Lainbach, where the water surface also loses its waviness. At higher discharges, KIEFFER (1984) noticed that the wave moved downstream. At even higher discharges, the wave amplitude was less than at medium discharge and acoustic reports indicated that most bedload transport did not occur when discharge was highest but rather during the phase with the very large wave. The wave-peak transfer observed by Kieffer was also seen at the Lainbach.

With the first bedload movement, the water surface should become sub-divided into many small waves which give the impression of "boiling". This phase is clearly developed at 18:25 and at 21:45 (see Fig. 6.79). Once bedload diminishes or ceases the surface should become organised into larger waves again. The phases before and after the suggested bedload transport phase support this. Fig. 6.81 c) indicates the chronological pattern of $K_3$ roughness distribution within the channel long profile during the course of the flood event. The frequency of $K_3$ roughness is again subdivided into 1 cm classes but this time the maximum roughness ranges up to 0.36 as compared to 0.24 at Squaw Creek. The largest roughness elements exist at the beginning of the flood, at 12:00 and at the end of the flood, at 05:32 and 10:00. Extremely low roughness values were obtained for the phase at 21:45. Since FAST suggests very low values corresponding with major and minor bedload pulses, this probably is also a period of major bedload transport. The fact that roughness is lowered during bedload transport had already been suggested by GILBERT in 1914.

Roughness peaks should occur in the periods in-between major bedload transport during periods of river bed build-up and adjustment. This has been re-affirmed from the Lainbach results. The roughness distribution varies very dynamically in the long profile, revealing a greater range than in the cross-profile (See section 6.4.2.1.2). The cause of this behaviour lies mainly in the position of the long profile within the main channel where, due to the higher probability of bedload transport, a larger obstacle has the chance of being removed and replaced again, such that the range in $K_3$ returns to previous values.

*6.4.2.1.2 Cross-sectional profile*

In cross-section, over the upper and lower bridges (Fig. 6.80), the changes in roughness, geometry and the water surface should be comparable to the longitudinal profile. At 18:20 and between 21:45 and 23:35, the river bed is smoothest. The times have to be considered as approximations of the measurements taken on the upper and lower bridges. In real time the measurements on the right and left bank are 30 min. apart. The changes seen at 23:35 are therefore half an hour earlier over the upper bridge. The cross-sectional measurements therefore indicate roughness states that are comparable to the longitudinal profile (Fig. 6.79). Thus roughness maximum and minimum occur at approximately the same time over the cross-sectional bridges as over the longitudinal bridges.

Figure 6.80 shows large undulating waves that exist at 14:50, but the waves become highly rippled and sub-divided into 5 minor waves at 18:20. At 19:20, the water surface becomes organised into three major waves again, whereas at 22:20, the water surface is very churned up ("boiling", Fig. 6.80). At 23:35, as was the case for the long profile (Fig. 6.79), the water surface amplitude has increased and it is beginning to become organised into waves again. By 09:38, the water surface approaches that at low stage.

The characteristics of geometry at the Lainbach are different to those at Squaw Creek. Unlike Squaw Creek, which consists of a bar, main channel and interface, the Lainbach has a clear and rapid transition between bar and channel and therefore the interface does not exist. In addition, during high stage at Lainbach, the channel widens considerably and occupies nearly all of the bar. This has repercussions for the development and geometry of flow cells. At Squaw Creek depth on the bar limits flow cell development, but at the Lainbach water depth is greater during the flood peak (40-50cm) so that cells can develop over the bar and channel during those periods.

The joint measurement of the river-bed and water surface allows development of a three-dimensional picture (F.A.S.T.) of the nature of flow cells and the

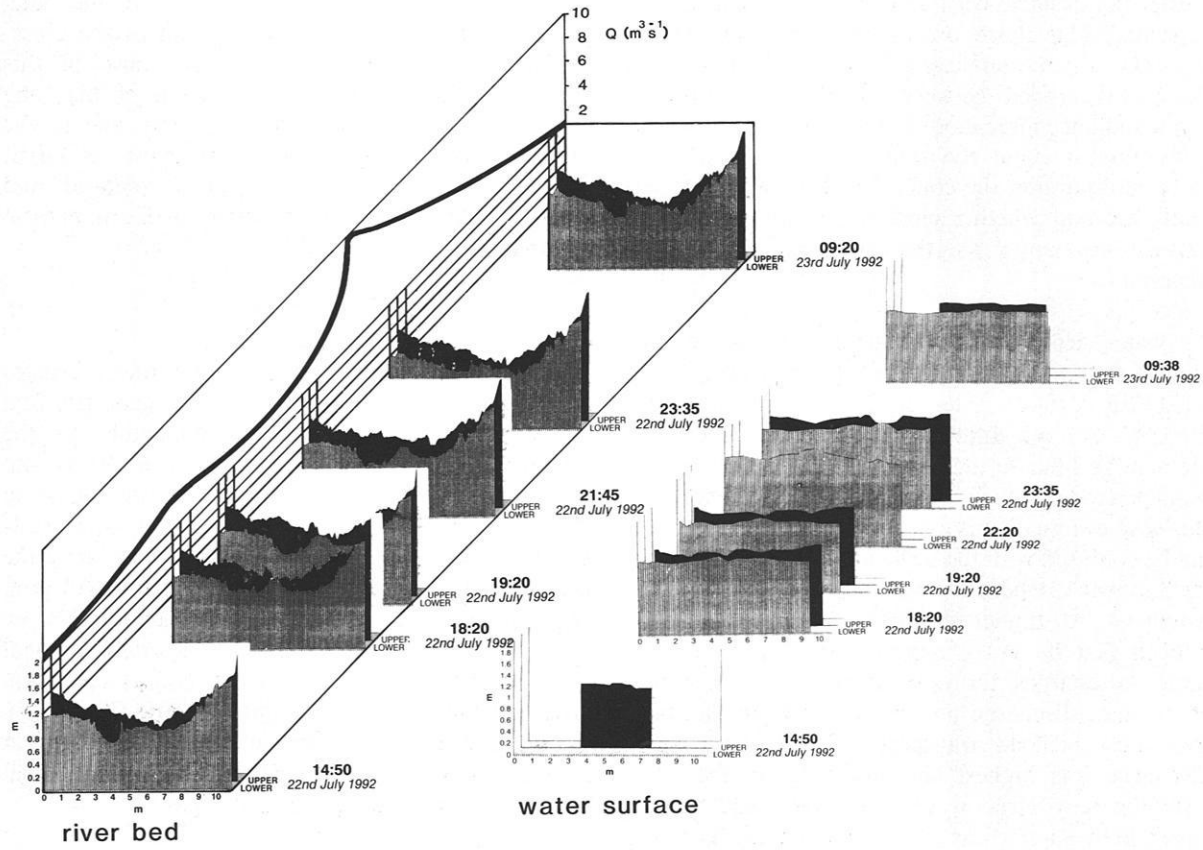


**Fig. 6.80** Temporal changes in cross-sectional river-bed adjustment and geometry over the upper and lower bridges (2 Tausendfüssler cross-sectional profiles taken simultaneously at each time) of the Lainbach during the flood of 22-23rd July 1992 (left-hand diagram). View is downstream. The water surface topography for the upper and lower cross-sectional profiles are plotted for the same temporal intervals and at the same location on the right-hand diagram. Heavy lines at the transect indicate measured sections, lighter lines in-between are interpolated. The discharge curve has been added for comparison.

possible bedload transporting phases as well as local bedload transport streets. The dynamics of the development, coalescence and destruction of spiral flow cells can be reconstructed from changes in the water surface from hour to hour monitored below the upper and lower bridge. The less dynamical behaviour of the upper bridge can be explained in terms of the bedrock outcrop forming part of the left profile. The following discussions are based on the diagrams in Appendix A4.

The fluctuations in intensity and lateral position of flow cells and the development of vortices according to roughness patterns have been confirmed in relevant studies made by GIBSON (1909) and LAPOINTE (1993). In the Lainbach the flow oscillations are influenced by the step-pool system, lateral bedrock outcrops and most importantly, the position of large boulders. A large boulder in the mid-channel location between the two bridges (Fig. 4.11 Ch. 4 Study Areas) causes the spirals to diverge. Along the lower bridge, another large boulder influences the field of scour to its lee. The deep scour around its flanks offers the opportunity for flow spirals to sweep deeper than normal and to cause more intensive changes.

Between 14:00-18:00, there was a 30-40 cm rise in water level over the upper and lower bridges, with a

maximum vertical wave amplitude of 20 cm (Fig. 6.82a). In this 4 hour period, the river bed was mainly depositional over the upper bridge. At 14:50, the water level over the bar surface was too shallow for flow cells to develop and only five cells were present in the main channel. The five flow cells are suggested from the three main waves built up over the channel, each approximately 2½ m across. Over the upper bridge there is also deposition in response to the first two waves but erosion at the third wave over the bar. Due to the cross-sectional shape of the upper section and its roughness distribution, spirals emerging from the upper bridge are depositional but cause major erosion below the lower bridge, where the geometrical constraints are different. Erosion over the right bar between the upper and lower bridge (view upstream) was caused by a small additional flow cell that died away towards the lower bridge. Deposition is associated with five spirals below the upper bridge. As they migrate downstream they expand within the large scour hollow on both sides of the large boulder in the lower section. The large size and vertical

a)

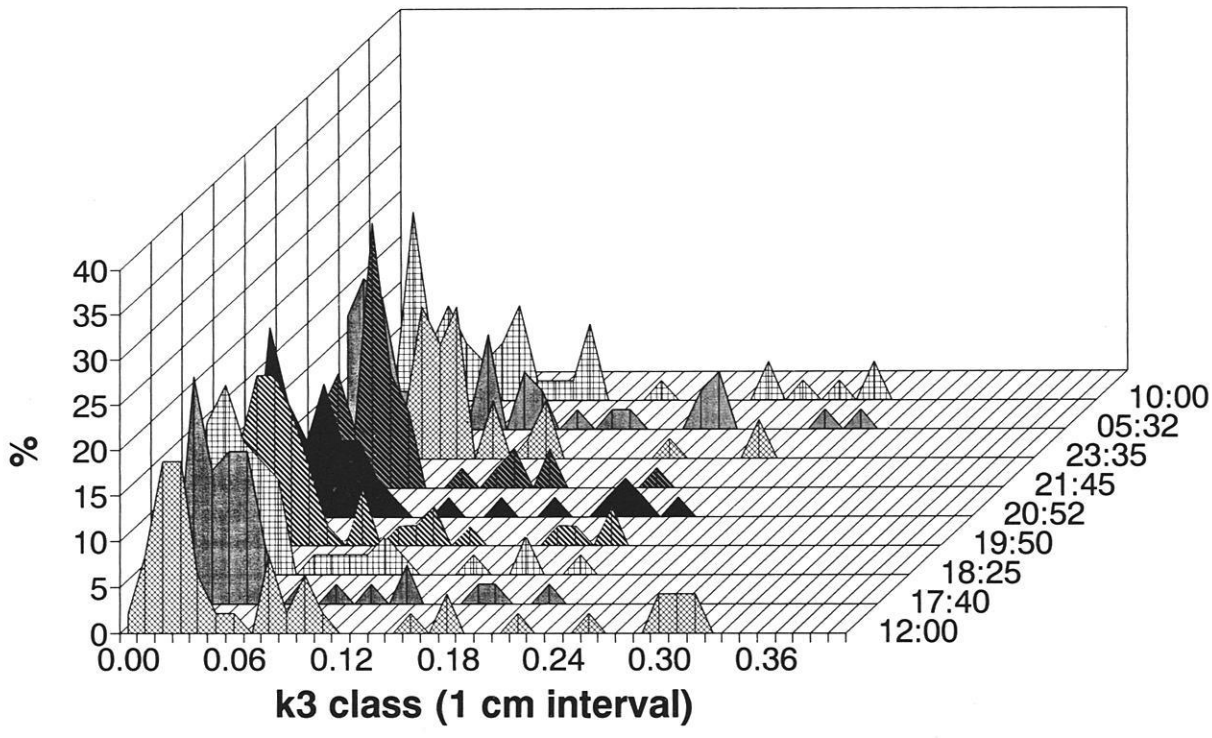


**Fig. 6.81** Temporal variability of $K_3$ roughness distribution at Lainbach, from 22-23rd July 1992 for **a)** long profile and in cross-section for **b)** upper bridge and **c)** lower bridge. Time sequence is from fore- to background. Class intervals are 1 cm. Notice maximum roughness lies at 0.36 as compared to 0.24 for Squaw Creek.

b)

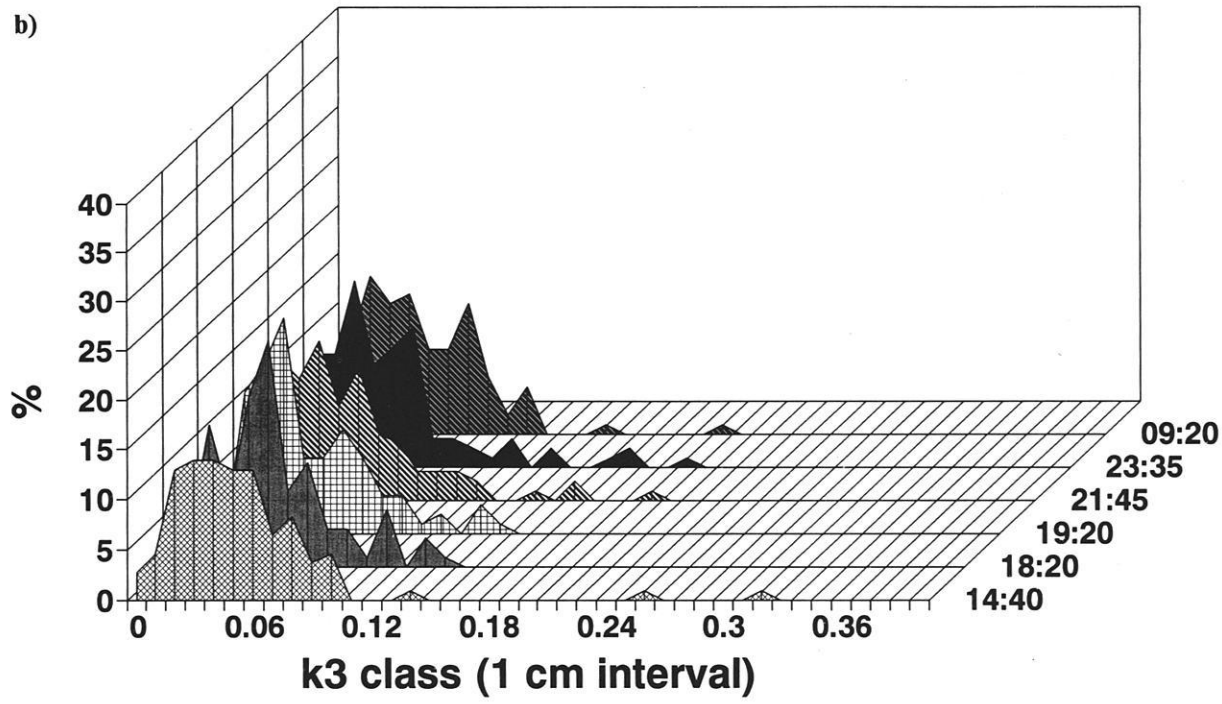
40
35
30
25
20
15
10
5
0
%
0
0.06
0.12
0.18
0.24
0.3
0.36
k3 class (1 cm interval)
09:20
23:35
21:45
19:20
18:20
14:40

c)

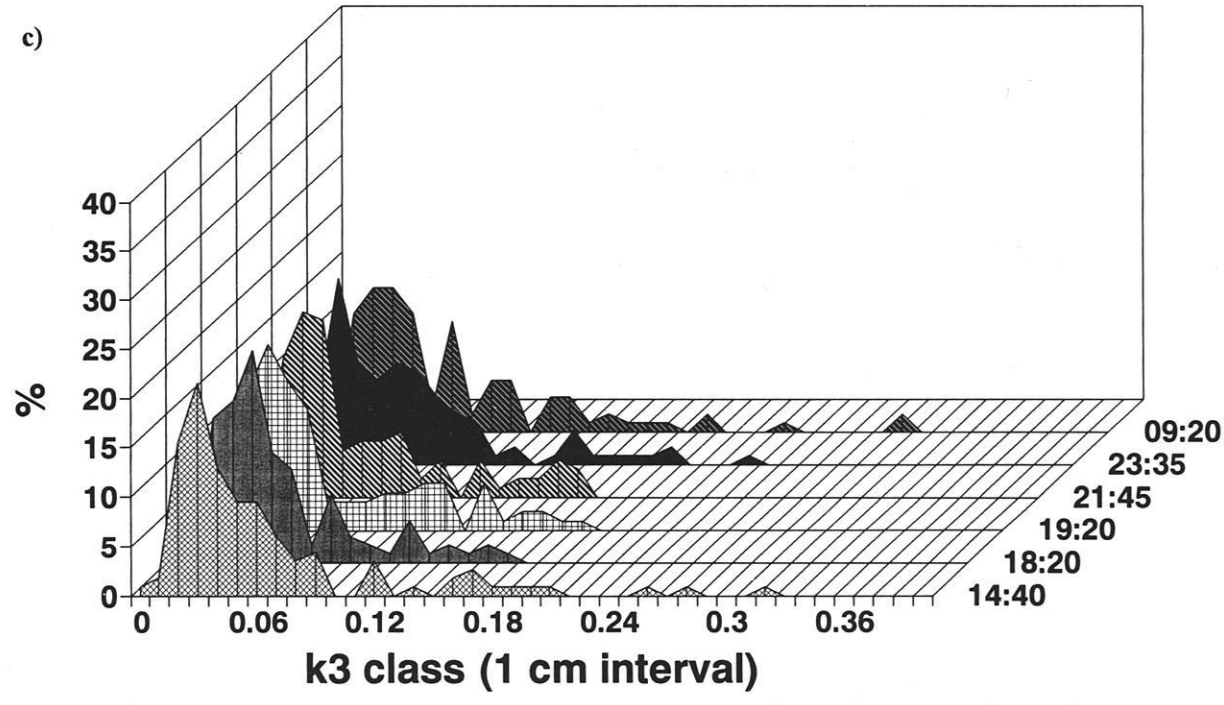
40
35
30
25
20
15
10
5
0
%
0
0.06
0.12
0.18
0.24
0.3
0.36
k3 class (1 cm interval)
09:20
23:35
21:45
19:20
18:20
14:40

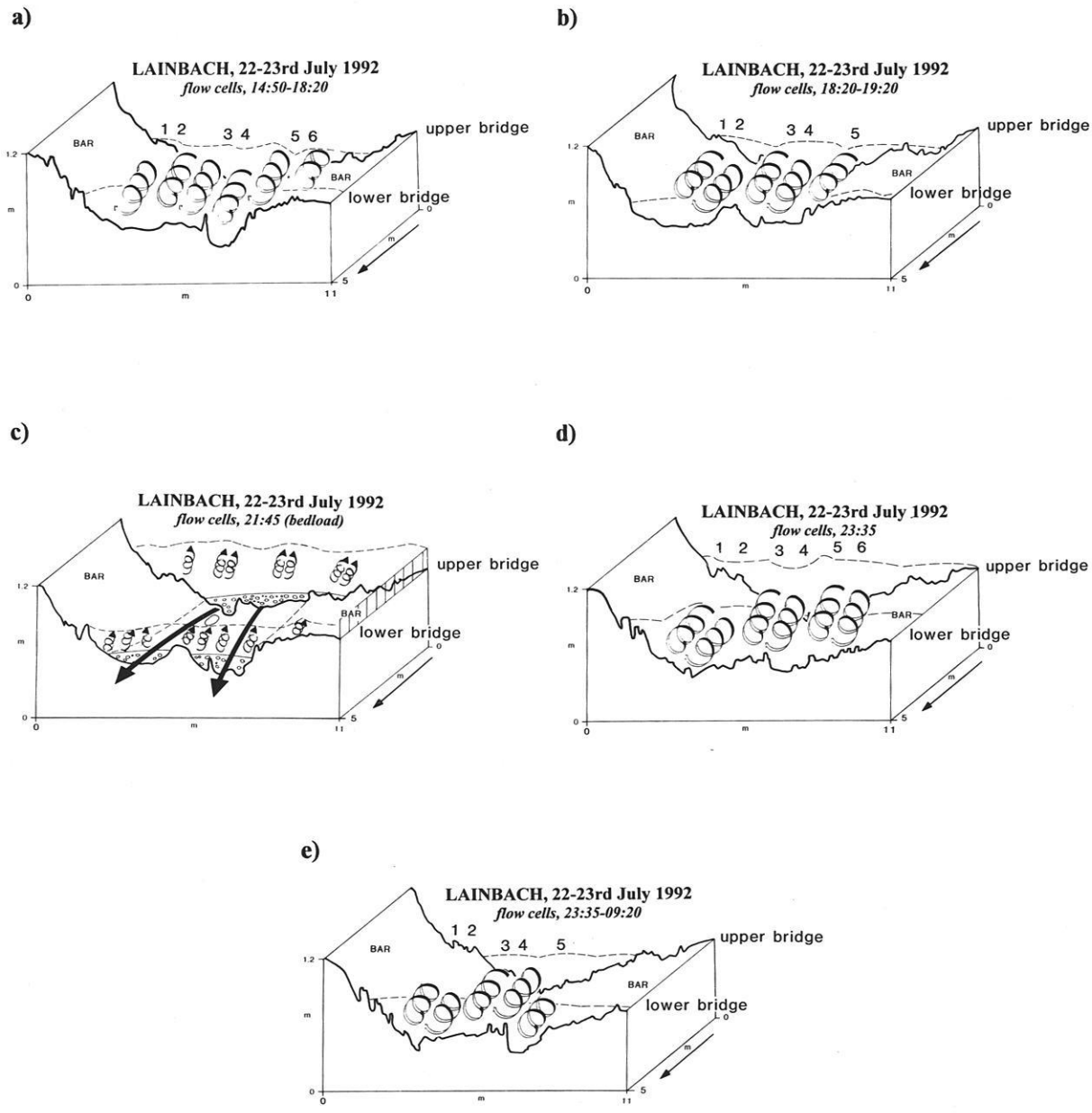


**Fig. 6.82** The three-dimensional development of spiral flow cells between the upper and lower bridges at the Lainbach for **a)** 14:50-18:00, small bedload pulse (river profiles at 14:50, **b)** 18:20-19:20 (river profiles at 18:20), **c)** 21:20-23:35, large bedload pulse (river profile at 21:20), **d)** at 23:35 just after pulse (river profile at 23:35), and **e)** between 23:35-09:20 (river profile at 09:20), re-adjustment during falling limb.

extend of the flow cells below the lower bridge allow cells to become more erosive, as will be seen in the next time step.

During the time from 18:00-19:00 (Fig. 6.82b), there is re-adjustment within the main channel, i.e. erosion with the decrease in stage, and deposition on the bar. With the build up of a small wave at 2m, and 6m there is erosion in the channel of the upper bridge but deposition on the bar with wave peak at 8m. Over the lower bridge there are also three wave peaks formed during the water level decrease, each 2.2m in length.

In the trough between the first and second wave there

is erosion, but deposition on the bar. With an 8 cm water level decrease there was on average, 15 cm of erosion. As at Squaw Creek, the erosional and depositional areas are neatly concave or convex in accordance with the wave patterns (see also Appendix A4, 18:20-19:20).

In the period between 18:00-19:00, the flow cells have to rotate in the opposite direction to induce the patterns of erosion and deposition monitored. Again this can be explained in terms of the more diverse geometry and roughness of the lower profile that has changed as a result of the flow cell patterns. Thus up to 18:20, the flow cells caused deposition in the main channel and erosion in the area between the right and left hand channel (looking upstream). The lateral displacement of the area of highest roughness i.e. further to the left, caused the left-most flow spiral from the 14:00-18:00 period to be destroyed and the remaining pairs of cells to migrate into its place. With the leftward migration, the gap produced was filled by an opposing cell. This meant that the flow cells were now causing the opposite behaviour, i.e. erosion in the location of former deposition.

The water surface topography formed the main criterion for establishing these dynamics. Over the upper bridge, the water surface corresponds to that of the lower and the adjustment of the river bed confirms a similar balance of convergence and divergence. The slight changes in the geometry and roughness conditions under the upper bridge are one reason for the changes occurring under the lower bridge. But the intensity of changes under the lower bridge could also be the reason for the spiral pattern to migrate upstream and influence the 50 $m^2$ area between the lower and upper bridge.

In the period between 19:20-21:45 (Fig. 6.82c), there is a rapid stage increase (41 cm at the upper bridge but only 19 cm at the lower). Under the first wave trough of the upper bridge there is approximately 12 cm erosion but beneath the second wave trough, 1.8 m in width, there is actually deposition on the river bed which matches the exact wave dimensions. At the lower transect, there is an exceptional water level drop along the mid-channel in relation to water level rise throughout the rest of the channel. The trough causes 8 cm of erosion but all the other minor wave peaks 1m apart correspond to areas of minor deposition. The diagram suggests the onset of the bedload transporting phase. The water and bed surfaces of the upper bridge were not measured during the transition phase. During this period of intensive bedload transfer the water surface is "boiling", induced by extreme turbulence over a layer of bedload. The depth of the bedload layer in Figure 6.88c) is estimated from the relationship between measured bed particles and river bed adjustment at Squaw Creek, taking into consideration the different particle density in the Lainbach.

During the major bedload pulse, it is assumed that more than one layer of particles is in motion and due to the larger particle size involved (obtained from photo-sieving) compared to Squaw Creek, an active bedload layer 15 cm in depth is estimated for the Lainbach. From the information on bed geometry and acoustic information obtained during the Tausendfüssler measurements, it is clear that two channels were active at the lower section but only one at the upper. The greater amount of material passing through the lower "pseudo-braided" section means that the bed at the lower bridge was much more active than that at the upper in adapting its geometry and roughness. The imbalance in erosion and deposition should therefore be considered in terms of bedload routing and depth.

Between 21:45-22:20, during the suggested bedload transporting phase, only the lower bridge was monitored. There was a build-up of a lateral wave, centrally located over the channel and a small wave over the bar, restricted by bar depth. This phase is actually associated with major deposition (28 cm) in the inner channel which could indeed signal the effects of large particles being transported within the main channel. In two other areas there is 10 cm of erosion in accordance with wave troughs at 1 m intervals. There is also bar erosion at a lateral trough.

Between 21:45-23:35 (Fig. 6.82d) there is a rapid increase in water level, 32 cm along the upper and only 22 cm over the lower. As usual the water surface and river bed changes are far more dynamic at the upper bridge than at the lower. The water surface at the upper bridge is subdivided into 6 waves. Along the 2-3m mark at the upper bridge there is deposition even though there is a wave trough here. Over the main channel there is 22 cm of erosion. The last two waves are related to erosion. At the lower bridge there are four main waves which are purely associated with large amounts of erosion (22 cm maximum).

Once bedload transport ceased, the extreme vertical differences in water surface topography suggest the renewed build-up of the flow cell system. This time the lower bridge has 6 flow cells again, in positions very similar to the original cells. The extra cell to the extreme left forms the required counterpart of the erosion-causing spiral. The reason for the wider dimensions and depth of flow cells arises because of the higher water levels at this stage which allow flow cells to develop even over the bar, given that the water

depth exceeded 30 cm at this time (ERGENZINGER et al 1993). Below the upper bridge, the same pattern holds true. With the increased water depths there is greater height available for cell expansion.

Between 23:35-09:20 (Fig. 6.82e) there is a major drop in water level, nearly of the same magnitude as during the rising limb. River bed adjustment is very minor at the upper bridge, with erosion and deposition remaining in balance. Over the bar and channel there is minor deposition. At the lower bridge there is general erosion within the main channel, with the result of re-adjustment to the initial state. On average, flow cells at the upper transect are 2-2.5 m across, and flow cells at the lower transect are 1.5-2.5 m across.

The continued erosional and depositional impact of the flow cells causes the topography of the profile to adjust back to their original boundaries. From the water surface topography, and information on river bed adjustment, it is clear that the flow cells were forced to wander back to the former conditions. This time the spirals shifted to the right (in the opposite direction to that at the beginning of the flood) so that the flow cells to the extreme right became extinguished. This explains the pronounced erosion in the main right-hand channel at the lower section and deposition in the left hand channel in the same section.

At the upper bridge, even fewer cells were in operation so there must have been flow cell formation midway between the two. Fewer flow cells remained at the end of the flood since bedload had ceased and water levels were lower than at the beginning of the monitoring session. Water depth is therefore an important determinant controlling the capacity and number of flow cells that will develop.

In the cross-sections, the behaviour at the lower bridge was more dynamic than at the upper bridge. This means that the changes in roughness distribution over the lower bridge were very similar to those in the long profile, whereas the upper bridge responded less dynamically (Fig. 6.81 b&c). Nevertheless the highest roughness values were obtained at the upper bridge at 14:40 at the beginning of the flood and at 09:20 towards the recession. During the periods in between, the lowest roughness range was obtained at 18:20, not as expected at 21:45. The lower variations in roughness values for the upper bridge can be explained in terms of its geometry (Fig. 6.80). Thus at the upper bridge there is a very smooth cross-profile with no clear inner channel.

At the lower bridge (Fig. 6.81 c), the roughness distribution was most attenuated at the beginning of the flood (14:40 and from 23:35 to 09:20). As anticipated, the lowest roughness was obtained for the 21:45 measurement period. The similarity of dynamics in cross-section and in long profile can be explained in terms of its geometry-induced roughness dynamics.

Thus, in contrast to the upper bridge, the lower bridge profile displays a well identified inner channel in addition to a smaller side channel; both were active during normal flow (Fig. 6.80). These geometrical differentiations enable the river bed to fluctuate more in the vertical dimension due to very localised infill and erosion. On the upper bridge, infill and erosion were more attenuated and spread over a wider area.

### 6.4.2.2 Temporal adjustment of geometry

*6.4.2.2.1 Longitudinal*

The temporal adjustment of geometry at the Lainbach was calculated as the rate of erosion and deposition in $m^2$ per hour from the Tausendfüssler measurement sessions. The procedure was the same as for Squaw Creek. In Fig. 6.83a, the rates of erosion are shown in the background. Most erosion occurred at 21:45, at the same time as bedload pulsed most intensively. Least erosion occurs at the beginning and end of the flood. In terms of deposition (Fig. 6.83 b), the opposite is true. Deposition is at its lowest during the postulated major bedload transport period as at Squaw Creek but is high at the beginning and end of the flood.

*6.4.2.2.2 Cross-sectional*

From the results at the upper and lower bridge, most adjustment occurred within the channel (Fig. 6.83 a). Most erosion occurs at the beginning of the flood and at 23:35. Most deposition (Fig. 6.83b) occurs at the upper bridge between 21:20-23:35 but between 19:20-20:30 at the lower bridge. Just as at Squaw Creek (5-6th June, 1991) within-reach processes are quite variable. River bed changes correspond least of all with discharge, i.e. at peak discharge the river bed is most stable.

Figure 6.84 shows that the river bed is adjusting in two main cycles. The most adjustment occurs as discharge begins to increase, suggesting the onset of bedload transport as at Squaw Creek. The next increase in adjustment corresponds with the descending limb at 21:45, which could correspond to the largest pulse observed at Squaw Creek during the same phase. A minor pulse could have occurred at

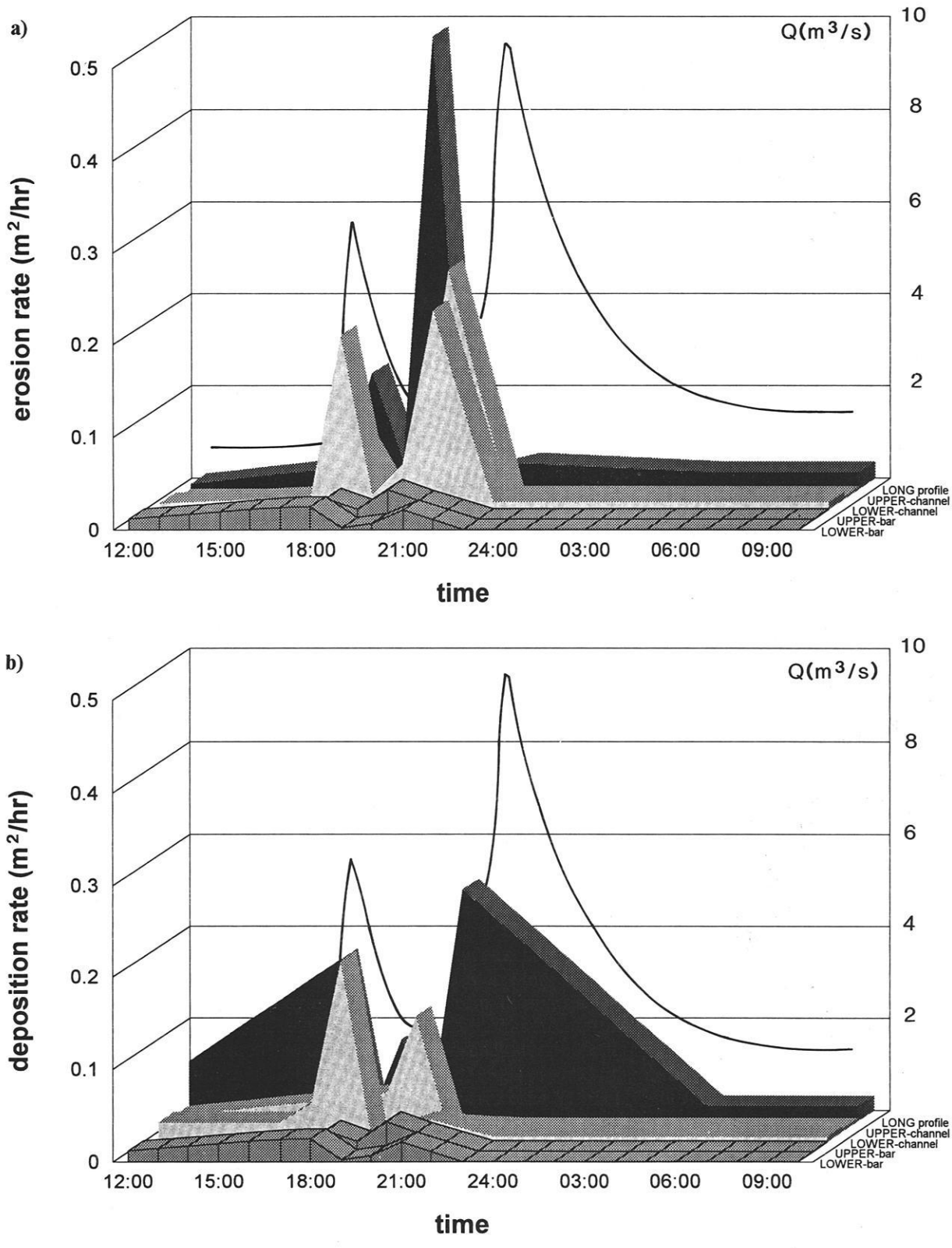


**Fig. 6.83** **a)** Hourly rates of erosion and **b)** rates of deposition along the long profile, upper and lower channel as well as bar area for the flood of 22-23rd July 1992 in the Lainbach. Values are calculated from the difference between two time-successive Tausendfüssler measurement series and as hourly, 10 cm (distance between 2 Tausendfüssler points) standardised area intervals ($m^2$/hr).

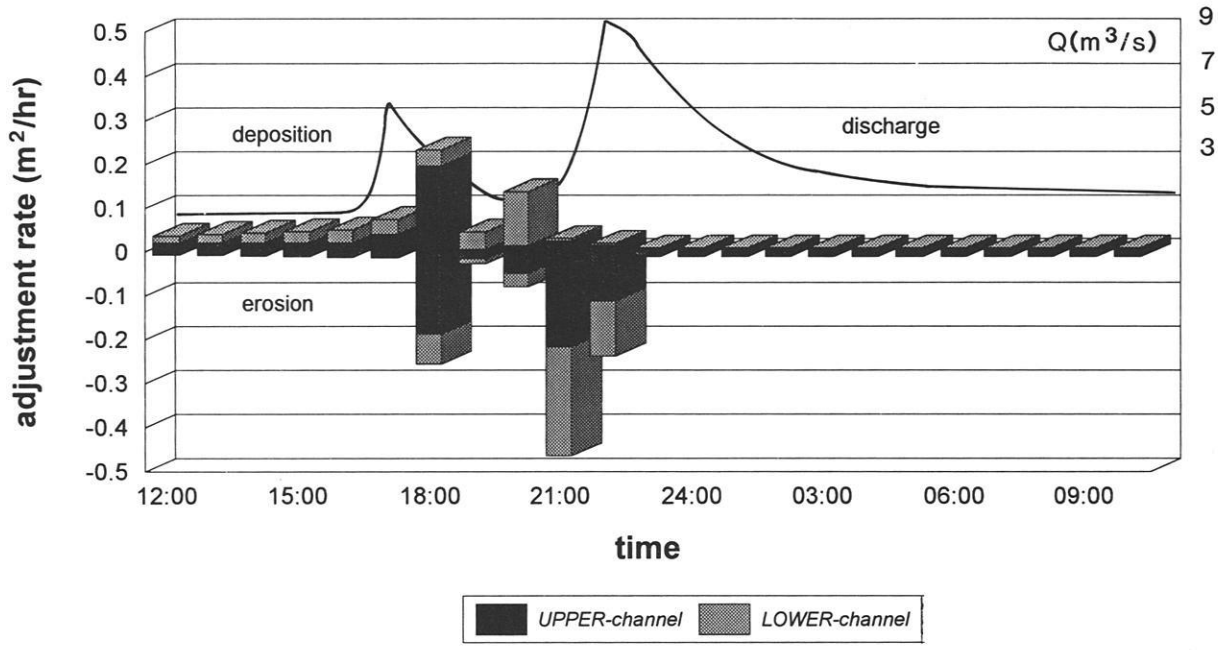


**Fig. 6.84** Hourly total rate of adjustment at upper and lower profile in the Lainbach, 22-23rd July 1992.

23:35 where a little adjustment occurred. The total amount of work was calculated as sediment volumes for all three bridge sections and are negatively correlated with the discharge hydrograph (Fig. 6.85 a & b). Both in terms of volumes of erosion as well as deposition, the lower bridge can be seen to be most active. The work volume achieved by the long profile constitutes more in terms of deposition than both the upper and lower bridge considered together. In terms of erosion, the long profile achieved 90% of the work. The work achieved by the bars is insignificant both for erosion and for deposition.

a)

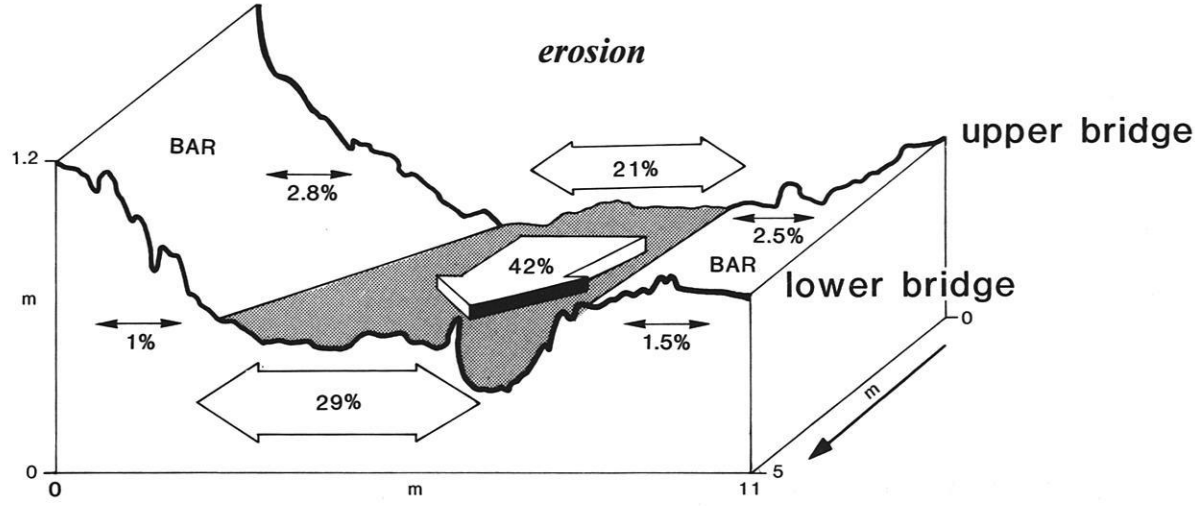


b)

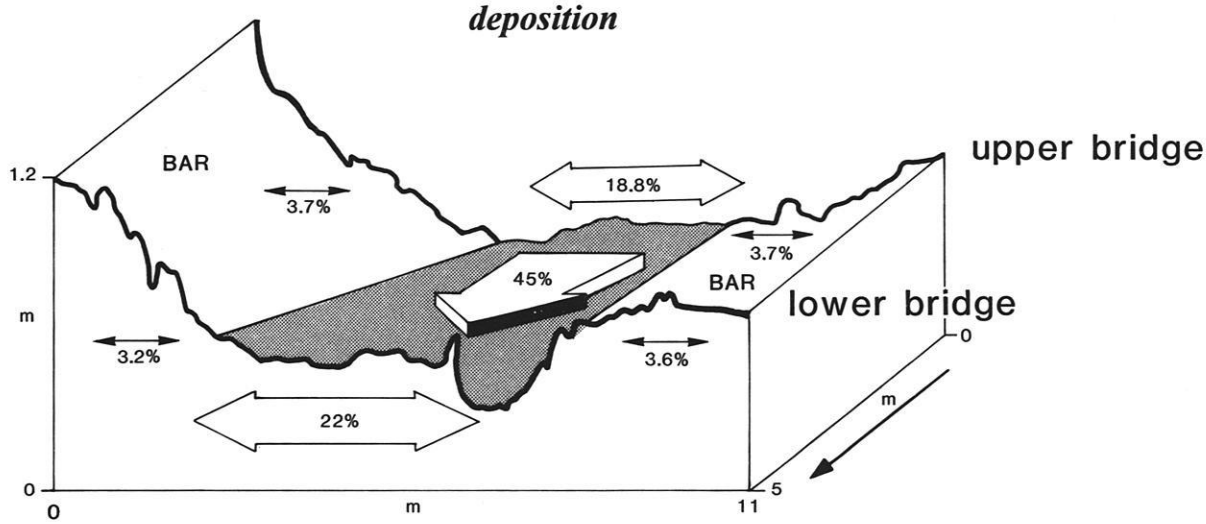


**Fig. 6.85** Calculation of total proportion of work in terms of **a)** erosion and **b)** deposition within the channel and on the bar of the upper and lower bridges (indicated by lateral arrows) and within the channel long profile (longitudinal arrow) in the Lainbach for the 22-23rd July 1992.

### 6.4.2.3 Comparison of $K_3$ and Manning coefficients

Since the $K_3$ values could not be spatially differentiated according to channel, interface and bar, an average $K_3$ value was calculated for the active cross-profile at the upper and lower bridge, as well as for the long profile. Comparison of the $K_3$ and Mannings coefficients were carried out for all three bridges (Fig. 6.86). The diagram shows that the long profile, due to its position within the main channel, was most dynamic. The upper cross-profile showed least variation and as demonstrated previously from the distribution of roughness frequency, the lower bridge behaved in a surprisingly similar manner to the calculated Mannings coefficient. It has to be pointed out that the 21:45 and 04:50 values for the upper and lower bridges are a calculated average.

$K_3$ fluctuates in the opposite direction from the discharge curve, whereas Manning goes inverse with $K_3$, indicating that both coefficients describe similar roughness conditions. Thus when the first peak discharge occurs, all values sink apart from Manning and where the second discharge peak occurs, the long profile indicates a drop in roughness. Since the upper profile was not measured at 21:45, the result could be misleading. From the lower profile there is no drop in roughness during the main peak, even though the river bed had generally become smoother. This could be due to the large particles in transit at the time. At 23:35 there is a slight drop in all roughness at all locations (including Manning as indicated from a rise in the curve) which may have been caused by a smaller bedload pulse on the descending flood limb. If the average $K_3$ value for all three bridges is divided by the Mannings n, a value of 0.9 is obtained throughout. Thus if the average velocity is to be estimated for the Lainbach, the following formula would apply:

$$\bar{u} = 1.12 K_3 R^{2/3} S^{1/2}$$

If CAVE (Coefficient for Average Velocity Estimation) (section 6.3.2.2.5 & Fig.6.87) is to be applied to the Lainbach, the grain to form transition and/or grain size has to be taken into account. Thus at Squaw Creek, there is a $D_{50}$ of 32mm on the gravel bar and a $K_3$ (20) of 0.04m. This results in a constant of 4 for the calculation of velocity. In the Lainbach, the $D_{50}$ lies at 125mm, or a $K_3$ (20) of 0.08m which allows for a constant of 1.12 in the velocity equation. In the Schmiedlaine, reconstructed velocities and a $K_3$ (20) of 0.1 formed the third point on the graph. The points are valid since they repeat their occurrence for different floods, and can be plotted (Fig. 6.87).

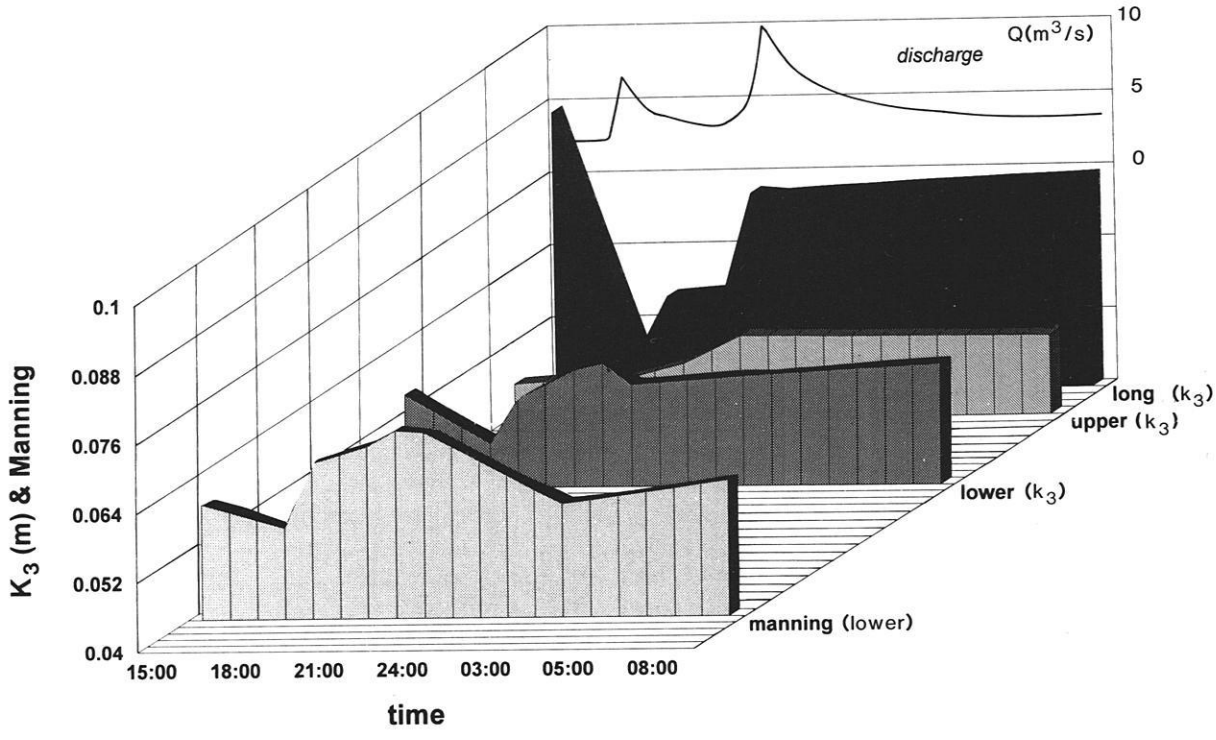


**Fig. 6.86** Comparison of $K_3$ and Mannings coefficients for the longitudinal, upper and lower cross-sectional bridges for the flood of 22-23rd July 1992 in the Lainbach.

In the relationship (Fig. 6.87) there is a multiple factor decrease in the coefficient for velocity with each average increase of $K_3$ (0.01) at the $K_3$ (20) transition. Thus the higher $K_3$ values and grain sizes result in a lower coefficient of velocity. From the relationship, the average velocity coefficient can be estimated for the Schmiedlaine.

### 6.4.3 Application of FAST (Fluid And Sediment Transfer) model to the Lainbach

The Lainbach study site data show that the conceptual model FAST can be successfully applied. If all the river bed and flow conditions are known during particular phases of a flood, then bedload and bedload intensity can be predicted for particular times. If a

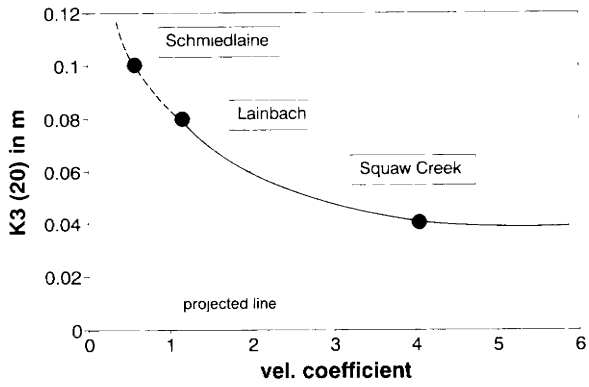


**Fig. 6.87** Relationship between $K_3$ (20) and coefficient of velocity for Squaw Creek and Lainbach. The estimated value for the Schmiedlaine has been marked.

certain roughness condition prevailed, then its relationship to river geometry and water surface conditions could verify whether or not bedload transport occurred, and to which intensity. This was tested from the acoustic measurements. By quantifying the parameters, all factors similar to those recorded on the 5-6th of June, 1991 at Squaw Creek can be plotted (Fig. 6.88). The figure assumes comparable model parameters to those of Fig. 6.77 (section 6.3.2.2). The right and left bank water surface gradients do not fluctuate as much as at Squaw Creek due to the shorter reach length involved (5m as compared to 30 m at Squaw Creek). There is an absence of large channel geometry effects at the Lainbach. An important similarity can however be observed between the Lainbach and Squaw Creek data.

Thus at the beginning of the flood, following the initial condition where gradients were equal, the gradient lines cross each other and the right bank is subject to a lower water surface gradient than the left bank (at 18:20). At this cross-over point there is considerable deposition and $K_3$ is at its lowest. This strongly suggests a bedload pulse if the FAST model is directly applied. In the next phase there is slight erosion. The water level gradients begin to rise steeply to a maximum, followed by a sudden decrease. This pulse is not recorded directly because during the pulse the particle volume into the system is approximately the same as that going out. This drop with the associated lower roughness values, as at Squaw Creek, most certainly indicates the largest bedload pulse during the event. The period is immediately followed by heavy erosion, a re-adjustment phenomenon also observed for both floods at Squaw Creek. After this, the water level gradients decrease gradually (Fig. 6.88), and erosion gradually decreases during the flood recession. Again these geometrical changes were recorded at Squaw Creek after the cessation of bedload transport. This evidence supports the untested suggestion by HEY (1982) that the hydraulic geometry and slope is controlled by the amount of bedload in transport.

The increase in roughness height at the beginning and end of the flood can be appreciated in terms of minimum stream power expenditure in association with the stabilisation of channel geometry (KIRKBY 1977, DAVIES & SUTHERLAND, 1980, CHANG 1980, BRIDGE & JARVIS 1982). When roughness and associated friction were high, sediment transport rates were low, probably in order to minimise energy expenditure. During intense bedload transport, roughness was low in order to minimise friction, again enabling bedload transport to occur with a minimum of extra energy expenditure. This complements the Lainbach and Squaw Creek data. BRIDGE & JARVIS (1982) found that energy slopes and friction coefficients were not constant from section to section. This explains the unequal balance in bedload results obtained for Squaw Creek but also the unequal balance in erosion and deposition obtained at the Lainbach. Each reach may have different responses in energy and friction.

Water surface gradients and acoustic descriptions from the insertion of the Tausendfüssler rod during the measurements supported the two bedload pulses suggested. During the bedload phase, the water became frothy or "boiling", the undulating waves were destroyed, and the number of clicks as gravel hit the rods increased. These measurements were quantified and measured frequently during the flood wave (see Appendix 3 & 4).

### 6.4.4 Summary

The results indicate that with quantitative as well as qualitative data, FAST was successfully applied to the Lainbach. As at Squaw Creek, the roughness, geometry and water surface conditions during flood waves were very similar at the beginning and the end of the flood. Both streams were very dynamic in between. Such dynamics have hitherto remained unrecorded. The river bed measurements at the beginning and end of the flood indicate a self-similarity that has obscured the real flood dynamics. During the course of a typical flood event, bedload transport will occur in characteristic phases that are associated with certain "symptoms" that are unmistakable, as has been suggested from the results of many flood waves. The sudden change in the roughness, channel dimensions and water surface configurations during a bedload pulse will very quickly re-adjust to the initial conditions. The physical laws governing this process have been simplified in the CAVE formula. Thus a certain roughness value on the river bed will always be balanced by a certain hydraulic radius (geometry) and slope (water surface in this case).

These data support the idea that the shape and size of a river channel is balanced by resisting forces (bed material size) and bed structure. The unequal increases in water surface gradient, width and depth are associated with the geometry and roughness of the channel. Whatever the type of interactions, the river cross-section detail cannot be generalised nor can the water surface be neglected. Shear values are unrealistic, since constant values cannot be used for the delicate balances of bedload transport, river bed roughness, channel geometry and flow hydraulics in nature. The CAVE formula should therefore not be seen as a solution to the river dynamics, even if it is based on a dynamical roughness coefficient. Not only do the solid and fluid interactions assume very different patterns in space but also in time. This underlines the need for further detailed spatial and temporal numerical experiments and not merely mathematical analyses or approximations. This thesis has shown that roughness and water surface conditions do not fluctuate simply with discharge, and that roughness cannot be assumed to be constant. Although the variations in energy expenditure can be considerable, the river system tends to stay in balance during a flood event.

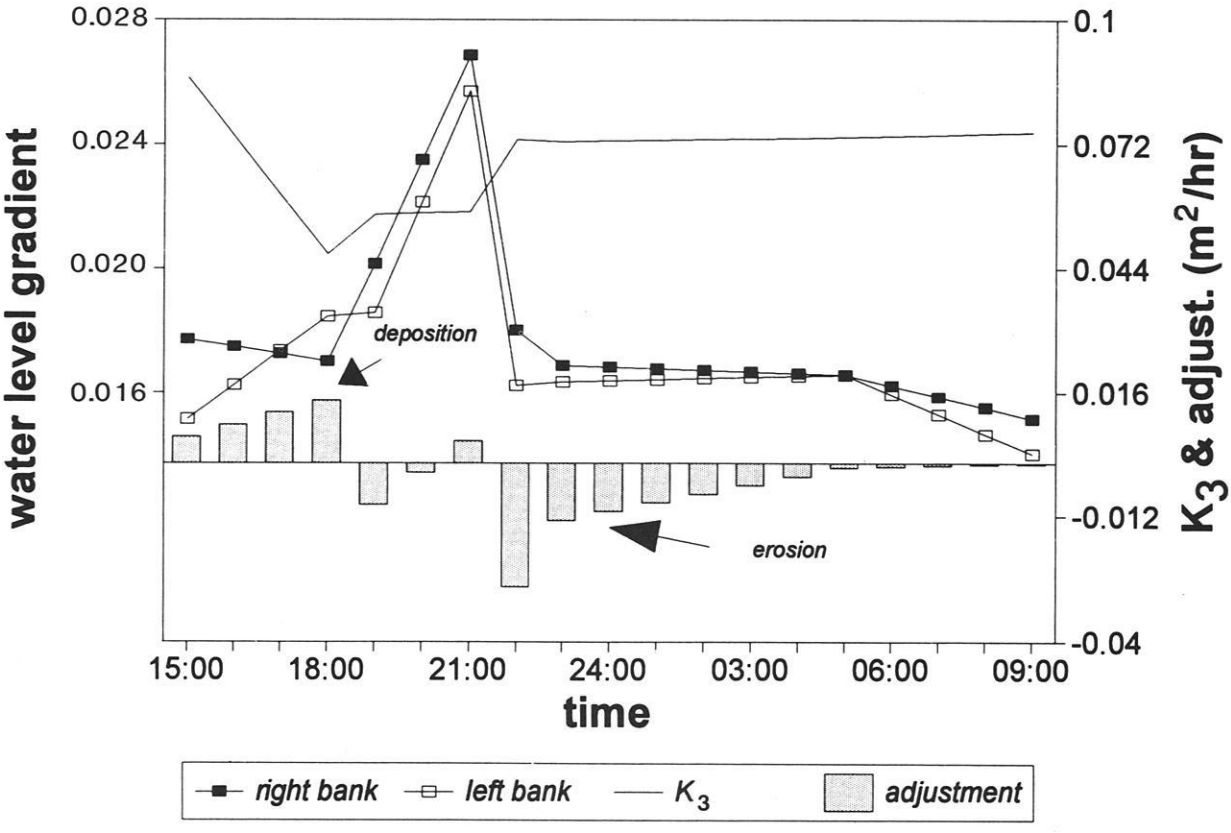


**Fig. 6.88** Changes in $K_3$ roughness against right and left bank water level gradient and total bed adjustment for the Lainbach, 22-23rd July 1992.

# 7. CONCLUSIONS

This study has analysed how the spatial and temporal dynamics of bed roughness and geometry are influenced by bedload and flow dynamics in three different mountain streams. For descriptions of spatial roughness, two new measuring techniques were utilised, the mini-Tausendfüssler, which measures roughness in section, and the photo-sieving technique, which determines single grain parameters. In order to determine relative roughness projection and to differentiate between form and grain roughness, both spatially and temporally, the new $K_3$ roughness approach was applied instead of the conventional Darcy-Weissbach or Manning's roughness coefficients. Temporal variations of $K_3$ roughness were obtained from a macro-Tausendfüssler and verified against the Manning 's coefficient.

- The complex temporal interrelationships between roughness, geometry, flow hydraulics and bedload transport have been tested at Squaw Creek, Montana, for two flood events and condensed in the FAST (Fluid And Sediment Transfer) model. Phases of measured bedload and non-bedload transport were differentiated according to the properties of the river bed and water surface topography at Squaw Creek. In the Lainbach, S. Germany, similarly distinct phases of river bed roughness, geometry and water surface adjustment could be distinguished. The FAST model was successfully applied in predictions of bedload and non-bedload transporting phases. Such temporal and three-dimensional dynamics are essential in explaining the spatial distribution of roughness.

- The spatial patterns of $K_3$ roughness investigated in detail on two differing gravel bars at Squaw Creek, a test bar in the Schmiedlaine, in the main channel and on the bar in the Lainbach, show that physical rules determine the relationship between longitudinal and lateral form roughness. In each case the cross-sectional roughness values obtained are higher than the longitudinal roughness. This pattern persists both at the micro-scale, i.e. within a bedform, and at the macro-scale, i.e. over a bar.

- Flow hydraulics and bedload dynamics govern the pattern of bed roughness development. Although these parameters could not be measured for all gravel bars during the actual events, the rules governing the size and distribution of roughness are very similar. The arrangement of roughness depends on the grain size and shape as well as the local gradient and channel form. Thus on the gravel bars studied, where flow is shallow, it is suggested that shear waves are responsible for local grain deposition, which separates and re-unites flow in a diamond pattern. The shear waves are suggested to develop where bedload transport is isolated. Due to the inability of roughness measurements to be taken within the channel, the distribution of roughness is discussed at larger intervals using the macro-Tausendfüssler device. In cross-section, roughness is isolated but well adapted to the lateral configuration of the bar. In the longitudinal profile, particles are arranged as individual cluster bedforms that are streamlined and will not project higher than the ellipsoidal outline of the grain assemblage itself.

- The river bed was defined in terms of a fractal approach, using ever-increasing $K_3$ roughness values from the cm to m scale. A good relationship exists between lateral and longitudinal roughness in all cases. From the distribution of the fractal relationship, the transition between grain to form roughness can be defined. The transition from grain to form roughness marks the threshold between single grains and bedforms such as clusters. The transition from form to system roughness marks the threshold between bedforms and river bed geometry or gradient. The river geometry and gradient reflect the type of river system (whether step-pool or shallow gravel bar). Lateral roughness transitions are higher than their longitudinal counterparts since in cross-section, the large $K_3$ intervals at the system roughness transition reflect the actual channel geometry. In contrast, the longitudinal system roughness intervals are strongly determined by the more gently decreasing reach gradients.

- Each individual fractal relationship depends on the grain size distribution. When the grain size distribution was related to the fractal transitions, it became clear that the lower percentiles of the grain size distribution were essential in forming the thresholds between grain to form roughness and that these transitions have not been adequately described in the literature. The $D_{50}$ and $D_{95}$ are not adequate roughness descriptors. A better descriptor is the relative roughness coefficient $K_3$. This coefficient should be considered in the future when analysing roughness.

- In the discussion on the much neglected topic of form roughness in steep-gradient, coarse-grained

streams, the example of clusters is treated in detail. Using the photo-sieving approach, several new methods of analysing roughness are tested for clusters in relation to their open-bed counterparts. The size difference between the form and grain roughness elements is considerable. Clusters contain the coarsest size fraction of the river bed. The year to year analyses of the spatial distribution and properties of cluster assemblages in relation to their surroundings on a gravel bar in the Schmiedlaine show that flow hydraulics may have a more significant influence on their distribution than sediment transport alone. For two time-sequential examples, the grain size distribution (using the b-axes by number method) remained identical from one year to the next for the general bar surface yet the organisation of particles within the clusters differed considerably. In order to establish these sensitive differences, the grain area was used as an indicator of roughness instead of the grain size. If the general grain size and grain area on the gravel bar did not change, yet the arrangement of cluster roughness did, then this is sufficient evidence to suggest that during the transport of similar grain sizes, the transport characteristics and associated flow hydraulics on the gravel bar differed considerably from year to year. Evidence from temporal nature of bedload transport suggests that even if similar grain sizes are in transit during one flood and the next, the river bed geometry and roughness respond very differently. It is the intensity of bedload that induces most important changes in roughness. The physical rules operating within the river system are sufficient to force the river bed to re-adjust back to a state very similar to the initial state at the end of the flood. Thus a gravel bar may maintain the same general roughness distribution if re-worked but with considerable variations in individual roughness arrangement.

- In the discussion on the spatial variability of form and system roughness in relation to flow, the variations in their distribution are attributed not only to gradient and grain size but also to bend curvature. The example for this study was supported by analyses form the Schmiedlaine. The type of bedform and bedform arrangement varies according to the bend curvature. Form roughness and new ideas on the formation of clusters are emphasised as are transverse ribs. Ultimately, the diamond arrangement of clusters on the gravel bar is subject to the diagonal crossing pattern of shear waves within the expansion zone between two bends. On the other hand, transverse ribs located within the main channel are influenced by the regular spacing of standing waves within the highly concentrated flow of the main channel. Parallel sequences of lateral cobble berms are related to the chronological deposition of clusters and coarse material in the outer bend under the decreasing flow energy of a flood recession.

- Because of the spatial variability of roughness in relation to flow, a unique technique was developed to transform clusters and open-bed material into flow orientation indicators. With the photo-sieving technique a wealth of single particle data presented over an entire gravel bar allows the orientation of particles as well as the whole cluster assemblages to be measured. The results show that while the coarser-grained clusters represent the recession of the flood wave (the most recent depositional stage), the open-bed material represents the high stage conditions when flood flow was fully developed. This relationship held true both for Squaw Creek and for the Schmiedlaine. In those cases where the size difference between clusters and open-bed material is less significant, clusters are prone to be very sensitive flow indicators.

- Flow significantly influences the planimetric and cross-sectional shape of roughness elements and their depositional angle of imbrication. For each cluster described along the longitudinal transects at Squaw Creek and Schmiedlaine a very clear ellipsoidal shape can be traced both in plan and in section. There is a well defined relationship between the plan and the section ellipsoid, which has implications for flow reconstructions. There are rules which determine and/or limit the length, width and height of clusters. Thus a short cluster will be longer than a tall one. On the gravel bars both at Squaw Creek and in the Schmiedlaine there is a transition from very high, short clusters to flatter, longer clusters as one proceeds downbar. This means that for tall clusters to develop, larger particles will have to be trapped in the proximal bar, whereas the smaller clusters pose fewer limitations on roughness length and develop freely on the medial to distal bar. The angle of imbrication of roughness elements is much higher than for the open-bed particles. This has implications for the stability of clusters in relation to open-bed material.

- Particle roundness and size had considerable influence on the density of and area covered by clusters. Thus where there are well rounded particles on the new bar at Squaw Creek, cluster density was high because cluster particles conform more frequently to the obstacle and are able to achieve long trains. By contrast, particles were

more angular in the channel and cluster density was lower. In the Schmiedlaine, where material was far more angular and grain sizes are larger, individual particles were far more prone to clustering. Nevertheless, cluster density was far lower than at Squaw Creek because the area covered by coarse-grained clusters was larger. Clusters, even if more frequent than at Squaw Creek, consisted of fewer particles. Thus very large angular material may actually prevent long clusters from forming.

- The spatial roughness arrangement is in most cases well ordered. In the Schmiedlaine, major roughness elements repeat at exactly 6 m intervals, which highlights the importance of the interaction between standing waves and large obstacles. The surprising regularity of the distribution of large roughness on steep river beds such as the Schmiedlaine was very clearly differentiated with the use of the relative $K_3$ roughness parameter. Direct comparison between $K_3$ roughness distributions and accompanying grain size variations show that the ordered arrangement of roughness is not revealed when relying on conventional grain size analyses.

- The temporal distribution of roughness and geometry can be subdivided into phases with the conceptual FAST model at Squaw Creek. Bedload transport and flow dynamics govern roughness and geometry conditions and vice versa. The FAST model identifies two main phase types: those with and those without abundant bedload transport. The attributes of the water surface and the pattern of flow development can be similarly subdivided into phases. During non-bedload transporting phases the regulated pattern of the river bed and water surface organisation responds to the development of flow cells. During bedload transporting phases, the water surface is in a "boiling" state and the flow cells are destroyed to give way to a two-layered flow. River bed roughness diminishes and energy is applied to efficient bedload transport. The appearance of the water surface (which indicates bed roughness) together with water slope changes can be classified into these two distinctive phases both at Squaw Creek and Lainbach. The water surface characteristics can be used to identify bedload transporting phases.

- The development of spiral flow cells monitored in a three-dimensional network at the Lainbach sheds light on the extreme variability of within-reach flow dynamics. The development, coalescence, shifting and decay of spiral flow vortices depends on channel geometry, water surface dynamics, flow depth, and most importantly whether bedload is in transit or not. The number of flow cells and their role in erosion and deposition vary spatially within a short distance as does the associated dynamics of river bed roughness. Changes in the volumes of erosion and deposition vary considerably depending on the cross-channel geometry and roughness distribution. Thus while one section of the river may be reacting very dynamically to the hydraulic and sedimentary processes, another section 5 m away may be undergoing far fewer changes. The same data and observations were gathered for bedload dynamics within a 30 m reach at Squaw Creek. There the volumes of material eroded and deposited within the reach also varied spatially and temporally. The ascending limb of the flood at Squaw Creek reflected an overall positive balance (deposition) while the descending limb reflected erosion. Just as at the Lainbach, it the final and largest bedload pulse caused major erosion. One explanation for the very localised changes in river bed roughness and associated geometry may be the localised nature of bedload transfer. As at Squaw Creek, phases where two or even four layers of particles are under way are very short-lived and restricted to the main bedload pulses. Extensive spatial and temporal measurements of bed adjustment and bedload transport from two flood waves showed that changes in river bed roughness are restricted to local areas of scour and infill determined by the development of flow cells

- The rules governing the relationship between velocity, roughness, geometry and the water surface gradient are determinable both for Squaw Creek and for the Lainbach. A very close relationship was obtained between the temporal changes of $K_3$ roughness and the well-known Manning coefficient for all flood flows in all study areas. During the flood flows, the constant relating velocity to $K_3$ roughness, hydraulic radius and water surface slope reaffirmed the limiting physical framework within which the river bed and roughness characteristics adjust during flood flows. The velocity constantly fluctuates according to roughness thresholds which are naturally influenced by the grain size characteristics within each study area. The amalgamation of all floods from all study areas with the related grain to form roughness transitions allowed the use of CAVE (Coefficient for Average Velocity Estimation) to establish a relationship between the $K_3$ (20) and the velocity constant. The $K_3$ roughness transition determined from the fractal analysis responds very sensitively to local roughness transitions.

# 8. ZUSAMMENFASSUNG

Die Untersuchungen der räumlichen und zeitlichen Dynamik der Rauheit und der Geometrie in Abhängigkeit von den Veränderungen von Geschiebetransport und Abfluß wurden in drei verschiedenen Gebirgsflüssen durchgeführt.

Zur Aufnahme der räumlicher Verteilung der Rauheit wurden zwei Meßtechniken weiter entwickelt. Die Rauheitsveränderungen in Längs- und Querprofilen erfolgten durch den "Tausendfüssler", die Eigenschaften einzelner Partikel wurden mit Hilfe des Photo-Siebtechnik erfaßt. Um die relativen Rauheiten und ihre räumlichen und zeitlichen Veränderungen besser beschreiben zu können, wurde die Bestimmung der Rauheitskoeffizienten nach Darcy-Weissbach oder Manning ergänzt durch den neuen Ansatz der $K_3$ Rauheit.

Die zeitlichen Veränderungen der Rauheit wurden mit Hilfe des Makro-Tausendfüsslers bestimmt und durch den Vergleich mit den Manning Rauheitkoeffizienten überprüft. Wesentliche Ergebnisse sind:

- Die komplexen zeitlichen Wechselwirkungen zwischen Rauheit, Geometrie, Fließdynamik und Geschiebetransport wurden während zweier Hochwässer am Squaw Creek in Montana beobachtet und gemessen und im FAST Modell zusammen gefaßt. FAST steht für Fluid And Sediment Transport. Auf Grund von topographischen Merkmalen der Sohle und der Wasseroberfläche lassen sich Phasen mit intensivem und Phasen mit sehr geringen Geschiebetransport unterscheiden. Am Lainbach in Oberbayern wurden die entsprechenden Phasen der Flußbettrauheit, der Geometrie und der Anpassung der Wasseroberfläche ebenfalls erkannt. Das FAST Model konnte hier erfolgreich zur Vorhersage der Phasen mit sehr starken oder sehr geringen Geschiebetransport eingesetzt werden. Zur Erklärung der räumlichen Verteilung der Rauheitsverhältnisse sind Vorstellungen über die zeitlichen Veränderungen der Primär- und Sekundärströmungen unabdingbar notwendig.

- Die räumliche Verteilung der $K_3$ Rauheiten wurde auf zwei unterschiedlichen Schotterbänken am Squaw Creek, einer Schotterbank und in der Hauptrinne der Schmiedlaine, sowie einer Schotterbank im Lainbach untersucht. Dabei ergeben sich Regeln über die Zusammenhänge zwischen den Form- und Kornrauheiten im Quer- und im Längsprofil. In allen Fällen ist die Rauheit im Querprofil höher als im Längsprofil. Dies gilt sowohl im Micromaßstab für eine einzelne Bettform, wie im Makromaßstab für eine gesamte Schotterbank.

- Die Dynamik der Fließvorgänge und des Geschiebetransportes bestimmt die Muster der Entwicklung der Bettrauheiten. Zwar konnten diese Parameter während der Abflußereignisse nicht auf allen Kiesbänken gemessen werden, doch die Regeln der Verteilung und das Ausmaß der Rauheiten sind für alle untersuchten Fälle sehr ähnlich. Die Anordnung der Rauheiten hängt sowohl von der Größe und Form der Partikel, als auch vom lokalen Gefälle und der Flußbettform ab. Überall dort, wo auf den Schotterbänken der Abfluß nur geringe Tiefe aufweist kommt es durch die dann auftretenden sich kreuzenden Scherwellen zu einer diamantförmigen Anordnung der Grobpartikel. Die Scherwellen können sich allerdings nur durchsetzen, wenn sich nur wenig Geschiebe lokal und einzeln bewegen. Im Gerinnebett können die zeitlichen und räumlichen Veränderungen der Rauheit durch den Makro-Tausendfüssler nur in grossen Zeitintervallen gewonnen werden. Im Querprofil der Schotterbank entspricht die Verbreitung der Rauheiten sehr gut dem lateralen Aufbau der Bank. Im Längsprofil ordnen sich die Partikel zu einzelnen Cluster-Bettformen. Die Cluster sind stromlinienförmig gebaut und erheben sich über die Schotterbank nur wenig höher als die maximale Breite im Grundriß.

- Wesentliche Eigenschaften der Rauheiten der Flußbetten wurden mit Hilfe eines fraktalen Ansatzes untersucht. $K_3$-Rauheiten wurden im Bereich zwischen Zentimetern und Metern bestimmt. In allen Maßstäben gibt es enge Zusammenhänge zwischen den Rauheitsbestimmungen im Längs- und Querprofil. Durch den fraktalen Ansatz ist es möglich, den Übergang zwischen Korn- und Formrauheit besser zu quantifizieren. Der Schwellwert liegt im Bereich des Übergangs von der Rauheit einzelner Partikel zur Rauheit geordneter Partikeleinheiten, den Clustern. Der Schwellwert beim Übergang von der Formrauheit zur Systemrauheit ergibt sich durch unterschiedliche Sohl- und Talformen (beispielsweise Step-pool System oder

Fließstrecken mit Schotterbänken). Im Querprofil sind die Unterschiede zwischen diesen Arten der Rauheit größer als im Längsprofil. Speziell bei den großen $K_3$ Abständen zur Bestimmung der Systemrauheit können größere Quergefälle durch Blöcke auftreten. Im Gegensatz dazu sind im Längsprofil, bedingt durch die lokal relativ geringen Gefälleverhältnisse, die entsprechenden $K_3$ Werte für die Systemrauheit niedrig

- Die Zusammenhänge im jeweiligen fraktalen System werden weitgehend von der Korngrößenverteilung bestimmt. Vergleicht man die Korngrößenverteilung mit den Diskontinuitäten im Bereich der fraktalen $K_3$ Werte so zeigt sich, daß die minderen Perzentile den Übergang von Korn- zu Formrauheit bestimmen. Der Übergang von Form- zu Systemrauheit liegt im Bereich oberhalb des $D_{75}$ Perzentiles. Die häufig für die Rauheit genutzten Perzentilwerte $D_{50}$ oder $D_{95}$ sind keine allgemein zutreffende Beschreibung der Rauheit und sollten durch genauere $K_3$ Aufnahmen ersetzt werden.

- Cluster wurden bisher in steilen Gebirgsbächen unzureichend untersucht. Durch die Photo-Siebtechnik ergeben sich auch hier neue Möglichkeiten der Analyse. Beispielsweise sind die Korngrößen der Cluster entscheidend gröber als die Partikel auf der umgebenden Sohle. Durch die mehrjährigen Beobachtungen auf einer Kießbank in der Schmiedlaine läßt sich zeigen, daß die hydraulischen Bedingungen für die Verteilung der Cluster von größerer Bedeutung sind als der Sedimenttransport. Während beispielsweise die Korngrößenzusammensetzung von Jahr zu Jahr gleich bleibt, verändert sich die Lage der Cluster entscheidend. Offensichtlich verändern sich die Fließbedingungen von Jahr zu Jahr und von Hochwasser zu Hochwasser bei etwa konstanter Korngrößenzusammensetzung des Geschiebes. Andererseits verursachen größere Geschiebewegungen große Veränderungen der Rauheit. Solange bestimmte Schwellwerte nicht überschritten werden, wird die Flußsohle gegen Ende der Hochwasserwelle immer wieder sich selbst ähnlich. Auch die Kiesbänke behalten Geometrie und Rauheit bei, selbst wenn Cluster erodiert und umgebaut werden.

- Die räumliche Veränderung von Form und Systemrauheit in Abhängigkeit von den Abflußbedingungen ist nicht nur eine Funktion von Gefälle und Korngrößenverteilung, sondern steht auch in starker Abhängigkeit von der Geometrie des Talgrundes. Das zeigt sich beispielsweise in der Anordnung der Cluster und der Querrippen. Die diamantförmige Ordung der Cluster auf der Schotterbank wird auf die Einflüsse von sich kreuzenden Scherwellen zurückgeführt, während die Querrippen sich durch stehende Wellen im Hauptgerinne bei Hochwasser formen. Blockige Flußuferwälle bilden sich zusammen mit sehr grobkörnigen Clustern, während der Rezession der Hochwasserwelle an der Aussenseite der Flußbiegungen.

- Durch die Photo-Siebanalyse können die Orientierungen der Schotter, Kiese und Cluster bestimmt werden. Es zeigt sich, daß die Orientierungen der Cluster die Abflußverhältnisse während der Rezession spiegeln, während die Oberflächen der Schotterbänke von der vorhergehende Hochwasserphase geprägt wird.

- Die Prägung der Form durch das fliessende Wasser ist bei den Clustern besonders deutlich. Im Grund- wie im Seitenriß dominieren Ellipsoidfiguren. Zwischen Clusterhöhe und Grundrißgeometrie gibt es enge Abhängigkeiten. Am Oberende von Schotterbänke, wo mehr Grobmaterial zur Verfügung steht, sind die Cluster größer, während am unteren Ende kleinere Cluster dominieren. Die Einregelung einzelner Steine der Cluster ist gegenüber dem Geschiebe auf der Schotterbank sehr viel größer. Diese hat große Folgen für die Stabilität der Rauheitsformen.

- Es kann auch gezeigt werden, daß die Rauhheitselemente sich oft räumlich zu Mustern ordnen. Auf der Kiesbank in der Schmiedlaine ist beispielsweise die Oberfläche im Abstand von 6m sehr rauh und grobkörnig. Dies ist eine Folge der Entwicklung von stehenden Wellen mit hohen Amplituden im entsprechenden Abstand. Diese Regelmäßigkeit konnte nur über die $K_3$ Analyse erschlossen werden, bei den entsprechenden Korngrößenanalysen ist der Befund viel weniger ausgeprägt.

- Die zeitliche Folge der Veränderungen von Rauheit und Geometrie kann mit dem am Squaw Creek entwickelten FAST-Modell interpretiert werden. Entscheidend für Rauheit und Geometrie sind die Zusammenhänge zwischen Geschiebetransport und Abflußvorgängen.

- Das FAST-Modell teilt den Hochwasserabfluß in Phasen mit wenig Geschiebetransport und Phasen mit viel Geschiebetrieb und verknüpft diese

Phasen mit speziellen Typen des Fließens. Während der Hochwasserphasen mit geringen oder fehlendem Geschiebetrieb wird die regelhafte Veränderunge des Flußbettes und die wellige Wasseroberfläche durch die Dynamik von Fließzellen verursacht. In den Phasen mit großen Geschiebtransport ist die Wasseroberfläche flacher und "kocht", die Fließzellen werden zerstört und durch ein Fließen in zwei Schichten abgelöst. Gleichzeitig nimmt die Rauheit der Sohle ab, dadurch steht dann mehr Energie für die Transportvorgänge zur Verfügung. Die Veränderung des Wasserspiegels ist ein eindeutiger Anzeiger für die Veränderung der Rauheitsverhältnisse. Beide Veränderungen stehen in Wechselwirkung mit typischen Schwankungen des Gefälles der Wasseroberfläche. Es ist sowohl am Squaw Creek, wie am Lainbach möglich, diese Dynamik mit den Phasen unterschiedlicher Geschiebeführung zu verknüpfen.

- Am Lainbach konnte in einem Testbereich die Entwicklung der Fließzellen drei-dimensional aufgenommen und dabei gleichzeitig die Veränderungen der Fließdynamik beobachtet werden. Bereits nach einer kurzen Fließstrecke kann sich die Zahl und die Lage der Fließzellen verändern. Daraus resultieren örtliche Veränderungen der Sohle durch Erosion oder Ablagerung und wechselnde Bettrauheiten. Je nach der Position im Querprofil und der Verteilung der jeweiligen Rauheiten schwanken die Beträge der Erosion und Ablagerung beträchtlich. Während beispielsweise im oberen Querprofil, bedingt durch die örtliche Hydraulik und dem Geschiebetrieb, große Veränderungen auftraten, erfolgten in dem nur 5m weiter unterhalb liegenden Querprofil die entsprechenden Veränderungen nur verzögert und abgeschwächt.

  Die Meßeinrichtungen am Squaw Creek erlauben es, für einen 30 m langen Sohlabschnitt den Ein- und den Austrag von magnetischem Grobgeschieben zu bestimmen. Während beispielsweise bei steigender Hochwasserwelle eine positive Bilanz mit Akkumulationstendenzen gemessen wurde, kam es bei der zweiten Phase mit großen Geschiebetransporten, zur Zeit der Rezession der Hochwasserwelle, zur Erosion im untersuchten Flußabschnitt. Über die untere Schwelle verließen mehr magnetische Steine den Flußabschnitt als über die oberere Schelle zugeliefert wurden. Eine der Hauptursachen für dieses differenzierte Verhalten ist die bei kleinen Hochwässern sehr typische räumliche Begrenzung der Transportvorgänge in einzelnen "Strassen". In diesen Bereichen können bei Geschiebepulsen kurzfristig auch bis zu drei oder vier Schotterlagen in Bewegung sein. In den Phasen mit einer Dominanz der Fließzellen lassen sich alle Veränderungen der Sohle konfluenten bzw. diffluenten sekundäre Strömungen zurückführen.

- Auf der Grundlage der Untersuchungen am Squaw Creek und am Lainbach lassen sich physikalische Regeln für die Beziehungen zwischen Geschwindigkeit, Geometrie und Wasserspiegelgefälle formulieren. In den Testgebieten ergeben sich für alle Hochwasserwellen sehr enge Beziehungen zwischen dem $K_3$ Rauheitsparameter und dem Manning Koeffizienten. Weiterhin läßt sich nachweisen, daß während der Hochwasserwellen zwischen der $K_3$ Rauheit, dem hydraulischen Radius und dem Gefälle funktionale Beziehungen bestehen. Die Dynamik vollzieht sich innerhalb eines engen Rahmens. Die Geschwindigkeiten verändern sich mit den Schwellwerten der Rauheit, die sich wiederum auf Grund der örtlichen vorhanden Korngrößenverteilungen ergeben. Auf Grund dieser Beziehungen ist es möglich, für alle drei Bäche in den jeweiligen Testgebieten, eine Beziehung zwischen dem jeweiligen $K_3$ (20) Parameter und der mittleren Geschwindigkeit zu ermitteln.

# 9. REFERENCES


Allen, J. R. L. (1968). The nature and origin of bedform hierarchies. Sedimentology, 10, (p.161-182).

Allen, J. R. L. (1983). River bedforms: progress and problems. In J. D. Collinson & J. Lewin (Eds.), Modern and ancient fluvial systems. Special Publication of the International Association of Sedimentologists Oxford: Blackwell Scientific Publications (p.19-33).

Allen, J. R. L. (1982a). Bedforms in supercritical and related flows: transverse ribs, rhomboidal features, and antidunes. In J. R. L. Allen (Eds.), Sedimentary structures: their character and physical basis Amsterdam: Elsevier, (p.383-416).

Allen, J. R. L. (1982b). Orientation of particles during sedimentation: shape fabrics. In J. R. L. Allen (Eds.), Sedimentary structures: their character and physical basis Amsterdam: Elsevier. (p.179-235).

Andrews, E. D. (1979). Hydraulic adjustment of the East Fork River, Wyoming to supply of sediment. In D. D. Rhodes & G. P. Williams (Eds.), Adjustments of the fluvial system Dubuque, Iowa, USA: Kendall Hunt (p.69-94).

Andrews, E. D. (1982). Bank stability and channel width adjustment, East Forking River, Wyoming. Water Research Research, 18, (p.1192-1194).

Andrews, E. D. (1983). Entrainment of gravel from naturally sorted riverbed material. Geological Society American Bulletin, 94, (p.1225-1231).

Andrews, E. D., & Erman, D. C. (1986). Persistence in the size distribution of surficial bed material during an extreme snow melt flood. Water Resources Research, 22(2), (p.191-197).

Andrews, E. D., & Parker, G. (1987). Formation of a coarse surface layer as the response to gravel mobility. In C. R. Thorne, J. C. Bathurst, & R. D. Hey (Eds.), Sediment transport in gravel-bed rivers Chichester: John Wiley & Sons. (p.269-328).

Andrele, R., & Abrahams, A. D. (1989). Fractal techniques and the surface roughness of talus slopes. Earth Surface Processes & Landforms, 14(3), 197-209.

Ashida, K., & Bayazit, M. (1973). Initiation of motion and roughness of flows in steep channels. In 15th Congress of the IAHR, Instanbul (p.475-484).

Ashida, K., Takahashi, T., & Sawada, T. (1981). Processes of sediment transport in a mountain stream channel. In Erosion and sediment transport in Pacific Rim steeplands (p.166-178). IAHS.

Ashmore, P. E. (1982). Laboratory modelling of gravel braided stream morphology. Earth Surface Processes & Landforms, 7, (p.201-225).

Ashworth, P. J., & Ferguson, R. I. (1989). Size-selective entrainment of bedload in gravel streams. Water Research Research, 25, (p.627-634).

Aubrey, D. G., Inman, D. L., & Winant, C. D. (1980). The statistical prediction of beach changes in Southern California. J. of Geophysical Research, 85(C6), (p.3264-3276).

Bagnold, R. A. (1956). The flow of cohesionless grains in fluids. Trans. Royal Soc. London, 249, (p.235-297).

Bagnold, R. A. (1973). The nature of saltation and of bedload transport in water. Proc. Royal Soc. London, 332 A, (p.473-504).

Bagnold, R. A., & Barndorff-Nielsen, O. (1980). The pattern of natural size distribution. Sedimentology, 27, (p.199-207).

Bänziger, R., & Bursch, H. (1990). Acoustic sensors for bedload transport in a mountain torrent. H, Lang, A. Musy (Eds.) In Hydrology in Mountain Regions, Lausanne: IAHS. 193 (p. 207-214).

Bänziger, R., & Bursch, H. (1991). Geschiebetransport in Wildbächen. Schweizer Ingenieur und Architekt, Heft 24.

Bathurst, J. C. (1978). Flow resistance of large scale roughness. American Soc. Civil Eng., 104(HY12), (p.1587-1603).

Bathurst, J. C. (1982a). Flow resistance in boulder-bed streams. In R. D. Hey, J. C. Bathurst, & C. R. Thorne (Eds.), Gravel-bed Rivers Chichester: J. Wiley & Sons (p.443-465).

Bathurst, J. C. (1982b). Theoretical aspects of flow resistance. In R. D. Hey, J. C. Bathurst, & C. R. Thorne (Eds.), Gravel-bed Rivers Chichester: J. Wiley & Sons (p.83-108).

Bathurst, J. C. (1985). Flow resistance estimation in mountain rivers. J. Hydraulic Engineering, 111(4), (p.625-643).

Bathurst, J. C., Graf, W. H., & Cao, H. H. (1982). Bedforms and flow resistance in steep gravel-bed channels. In B. M. Sumer & A. Müller (Eds.), Mechanics of Sediment Transport Rotterdam: Balkema. (p.215-21).

Bathurst, J. C., Thorne, C. R., & Hey, R. D. (1977). Direct measurements of secondary currents in river bends. Nature, 269(5628), (p.504-506).

Bathurst, J. C., Thorne, C. R., & Hey, R. D. (1979). Secondary flow and shear stress at river bends. J. of Hydr. Div., Am. Soc. Civil Engr., 105 (HY10), (p.1277-1295).

Bayazit, M. (1978). Scour of bed material in very rough channels. J. Hydraul. Div., Am. Soc. Civ. Eng., 104 (HY9), (p.1345-13499.

Bayazit, M. (1982). Flow structure and sediment transport mechanics in steep channels. In B.M. Sumer & A. Müller (Eds.), Mechanics of sediment transport, Balkema (p.197-206).

Becht, M. (1989). Der Einfluß von Muren, Schneeschmelze und Regenniederschlägen auf die Sedimentbilanz eines randalpinen Wildbachgebietes. Die Erde, 120, (p.189-202).

Bell, R. G., & Sutherland, A. J. (1983). Non-equilibrium bedload transport by steady flows. J. Hydr. Eng., Am. Soc. Civil Engr., 109, (p.351-365).

Bhowmik, N. (1979). Hydraulics of flow in the Kaskaskia River, Illinois (Report of Investigation, Urbanan III No. 91). Illinois State Water Survey.

Bhowmik, N. G. (1982). Shear stress distribution and secondary currents in straight open channels. In R. D. Hey, J. C. Bathurst, & C. R. Thorne (Eds.), Gravel-bed Rivers J.Wiley and Sons (p.31-61).

Billi, P. (1987). Sediment storage, bed fabric and particle features of two mountain streams at Plynlimon (mid-Wales) No. 97. University of Florence.

Billi, P. (1988). A note on cluster bedform behavior in a gravel-bed river. Catena, 15(5), (p.473-481).

Bluck, B. J. (1987). Bedforms and clast size changes in gravel bed rivers. In K. S. Richards (Eds.), River channels: environment and process Oxford: Basil Blackwell (p.159-78).

Bogardi, J. (1974). Sediment transport in alluvial streams. Budapest: Akademiai Kiado.

Boothroyd, J. C., & Ashley, G. (1975). Process, bar morphology and sedimentary structures on braided outwash fans, north-eastern Gulf of Alaska. In A. V. Jopling & B. C. McDonald (Eds.), Glaciofluvial and glaciolacustrine environments Society of Economic Paleontologists and Mineralogists Special Publication (p.193-222).

Bray, D. I. (1982). Flow resistance in gravel-bed rivers. In R. D. Hey, J. C. Bathurst, & C. R. Thorne (Eds.), Gravel-Bed Rivers New York: John Wiley (p.109-137).

Bray, D. I., & Church, M. (1980). Armoured versus paved gravel-beds. J. Hydraul. Div., Am. Soc. Civil Eng., 106 (HY11), (p.1937-1940).

Brayshaw, A. C. (1984). The characteristics and origin of cluster bedforms in coarse-grained alluvial channels. In C. H. Koster & R. H. Stell (Eds.), Sedimentology of gravels and conglomerates Canadian Society of Petroleum Geologists (p.77-85).

Brayshaw, A. C. (1985). Bed microtopograhy and entrainment thresholds in gravel-bed rivers. Geological Soc. American Bull., 96, (p.218-223).

Brayshaw, A. C., Frostick, L. E., & Reid, I. (1983). The hydrodynamics of particle clusters and sediment entrainment in coarse alluvial channels. Sedimentology., 30, (p.137-143).

Bridge, J. S. (1991). A revised model for water flow, sediment transport, bed topography and grain sorting in natural river bends. Water Resources Research, 28(4), (p.999-1013).

Bridge, J. S., & Jarvis, J. (1982). The dynamics of a river bend: a study in flow and sedimentary processes. Sedimentology, 29, (p.499-541).

Brotherston, D. I. (1979). On the origins and characteristics of river channel patterns. Journal of Hydrology, 44, (p.211-230).

Brush, L. M. (1965). Experimental work on primary sedimentary structures. In G. V. Middleton (Ed.), Primary sedimentary structures and their hydrodynamic interpretation, Spec. Publ. 12 Tulsa, USA: Society of Economic Paleontologists and Mineralogists (p.17-25).

Buffington, J. M., Dietrich, W. E., & Kirchner, J. W. (1992). Friction angle measurements on a naturally formed gravel streambed: implications for critical boundary shear stress. Water Resources Research, 28(2), (p.411-425).

Bunte, K. (1990). Experiences and results from using a big-frame bedload sampler for coarse material bedload. In H.Lang & A.Musy (Ed.), Hydrology in Mountainous Regions, Lausanne: IAHS 193 (p.223-230).

Bunte, K. (1992a). Particle number grain-size composition of bedload in a mountain stream. In P. Billi, R. D. Hey, C. R. Thorne, & P. Tacconi (Eds.), Dynamics of gravel-bed rivers (pp. 55-72). Chichester: John Wiley and Sons.

Bunte, K. (1992b) Untersuchungen der zeitlichen Variation des Grobgeschiebetransportes und seiner Korngrößenzusammensetzung (Squaw Creek, Montana, USA). Ph.D. thesis, Unpublished, Dept. of Geography, Free University of Berlin.

Carling, P. A. (1989). Hydrodynamic models of boulder berm deposition. Geomorphology, 2, (p.319-340).

Carling, P. A., & Reader, N. A. (1982). Structure, composition and bulk properties of upland stream gravels. Earth Surface Processes & Landforms, 7, (p.349-365).

Carson, M. A., & Griffiths, G. A. (1985). Tractive

stress and the onset of bed particle movement in gravel stream channels: different equations for different purposes. Journal of Hydrology, 79, (p.375-388).

Carson, M. A., & Griffiths, G. A. (1987). Bedload Transport in Gravel Channels. Journal of Hydrology, 26(1), (p.1-151).

Chang, H. H. (1980). Geometry of gravel streams. J. Hydr. Div., Am. Soc. Civil Engr, 106 (HY9), (p.1443-1456).

Chin, A. (1989). Step pools in stream channels. Progress Physical Geography, 13 (p.391-407).

Chiu, C. L. (1982). Modelling channel flow pattern. In R. D. Hey, J. C. Bathurst, & C. R. Thorne (Eds.), Gravel-bed Rivers Chichester: J. Wiley & Sons (p.63-80).

Church, M. (1985). Bedload in gravel-bed rivers: observed phenomena and implications for computation. In Proc. Ann. Conf. Canadian Society for Civil Engineering and 7th Canadian Hydrotech. Conf. Saskatoon, Canada, Vol 1B, (p. 17-37).

Church, M., & Gilbert, R. (1975). Proglacial fluvial and lacustrine environments. In A. V. Jopling & B. C. McDonald (Eds.), Glaciofluvial and glaciolacustrine sedimentation New York: Society of Economic Paleontologists and Mineralogists (p.22-100).

Church, M., & Jones, D. (1982). Channel bars in gravel-bed rivers. In R. D. Hey, J. C. Bathurst, & C. R. Thorne (Eds.), Gravel-bed Rivers Chichester: J. Wiley and Sons (p.291-324).

Church, M., Wolcott, J.F. and Maizels, J. (1990) Paleovelocity: a parsinonious proposal. Earth Surface Processes & Landforms V. 15, (p.475-80).

Church, M., Wolcott, J. F., & Fletscher, W. K. (1991). A test of equal mobility in fluvial sediment transport: behaviour of the sand fraction. Water Resources Research, 27(11), (p.2941-2951).

Church, M. A., McLean, D. G., & Wolcott, J. F. (1987b). River bed gravels: sampling and analysis. In C. R. Thorne, J. C. Bathurst, & R. D. Hey (Eds.), Sediment transport in gravel bed rivers Chichester: J. Wiley and Sons (p.43-88).

Clifford, N. J., Robert, A., & Richards, K. S. (1992). Estimation of flow resistance in gravel-bedded rivers: a physical explanation of the multiplier of roughness length. Earth Surface Processes & Landforms, 17, (p.111-126).

Costa, J. E. (1983). Paleohydraulic reconstruction of flash flood peaks from boulder deposits in the Colorado Front Range. Bull. Geological Soc. American, 94, (p.986-1004).

Cunningham, A. (1883). Recent hydraulic experiments. Minutes of Proceedings, Inst. of Civil Engineers, 71.

Custer, S. G., Ergenzinger, P., Anderson, B. C., & Bugosh, N. (1987). Electro-magnetic detection of Pebble Transport in Streams: A method for measurement of sediment-transport waves. In F. Ethridge, R. M. Flores, & M. Harvey (Ed.), Recent Developments in Fluvial Sedimentology, Tulsa (pp. 21-26).

Dal Cin, R. (1968). Pebble clusters, their origin and utilisation in the study of paleo-currents. Sedimentary Geology 2, (p.233-242).

Davies, T. R., & Sutherland, A. J. (1980). Resistance to flow past deformable boundaries. Earth Surface Processes & Landforms, 5, (p.175-179).

Davies, T. R. H. (1980). Bedform spacing and flow resistance. J. of Hydr. Div., Am. Soc. Civil Engr., 106 (HY3), (p.423-433).

Davies, T. R. H. (1982). Lower flow regime bedforms: rational classification. J. Hydr. Research. Am. Soc. Civil Eng., 108 (HY3), (p.343-360).

de Jong, C. (1991). A re-appraisal of the significance of obstacle clasts in cluster bedform dispersal. Earth Surface Processes & Landforms, 16(8), (p.737-744).

de Jong, C. (1992a). Discussion on: Microform roughness elements and the selective entrainment and entrapment of particles in gravel-bed rivers. In R. D. H. P.Billi C.R.Thorne, P.Tacconi. (Ed.), Dynamics of Gravel Bed Rivers, Florence: J. Wiley and Sons (p.267-272) .

de Jong, C. (1992b). The dynamics of a catastrophic flood/multiple debris flow in the Schmiedlaine, S.Germany. In D. E. Walling, T. R. Davies, & B. Hasholt (Ed.), Erosion, Debris Flows and Environment in Mountain Regions, Chengdu: IAHS 209 (p. 237-245.).

de Jong, C. (1992c). Measuring changes in micro and macro roughness on mobile gravel beds. In J. Bogen, D. E. Walling, & T. Day (Ed.), Erosion and Sediment Transport Monitoring Programmes in River Basins, 210 Oslo: IAHS (p.31-40.).

de Jong, C. (1992d). Micro-profiling of mobile gravel beds. In J. Bogen (Ed) Erosion and Sediment Transport Monitoring Programmes in River Basins, Oslo: IAHS (p.63-67).

de Jong, C. (1992e). Thresholds for channel change on two contrasting proglacial river fans, West Greenland. Geografiska Annaler, 74A(1), (p.1-12).

de Jong, C., & Ergenzinger, P. (1992). Unsteady flow, bedload transport and bed geometry responses in steep mountain torrents. In P. Larsen & N. Eisenhauer (Ed.), 5th International Symposium

on River Sedimentation. Sediment Management, Vol. 1 Karlsruhe: ISRS (p.185-192.).

Diepenbroek, M. (1992) Die Beschreibung der Korngestalt mit Hilfe der Fourier-Analyse. Ph.D. thesis. Unpublished, Dept. of Geology, Free University of Berlin.

Diepenbroek, M., Bartholomä, A., & Ibbeken, H. (1992). How round is round? A new approach to the topic 'roundness' by Fourier grain shape analysis. Sedimentology, 39, (p.411-422).

Diepenbroek, M., & de Jong, C. (1993). Quantification of textural particle characteristics by image analysis - examples from active and paleo-surfaces in steep, coarse-grained mountain environments. In P. Ergenzinger & K. Schmidt (Ed.), Dynamics and Geomorphology of Mountain Rivers. Benediktbeuern: Springer Verlag, (p.301-314).

Dietrich, W. E., Kirchner, J. W., Ikeda, H., & Iseya, F. (1990). Sediment supply and the development of the coarse surface layer in gravel-bedded rivers. Nature, 340, (p.215-217).

Dietrich, W. E., Smith, N. D., & Dunne, T. (1979). Flow and sediment transport in a sand-bedded meander. Journal of Geology, 87, (p.305-315).

Dingler, J. R., Boylls, J. C., & Lowe, R. L. (1977). A high frequency sonar for profiling small scale subaqueous bedforms. Marine Geology, 24, (p.279-288).

Dobin, K. (1985). Geologische Karte von Bayern 1:25 000. Blatt Kochel. Bayerisches Geologisches Landesamt, München.

Drake, T. G., Schreve, R. L., Dietrich, W. E., Whiting, P. J., & Leopold, L. B. (1987). Bedload transport of fine gravel observed by motion-picture photography. Journal of Fluid Mechanics, 192, (p.193-217).

Egashira, S., & Ashida, K. (1991). Flow resistance and sediment transportation in streams with step-pool bed morphology. In A. Armanini, G. Di Silvio, & (Ed.), Fluvial Hydraulics of Mountain Regions, 37, Trento, Italy: Springer-Verlag (p.45-58).

Egiazaroff, I. V. (1965). Calculations of nonuniform sediment concentrations. J. Hydr. Div., Am. Soc. Civil Engr., 91, (p.425-438).

Einstein, H. A. (1950). The bedload function for sediment transportation in open channel flows. Soil Conservation Service, Tech. Bull., United States Dept. of Agri., Washington D.C., 1026, (pp.78)

Einstein, H. A., & Barbarossa, N. L. (1951). River channel roughness. Proc. American Society Civil Eng.. (pp.12)

Einstein, H. A., & Li, H. (1958). Secondary currents in straight channels. Transactions American Geophysical Union, 39(6), (p.1058-1088).

Einstein, H. A., & Shen, S. W. (1964). A study of meandering in straight alluvial channels. Journal of Geophysical Research, 69, (p.5239-5247).

Emmett, W. W. (1975). The channels and waters of the Upper Salmon River area, Idaho. Geological Survey Professional Paper, 870(A), (pp.116).

Engelund, F. (1974). Flow and bed topography in channel bends. J. Hydr. Div., Am. Soc. Civil Eng., 100(HY11), (p.1631-1648).

Ergenzinger, P. (1987). Chaos and order: the channel geometry of gravel-braided rivers. Catena Supplement, 10, (p.85-98).

Ergenzinger, P. (1988). The nature of coarse material bed load transport. In M.P.Bordas, D.E. Walling (Ed) Sediment budgets, 174 Porto Allegro: (p.207-216).

Ergenzinger, P. (1992). River bed adjustments in a step-pool system: Lainbach, Upper Bavaria. In P. Billi, R.D. Hey, C. R. Thorne, & P. Tacconi (Eds.), Dynamics of Gravel Bed Rivers Chichester: J.Wiley and Sons (p.415-430).

Ergenzinger, P. & Conrady, J. (1982). A new tracer technique for measuring bedload in natural channels. Catena V. 9, (p.77-80).

Ergenzinger, P., & Custer, S. G. (1983). Determination of bedload transport using naturally magnetic tracers. First experiences at Squaw Creek, Gallatin County, Montana. Water Resources Research, 19(1), (p.187-193).

Ergenzinger, P., de Jong, C., & Christaller, G. (1994). Interrelationships between bedload transfer and river bed adjustment in mountain rivers. In M. Kirkby (Ed.), Theory in Geomorphology, Leeds: John Wiley and Sons (p.141-158).

Ergenzinger, P., & Jüpner, R. (1992). Using COSSY (CObble Satellite SYstem) for measuring the effects of lift and drag forces. In J. Bogen, D. E. Walling, & T. Day (Ed.), Erosion and sediment transport monitoring programmes in river basins, Oslo: IAHS. 210 (p.41-49).

Ergenzinger, P., & Schmidt, K. H. (1990 Aug.). Stochastic elements of bedload transport in a step-pool mountain river. In O. Sinniger & M. Monbaron (Ed.), Hydrology in Mountain Region. II Artificial Reservoirs; Water and Slopes, II, Lausanne: IAHS, Spec. Publ. 119 (p.39-46).

Ergenzinger, P., & Stüve, P. (1989). Räumliche und zeitliche Variabilität der Fliesswiderstände in einem Wildbach: Der Lainbach bei Benediktbeuern in Oberbayern. Göttinger Geographische Abbhandlungen, 86, (p.61-79).

Fahnstock, R. D. (1963). Morphology and hydrology of a glacial stream - White River, Mt. Rainer,

Washington. Prof. Paper, United States Geol. Survey, 422-A, (pp.67).

Felix, P. K., Priesmeier, H. V., & Wilhelm, F. (1988). Abfluß in Wildbächen. Untersuchungen im Einzugsgebiet des Lainbaches bei Benediktbeuern. Münchner Geographische Abhandlungen, B(6) (pp.550).

Fenton, J. D., & Abbott, J. E. (1977). Initial movement of grains on a stream bed: the effect of relative protrusion. Proc. Royal Soc. London, A 352, (p.523-537).

Ferguson, R. I., Ashmore, P. E., Ashworth, P. J., Paola, C., & Prestegaard, K. L. (1992). Measurements in a braided river chute and lobe. 1. Flow pattern, sediment transport and channel change. Water Resources Research, 28(7), (p.1877-1886).

Forster, F., Keller, H.M., Rickenmann, D. & Röthlisberger, G. (1993). Hochwasser, R. Schluepfer (Ed.), Naturgefahren. Forum für Wissen, Birmensdorf, WSL, (p.23-33).

Furbish, D. J. (1987). Conditions for the geometric similarity of coarse stream-bed roughness. Mathematical Geology, 19, (p.291-307).

Gessler, J. (1965a). Der Geschiebetriebbeginn bei Mischungen untersucht an natürlichen Abpflasterungserscheinigungen in Kanälen. Mitteilungen VAW, ETH, Zürich, 69.

Gessler, J. (1990). Friction factors of armoured river beds. J. of Hydr. Div., Am. Soc. Civ. Eng., 116(4), (p.531-43).

Gibson, A. H. (1909). On the depression of the filament of maximum velocity in a stream flowing through a natural channel. Proc. of the Royal Society, 82(Series A), (p.149-159).

Gilbert, G. K. (1914). The transportation of debris by running water. Prof. Paper, United States Geol. Survey, 86, (pp.363).

Gomez, B. (1983). Temporal variations in bedload transport rates: the effect of progressive bed armouring. Earth Surface Processes & Landforms, 8, (p.41-54).

Gomez, B., Naff, R. L., & Hubbell, D. W. (1989). Temporal variation in bedload transport rates associated with the migration of bedforms. Earth Surface Processes & Landforms, 14, (p.135-156).

Goudie, A. (1981). Geomorphological Techniques. London: George Allen and Unwin.

Görtler, H. (1941). Instabilität laminarer Grenzschichten in konkaven Wänden gegenüber gewissen drei-dimensionalen Strömungen. 2. Angewandte Mathematische Med. 21. (p.250-252)

Graf, W.H. (1971). Hydraulics of sediment transport, McCraw Hill Book Co., Series in Water Resources and Environmental Engineering. London (pp.513).

Graf, W. H. (1989). Flow resistance over a gravel bed: its consequence on initial sediment movement. In G. di Silvio & A. Armanini (Ed.), Fluvial Hydraulics of Mountain Regions, Trent, Italy: Springer Verlag (p.17-32).

Grant, G. E., Swanson, F. J., & Wolman, M. G. (1990). Pattern and origin of stepped-bed morphology in high gradient streams, Western Cascades, Oregon. Geological Society of American Bulletin, 102, (p.340-352).

Grass, A. J. (1971). Structural features of turbulent flow over smooth and rough boundaries. Journal of Fluid Mechanics, 50, (p.233-255).

Grass, A. J., Stuart, R. J., & Mansour-Thrani, M. (1991). Vortical structures and coherent motion in turbulent flow over smooth and rough boundaries. Philosophical Transactions Ryoal Soc. London, A(336), (p.35-65).

Griffiths, G. A. (1981). Flow resistance in coarse gravel bed rivers. J. Hydr. Div., Am. Soc. Civil Eng., 107(HY7), (p.899-918).

Griffiths, G. A. (1989). Form resistance in gravel channels with mobile beds. J. of Hydr. Eng., Am. Soc. Civil Eng, 115(3), (p.340-55).

Gustavson, T. C. (1974). Sedimentation on gravel outwash fans, Malaspina Foreland Alaska. Journal of Sedimentary Petrology, 44, (p.374-89).

Haines-Young, R. H., & Petch, J. R. (1980). The challenge of critical rationalism for methodology in physical geography. Progress in Physical Geography, 4(1), (p.63-77).

Haizhou, T., & Graf, W. H. (1993). Friction in unsteady open-channel flow over gravel beds. Journal of Hydraulic Research, 31(1), (p.99-110).

Hammann de Salazar, K. (1992). Experimentelle Untersuchungen zur Charakterisierung des Strömungsfeldes über rauhen Sohlen (Diplomarbeit im Fach Physik) Institut für Wasserbau und Kulturtechnik, Universität Karlsruhe.

Hassan, M. A. (1990). Scour, fill and burial depth of coarse material in gravel bed streams. Earth Surface Processes & Landforms, 15, (p.341-356).

Hassan, M. A., & Reid, I. (1990). The influence of microform bed roughness elements on flow and sediment transport in gravel bed rivers. Earth Surface Processes & Landforms, 15(8), (p.739-750).

Hassan, M. A., Schick, A. P., & Laronne, J. B. (1984). The recovery of flood dispersed coarse sediment particles. Catena Supplement, 5, (p.153-162).

Hayward, J. A. (1980). Hydrology and stream

sediment from Torlesse stream catchment. No. No. 17). Tussock Grasslands and Mountain Lands Institute Lincoln College, New Zealand.

Hayward, J. A., & Sutherland, A. J. (1974). The Torlesse stream vortex-tube sediment trap. Journal of Hydrology, 13, (p.41-53).

Hellstrom, B. (1948). Discussion of "Macroturbulence in natural stream flow". Transactions American Geophys. Union, Vol. 29, No.2, p.272-273.

Hey, R.D. (1975). Design discharge for natural channels, Science, Technology and Environmental Management, R.D. Hey and T.D. Davies (eds), Saxon House, UK, p.73-88.

Hey, R. D. (1979). Flow resistance in gravel-bed rivers. J. Hydr. Div., Am. Soc. Civil Eng, 105 (NY4), (p.365-379).

Hey, R. D. (1982). Design equations for mobile gravel-bed rivers. In R. D. Hey, J. C. Bathurst, & C. R. Thorne (Eds.), Gravel-bed Rivers Chichester: J. Wiley & Sons (p. 553-580).

Hey, R. D. (1986). Stable channels with mobile beds. J. of Hydr. Eng., Am. Soc. Civil Eng., 112(8), (p.671-89).

Hey, R. D. (1987). River dynamics, flow regime and sediment transport. In C. R. Thorne, J. C. Bathurst, & R. D. Hey (Eds.), Sediment transport in gravel bed rivers (pp. 17-42). Chichester: J. Wiley and Sons.

Hey, R. D. (1988). Bar form resistance in gravel-bed rivers. J. of Hydr. Eng., Am. Soc. Civil Eng., 114(12), (p.1498-508).

Hey, R. D., & Thorne, C. D. (1983). Accuracy of surface samples from gravel bed material. J. of Hydr. Eng. Am. Soc. Civil Eng., 109(6), (p.842-51).

Hodges, W. K. (1982). Hydraulic characteristics of a badland pseudo-pediment slope system during simulated rainstorm experiments. In R. Bryan & A. Yair (Eds.), Badland Geomorphology Norwich: Geo Books (p.127-153).

Hoey, T. (1992). Temporal variations in bedload transport rates and sediment storage in gravel-bed rivers. Progress in Physical Geography, 16(3), (p.319-338).

Humboldt, A. von (1845-1858). Kosmos. Entwurf einer physischen Weltbeschreibung. B. I-IV.

Ibbeken, H. (1974). A simple sieving and splitting device for field analysis of coarse-grained sediments. Journal Sedimentary Petrology, 44(3), (p.939-946).

Ibbeken, H., & Schleyer, R. (1986). Photo-sieving: a method for grain size analysis of coarse-grained, unconsolidated bedding surfaces. Earth Surface Processes & Landforms, 11, (p.59-77).

Ikeda, S., & Kimura, Y. (1987). Stable channel cross section of straight rivers. In W. R. White (Ed.), Fluvial Hydraulics in Mountain Regions Lausanne: IAHR, (p.339-345).

Ikeda, S., & Nishmura, T. (1986). Flow and bed profile in meandering sand-silt rivers. J. Hydr. Eng., Am. Soc. Civ. Eng., 112(7), (p.562-579).

Iseya, F., & Ikeda, H. (1987). Pulsations in bedload transport rates induced by a longitudinal sediment sorting. Geografiska Annaler, 69A(1), (p.15-27).

Jackson, W. L., & Beshta, R. L. (1982). A model of two-phase bedload transport in an Oregon coast range stream. Earth Surface Processes & Landforms, 7, (p.517-527).

Jaeggi, M. N. R. (1987). Effect of flow variability (unsteadiness and nonuniformity) in erodible channels. In W. R. White (Ed.), Fluvial Hydraulics, Lausanne: IAHR (pp.117-123).

James, C. S. (1991). Entrainment of spheres -an experimental study of the effect of bed roughness on sediment sorting by entrainment. In M. Marzo & C. Puigdefabregas, Alluvial Sedimentation, Barcelona: Spec. Publ. 17, IAS, Blackwell Scientific Publications, (p.3-10).

Jarrett, R. D. (1984). Hydraulics of high gradient streams. J. Hydr. Eng., Am. Soc. Civil Engr., 110(11), (p.1519-1539).

Johansson, C. E. (1963). Orientation of pebble clusters in running water: a laboratory study. Geografiska Annaler, 45A, (p.85-112).

Johansson, C. E. (1976). Structural studies of frictional sediments. Geografiska Annaler, 58 (Series A), (p.201-301).

Karcz, I. (1968). Fluviatile obstacle marks from the wadis of the Negev (Southern Israel). Journal Sedimentary Petrology, 38, (p.1000-1012).

Karcz, I. (1981). Reflections on the origin of small-scale longitudinal streambed scours. In M. A. Morisawa (Eds.), Fluvial Geomorphology London: George Allen and Unwin (p.149-173).

Karman, V., T., & Rubach, H. (1912). Über den Mechanismus des Flüssigkeits und Luftwiderstandes. Physik Zeitschrift, 2, (p.49-59).

Keller, A., & Melhorne, N. (1978). Rhythmic spacing and origin of pools and riffles. Bull. Geological Soc. of America, 89, (p.723-30).

Keller, E. A. (1971). Areal sorting of bed-load materials: the hypothesis of velocity reversal. Bull. Geological Soc. America, 82, (p.753-756).

Keller, E. A. (1972). Development of alluvial stream channels: a five stage model. Bull. Geological Soc. of America, 83, (p.1531-1536).

Keller, E. A., & Tally, Z. (1979). Effects of large organic debris on channel form and fluvial processes in the coastal Redwood environment.

In D. D. Rhodes & G. P. Williams (Eds.), Adjustments of the fluvial system Dubuque, Iowa, USA: Kendall Hunt (p.169-196).

Keulegan, G. H. (1938). Laws of turbulent flow in open channels. Journal of Natural Bureau of Standard Washington D.C. Research Paper, 1151 (21), 707-741.

Kieffer, S. (1985). The 1983 hydraulic jump in Crystal Rapids: Implications for river managing and geomorphic evolution in the Grand Canyon. Journal of Geology, 93, (P.385-406).

Kirchner, J. W., Dietrich, W. E., Iseya, F., & Ikeda, H. (1990). The variability of critical shear stress, friction angle and grain protrusion in water-worked sediments. Sedimentology, 37, (p.647-672).

Klingeman, P.C. & Matin, H (1993). Incipient motion in gravel-bed rivers. Hydraulic Engineering ASCE (Eds) W. Shen, S.T. Su, and F. Wen. Vol. 1., San Francisco, (p.707-712).

Knight, D. W., & MacDonald, J. A. (1979). Open channel flow with varying bed roughness. J Hydr. Div, Am. Soc. Civil Engr., 105 (HY9), (p.1167-1183).

Knight, D.W. (1989). Hydraulics of flood channels. K. Beven & P. Carling (Eds.), Floods: hydrological, sedimentological and geomorphological implications. J. Wiley and Sons., (p.83-105).

Knighton, A. D. (1983). Models of stream bed topography at the reach scale. Journal of Hydrology, 60, (p.105-121).

Komar, P. D. (1987). Selective grain entrainment by a current from a bed of mixed sizes: a reanalysis. Journal Sedimentary Petrolology, 57, (p.203-211).

Komar, P. D., & Li, Z. (1988). Applications of grain pivoting and sliding analyses to selective entrainment of gravel and to flow-competence evaluations. Sedimentology, 35, (p.681-695).

Komar, P. D., & Shih, S.-M. (1992). Equal mobility versus changing bedload grain size in gravel-bed streams. In P. Billi, R. D. Hey, C. R. Thorne, & P. Tacconi (Eds.), Dynamics of gravel-bed rivers Chichester: John Wiley and Sons (p.73-106).

Koster, E. H. (1978). Transverse ribs: their characteristics, origin and paleohydraulic significance. In A. D. Miall (Eds.), Fluvial Sedimentology Canadian Society of Petroleum Geologists (p.161-86).

Kuhnle, R. A., & Southard, J. B. (1988). Bedload transport fluctuations in a gravel-bed laboratory channel. Water Resources Research, 25(2), (p.247-260).

Langbein, W.B. & Leopold, C.B. (1968) River channel bars and dunes in the theory of kinematic waves. US Geological Survey Prof. Paper. 122-L. (p-1-20).

Lamberti, A., & Paris, E. (1992). Analysis of armouring processes through laboratory experiments. In P. Billi, R. D. Hey, C. R. Thorne, & P. Tacconi (Eds.), Dynamics of Gravel-bed Rivers Chichester: John Wiley and Sons Ltd (p.227-250).

Lane, E. W., & Carson, E. J. (1954). Some observations on the effect of particle shape on the movement of coarse sediment. Trans. American Geophysical Union, 35, (p.453-462).

Lapointe, M. (1993) Monitoring alluvial sand suspension by eddy correlation. Earth Surface Processes & Landforms Vol. 18, (p.157-175).

Laronne, J. B., & Carson, M. A. (1976). Interrelationships between bed morphology and bed-material transport for a small, gravel-bed channel. Sedimentology, 23, (p.67-85).

Laronne, J. B., & Duncan, M. J. (1992). Bedload transport paths and gravel bar formation. In P. Billi, R. D. Hey, C. R. Thorne, & P. Tacconi (Eds.), Dynamics of Gravel Bed Rivers, Chichester: (p.177-202).

Lawrence, G. A. (1987). Steady flow over an obstacle. J. Hydr. Eng., Am. Soc. Civil Engr., 113(8), (p.981-991).

Lekash, J., & Schick, A. P. (1983). Evidence for transport of bedload in waves: analysis of fluvial sediment samples in a small upland stream channel. Catena, 10, (p.267-279).

Leliavsky, S. (1955). An introduction to Fluvial Hydraulics. London: Constable & Co.

Leopold, L. B. (1982). Water Surface Topography in River Channels and Implications for Meander Development. In R. D. Hey, J. C. Bathurst, & C. R. Thorne (Eds.), Gravel-Bed Rivers, J.Wiley and Sons (p.359-383).

Leopold, L. B. (1992). Sediment size that determines channel morphology. In P. Billi, R. D. Hey, C. R. Thorne, & P. Tacconi (Eds.), Dynamics of Gravel Bed Rivers Chichester: J.Wiley and Sons (p.297-312).

Leopold, L. B., & Emmett, W. W. (1981). Some observations on the movements of cobbles on a streambed. In Erosion and Sediment Transport Measurement, 133, Florence: IAHS (p.49-59).

Leopold, L. B., & Emmett, W. W. (1982). Bedload trap, East Fork River. In L. B. Leopold (Ed.), Am. Geomorph. Field Group. Field Trip Guidebook, Pinedale, Wyoming.

Leopold, L. B., & Maddock, T. (1953). The hydraulic geometry of stream channels and some physiographic implications. US Geol. Survey Professional Paper, 252, (pp.57).

Leopold, L. B., & Wolman, M. G. (1957). River

channel patterns: braided, meandering and straight. Professional Paper. United States Geological Survey, 282 B, (p.39-85).

Leopold, L. B., Wolman, M. G., & Miller, J. P. (1964). Fluvial Processes in Geomorphology. San Francisco: W.H. Freeman Co., (pp.522).

Leviasky, S. (1955). An introduction to fluvial hydraulics, Dover Publi. New York.

Lewin, J. L. (1976). Initiation of bedforms and meanders in coarse-grained sediment. Geological Soc. American Bull., 87, (p.281-317).

Li, Z. & Komar, P.D. (1986). Laboratory measurements of privoting angles for applications to selective entrainment of gravel in a current. Sedimentology, 33, (p.413-423).

Lisle, T. (1986). Stabilisation of a gravel channel by large streamwise obstructions and bedrock bends, Jacoby Creek, north-western California. Geological Soc. American Bull., 97, (p.999-1011).

Mandelbrot, B. (1987). Die fraktale Geometrie der Natur. Basel Boston: Birkhauser Verlag (pp.491).

McCarroll, D. (1992). A new instrument and techniques for the field measurement of rock surface roughness. Zeitschrift für Geomorphologie, N.F., 36(1), (p.69-79).

McDonald, B. C., & Banerjee, I. (1971). Sediments and bedforms on a braided outwash plain. Canadian Journal of Earth Sciences, 8, (p.1282-301).

McDonald, B. C., & Day, T. J. (1978). An experimental flume study on the formation of transverse ribs. Current Research (A): Geological Surv. Canada Pap., 78-1A, (p.441-451).

Miller, J. P., & Leopold, L. B. (1963). Simple measurements of morphological changes in river channels and hill slopes. Arid Zone Research, 20, (p.421-427).

Milne, J. A. (1982a). Bed-material size and the riffle-pool sequence. Sedimentology, 29, (p.267-278).

Milne, J. A. (1982b). Bedforms and bend-arc spacing of some coarse-bedload channels in upland Britain. Earth Surface Processes & Landforms, 7, (p.227-40).

Mosley, M. P. (1981). Semi-determinate hydraulic geometry of river channels. South Island, New Zealand. Earth Surface Processes and Landforms, 6, (p.127-137).

Moss, A. J., Green, P., & Hutka, J. (1982). Small channels: their experimental formation, nature and significance. Earth Surface Processes & Landforms, 7, (p.401-415).

Mülhofer, L. (1933). Untersuchungen über die Schwebstoff und Geschiebeführung des Inn nächst Kirchbichl (Tirol). Die Wasserwirtschaft, 1-6, (p.1-23).

Naden, P. M., & Brayshaw, A. C. (1987). Small and medium scale bedforms in gravel-bed rivers. In K. S. Richards (Eds.), River channels: environment and process Oxford: Basil Blackwell (p.249-71).

Nakagawa, H., Tsujimoto, T., & Shimizu, Y. (1988). Velocity profile of flow over rough permeable beds. In 6th Congress of Asian and Pacific Regional Division of IAHR, Kyoto, Japan (p. 449-456).

Nelson, J.M. & Smith, J.D. (1989). Mechanics of flow over ripples and dunes. Journal Geophysical Research, 24, (p.8146-8162).

Newson, M. (1992). Twenty years of systematic physical geography: issues for a "New Environmental Age". Progress in Physical Geography, 16(2), (p.209-221).

Nezu, I., & Rodi, W. (1986). Open-channel flow measurements with a laser doppler anemometer. J. of Hydr. Eng., Am. Soc. Civil Eng., 112 (HY 5), (p.335-355).

Nikuradse, J. (1933). Strömungsgesetze in rauhen Rohren. Ver. Deut. Ing. Forschungsheft, (pp.361).

Osterkamp, W. R. (1978). Gradient, discharge and particle size relations of alluvial channels in Kansas with observations on braiding. American Journal of Science, 278, (p.1253-1268).

Paola, C., Gust, G., & Southard, J. B. (1986). Skin friction behind isolated hemispheres and the formation of obstacle marks. Sedimentology, 33, (p.279-293).

Parker, G. & Sutherland, A.J. (1990), Fluvial armour, J. of Hydr. Res., Am. Soc. Civil Eng. 28, (p.529-49).

Parker, G. (1979). Hydraulic geometry of active gravel beds. J. of Hydr. Div., Am. Soc. Civil Eng., 105 (HY 9), (p.1185-1201).

Parker, G., Dhamotharan, S., & Stefan, H. (1982). Model experiments on mobile paved gravel bed streams. Water Resources Research, 19, (p.1395-1408).

Parker, G., Klingeman, P.C. and McClean, D.G. (1982). Bedload and size distribution in paved gravel-bed streams. J. Hydraul. Div., Am. Soc. Civ. Eng. 108 (HY4), (p.544-571).

Petit, F. (1990). Evaluation of grain shear stresses required to initiate movement of particles in natural rivers. Earth Surface Processes & Landforms, 15, (p.135-148).

Phillips, J. D. (1990). The instability of hydraulic geometry. Water Resources Research, 26(4), (p.739-744).

Press, H., & Schröder, R. (1966). Hydromechanik im Wasserbau. Berlin-München: Wilhelm Ernst & Sohn.

Prestegaard, K. L. (1983). Bar resistance of gravel-bed streams at bankfull stage. Water Resources Research, 19 (HY10), (p.472-76).

Profitt, G.T. & Sutherland, A.J. (1983). Transport of non-uniform sediment. J. Hydraulic Research 21(1), (p.33-43).

Rachocki, A. H. (1981). Alluvial fans. John Wiley & Sons, University of Gdansk (pp. 161).

Reid, I., & Frostick, L. E. (1986). Dynamics of bedload transport in Turkey Brook, a coarse-grained alluvial channel. Earth Surface Processes & Landforms, 11, (p.143-155).

Reid, I., & Frostick, L. E. (1987). Toward a better understanding of bedload transport. In F. G. Ethridge, R. M. Flores, & M. D. Harvey (Ed.), Recent developments in fluvial geomorphology, 39 Tulsa U.S.A. Society of Economic Paleontologists and Mineralogists (pp. 13-19).

Reid, I., Frostick, L. E., & Brayshaw, A. C. (1992). Microform roughness elements and the selective entrainment and entrapment of particles in gravel-bed rivers. In P. Billi, R. D. Hey, C. R. Thorne, & P. Tacconi (Eds.), Dynamics of Gravel Bed Rivers Chichester: J.Wiley and Sons (p. 253-276).

Reid, I., Frostick, L. E., & Layman, J. T. (1985). The incidence and nature of bedload transport during flood flows in coarse-grained alluvial channels. Earth Surface Processes & Landforms, 10(1), (p.33-44).

Richards, K. S. (1978). Channel geometry in the riffle pool system. Geografiska Annaler, 60A, (p.345-354).

Richards, K. S. (1976). The morphology of riffle pool sequences. Earth Surface Processes & Landforms, 1(1), (p.71-88).

Richards, K. S. (1978). Simulation of flow geometry in a riffle-pool system. Earth Surface Processes & Landforms, 3(4), (p.23-27).

Richardson, E. V., & McQuivey, R. S. (1968). Measurement of turbulence in water flow. Journal of Hydraulics Division. ASCE, 94(HY2), (p.411-429).

Rickenmann, D. (1992). Bedload transport and discharge in the Ehrlenbach stream. In P. Ergenzinger & K.-H. Schmidt (Ed.), Dynamics and Geomorphology of Mountain Streams, Benediktbeuern: Springer (p.53-66).

Robert, A. (1988). Statistical analysis of sediment bed profiles in alluvial channels. Mathematical Geology, 20(3), (p.205-225).

Robert, A. (1990). Boundary roughness in coarse-grained channels. Progress Physical Geography, 14(1), (p.42-70).

Robert, A. (1991). Fractal properties of simulated bed profiles in coarse-grained channels. Mathematical Geology, 23(3), (p.367-382).

Robert, A. and Richards, K. (1988). On the modelling of sand bedforms using the semivariogram. Earth Surface Processes & Landforms, 13, (p.459-473).

Robert, A., & Roy, A. G. (1990). On the fractal interpretation of the mainstream length-drainage area relationship. Water Resources Research, 26(5), (p.839-842).

Roy, A. G., & Robert, A. (1990). Fractal techniques and the surface roughness of talus slopes: a comment. Earth Surface Processes & Landforms, 15, (p.283-285).

Rubin, D.M, Schmidt, J.C. & Moore, J.M (1990). Origin, structure and evolution of a re-attachment bar, Colorado River, Grand Canyon, Arizona. Journal of Sedimentary Petrology, Vol. 60, N. 6, (p.982-991).

Saunderson, H. C. (1992). Multiquadric interpolation of fluid speeds in a natural river channel. Computers Mathematics Applications, 24(12), (p.187-193).

Sawada, T., Ashida, K., & Takahashi, T. (1983). Relationship between channel pattern and sediment transport in a steep gravel bed river. Zeitschrift für Geomorphologie, N.F. Suppl. Band 46, (p.55-66).

Sayre, W. W., & Alberston, M. L. (1961). Roughness spacing in rigid open channels. J. Hyd. Div., Am. Soc. Civ. Eng., 87, (p.121-150).

Schlichting, H. (1958). Grenzschicht-Theorie. Karlsruhe: Braun.

Schumm, S. A. (1960). The shape of alluvial channels in relation to sediment type. US Geol. Survey Prof. Paper, 352(B), (p.17-30).

Shen, H.W., Fehlman, H.M. & Mendoza, C. (1990). Bedform resistance in open-channel flow. J. of Hydr. Eng., Am. Soc. Civ. Eng., 116 (6), (p.799-815).

Shih, S., & Komar, P. D. (1990). Differential bedload transport rates in a gravel-bed stream: a grain size distribution approach. Earth Surface Processes & Landforms, 15, (p.539-552).

Simons, D. B., Richardson, E. V., & Nordin, C. F. (1965). Sedimentary structures generated by flow in alluvial channels. In G. V. Middleton (Ed.), Primary sedimentary structures and their hydrodynamic interpretation, Spec. Publ. 12 Tulsa, USA: Society of Economic Paleontologists and Mineralogists (p.34-53).

Spieker, R., & Ergenzinger, P. (1990). New developments in measuring bed load by the magnetic tracer technique. In D. E. Walling, A. Yair, & S. Berkowicz (Ed.), Erosion,

transport and deposition processes, 189 Jerusalem (p.169-178).

Spurk, J. H. (1989). Strömungslehre - Einführung in die Theorie der Strömung. Berlin: Springer Verlag, (pp.482).

Statzner, B. (1988). Growth and Reynold's number of lotic macroinvertebrates: a problem for adaptation of shape to drag. Oikos, 51, (p.84-87).

Statzner, B., & Holm, T. F. (1989). Morphological adaptation of shape to flow: Microcurrents around loci macroinvertebrates with known Reynold's numbers at quasi-natural flow conditions. Oecologia. 78, Springer, (p. 145-157).

Stearns, F. P. (1883). On the current meter, together with a reason why the maximum velocity of water flowing in open channels is below the surface. Trans. Am. Soc. Civ. Eng., 12, (p.5-8).

Sutherland, A. J. (1967). Proposed mechanism for sediment entrainment by turbulent flows. Journal of Geophysical Research, 72, (p.6183-6194).

Sutherland, A. J. (1987). Static armour layers by selective erosion. In C. R. Thorne, J. C. Bathurst, & R. D. Hey (Eds.), Sediment transport in gravel-bed rivers, Chichester: John Wiley and Sons (p.243-268).

Sutherland, A. J., & Griffiths, G. A. (1975). Non-steady bed load transport by translation waves. Sau Paulo: IAHR (p.196-203).

Tacconi, P., & Billi, P. (1987). Bedload transport measurements by the vortex-tube trap on Virginio Creek, Italy. In C.R.Thorne, J.C.Bathurst, & R.D.Hey (Eds.), Gravel-bed Rivers, Chichester: John Wiley and Sons, (p. 583-616).

Tait, S. J., & Willetts, B. B. (1992). Characterisation of armoured bed surfaces. Proceedings International Grain Sorting Seminar, Mitteilungen der V.A.W. 117, (p.207-225).

Tait, S. J., Willetts, B. B., & Maizels, J. K. (1992). Laboratory observations of bed armouring and changes in bedload composition. In P. Billi, R. D. Hey, C. R. Thorne, & P. Tacconi (Eds.), Dynamics of Gravel-bed Rivers, Chichester: John Wiley and Sons Ltd (p.205-225).

Takahashi, T. (1991). Debris flow. In IAHR Monograph Fluvial Hydraulics Rotterdam, A.A.Balkema (p.121-154).

Teisseyre, J. G. (1977). Pebble clusters as a directional structure in fluvial gravels: modern and ancient examples. Geologia Sudetica, 12, (p.79-92).

Thompson, A. (1986). Secondary flows and the pool-riffle unit: a case study of the processes of meander development. Earth Surface Processes & Landforms, 11, (p.631-641).

Thorne, C.R. & Hey, R.D. Direct measurements of secondary currents at a meander inflexion point, Nature, Vol. 280, No. 5719, (p.226-228).

Turcotte, D. L. (1992). Fractals and chaos in geology and geophysics. Cambridge: Cambridge University Press.

Vaughin, D. M. (1990). Flood dynamics of a concrete-lined, urban stream in Kansas City, Missouri. Earth Surface Processes & Landforms, 15, (p.525-537).

Vanoni, V.A. (1946). Transportation of suspended sediment by water. Am. Soc. Civil. Engrs. Trans. No. II, (p.67-133).

Vincent, J. (1967). Effect of bedload movement on the roughness coefficient value. In 12th Congress of the International Association for Hydraulic Research, Fort Collins, USA: IAHR.

Wang, J., Dong, Z., Chen, C., & Xia, Z. (1993). The effects of bed roughness on the distribution of turbulent intensities in open channel flow. J. of Hydraul. Research., 31(1), (p.89-98).

Whiting, P. J., & Dietrich, W. E. (1990). Boundary shear stress and roughness over mobile alluvial beds. J. of Hydr. Eng., Am. Soc. Civil Engr., 116(12), (p.1495-1505).

Whiting, P. J., Dietrich, W. E., Leopold, L. B., Drake, T. G., & Shreve, R. L. (1988). Bedload sheets in heterogeneous sediments. Geology, 16, (p.105-108).

Whittaker, J. G. (1987). Sediment transport in step-pool streams. In C. R. Thorne, J. C. Bathurst, & R. D. Hey (Eds.), Sediment transport in gravel bed rivers, Chichester: John Wiley & Sons (p.545-579).

Whittaker, J. G., & Davies, T. R. H. (1982). Erosion and sediment transport processes in step-pool mountain torrents. In Recent Developments in the Explanation and Prediction of Erosion and Sediment Yield, 137, Exeter, England: IAHS (p.99-104).

Whittaker, J. G., & Jaeggi, M. N. R. (1982). Origin of step-pool systems in mountain streams. J. of Hydr. Div., Am. Soc. Civil Engr., 108 (HY6), (p.758-73).

Wiberg, P. L., & Smith, J. D. (1987b). Initial motion of coarse sediment in streams of high gradient. In Corvallis Symposium, 165, Corvallis: IAHS, (p.299-308).

Wiberg, P. L., & Smith, J. D. (1987). Calculations of critical shear stress for motion of uniform and heterogeneous sediments. Water Resources Research, 23(8), (p.1471-1480).

Wiberg, P. L., & Smith, J. D. (1991). Velocity distribution and bed roughness in high

gradient streams. Water Resources Research, 27(5), (p.825-838).

Willetts, B. B., & Naddeh, K. F. (1987). Measurements of lift on spheres fixed in low Reynolds number flows. J. of Hydraulic Research, 24(5), (p.425-435).

Willetts, B. B., & Rice, M. A. (1986). Collision in aeolian transport: the saltation/creep link. In W. G. Nickling (Ed.), Aeolian Geomorphology - Annual Binghampton Geomorphology Symposium, 17, Allen & Unwin, (p.1-17).

Williams, G. P. (1983). Paleohydrological methods and some examples from Swedish fluvial environments - cobble and boulder deposits. Geografiska Annaler, 54A, (p.227-243).

Williams, J. J., Thorne, P. D., & Heathershaw, A. D. (1989). Comparisons between acoustic measurements and predictions of the bedload transport of marine gravels. Sedimentology, 33, (p.973-979).

Wolcott, J., & Church, M. (1991). Strategies for sampling spatially heterogeneous phenomena: the examples of river gravels. Journal of Sedimentary Petrology, 61(4), (p.534-543).

Wolman, M. G. (1954). A method for sampling coarse river-bed material. Trans. American Geophysical Union, 35(6-1), (p.951-956).

Yalin, M. S. (1992). River mechanics. Oxford, New York, Seoul, Tokyo: Pergamon Press (pp.220).

Yang, C. T. (1971). Formation of riffles and pools. Water Resources Research, 7, (p.1567-1574).

Yen, C.-L., & Yen, B. C. (1971). Water Surface Configuration in Channel Bends. J. Hyd. Div. Am. Soc. Civ. Eng., 97, (p.303-321).

Zanke, U. (1982). Grundlagen der Sediment Bewegung. Berlin: Springer.

Zgheib, P. W. (1990). Large bed element channels in steep mountain streams. In Sinniger,O. and Monbaron, M. (Ed.) Hydrology in Mountain Regions - Vol. II Artificical reservoirs, Water and Slopes, Spec. Publ. 194, (p.277-283). Lausanne: IAHS.

# APPENDICES A1-A4

**Appendix A1 Squaw Creek, 23-24th May 1991. River bed and water level adjustment.**

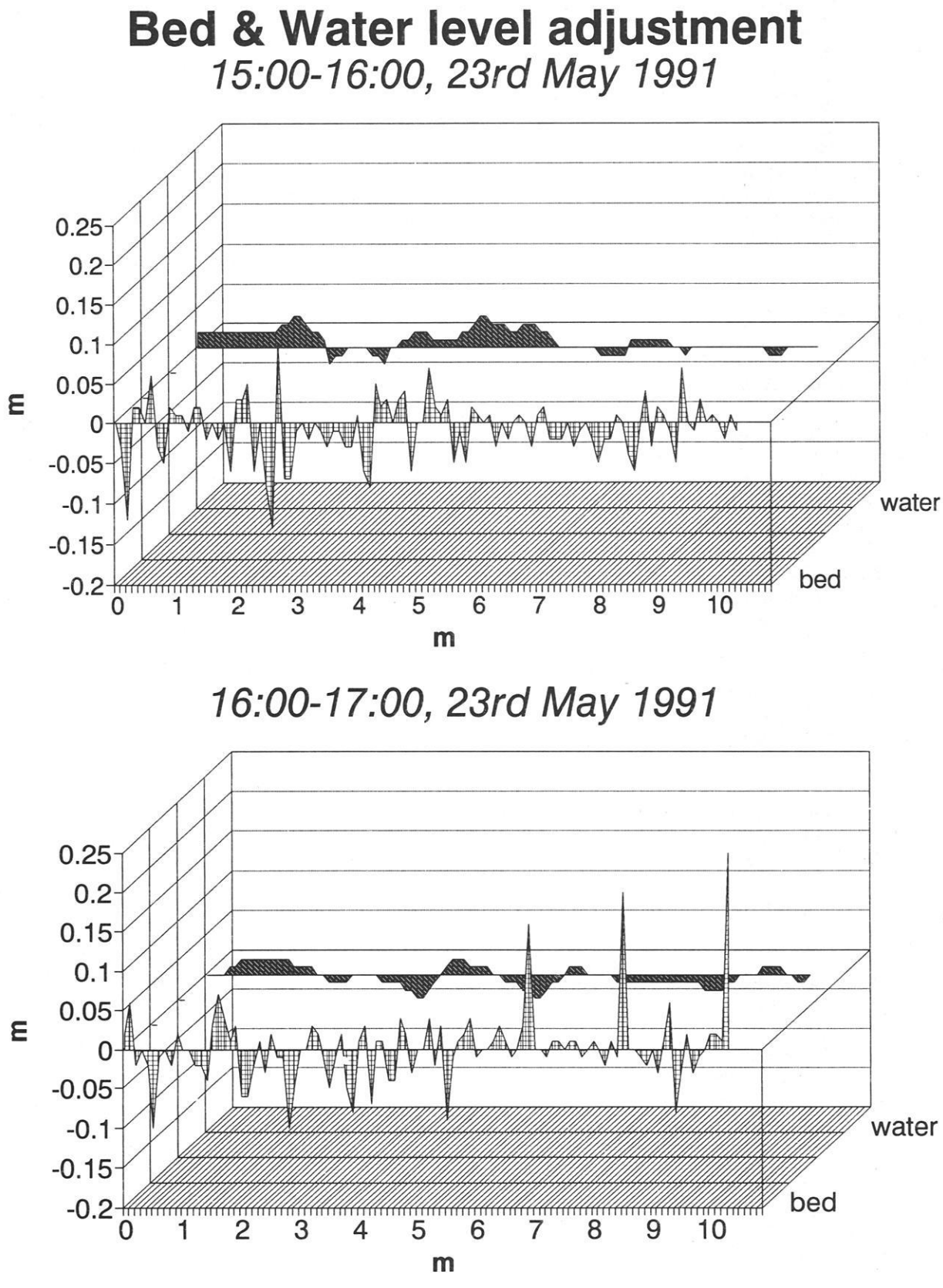

# Bed and water level adjustment

*17:00-18:00, 23rd May 1991*

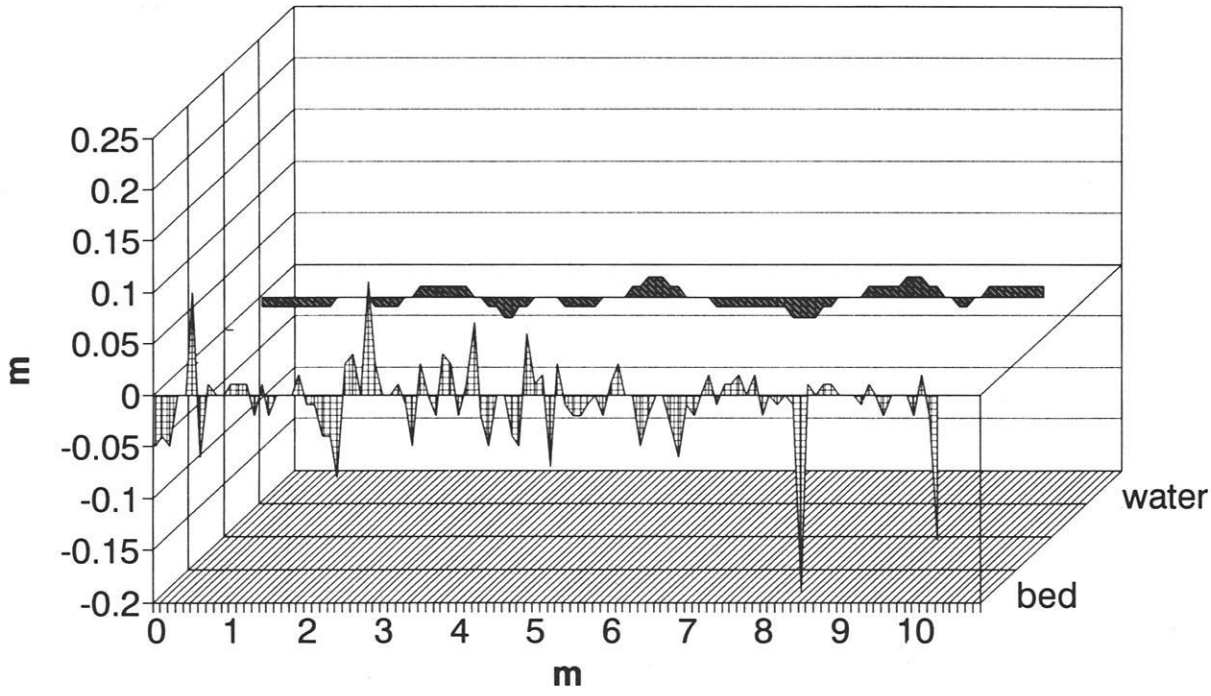


# Bed and water level adjustment

*18:00-19:00, 23rd May 1991*

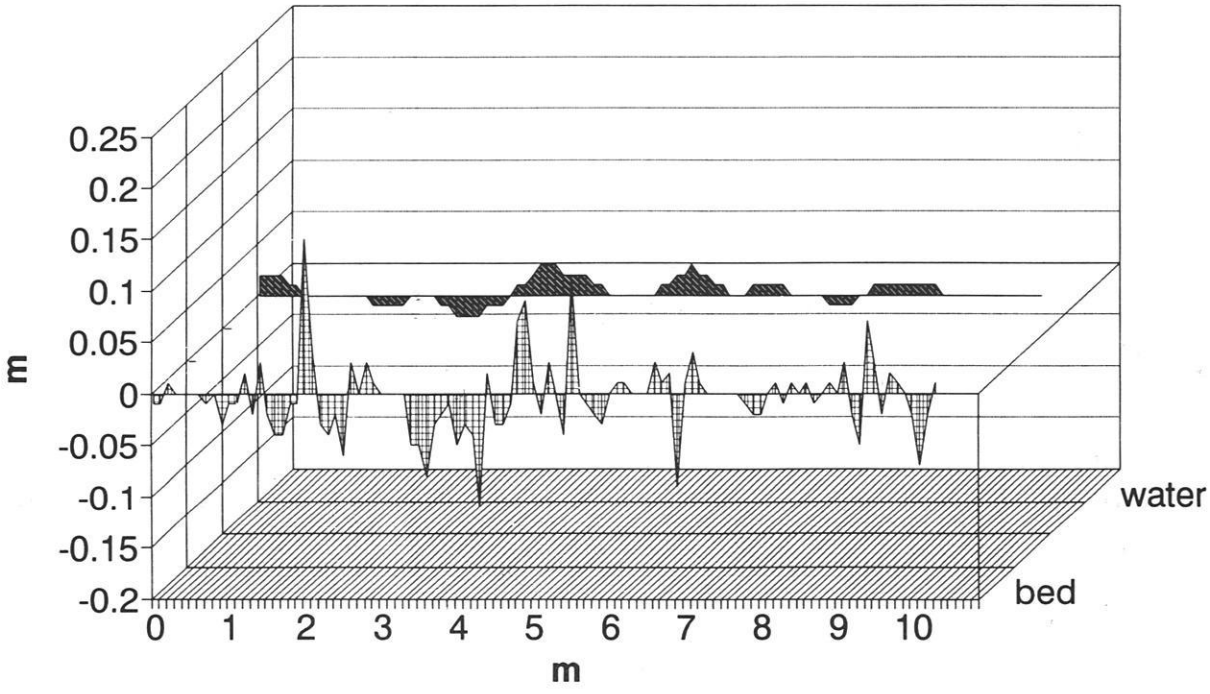

# Bed and water level adjustment

*19:00-20:00, 23rd May 1991*

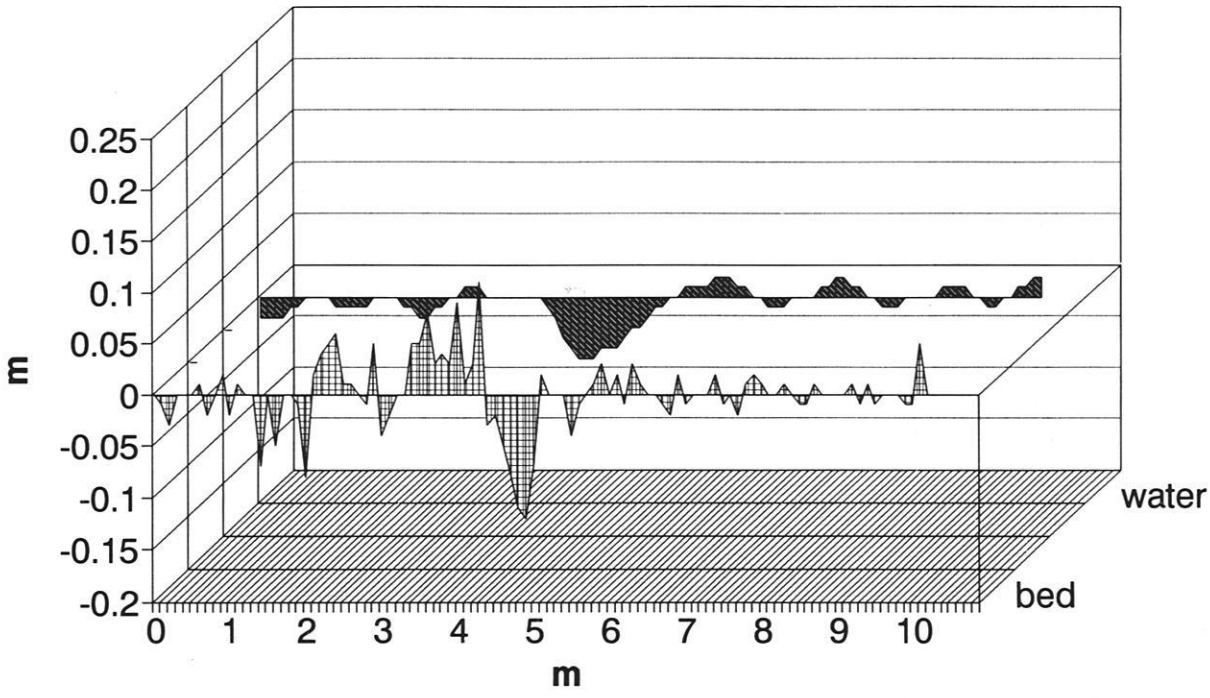


# Bed and water level adjustment

*20:00-21:00, 23rd May 1991*

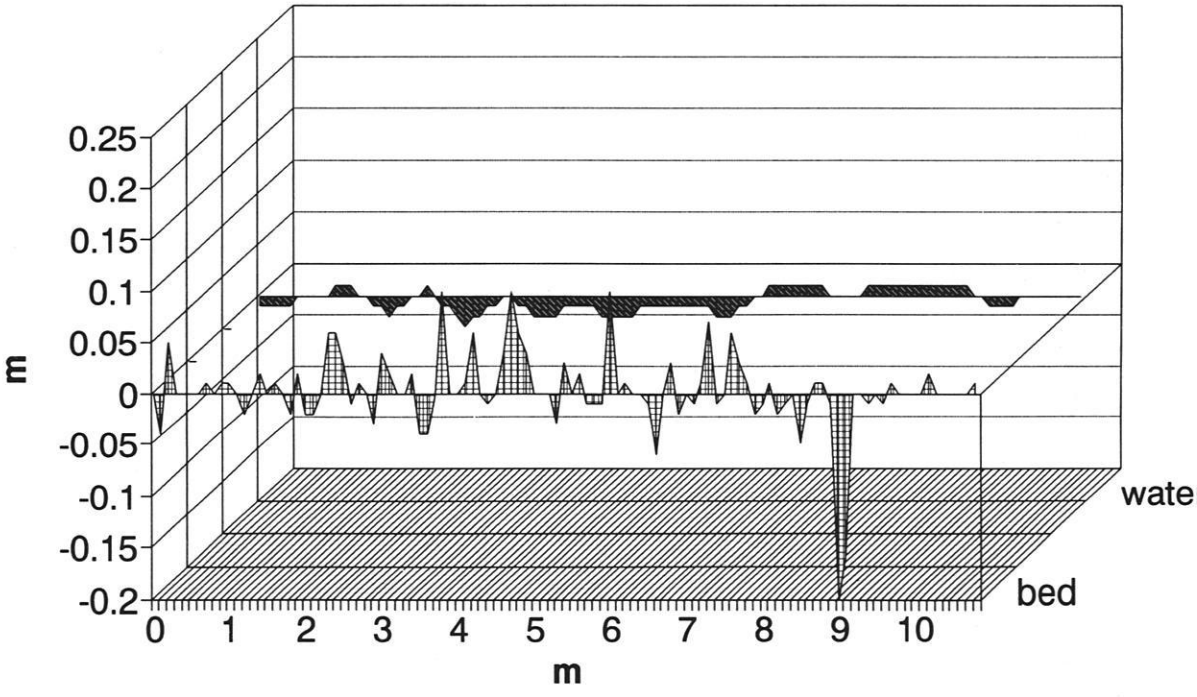

# Bed and water level adjustment

*21:00-22:00, 23rd May 1991*

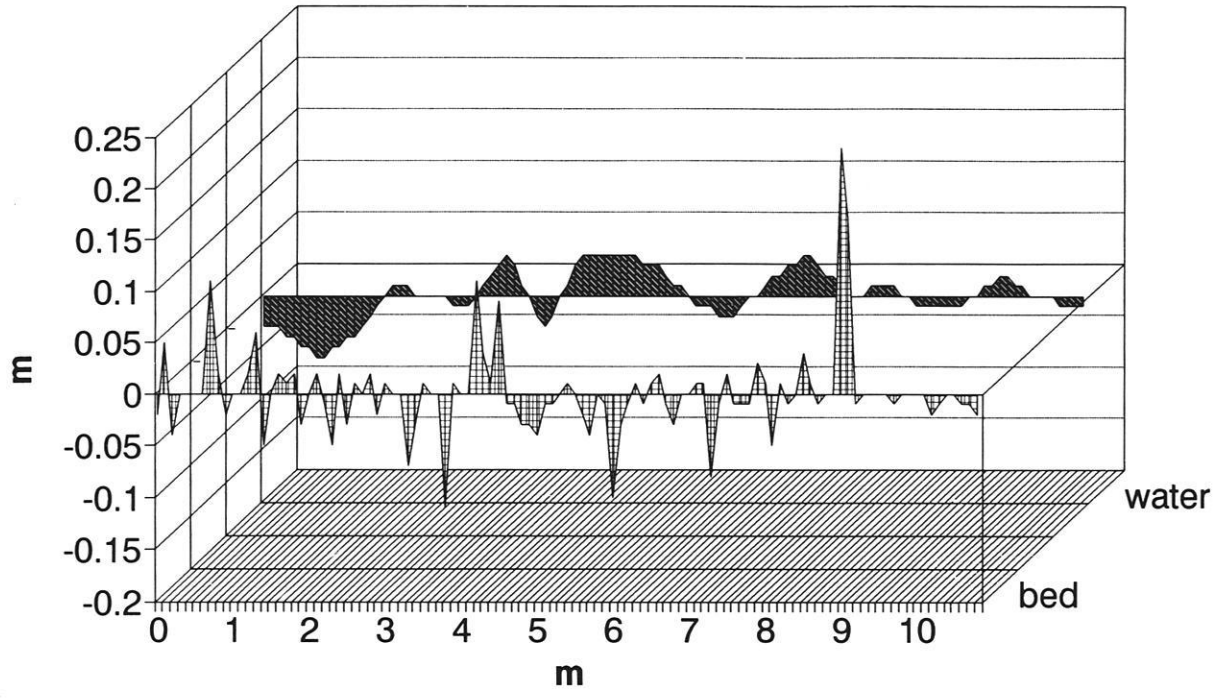


# Bed and water level adjustment

*22:00-23:00, 23rd May 1991*

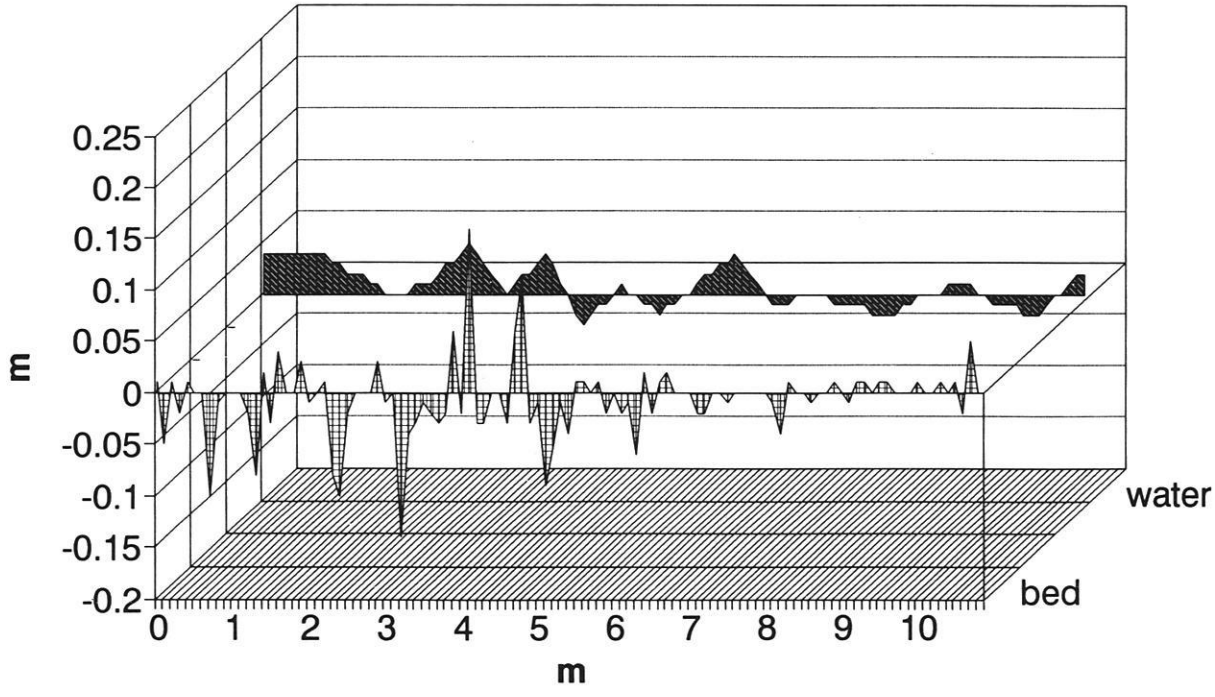

# Bed and water level adjustment

*23:00-24:00, 23rd May 1991*

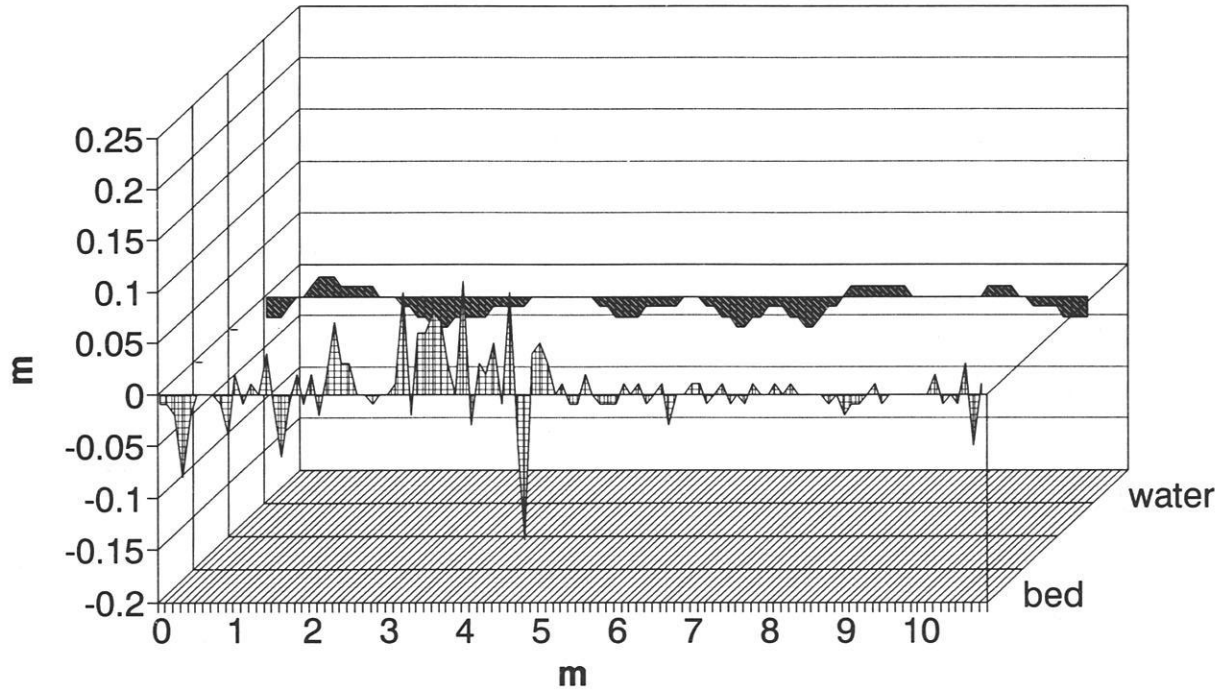


# Bed and water level adjustment

*24:00-02:00, 23rd May 1991*

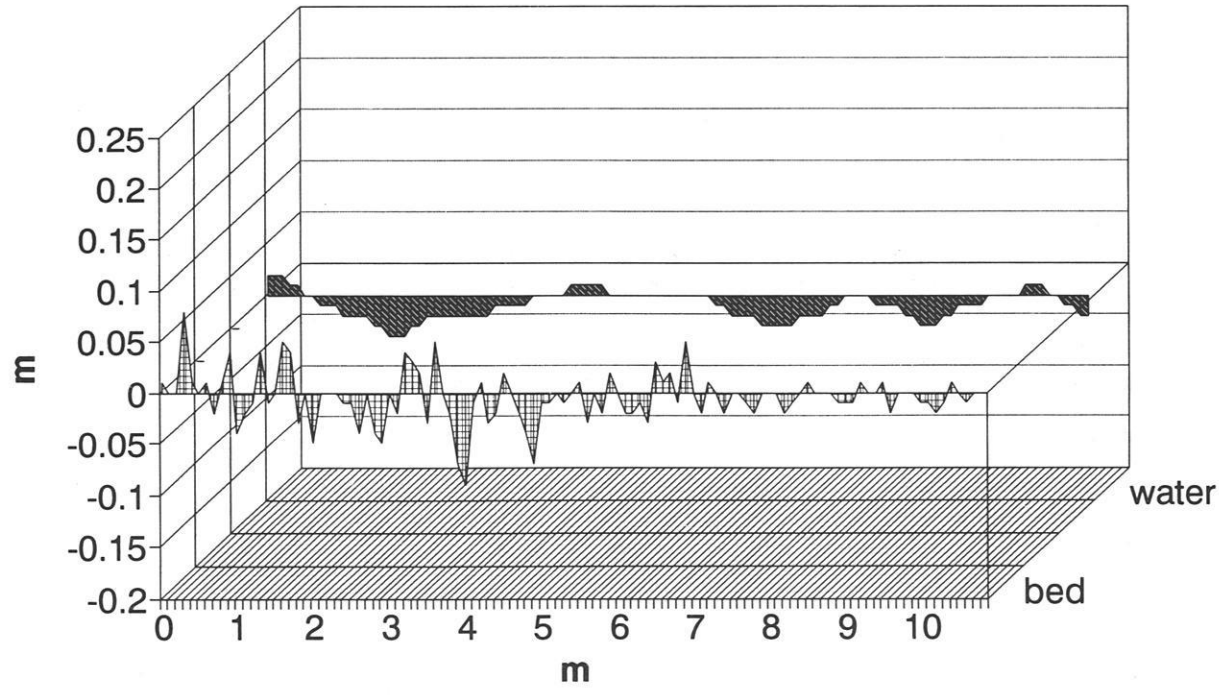

# Bed and water level adjustment

*02:00-04:00, 24th May 1991*

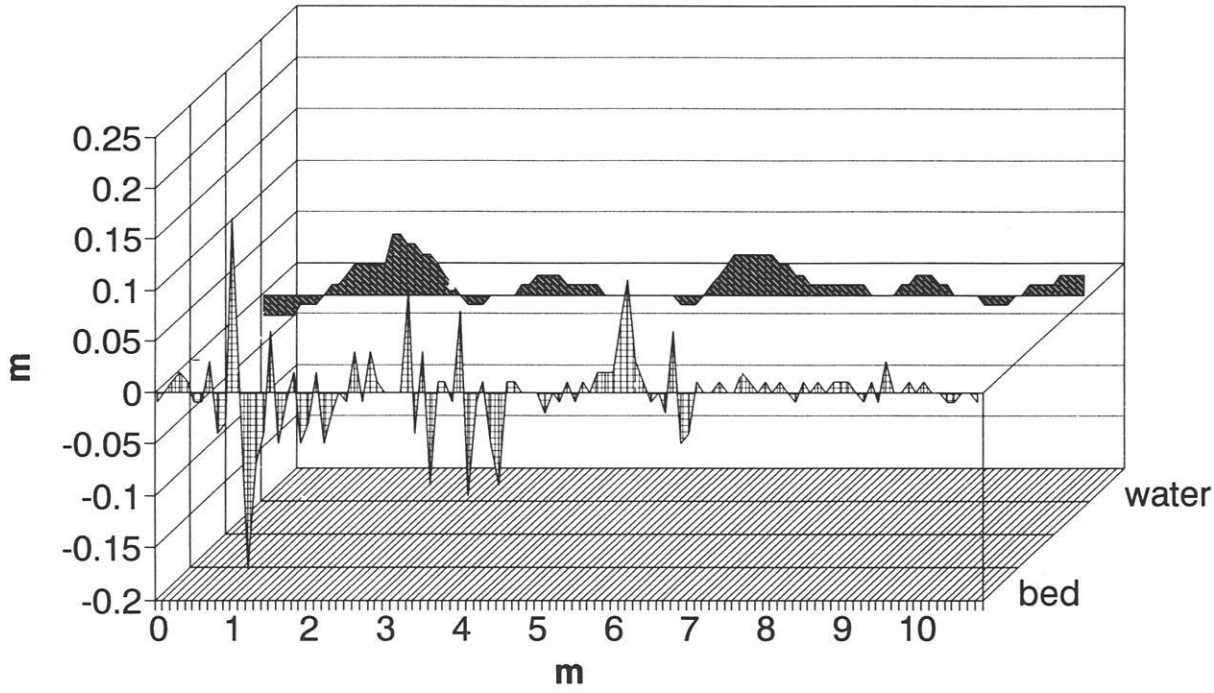


# Bed and water level adjustment

*04:00-06:00, 24th May 1991*

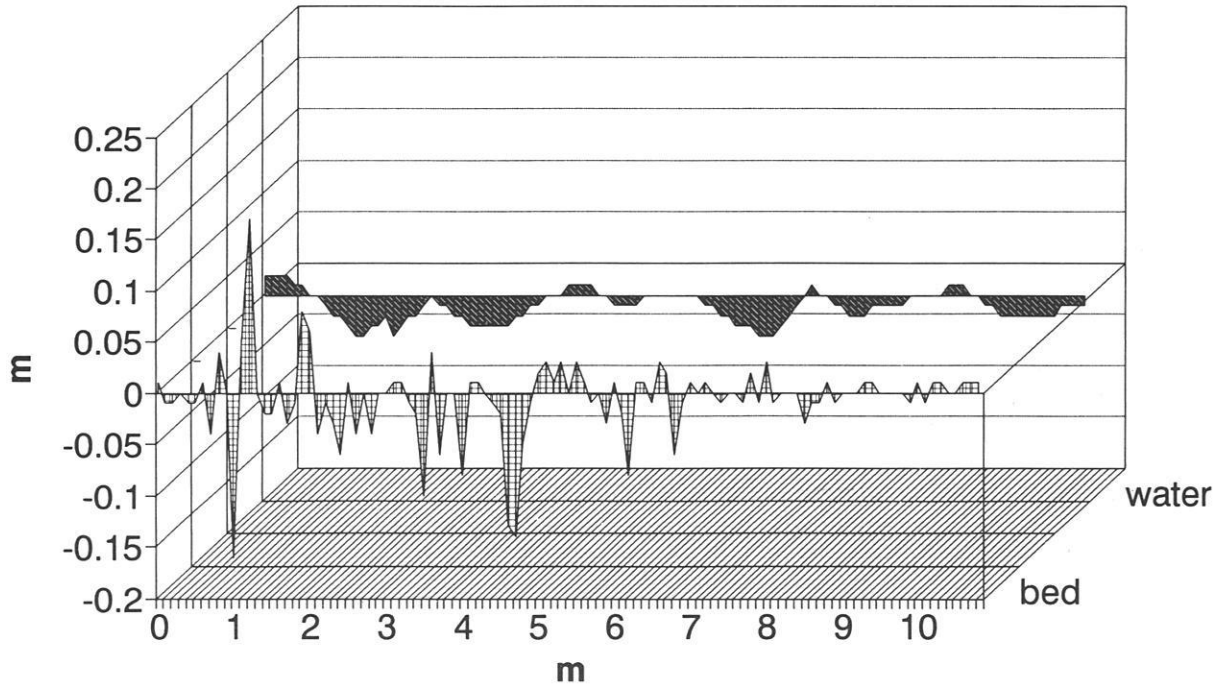

# Bed and water level adjustment

*06:00-09:00, 24th May 1991*

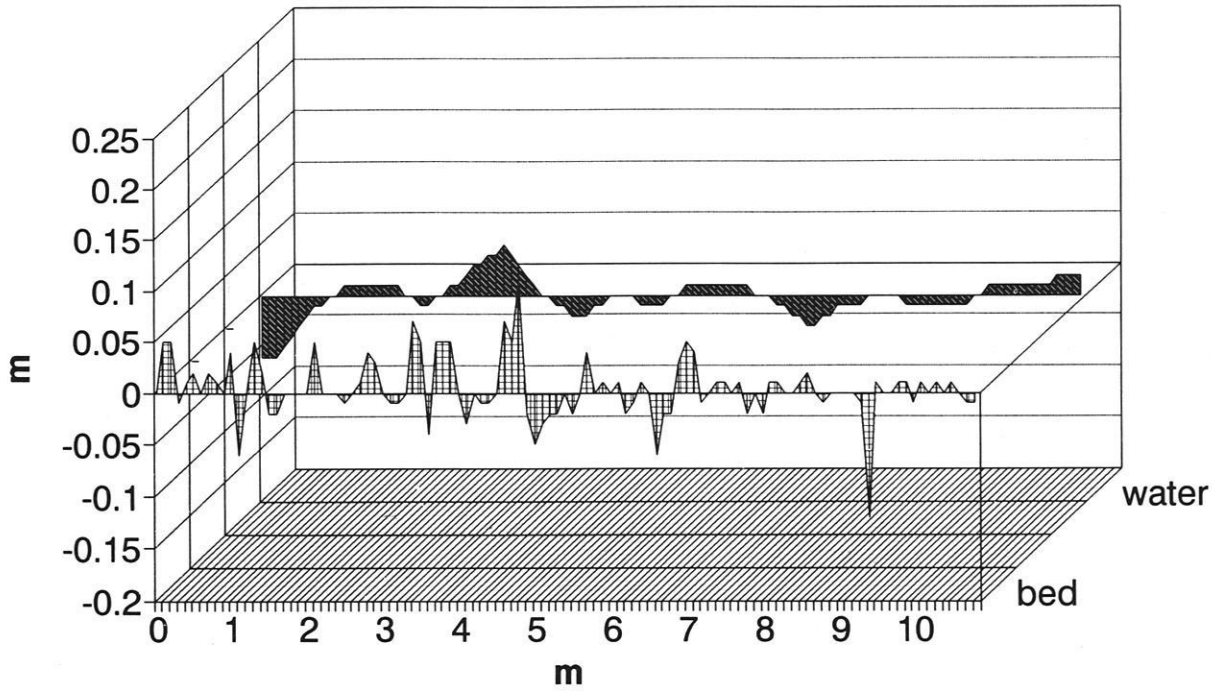


# Bed and water level adjustment

*09:00-12:00, 24th May 1991*

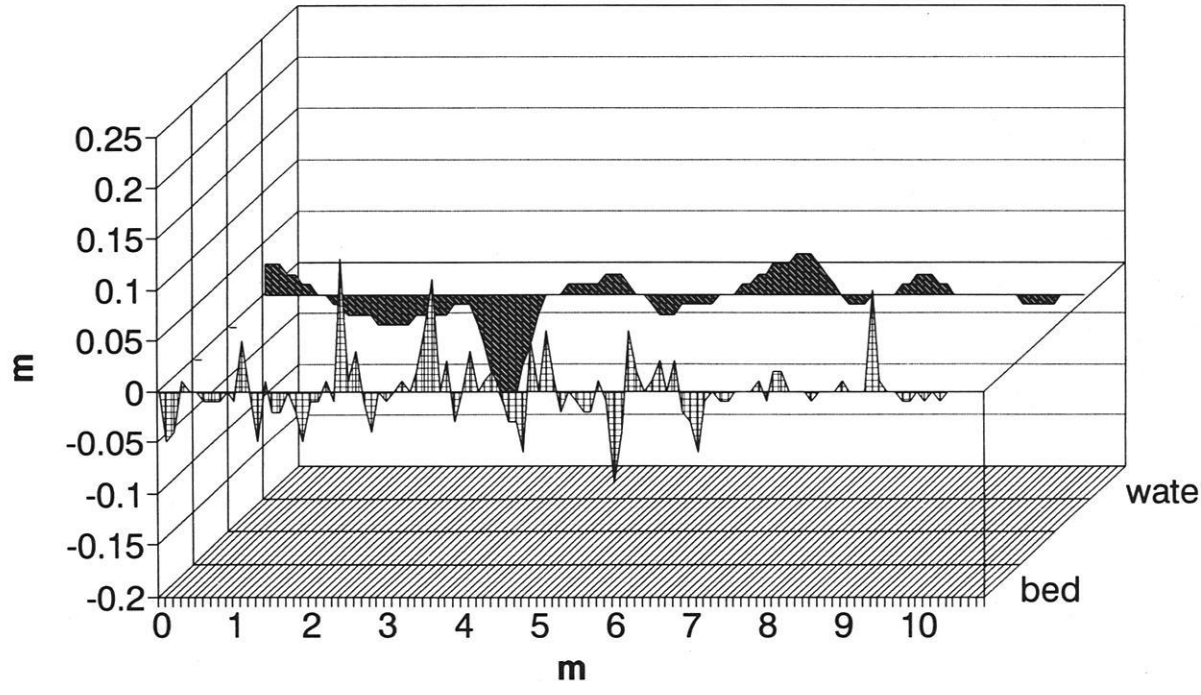

# Bed and water level adjustment

*12:00-15:00, 24th May 1991*

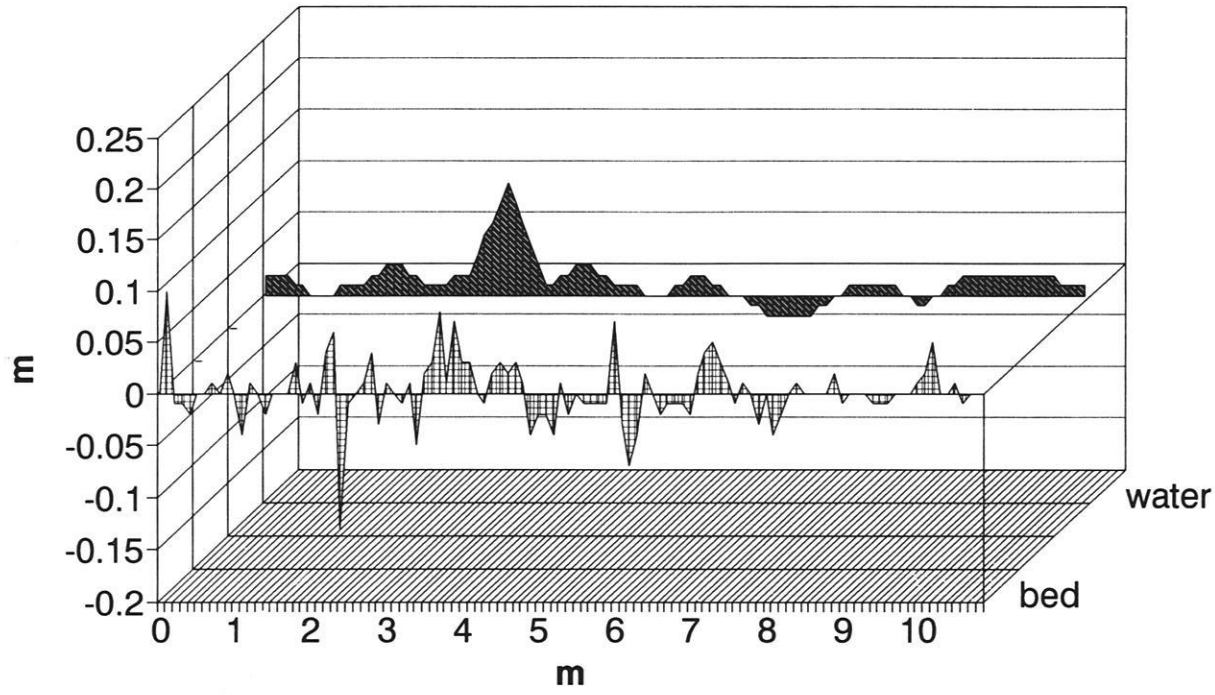

**Appendix A2** **Squaw Creek, 5-6th June 1991. River bed and water level adjustment against bedload input & output**

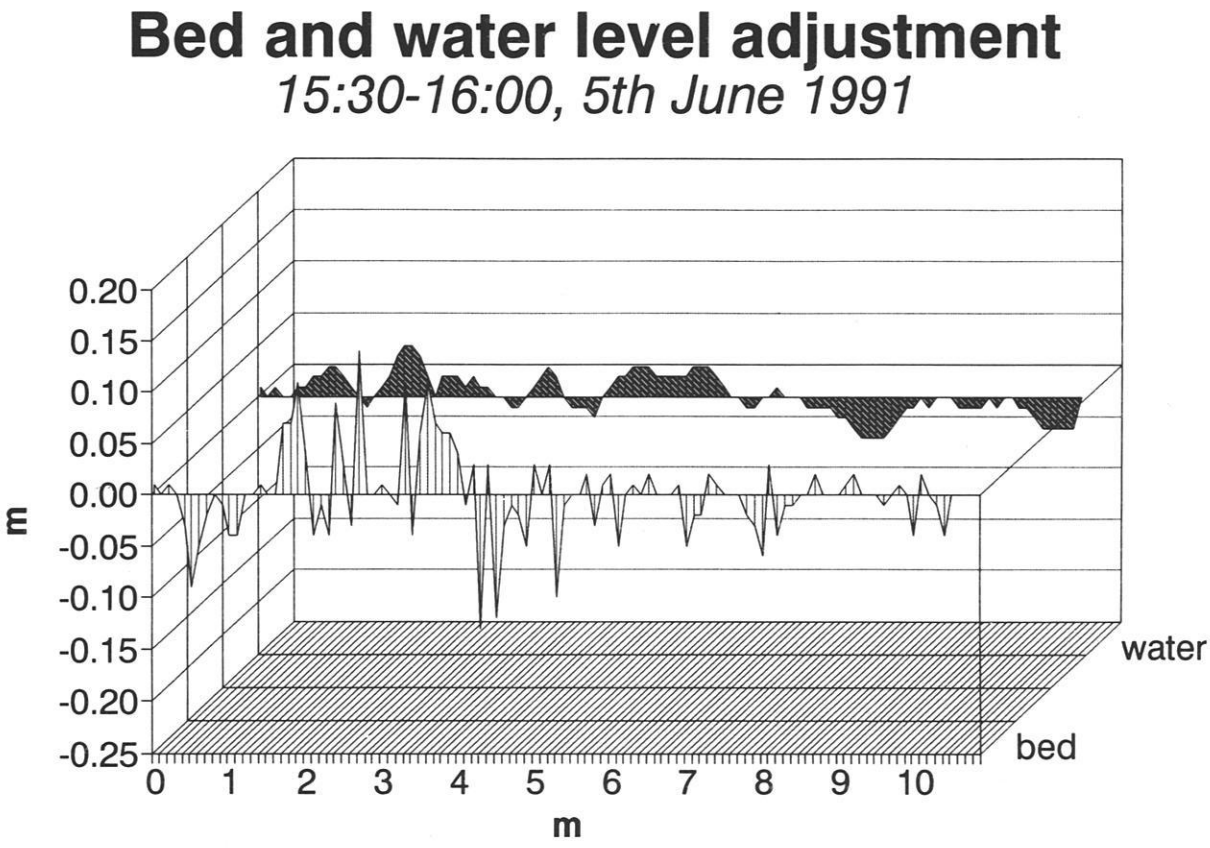


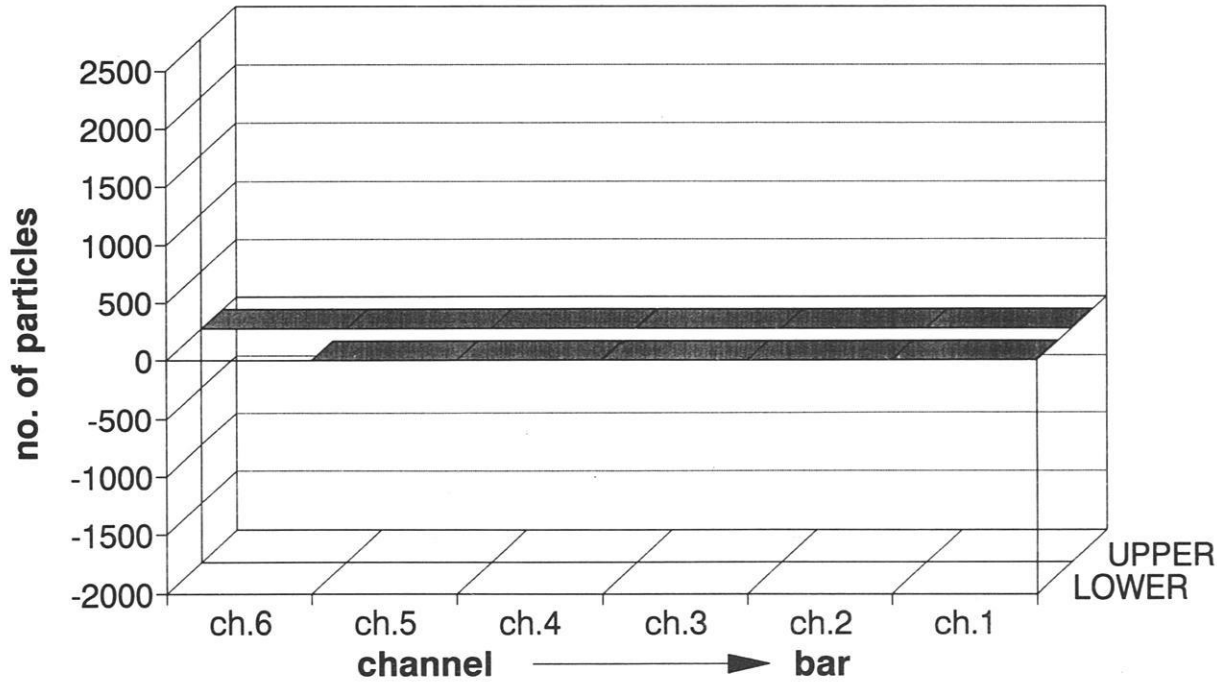

# Bed and water level adjustment

*16:00-16:30, 5th June 1991*

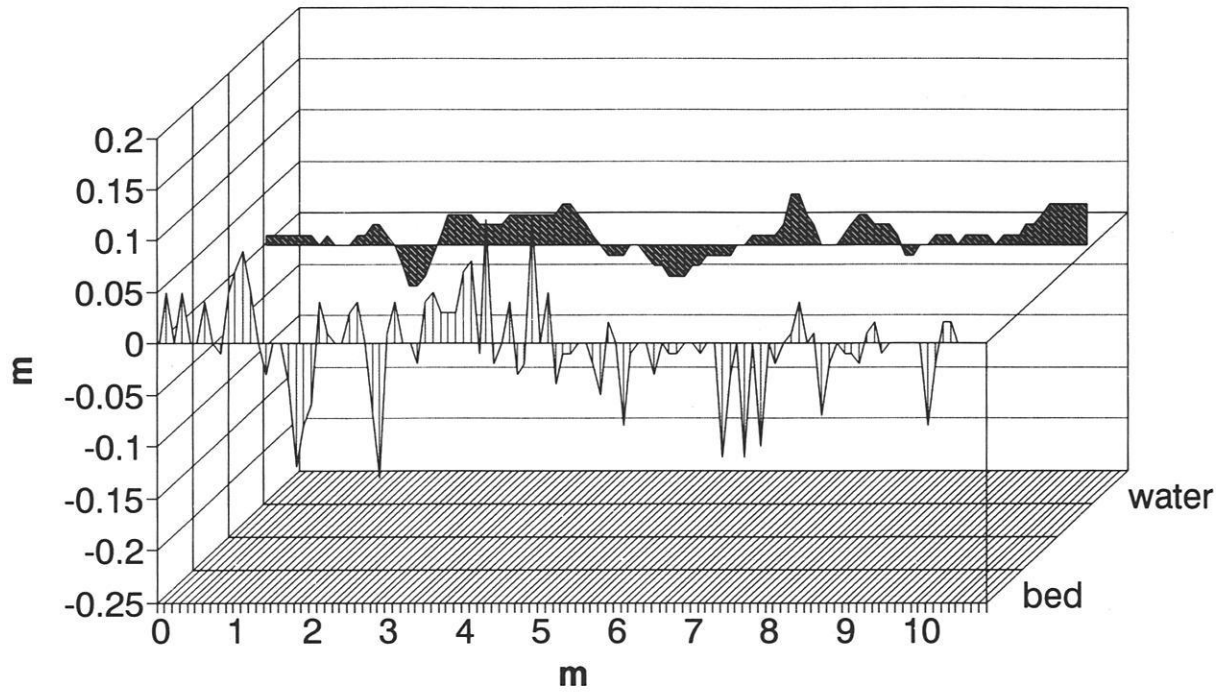


# Squaw Creek, 5th June 1991

*input/output 16:00-16:45*

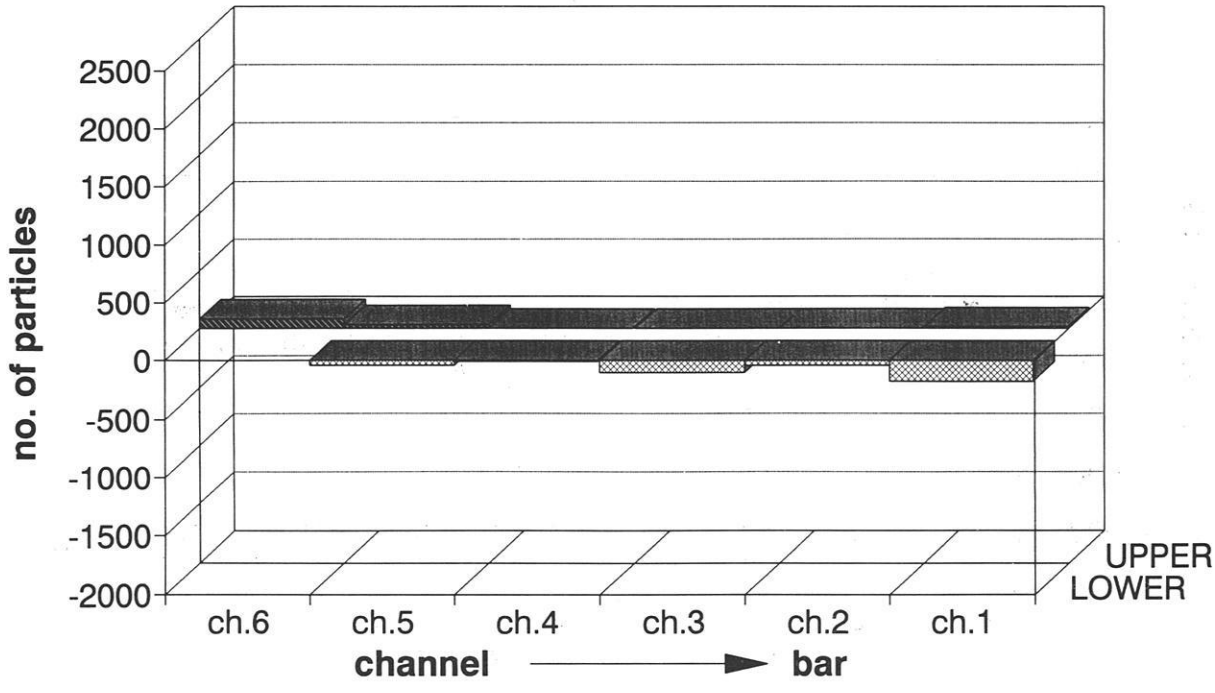

# Bed and water level adjustment

*16:30-17:25, 5th June 1991*

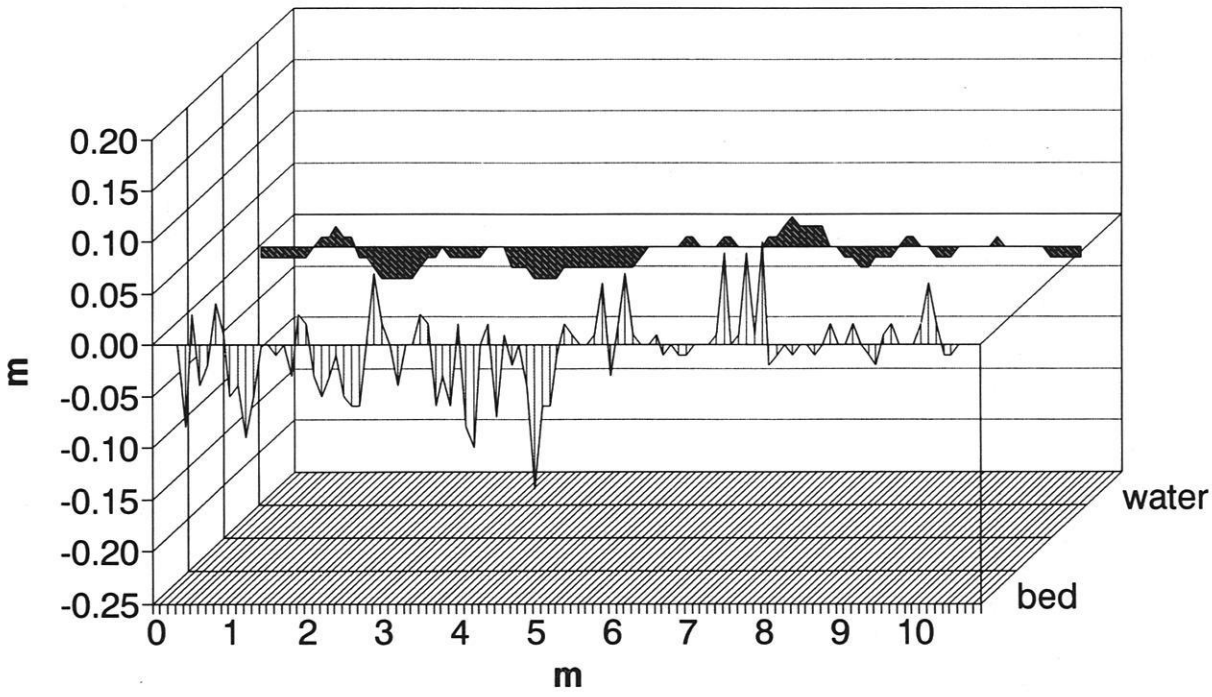


# Squaw Creek, 5th June 1991

*input/output 16:45-17:25*

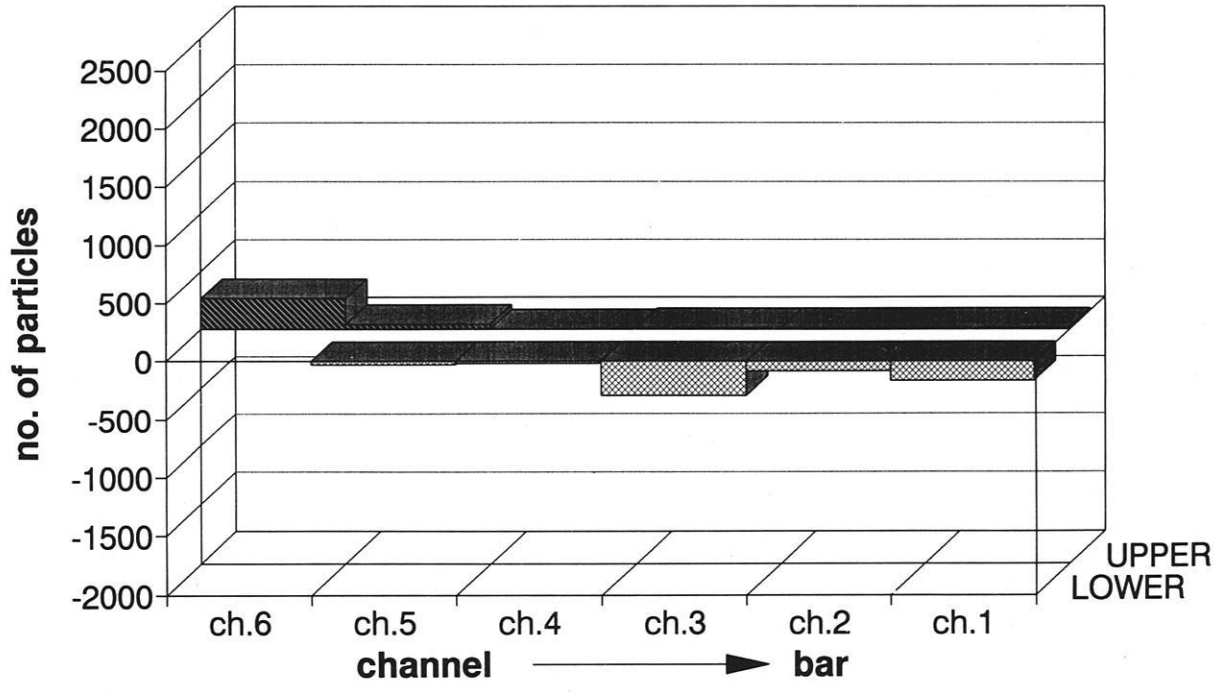

# Bed and water level adjustment

*17:25-18:30, 5th June 1991*

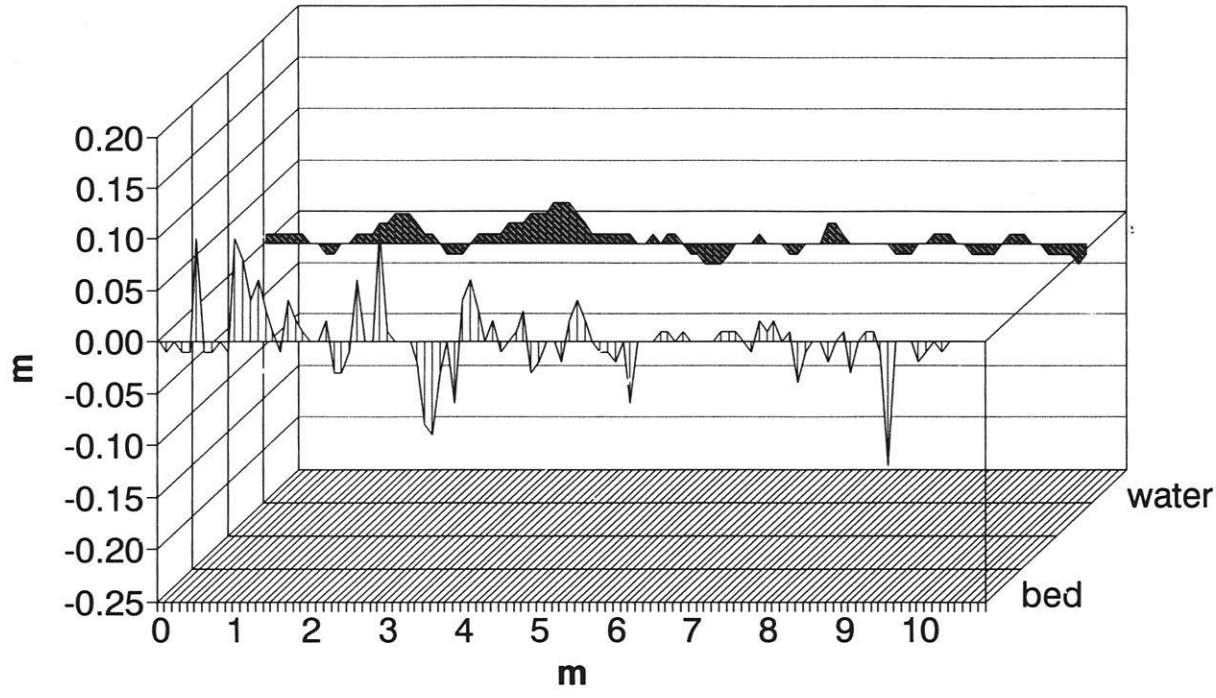


# Squaw Creek, 5th June 1991

*input/output 17:25-18:30*

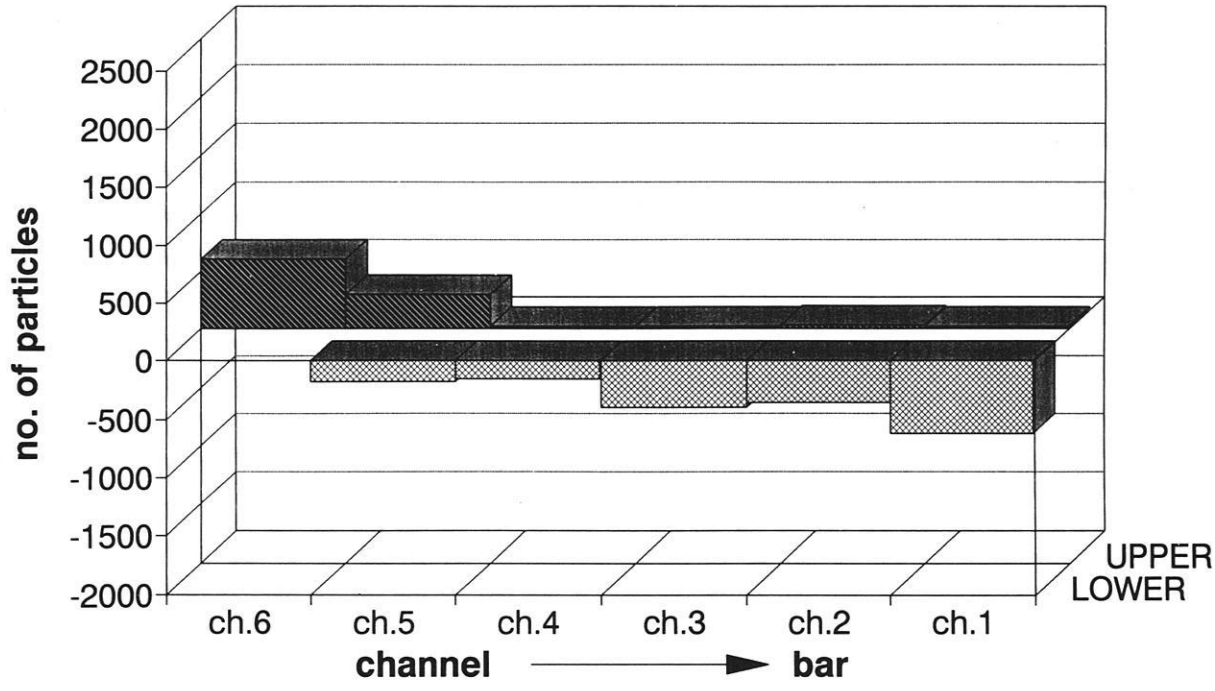

# Bed and water level adjustment

*18:30-19:30, 5th June 1991*

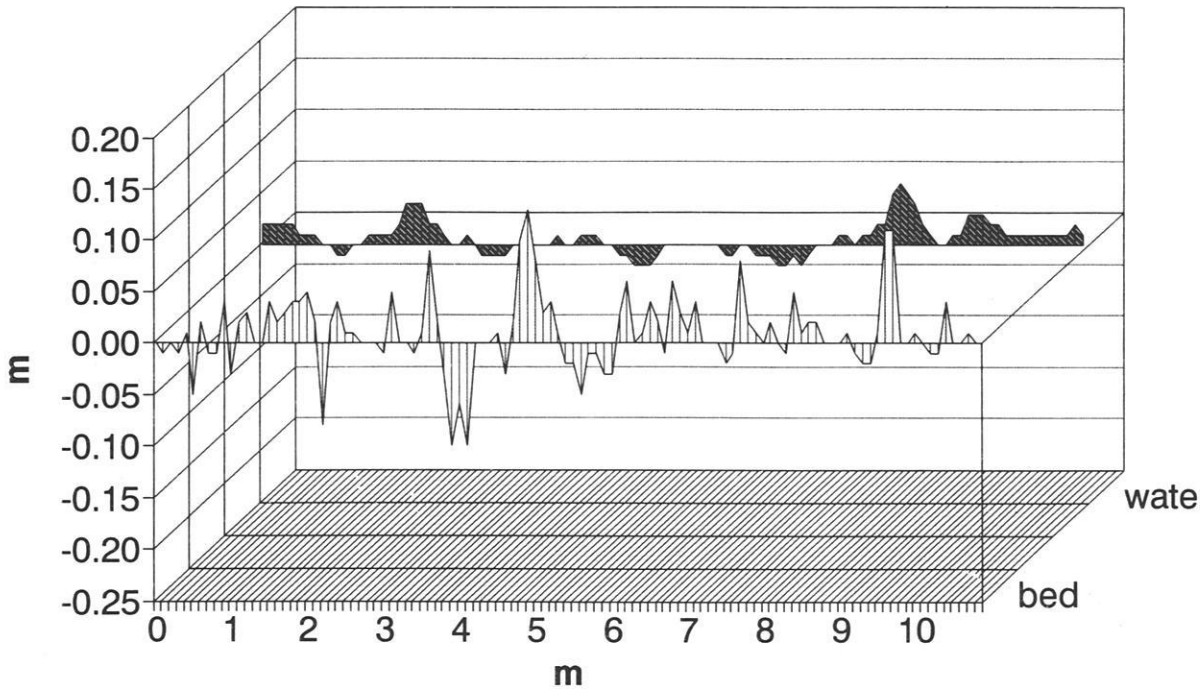


# Squaw Creek, 5th June 1991

*input/output 18:30-19:30*

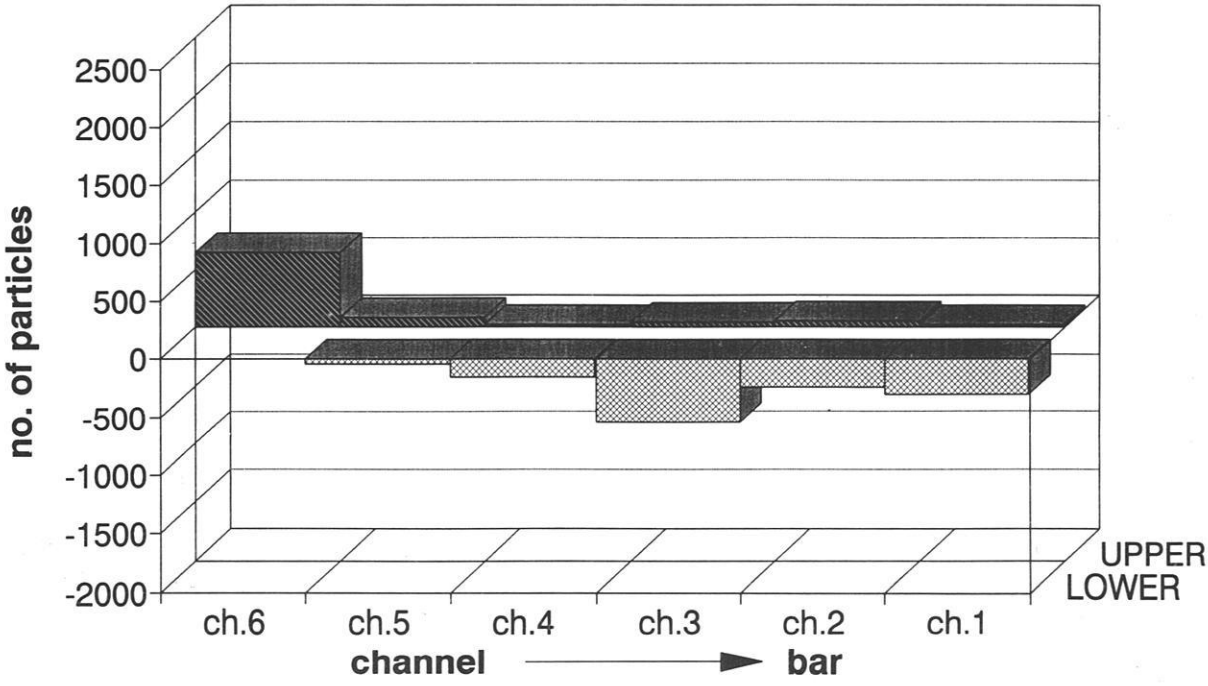

# Bed and water level adjustment

*19:30-20:30, 5th June 1991*

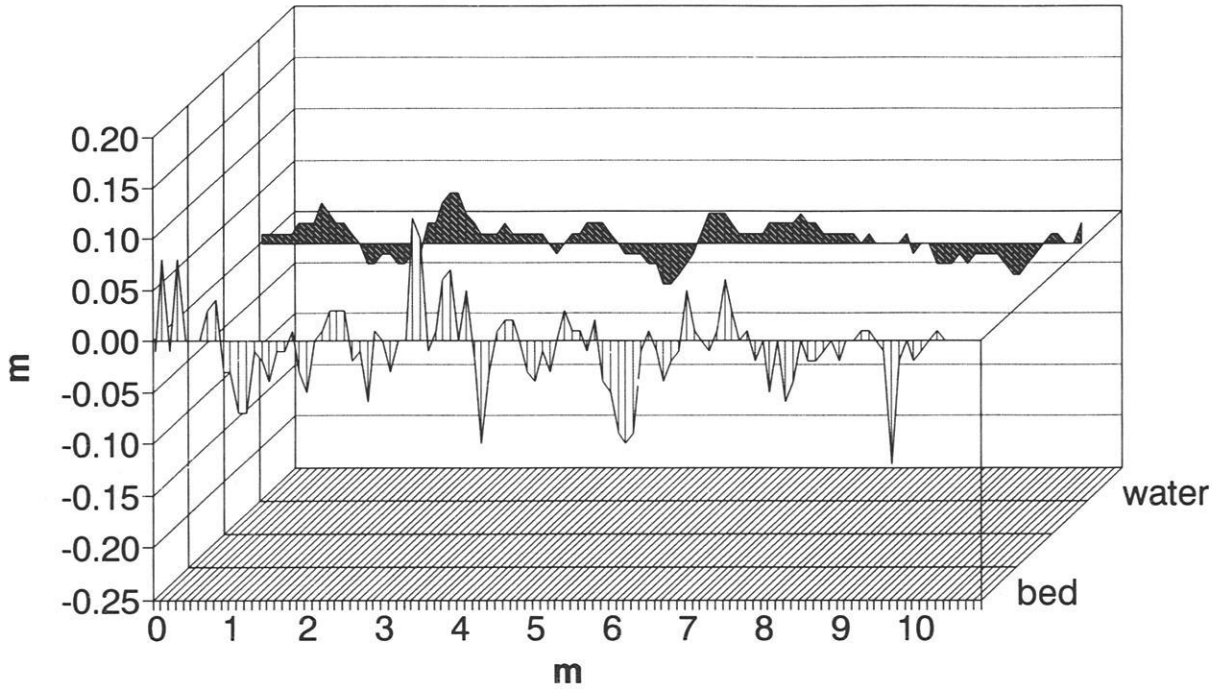


# Squaw Creek, 5th June 1991

*input/output 19:30-20:30*

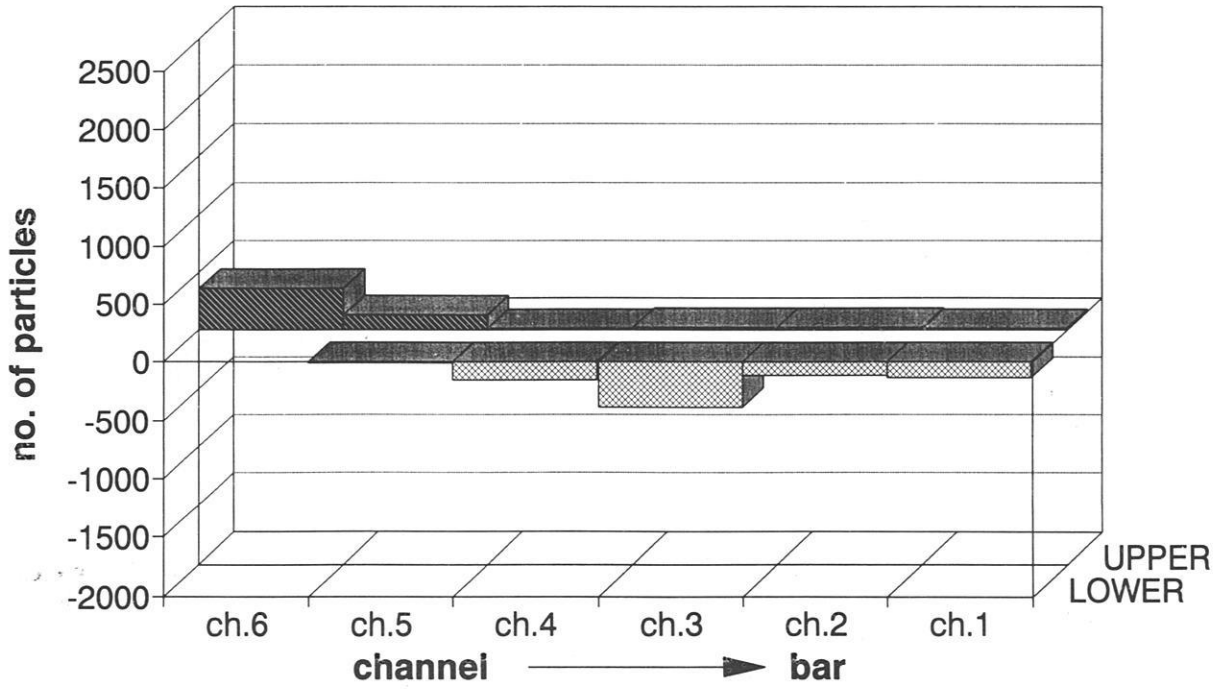

# Bed and water level adjustment

*20:30-21:30, 5th June 1991*

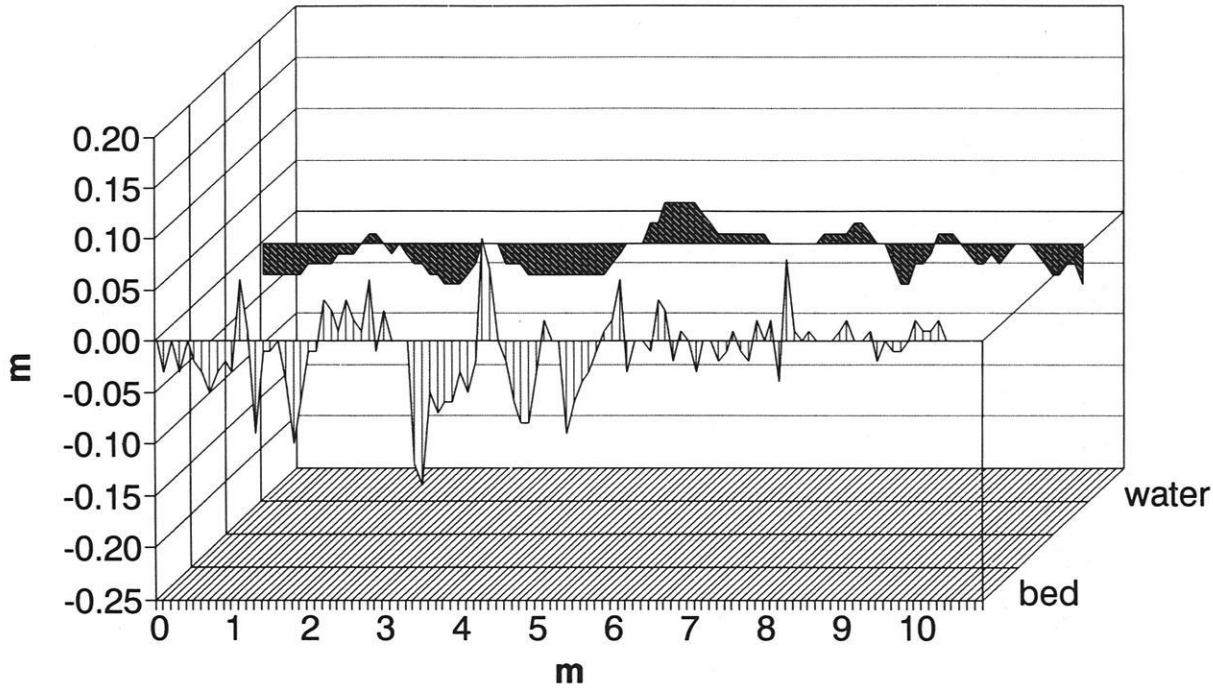


# Squaw Creek, 5th June 1991

*input/output 20:30-21:30*

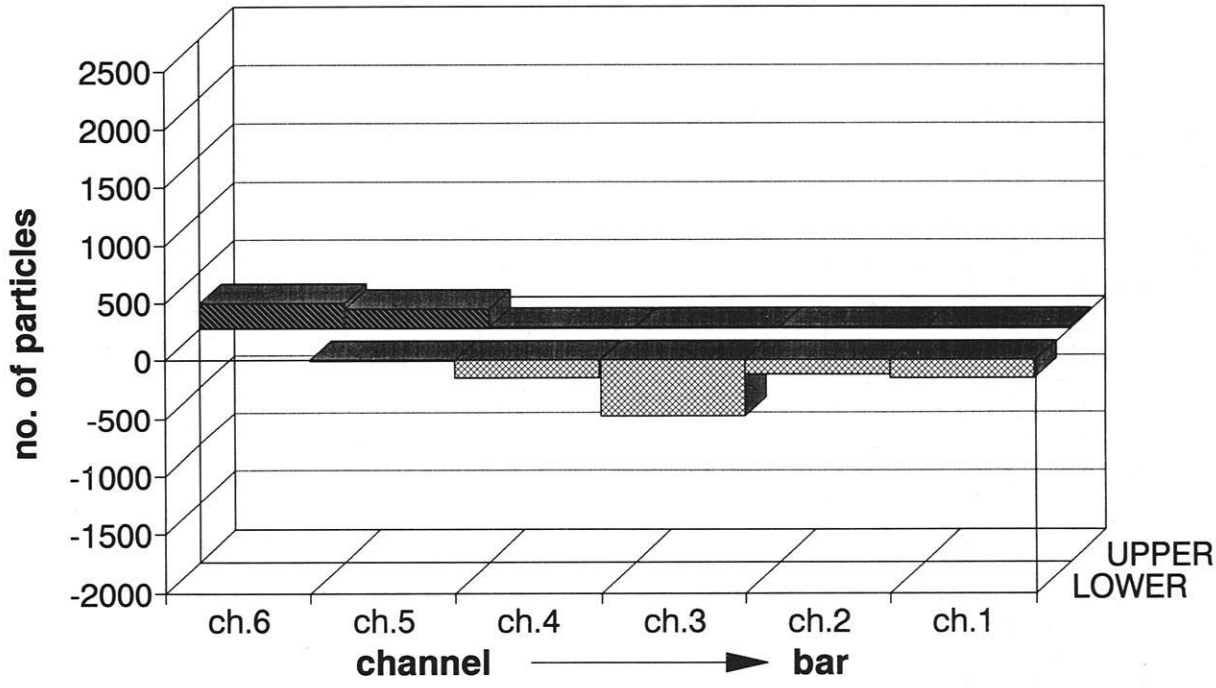

# Bed and water level adjustment

*21:30-22:30, 5th June 1991*

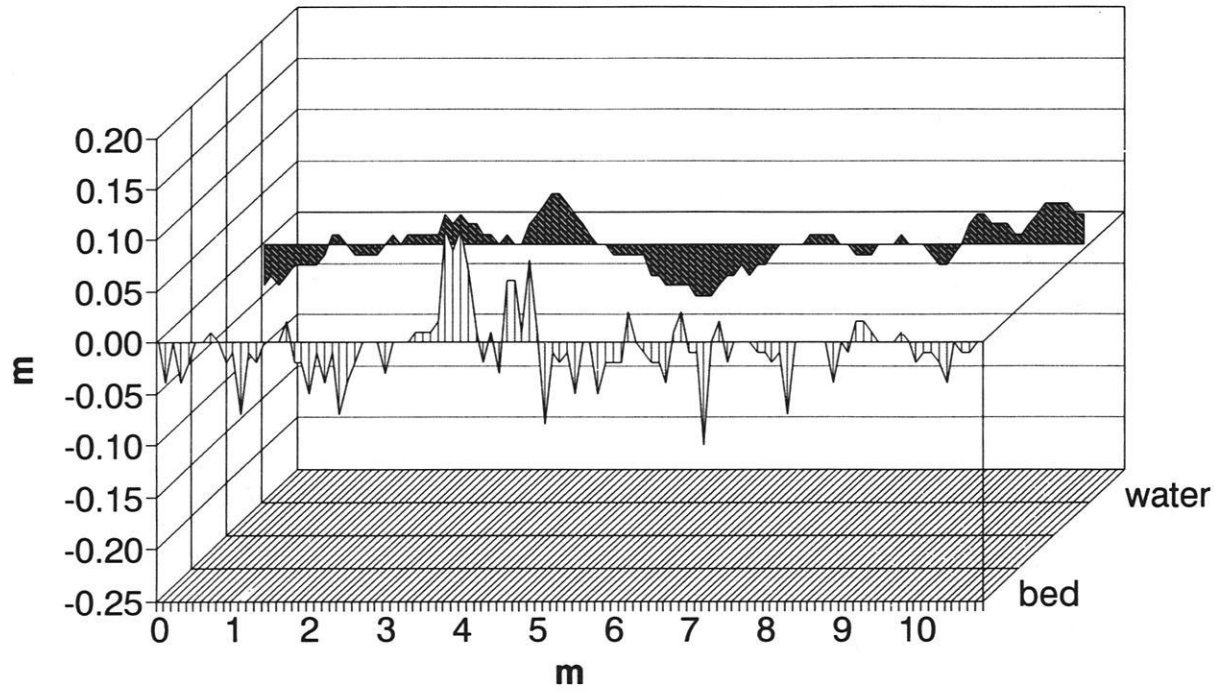


# Squaw Creek, 5th June 1991

*input/output 21:30-22:30*

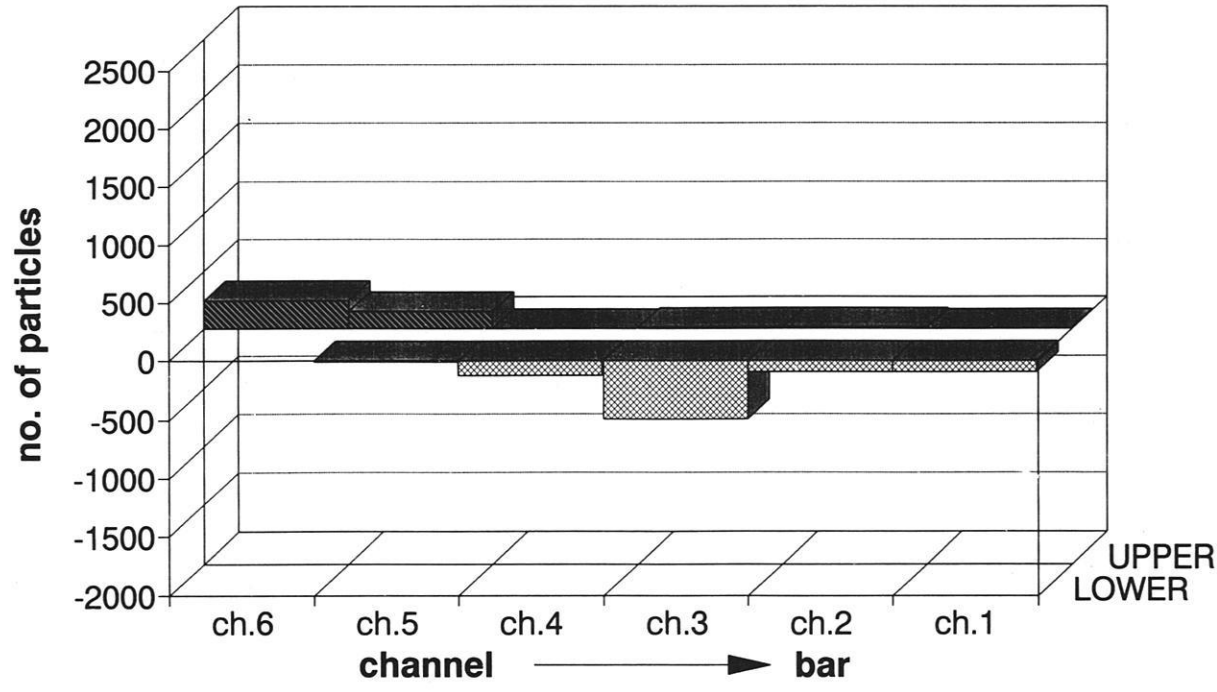

# Bed and water level adjustment

*22:30-23:30, 5th June 1991*

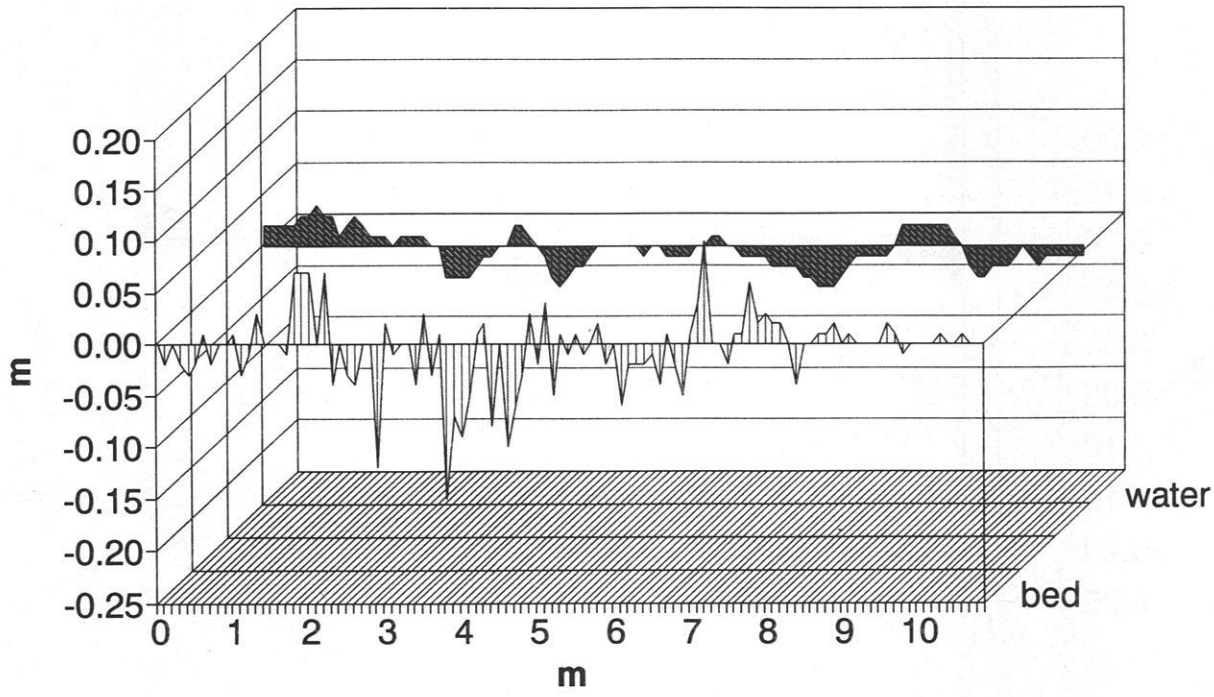


# Squaw Creek, 5th June 1991

*input/output 22:30-23:30*

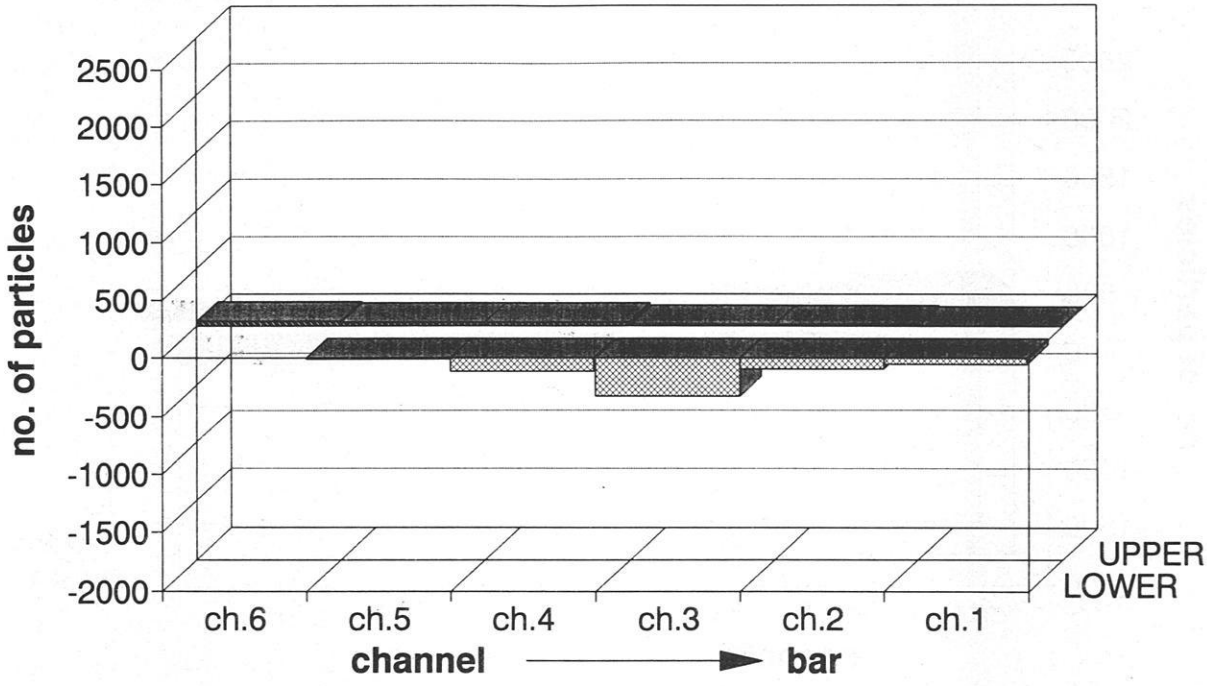

# Bed and water level adjustment

*23:30-00:30, 5th June 1991*

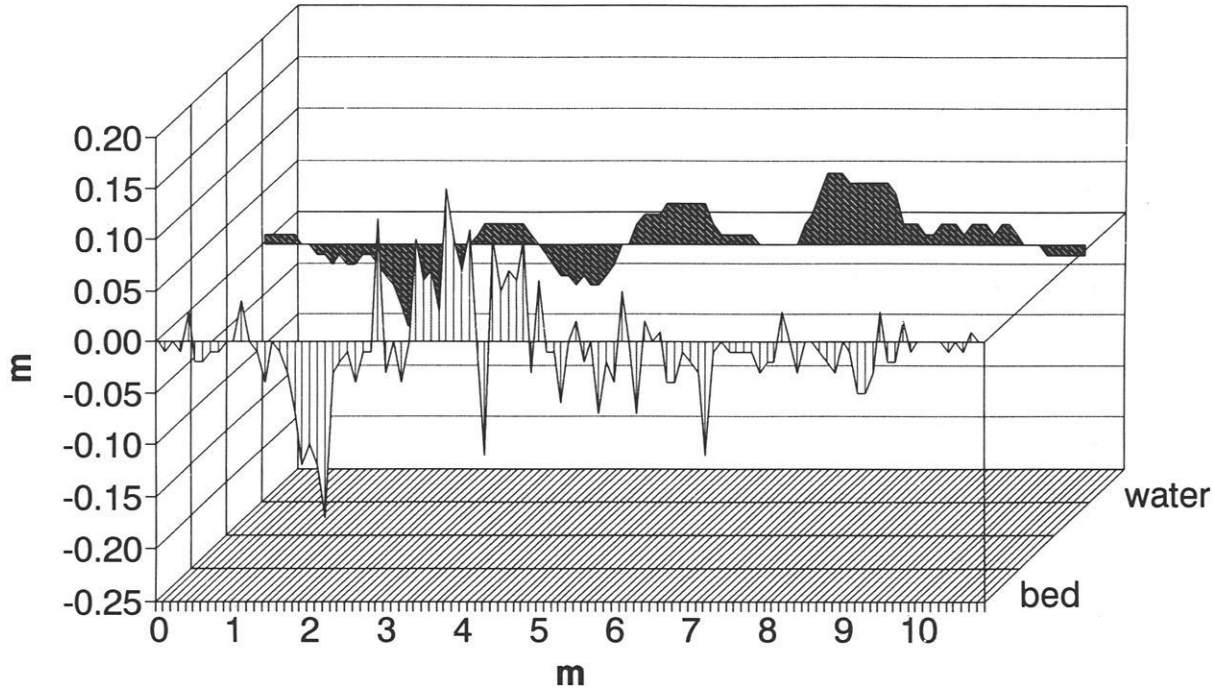


# Squaw Creek, 5th June 1991

*input/output 23:30-00:30*

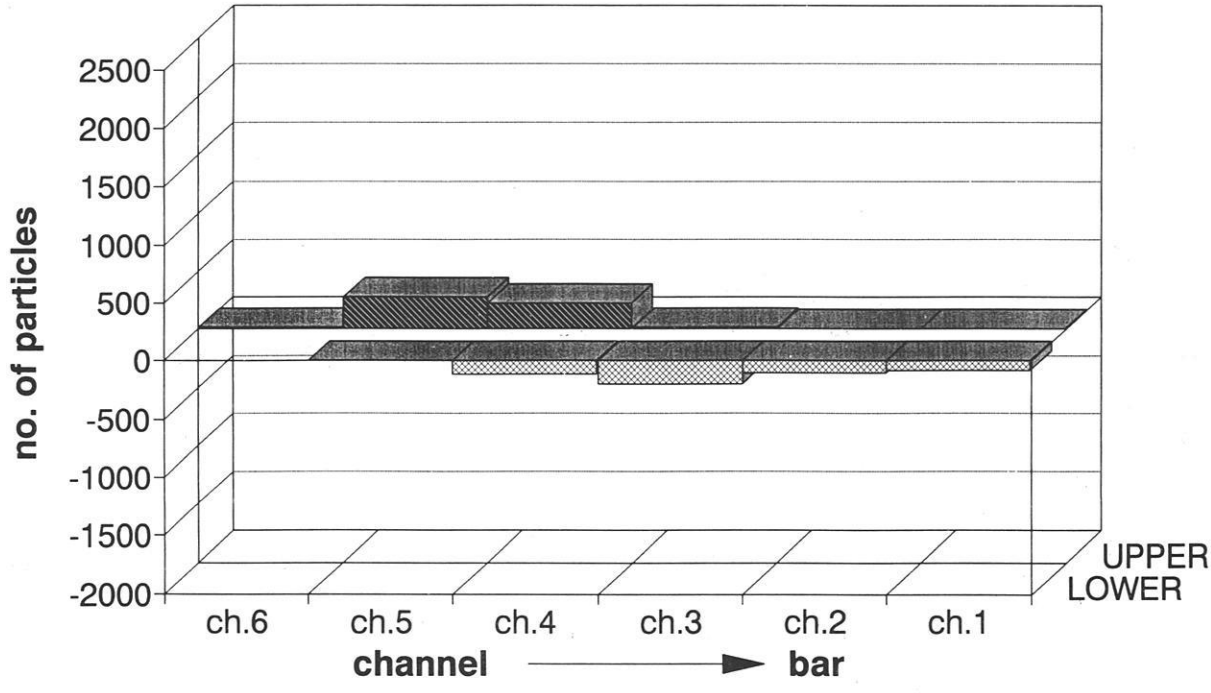

# Bed and water level adjustment

*00:30-01:30, 6th June 1991*

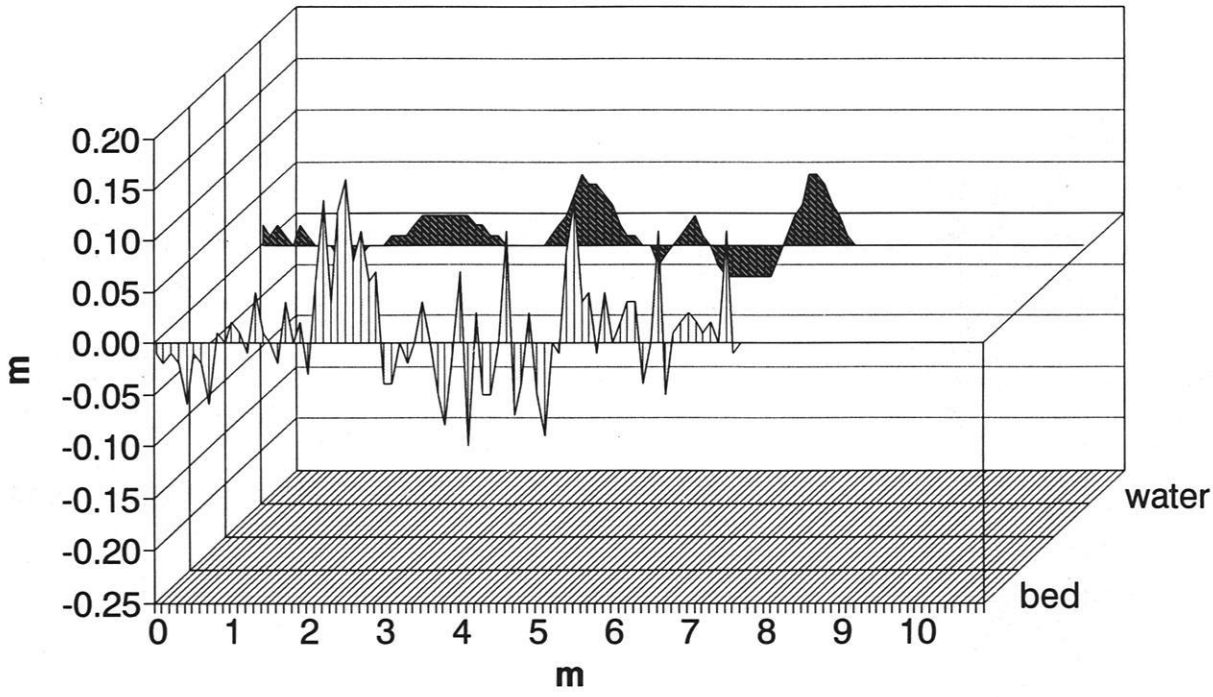


# Squaw Creek, 6th June 1991

*input/output 00:30-01:30*

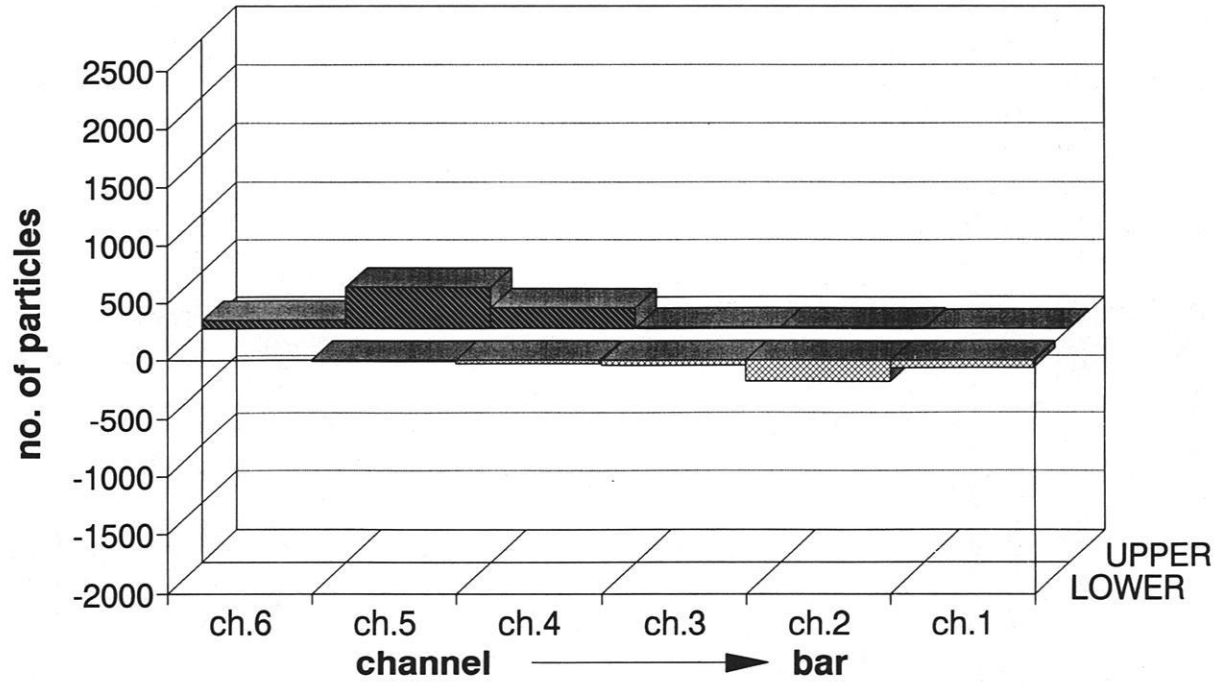

# Bed and water level adjustment

*01:30-02:11, 6th June 1991*

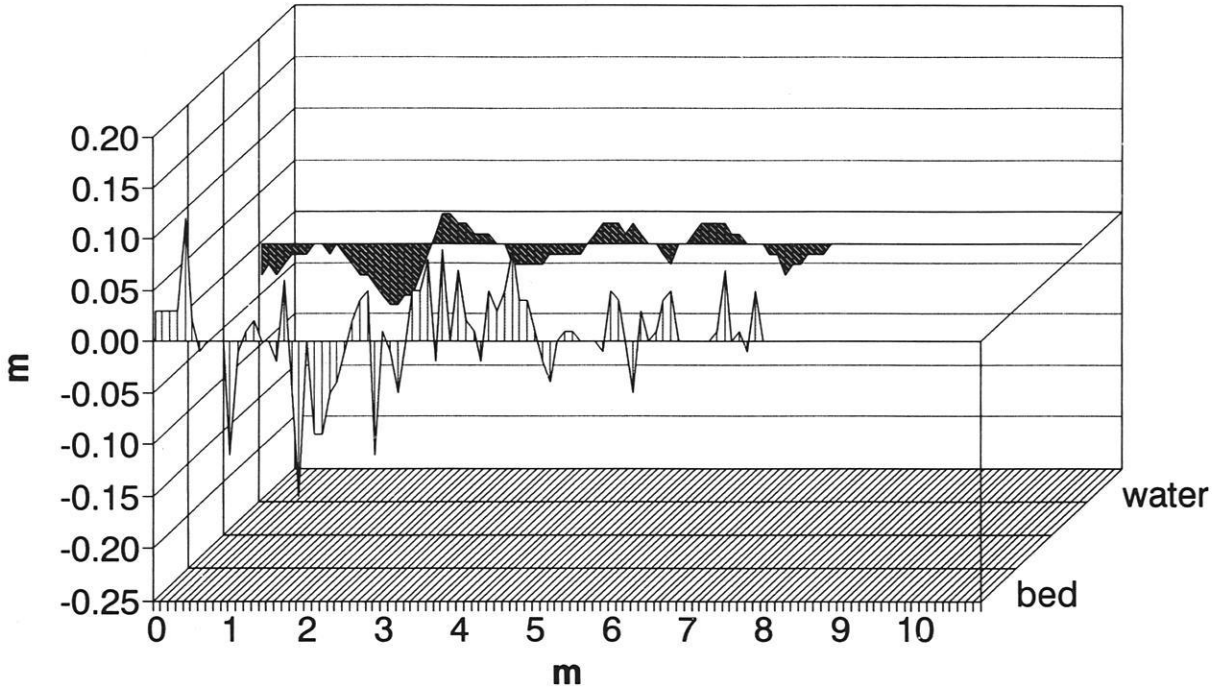


# Squaw Creek, 6th June 1991

*input/output 01:30-02:30*

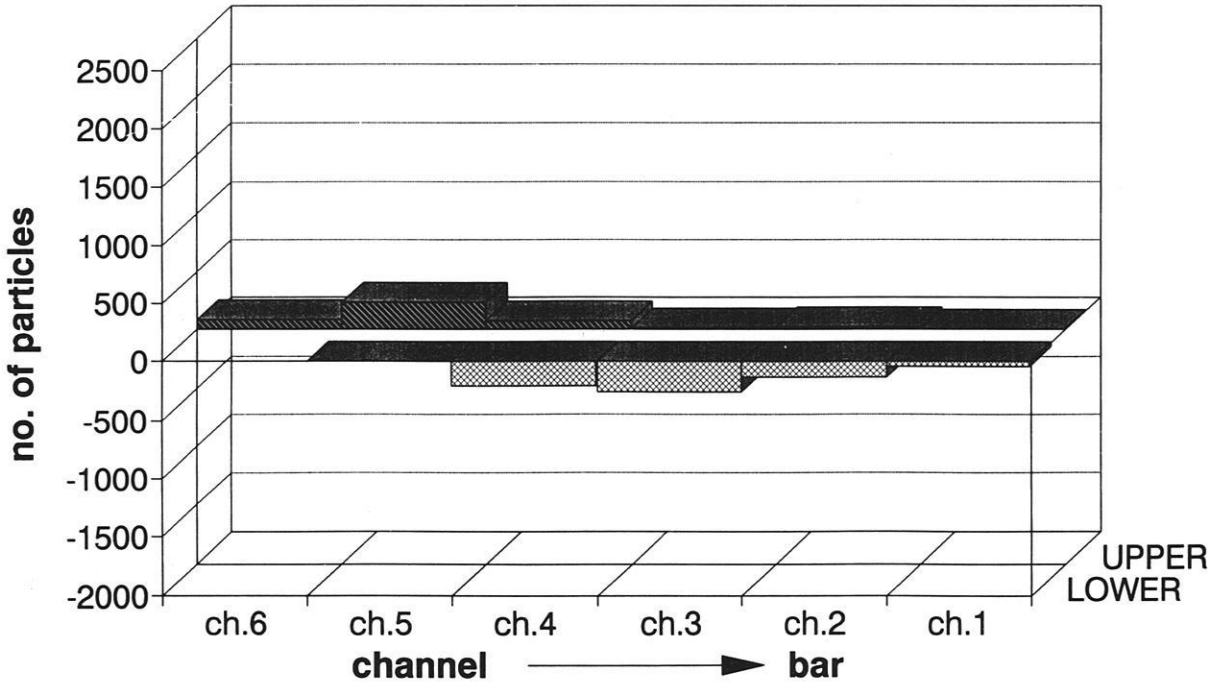

# Bed and water level adjustment

*02:11-03:00, 6th June 1991*

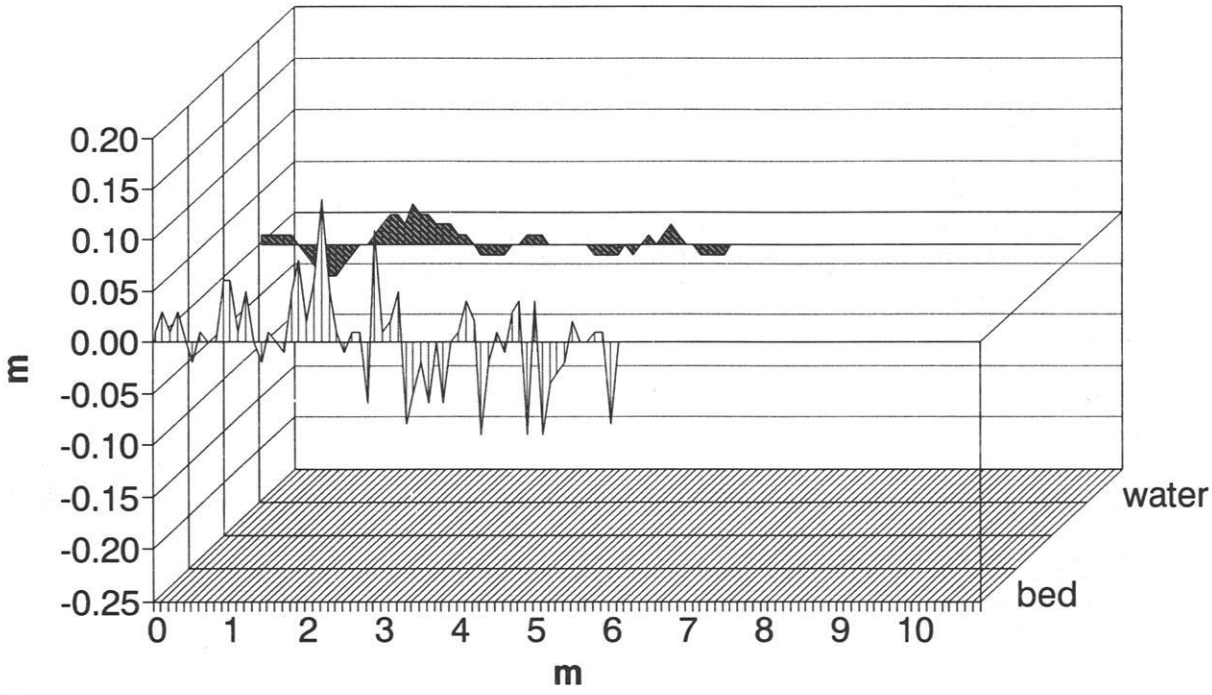


# Squaw Creek, 6th June 1991

*input/output 02:30-03:00*

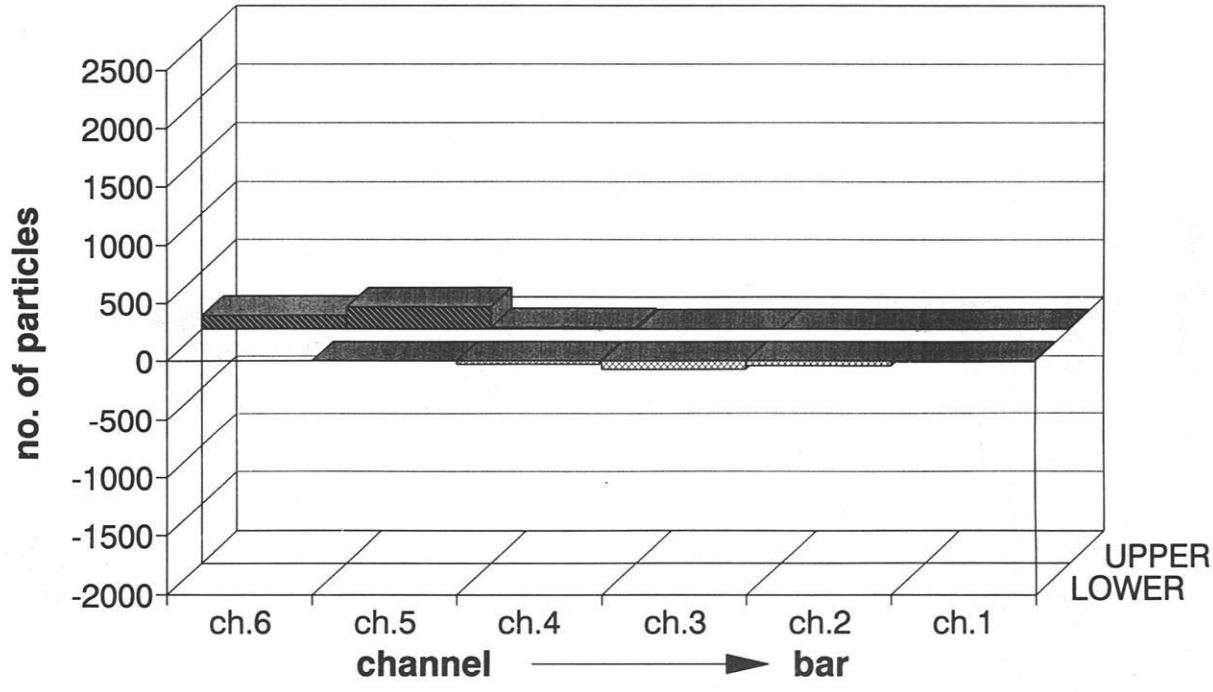

# Bed and water level adjustment

*03:00-03:45, 6th June 1991*

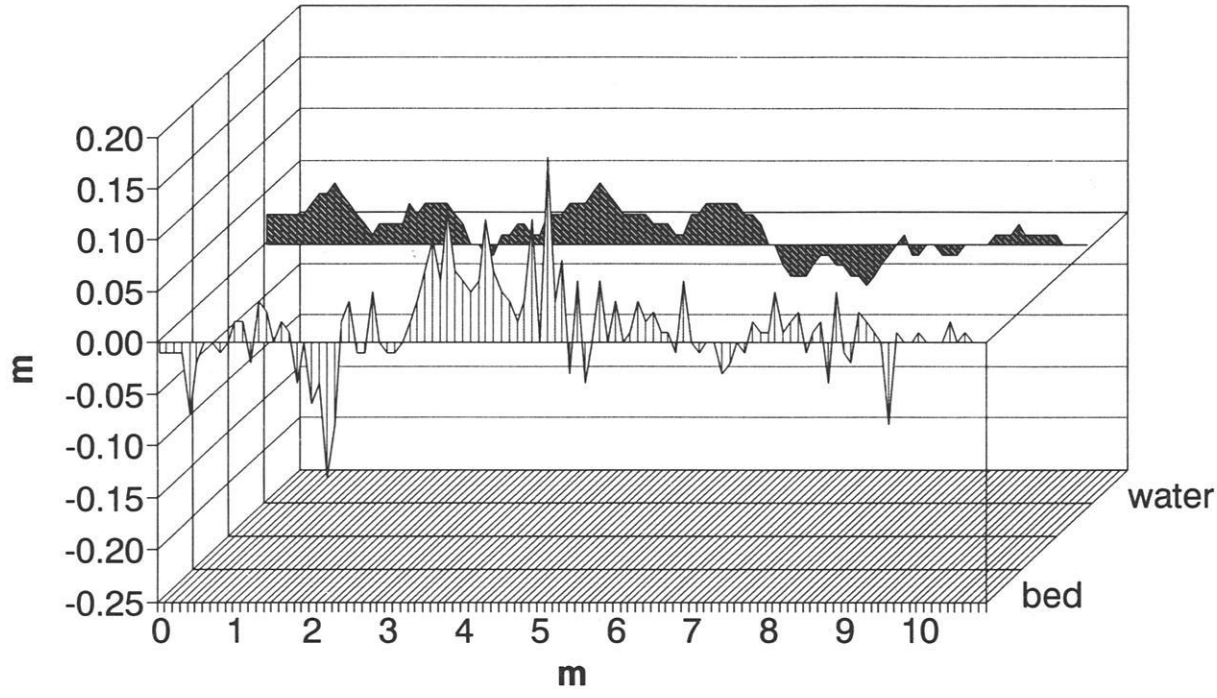


# Squaw Creek, 6th June 1991

*input/output 03:00-03:45*

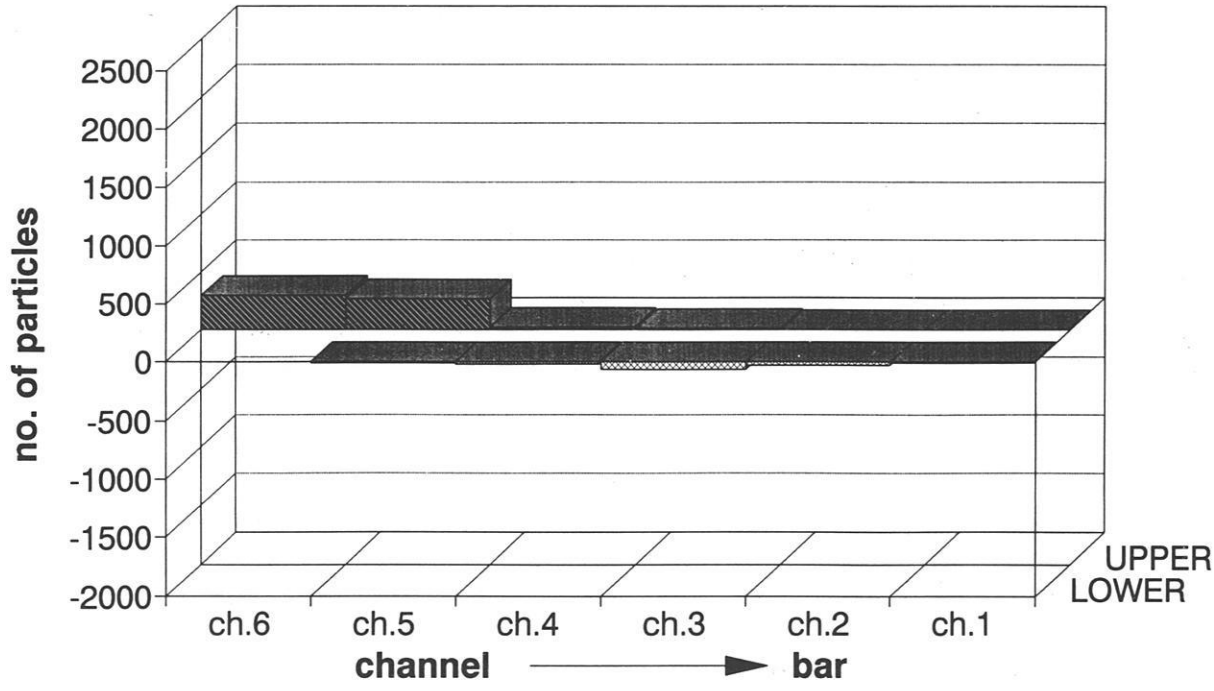

# Bed and water level adjustment

*03:45-06:00, 6th June 1991*

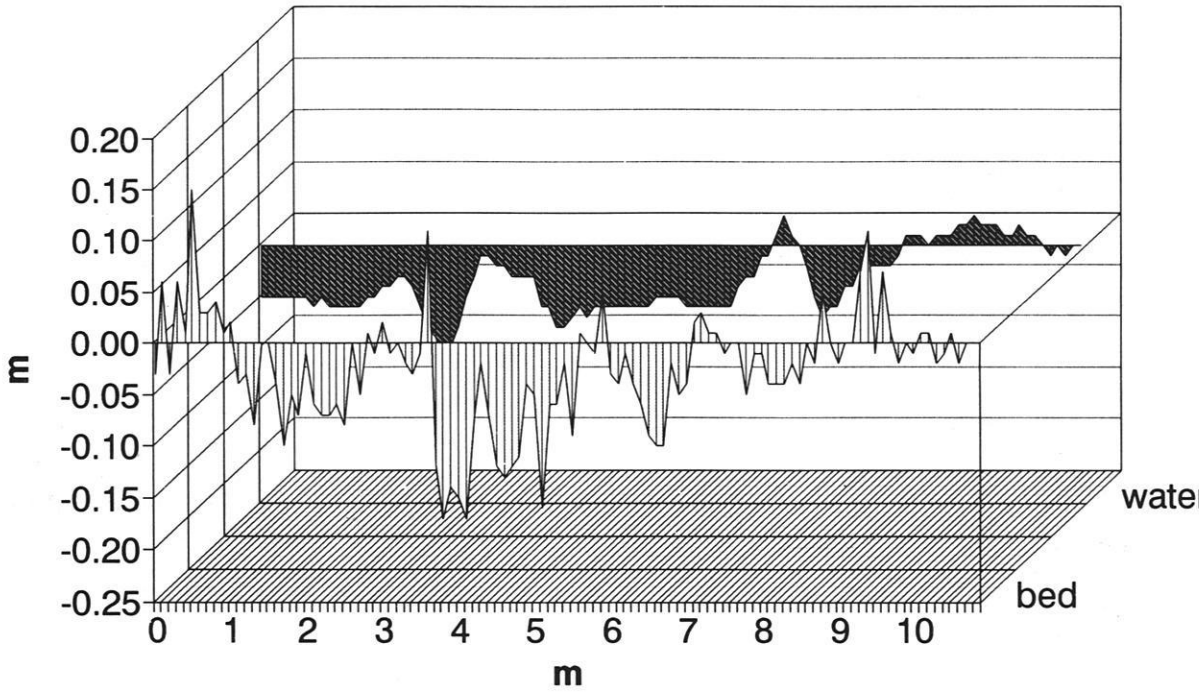


# Squaw Creek, 6th June 1991

*input/output 03:45-06:00*

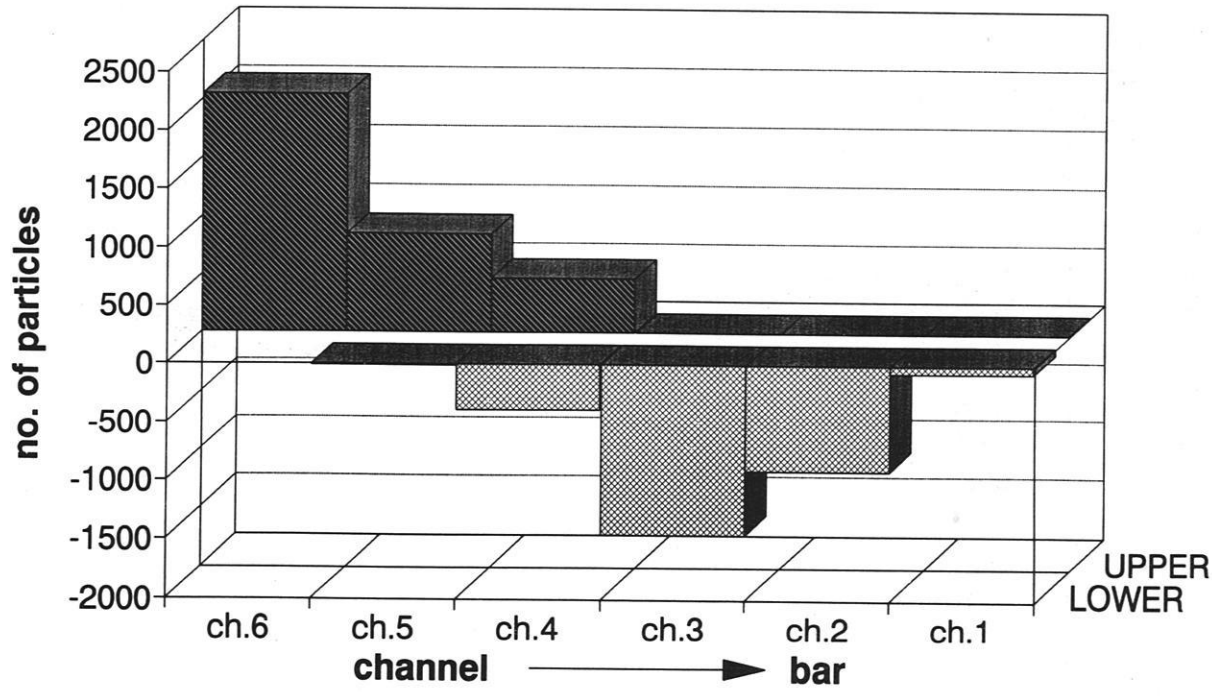

# Bed and water level adjustment

*06:00-06:45, 6th June 1991*

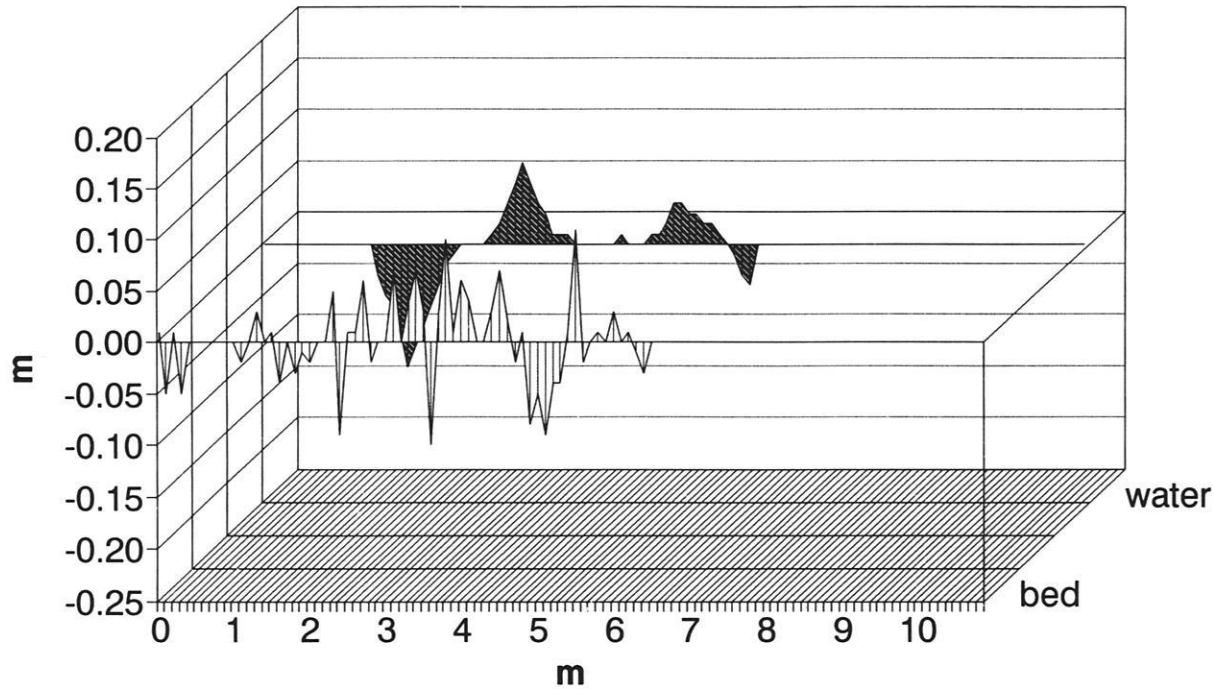


# Squaw Creek, 6th June 1991

*input/output 06:00-06:45*

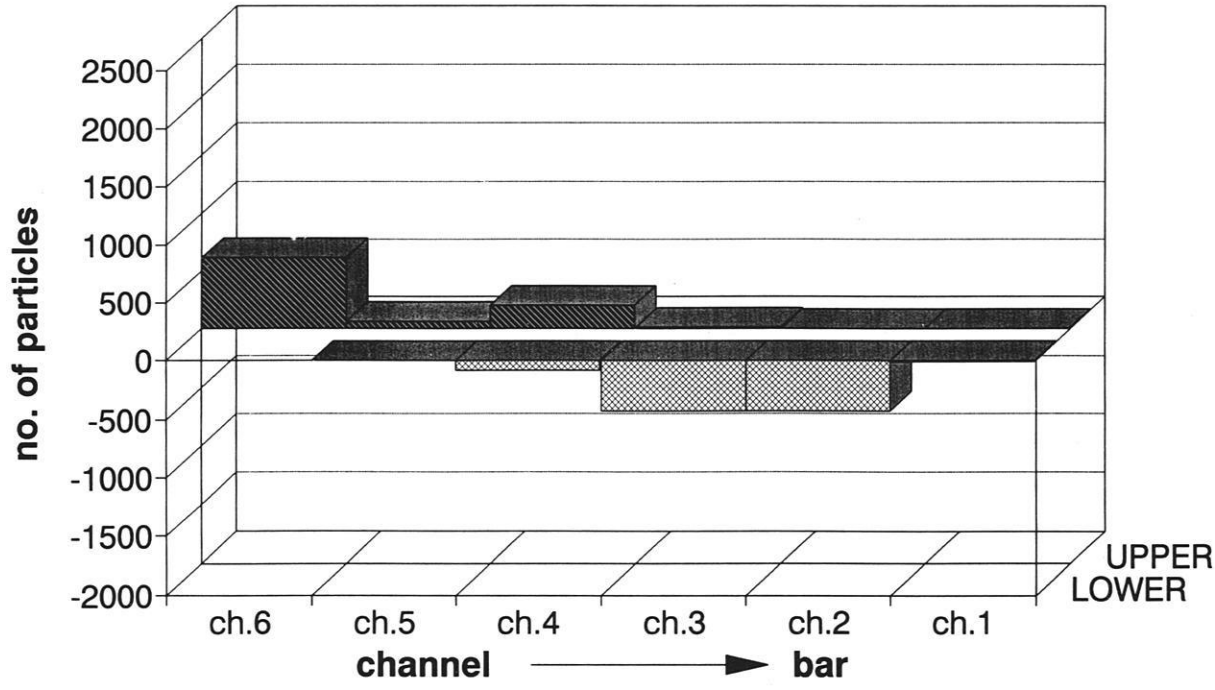

# Bed and water level adjustment

*06:45-07:10, 6th June 1991*

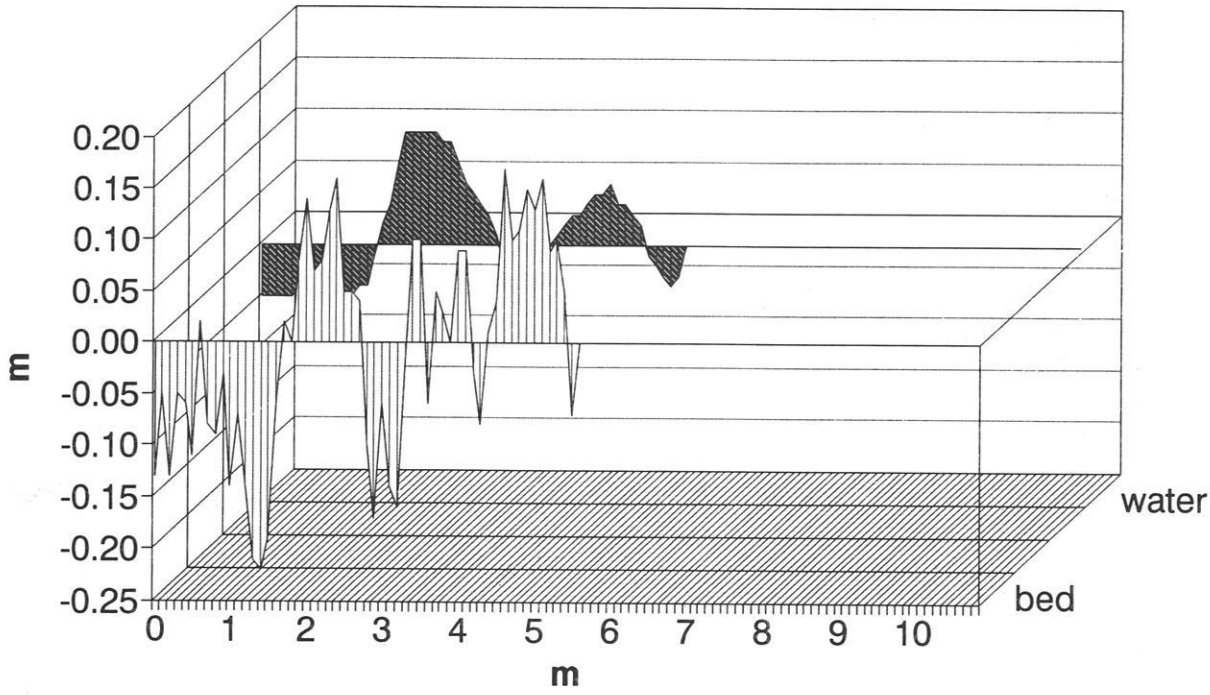


# Squaw Creek, 6th June 1991

*input/output 06:45-07:10*

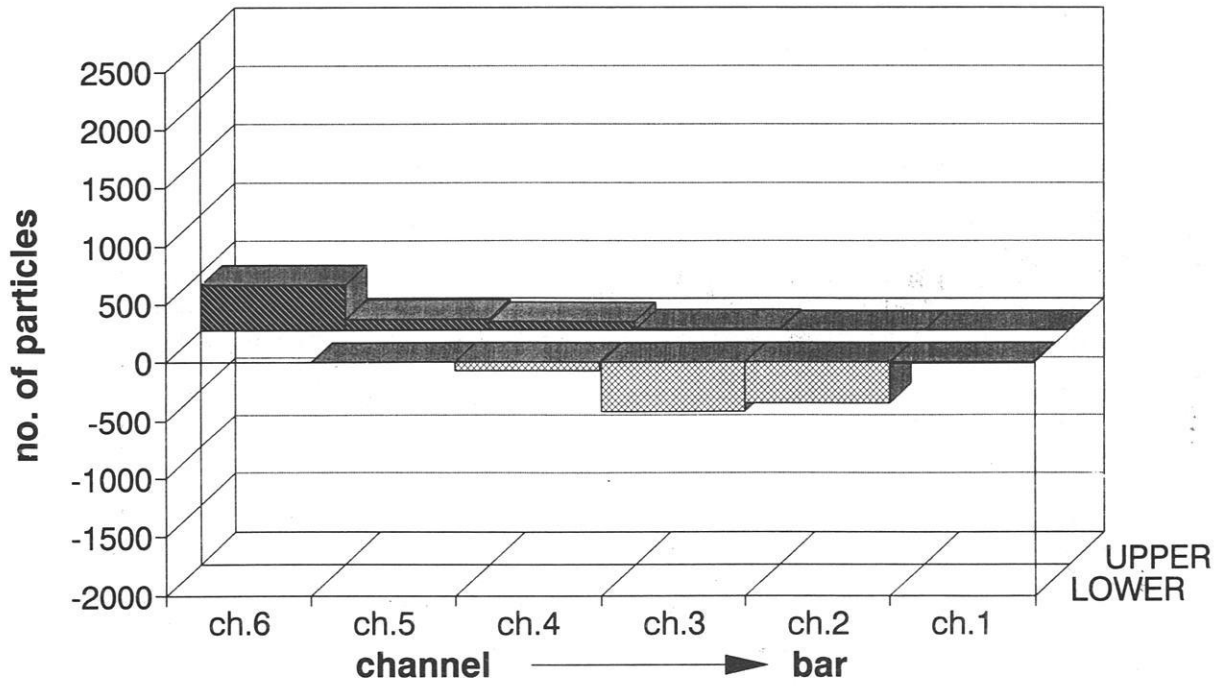

# Bed and water level adjustment

*07:10-10:07, 6th June 1991*

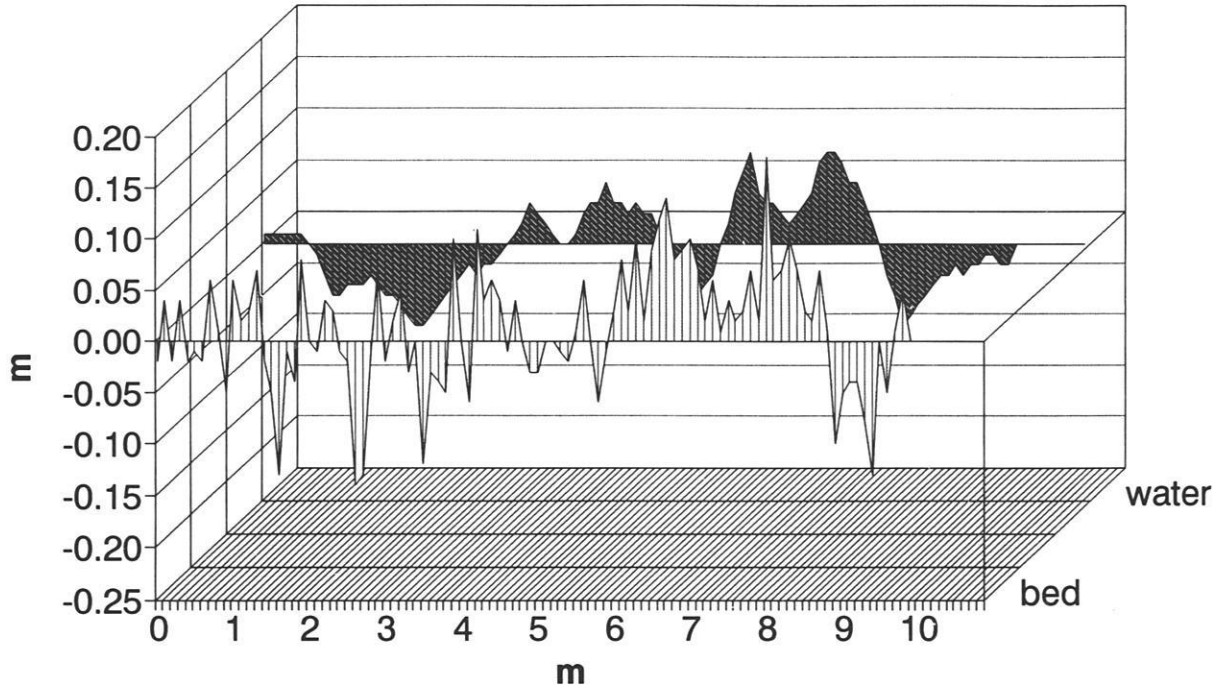


# Squaw Creek, 6th June 1991

*input/output 07:10-10:00*

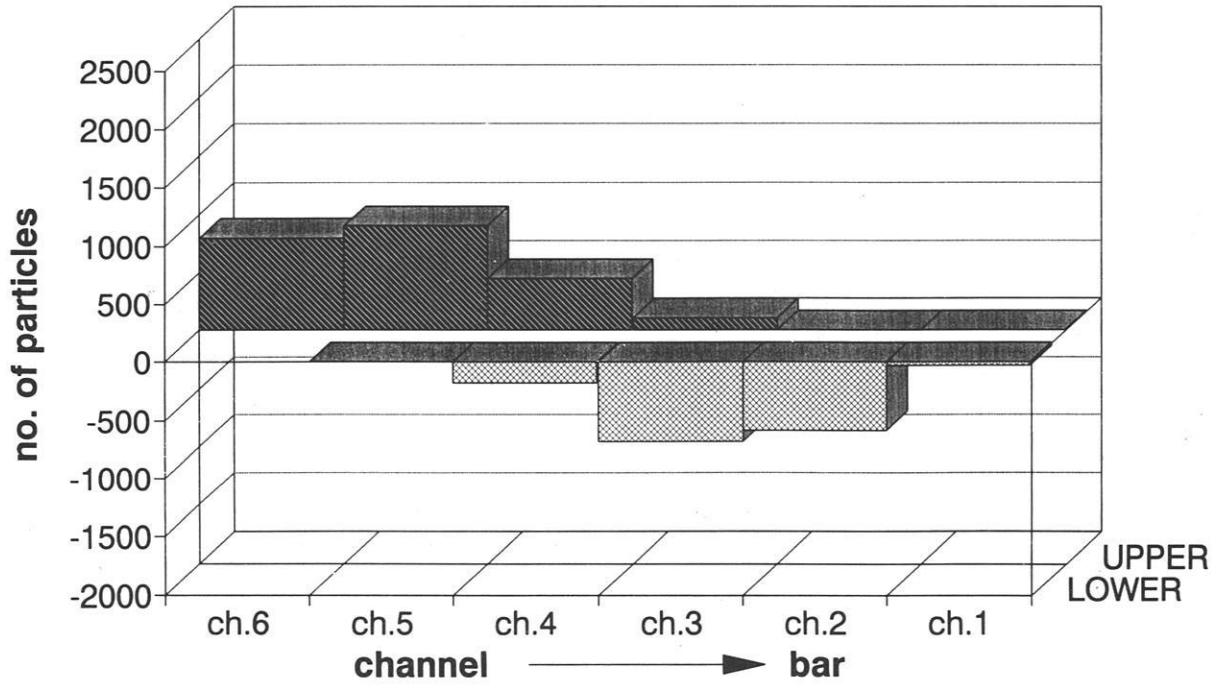

# Bed and water level adjustment

*10:07-13:08, 6th June 1991*

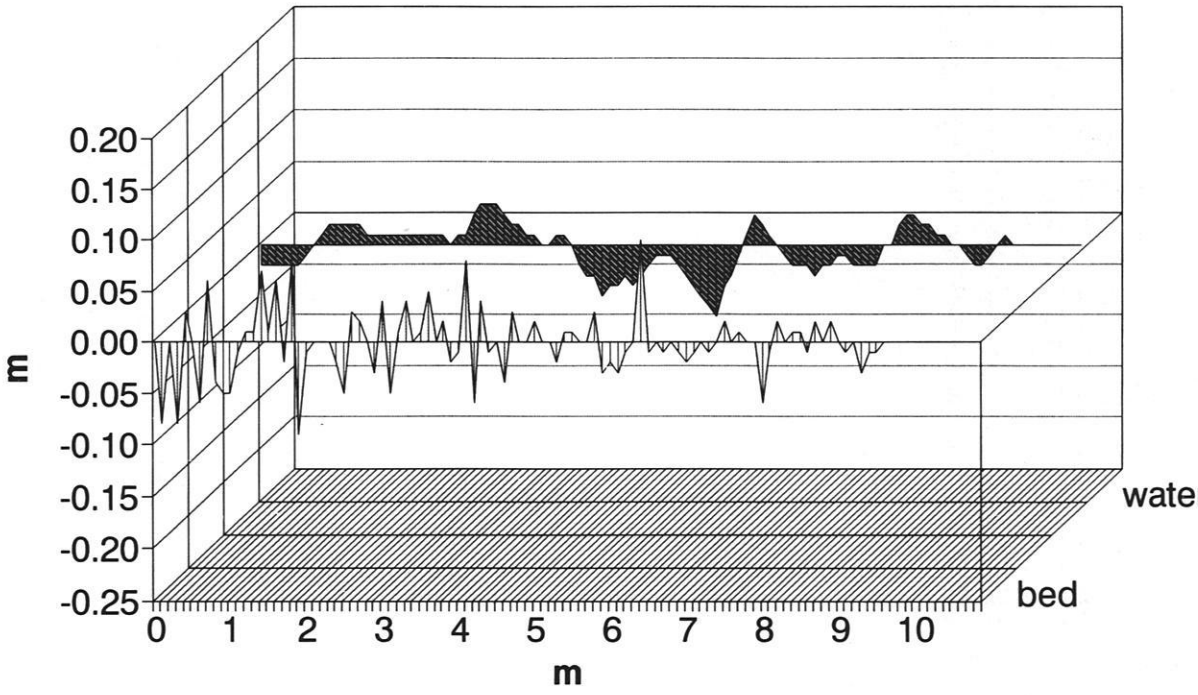


# Squaw Creek, 6th June 1991

*input/output 10:00-13:00*

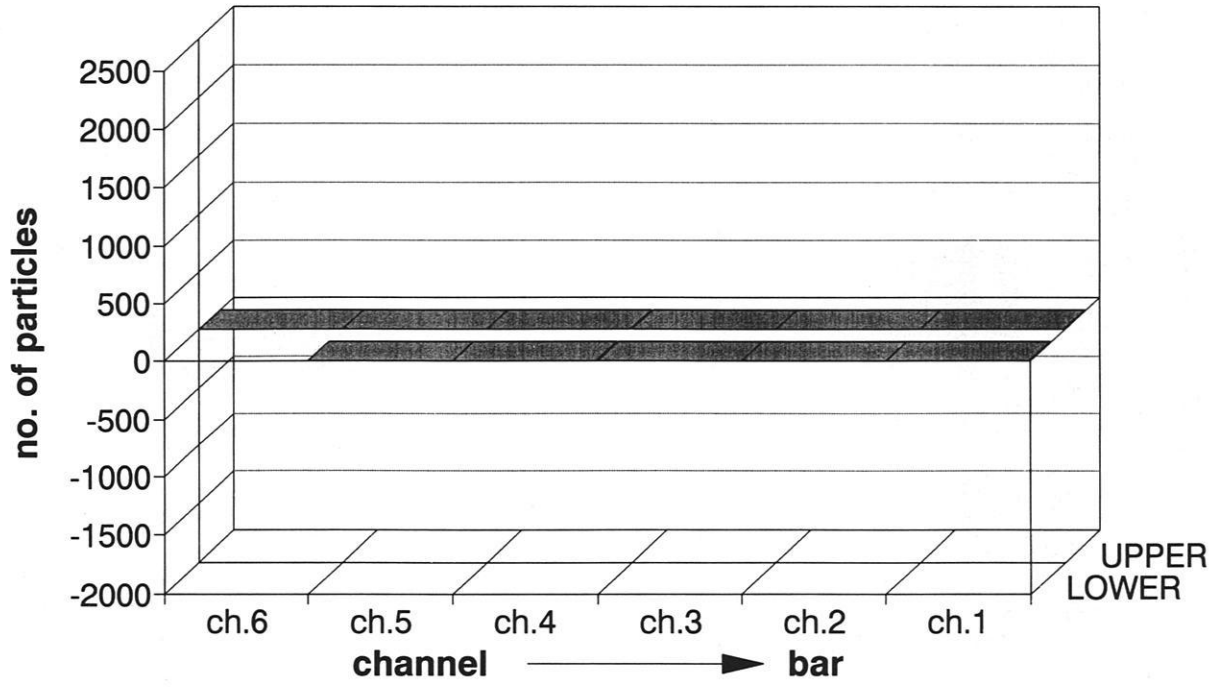

# Bed and water level adjustment

*13:08-15:05, 6th June 1991*

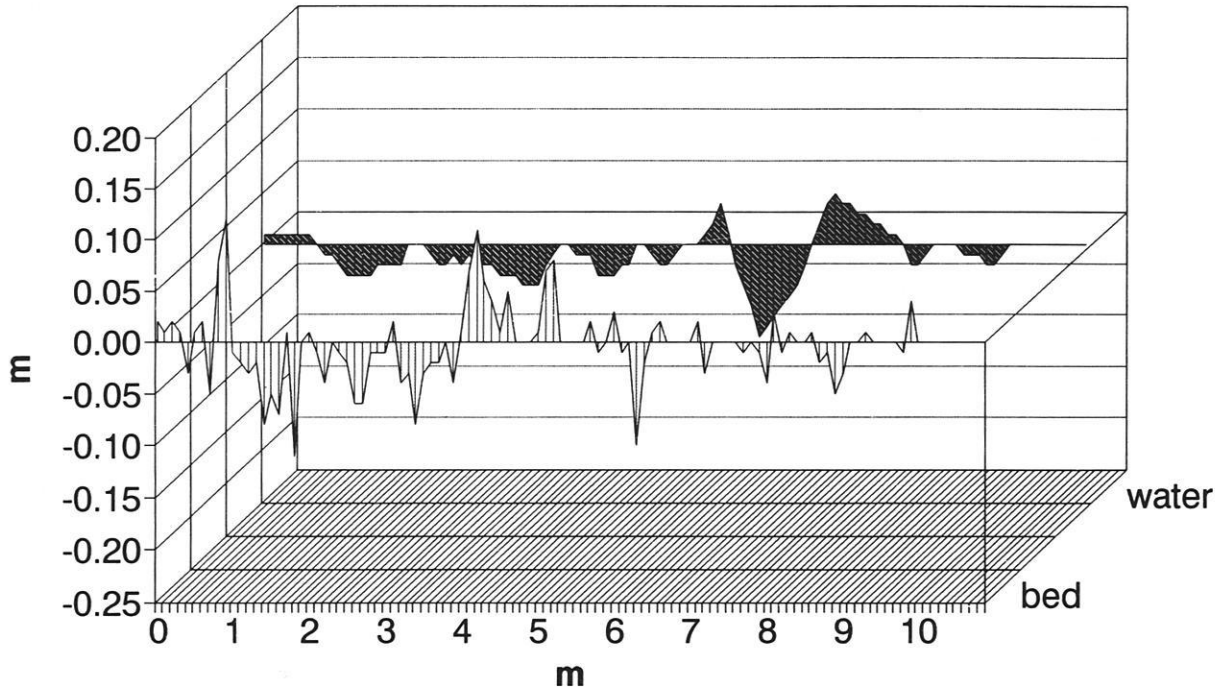


# Squaw Creek, 6th June 1991

*input/output 13:00-15:10*

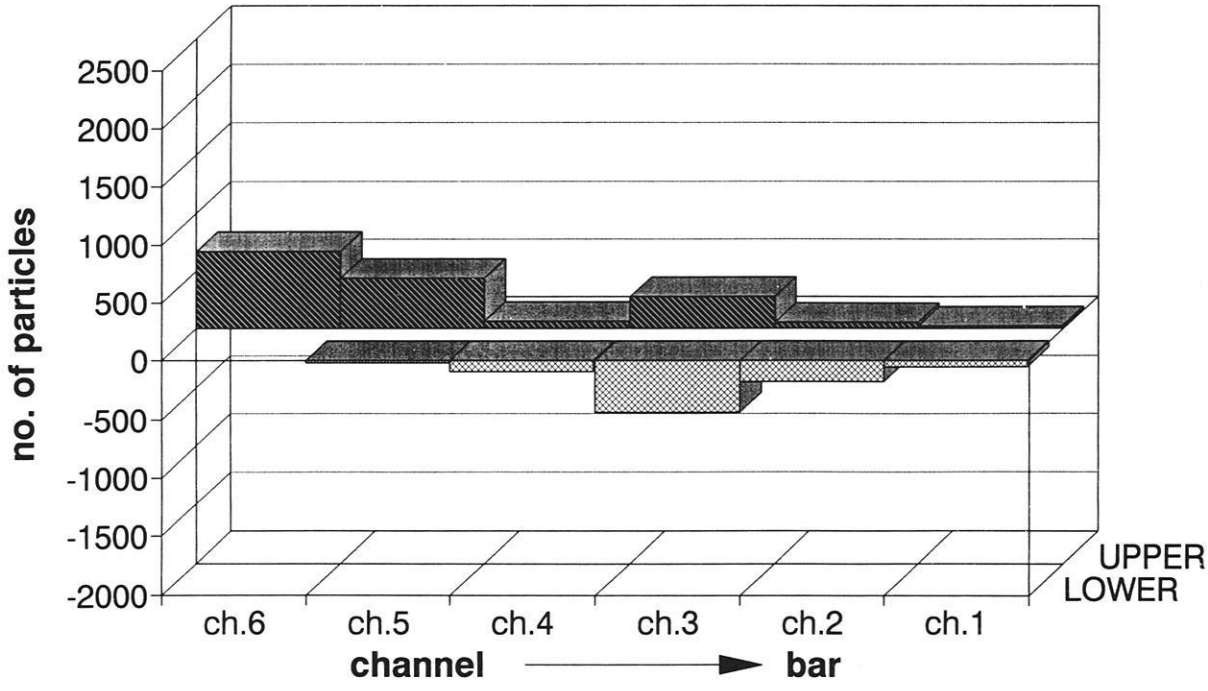

**Appendix A3** **Lainbach, 22-23rd July 1992. Long profile: river bed and water level adjustment**

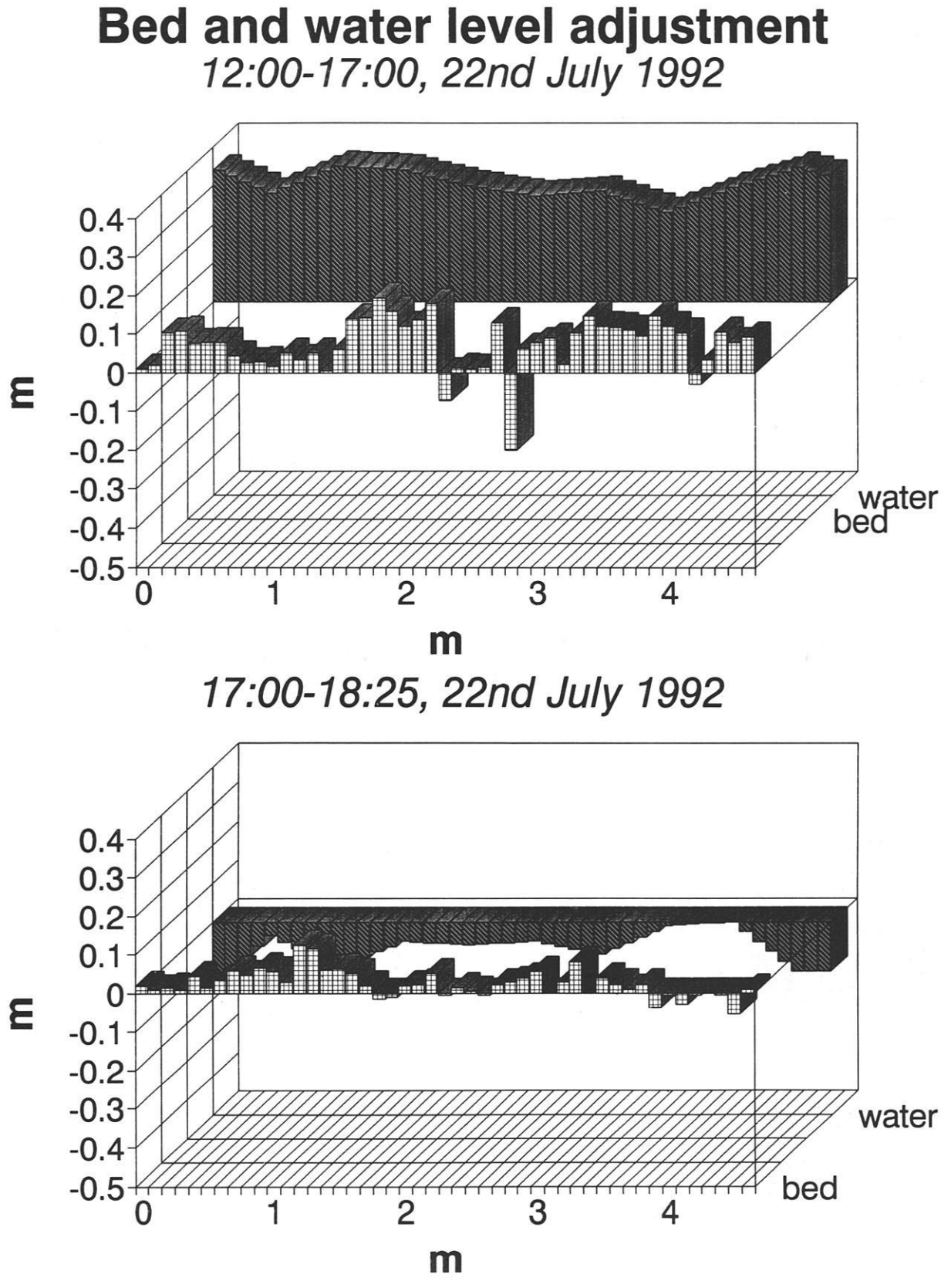

# Bed and water level adjustment

*18:25-19:50, 22nd July 1992*

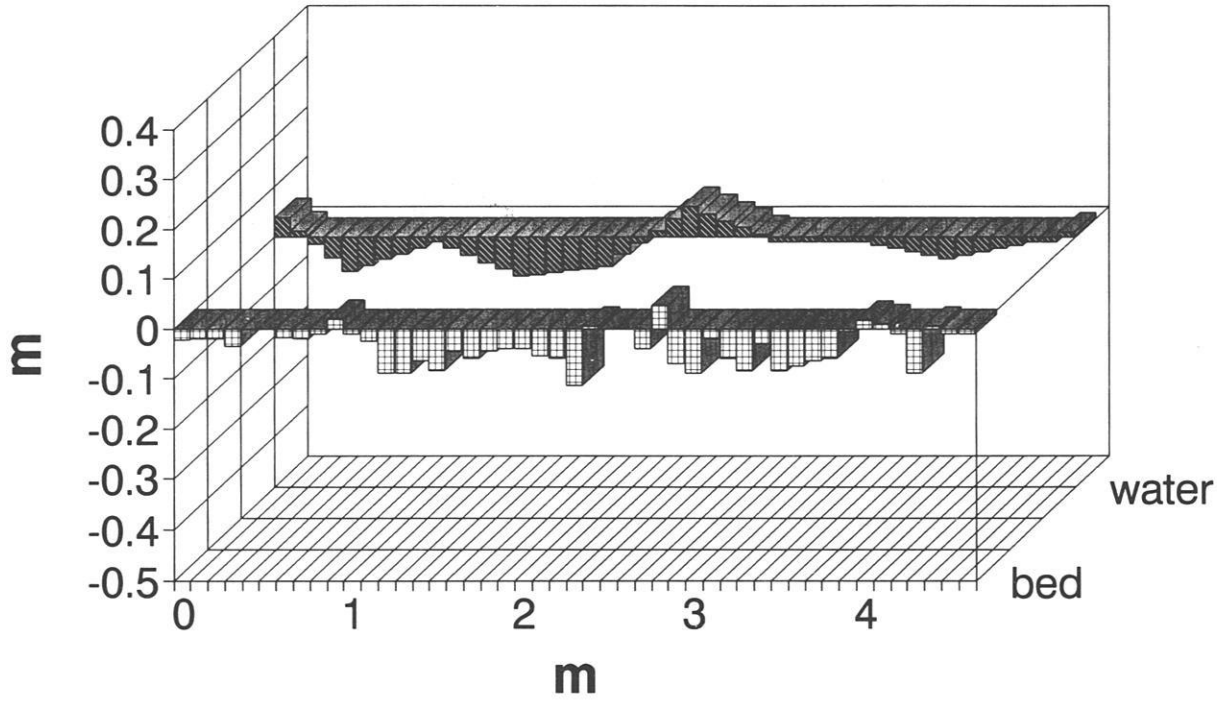


# Bed and water level adjustment

*19:50-20:52, 22nd July 1992*

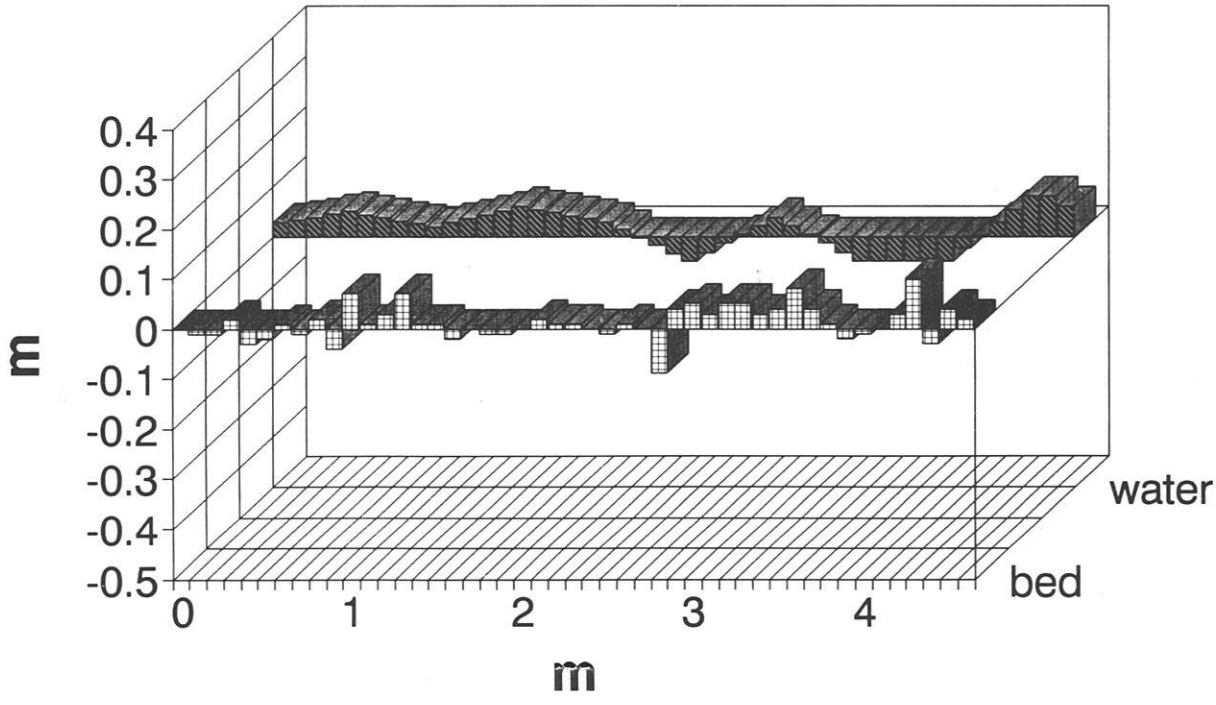

## Bed and water level adjustment

*20:52-21:45, 22nd July 1992*

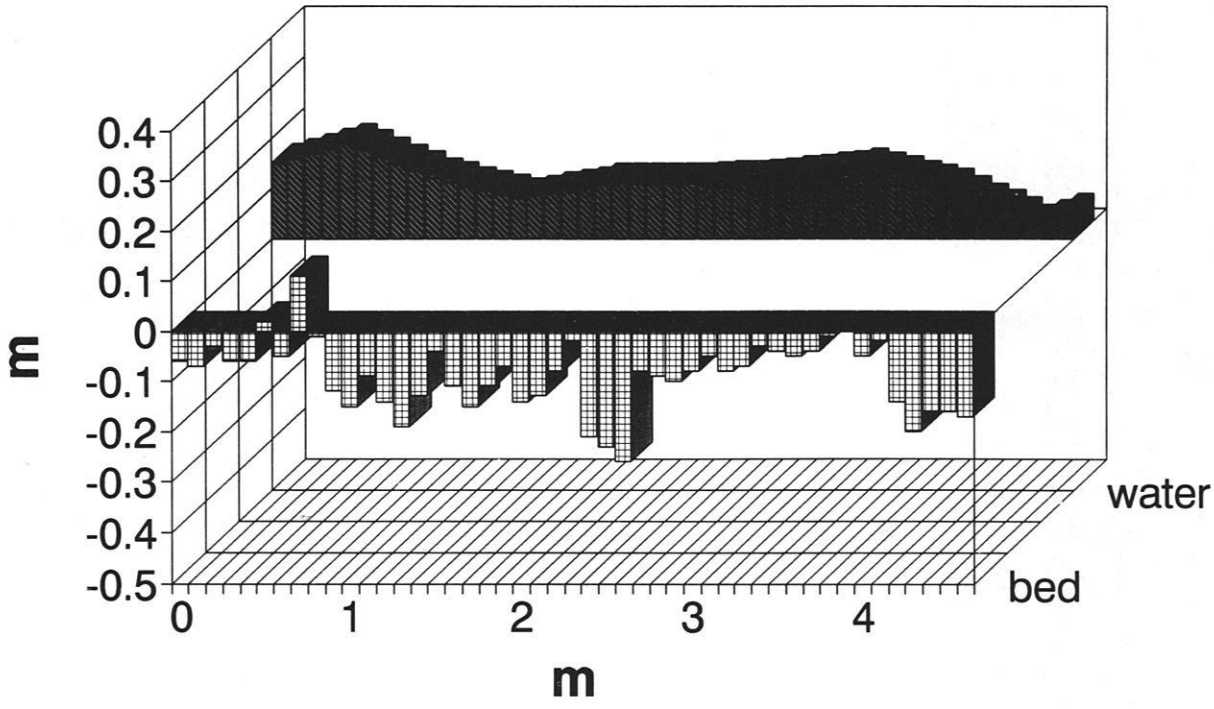


## Bed and water level adjustment

*21:45-23:35, 22nd July 1992*

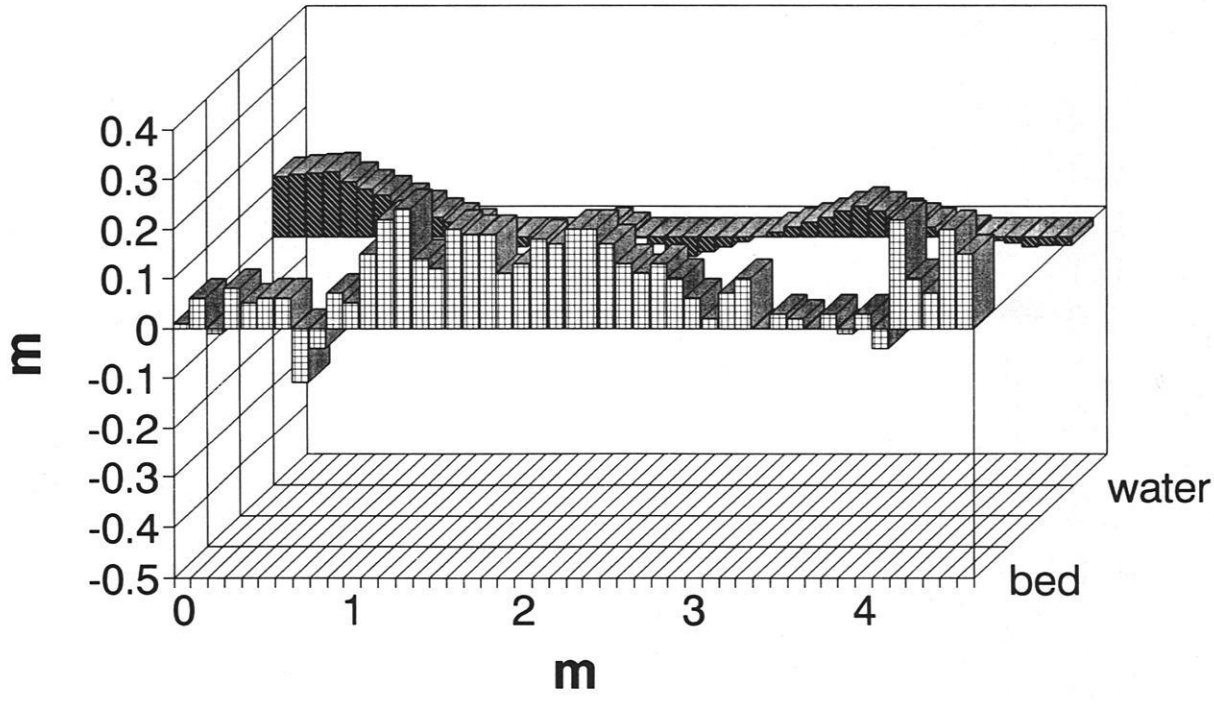

# Bed and water level adjustment

*23:35-05:32, 23rd July 1992*

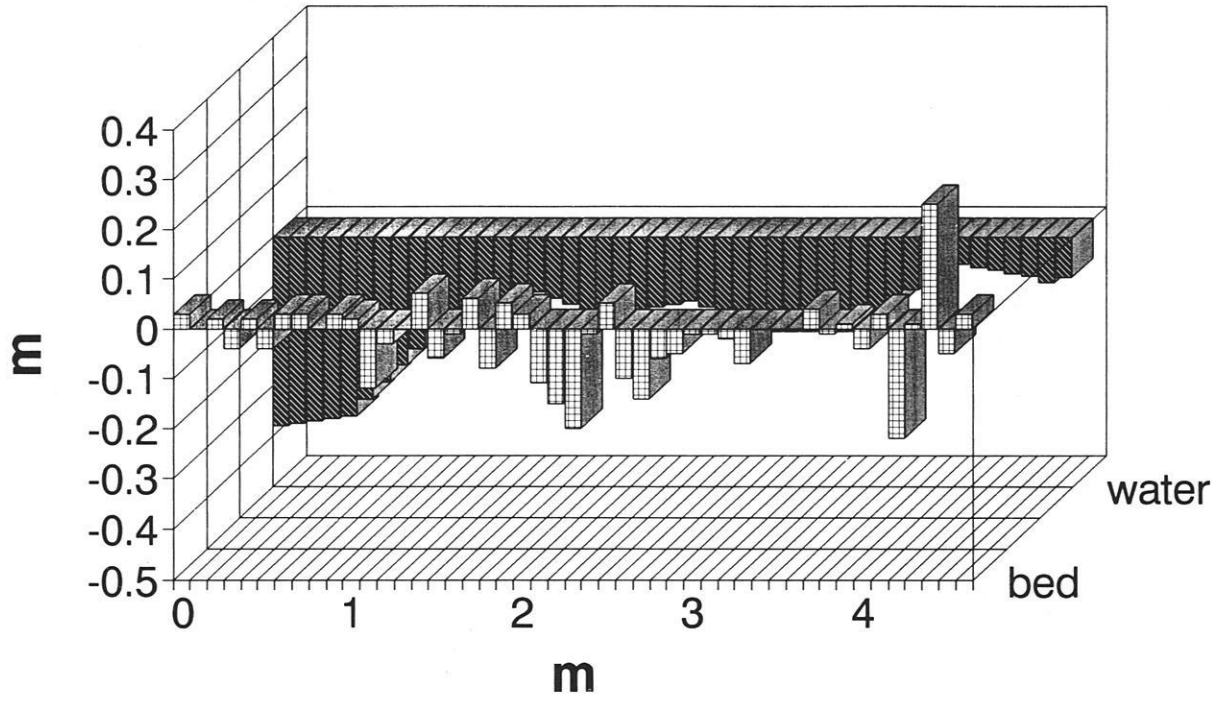


# Bed and water level adjustment

*05:32-10:00, 23rd July 1992*

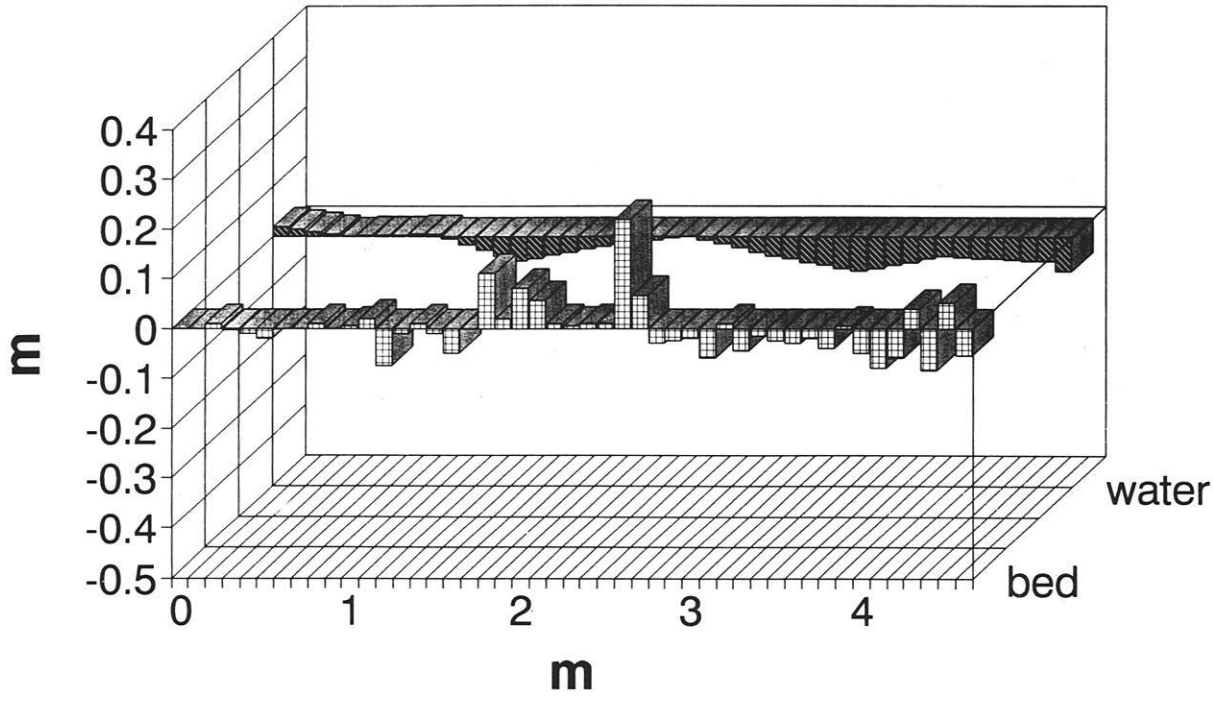

**Appendix A4** **Lainbach, 22-23rd July 1992. Upper & lower bridge (cross-profiles): river bed and water level adjustment**

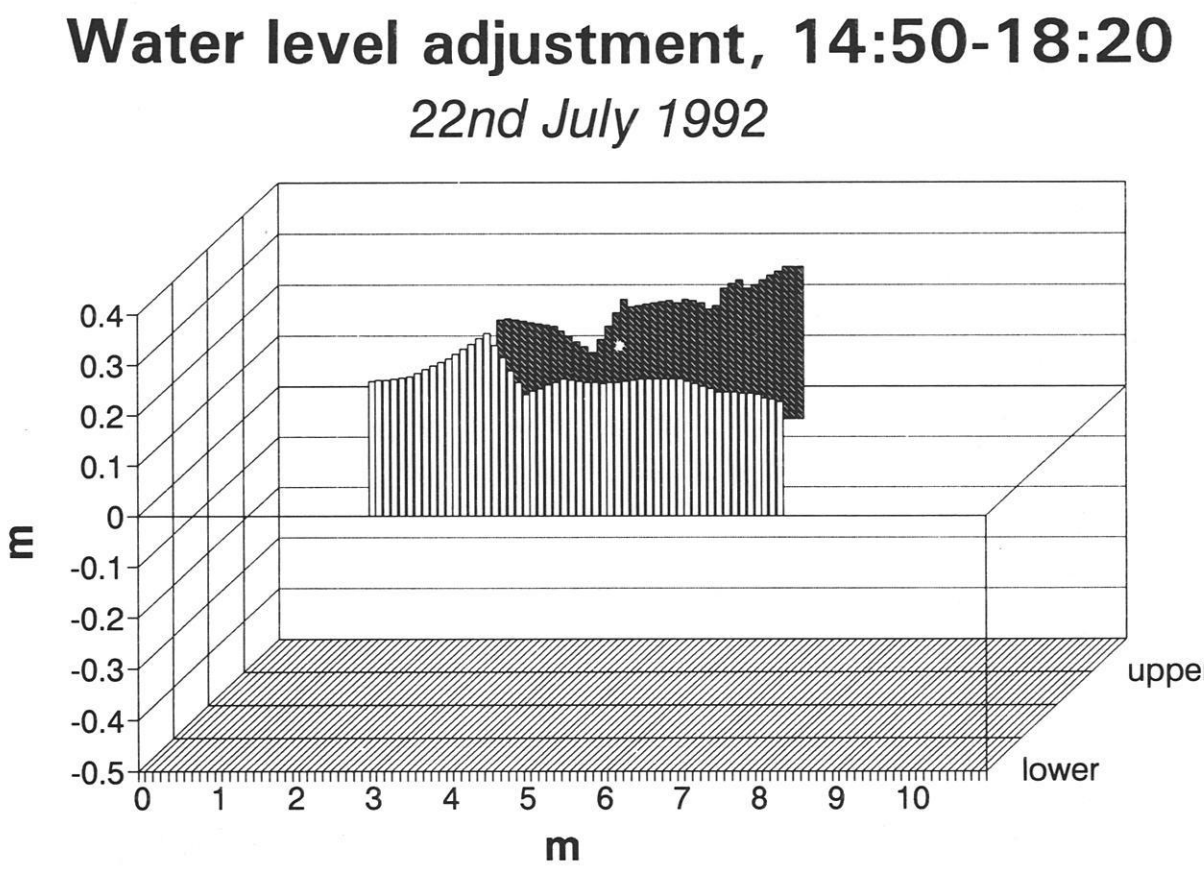


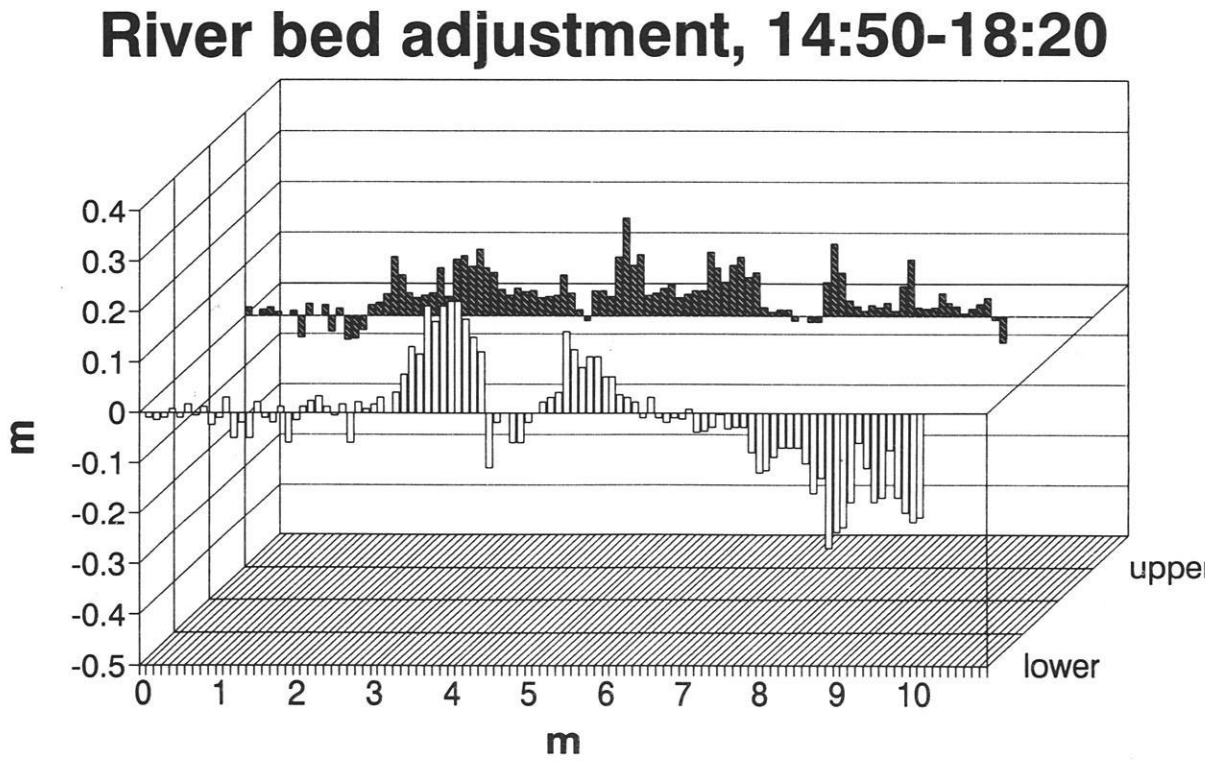

# Water level adjustment, 18:20-19:20

*22nd July 1992*

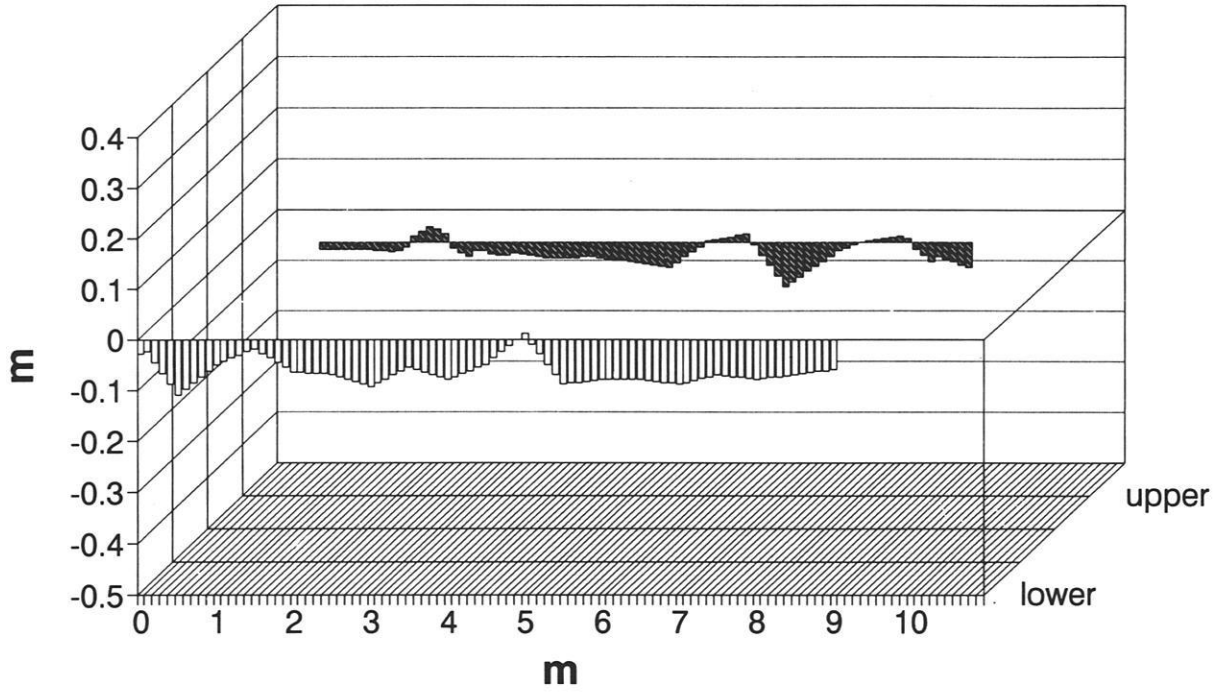


# River bed adjustment, 18:20-19:20

*22nd July 1992*

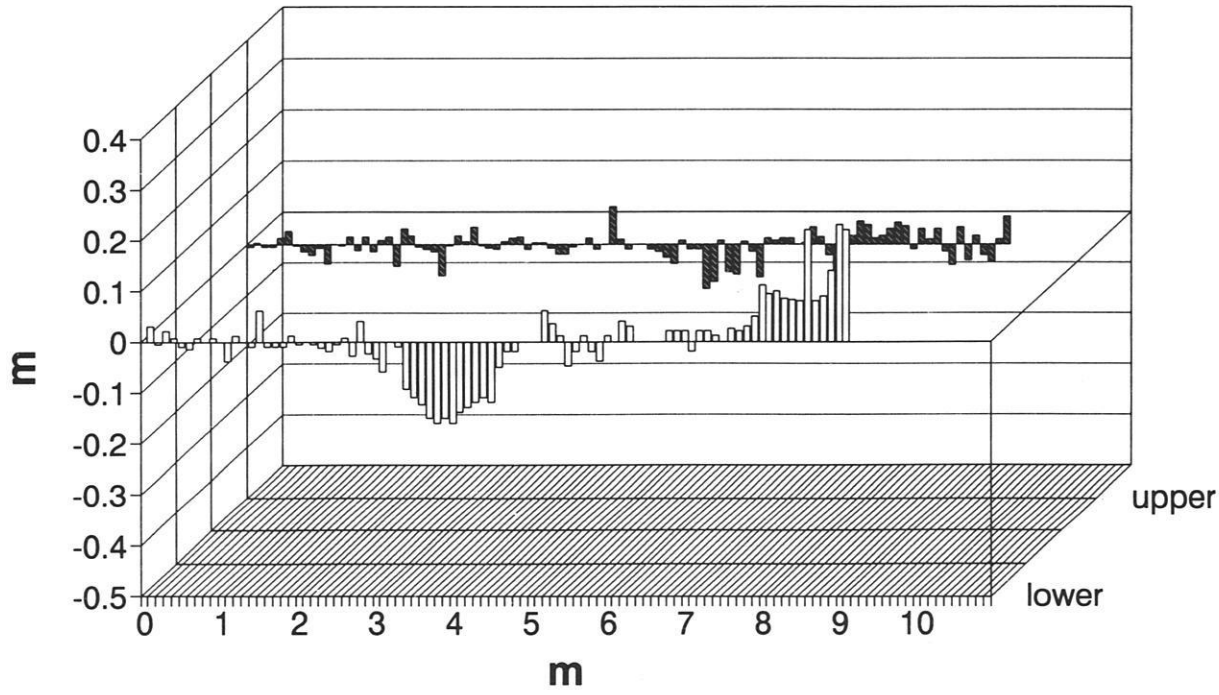

# Water level adjustment, 19:20-21:45

*22nd July 1992*

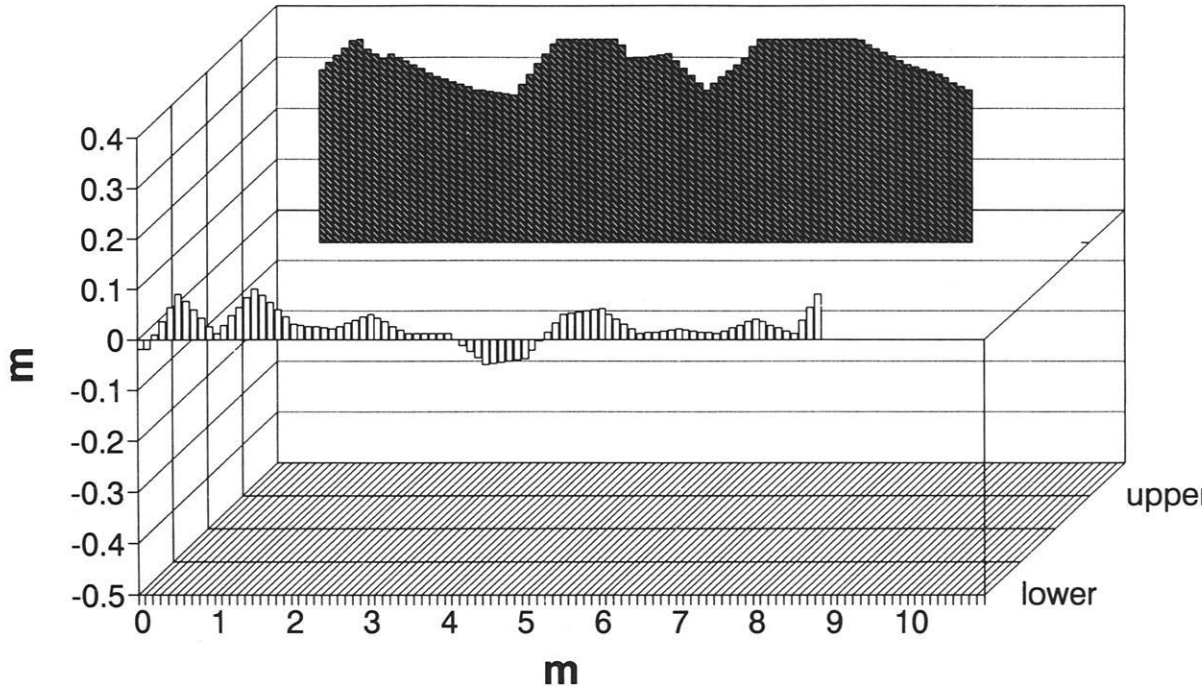


# River bed adjustment, 19:20-21:45

*22nd July 1992*

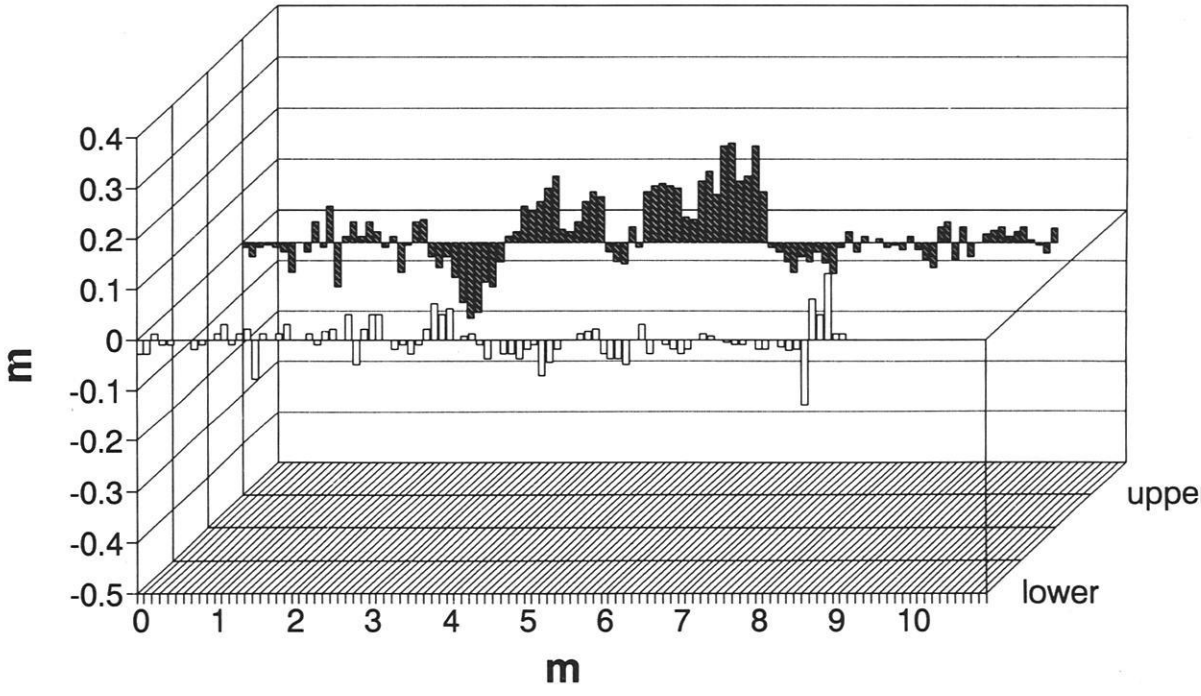

# Water level adjustment, 21:45-22:20

*22nd July 1992*

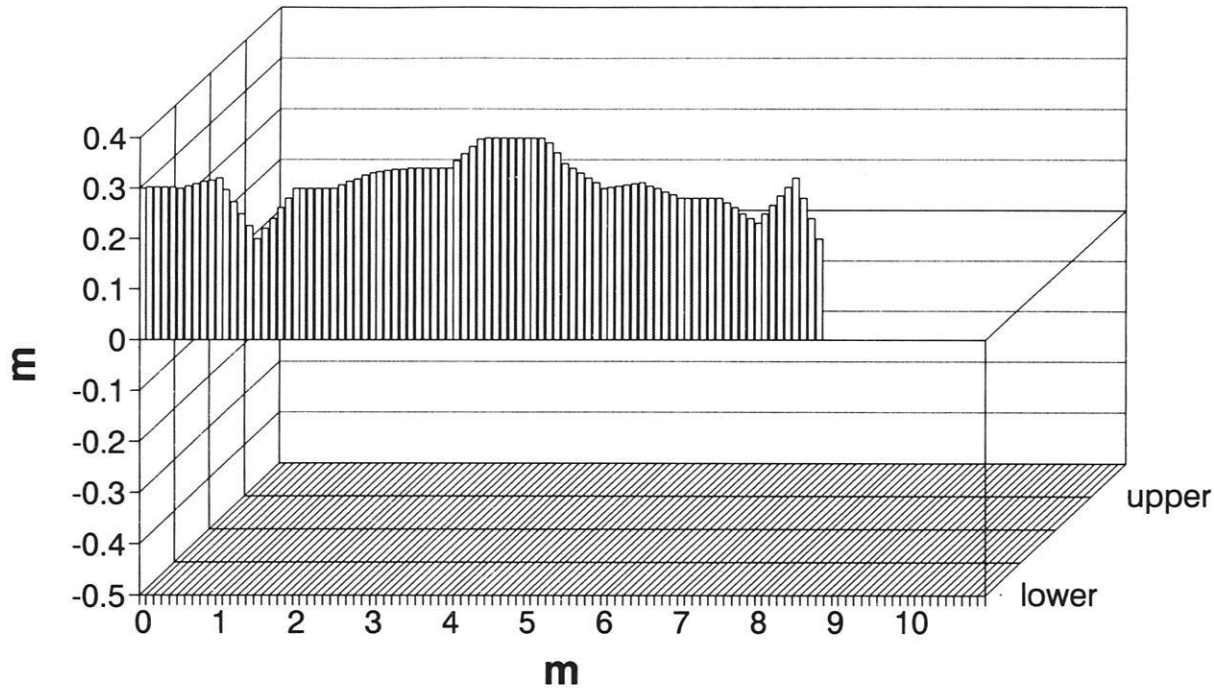


# River bed adjustment, 21:45-22:20

*22nd July 1992*

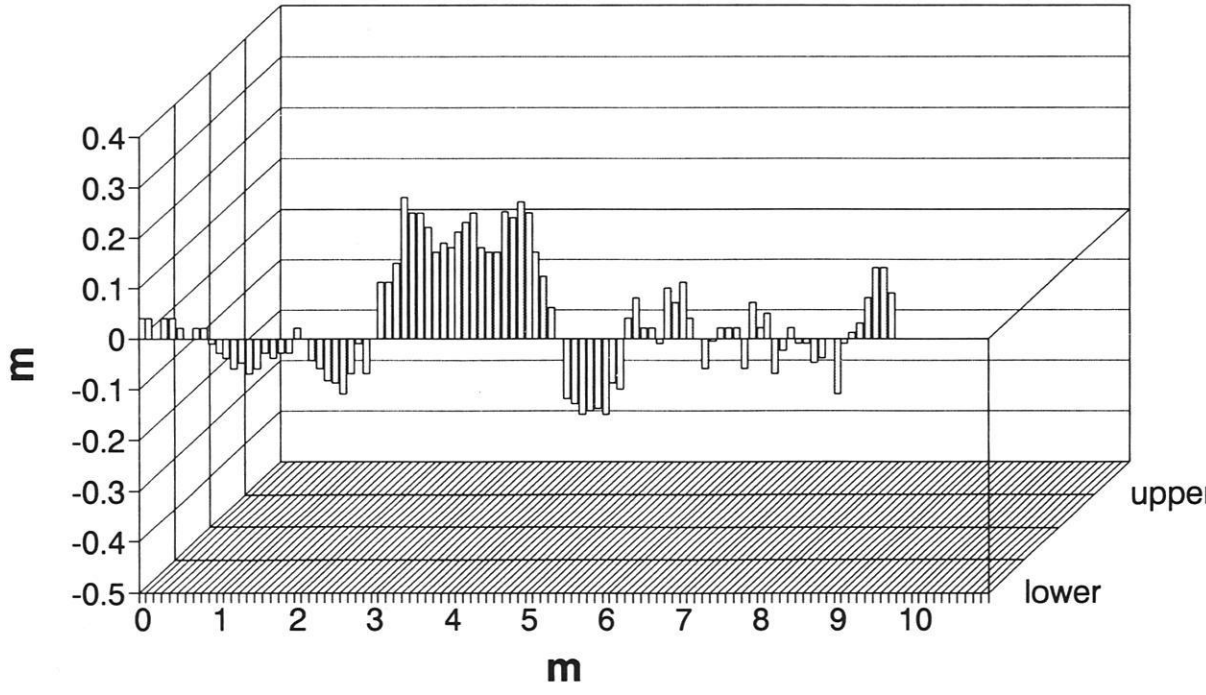

# Water level adjustment, 22:20-23:35

*22nd July 1992*

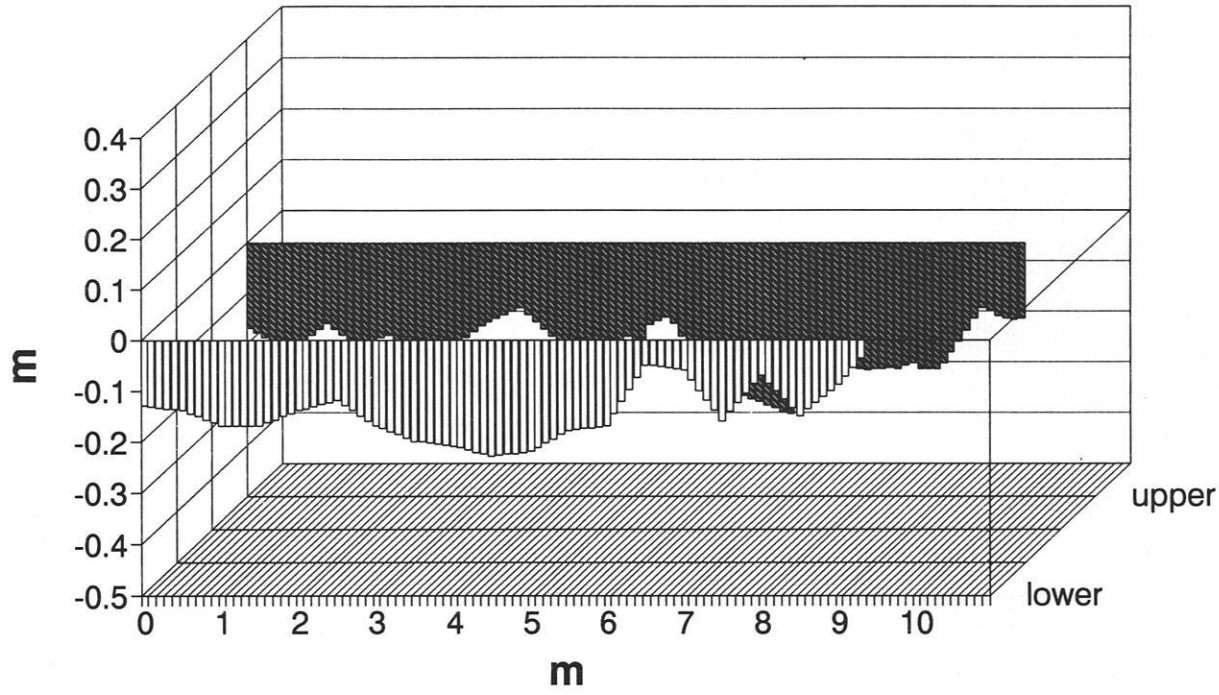


# River bed adjustment, 22:20-23:35

*22nd July 1992*

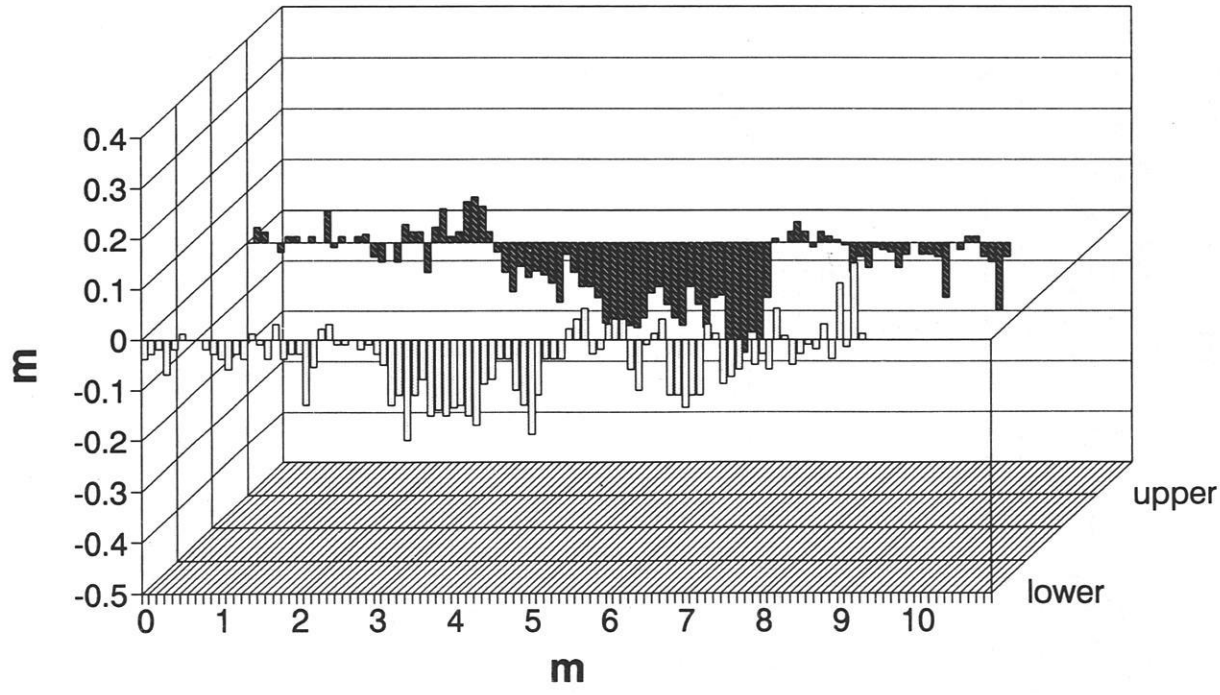

# Water level adjustment, 23:35-09:20

*22nd July 1992*

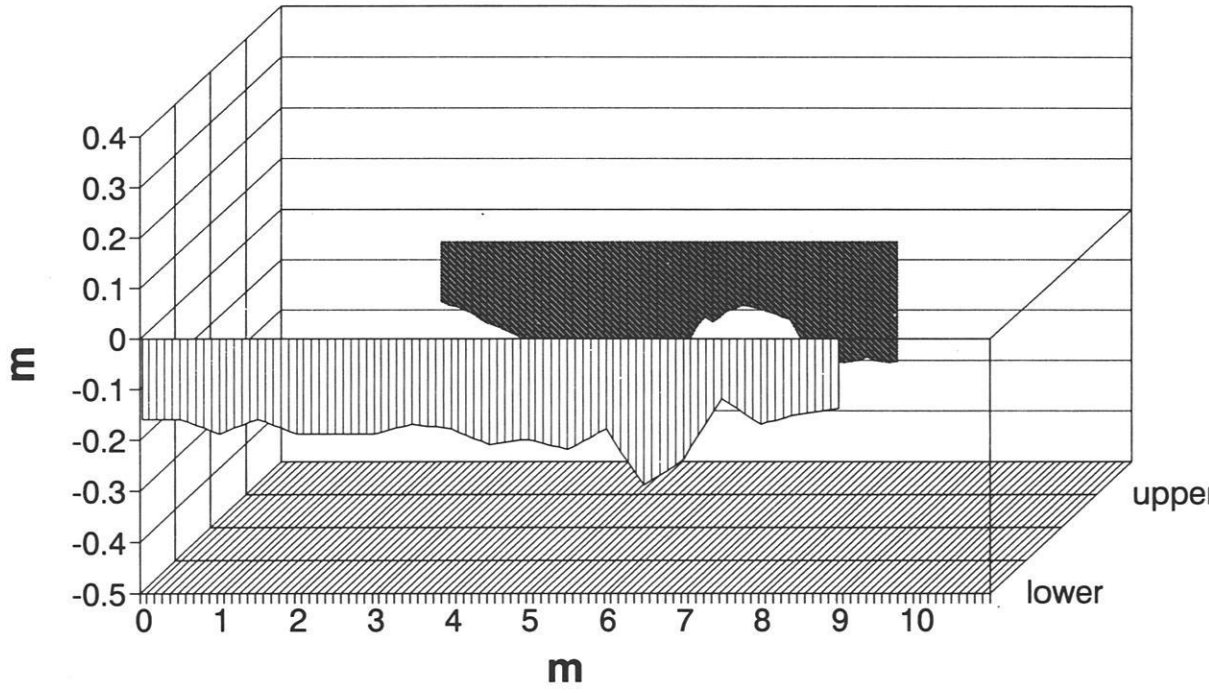


# River bed adjustment, 23:35-09:20

*22nd July 1992*

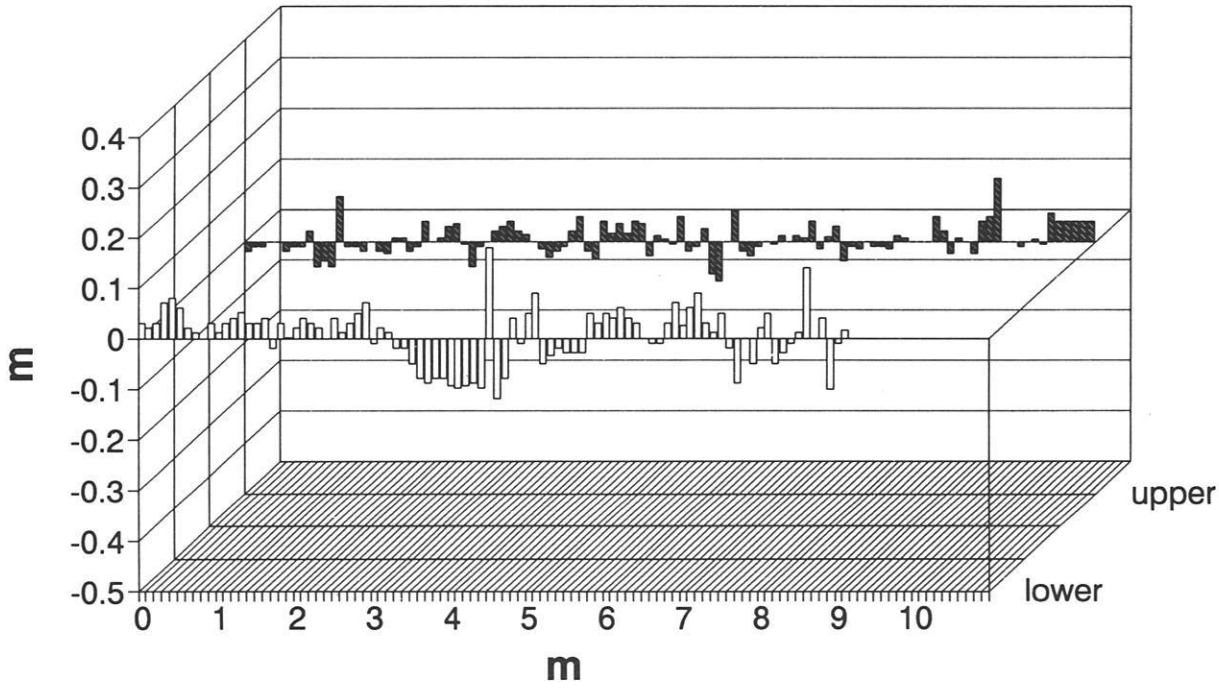

## Berliner Geographische Abhandlungen

Im Selbstverlag des Instituts für Geographische Wissenschaften der Freien Universität Berlin,
Grunewaldstr. 35, D-12165 Berlin (Preise zuzüglich Versandspesen)
Postanschrift: Geomorphologisches Laboratorium, Altensteinstr. 19, D 14195 Berlin

---

Heft 1: HIERSEMENZEL, Sigrid-Elisabeth (1964)
Britische Agrarlandschaften im Rhythmus des landwirtschaftlichen Arbeitsjahres, untersucht an 7 Einzelbeispielen. - 46 S., 7 Karten, 10 Diagramme.
ISBN 3-88009-000-9 (*vergriffen*)

Heft 2: ERGENZINGER, Peter (1965)
Morphologische Untersuchungen im Einzugsgebiet der Ilz (Bayerischer Wald). - 48 S., 62 Abb.
ISBN 3-88009-001-7 (*vergriffen*)

Heft 3: ABDUL-SALAM, Adel (1966)
Morphologische Studien in der Syrischen Wüste und dem Antilibanon. - 52 S., 27 Abb. im Text, 4 Skizzen, 2 Profile, 2 Karten, 36 Bilder im Anhang.
ISBN 3-88009-002-5 (*vergriffen*)

Heft 4: PACHUR, Hans-Joachim (1966)
Untersuchungen zur morphoskopischen Sandanalyse. - 35 S., 37 Diagramme, 2 Tab., 21 Abb.
ISBN 3-88009-003-3 (*vergriffen*)

Heft 5: Arbeitsberichte aus der Forschungsstation Bardai/Tibesti. I. Feldarbeiten 1964/65 (1967)
65 S., 34 Abb., 1 Karte.
ISBN 3-88009-004-1 (*vergriffen*)

Heft 6: ROSTANKOWSKI, Peter (1969)
Siedlungsentwicklung und Siedlungsformen in den Ländern der russischen Kosakenheere. - 84 S., 15 Abb., 16 Bilder, 2 Karten.
ISBN 3-88009-005-X (DM 15,-)

Heft 7: SCHULZ, Georg (1969)
Versuch einer optimalen geographischen Inhaltsgestaltung der topographischen Karte 1 : 25 000 am Beispiel eines Kartenausschnittes. - 28 S. 6 Abb. im Text, 1 Karte im Anhang.
ISBN 3-88009-006-8 (DM 10,-)

Heft 8: Arbeitsberichte aus der Forschungsstation Bardai/Tibesti. II. Feldarbeiten 1965/66 (1969)
82 S., 15 Abb., 27 Fig., 13 Tafeln, 11 Karten.
ISBN 3-88009-007-6 (DM 15,-)

Heft 9: JANNSEN, Gert (1970)
Morphologische Untersuchungen im nördlichen Tarso Voon (Zentrales Tibesti). - 66 S., 12 Abb., 41 Bilder, 3 Karten.
ISBN 3-88009-008-4 (DM 15,-)

Heft 10: JÄKEL, Dieter (1971)
Erosion und Akkumulation im Enneri Bardague-Araye des Tibesti-Gebirges (zentrale Sahara) während des Pleistozäns und Holozäns. - Arbeit aus der Forschungsstation Bardai/Tibesti, 55 S., 13 Abb., 54 Bilder, 3 Tab., 1 Nivellement (4 Teile), 60 Profile, 3 Karten (6 Teile).
ISBN 3-88009-009-2 (*vergriffen*)

Heft 11: MÜLLER, Konrad (1971)
Arbeitsaufwand und Arbeitsrhythmus in den Agrarlandschaften Süd- und Südostfrankreichs: Les Dombes bis Bouches-du-Rhône. - 64 S., 18 Karten, 26 Diagramme, 10 Fig., zahlreiche Tabellen.
ISBN 3-88009-010-6 (DM 25,-)

Heft 12: OBENAUF, K. Peter (1971)
Die Enneris Gonoa, Toudoufou, Oudingueur und Nemagayesko im nordwestlichen Tibesti. Beobachtungen zu Formen und Formung in den Tälern eines ariden Gebirges. - Arbeit aus der Forschungsstation Bardai/Tibesti. 70 S., 6 Abb., 10 Tab., 21 Photos, 34 Querprofile, 1 Längsprofil, 9 Karten.
ISBN 3-88009-011-4 (DM 20,-)

Heft 13: MOLLE, Hans-Georg (1971)
Gliederung und Aufbau fluviatiler Terrassenakkumulation im Gebiet des Enneri Zoumri (Tibesti-Gebirge). - Arbeit aus der Forschungsstation Bardai/Tibesti. 53 S., 26 Photos, 28 Fig., 11 Profile, 5 Tab., 2 Karten.
ISBN 3-88009-012-2 (DM 10,-)

Heft 14: STOCK, Peter (1972)
Photogeologische und tektonische Untersuchungen am Nordrand des Tibesti-Gebirges, Zentral-Sahara, Tchad. - Arbeit aus der Forschungsstation Bardai/Tibesti. 73 S., 47 Abb., 4 Karten.
ISBN 3-88009-013-0 (DM 15,-)

Heft 15: BIEWALD, Dieter (1973)
Die Bestimmungen eiszeitlicher Meeresoberflächentemperaturen mit der Ansatztiefe typischer Korallenriffe. - 40 S., 16 Abb., 26 Seiten Fig. und Karten.
ISBN 3-88009-015-7 (DM 10,-)

Heft 16: Arbeitsberichte aus der Forschungsstation Bardai/Tibesti. III. Feldarbeiten 1966/67 (1972)
156 S., 133 Abb., 41 Fig., 34 Tab., 1 Karte.
ISBN 3-88009-014-9 (DM 45,-)

**Berliner Geographische Abhandlungen**
Im Selbstverlag des Instituts für Geographische Wissenschaften der Freien Universität Berlin,
Grunewaldstr. 35, D-12165 Berlin (Preise zuzüglich Versandspesen)
Postanschrift: Geomorphologisches Laboratorium, Altensteinstr. 19, D 14195 Berlin

---

Heft 17: PACHUR, Hans-Joachim (1973)
Geomorphologische Untersuchungen im Raum der Serir Tibesti (Zentralsahara). - Arbeit aus der Forschungsstation Bardai/ Tibesti. 58. S., 39 Photos, 16 Fig. und Profile, 9 Tab., 1 Karte.
ISBN 3-88009-016-5 (DM 25,-)

Heft 18: BUSCHE, Detlef (1973)
Die Entstehung von Pedimenten und ihre Überformung, untersucht an Beispielen aus dem Tibesti-Gebirge, Republique du Tchad. - Arbeit aus der Forschungsstation Bardai/Tibesti. 130 S., 57 Abb., 22 Fig., 1 Tab., 6 Karten.
ISBN 3-88009-017-3 (DM 40,-)

Heft 19: ROLAND, Norbert W. (1973)
Anwendung der Photointerpretation zur Lösung stratigraphischer und tektonischer Probleme im Bereich von Bardai und Aozou (Tibesti-Gebirge, Zentral-Sahara). - Arbeit aus der Forschungsstation Bardai/Tibesti. 48 S., 35 Abb., 10 Fig., 4 Tab., 2 Karten.
ISBN 3-88009-018-1 (DM 20,-)

Heft 20: SCHULZ, Georg (1974)
Die Atlaskartographie in Vergangenheit und Gegenwart und die darauf aufbauende Entwicklung eines neuen Erdatlas. - 59 S., 3 Abb., 8 Fig., 23 Tab., 8 Karten.
ISBN 3-88009-019-X (DM 35,-)

Heft 21: HABERLAND, Wolfram (1975)
Untersuchungen an Krusten, Wüstenlacken und Polituren auf Gesteinsoberflächen der nördlichen und mittleren Sahara (Libyen und Tchad). - Arbeit aus der Forschungsstation Bardai/Tibesti. 71 S., 62 Abb. 24 Fig., 10 Tab.
ISBN 3-88009-020-3 (DM 50,-)

Heft 22: GRUNERT, Jörg (1975)
Beiträge zum Problem der Talbildung in ariden Gebieten, am Beispiel des zentralen Tibesti-Gebirges (Rep. du Tchad). - Arbeit aus der Forschungsstation Bardai/Tibesti. 96 S., 3 Tab., 6 Fig., 58 Profile, 41 Abb., 2 Karten.
ISBN 3-88009-021-1 (DM 35,-)

Heft 23: ERGENZINGER, Peter Jürgen (1978)
Das Gebiet des Enneri Misky im Tibesti-Gebirge, République du Tchad - Erläuterungen zu einer geomorphologischen Karte 1 : 200 000. - Arbeit aus der Forschungsstation Bardai/Tibesti. 60 S., 6 Tab., 24 Fig., 24 Photos, 2 Karten.
ISBN 3-88009-022-X (DM 40,-)

Heft 24: Arbeitsberichte aus der Forschungsstation Bardai/Tibesti. IV. Feldarbeiten 1967/68, 1969/70, 1974 (1976)
73 S., 24 Fig., 79 Abb., 12 Tab., 2 Karten.
ISBN 3-88009-023-8 (DM 30,-)

Heft 25: MOLLE, Hans-Georg (1979)
Untersuchungen zur Entwicklung der vorzeitlichen Morphodynamik im Tibesti-Gebirge (Zentral-Sahara) und in Tunesien. - Arbeit aus der Forschungsstation Bardai/Tibesti. 104 S., 22 Abb., 40 Fig., 15 Tab., 3 Karten.
ISBN 3-88009-024-6 (DM 35,-)

Heft 26: BRIEM, Elmar (1977)
Beiträge zur Genese und Morphodynamik des ariden Formenschatzes unter besonderer Berücksichtigung des Problems der Flächenbildung am Beispiel der Sandschwemmebenen in der östlichen Zentralsahara. - Arbeit aus der Forschungsstation Bardai/Tibesti. 89 S., 38 Abb., 23 Fig., 8 Tab., 155 Diagramme, 2 Karten.
ISBN 3-88009-025-4 (DM 25,-)

Heft 27: GABRIEL, Baldur (1977)
Zum ökologischen Wandel im Neolithikum der östlichen Zentralsahara. - Arbeit aus der Forschungsstation Bardai/Tibesti. 111 S., 9 Tab., 32 Fig., 41 Photos, 2 Karten.
ISBN 3-88009-026-2 (DM 35,-)

Heft 28: BÖSE, Margot (1979)
Die geomorphologische Entwicklung im westlichen Berlin nach neueren stratigraphischen Untersuchungen. - 46 S., 3 Tab., 14 Abb., 25 Photos, 1 Karte.
ISBN 3-88009-027-0 (*vergriffen*)

Heft 29: GEHRENKEMPER, Johannes (1978)
Rañas und Reliefgenerationen der Montes de Toledo in Zentralspanien. - 81 S., 68 Abb., 3 Tab., 32 Photos, 2 Karten.
ISBN 3-88009-028-9 (DM 20,-)

Heft 30: STÄBLEIN, Gerhard (Hrsg.) (1978)
Geomorphologische Detailaufnahme. Beiträge zum GMK-Schwerpunktprogramm I. - 90 S., 38 Abb. und Beilagen, 17 Tab.
ISBN 3-88009-029-7 (DM 18,-)

Heft 31: BARSCH, Dietrich & LIEDTKE, Herbert (Hrsg.) (1980)
Methoden und Anwendbarkeit geomorphologischer Detailkarten. Beiträge zum GMK-Schwerpunktprogramm II. - 104 S., 25 Abb., 5 Tab.
ISBN 3-88009-030-0 (DM 17,-)

**Berliner Geographische Abhandlungen**
Im Selbstverlag des Instituts für Geographische Wissenschaften der Freien Universität Berlin,
Grunewaldstr. 35, D-12165 Berlin (Preise zuzüglich Versandspesen)
Postanschrift: Geomorphologisches Laboratorium, Altensteinstr. 19, D 14195 Berlin

---

Heft 32: Arbeitsberichte aus der Forschungsstation Bardai/Tibesti. V. Abschlußbericht (1982)
182 S., 63 Fig. und Abb., 84 Photos, 4 Tab., 5 Karten.
ISBN 3-88009-031-9 (DM 60,-)

Heft 33: TRETER, Uwe (1981)
Zum Wasserhaushalt schleswig-holsteinischer Seengebiete. - 168 S., 102 Abb., 57 Tab.
ISBN 3-88009-033-5 (DM 40,-)

Heft 34: GEHRENKEMPER, Kirsten (1981)
Rezenter Hangabtrag und geoökologische Faktoren in den Montes de Toledo. Zentralspanien. - 78 S., 39 Abb., 13 Tab., 24 Photos, 4 Karten.
ISBN 3-88009-032-7 (DM 20,-)

Heft 35: BARSCH, Dietrich & STÄBLEIN, Gerhard (Hrsg.) (1982)
Erträge und Fortschritte der geomorphologischen Detailkartierung. Beiträge zum GMK-Schwerpunktprogramm III. - 134 S., 23 Abb., 5 Tab., 5 Beilagen.
ISBN 3-88009-034-3 (DM 30,-)

Heft 36: STÄBLEIN, Gerhard (Hrsg.) (1984):
Regionale Beiträge zur Geomorphologie. Vorträge des Ferdinand von Richthofen-Symposiums, Berlin 1983. - 140 S., 67 Abb., 6 Tab.
ISBN 3-88009-035-1 (DM 35,-)

Heft 37: ZILLBACH, Käthe (1984)
Geoökologische Gefügemuster in Süd-Marokko. Arbeit im Forschungsprojekt Mobilität aktiver Kontinentalränder. - 95 S., 61 Abb., 2 Tab., 3 Karten.
ISBN 3-88009-036-X (DM 18,-)

Heft 38: WAGNER, Peter (1984)
Rezente Abtragung und geomorphologische Bedingungen im Becken von Ouarzazate (Süd-Marokko). Arbeit im Forschungsprojekt Mobilität aktiver Kontinentalränder. - 112 S., 63 Abb., 48 Tab., 3 Karten.
ISBN 3-88009-037-8 (DM 18,-).

Heft 39: BARSCH, Dietrich & LIEDTKE, Herbert (Hrsg.) (1985)
Geomorphological Mapping in the Federal Republic of Germany. Contributions to the GMK priority program IV. - 89 S., 16 Abb., 5 Tab.
ISBN 3-88009-038-6 (DM 22,50)

Heft 40: MÄUSBACHER, Roland (1985)
Die Verwendbarkeit der geomorphologischen Karte 1 : 25 000 (GMK 25) der Bundesrepublik Deutschland für Nachbarwissenschaften und Planung. Beiträge zum GMK-Schwerpunktprogramm V. - 97 S., 15 Abb., 31 Tab., 21 Karten.
ISBN 3-88009-039-4 (DM 18,-)

Heft 41: STÄBLEIN, Gerhard (Hrsg.) (1986)
Geo- und biowissenschaftliche Forschungen der Freien Universität Berlin im Werra-Meißner-Kreis (Nordhessen). Beiträge zur Werra-Meißner-Forschung I. - 265 S., 82 Abb., 45 Tab., 3 Karten.
ISBN 3-88009-040-8 (DM 28,-)

Heft 42: BARSCH, Dietrich & LESER, Hartmut (Hrsg.) (1987)
Regionale Beispiele zur geomorphologischen Kartierung in verschiedenen Maßstäben (1 : 5 000 bis 1 : 200 000). Beiträge zum GMK-Schwerpunktprogramm VI. - 80 S., 10 Abb., 9 Beilagen.
ISBN 3-88009-041-6 (DM 35,-)

Heft 43: VAHRSON, Wilhelm-Günther (1987)
Aspekte bodenphysikalischer Untersuchungen in der libyschen Wüste. Ein Beitrag zur Frage spätpleistozäner und holozäner Grundwasserbildung. - 92 S., 12 Abb., 56 Fig., 7 Tab., 1 Karte.
ISBN 3-88009-042-4 (DM 18,-)

Heft 44: PACHUR, Hans-Joachim & RÖPER, Hans-Peter (1987)
Zur Paläolimnologie Berliner Seen. - 150 S., 42 Abb., 28 Tab.
ISBN 3-88009-043-2 (DM 30,-)

Heft 45: BERTZEN, Günter (1987)
Diatomeenanalytische Untersuchungen an spätpleistozänen und holozänen Sedimenten des Tegeler Sees. - 150 S., 19 Fig., 2 Tab., 38 Abb., 7 Anlagen
ISBN 3-88009-044-0 (DM 30,-)

Heft 46: FRANK, Felix (1987)
Die Auswertung großmaßstäbiger Geomorphologischer Karten (GMK 25) für den Schulunterricht. Beiträge zum GMK-Schwerpunktprogramm VII. - 100 S., 29 Abb., Legende der Geomorphologischen Karte 1 : 25 000 (GMK 25).
ISBN 3-88009-045-9 (DM 18,-)

Heft 47: LIEDTKE, Herbert (Hrsg.) (1988)
Untersuchungen zur Geomorphologie der Bundesrepublik Deutschland - Neue Ergebnisse der Geomorphologischen Kartierung. Beiträge zum GMK-Schwerpunktprogramm VIII. - 225 S., 77 Abb., 12 Tab.
ISBN 3-88009-046-7 (DM 60,-)

**Berliner Geographische Abhandlungen**
Im Selbstverlag des Instituts für Geographische Wissenschaften der Freien Universität Berlin,
Grunewaldstr. 35, D-12165 Berlin (Preise zuzüglich Versandspesen)
Postanschrift: Geomorphologisches Laboratorium, Altensteinstr. 19, D 14195 Berlin

---

Heft 48: MÖLLER, Klaus (1988)
Reliefentwicklung und Auslaugung in der Umgebung des Unterwerra-Sattels (Nordhessen). - 187 S., 55 Abb., 20 Tab., 2 Karten.
ISBN 3-88009-047-5 (DM 25,-)

Heft 49: SCHMIDT, Karl-Heinz (1988)
Die Reliefentwicklung des Colorado Plateaus. - 183 S., 50 Abb., 17 Photos, 20 Tab., 2 Karten.
ISBN 3-88009-048-3 (DM 60,-)

Heft 50: STÜVE, Peter (1988)
Die Schneeschmelze eines nordskandinavischen Einzugsgebietes ermittelt über die räumlich-zeitliche Variation des Strahlungs- und Energiehaushalts. - 119 S., 42 Abb., 13 Tab., 21 Karten.
ISBN 3-88009-050-1 (DM 30,-)

Heft 51: BÖSE, Margot (1989)
Methodisch-stratigraphische Studien und paläomorphologische Untersuchungen zum Pleistozän südlich der Ostsee. - 114 S., 54 Abb., 17 Tab., 1 Bild.
ISBN 3-88009-051-3 (DM 25,-)

Heft 52: WALTHER, Michael (1990)
Untersuchungsergebnisse zur jungpleistozänen Landschaftsentwicklung Schwansens (Schleswig-Holstein). - 143 S., 60 Abb., 4 Tab., 9 Fotos.
ISBN 3-88009-052-1 (DM 20,-)

Heft 53: KARRASCH, Heinz (Hrsg.) (1990)
Prozeßabläufe bei der Landschafts- und Landesentwicklung: Methoden, Ergebnisse, Anwendungen. Festschrift für Wilhelm Wöhlke zum 65. Geburtstag. - 300 S., 121 Abb., 35 Tab.
ISBN 3-88009-053-X (DM 80,-)

Heft 54: KRÖPELIN, Stefan (1993)
Zur Rekonstruktion der spätquartären Umwelt am Unteren Wadi Howar (Südöstliche Sahara / NW-Sudan). - 293 S., 53 Abb., 47 Tab., 92 Fotos und Fototafeln, 1 Satellitenbildmosaik.
ISBN 3-88009-054-6 (DM 35,-)

Heft 55: WÜNNEMANN, Bernd (1993)
Ergebnisse zur jungpleistozänen Entwicklung der Langseerinne Südangelns in Schleswig-Holstein. - 167 S., 59 Abb., 8 Tab., 15 Bilder.
ISBN 3-88009-056-4 (DM 20,-)

Heft 56: JACOBSHAGEN, Volker, MÖLLER, Klaus & JÄKEL, Dieter (Hrsg.) (1993)
Hoher Meißner und Eschweger Becken. Geowissenschaftliche und vegetationskundliche Charakteristik einer Nordhessischen Landschaft. (In Vorbereitung).
ISBN 3-88009-057-2

Heft 57: HOFMANN, Jürgen (1993)
Geomorphologische Untersuchungen zur jungquartären Klimaentwicklung des Helan Shan und seines westlichen Vorlandes (Autonomes Gebiet Innere Mongolei/VR China). - 187 S., 46 Abb., 23 Tab., 85 Photos, 7 Beilagen.
ISBN 3-88009-058-0 (DM 25,-)

Heft 58: SCHULZ, Georg (1994)
Die pleistozäne Vergletscherung der Anden Perus und Boliviens abgeleitet aus Formen einer flächendeckend-integrativen Höhenlinienanalyse. 156 S., 86 Abb., 5 Tab., 2 Karten.
ISBN 3-88009-059-9 (DM 68,-).

Heft 59: DE JONG, Carmen (1995)
Temporal and spatial interactions between river bed roughness, geometry, bedload transport and flow hydraulics in mountain streams - examples from Squaw Creek, Montana (USA) and Lainbach/Schmiedlaine, Upper Bavaria (Germany). 229 S., 255 Abb., 7 Tab.
ISBN 3-88009-060-2 (DM 60,-).